Muskoka and Shawanaga domains, Central Gneiss Belt, Grenville Province, Ontario: Geochemical and geochronological constraints on pre-Grenvillian and Grenvillian geological evolution

by

Trond Slagstad

Submitted in partial fulfillment of the requirements

for the degree of Doctor of Philosophy

at

Dalhousie University

Halifax, Nova Scotia

April 2003

0-612-79409-1

Canadä

DALHOUSIE UNIVERSITY

FACULTY OF GRADUATE STUDIES

The undersigned hereby certify that they have read and recommend to the Faculty of
Graduate Studies for acceptance a thesis entitled "Muskoka and Shawanaga domains,
Central Gneiss Belt, Grenville Province, Ontario: Geochemical and geochronological
constraints on pre-Grenvillian and Grenvillian geological evolution" by Trond Slagstad in
partial fulfillment for the degree of Doctor of Philosophy.

Dated: _____March 11, 2003_____

External Examiner: ___███████████████████___

Research Supervisor: ___███████████████████___

Examining Committee: ___███████████████████___

___███████████████████___
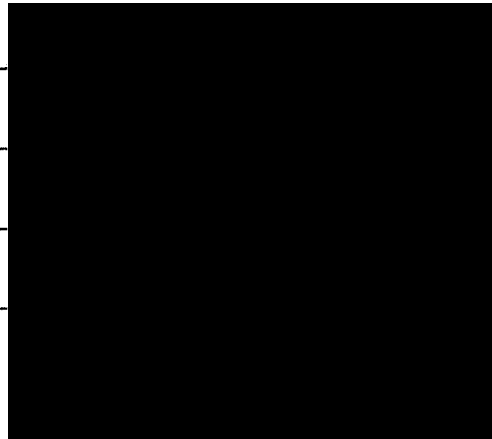
DALHOUSIE UNIVERSITY

DATE: <u>13 March, 2003</u>

AUTHOR: <u>Trond Slagstad</u>

TITLE: <u>Muskoka and Shawanaga domains, Central Gneiss Belt, Grenville Province,</u>
<u>Ontario: Geochemical and geochronological constraints on pre-Grenvillian</u>
<u>and Grenvillian geological evolution</u>

DEPARTMENT OR SCHOOL: <u>Earth Sciences</u>

DEGREE: <u>Ph.D</u>   CONVOCATION: <u>May</u>   YEAR: <u>2003</u>

Table of contents

v

List of figures

xi

List of tables

Abstract

The Muskoka and Shawanaga domains in the Central Gneiss Belt, southwestern Grenville Province, Ontario comprise ca. 1500-1350 Ma migmatitic orthogneisses and volumetrically minor paragneisses that were deformed and metamorphosed under upper amphibolite- to granulite-facies conditions during the Grenvillian orogeny between ca. 1090 and 1050 Ma. The objectives of this study are: i) to determine the tectonic setting and petrogenesis of the protoliths to the high-grade gneisses; and ii) to investigate the petrogenesis of the migmatites and its possible relationship to deformation. The new field, geochemical, petrographic, and geochronological data is used to test and further constrain current models for the evolution of the Laurentian margin between ca. 1500 and 1000 Ma.

The geochemical and geochronological data show that volumetrically dominant calc-alkaline rocks in the Muskoka domain, shown earlier to range in age from ca. 1480 to 1450 Ma, are spatially and temporally associated with A-type granite and charnockite. The calc-alkaline rocks probably formed in a juvenile continental arc at the southeastern (present-day coordinates) Laurentian margin, and the association with A-type rocks is interpreted to reflect intra-arc extension. Granulite-facies metamorphism in the Central Gneiss Belt was coeval with or slightly post-dated emplacement of the calc-alkaline and A-type rocks. The high-grade metamorphism could reflect increased heat flow resulting from arc/back-arc extension or the waning stages of voluminous arc magmatism, or from arc-continent collision, for which there is little direct evidence.

Petrographic observations from two types of migmatite in the Muskoka domain suggest that the large proportion of leucosome (up to 40-50 vol.%) is unlikely to have formed by dehydration melting alone, suggesting that partial melting took place in response to influx of externally derived fluids. The two types of migmatite contain leucosomes that, based on whole-rock geochemical data, are interpreted to represent disequilibrium and equilibrium melts. The disequilibrium melts formed in strongly migmatitic, granodioritic host rocks that display evidence of syn-melting deformation, whereas the equilibrium melts formed in less migmatitic, dioritic host rocks that lack evidence of syn-melting deformation. Based on field observations, geochemical data, and experimental studies by others, the disequilibrium melts are interpreted to have formed as a result of rapid, deformation-enhanced melt segregation. The less migmatitic dioritic host rocks were stronger, effectively shielding the melts from deformation, and the resulting slow melt segregation rates resulted in melts with equilibrium compositions.

Leucosome in the Muskoka and Shawanaga domains, dated at ca. 1068 and 1055 Ma, respectively, is typically associated with southeast-directed, normal-sense shear bands. The geochronological data, however, suggest that the orogen was undergoing northwest-directed convergence at those times. One interpretation is that the Muskoka and Shawanaga domains represent mid-crustal zones of channel flow in which ductile material was transported from the core toward the exterior of the orogen.

Acknowledgements

1. Introduction

1.1. Introduction

The Grenville Province in eastern Canada is part of the middle to late Mesoproterozoic Grenville orogen, extending across the North American continent from Mexico and Texas in the southwest to Labrador and Greenland in the northeast (Fig. 1.1a). The orogen is further represented by inliers in the Paleozoic Appalachian and Caledonian orogens, and the Sveconorwegian Province in southern Norway and Sweden is believed to represent its continuation into northern Europe (e.g., Gower et al., 1990; Cosca et al., 1998; Fig. 1.1b). In addition, reconstructions of Rodinia (e.g., Dalziel, 1991; Hoffmann, 1991; Moores, 1991; Borg and DePaolo, 1994; Weil et al., 1998) suggest a further continuation of the belt from Central America through Antarctica and eastern India to Australia. The Grenville orogen, and coeval orogens elsewhere in the world, appear to have been part of a worldwide orogenic system formed during assembly of a late Mesoproterozoic to early Neoproterozoic supercontinent, generally referred to as Rodinia (McMenamin and McMenamin, 1990). The term 'Grenville orogen' is used here to denote the entire orogen as outlined above, whereas 'Grenville Province' is used specifically to denote the part of the Grenville orogen exposed in eastern Canada (Fig. 1.2 inset).

The Grenville orogen is generally believed to have formed as a result of continent-continent and/or continent-arc collision(s) (e.g., Rivers, 1997). The southwestern Grenville Province in Ontario, which is the area of study (Fig. 1.2), exposes mid- to lower-crustal levels (Culshaw et al., 1997) of what is believed to have been a Himalayan-scale orogen (e.g., Dewey and Burke, 1973; Windley, 1986; Hanmer, 1988), formed between ca. 1.2-1.0 Ga. The Grenville Province is underlain by high-grade gneisses and migmatites, ranging in age from Archean to Mesoproterozoic (Rivers, 1997), that probably formed in continental/island arc and back-arc settings (e.g., Rivers and Corrigan, 2000). Older rocks, confined to the western parts of the Province close to the foreland, are interpreted to represent the reworked pre-Grenvillian margin of Laurentia,

1
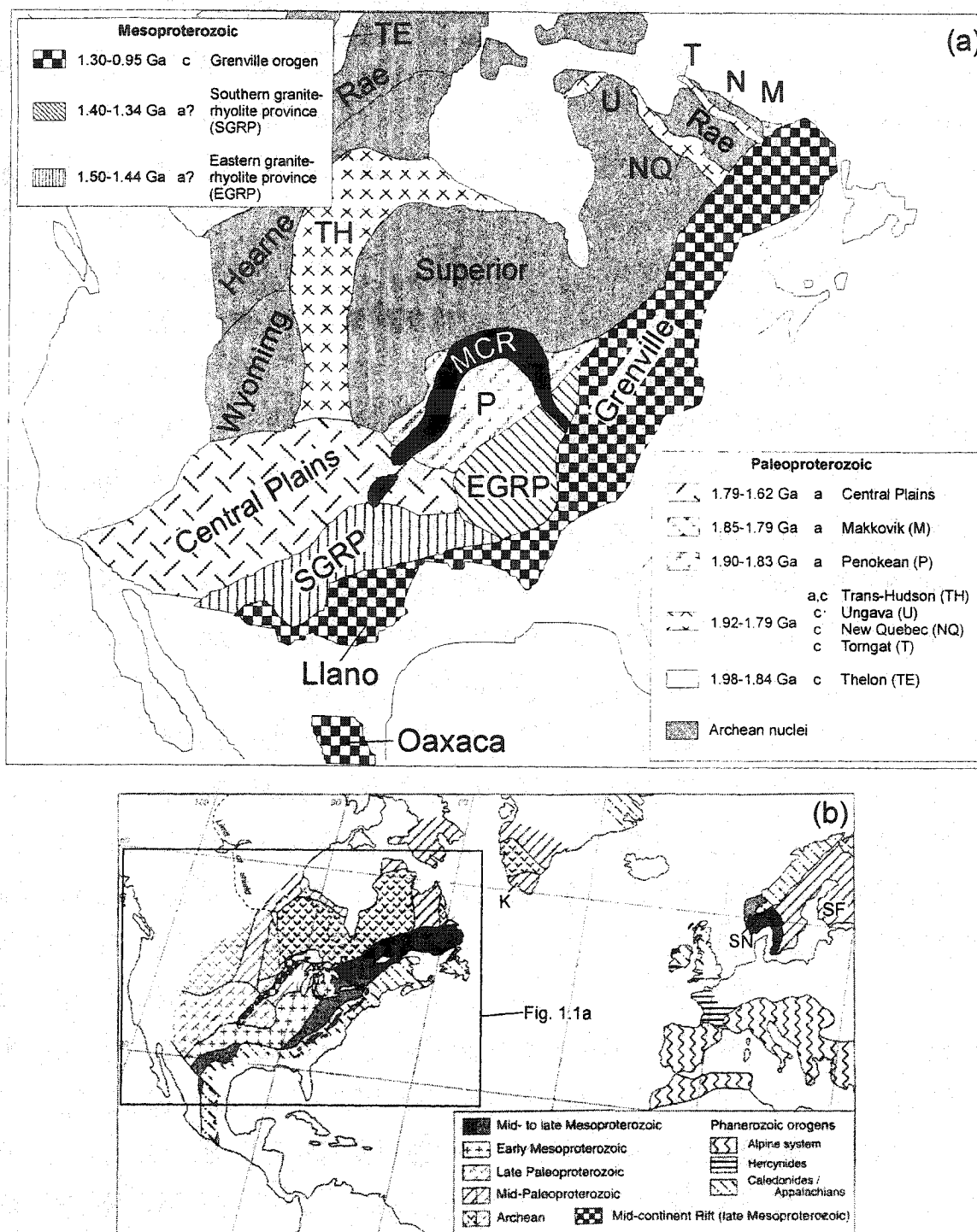
Fig. 1.1 (a) Precambrian geology of North America, from Rivers (1997), modified after Hoffman (1989). MCR (black fill)- Mid-continent rift (1.1-1.09 Ga). Present-day coastline of North America shown for reference. Patterns, names, age ranges, and abbreviations explained in the legend, except 'a' - accretionary and 'c' collisional orogen, respectively. (b) Map showing the extent of the Grenville orogen (gray fill) in North America and the North Atlantic region. From Davidson (1998). Abbreviations: N=Nain, K=Ketilidian orogen, SN=Sveconorwegian province, SF=Svecofennian province.
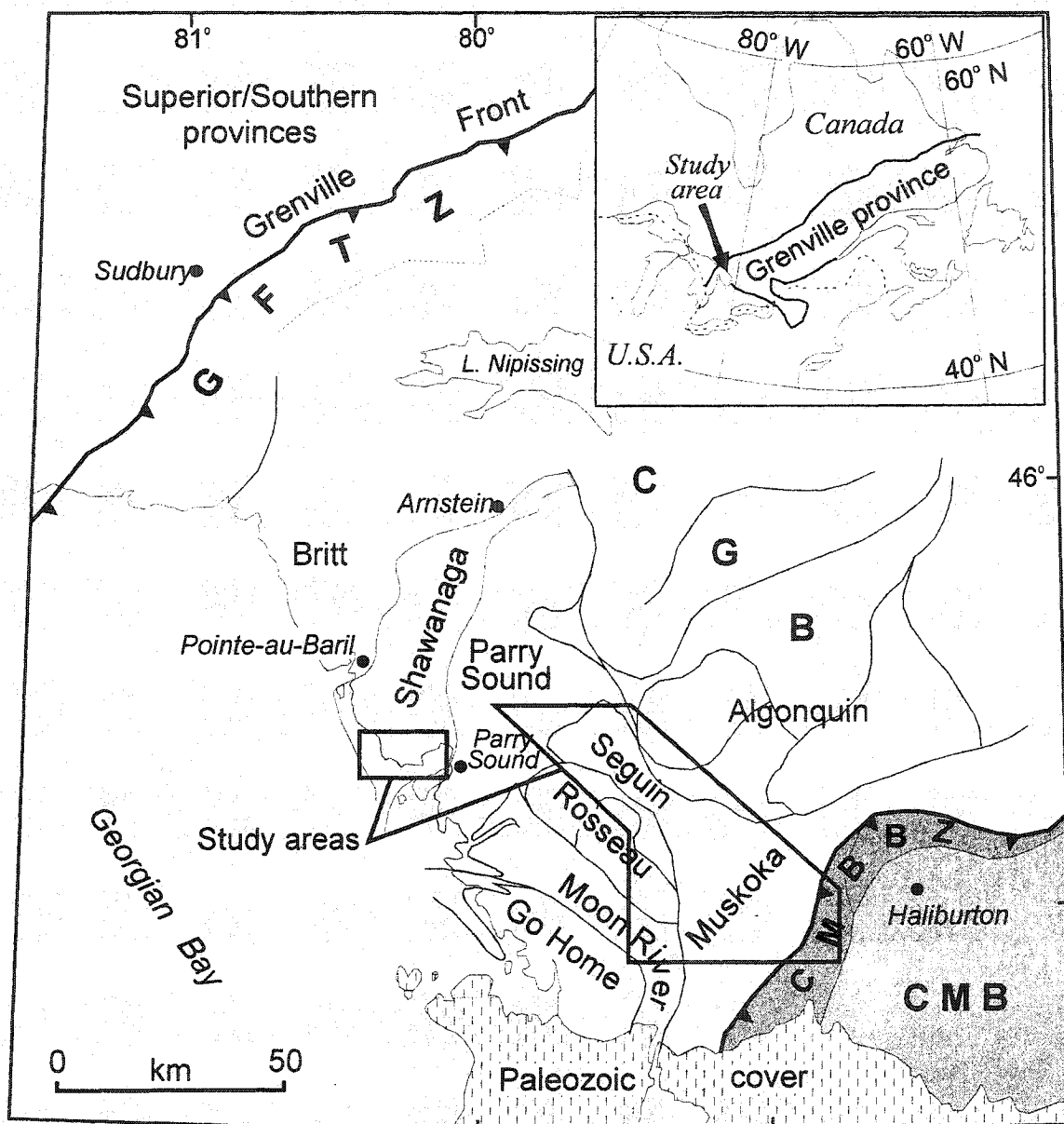
Fig. 1.2 Simplified geological map of the study area in the southwestern Grenville Province, Ontario. Inset map shows location of study area in the Grenville Province in eastern Canada. Heavy barbed lines indicate major thrust boundaries. Thin lines represent domain boundaries after Culshaw *et al.* (1983, 1988, 1989, 1990), Davidson (1984), and Davidson and van Breemen (1988), modified by Culshaw *et al.* (1997). Abbreviations: GFTZ=Grenville Front Tectonic Zone, CGB=Central Gneiss Belt, CMB=Central Metasedimentary Belt, CMBBZ=Central Metasedimentary Belt boundary thrust zone .

whereas younger rocks, dominantly located to the southeast, are believed to be allochthonous with regard to Laurentia (e.g., Carr *et al.*, 2000). The Grenville Province, therefore, not only offers an opportunity to study mid- to lower-crustal processes in large orogens, but can also provide information about the preceding geological history of the southeastern margin of Laurentia.

This thesis reports the results of two seasons of field work along and east of Georgian Bay in Ontario, including geochemical, petrological, and geochronological investigations of high-grade, mostly migmatitic, gneisses in the Muskoka and Shawanaga domains, Central Gneiss Belt (CGB), Ontario. The Muskoka domain constitutes the immediate footwall to the Central Metasedimentary Belt boundary thrust zone, a crustal-scale shear zone marking the boundary between allochthonous rocks with Laurentian affinities and allochthonous rocks lacking clear evidence of contiguity to Laurentia. The Shawanaga domain forms the hanging wall to the Shawanaga shear zone, marking the boundary between allochthonous rocks with Laurentian affinities and parautochthonous rocks. The structural settings of the Muskoka and Shawanaga domains make them important targets for investigations of Grenvillian and pre-Grenvillian orogenic processes and evolution.

Although the large geochronological database for the CGB in Ontario suggests a major crustal forming event at ca. 1450 Ma, little is known about the tectonic setting and evolution of the CGB at this time. The geochemical data presented in Chapter 2, combined with new geochronological data presented in Chapter 5, allow current tectonic models for the pre-Grenvillian evolution of the CGB to be refined and demonstrate the importance of considering geochemistry in addition to geochronology when undertaking investigations of high-grade terranes.

Evidence of partial melting in the form of migmatites is common in the CGB. Earlier petrographic investigations of the migmatites provide some information about their petrogenesis (Timmermann *et al.*, 2002); however, the relatively simple mineralogy of the migmatites limits our understanding of partial melting reactions in these rocks. The geochemical and petrographic data presented in Chapter 3 allow new interpretations

to be made regarding the relationship between partial melting and deformation and of the role of fluids during melting. Combined with new field observations presented in Chapter 4, and geochronological data discussed in Chapter 5, inferences can also be made regarding the temporal and mechanical relationship between partial melting and orogenic evolution.

1.2. Geological background

1.2.1. Pre-Grenvillian tectonic evolution of the southeastern margin of Laurentia

Following the amalgamation of Archean microcontinents or nuclei, the geological evolution of the North American craton spanned almost a billion years, ending with the Grenvillian orogeny at approximately 1.0 Ga (Fig. 1.1). Van Schmus *et al.* (1993) and Davidson (1998) presented extensive reviews of the late Paleoproterozoic and Mesoproterozoic evolution of Laurentia and the Grenville Province, and only a brief overview is presented here with emphasis on the Mesoproterozoic era. In recent years it has become clear that the geological evolution of Baltica during this time period was closely linked to that of Laurentia (Gower *et al.*, 1990; Gower, 1992); however, for the sake of brevity, the Laurentia-Baltica connection is referred to only in passing.

Late Paleoproterozoic evolution

Amalgamation of the proto-North American craton by collisions between Archean microcontinents in the period 1.9-1.8 Ga formed orogens, such as the Trans-Hudson orogen (Lewry and Stauffer, 1990), that are now internal to Laurentia (Hoffmann, 1989) (Fig. 1.1b). Coeval arc accretion and orogenesis took place along the southeastern margin of the craton, represented by the ca. 1.9-1.8 Ga Penokean, Makkovikian, and Ketilidian orogens in North America and Greenland, and the Svecofennian orogen in Baltica (Gower *et al.*, 1990 and references therein). Continued crustal growth between ca. 1.8-1.6 Ga is represented by the Central Plains orogen (Sims and Peterman, 1986), which consists of the ca. 1.8-1.7 Ga Yavapai, and the ca. 1.7-1.6 Ga Mazatzal orogens (e.g., Van Schmus *et al.*, 1996). The Yavapai-Mazatzal orogens are considered to represent accreted arc terranes (e.g., Condie, 1986; Condie and Chomiak, 1996), whereas

rocks of similar age to the northeast along the Laurentia-Baltica margin have anorogenic characteristics, e.g. the Killarney Complex in Southern Ontario (van Breemen and Davidson, 1988; Clifford, 1990) and the Transscandinavian Igneous Belt in Sweden and central Norway (Lindh and Persson, 1990; Roberts *et al.*, 1999). Thus, the tectonic regime along the Laurentia-Baltica margin at this time is not entirely clear, and may have varied along its length (cf., Gower, 1992).

Early Mesoproterozoic evolution

The first 100 My of the Mesoproterozoic era, between 1.6 and 1.5 Ga, was a period of relative quiescence, followed by two periods of widespread granitic and rhyolitic magmatism in the midcontinental USA, forming the Eastern (ca. 1470±30 Ma) and Southern (ca. 1370±30 Ma) granite-rhyolite provinces (e.g., Van Schmus *et al.*, 1996). The Central Plains orogen was intruded by abundant granite plutons during the same time periods, in particular during formation of the Eastern granite-rhyolite province. The granite-rhyolite provinces are generally buried by younger strata, with only a few known exposures; thus, the study of these provinces has relied heavily on subsurface drill-cores and some seismic data.

The granite-rhyolite provinces dominantly comprise rhyolites and epizonal and mesozonal granite plutons that are lithologically and chemically similar in both provinces. Other rock types are subordinate and in many cases younger. The tectonic setting of these provinces is debated. The granites and rhyolites have A-type geochemical characteristics (e.g., Anderson, 1983; Lidiak, 1996), and are largely undeformed and unmetamorphosed. Based on these characteristics, a number of authors (e.g., Anderson, 1983; Hoffmann, 1989; Kisvarsanyi and Kisvarsanyi, 1990; Windley, 1993) have inferred an anorogenic setting related to continental rifting or supercontinent break-up. Other interpretations recognize that ca. 1.4 Ga granite plutons intruded older crust north and northwest of the granite-rhyolite provinces during regional contractional deformation (Kirby *et al.*, 1995; Nyman and Karlstrom, 1997), suggesting an active margin setting. Bowring *et al.* (1991) observed that some of the rocks in the St. Francois Mountains, Missouri, have relatively juvenile Nd isotopic compositions and argued for

partial melting of an accreted arc terrane formed at ca. 1.5 Ga. Kay *et al.* (1989) proposed a similar model by analogy with the Paleozoic to Mesozoic rhyolite provinces in southern South America. Later, Van Schmus *et al.* (1996) identified a relatively sharp Nd model age boundary within the granite-rhyolite provinces. North and northwest of this boundary the rocks have Paleoproterozoic model ages (>1.55 Ga) whereas rocks to the south and southeast have early Mesoproterozoic (<1.55 Ga) model ages. Recognizing that the granites and rhyolites probably represent crustal melts, Van Schmus *et al.* (1996) suggested that the rocks with the youngest model ages formed by partial melting of juvenile assemblages that were accreted onto the continental margin shortly before the melting event. Menuge *et al.* (2002) proposed a similar model, involving a juvenile, calc-alkaline, arc-related source. A significant problem with all of these models is, however, the lack of identifiable source rocks in the midcontinental United States.

1.2.2. The Grenville Province

In the beginning of the last century, Wilson (1918, 1925) recognized the Grenville Province as different from the rest of the Canadian Shield and separated from rocks to the northwest by "...an extended belt of banded gneisses...". Derry (1950) later recognized this "extended belt of banded gneisses" as the northwest boundary of the Grenville Province, and referred to it as the "Grenville Front". This term is still widely used by workers in the Grenville Province. Davidson (1998) presents a more detailed discussion on the history of geological investigations in the Grenville Province.

Over the last decade or so, several papers have summarized the available geological data for the Grenville Province in Ontario (e.g., Rivers *et al.*, 1989; Easton, 1992; Davidson, 1995; Culshaw *et al.*, 1997; Rivers, 1997; Carr *et al.*, 2000; Ketchum and Davidson, 2000). The ensuing discussion is only intended to summarize the data relevant for the thesis.

Alternative subdivisions of the Grenville Province

Various workers have proposed different subdivisions of the Grenville Province. The subdivisions differ in detail, and it is necessary to select the subdivision best suited for the problem at hand, depending, for example, on whether investigations are conducted

on a province-wide, regional, or local scale. The subdivisions are presented chronologically according to publication year.

Wynne-Edwards (1972). The subdivision most commonly employed by workers in the southwestern Grenville Province is the one proposed by Wynne-Edwards (1972) (Fig. 1.2). He described the Grenville Province in Ontario in terms of three major divisions: (i) The Grenville Front Tectonic Zone (GFTZ) is a crustal-scale shear zone marking the northwestern boundary of the orogen. Thrusting along this shear zone occurred late in the Grenvillian orogeny, at ca. 990 Ma (Haggart *et al.*, 1993; Krogh, 1994). (ii) Overlying the GFTZ is the Central Gneiss Belt (CGB) which dominantly comprises rocks of the Laurentian craton (pre-1400 Ma) and younger supracrustal sequences deposited along its margin, reworked at high-grade during Grenvillian orogenesis. (iii) To the southeast, overlying the CGB, is the Central Metasedimentary Belt (CMB) which consists of post-1400 Ma magmatic arcs and marginal basins (Easton, 1992; Davidson, 1995; Carr *et al.*, 2000), accreted to Laurentia during the Grenvillian orogeny. Separating the CGB and CMB is the crustal-scale Central Metasedimentary Belt boundary thrust zone (CMBBZ, Hanmer and McEachern, 1992). Although there is general agreement that emplacement of the CMB over the CGB took place along the CMBBZ, the timing of this event is debated. Hanmer and McEachern (1992) and Corriveau and van Breemen (2000) argued, based on dating of syntectonic pegmatite dikes in the CMBBZ, that the CMB was emplaced onto the Laurentian margin at ca. 1190 Ma, and that the shear zone was reactivated at ca. 1080-1060 Ma. In contrast, Timmermann *et al.* (1997) and Culshaw *et al.* (1997) pointed out that the Laurentian footwall in Ontario did not undergo high-grade metamorphism until ca. 1080 Ma, and that the only Grenville-age tectonic activity in the Laurentian craton preceding the 1080 Ma metamorphism was the intrusion of coronitic gabbro at 1170-1150 Ma (Davidson and van Breemen, 1988; Heaman and LeCheminant, 1993). They suggested that the early phase of deformation and metamorphism in the CMBBZ was a result of offshore tectonism prior to emplacement of the CMB onto the Laurentian craton. Timmermann (1998) discussed this controversy in greater detail.

Rivers et al. (1989). Rivers *et al.* (1989) divided the Grenville Province into three major units (Fig. 1.3): (i) the Parautochthonous Belt closest to the Grenville Front, comprising variably reworked and displaced equivalents of older shield provinces to the northwest; (ii) the Allochthonous Polycyclic Belt, comprising rocks with a pre-Grenvillian history of deformation and metamorphism, but which cannot be correlated with rocks outside the province; (iii) the Allochthonous Monocyclic Belt, dominated by supracrustal rocks which experienced only Grenvillian deformation, metamorphism, and plutonism. The Shawanaga and Muskoka domains (Fig. 1.2), which are the focus of this thesis, were assigned to the Allochthonous Polycyclic Belt. Field and geochronological work, however, has not revealed any evidence of pre-Grenvillian deformation or metamorphism in these units (Culshaw *et al.*, 1994; Ketchum, 1995; Timmermann, 1998). Thus, they are not 'polycyclic' but rather 'monocyclic', as defined by Rivers *et al.* (1989), and the subdivision of Rivers *et al.* (1989) is not directly applicable to the investigated area. Hoffman (1989) proposed the terms northwestern zone, central zone, and southeastern terranes, that differ slightly, but encompass the same elements as the subdivision proposed by Rivers *et al.* (1989).

Culshaw et al. (1997). Culshaw *et al.* (1997) proposed a detailed subdivision for the CGB east of Georgian Bay, based on the present-day structural distribution of domains (Fig. 1.4). Structural level 1 (Britt domain) (structural levels after Culshaw *et al.* (1983) and Ketchum and Davidson (2000)) is the lowermost structural level and corresponds to the Parautochthonous Belt of Rivers *et al.* (1989), comprising Archean and late Paleoproterozoic to early Mesoproterozoic orthogneisses with a pre-Grenvillian history of deformation and metamorphism. Structural level 2 is the lowermost allochthonous level and forms the hanging wall to the Allochthon Boundary Thrust (ABT) (Ketchum and Davidson, 2000). Domains in structural level 2 include the Algonquin, Lower Rosseau, and Lower Go Home domains, comprising late Paleoproterozoic and early Mesoproterozoic orthogneisses that yield pre-Grenvillian metamorphic ages, but, in contrast to structural level 1, lack evidence of an Archean geological history. Structural level 3 includes the Shawanaga, Upper Rosseau, and Upper Go Home domains, which appear to lack late Paleoproterozoic rocks as well as a pre-
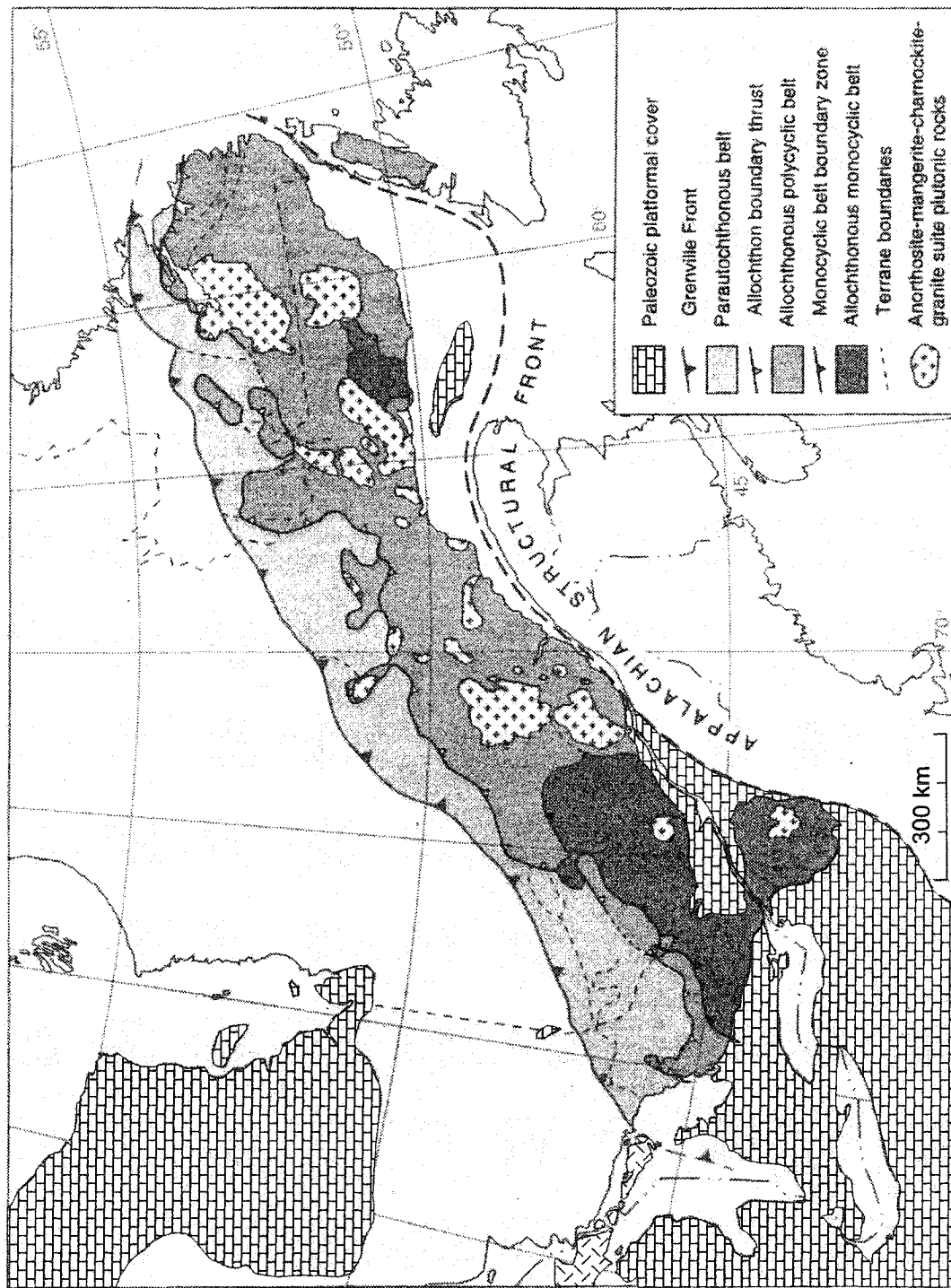
Fig. 1.3 Subdivisions of the Grenville Province proposed by Rivers *et al.* (1989). Modified after Davidson (1998).

Legend:
- Paleozoic platformal cover
- Grenville Front
- Parautochthonous belt
- Allochthon boundary thrust
- Allochthonous polycyclic belt
- Monocyclic belt boundary zone
- Allochthonous monocyclic belt
- Terrane boundaries
- Anorthosite-mangerite-charnockite-granite suite plutonic rocks
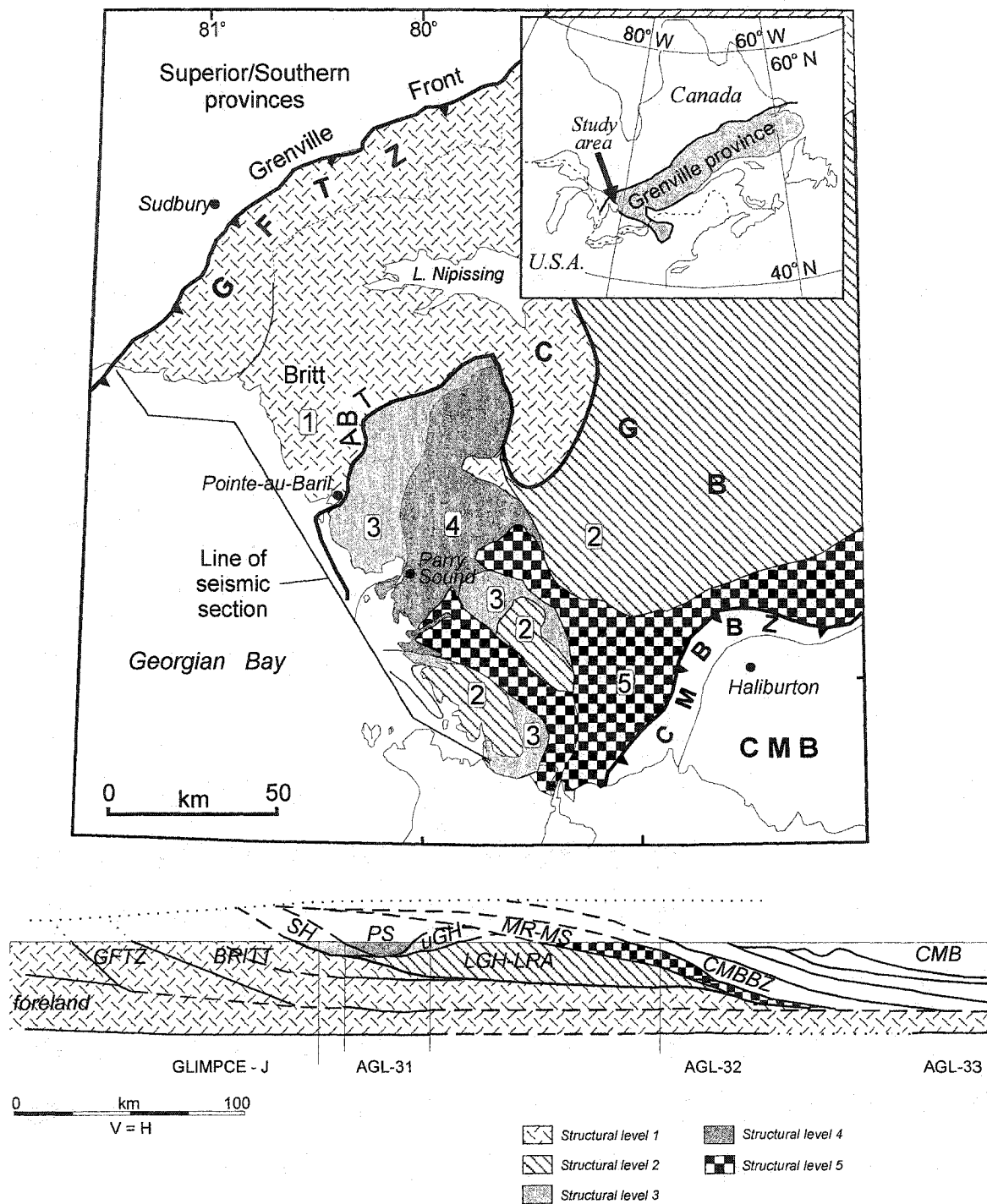
Fig. 1.4 Structural levels (SL) in the western CGB, modified after Culshaw *et al.* (1997) and Ketchum and Davidson (2000). Seismic interpretation after White *et al.* (2000). SL 1: Britt and Nepewassi domains, SL 2: Algonquin, Lower Rosseau (LRA), and Lower Go Home (LGH) domains, SL 3: Shawanaga (SH), Ahmic, Upper Rosseau, and Upper Go Home (UGH) domains, SL 4: Parry Sound (PS) domain, SL 5: Muskoka (MS) domain, Seguin and Moon River (MR) subdomains. Other abbreviations: GFTZ=Grenville Front Tectonic Zone, ABT=Allochthon Boundary Thrust, CMBBZ=Central Metasedimentary Belt boundary thrust zone, CMB=Central Metasedimentary Belt

Grenvillian metamorphic history. Structurally upper and lower bounding shear zones of Structural level 3 commonly contain pods or lenses of retrogressed eclogites and anorthosites (e.g., Davidson, 1990; Ketchum and Krogh, 1997). Structural level 4 consists of the Parry Sound domain, which comprises granulites and anorthosites dated at ca. 1425-1315 and 1163 Ma, metamorphosed at ca. 1160 and 1120 Ma (van Breemen *et al.*, 1986; Wodicka, 1994; Wodicka *et al.*, 1996). The Parry Sound domain represents somewhat of an anomaly in the CGB in terms of plutonic and metamorphic ages, and has been interpreted to represent an allochthonous slice (Davidson *et al.*, 1982) from the CMBBZ or Adirondack Highlands to the southeast (Wodicka *et al.*, 1996). Structural level 5 is the uppermost structural level in the CGB, in the immediate footwall to the CMBBZ, and consists of the Muskoka domain and contiguous Seguin and Moon River subdomains, apparently lacking late Paleoproterozoic rocks or evidence of a pre-Grenvillian metamorphic history.

Carr et al. (2000). The most recent subdivision proposed for the southwestern Grenville Province is that of Carr *et al.* (2000). They proposed a tripartite subdivision into (Fig. 1.5): (i) Pre-Grenvillian Laurentia and its margin, comprising ca. 1740 and 1450 Ma continental arc plutons and associated supracrustal rocks, corresponding to the Grenvillian foreland or Southern Province and CGB of Wynne-Edwards (1972), (ii) Composite Arc Belt comprising allochthonous ca. 1300-1250 Ma volcanic arcs and sedimentary rocks, corresponding to the CMB of Wynne-Edwards (1972), (iii) Frontenac-Adirondack Belt, comprising supracrustal and granitoid rocks and anorthosites, corresponding to the Central Granulite Terrane of Wynne-Edwards (1972).

The two subdivisions used in this thesis will be the ones proposed by Wynne-Edwards (1972) and Culshaw *et al.* (1997). The former is particularly useful as a reference frame for discussing pre-Grenvillian events, whereas the latter is preferred when discussing Grenvillian tectonic events and evolution.

Late Paleoproterozoic and early Mesoproterozoic rocks in Ontario

Geochronological work has shown that much of the CGB formed during two major
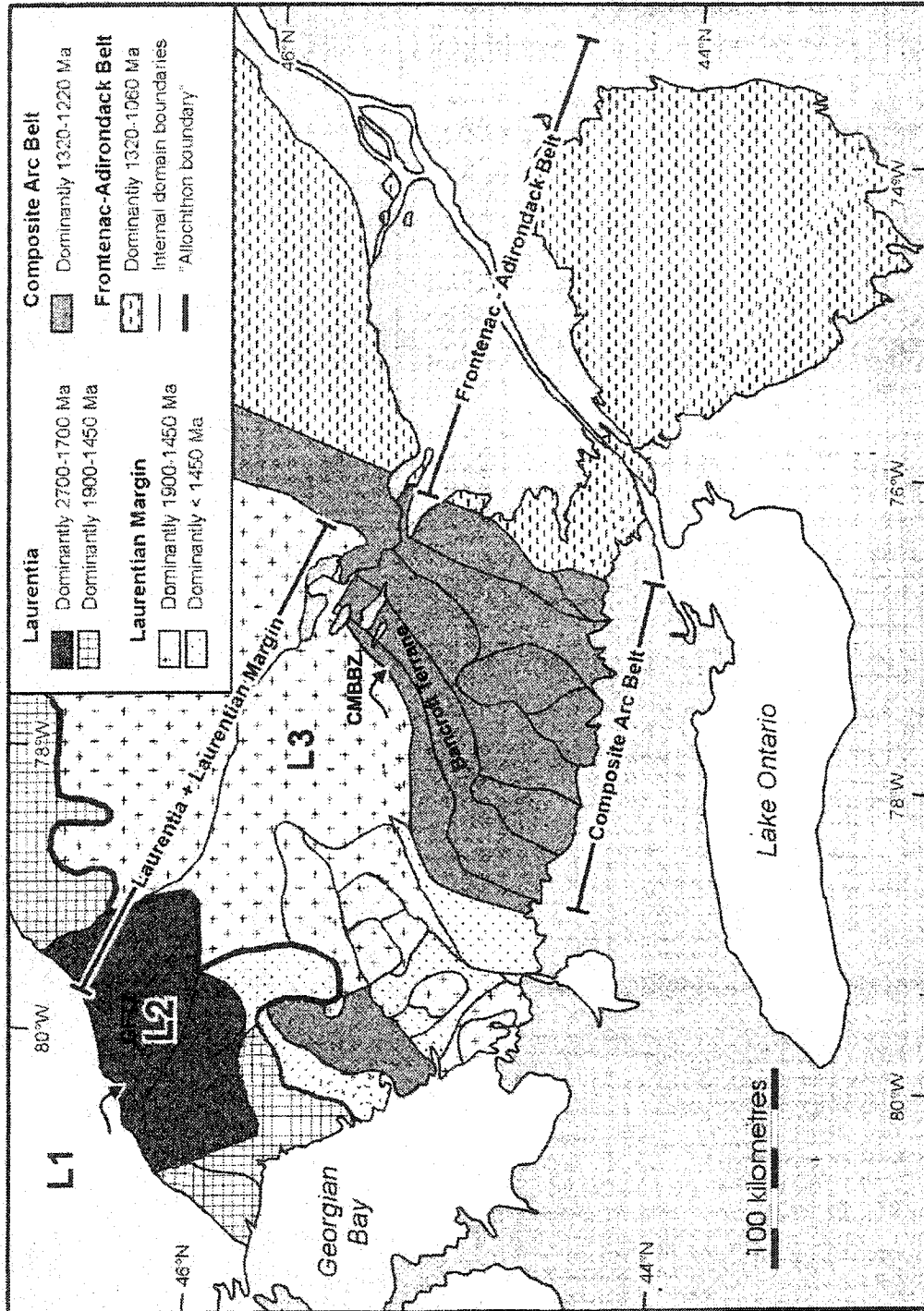
Fig. 1.5 Subdivision proposed by Carr *et al.* (2000). L1: Laurentian foreland northwest of the Grenville Front; L2: Archean crust with 1740 and 1450 Ma plutons; L3: 1800-1680 Ma supracrustal rocks with ca. 1450 Ma continental arc granitoids.

magmatic episodes at 1750-1600 and 1470-1350 Ma. Van Breemen and Davidson (1988) and Corrigan et al. (1994) obtained ages falling in both age intervals from orthogneisses in the western part of the CGB and the adjacent foreland, and pointed out that the older and younger age intervals coincide with the Central Plains orogeny and formation of the midcontinental granite-rhyolite provinces, respectively. Culshaw and Dostal (1997, 2002) and Rivers and Corrigan (2000) suggested a tectonic setting involving continental arc and back-arc magmatism for the late Paleoproterozoic and early Mesoproterozoic Laurentian margin represented in the Grenville Province, and Culshaw and Dostal (2002) presented data suggesting that rifting may have been complete, forming a new ocean of unknown extent southeast of Laurentia, possibly represented by the CMB.

Tectonic models for Grenvillian orogenesis

As discussed above, the Grenvillian orogeny appears to have been the result of continent-continent and/or continent-arc collisions that formed the supercontinent Rodinia. Comparisons have been made to the Himalayas, and most models propose collision and subduction of the pre-Grenvillian Laurentian margin beneath arc terranes and/or continents (unidentified) to the southeast (e.g., Carr et al., 2000). The ensuing discussion focuses on tectonic processes relevant to the study area in the southwestern Grenville Province.

The southwestern Grenville Province is often described as a collage of tectonically stacked units or domains. Separating the domains are high-strain zones interpreted to represent ductile shear zones along which the domains or thrust sheets were emplaced (e.g., Davidson et al., 1982; Culshaw et al., 1983). Over the last 5-10 years, however, it has become increasingly clear that the processes by which the domains were assembled may have varied significantly between different areas. As a result, controversies have arisen between groups working in different areas of the southwestern Grenville Province. Jamieson et al. (1992, 1995), Bussey et al. (1995), Wodicka et al. (1996), Timmermann et al. (1997), and Culshaw et al. (1997) suggested, based on field and geochronological data, that the domains along Georgian Bay were assembled by dominantly forward-

propagating, piggyback thrusting, with intermittent out-of-sequence thrusting. An important corollary of this model is that events identified from geochronology need not have taken place *in situ*. In contrast, Nadeau and Hanmer (1992), working in the Huntsville area, proposed a break-back model for assembly of the Seguin subdomain and underlying Algonquin domain. In an attempt to reconcile these apparently mutually exclusive models, Ketchum and Davidson (2000) noted that tectonic assembly was dominated by transport of structural levels rather than individual domains. They furthermore noted that tectonic assembly of the Algonquin domain may have taken place before ca. 1100 Ma (Nadeau, 1990; Nadeau and Hanmer, 1992), prior to thrusting on the CMBBZ at 1080-1040 Ma. Ketchum and Davidson (2000), therefore, proposed that assembly of the Algonquin domain could represent a period of orogenic construction within structural level 2, preceding the larger scale forward-propagating sequence proposed by Culshaw *et al.* (1997) in which each structural level behaved essentially as a single entity. The two models differ in both timing and scale, and thus cannot be compared directly.

1.2.3. Geology of the Muskoka and Shawanaga domains

Pre-Grenvillian history (protoliths)

The main lithology of the Muskoka domain is gray orthogneiss ranging in composition from gabbro and diorite to granite (Culshaw *et al.*, 1983; Timmermann, 1998). U-Pb zircon dates from the gray gneisses in the Muskoka domain and contiguous Seguin subdomain suggest that they formed in the interval 1480-1430 Ma (Timmermann *et al.*, 1997; Nadeau and van Breemen, 1998; McMullen, 1999). In addition, a small granite body yielded a younger age of ca. 1390 Ma (Timmermann *et al.*, 1997), which, based on data presented in Chapter 5, may have to be revised. The 1480-1430 Ma gray gneisses are generally assumed to have formed along the active Laurentian continental margin (e.g., Nadeau and van Breemen, 1998; Rivers and Corrigan, 2000).

Culshaw *et al.* (1988, 1989, 1994) divided the Shawanaga domain into five units or gneiss associations: the Shawanaga pluton, Ojibway, Sand Bay, and Lighthouse gneiss associations, and the 'marginal orthogneiss'. The granodioritic Shawanaga pluton and

gray orthogneisses of the Ojibway gneiss association have yielded protolith ages of ca. 1460 Ma (T. E. Krogh, unpublished data), similar to the Muskoka domain. The overlying Sand Bay gneiss association comprises interlayered pink rhyolitic and gray quartzofeldspathic gneisses with an age of ca. 1360 Ma, inferred from dating of detrital zircons (T. E. Krogh, unpublished data). Culshaw and Dostal (1997) and Rivers and Corrigan (2000) suggested that the Sand Bay gneiss association may represent rocks deposited in an ensialic back-arc basin, behind an arc situated at the Laurentian margin. The identity of the proposed arc is unknown. Recent dating of detrital zircons suggests that the lower unit of the Lighthouse gneiss association (cf., Culshaw and Dostal, 2002) may be considered part of the Sand Bay gneiss association, whereas the upper unit appears to have a different, uncertain affinity (Raistrick, 2003). The 'marginal orthogneiss' is a megacrystic granitoid orthogneiss dated at 1346+69/-39 Ma (van Breemen *et al.*, 1986), however, the large error in the age of this unit makes interpretations regarding its tectonic significance uncertain.

Grenvillian metamorphism

Timmermann (1998) and Timmermann *et al.* (2002) documented widespread Grenvillian upper amphibolite-facies metamorphism and partial melting, with local coeval granulite-facies metamorphism, and determined peak metamorphic conditions in the Muskoka domain to 750-850°C and 1000-1150 MPa during the interval 1080-1060 Ma. Ketchum and Krogh (1997) obtained ages of 1120 to 1090 Ma from retrogressed eclogite bodies in the Shawanaga domain, and Bussey *et al.* (1995) reported metamorphic ages in the interval 1080-1070 Ma from the Ahmic domain, at the same structural level as the Shawanaga domain. These data suggest that high-pressure metamorphism in the Shawanaga domain preceded metamorphism in the Muskoka domain, but that peak conditions persisted and overlapped in the two domains, consistent with the tectonic model of Culshaw *et al.* (1997). P-T estimates of peak metamorphism are 1050-1100 MPa and 830°C for the uppermost structural level of the Shawanaga domain (Lighthouse gneiss association), and 750-850 MPa and 685-700°C for the structurally lower Ojibway gneiss association (Wodicka *et al.*, 2000).

1.3. Objectives

The thesis involves investigations of ca. 1.48-1.36 Ga gneisses in the Muskoka and Shawanaga domains (Fig. 1.2), metamorphosed under upper amphibolite- to locally granulite-facies conditions during Grenvillian orogenesis, using a combination of geochemical, geochronological, and petrographic techniques. The techniques include, in addition to field work and petrography, XRF and ICP-MS whole rock geochemical analysis, and TIMS and SHRIMP U-Pb zircon dating.

1.3.1. Pre-Grenvillian events

As discussed above, the investigated rocks probably formed at or close to the Laurentian margin between ca. 1.48 and 1.36 Ga, coeval with magmatic activity along the paleomargin of Laurentia from Labrador through the midcontinental USA. One of the main objectives of the thesis is to determine the petrogenesis and tectonic significance of the protoliths to the investigated gneisses using a combination of geochemical and geochronological techniques. Recent models of the tectonic evolution of Laurentia during this interval suggest an active continental margin (Rivers and Corrigan, 2000); however, few geochemical data are available to support this model (Culshaw and Dostal, 1997, 2002). This thesis represents the first extensive geochemical investigation of the area and is intended to test and refine the proposed model. The results also have implications for the applicability of geochemical data to high-grade terranes.

1.3.2. Grenvillian events

Grenvillian overprinting involved moderate to strong ductile deformation and moderate to extensive partial melting over much of the investigated area. In recent years it has become increasingly clear that partially molten rocks may influence the way orogens evolve by lowering the strength of the rocks (e.g., Hollister and Crawford, 1986; Rutter, 1997). An important objective of the thesis is to determine how the migmatites formed (partial melting processes) and the relationship between migmatization and tectonic processes or events.

In summary, the main objectives are to:

- Determine the petrogenesis of the protoliths to high-grade gneisses in the Muskoka and Shawanaga domains and their significance for the tectonic evolution of Laurentia between ca. 1.5 and 1.35 Ga.

- Determine how the migmatites formed and their relationship to Grenvillian tectonism.

1.4. Thesis structure and organization

1.4.1. Relationship to published work

The chapters in this thesis are written as independent but complementary manuscripts. Some repetition of background material is, therefore, unavoidable.

Chapter 2 presents geochemical data from protoliths to high-grade gneisses in the Muskoka and Shawanaga domains and discusses the pre-Grenvillian tectonic evolution of the southwestern Grenville Province. This chapter is written as a journal manuscript and has been accepted for publication in *Proterozoic Evolution of the Grenville Orogen in North America, GSA Special Paper*. Co-authors are Nick Culshaw, Rebecca Jamieson, and John Ketchum. The paper includes geochronological data from one sample (charnockitic gneiss) that for the purpose of thesis organization are discussed in Chapter 5 along with the other geochronological data. I have interpreted the geochemical data and done the trace element modeling myself, with helpful suggestions from Barrie Clarke. Nick Culshaw and Rebecca Jamieson contributed significantly to the ideas and interpretations regarding tectonic evolution. John Ketchum conducted the geochronological analyses (TIMS).

Chapter 3 discusses the petrogenesis of migmatites in the Muskoka domain, and shows that deformation may influence the compositions of partial melts at mid-crustal levels. This chapter represents a manuscript in preparation intended for publication in *The Journal of Petrology*, co-authored by Rebecca Jamieson and Nick Culshaw. The paper will contain mineral compositional data from SEM analyses currently underway at the Geological Survey of Norway (NGU). I have interpreted the geochemical data and done the trace element modeling myself, whereas interpretations regarding the role of

fluids, in particular the possible presence of low-aH_2O fluids, and tectonic significance of partial melting have benefited greatly from discussions with the co-authors.

Chapter 4 describes field relationships, petrography, geochemistry, and petrogenesis of leucosome-rich metatexite, diatexite, granite, and pegmatite in the southern Shawanaga domain, immediately below the Parry Sound domain. Barrie Clarke and Rune Larsen at NGU have both been a great help in the work with this chapter; in particular, the interpretations of the granite-pegmatite relationship have benefited greatly from discussions with Clarke and Larsen. In addition, this chapter relies on previous mapping conducted by Nick Culshaw and co-workers (Culshaw *et al.*, 1988, 1989, 1990) as well as more detailed mapping in a limited area conducted by myself.

Chapter 5 presents and discusses SHRIMP and ID-TIMS U-Pb zircon geochronological data from the Muskoka and Shawanaga domains. The results from the TIMS analyses have already been published (see above). This chapter is written as a manuscript, albeit in greater detail than will be possible in a journal paper. Mike Hamilton, Rebecca Jamieson, and Nick Culshaw will be co-authors on the planned paper. Mike Hamilton conducted the SHRIMP analyses, but I have for the most part interpreted the results myself with helpful input from the co-authors and Bernard Bingen at NGU.

1.4.2. Originality

I have for the most part interpreted the field, petrographic, geochemical, and geochronological data myself, but with important input from the thesis committee as well as other collaborators mentioned in the Acknowledgements. I have done most of the writing, with minor corrections or revisions done by others (thesis committee). Analytical work was conducted at St. Mary's University, Halifax (XRF by David Slauenwhite), Memorial University of Newfoundland (ICP-MS by Pam King), SHRIMP geochronology at the GSC in Ottawa by Mike Hamilton, and ID-TIMS geochronology at the Royal Ontario Museum in Toronto by John Ketchum. I mainly did the sample preparation and zircon separation myself, with some help mentioned in the Acknowledgements. Much of the work presented herein is based on mapping conducted in the 1980's and early 1990's by Nick Culshaw, Tony Davidson, and co-workers

(Culshaw *et al.*, 1983, 1988, 1989, 1990, 1994; Davidson and Morgan, 1980; Davidson *et al.*, 1982, 1985).

2. Protolith geochemistry, Muskoka and Shawanaga domains

2.1. Introduction

Continental growth processes include formation of juvenile magmatic crust at or near the continental margin, accretion of outboard terranes (Bickford, 1988; Condie and Chomiak, 1996), and continental collision (e.g., Yin and Harrison, 2000 and references therein). Where these processes are superimposed, evidence of successive continental growth is likely to be obscured by subsequent accretionary or collisional orogenesis. Unraveling the pre-orogenic history of strongly deformed, metamorphosed, and dismembered rocks in accretionary and collisional orogenic belts, ancient as well as recent, is a daunting task (cf., van Staal et al., 1998). In addition to the effects imposed by accretion and continental collision, rocks incorporated in orogenic belts typically span several hundred million years in age, come from a variety of tectonic settings and geographical locations, and may have been involved in several orogenic cycles. This problem, inherent in most large orogenic belts, may be nowhere better illustrated than in the pervasively deformed Central Gneiss Belt (CGB) of the southwestern Grenville Province in Ontario.

The CGB is commonly described as a collage of tectonically stacked lithotectonic units or domains, assembled by northwest-directed thrusting during Grenvillian orogenesis (Davidson et al., 1982; Rivers et al., 1989; Nadeau and Hanmer, 1992; Culshaw et al., 1997). Discrete domains, identified based on contrasting lithologies, structural style, metamorphic history, and in some cases geophysical properties, are separated by zones of straight gneisses (S tectonites with a pronounced layering, after Davidson et al., 1982) interpreted to represent ductile shear zones (Davidson et al., 1982; Culshaw et al., 1983, 1997). The CGB exposes high-grade gneisses with protolith ages ranging from Archean to late Mesoproterozoic (Ketchum and Davidson, 2000), which include reworked continuations of Archean, early and mid Paleoproterozoic, and Mesoproterozoic orogens (Rivers, 1997 and references therein), representing a variety of probably arc-related tectonic settings, from continental and island arc to intra-arc and

back-arc (Culshaw and Dostal, 1997, 2002; Rivers, 1997; Carr *et al.*, 2000; Rivers and Corrigan, 2000). Some units are clearly allochthonous with respect to the surrounding units (Wodicka *et al.*, 1996), and some protoliths were strongly deformed and metamorphosed prior to Grenvillian orogenesis (Corrigan *et al.*, 1994; Ketchum *et al.*, 1994).

Studies of the pre-orogenic history of rocks in orogenic belts rely heavily on geochronology (e.g., Ketchum *et al.*, 1997; Gebauer, 1999; Söderlund *et al.*, 2002). Geochronological data are necessary in order to identify the sequence of events and correlate rocks that may have formed during the same geological event, and in many cases, the robust U-Pb zircon system preserves evidence of several past tectonic events. However, in most cases determining the petrogenesis and tectonic significance of a rock requires information about its composition, in addition to its age. Here, we present new geochemical and geochronological data from a variety of rock types from the CGB in order to constrain their petrogenesis and tectonic setting, and discuss likely tectonic models for the pre-Grenvillian evolution of the area between ca. 1500 and 1350 Ma.

Apart from the detailed studies of Culshaw and Dostal (1997, 2002), proposed tectonic models for the early Mesoproterozoic evolution of the Grenville Province are typically relatively broad in scope. For example, Rivers and Corrigan (2000) proposed an 'Andean'-type model involving continuous subduction of oceanic crust beneath the Laurentian margin, with alternating periods of back-arc extension and compression. Although we agree with their general interpretation, the data presented here suggest differences in detail, and have different implications for the early Mesoproterozoic geological and magmatic evolution of the North American midcontinent region.

The main contributions of this paper are to: (i) demonstrate the robustness of the geochemical system in strongly deformed and metamorphosed rocks, (ii) show that in addition to geochronology, geochemistry should be considered in studies of pre-orogenic history, (iii) propose a detailed model for the pre-Grenvillian, early Mesoproterozoic tectonic history of the southwestern Grenville Province, and (iv) add to the understanding of the evolution of the Laurentian margin during the Mesoproterozoic. Coupled with

relatively good exposure, simple logistics, a relatively well-understood Grenvillian history, and large geochronological database, the selected study area (Fig. 2.1) is well suited for studies aimed at understanding the pre-Grenvillian history of the CGB.

2.2. Regional geology

Wynne-Edwards (1972) described the Grenville Province in Ontario in terms of three major divisions (Fig. 2.1): the Grenville Front Tectonic Zone, Central Gneiss Belt (CGB), and Central Metasedimentary Belt (CMB), the latter two separated by the Central Metasedimentary Belt boundary thrust zone (CMBBZ). The Grenville Front Tectonic Zone is a southeast-dipping crustal-scale thrust zone, active at ca. 1.0 Ga (Haggart et al., 1993; Krogh, 1994), that marks the northwestern limit of Grenvillian deformation and metamorphism. The CGB structurally overlies the Grenville Front Tectonic Zone and comprises late Paleoproterozoic to early Mesoproterozoic high-grade gneisses that formed along the southeastern margin of the pre-Grenvillian Laurentian craton and were penetratively deformed and tectonically stacked during Grenvillian orogenesis (Culshaw et al., 1997). The CMB structurally overlies the CGB and comprises post-1.4 Ga arc and back-arc assemblages interpreted to have formed outboard of the southeastern margin of Laurentia (Carr et al., 2000 and references therein). Emplacement of the CMB onto the CGB took place by thrusting along the CMBBZ during Grenvillian orogenesis, although the timing of this event is debated. McEachern and van Breemen (1993) and Corriveau and van Breemen (2000) suggested that collision started around 1.2 Ga, whereas Culshaw et al. (1997) and Timmermann et al. (1997), citing the lack of geochronological evidence for metamorphism prior to ca. 1080 Ma in the CGB in Ontario, argued for continental collision at ca. 1090-1080 Ma. The Parry Sound domain (Fig. 2.1) is now located within the CGB, but is interpreted to represent a thrust-slice originating within the CMBBZ or correlative rocks to the southeast (Wodicka et al., 1996).

The CGB can be divided into two parts, separated by the Allochthon Boundary Thrust (Fig. 2.1). Northwest of the Allochthon Boundary Thrust, the CGB comprises orthogneisses and minor paragneisses, the protoliths of which formed during two major

Units of Laurentian affinity

☐ parautochthonous polycyclic rocks

⊞ transported polycyclic rocks

▓ post-1500 Ma monocyclic rocks
(Laurentian margin)

Composite Arc Belt

▨ Central Metasedimentary Belt

▤ Central Metasedimentary Belt
boundary thrust zone,
Parry Sound domain
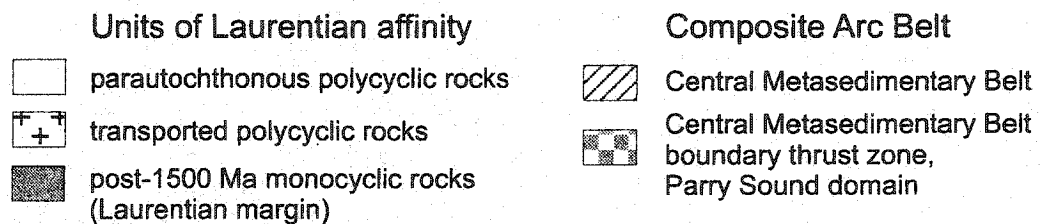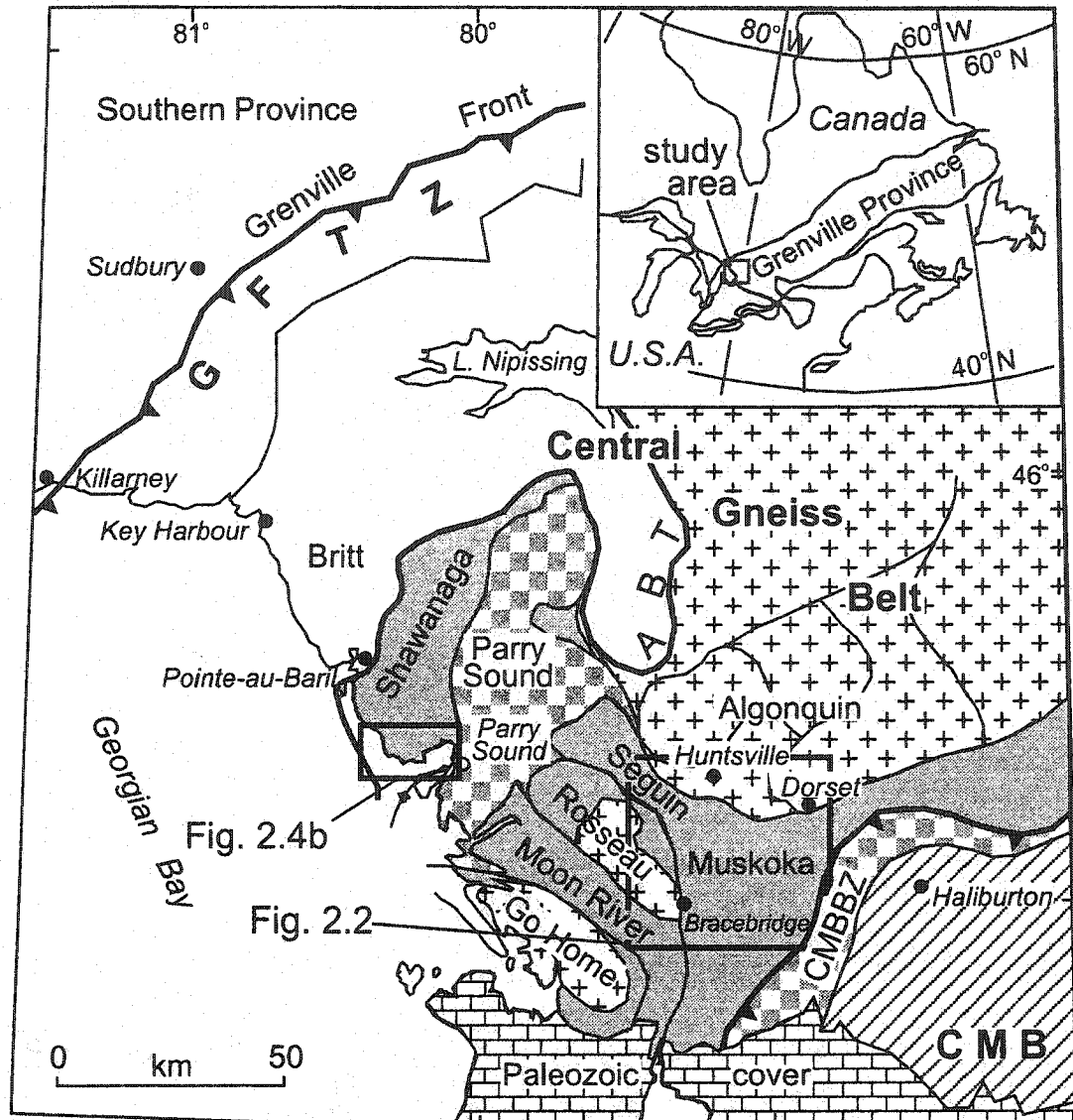
Fig. 2.1 Lithotectonic domains within the Central Gneiss Belt, southwestern Grenville Province, Ontario. Heavy barbed lines indicate major thrust boundaries; heavy line indicates Allochthon Boundary Thrust (from Ketchum and Davidson, 2000); thin lines represent domain boundaries after Culshaw et al. (1983, 1988, 1989. 1990), Davidson (1984), and Davidson and van Breemen (1988), modified by Culshaw et al. (1997) and Ketchum and Davidson (2000). Composite ArcBelt defined by Carr et al. (2000). Abbreviations: ABT=Allochthon Boundary Thrust, GFTZ=Grenville Front Tectonic Zone, CMB=Central Metasedimentary Belt, CMBBZ=Central Metasedimentary Belt boundary thrust zone.

magmatic episodes at ca. 1750-1600 and 1470-1340 Ma (e.g., Rivers, 1997; Ketchum and Davidson, 2000). Despite extensive reworking during Grenvillian metamorphism and deformation, evidence for multiple phases of pre-Grenvillian tectonism, including significant >1700 Ma and ca. 1450-1350 Ma events, is locally preserved (van Breemen and Davidson, 1988; Tuccillo *et al.*, 1992; Corrigan *et al.*, 1994; Dudás *et al.*, 1994; Ketchum *et al.*, 1994; Jamieson *et al.*, 2001). Krogh *et al.* (1996) proposed the term Pinwarian orogeny for the ca. 1450 Ma event. In contrast, southeast of the Allochthon Boundary Thrust, Culshaw *et al.* (1997) and Timmermann *et al.* (1997) found no clear evidence for a pre-Grenvillian metamorphic history in the Shawanaga and Muskoka domains, hence they are 'monocyclic' according to the terminology of Rivers *et al.* (1989). Following Rivers *et al.* (1989), we define Grenvillian orogenesis to include tectonic, metamorphic, and plutonic events that took place at or outboard of the Laurentian margin between ca. 1190 and 970 Ma. The distribution of lithological units, structures, and metamorphic grades in the investigated area is largely the result of Grenvillian tectonic processes (e.g., Culshaw *et al.*, 1997; Timmermann *et al.*, 1997; Carr *et al.*, 2000).

The times of protolith formation in the CGB coincided with major crustal-forming events in the North American midcontinent (Condie, 1986; Bickford, 1988; Van Schmus *et al.*, 1996), and several authors have proposed that events in the CGB and adjacent foreland can be correlated with events in the midcontinent region (Davidson, 1986; Easton, 1986; Bickford, 1988; van Breemen and Davidson, 1988; Rivers and Corrigan, 2000; Culshaw and Dostal, 2002). The ca. 1.9-1.6 Ga Penokean, Yavapai-Mazatzal, Killarnean, and Makkovikian orogenies involved formation and accretion of juvenile crust along the southeastern margin of Laurentia (Condie, 1986; Dickin and McNutt, 1990; Davidson *et al.*, 1992; Culshaw *et al.*, 2000). Subsequently, in the intervals 1500-1440 and 1400-1340 Ma, the Eastern and Southern granite-rhyolite province, respectively, formed along the southeastern margin of Laurentia (Bickford, 1988; Van Schmus *et al.*, 1996). The tectonic setting of the granite-rhyolite provinces is debated. Early models focused on the A-type composition of the rocks and their relative lack of

deformation, suggesting an anorogenic setting (e.g., Anderson, 1983; Hoffmann, 1989; Kisvarsanyi and Kisvarsanyi, 1990; Windley, 1993). More recent models, however, emphasize that many of the granites and rhyolites have Nd model ages that are only slightly older than their crystallization ages, suggesting derivation from juvenile continental crust (e.g., Van Schmus et al., 1996; Menuge et al., 2002). The latter authors suggested that the granites and rhyolites most likely formed in an ensialic back-arc setting following accretion of juvenile crust to the Laurentian margin. A problem with this model, however, is that the substrate (i.e., potential source) to the granites and rhyolites is unexposed in the midcontinent region. As pointed out by Culshaw and Dostal (2002), the CGB may represent the reworked and telescoped continuation of the midcontinental granite-rhyolite provinces; work in this area may, therefore, contribute to understanding the Mesoproterozoic evolution of the Laurentian margin as a whole.

2.3. Geology of the study area

The term *domain* is widely used in Grenville literature for segments of crust that, on the basis of lithology, structure, metamorphic grade, geological history, and geophysical signature, are sufficiently distinct to set them apart from adjacent segments (Davidson, 1995). *Domain* is preferred over *terrane* because some tectonic connotations of the latter do not apply in the area; for example, most domains are not bounded by sutures (cf., Coney et al., 1980), and on palinspastic reconstruction many Grenville domains restore together as a single entity (Culshaw et al., 1997).

The investigated rocks were strongly deformed under upper amphibolite-to granulite-facies conditions during Grenvillian orogenesis and generally form layered gneisses lacking primary igneous or sedimentary structures, although some rocks contain primary megacrystic K-feldspar. For simplicity, we generally omit the prefix "meta" and the generic term "gneiss", and instead use protolith names as defined by modal compositions. The only exception is the 'gray gneiss' described below that warrants a distinct grouping because it encompasses a range of protolith compositions with similar geochemical characteristics.

2.3.1. Muskoka and Seguin domains

Gray gneiss

The Muskoka domain and contiguous Seguin subdomain (Fig. 2.2, hereafter collectively referred to as the Muskoka domain) constitute the uppermost structural level (level 5, Ketchum and Davidson, 2000) of the CGB, in the immediate footwall to the CMBBZ (Fig. 2.2). The Muskoka domain is dominated by moderately east- to southeast-dipping, gray, migmatitic orthogneisses that range in composition from gabbro and diorite through granodiorite to volumetrically subordinate granite (Table 2.1, Fig. 2.3). Granodioritic, dioritic, and/or granitic orthogneisses are locally interlayered, imparting the gneisses with a cm-scale banded appearance. By analogy with other gneiss terranes (e.g., Passchier *et al.*, 1990), the interlayering is most likely the result of ductile deformation of igneous features. Protolith ages for the gray gneisses range from ca. 1480 to 1430 Ma (Timmermann *et al.*, 1997; Nadeau and van Breemen, 1998; McMullen, 1999), but most ages cluster around 1450 to 1460 Ma. The gneisses were metamorphosed under upper amphibolite- to local granulite-facies conditions during Grenvillian orogenesis (Timmermann *et al.*, 2002), and typically include 30-40 vol.% leucosome measured on a series of vertical cross-sections (Slagstad, unpublished data). The leucosomes appear to be *in situ* at the outcrop scale, indicated by ubiquitous, spatially associated melanosomes.

Mafic enclaves. Elongate mafic enclaves (boudins), ranging in size from a few decimeters up to several meters and concordant with the Grenvillian fabric are common throughout the Muskoka domain. Nadeau (1990) and Timmermann (2002) interpreted the mafic enclaves to represent disrupted and boudinaged dikes, however, they do not appear to cut any preexisting fabrics or layering and an origin as xenoliths or cognate inclusions (e.g., Dorais *et al.*, 1990; Kay *et al.*, 1990) cannot be discounted. The composition of the mafic enclaves is unlike that of the Sudbury metadiabase (ca. 1.24 Ga, Dudás *et al.*, 1994) as summarized by Ketchum and Davidson (2000), compatible with the hypothesis that Sudbury metadiabase is restricted to rocks in the footwall of the Allochthon Boundary Thrust (Culshaw *et al.*, 1997; Ketchum and Davidson, 2000).
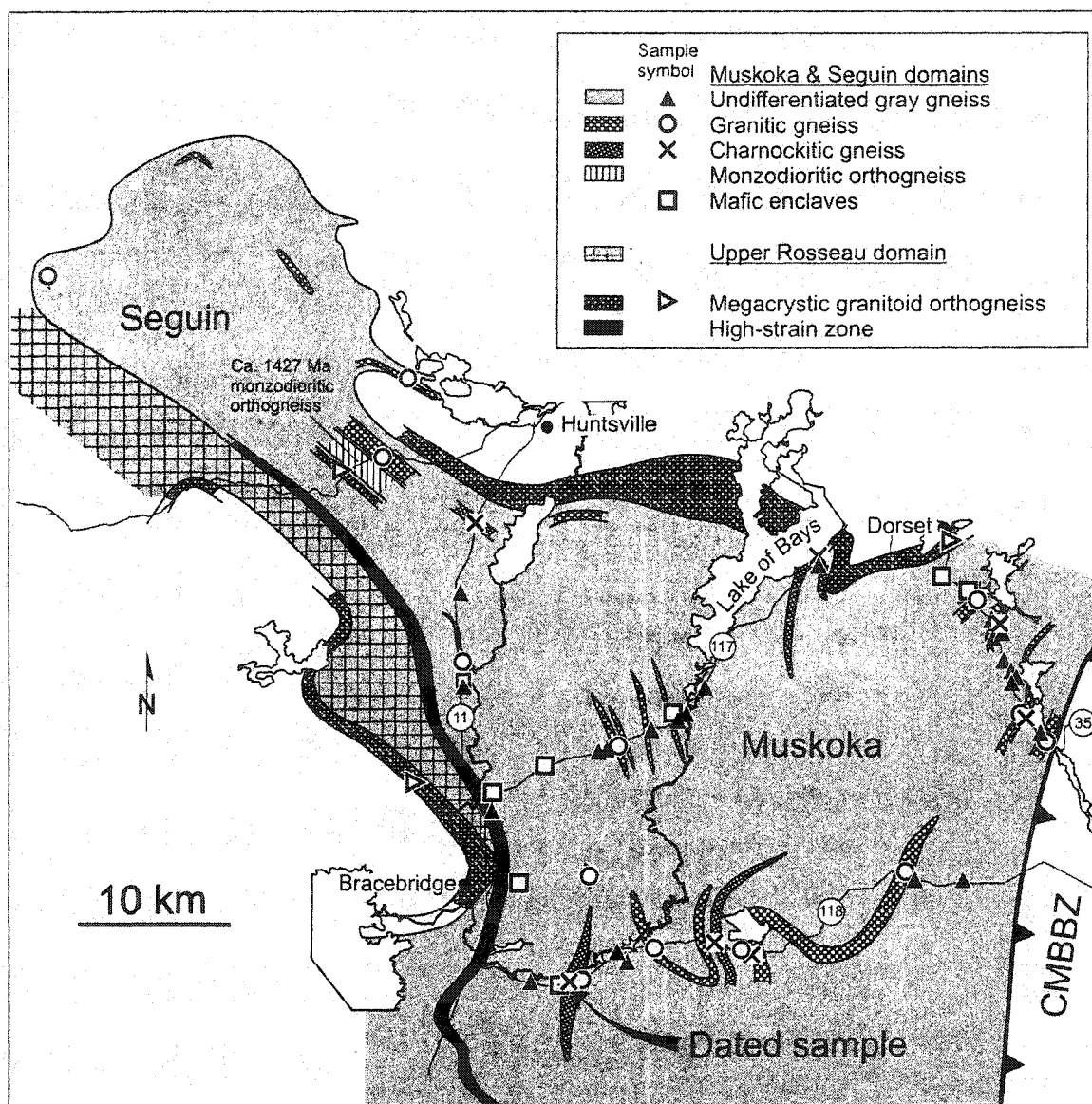
Fig. 2.2 Geological map of the Muskoka domain and contiguous Seguin subdomain showing dominant lithological units, sample-locations and -symbols; major highways, towns, and lakes are included as geographical reference. UTM coordinates (zone 17) for dated charnockite sample: 640 050E 4980 550N. The ca. 1427 Ma monzodioritic orthogneiss is the youngest protolith age obtained from the Muskoka domain (Nadeau and van Breemen (1998).
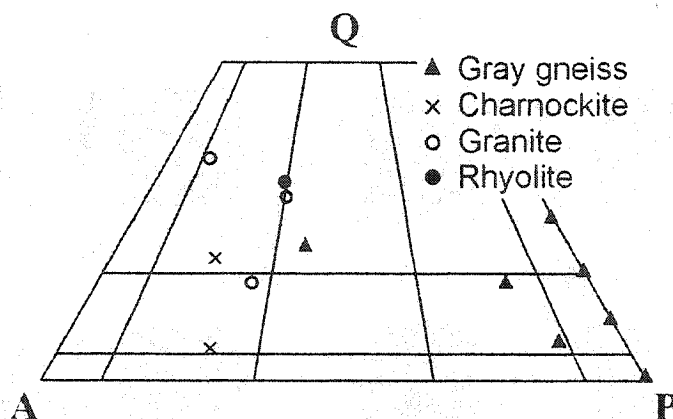
Fig. 2.3 Streckeisen (1973) classification diagram.

Table 2.1 Modes of representative protolith samples.

	Gray gneiss						
	M100716	M2707-11	M10075-1	M03083B-M	M03083-M	M2707-16	M2707-10
n	400	500	500	500	500	400	400
Qtz	16.7	24.0	9.6	15.0	6.4	23.2	
Pl	63.5	52.6	72.2	53.8	69.4	28.3	46.3
Kfs				11.0	9.0	40.0	
Hbl	7.8	16.6	4.4	11.6	7.0		37.5
Bt	8.6	5.4	11.6	6.8	7.0	5.7	8.0
Opx							
Cpx							
Grt							
Ttn							
Opaq	2.4	0.8		1.6	1.2	2.8	8.2
Ap	acc.	acc.	acc.	acc.	acc.		
Zrn	acc.	acc.	acc.		acc.		
Aln							

	Granitic gneiss			Charnockite		Rhyolite
	M100710-2	M150712	M150724	M080721-1	M18072	S02063
n	510	500	500	500	500	400
Qtz	32.4	41.8	17.6	5.4	20.6	37.3
Pl	21.8	7.0	25.0	23.0	15.6	21.3
Kfs	39.6	50.8	55.0	63.2	53.2	41.0
Hbl	2.4		0.6		acc.	
Bt	1.4		1.4			acc.
Opx		acc.		0.8		
Cpx				2.0	3.2	
Grt			acc.	1.0		acc.
Ttn						
Opaq	2	acc.	acc.	4.2	3.4	acc.
Ap	acc.	acc.		acc.	acc.	
Zrn	acc.	acc.		acc.	acc.	
Aln	acc.					
Unknown					3	

Determined by point-counting (n denotes number or points). acc.=accessory phase (<0.25 vol.%).

Charnockitic gneiss

Dark green, two-pyroxene charnockitic gneiss constitutes a volumetrically minor part of the Muskoka domain (Fig. 2.2). The charnockitic gneiss typically forms relatively small bodies, up to a few hundred meters across, that may extend along strike for several kilometers, although there is insufficient outcrop to map out individual bodies for more than a few hundred meters. The charnockitic gneisses are recognized in the field based on their green color and textural homogeneity. Leucosome is generally absent, in marked contrast to surrounding rocks. Their modal mineralogy corresponds to two- pyroxene granite to quartz syenite (Fig. 2.3), but for simplicity, they are referred to as charnockite. In one outcrop, the charnockite contains a 0.5 m thick mafic sheet that is geochemically indistinguishable from the mafic enclaves. As discussed in Chapter 5, the age of the charnockite is relatively poorly constrained at 1449+20/-17 Ma, i.e., similar to the gray gneisses.

Granitic gneiss

Pink to orange, granitic (granite to quartz syenite, Fig. 2.3) orthogneiss forms bodies similar in size and distribution to the charnockites (Fig. 2.2), but does not contain pyroxene. The granites are sparsely migmatitic, with significantly less leucosome than the surrounding gray gneisses. Timmermann *et al.* (1997) dated one granite body at 1394±13 Ma, however, recent SHRIMP data from a different, but geochemically similar granite elsewhere in the Muskoka domain yielded an age of ca. 1470±40 Ma (M. Hamilton, pers. comm., 2002), similar to the gray gneiss and charnockite.

2.3.2. Megacrystic orthogneiss

Lake of Bays suite

A unit of K-feldspar megacrystic granitoid orthogneiss, several hundred meters thick and traceable for several tens of kilometers, separates the Upper Rosseau and Muskoka domains from the underlying domains (Fig. 2.2). Similar megacrystic orthogneisses do not appear to be present in the Upper Rosseau domain, and they are sparse in the Muskoka and Shawanaga domains. Where dated, the megacrystic

orthogneisses have yielded ages similar to the gray gneisses (Nadeau and van Breemen, 1998; Timmermann, 1998; McMullen, 1999). In this paper, we refer to these megacrystic orthogneisses as the Lake of Bays suite.

Mann Island granodiorite and Britt pluton

Megacrystic orthogneisses are common at lower structural levels of the CGB in Ontario (Carr *et al.*, 2000). For comparative purposes, we sampled several megacrystic granitoid plutons outside the main study area. In the Britt domain, we sampled the Britt pluton (1456.5+8.5/-5.9 Ma; van Breemen *et al.*, 1986) and Mann Island granodiorite (1442+7/-6 Ma; Corrigan *et al.*, 1994). Both of these plutons intruded older, ca. 1.7 Ga, Laurentian continental crust (Culshaw *et al.*, 1988; Corrigan *et al.*, 1994).

'Marginal orthogneiss'

In the Shawanaga domain (discussed below), a megacrystic orthogneiss commonly referred to as 'marginal orthogneiss' (van Breemen *et al.*, 1986) was sampled. The 'marginal orthogneiss' immediately underlies the Parry Sound shear zone, and has yielded an imprecise age of 1346+69/-39 Ma (van Breemen *et al.*, 1986).

2.3.3. Shawanaga domain

The Shawanaga domain is situated in the hanging wall to the Shawanaga shear zone (Figs. 2.1, 2.4) (Culshaw *et al.*, 1994; Ketchum, 1995), which in this area is interpreted to represent an extension of the province-wide Allochthon Boundary Thrust (Ketchum and Davidson, 2000). Culshaw *et al.* (1988, 1989, 1994, 1997) divided the Shawanaga domain into five units or gneiss associations: the Shawanaga pluton, Ojibway gneiss association, Sand Bay gneiss association, Lighthouse gneiss association, and the 'marginal orthogneiss' noted above. The Sand Bay gneiss association was the main target of study in the Shawanaga domain, whereas the Ojibway gneiss association and Shawanaga pluton were only investigated on a reconnaissance level (two samples from each).

Shawanaga pluton

The Shawanaga pluton (Davidson *et al.*, 1982; Culshaw *et al.*, 1994), dated at 1460

+12/-8 Ma (T. E. Krogh, unpublished data), is a migmatitic, garnet-amphibole-biotite granodiorite with minor granite and leucogranite, that lies within the Shawanaga shear zone (Ketchum, 1995).

Ojibway gneiss association

The Ojibway gneiss association structurally overlies the Shawanaga pluton and extends southeastward to within a few kilometers of the Parry Sound domain (Culshaw *et al.*, 1994). Like the Muskoka domain, it is dominated by gray, migmatitic, upper amphibolite-facies dioritic to granodioritic orthogneiss (Culshaw *et al.*, 1994), with a protolith age of 1466±11 Ma (T. E. Krogh, unpublished data). The Ojibway gneiss association also contains small granite and megacrystic granitoid bodies, similar to those in the Muskoka domain.

Sand Bay gneiss association.

The Sand Bay gneiss association (Culshaw *et al.*, 1989) comprises a supracrustal assemblage, dominated by fine-grained, pink, migmatitic, quartzofeldspathic gneisses interpreted to be of volcanic (rhyolitic) origin based on compositional data (Culshaw and Dostal, 1997). Gray quartzofeldspathic gneiss, plagioclase-quartz-biotite schist (Dillon schist, Culshaw *et al.*, 1989) and minor calc-silicate, quartzite, and amphibolite are interlayered with the rhyolites. The contact with the Ojibway gneiss association is isoclinally folded and may be a deformed unconformity or décollement (Culshaw *et al.*, 1994). Detrital zircons from quartzites within the Sand Bay gneiss association yielded ages ranging from >2000-1382 Ma (T. E. Krogh, unpublished data), indicating a Laurentian source. The mineralogical and chemical composition of the Dillon schist suggests derivation from an immature, calcareous, epiclastic sediment (Culshaw and Dostal, 1997), and detrital zircons suggest a contribution from a proximal volcanic source at ca. 1364 Ma (T. E. Krogh, unpublished data). Thin megacrystic granitoid orthogneiss sheets, found in a few places in the Sand Bay gneiss association, are considered with the 'marginal orthogneiss' in the following discussion.
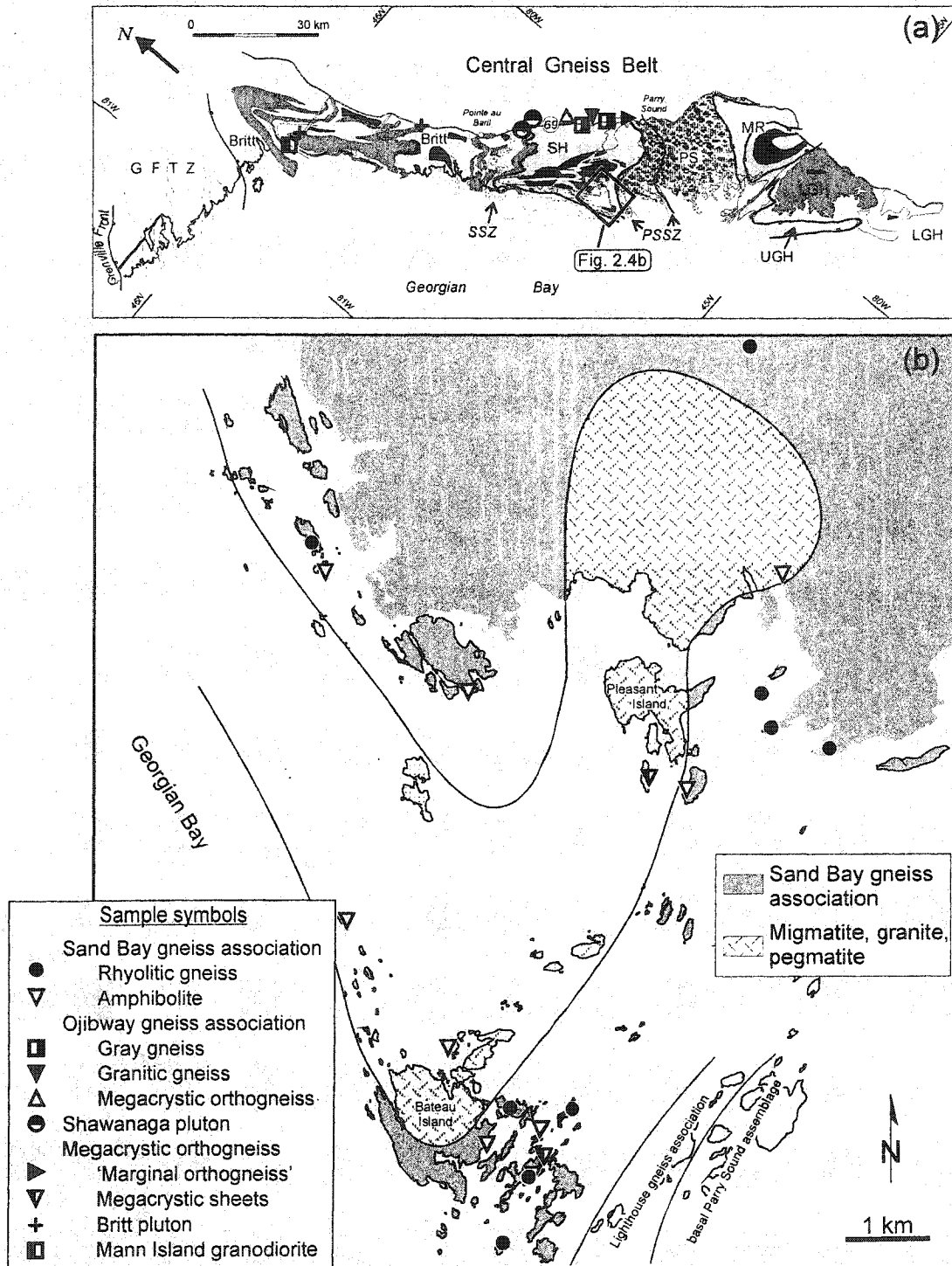
Fig. 2.4 Geological map, sample-locations and -symbols of (a) the CGB along Georgian Bay, from Culshaw and Dostal (2002), and (b) the southwestern part of the Shawanaga domain. Locations of the 'Lighthouse gneiss association' and 'basal Parry Sound assemblage' after Culshaw and Dostal (2002). The 'Migmatite, granite, pegmatite' unit in (b) consists of leucosome-rich migmatites, granites, and heterogeneous pegmatites (Chapter 4). Abbreviations: SSZ=Shawanaga Shear Zone, PSSZ=Parry Sound Shear Zone, UGH and LGH=Upper and Lower Go Home domain, MR=Moon River subdomain, PS= Parry Sound domain, SH=Shawanaga domain.

Amphibolite. Culshaw and Dostal (1997) interpreted the amphibolites in the Sand Bay gneiss association to represent basaltic extrusions, coeval with the rhyolites in the Sand Bay gneiss association. The amphibolites are compositionally similar to the mafic enclaves in the Muskoka domain and they are referred to collectively as metabasites below.

Lighthouse gneiss association.

The Lighthouse gneiss association (Culshaw and Dostal, 2002), in the immediate footwall to the Parry Sound shear zone, is the structurally uppermost supracrustal unit of the Shawanaga domain. It includes interlayered pelitic and psammitic gneiss, quartzofeldspathic gneiss, and amphibolite (Wodicka *et al.*, 2000; Culshaw and Dostal, 2002).

Geochemical investigations of the Sand Bay and Lighthouse gneiss associations by Culshaw and Dostal (1997, 2002) suggested the presence of a bimodal suite of continental tholeiitic basalts and rhyolites in the Sand Bay gneiss association, and a progression toward more ocean-floor-like (N- to E-type MORB) compositions in the lower and upper Lighthouse gneiss association. Culshaw and Dostal (1997, 2002) interpreted this progression to be compatible with progressive rifting in or behind a continental margin arc, however, it has not yet been established that the Sand Bay and Lighthouse gneiss associations are genetically related. Recent dating of detrital zircons from the Lighthouse gneiss association suggests that the lower unit is related to the Sand Bay gneiss association, whereas the upper unit is distinct (Raistrick, 2003).

2.4. Geochemistry

2.4.1. Analytical and sampling procedures

Major and trace elements were determined on fused glass beads and pressed powder pellets, respectively, using standard X-ray fluorescence (XRF) techniques at St. Mary's University, Halifax. Rare earth elements (REEs), Hf, and Th were determined at Memorial University, Newfoundland, by inductively coupled plasma-mass spectrometry (ICP-MS) using a Na_2O_2 sintering technique. Dostal *et al.* (1986) and Longerich *et al.*

(1990) discussed the analytical procedures, uncertainties, and precision of the XRF and ICP-MS analyses, respectively (see also Appendix A). Analytical results are presented in Appendix B.

Samples were collected from variably migmatitic outcrops. We have no field, petrographic, or geochemical data to suggest that sparsely migmatitic outcrops lost melt; in particular, the compositions of these rocks are not residual (cf., Solar and Brown, 2001). The more typical, strongly migmatitic outcrops present a greater challenge, because the bulk compositions may have been affected by gain or loss of melt. Samples from these outcrops lack leucosome on the hand sample scale, although they generally show grain-scale evidence (cf., Sawyer, 1999) of melting (Timmermann *et al.*, 2002). On the basis of textural evidence, Timmermann *et al.* (2002) concluded that partial melting in these rocks involved incongruent breakdown of biotite, producing abundant new hornblende. Evidence of this process is lacking from the sampled rocks (Slagstad, unpublished data) suggesting that they did not undergo significant melting. We conclude that only small amounts of melt, if any, were added to or segregated from the sampled rocks, and that they therefore represent a good approximation to protolith compositions.

2.4.2. Element mobility

The chemical compositions of highly metamorphosed orthogneisses have been used to determine petrogenesis and paleotectonic setting of their igneous protoliths, based on the assumption that the concentrations of the elements under consideration remained essentially unchanged during metamorphism and deformation. In general, low-field-strength elements (Sr, K, Rb, and Ba) are considered mobile, whereas high-field-strength elements (REEs, Y, Th, Zr, Hf, Ti, Nb, and P) and some transition metals (Ni, V, and Cr) are considered immobile (Rollinson, 1993). Element mobility should produce widely scattered patterns in normalized-element plots; however, most elements display no such scatter in the primitive mantle-normalized diagrams presented here, and the rocks have compositions similar to fresh, unmetamorphosed rocks (see following sections). Notable exceptions are Th in the gray gneisses and Ba in the metabasites that display significant variation, possibly because of mobilization. In addition, the distinct differences between

suites of rocks in these diagrams indicate only limited element mobility. Another way to assess whether or not a suite of rocks shows a coherent relationship that can be interpreted in terms of magmatic evolution is to use Pearce element ratios (Pearce, 1968), in which the molar ratios of compatible/incompatible elements are plotted against each other. Pearce element ratio diagrams for the gray gneisses and metabasites indicate that the major element variation within these two suites is similar to that expected for a related suite of magmatic rocks, and the same conclusion can be drawn from Harker variation diagrams (see following sections).

Despite the potential problems associated with both migmatization and element mobility, the consistency of the geochemical data and similarity to unmetamorphosed magmatic rocks suggest a reasonable approximation to original protolith compositions, therefore allowing for a plausible interpretation of petrogenesis and paleotectonic setting.

2.4.3. Muskoka and Seguin domains

Gray gneiss

The gray gneisses range in SiO_2 from 46.7 to 71.3 wt.%. They follow a calc-alkaline trend on the AFM diagram of Irvine and Baragar (1971) and have $FeO_t/(FeO_t+MgO)$ ratios <0.80 (Fig. 2.5a), typical of calc-alkaline rocks (Frost *et al.*, 2001). In the alumina-saturation diagram, the rocks straddle the boundary between metaluminous and slightly peraluminous compositions (Fig. 2.5d), with A/CNK<1.1, and A/NK>1.2. Harker diagrams (Fig. 2.6) display relatively well defined negative trends for most major elements (positive for K_2O), although there is some scatter in K_2O and Al_2O_3 values and substantial scatter in Na_2O values. The scatter in K_2O and Na_2O may reflect mobilization by secondary processes, although the preservation of a clear positive trend for K_2O suggests limited mobility. Similar scatter in Al_2O_3 was noted by Clynne (1990) in fresh, mafic to intermediate lavas from the Lassen Volcanic Center in California, and may, thus, be a magmatic feature rather than a result of element mobility. Fig. 2.7 shows Pearce element ratio diagrams of Al/K vs. (2Ca+Na)/K and Ti/K vs. P/K; we chose K as the conserved element in the denominator because it is incompatible in the fractionating
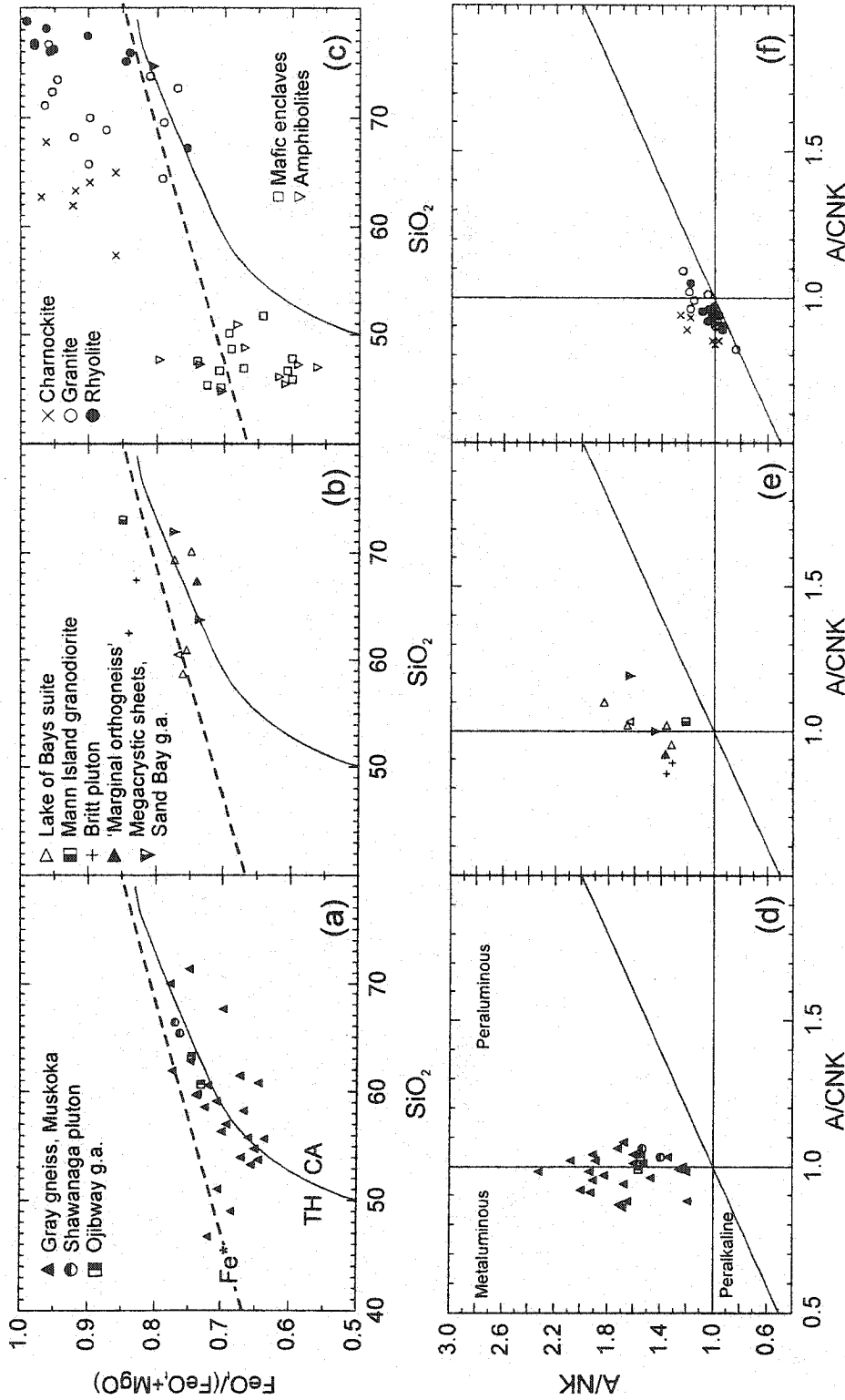
Fig. 2.5 (a-c) Silica contents *vs.* iron-enrichment ($FeO_t/(FeO_t+MgO)$). (d-f) A/CNK (mole $Al_2O_3/(CaO+Na_2O+K_2O)$) vs. A/NK (mole $Al_2O_3/(Na_2O+K_2O)$) diagrams. (a, d) gray gneiss, Muskoka domain, Ojibway gneiss association, and Shawanaga pluton; (b, e) Lake of Bays suite, 'marginal orthogneiss', megacrystic sheets in Sand Bay gneiss association, Britt pluton, Mann Island granodiorite; (c, f) charnockite, granite, rhyolite, and metabasites. Boundaries after Miyashiro (1974) (a-c) and Maniar and Piccoli (1989) (d-f). The dashed line in (a-c) is the Fe* line of Frost *et al.* (2001) separating 'ferroan' (~tholeiitic) and 'magnesian' (~calc-alkaline) rocks at higher and lower ($FeO_t/(FeO_t+MgO)$), respectively. Most A-type granites classify as 'ferroan' (Frost *et al.*, 2001).
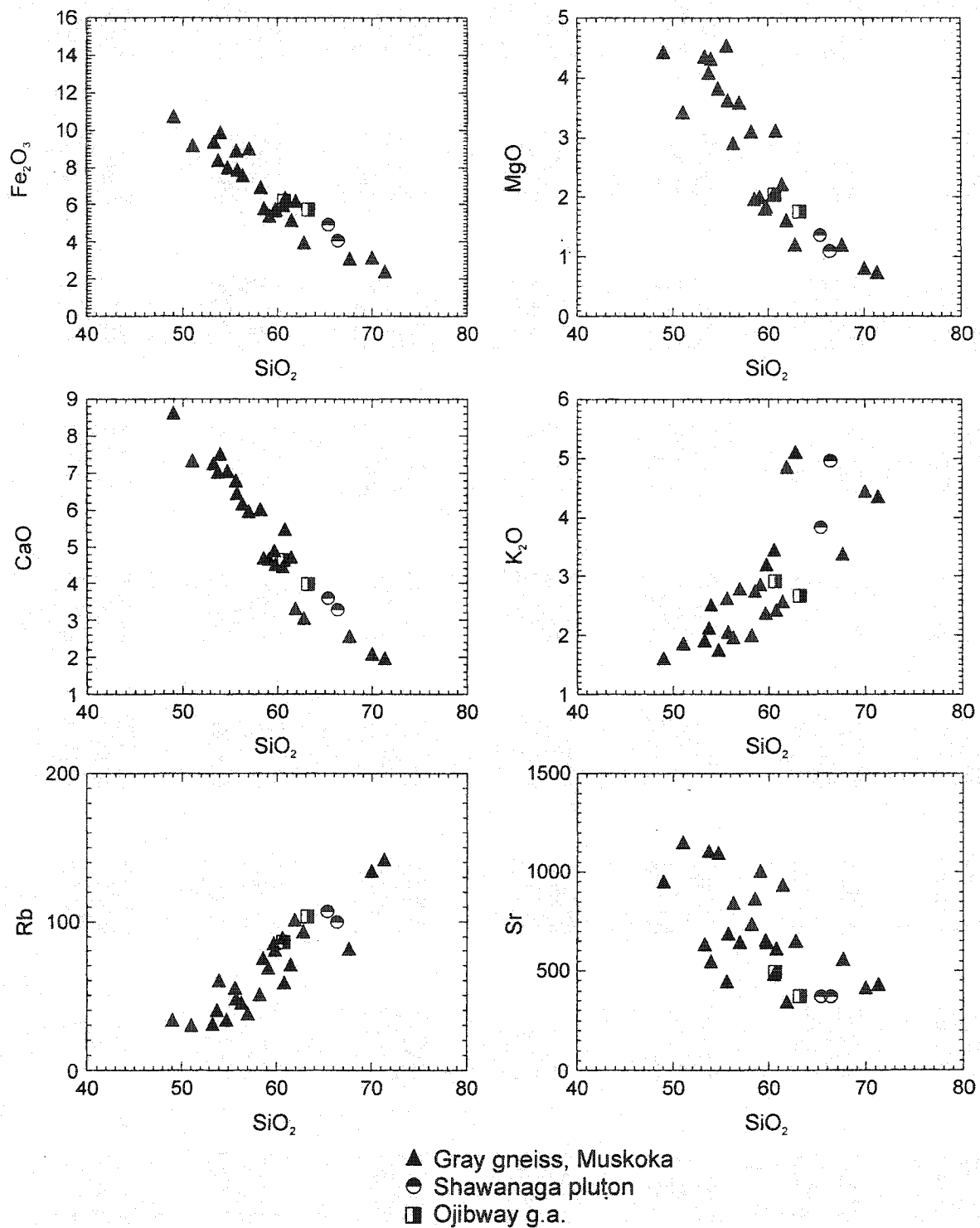
Fig. 2.6 Selected Harker diagrams for the gray gneisses in Muskoka domain, Shawanaga pluton, and Ojibway gneiss association, showing relatively well defined trends with SiO_2.
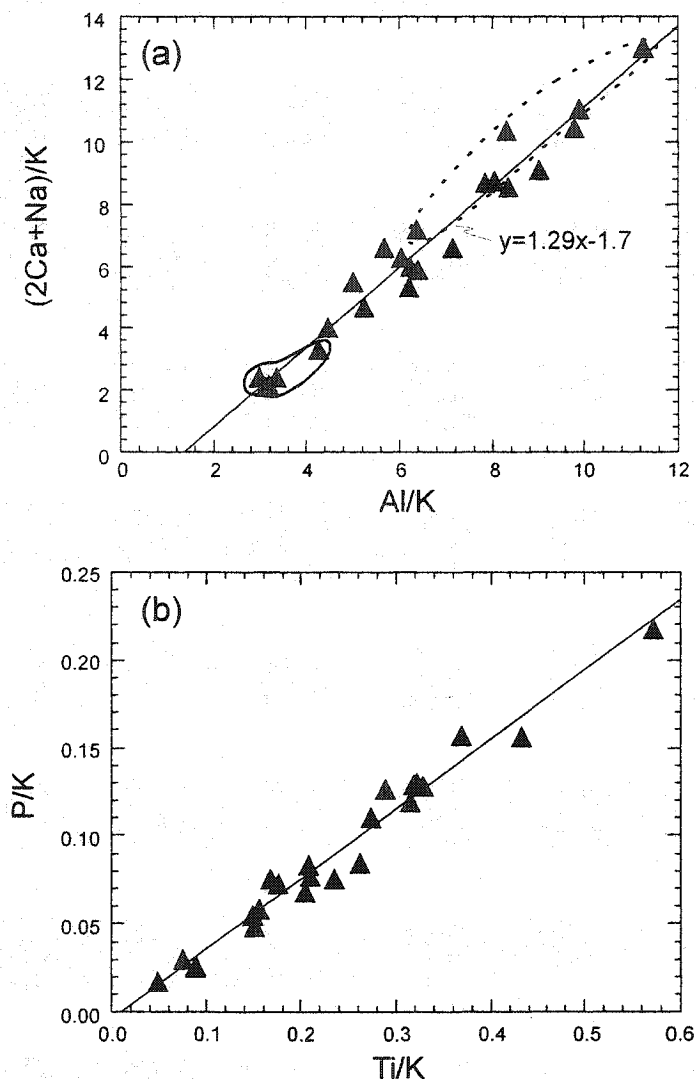
Fig. 2.7 (a) Pearce element ratio diagram of mole Al/K vs. (2Ca+Na)/K for the gray gneisses (Muskoka domain) yielding a slope of 1.29, suggesting fractionation of plagio-clase and clinopyroxene in a ratio of (mole Pl/Pl+Cpx) 3:4 (Russell and Nicholls, 1988). The dashed line encloses samples used as the starting composition (<55 wt.% SiO_2) for trace element modeling (stage 1, Fig. 2.14a); the solid line encloses samples representing the most felsic gray gneisses (avg. SiO_2=70 wt.%) (stage 2, Fig. 2.14b). (b) Pearce element ratio diagram of mole Ti/K vs. P/K, suggesting fractionation of apatite and Fe-Ti oxides.

assemblage (increases with increasing SiO_2) and appears not to be strongly affected by mobilization. The linear trends displayed in these diagrams are compatible with the gray gneisses being part of the same suite of magmatic rocks, and suggest that the geochemical variation within the suite is related to magmatic evolution rather than element mobility. Trace elements such as Sr and V (compatible in plagioclase and Fe-Ti oxides, respectively) show negative trends with SiO_2, whereas Rb increases with increasing SiO_2.

The REE patterns (Fig. 2.8a inset) are moderately fractionated, with small to moderate negative Eu anomalies (($Eu/Eu^*)_N$=0.54-0.80) that display a shallow negative trend with increasing SiO_2. Rare earth fractionation (($La/Yb)_N$) increases from 5.4 to 12.7 and ($La/Sm)_N$ from 1.8 to 4.8 with increasing SiO_2. Light (L)REEs are not correlated with SiO_2, whereas heavy (H)REEs and particularly middle (M)REEs show well defined negative trends. The primitive mantle-normalized variation diagram (Fig. 2.8a) shows that the rocks have trace element abundances typical of magmatic arcs (e.g., Brown et al., 1984), with distinct negative Nb, and small negative P and Ti anomalies. However, Zr values range from 200 to 400 ppm, significantly higher than most arc-related rocks. The rocks plot in the magmatic arc field in the Y+Nb vs. Rb tectonic discrimination diagram of Pearce et al. (1984) (Fig. 2.9a), consistent with their calc-alkaline character and trace element composition.

Charnockites

The charnockites range in SiO_2 from 62 to 68 wt.%, and are high in alkalis (Na_2O + K_2O = 9.8-11.4) and iron ($FeO_t/(FeO_t+MgO)$=0.86-0.97) (Fig. 2.5c). Total REE contents are high and the REE patterns are moderately fractionated (($La/Yb)_N$=4.2 to 15.8) with a large scatter of Eu anomalies (($Eu/Eu^*)_N$=0.3-1.5) (Fig. 2.10a inset). Barium also shows significant scatter, which could reflect element mobility. However, Ba and ($Eu/Eu^*)_N$ display a well defined linear trend, and the scatter in Ba and Eu anomalies may be better explained by K-feldspar accumulation than by element mobility. In the primitive mantle-normalized diagram (Fig. 2.10a), the charnockites are depleted in Th and Nb relative to the LREEs, and have large negative Sr, P, and Ti anomalies. Except for one sample, the

charnockites plot in the field of within-plate granites in tectonic discrimination diagrams (Fig. 2.9c).

Granites

The granites range in SiO_2 from 64 to 76 wt.% and are, like the charnockites, high in alkalis ($Na_2O + K_2O$ = 8.6-10.6) and iron (FeO_t/FeO_t+MgO=0.77-0.98 (Fig. 2.5c). They have moderately fractionated REE patterns with $(La/Yb)_N$ = 9.5-16.4, and large negative Eu anomalies ($(Eu/Eu^*)_N$=0.23-0.56) (Fig. 2.10b inset). Total REE contents are high and comparable to the charnockites, whereas other incompatible elements (particularly Zr, Y, and Hf) are lower. In the primitive mantle-normalized diagram (Fig. 2.10b), the granites are characterized by negative Nb and Eu, and large, negative Sr, P and Ti anomalies. In tectonic discrimination diagrams, the granites straddle the boundary between within-plate and arc settings (Fig. 2.9c).

2.4.4. Megacrystic orthogneiss

Lake of Bays suite and 'marginal orthogneiss'

Samples from the Lake of Bays suite range in SiO_2 from 59 to 70 wt.%, and the 'marginal orthogneiss' and associated megacrystic sheets in the Sand Bay gneiss association range from 64 to 67 wt.%. Despite the apparent age difference between the Lake of Bays suite and the 'marginal orthogneiss', their major and trace element compositions are indistinguishable from each other and from the gray gneisses (Figs. 2.5, 2.8, 2.9). One sample of a megacrystic orthogneiss from the Ojibway gneiss association is also geochemically similar to the Lake of Bays suite.

Mann Island granodiorite and Britt pluton

The Mann Island granodiorite and Britt pluton range in SiO_2 from 62 to 73 wt.% SiO_2 and are enriched in iron ($FeO_t/(FeO_t+MgO)$=0.83-0.85) relative to the Lake of Bays suite and 'marginal orthogneiss' that have ($FeO_t/(FeO_t+MgO)$) ratios between 0.74 and 0.77, typical of calc-alkaline rocks (Fig. 2.5b). The Mann Island granodiorite and Britt pluton are enriched in incompatible elements relative to the Lake of Bays suite and 'marginal orthogneiss' (Fig. 2.8c); they plot in the field of within-plate granites or straddle
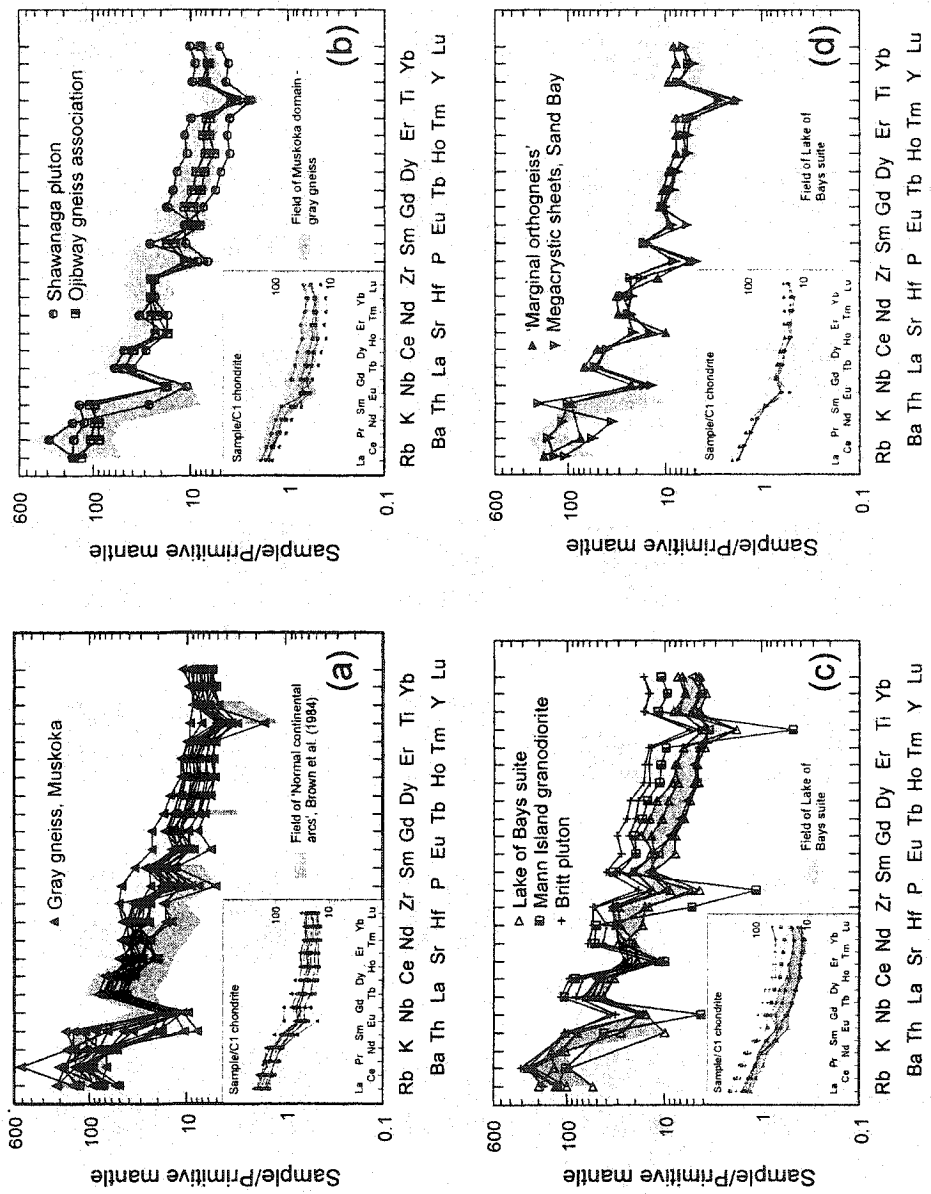
Fig. 2.8 Primitive mantle- and chondrite-normalized (inset) trace element variation diagrams for (a) gray gneisses, Muskoka domain; (b) Shawanaga pluton and Ojibway gneiss association, (c) Lake of Bays suite, Britt pluton, Mann Island granodiorite; (d) 'marginal orthogneiss' and megacrystic sheets in Sand Bay gneiss association. Normalization factors after Sun and McDonough (1989). Gray fields in (a) represent 'Normal continental arcs' as defined by Brown *et al.* (1984); note that Brown *et al.* used normalization factors from Wood (1979) but that this has a negligible effect on the normalized values as compared to the normalization factors of Sun and McDonough (1989). (Eu/Eu*)$_N$=(Eu$_N$)/((Sm$_N$+Gd$_N$)/2), where lowercase N denotes chondrite-normalized.
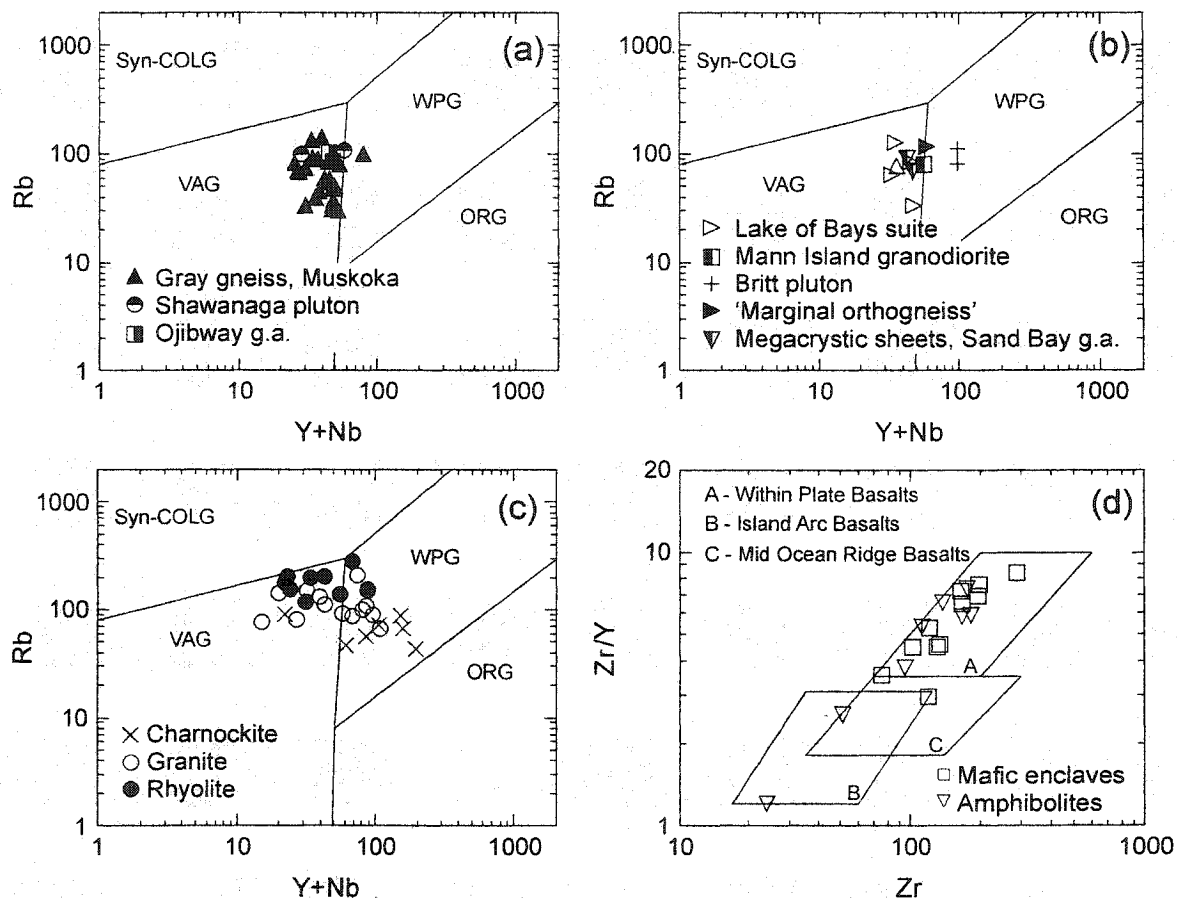
Fig. 2.9 Y+Nb vs. Rb tectonic discrimination diagram (Pearce *et al.*, 1984) for (a) gray gneisses in Muskoka domain, Shawanaga pluton, and Ojibway gneiss association; (b) megacrystic granitoid orthogneisses; and (c) charnockite, granite, and rhyolite. (d) Zr vs. Zr/Y tectonic discrimination diagram (Pearce and Cann, 1973) for the metabasites.
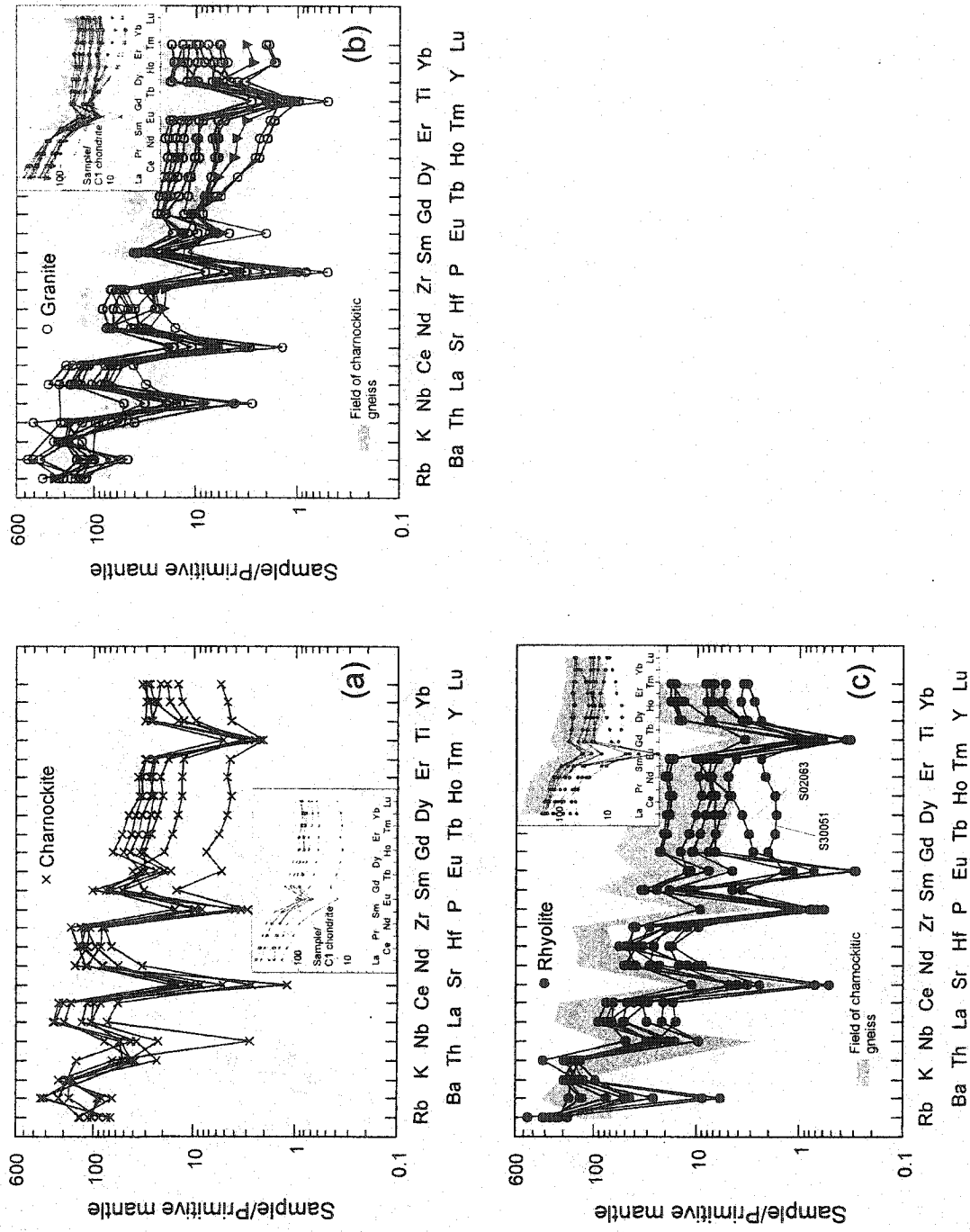
Fig. 2.10 Primitive mantle- and chondrite-normalized (inset) trace element variation diagrams for (a) charnockites; (b) granites, Muskoka domain and Ojibway gneiss association; and (c) rhyolites. Normalization factors after Sun and McDonough (1989).
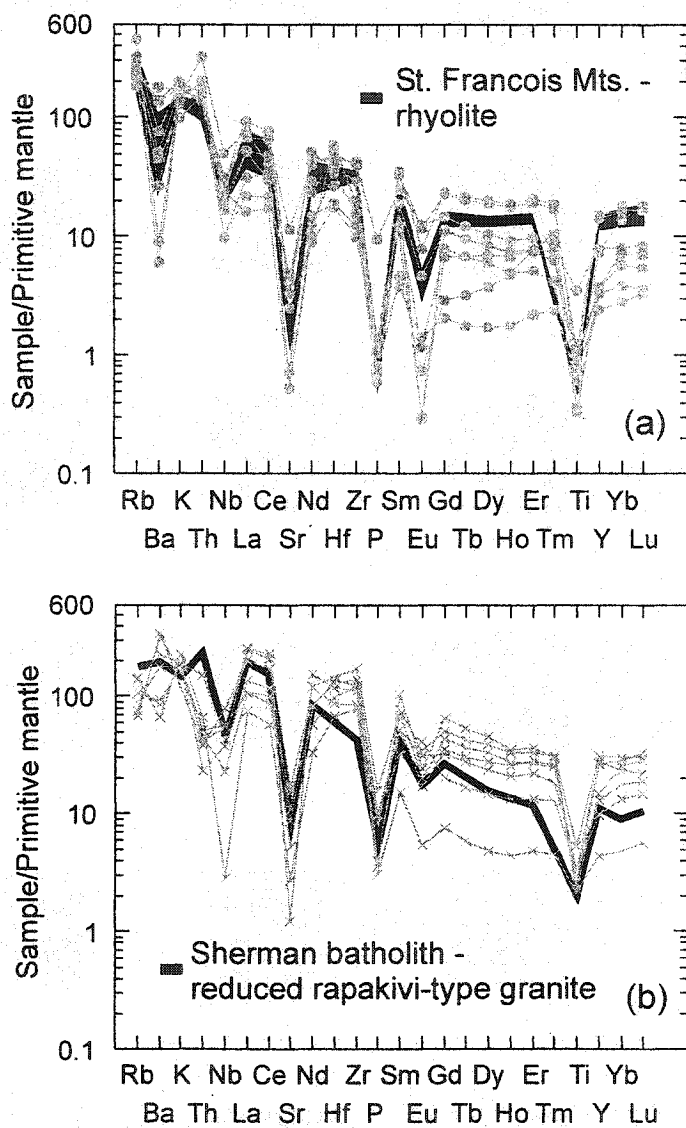
Fig. 2.11 (a) Trace element composition of Sand Bay rhyolite compared to that of rhyolite from the Eastern granite-rhyolite province, St. Francois Mountains (Menuge *et al.*, 2002). (b) Trace element composition of the charnockite compared to that of the Sherman batholith (Frost *et al.*, 1999).

the boundary between within-plate and arc settings in tectonic discrimination diagrams (Fig. 2.9b).

2.4.5. Shawanaga domain

Shawanaga pluton and Ojibway gneiss association

The four samples of Shawanaga pluton and Ojibway gneiss association contain 61-66 wt.% SiO_2 and resemble the gray gneisses in terms of major and trace element concentrations (Figs. 2.5, 2.6, 2.8, 2.9). The REE patterns are moderately fractionated ($(La/Yb)_N$=6.7-9.6) with negative to positive Eu-anomalies ($(Eu/Eu^*)_N$=0.4-1.3).

Sand Bay rhyolites

The rhyolites range from 67 to 79 wt.% SiO_2; all but one sample have SiO_2>75 wt.% (Fig. 2.5c). The very high SiO_2 could reflect silicification, however, we note that the composition of the rhyolites is comparable to little altered, non-metamorphosed rhyolites elsewhere (cf., Menuge *et al.*, 2002) (Fig. 2.11a). Like the charnockites and granites in Muskoka domain, the rhyolites are high in iron ($FeO_t/(FeO_t+MgO)$ typically >0.85) and alkalis ($Na_2O + K_2O$ = 7.5-9.5). The REE patterns are weakly to moderately fractionated ($(La/Yb)_N$=2.3-8.3), with large, negative Eu anomalies ($(Eu/Eu^*)_N$=0.02-0.64) (Fig. 2.10c inset). Two of the rhyolite samples (S30051 and S02063) have birdwing-shaped REE patterns with strongly negatively sloping LREEs and positively sloping HREEs, whereas other element abundances are similar to the other rhyolites. The geological significance, if any, of these two samples is unknown. A possible interpretation is that they are related to severe hydrothermal alteration (Blein *et al.*, in press), but this possibility has not been investigated in detail here. In the primitive mantle-normalized diagram (Fig. 2.10c), the rhyolites are characterized by strong Th enrichment (significantly higher than for the charnockites and granites), moderately negative Nb, and large negative Sr, P and Ti anomalies. The rocks straddle the boundary between arc and within-plate settings in tectonic discrimination diagrams (Fig. 2.9c).

2.4.6. Metabasites

The mafic enclaves from the Muskoka domain and amphibolites from the Sand Bay

gneiss association are geochemically indistinguishable, and they are, therefore, considered together. However, we emphasize that the geochemical similarity does not necessarily mean that they are the same age.

The metabasites range in SiO_2 from 44.8 to 51.0 wt.% with Mg# (mole $MgO/(MgO+FeO_t)$) generally between 0.40 and 0.60, and can be classified as subalkaline basalt to basaltic andesite (Winchester and Floyd, 1977). Titanium, Fe_2O_3, and V increase with decreasing Mg#, whereas Ni and Cr decrease (Fig. 2.12a). Elements such as Rb, Ba, and Sr show significant scatter (Fig. 2.13), suggesting secondary alteration. The $FeO_t/(FeO_t+MgO)$ vs. SiO_2 (Fig. 2.5c) and FeO_t/MgO vs. TiO_2 diagrams (Miyashiro, 1974) clearly illustrate the tholeiitic nature of the metabasites. The Si/Ti vs. 0.5*(Mg+Fe)/Ti Pearce element ratio diagram is consistent with fractionation of phases such as pyroxenes and olivine (cf., Russell and Nicholls, 1988) (Fig. 2.12b).

The metabasites have weakly fractionated REE patterns with $(La/Yb)_N$=2.3-4.9, similar to continental flood basalts (Fig. 2.13a). Th/La ratios are low, averaging 0.09, arguing against significant crustal contamination; however, evidence of Th mobility in some rocks makes this interpretation highly uncertain. Total REE contents increase and $(Eu/Eu^*)_N$ decreases slightly with decreasing Mg# (Fig. 2.12c), whereas $(La/Yb)_N$ remains constant. In the MORB-normalized diagram (Fig. 2.13), most samples display enrichment in all elements from Th to Sm, and depletion in Y, Yb, and Cr. Most samples have a negative Nb anomaly. In tectonic discrimination diagrams the majority of metabasites plot in the field of within-plate basalts (Fig. 2.9d). One distinct sample (S20066-2) from the Sand Bay gneiss association has a slightly LREE-depleted pattern, similar to ocean floor basalts; however, the geological significance of this sample is unknown.

2.5. Petrogenesis

It is convenient to divide the discussion of petrogenesis into three parts, based on geochemical composition: i) rocks with typical arc geochemical characteristics (gray gneiss); ii) rocks with A-type (defined below) geochemical characteristics (charnockite,
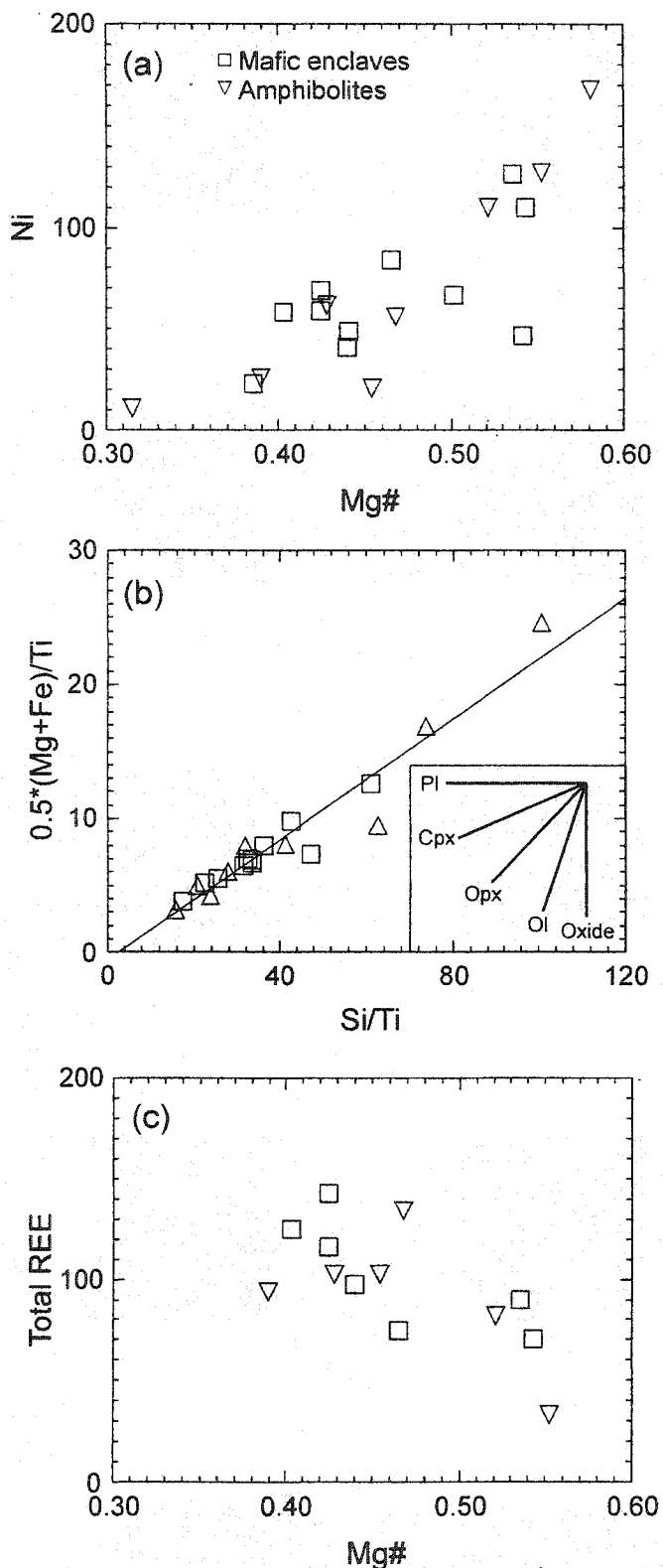
Fig. 2.12 Metabasite variation diagrams. (a) Mg# (mole Mg/(Mg+Fe)) vs. Ni.
(b) Pearce element ratio diagram of mole Si/Ti vs. 0.5*(Mg+Fe)/Ti. Inset shows slopes
expected for the fractionation of plagioclase, pyroxene, olivine, and oxides after Russell
and Nicholls (1988). (c) Mg# vs. total REE contents.
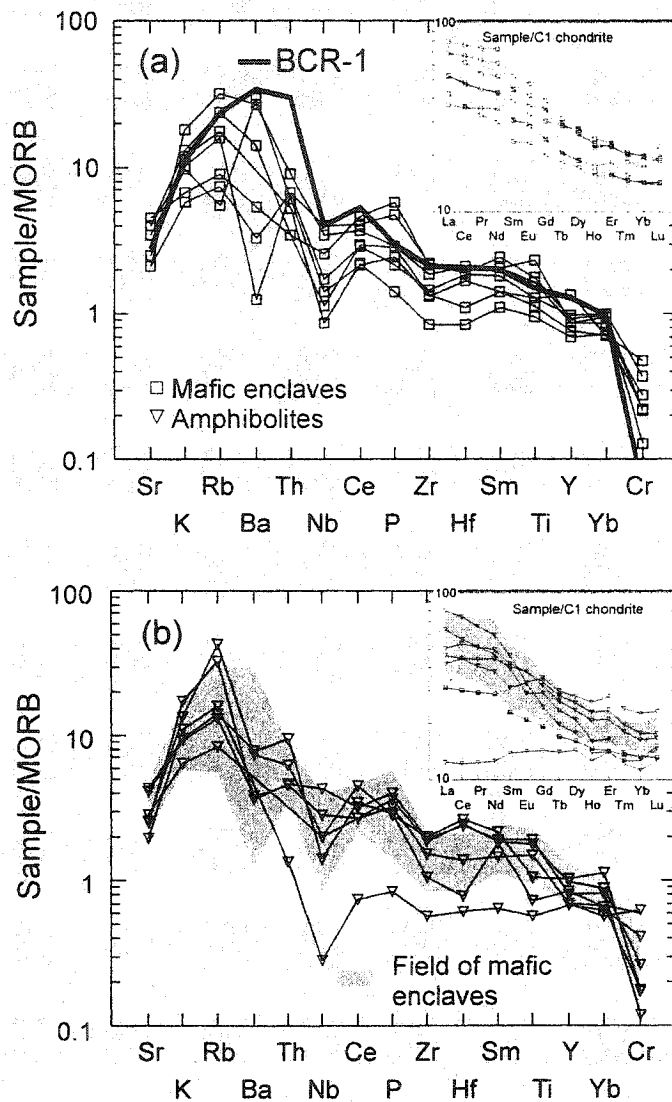
Fig. 2.13 MORB-normalized trace element variation diagram, (a) mafic enclaves, Muskoka domain; (b) amphibolites, Sand Bay gneiss association. Normalization factors after Pearce (1982). The composition of the Columbia River continental flood basalt (BCR-1) (Govindaraju, 1994) is shown in (a) for comparison. The composition of the metabasites is normalized to MORB rather than primitive mantle to facilitate comparison with basalt/amphibolite compositions reported elsewhere, typically normalized to MORB.

granite, and rhyolite); and iii) metabasites (mafic enclaves from Muskoka domain and amphibolites from Shawanaga domain). The megacrystic orthogneisses, Shawanaga pluton, and Ojibway gneiss association were investigated only on a reconnaissance level and a detailed treatment of their petrogenesis is not warranted.

2.5.1. Gray gneiss

A positive correlation between MgO and CaO and decreasing Ni and Sr with decreasing MgO indicates fractionation of plagioclase and clinopyroxene (cf., Devine, 1995). Russell and Nicholls (1988) proposed that the molar proportions of plagioclase to clinopyroxene could be determined from the slope in the Al/K vs. (2Ca+Na)/K diagram. The slope for the gray gneisses in this diagram is 1.29 (Fig. 2.7a), which corresponds to a (molar) plagioclase/(plagioclase+clinopyroxene) ratio of ca. 3:4. Alternatively, Ti and P can be used as the conserved element (denominator) if Fe-Ti oxides and apatite are absent from the fractionating assemblage, in which case Ti/K vs. P/K will define a tight cluster, or ideally a point (Russell and Nicholls, 1988). Plotting Ti/K vs. P/K yields a well defined linear trend for the gray gneisses (Fig. 2.7b), suggesting that Ti and P were compatible. We therefore assume that Fe-Ti oxides and apatite, in addition to plagioclase and clinopyroxene, were part of the fractionating assemblage. Increasing $(La/Yb)_N$ and $(La/Sm)_N$ with increasing SiO_2 may indicate fractionation of hornblende (cf., Arth and Barker, 1976).

Europium anomalies normally become more negative with increasing fractionation if plagioclase is involved and could be used as an argument against the model proposed above. However, Gertisser and Keller (2000) did not observe well developed negative Eu anomalies in the calc-alkaline Aeolian Arc, where it can be shown petrographically that plagioclase was the dominant fractionating phase. They interpreted the lack of negative Eu anomalies to reflect relatively high oxygen fugacities during differentiation.

To test whether fractional crystallization of plagioclase, clinopyroxene, Fe-Ti oxides, hornblende, and apatite can explain the gray gneiss compositions, we modeled changes in REEs, Rb, and Sr concentrations assuming Rayleigh fractional crystallization in which cumulate phases are immediately removed from interaction with the melt after

they form (e.g., Hanson, 1978). Table 2.2 presents the partition coefficients and Appendix F the equations used in the modeling. Appendix F also discusses the effects of analytical error and partition coefficients on the petrogenetic interpretations made herein. Rubidium and Sr were included because they are important petrogenetic indicators and show relatively well defined trends in bivariate diagrams, suggesting limited mobility. In contrast, Ba shows significant scatter, possibly indicating secondary mobilization, and was not included.

Trace element modeling presents a number of uncertainties (see Rollinson, 1993 for a review). One of the most obvious is probably the mineral/melt partition coefficient used in the modeling. Melt composition is the most important single factor controlling partition coefficients. Available data permitting, we took melt composition (assumed similar to rock composition) into account when selecting a partition coefficient; for example, the fractional crystallization modeling for the gray gneisses is done in two stages to account for evolving melt composition. However, the partition coefficients also depend on a number of other factors on which we have few constraints, including temperature, pressure, oxygen activity, crystal chemistry, and water content. An additional complexity is that most of the investigated rocks are plutonic, thus, their composition probably does not represent melt composition but rather magma composition (melt plus entrained cumulate and/or residual minerals). Despite these uncertainties, trace element modeling is useful for assessing and in some cases refining petrogenetic models based on major element geochemistry, field observations, and experimental data.

Fractional crystallization modeling of the gray gneisses was performed in two stages to account for changing partition coefficients between mafic/intermediate and felsic compositions. The average composition of the most mafic gray gneisses (all samples with <55 wt.% SiO_2, see Fig. 2.7a) was used as the starting composition for stage 1 whereas the daughter composition was taken to be intermediate gray gneiss with average 59 wt.% SiO_2. A good fit between model melt and intermediate gray gneiss was achieved after ca. 30% crystallization (fractionating assemblage and abundances given in Fig. 2.14). The model melt after 30% crystallization in stage 1 was taken to be the

Table 2.2 Partition coefficients used in modeling Rayleigh fractional crystallization of gray gneiss.

	Stage 1					Stage 2					
	Pl	Cpx	Hbl	Magnetite	Ap	Pl	Cpx	Hbl	Magnetite	Ap	Zrn
Ref.	1	2	1	1	2	2	3	4	1	2	2
Rb	0.04	0.03[1]	0.014	0.01[7]		0.048[3]	0.031[7]		0.01[7]		
Sr	4.4	0.1283[6]	0.022	0.01[7]		2.84[3]	0.060[7]		0.01[7]		
La	0.4	0.0536[6]	0.74	0.22	20[8]	0.302[5]	0.12[9]	0.6[9]	0.22	20[8]	(2)
Ce	0.27	0.07	1.52	0.26	34.7	0.24	0.15	0.9	0.26	34.7	2.64
Nd	0.21	0.12	4.26	0.30	57.1	0.17	0.31	2.8	0.30	57.1	2.20
Sm	0.13	0.18	7.77	0.35	62.8	0.13	0.50	3.99	0.35	62.8	3.14
Eu	2.15	0.18	5.14	0.26	30.4	2.11	0.51	3.44	0.26	30.4	3.14
Gd	0.097	0.19	10	0.32	56.3	0.09	0.61	5.47	0.32	56.3	12
Tb	0.09	0.315[1]	11	0.28	(55)	(0.09)	(0.65)	(6)	0.28	(55)	(30)
Dy	0.064	0.21	13	0.28	50.7	0.086	0.68	6.19	0.28	50.7	45.7
Ho	0.057[5]	(0.3)	(12)	(0.25)	(40)	(0.085)	(0.66)	(6)	(0.25)	(40)	(100)
Er	0.055	0.17	12	0.22	37.2	0.084	0.65	5.94	0.22	37.2	135
Tm	(0.05)	(0.16)	(10)	(0.2)	(30)	(0.08)	(0.63)	(5)	(0.2)	(30)	(200)
Yb	0.049	0.16	8.4	0.18	23.9	0.077	0.62	4.9	0.18	23.9	270
Lu	0.046	0.13	6	0.18	20.2	0.062	0.56	4.51	0.18	20.2	323

References: 1) Martin (1987); 2) Arth and Hanson (1975); 3) Arth (1976); 4) Arth and Barker (1976); 5) Fujimaki et al. (1984); 6) Smith and Humphris (1998); 7) Rollinson (1993); 8) Barbey et al. (1989); 9) Borg and Clynne (1998);. Values in parentheses are assumed by extrapolation.

Table 2.3 Partition coefficients used in modeling equilibrium partial melting of gray gneiss producing granite and rhyolite.

	Pl	Cpx	Opx	Mag	Ap	Zrn	Aln
Ref.	1	2	2	2	3	3	4
Rb	0.09	0.0019	0.001	0.01			
Sr	4.5 [33]	0.12	0.02	0.01			
La	0.38	0.16	0.016	0.01	20^1	(2)	2827
Ce	0.27	0.21	0.019	0.01	34.7	2.64	2494
Nd	0.21	0.45	0.03	0.01	57.1	2.2	1840
Sm	0.13	0.8	0.042	0.01	62.8	3.14	977
Eu	2.15 [7.9]	0.85	0.052	0.01	30.4	3.14	100
Gd	0.1	1.1	0.066	0.01	56.3	12	440^1
Tb	0.095^2	1.3	0.08	0.01	(55)	(30)	311
Dy	0.064	1.45	0.12	0.01	50.7	45.7	150
Ho	(0.06)	1.4	0.16	0.01	(40)	(100)	(100)
Er	0.0588^5	1.3	0.2	0.01	37.2	135	(60)
Tm	(0.055)	1.2	0.25	0.01	(30)	(200)	(50)
Yb	0.049	1.1	0.36	0.01	23.9	270	37
Lu	(0.045)	1	0.45	0.01	20.2	323	44

References: 1) 1) Barbey *et al.* (1989); 2) Borg and Clynne (1998); 3) Arth and Hanson (1975); 4) Mahood and Hildreth (1983); 5) Arth and Barker (1976). Values in parentheses are assumed by extrapolation. Values in brackets from Nash and Crecraft (1985), used in modeling rhyolite (Fig. 2.15c).

Table 2.4 Partition coefficients used in modeling fractional crystallization and partial melting of a basaltic magma and rock, respectively, producing charnockite.

Ref.	Fractional crystallization				Partial melting		
	Pl	Ol	Hbl	Cpx	Pl	Cpx	Opx
	1	1	2	1	2	2	2
La	0.0415	0.000007	0.74	0.0536	0.13	0.1	0.002
Ce	0.0297	0.00001	1.52	0.0858	0.11	0.2	0.003
Sr	1.61	0.0030	0.022	0.1283	2.0	0.2	0.017
Nd	0.023	0.00007	4.26	0.1873	0.07	0.4	0.0068
Sm	0.0177	0.0007	7.77	0.2910	0.05	0.6	0.010
Eu	0.168 [2.15[2]]	0.00095	5.14	0.35	1.3	0.6	0.013
Gd	0.012	0.0012	10	0.40	0.04	0.7	0.016
Tb	(0.01)	0.0016[2]	11	(0.4)	0.037	0.7	0.019
Dy	0.0090	0.0040	13	0.442	0.031	0.7	0.022
Ho	(0.085)	(0.007)	(12)	(0.4)	0.03[3]	(0.65)	(0.03)
Er	0.0079	0.0090	12	0.3870	0.026	0.6	0.030
Tm	(0.075)	(0.01)	(10)	(0.4)	0.02[3]	(0.6)	(0.04)
Yb	0.0070	0.023	8.4	0.43	0.024	0.6	0.049
Lu	(0.065)	(0.02)	6	(0.4)	0.023	0.6	0.028

References: 1) Smith and Humphris (1998); 2) Martin (1987); 3) Borg and Clynne (1998). Values in parentheses are assumed by extrapolation. Value in brackets demonstrates range in published partition coefficients for Eu in plagioclase; both values are used in the modeling.

starting composition for stage 2 modeling and the daughter for stage 2 was represented by the felsic gray gneisses (avg. 70 wt.% SiO_2, see Fig. 2.7b). A good fit between model melt and felsic gray gneiss was achieved after 30-50% crystallization (see Fig. 2.14 for details). Total fractionation for stage 1 and 2 was 50-65%.

Both stages are dominated by plagioclase, clinopyroxene, and Fe-Ti oxide (magnetite). Hornblende constitutes a minor part of the model fractionating assemblage, and apatite occurs in trace amounts. Minor zircon was included in stage 2 to account for the depletion in HREEs. The results of the modeling are compatible with the major element data (Pearce element ratios) suggesting that the gray gneisses may have evolved from the dioritic members of the suite by fractional crystallization of plagioclase, clinopyroxene, Fe-Ti oxides, minor hornblende, and trace amounts of apatite. Minor zircon fractionation appears to have affected the most felsic samples.

2.5.2. A-type granites (charnockite, granite) and rhyolite

The charnockites, granites, and rhyolites have high $FeO_t/(FeO_t + MgO)$, high alkalis decreasing with SiO_2, high Zr, Y, Hf, REEs (except Eu), and Ga/Al, and low MgO, CaO, and Sr, characteristic of A-type granites (Loiselle and Wones, 1979; Whalen et al., 1987; Eby, 1990). A-type granites are typically interpreted to have been emplaced at middle to upper crustal levels in extensional tectonic settings, and are characterized by high magmatic temperatures (Clemens et al., 1986; Creaser et al., 1991) and low fH_2O and fO_2. It is not possible to determine primary fH_2O or fO_2 values for the upper amphibolite- to granulite-facies rocks described here, however, abundant pyroxene in the charnockites, the scarcity of hydrous minerals in general, and the paucity of leucosome by comparison with the adjacent gray gneisses, suggests that their protoliths were H_2O-deficient. Both the charnockites and granites form discrete bodies and are petrographically and geochemically distinct from the surrounding gray gneisses, suggesting that their petrological and geochemical features are unlikely to result from Grenvillian metamorphic processes. Magmatic temperatures can be estimated using the zircon saturation thermometer of Watson and Harrison (1983). As discussed in the Geochronology section, the charnockites contain abundant euhedral zircons that lack
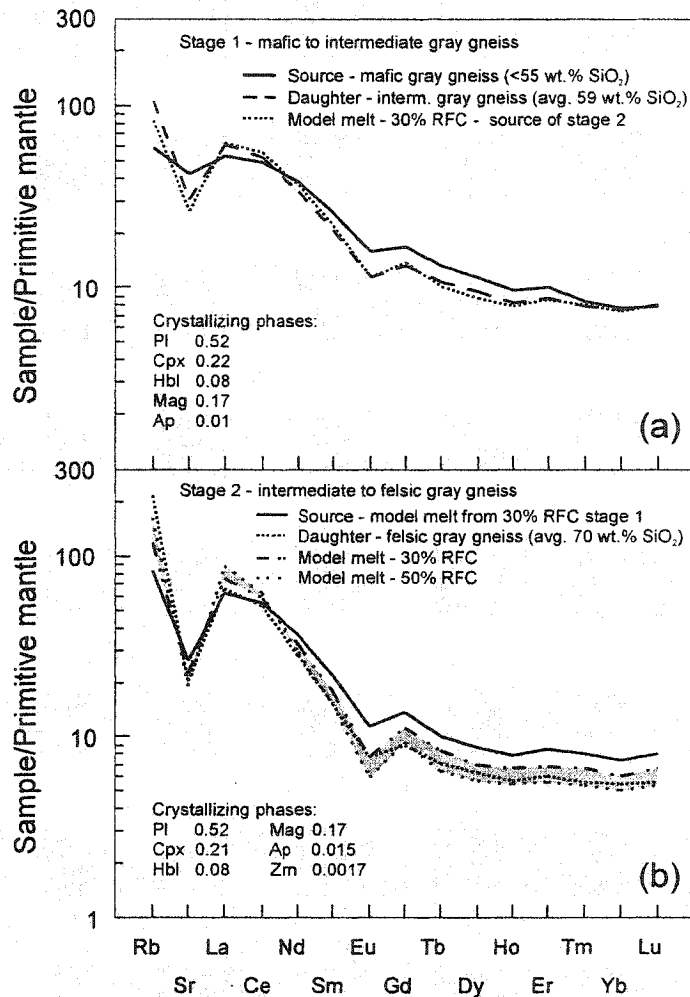
Fig. 2.14 Modeling results for Rayleigh fractional crystallization of a mafic to intermediate magma (a) and an intermediate to felsic magma (b), simulating the evolution of the gray gneisses. Abundances of crystallizing phases given as weight proportions. Mineral abbreviations after Kretz (1983) and normalization factors after Sun and McDonough (1989) in this and other figures, RFC=Rayleigh Fractional Crystallization.

distinct inherited cores or metamorphic overgrowths; it is, therefore, possible that they crystallized from the charnockite magma, meaning that the calculated temperatures may reflect the liquidus temperature of the magma. Temperatures fall in a narrow range between 931 and 968°C, consistent with the magmatic temperatures associated with A-type granites (e.g., Creaser and White, 1991). Zircon saturation temperatures for the granites range from 866-964°C, with an average of 904°C, whereas the rhyolites yield temperatures in the range 755-891°C, with an average of 819°C.

High magmatic temperatures of A-type granites can be explained by intrusion and crystallization of mantle-derived mafic magmas (e.g., Creaser et al., 1991), by high geothermal gradients characteristic of areas undergoing crustal extension (e.g., Sandiford and Powell, 1986), or by a combination of both. Commonly invoked petrogenetic models for A-type granites include partial melting of a residual granulitic source that has previously generated an I-type granite (Collins et al., 1982; Clemens et al., 1986), partial melting of crustal igneous rocks of tonalitic to granodioritic composition (Cullers et al., 1981; Anderson, 1983; Creaser et al., 1991; Patiño Douce, 1997), and extreme differentiation (with or without assimilation) or partial melting of underplated tholeiitic basalts (Turner et al., 1992; Frost et al., 1999). A short review of the various models and a discussion on their applicability to the investigated charnockite, granite, and rhyolite follows.

Partial melting of a residual source

Clemens et al. (1986), Whalen et al. (1987), and Landenberger and Collins (1996) proposed that A-type granites form by partial melting of a granulite-facies meta-igneous source that has previously yielded a hydrous, I-type granitic melt. The model was proposed to explain the low magmatic water activity and high magmatic temperatures of A-type granites, but has been disputed by several authors, based on the chemical composition of A-type granites and experimental data (e.g., Creaser et al., 1991; Cullers et al., 1993; Patiño Douce, 1997). For example, strong iron enrichment appears to be characteristic of A-type granites (e.g., Frost et al., 2001). However, as pointed out by Creaser et al. (1991), partial melts invariably have higher Fe/Mg ratios than the mafic

silicates with which they are in equilibrium. Thus, mafic residual silicates such as pyroxene and amphibole should become enriched in Mg after extraction of an I-type melt. Such a residue is unlikely to subsequently yield melts with higher Fe/Mg ratios than that of the I-type melt produced during the first melting episode (Creaser *et al.*, 1991). Following these authors, we consider granulite-facies, residual rocks an unlikely source for the charnockite, granite, and rhyolite.

Partial melting of a tonalitic to granodioritic source (gray gneiss)

Several authors have suggested that granites and rhyolites with A-type characteristics may form by 10-40% partial melting of a tonalitic to granodioritic, calk-alkaline source (Anderson and Cullers, 1978; Anderson, 1983; Creaser *et al.*, 1991; Patiño Douce, 1997; Menuge *et al.*, 2002). These granites and rhyolites typically have $SiO_2 > 70$ wt.% and $FeO_t < 4$ wt.%. In contrast, A-type granites with inferred mantle-derived sources (e.g., Nédélec *et al.*, 1995; Frost *et al.*, 1999) typically have $SiO_2 < 70$ wt.% and $FeO_t > 6$ wt.%. The granites and rhyolites, but not the charnockites, are compositionally similar to A-type granites inferred to have formed by partial melting of a tonalitic or granodioritic source (Fig. 2.11A). To test whether this model is feasible, we used the average gray gneiss (57% SiO_2) as the starting composition for petrogenetic modeling. The modeling assumed equilibrium batch melting, i.e., the melt and residue remained in equilibrium as melting proceeded (e.g., Hanson, 1978). Fig. 2.15 presents the results and details of the modeling, Table 2.3 the partition coefficients, and Appendix F the equations. A good fit between model melt and observed compositions, except Eu in rhyolite and Sr in rhyolite and granite, was obtained by 10-40% partial melting, leaving a granulitic residue consisting of quartz, plagioclase, pyroxenes, and Fe-Ti oxide. Minor apatite and zircon were included in the residue for the granites, and apatite, zircon, and allanite for the rhyolites. These are common accessory minerals in granitic systems, and partition coefficients of otherwise incompatible elements (e.g., REEs) may be extremely high in these phases (Tindle *et al.*, 1988; Wark and Miller, 1993; Bea, 1996). Thus, although they have little petrogenetic significance, they may effectively determine the trace element composition of a magma. The above results must, therefore, be treated
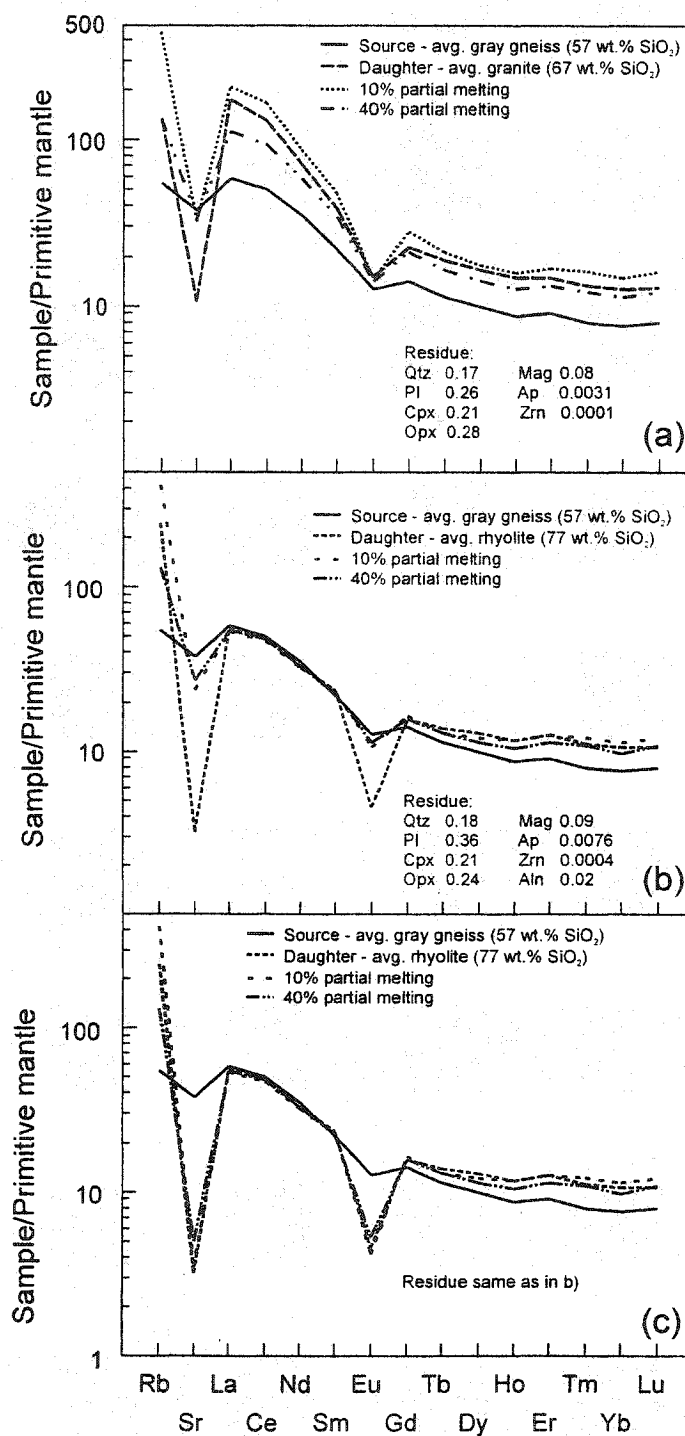
Fig. 2.15 Modeling results for equilibrium partial melting of intermediate gray gneiss. (a) the model melt obtained by 10-40% partial melting is similar to the granites for the REEs but enriched in Sr and Rb. (b) the model melt obtained by 10-40% partial melting is similar to the rhyolites for most trace elements except for enrichment in Eu and Sr. The results presented in (a) and (b) were obtained using partition coefficients appropriate for felsic systems. (c) identical to (b) except for significantly higher partition coefficients for Eu and Sr in plagioclase, probably more appropriate for high-silica rhyolites (Nash and Crecraft, 1985). The model melt thus obtained is compositionally similar to the rhyolites. Abundances of crystallizing phases given as weight proportions.

with caution. The model results shown in Figs. 2.15a, b are based on partition coefficients appropriate for granitic systems (i.e., $SiO_2 \sim 70$ wt.%) (Table 2.3). However, some studies have shown that partition coefficients for Sr and Eu in plagioclase can be significantly higher in high-silica (i.e., $SiO_2 \sim 75$ wt.%) rhyolites (e.g., Nash and Crecraft, 1985). The rhyolites investigated here can be regarded as high-silica rhyolites and employing partition coefficients from Nash and Crecraft (1985) (Table 2.3) yields a good fit between model melt and rhyolite (Fig. 2.15c). In summary, partial melting of an intermediate calc-alkaline source is not feasible for producing the charnockites, but remains a possibility for the granites and appears likely for the rhyolites. A likely source of the granites and rhyolites is the abundant gray gneiss in the Muskoka domain and Ojibway gneiss association, although other, similar sources are equally possible. Isotopic data are needed to determine the nature of the source of the granites and rhyolites.

Differentiation from, or partial melting of, a mafic source

A-type granites, similar in composition to the charnockites, have been described from Madagascar (Nédélec *et al.*, 1995) and Wyoming (Frost *et al.*, 1999). In the Madagascar example, Nédélec *et al.* (1995) proposed that A-type granites (syenites) formed from a mantle-derived mafic magma by fractional crystallization, with hornblende as a major fractionating phase. Frost *et al.* (1999) proposed partial melting of pre-existing tholeiites or more probably their differentiates as the most feasible petrogenetic model for the Sherman batholith in Wyoming. We interpret the charnockites to have formed in a similar way to the Sherman batholith, based on their similar composition (Fig. 2.11b). The metabasites have compositions compatible with an origin as underplated basaltic magmas, discussed further below. Although the amphibolites in the Sand Bay gneiss association are interpreted to be coeval with the rhyolites and, thus, significantly younger than the charnockites, the mafic enclaves in Muskoka domain may represent a potential source. This model is tested using trace element modeling; partition coefficients are given in Table 2.3.

The modeling yields interesting but inconclusive results (Fig. 2.16). The charnockites could have formed by 80-90% Rayleigh fractional crystallization of a mafic

magma, fractionating plagioclase, olivine, clinopyroxene, and minor hornblende (Fig. 2.16a). Equilibrium partial melting of a mafic enclave yields a model melt composition that is depleted in REEs relative to the average charnockite (Fig. 2.16b). Alternatively, the charnockites could have formed via a two-stage process involving fractional crystallization of a mafic magma, followed by partial melting of the fractionated rock, i.e., similar to the model proposed by Frost et al. (1999) for the Sherman batholith. This alternative was modeled in two stages (Fig. 2.16c): stage 1 involved 40% Rayleigh fractional crystallization of a mafic magma, fractionating the same minerals in similar proportions as shown in Fig. 2.16a. The model melt composition thus obtained was used as the starting composition for partial melting calculations; the results show that 10-30% partial melting of the fractionated rock, leaving a residue comprising plagioclase, clinopyroxene, and orthopyroxene, produces model melts similar to the charnockites. The degree of fractionation during stage 1, arbitrarily set at 40%, determines the REE contents but not the REE pattern used as the starting composition for stage 2. Selecting a different value, for example 20%, gives similar results but requires lower degrees of partial melting (<10%). Thus, the fractionating assemblage during stage 1 and the residue during stage 2 are the main controlling factors on the model results, not the degree of fractionation. In contrast to the model proposed by Nédélec et al. (1995), hornblende appears to have been relatively insignificant, consistent with the anhydrous nature of these rocks.

Frost et al. (1999) cited the lack of intermediate compositions between mafic rocks and granites as evidence against a fractional crystallization model for the Sherman batholith. Grove and Donnelly-Nolan (1986) suggested that compositional gaps could result from shallow temperature vs. composition slopes on liquidus surfaces, allowing large degrees of crystallization and compositional change over small temperature intervals. Turner et al. (1992) suggested that the gap between basaltic magmas and A-type granites could be explained by this mechanism. However, the mechanism was originally proposed to explain the commonly observed gap between andesitic and silicic lavas (~60-70% SiO_2) from a single calc-alkaline volcano (e.g., Hildreth, 1981; Bacon and Druitt, 1988), and is not necessarily applicable to A-type granites in general. We
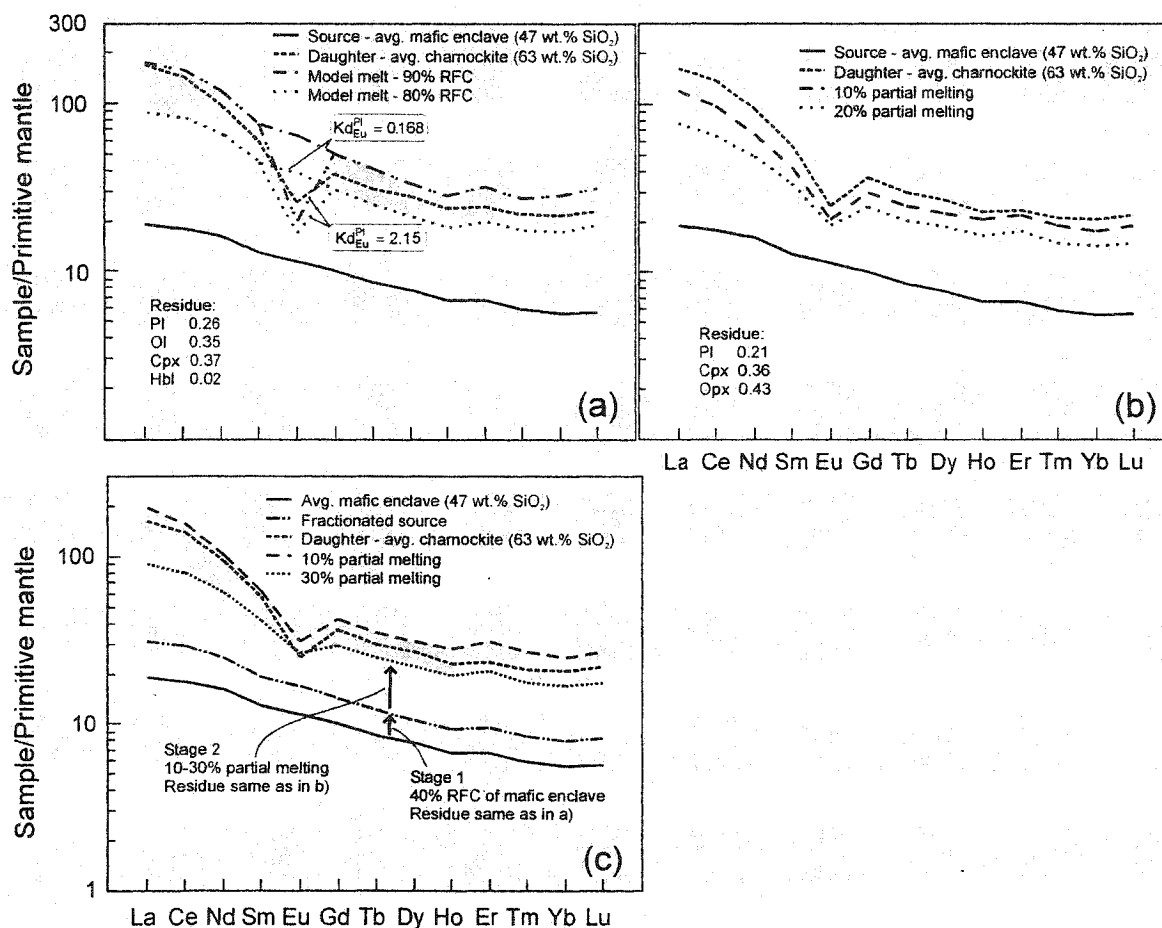
Fig. 2.16 Three possible models for relating the mafic enclaves and the charnockites. (a) Rayleigh fractional crystallization of a basaltic magma (mafic enclave). The fit between model melt and charnockite is good for most elements after 80-90% fractional crystallization, whereas the fit for Eu depends on the partition coefficient for Eu in plagioclase. A partition coefficient of 0.168 (Smith and Humphris, 1998) produces a model melt that is too high in Eu, whereas a partition coefficient of 2.15 (Martin, 1987) produces a model melt depleted in Eu. Both partition coefficients were reported to be appropriate for mafic systems and exemplify some of the inherent problems in trace element modeling. (b) Equilibrium partial melting of a basaltic source (mafic enclave). The modeling shows that low-degrees of partial melting (10-20%) of a basaltic source produces model melts that are depleted in REEs relative to the charnockites.
(c) equilibrium partial melting of a fractionated mafic enclave. The source for this model was taken to be the model melt obtained after 40% Rayleigh fractional crystallization of a basaltic magma (mafic enclave), fractionating the same phases and in similar proportions as in (a). Low degrees (10-30%) of partial melting of this fractionated source, leaving a residue similar to (b), yielded a model melt similar to the charnockites. Abundances of crystallizing and residual phases given as weight proportions.

therefore conclude that partial melting of underplated tholeiitic basaltic rocks or their fractionated derivatives is the most likely petrogenetic model for the charnockites.

Eby (1990) proposed that the source of A-type granites could be identified as having a composition similar to oceanic island basalts or island arc and continental arc basalts, based on Y/Nb ratios <1.2 and >1.2, respectively. With a few exceptions, the charnockites, granites, and rhyolites have Y/Nb ratios >1.2, consistent with derivation from a subduction-influenced source such as the mafic enclaves (see below) or gray gneisses. Isotopic data would help to refine the petrogenetic model(s) for these rocks.

Metabasites

The geochemistry of the metabasites, particularly decreasing Ni and Cr, and increasing total REE contents and constant $(La/Yb)_N$ with decreasing Mg#, is consistent with low-pressure fractionation of phases such as olivine and pyroxene that do not fractionate the REEs significantly (e.g., Rollinson, 1993). Shallowly decreasing Al_2O_3, CaO, and $(Eu/Eu^*)_N$ with decreasing Mg# suggests limited plagioclase fractionation. Increasing Ti, Fe, and V, and constant $(La/Yb)_N$ with decreasing Mg#, indicate a lack of Fe-Ti oxides and amphibole in the fractionating assemblage. This result is consistent with the results from the Pearce element ratio diagram (Fig. 2.12b).

The metabasites are enriched in incompatible elements relative to MORB (Fig. 2.13), except Y, Yb, and Cr, typical of within-plate basalts, and have a distinct negative Nb anomaly, characteristic of arc settings. At least three models can account for the low Nb contents: 1) the metabasites are arc-related (Pearce and Peate, 1995), 2) their composition was influenced by crustal assimilation (Davidson *et al.*, 1987), or 3) they were derived from previously subduction-influenced mantle (Barnes *et al.*, 1999). An arc setting cannot be discounted for the mafic enclaves in the Muskoka domain based on composition, in contrast, amphibolites (metamorphosed basalt flows) of similar composition in the supracrustal Sand Bay gneiss association are more likely to have formed in a back-arc rather than an arc setting (Culshaw and Dostal, 1997). Assimilation of crustal rocks into mafic magma should be accompanied by fractional crystallization

(e.g., DePaolo, 1981). As argued above, the metabasites did not fractionate Fe-Ti oxides, thus Nb should have been incompatible in any fractionating assemblage. We conclude that crustal assimilation cannot explain either the low Nb contents or the low Th/La ratios observed in these rocks. Instead, we suggest that the source of the metabasites was previously subduction-influenced mantle, enriched by fertile asthenospheric mantle invading the mantle wedge as a result of extension and rifting (cf., Gill, 1984; Hochstaedter *et al.*, 1990).

2.6. Tectonic significance

2.6.1. Gray gneiss

Calc-alkaline rocks are characteristic products of magmatism at convergent plate boundaries, and an arc origin for the gray gneisses in the Muskoka domain is supported by their trace element compositions. We suggest that the Shawanaga pluton and Ojibway gneiss association also formed part of the 'Muskoka-Ojibway' arc, based on similarities in composition and age. The proposed proximity of the Muskoka and Shawanaga domains prior to Grenvillian orogenesis is compatible with the restored, pre-Grenvillian cross section of Culshaw *et al.* (1997). Whether the rocks formed in an evolved island arc, on a rifted continental fragment, or in a continental arc is not easily discerned from the geochemical data. Some constraints are: 1) Nd model ages in the Muskoka domain and Ojibway gneiss association (Dickin and McNutt, 1990) are similar to or slightly older than crystallization ages, suggesting a setting where the magma interacted with older continental crust, consistent with a continental arc or rifted continental fragment setting.; 2) there are no clear indicators of an intervening ocean or back-arc basin between the arc and older Laurentian crust (cf., Saunders *et al.*, 1979), which appears to support a continental arc setting; and 3) extension-related magmatism at, or inboard of, the Laurentian margin, simultaneous with formation of the 'Muskoka-Ojibway' arc, is indicated by the ca. 1450 Ma Britt pluton and Mann Island granodiorite (see below) intruding older continental crust in the CGB and Grenville foreland, favoring a continental arc setting. We note, however, that one amphibolite from the Sand Bay gneiss association has a composition compatible with an oceanic setting, and that the

geological and tectonic significance of the Lighthouse gneiss association in the footwall of the Parry Sound domain is as yet poorly understood. We conclude that the 'Muskoka-Ojibway' arc, with associated ensialic back-arc extension, was located at the southeastern margin of Laurentia at ca. 1480-1430 Ma, although we cannot exclude a more distal position, for example on a fragment of rifted continental crust (e.g., Okamura *et al.*, 1998).

2.6.2. Megacrystic orthogneiss

Lake of Bays suite

The Lake of Bays suite is interpreted to have formed in a continental magmatic arc, coevally with the gray gneisses in the Muskoka domain and Ojibway gneiss association. Culshaw *et al.* (1989) also identified megacrystic orthogneisses of similar age (ca. 1460 Ma, Krogh, 1991) in the Go Home domain (Fig. 2.1), contiguous with the Muskoka and Shawanaga domains on restored, pre-Grenvillian cross sections (Culshaw *et al.*, 1997). The 'marginal orthogneiss', including thin sheets of megacrystic orthogneiss in the Sand Bay gneiss association, is compositionally indistinguishable from the Lake of Bays suite. However, the lack of a precise age from the 'marginal orthogneiss' makes it difficult to correlate these units.

Mann Island granodiorite and Britt pluton

Despite their similar age, the Mann Island granodiorite and Britt pluton have within-plate characteristics and intruded pre-1450 Ma continental crust, in contrast to the arc-related signature and lack of older crust typical of the Lake of Bays suite. Following Culshaw *et al.* (2002), we consider the most likely tectonic setting for the Mann Island granodiorite and Britt pluton to be the back-arc region of the postulated ca. 1480-1430 Ma continental arc.

2.6.3. A-type granites (charnockite, granite) and rhyolite

Although the charnockite and granite are geochemically distinct from the surrounding gray gneisses, the imprecise geochronological data suggest that they formed at about the same time and the lack of any evidence for tectonic contacts suggests that

they formed in the same general setting. The charnockites have geochemical characteristics indicating derivation from mantle-derived underplated magmas or rocks. Although the geochemical data do not clearly distinguish the process by which they formed, the apparent lack of intermediate precursors to the charnockites favors partial melting rather than fractional crystallization. Lithospheric thinning associated with continued underplating may have provided the heat necessary to melt the previously underplated rocks (e.g., Frost and Frost, 1997). The granites formed at the same time as the charnockites, apparently by partial melting of a crustal source. Although the Sherman batholith (Frost et al., 1999) is about the same age as the charnockite and granite from the Muskoka domain, there is no evidence that its emplacement was spatially or temporally associated with arc magmatism, and Frost et al. (1999) interpreted it to be related to continental rifting. The model proposed for the Muskoka charnockite and granite implies the presence of a tholeiitic basaltic underplate to provide source material and, possibly, heat. The mafic enclaves in the Muskoka domain have the appropriate composition to be related to the postulated underplating magmas; however, they may also be younger. The most likely tectonic setting for such an underplate is in an extensional tectonic regime, suggesting that in addition to extension in the back-arc region (Britt pluton and Mann Island granodiorite), the arc itself may have undergone extension at ca. 1450 Ma. Unfortunately, the timing of arc-related and A-type magmatism are relatively poorly constrained, making it difficult to propose more detailed tectonic models.

The Sand Bay rhyolites probably formed by partial melting of intermediate calc-alkaline rocks, and lithospheric thinning and associated basaltic underplating, represented by the coeval amphibolites, is considered the most likely heat source for crustal melting. Our data support the conclusions of previous workers (e.g., Culshaw and Dostal, 1997; Rivers and Corrigan, 2000) that the Sand Bay rhyolites formed in an extensional, back-arc setting at ca. 1360 Ma.

2.6.4. Metabasites

Bruhn et al. (1978) described basaltic rocks from southernmost South America with a similar combination of within-plate and arc characteristics and interpreted them to be

related to initial stages of back-arc rifting. A significant finding of this study is the complete compositional overlap between mafic enclaves in the Muskoka domain and amphibolites in the Sand Bay gneiss association. The interlayering of rhyolites and amphibolites in the Sand Bay gneiss association (Culshaw and Dostal, 1997) suggests an age of ca. 1360 Ma for the amphibolites. In the absence of radiometric dates from mafic enclaves in the Muskoka domain, the overlap in composition between mafic enclaves and amphibolites could be interpreted in one of two ways: either the mafic enclaves and amphibolites represent two temporally distinct, but tectonically similar, events, or, they formed during the same event at ca. 1360 Ma.

2.7. Discussion

The geochemical data presented here, coupled with previously obtained geochronological data, suggest the following tectonic evolution for this part of the southeastern Laurentian margin:

2.7.1. 1480-1430 Ma

Arc-related magmatic activity at around 1450 Ma in the Muskoka domain, most likely at the Laurentian continental margin, is relatively well established based on abundant geochronological data (e.g., Timmermann et al., 1997; Nadeau and van Breemen, 1998; McMullen, 1999) and recent geochemical data (McMullen, 1999; this study). Protolith ages of orthogneisses in the Muskoka domain range from ca. 1480 to 1430 Ma, it is, however, worth noting that the younger age limit comes from a "monzodioritic orthogneiss" dated at ca. 1427 Ma by Nadeau and van Breemen (1998) (Fig. 2), whereas other published protolith ages are >1450 Ma. The monzodioritic orthogneiss contains orthopyroxene and clinopyroxene, unlike the arc-related rocks described herein that lack pyroxene. Thus, the tectonic significance of the monzodioritic orthogneiss and the duration of arc magmatism are currently uncertain.

A new finding of this study is that the arc-related rocks may be temporally and spatially related to A-type granites, suggesting intra-arc extension during all or part of this stage of its evolution. In addition to intra-arc extension, the new geochemical data,

coupled with published geochronological data, suggest that back-arc magmatism affected the Britt domain at ca. 1450 Ma (van Breemen *et al.*, 1986; Corrigan *et al.*, 1994). Furthermore, Nadeau and van Breemen (1998) suggested that the Algonquin domain was situated in the back-arc of the Muskoka arc. We conclude that a broad, arc-related extensional regime, for example related to slab roll-back, dominated the southeastern Laurentian margin at ca. 1450 Ma.

Between ca. 1450 and 1430 Ma, the Britt domain, and possibly Algonquin domain, underwent granulite-facies metamorphism (Ketchum *et al.*, 1994; Nadeau and van Breemen, 1998; Timmermann, 1998) followed by an apparent hiatus in magmatic activity in the CGB. As noted below, the tectonic setting of the high-grade metamorphism is not clear at present.

2.7.2. 1430-1360 Ma

Evidence of geologic activity between ca. 1430 and 1360 Ma in the CGB is sparse. Carr *et al.* (2000) and Culshaw *et al.* (2002) suggested that magmatism may have migrated to a more outboard position of the Laurentian margin at this time. Arc magmatism at this time may be represented by orthogneisses of varied composition in the Parry Sound domain and CMBBZ. For example, magmatism in the Parry Sound domain, which began at ca. 1425 Ma (van Breemen *et al.*, 1986) and continued until ca. 1160 Ma (van Breemen *et al.*, 1986; Wodicka, 1994; Wodicka *et al.*, 1996), produced rocks ranging from granite to anorthosite. The magmatic evolution in the Parry Sound domain has not been studied in detail, but the nearly continuous record of granitoid magmatism with intermittent anorthositic magmatism may point to an evolving arc involving several phases of extension. The relationship, if any, between Laurentia and the Parry Sound domain is unknown, but dating of detrital zircons from a quartzite (<1436 Ma) in the basal Parry Sound assemblage is compatible with a Laurentian source for some of the clastic sediments (Wodicka *et al.*, 1996).

2.7.3. <1360 Ma

The Sand Bay gneiss association is widely regarded to have formed at ca. 1360 Ma in a back-arc setting at or near the outermost edge of the Laurentian margin (Culshaw and

Dostal, 1997; Rivers and Corrigan, 2000; this study).

2.7.4. Outstanding problems and suggestions for further work

Although the points listed above are compatible with a wide range of data, and are broadly consistent with "continental arc" models proposed previously (e.g., Rivers and Corrigan, 2000), we regard detailed tectonic models for the late Paleoproterozoic to early Mesoproterozoic evolution of the CGB as premature. Instead, we point out some outstanding problems and discuss ways to test them. The main unresolved issues raised by this work are:

1) *Relationship between arc-related and A-type rocks in Muskoka domain.* The timing of arc and A-type magmatism in the Muskoka domain is only loosely constrained to between 1480 and 1430 Ma, The lack of precise age constraints on the duration of arc magmatism and the temporal relationship between arc and A-type magmatism makes models for this time period highly speculative.

2) *Significance of granulite-facies metamorphism between 1450 and 1430 Ma.* Ketchum *et al.* (1994) suggested that granulite-facies metamorphism at 1450-1430 Ma may have resulted from accretion of a juvenile arc at this time, however, other interpretations are also possible. For example, Sandiford and Powell (1986) suggested that rocks at lower crustal levels in regions characterized by extension and thinning of the continental crust can undergo granulite-facies metamorphism as a result of the high heat flow associated with such tectonic settings. Dunphy and Ludden (1998) and St-Onge *et al.* (2000) argued that granulite-facies metamorphism in the Trans-Hudson orogen in northern Québec resulted from heat related to arc plutonism, an interpretation that may also be applicable in the CGB considering the apparent overlap in magmatic and metamorphic ages. A fourth possible interpretation, essentially a modification of the accretion model proposed by Ketchum *et al.* (1994), involves a change in tectonic regime from extension to convergence leading to crustal thickening and granulite-facies metamorphism in the former back-arc region (cf., Collins, 2002). In this case, the change from extension to contraction could have been controlled by a number of factors

including the age of the subducting oceanic crust (e.g., old, dense crust favoring slab roll-back and extension, Molnar and Atwater, 1978), subduction of oceanic plateaus or seamounts inducing shortening (Gutscher *et al.*, 2000), and changes in the rate and/or angle of convergence (Royden, 1993; Waschbusch and Beaumont, 1996; Pope and Willett, 1998). The 1450-1430 Ma granulite-facies metamorphism in the Britt and Algonquin domains can, therefore, be interpreted in a number of ways with very different tectonic implications, including accretion/convergence, extension, and arc magmatism, all compatible with the "continental arc" model proposed by Rivers and Corrigan (2000).

3) *Relationship between Parry Sound domain/CMBBZ and the Laurentian margin.* The Parry Sound domain and CMBBZ may represent magmatic activity along the Laurentian margin following arc magmatism and high-grade metamorphism between 1480 and 1430 Ma. However, the magmatic evolution and paleogeographic location of the Parry Sound domain and CMBBZ, and their relationship with Laurentia, are relatively unconstrained, which makes interpretations of the evolution along the Laurentian margin between 1430 and 1360 Ma uncertain.

4) *Significance of back-arc magmatism in Sand Bay gneiss association.* The Sand Bay gneiss association appears to have formed in a back-arc setting at the Laurentian margin. The identity of the active arc at that time is unknown; possibilities include the Parry Sound domain, CMBBZ, or another, unidentified arc. In the latter case it is possible that the arc rifted from the Laurentian margin (e.g., Culshaw and Dostal, 1997) but was not subsequently re-accreted.

This paper and the work of Culshaw and Dostal (1997, 2002) have shown that geochemical data from high-grade metamorphic rocks can yield significant information about the petrogenesis and tectonic setting of their protoliths that cannot be obtained in any other way. In principle, therefore, answers to several of the problems outlined above could be obtained by further geochemical and associated geochronological work.

1) The temporal relationship between arc-related and A-type plutonic rocks in the

Muskoka domain could be better constrained with further geochronological work, provided that geochemical data are used to determine the tectonic significance of the dated rocks. The results from integrated geochemical/geochronological studies are likely to improve our understanding of arc evolution significantly. A similar approach should be applied to the Parry Sound domain and CMBBZ in order to address the tectonic significance of the meta-igneous rocks in these areas. Furthermore, additional Sm-Nd isotopic data from the rocks described in this paper, and those in the Parry Sound domain and CMBBZ, could yield information about the source to the A-type granites and the substrate upon which the Muskoka arc and Parry Sound/CMBBZ (arcs?) formed. Information about the substrate to the arc-related rocks is important for relating the rocks to the Laurentian margin or to more outboard, possibly oceanic settings, and similar information could come from dating of detrital or inherited zircons. Evidence for spatial separation between Laurentia and the inferred arcs may come from the identification of accretion-related structures or lithological assemblages (e.g., ophiolites) characteristic of suture zones.

2) Granulite-facies metamorphism in the Britt and Algonquin domains between 1450 and 1430 Ma is compatible with a range of tectonic models, including accretion/convergence, extension, and arc magmatism. The most reliable test for distinguishing between accretion/convergence and extension is to determine the P-T-t path for the metamorphic event. The predicted P-T-t paths for extension-related metamorphism involve heating to granulite-facies conditions at constant or decreasing pressure, followed by cooling at constant or increasing pressure (Sandiford and Powell, 1986), in contrast to P-T-t paths from metamorphic belts formed during crustal thickening (England and Thompson, 1984). However, superimposed high-grade Grenvillian metamorphism makes extracting pre-Grenvillian P-T information difficult, if not impossible (e.g., Ketchum et al., 1994). Determining if granulite-facies assemblages formed in response to arc magmatism requires better constraints on both the age of granulite-facies metamorphism and the duration of arc magmatism. If arc magmatism ceased

prior to granulite-facies metamorphism any connection between arc magmatism and granulite-facies metamorphism can be discounted.

Our interpretation is generally similar to the model proposed by Rivers and Corrigan (2000), but differs in detail. For example, our data indicate that some of their "arc-related" plutons in the CGB actually formed in a back-arc setting, and we have also identified A-type metaplutonic rocks that may have formed in extensional intra-arc settings (e.g., charnockite and granite in the Muskoka domain). Following Kay *et al.* (1989) and Menuge *et al.* (2002), we prefer a back-arc setting for the granite-rhyolite provinces in the midcontinent region, in contrast to the "continental arc" interpretation proposed by Rivers and Corrigan (2000). The substrate to the granite-rhyolite provinces is not exposed, and hence the source regions of the magmas have not been positively identified, although they are inferred to have been previously accreted juvenile arcs (e.g., Kay *et al.*, 1989; Van Schmus *et al.*, 1996; Menuge *et al.*, 2002). Based on the temporal, spatial, and petrogenetic links between arc-related and A-type rocks identified in this study, we suggest that rocks exposed in the CGB, for instance in the Muskoka domain, could represent good analogues for the hidden substrate that was the source(s) of A-type silicic rocks in the granite-rhyolite provinces. Our data support a correlation between the CGB and granite-rhyolite provinces, and we agree with Culshaw and Dostal (2002) that the CGB represents the tectonically reworked and stacked equivalent of the Proterozoic midcontinental USA. We suggest that further efforts to resolve the Mesoproterozoic evolution of the midcontinent region could benefit from including CGB rocks in future investigations.

3. Migmatite petrogenesis, Muskoka domain

3.1. Introduction

The Muskoka domain in the southwestern Grenville Province comprises orthogneisses whose protoliths range in composition from gabbroic to granitic (Chapter 2). The orthogneisses are highly migmatitic with apparently *in situ* leucosome-abundances locally exceeding 40-50 vol.%. Most of the migmatites are deformed and many outcrops display features, such as leucosome-filled shear bands and leucosome patches in boudin necks, that suggest melting coeval with deformation. These observations pose two questions: i) why was so much leucosome produced? (i.e., melting reaction), and ii) what was the relationship between partial melting and deformation? Question ii) can be further subdivided into two questions: a) how did deformation affect migmatite petrogenesis?, and b) how did the presence of partial melt affect the deformational behavior of the rocks?. Question a) is dealt with in this chapter, which focuses on migmatite petrogenesis, whereas b) is discussed in detail in Chapter 6.

Nearly all migmatites are characterized by some degree of segregation of melts from their residues (e.g., Brown *et al.*, 1995; Sawyer, 1996). Up until recently, separation of felsic melt from its source was widely believed to occur when the proportion of melt exceeded some critical threshold causing loss of cohesion along grain-grain contacts in the source, resulting in diapiric rise of the low-density, low-viscosity melt (Wickham, 1987b; Rutter and Wyllie, 1988; Fountain *et al.*, 1989; Harris *et al.*, 1993). This threshold has been variably referred to as 'rheologic critical melt percentage' (RCMP, Arzi, 1978) or 'critical melt fraction' (CMF, van der Molen and Paterson, 1979). The RCMP/CMF concept has recently been disputed on experimental grounds, and in many high-grade rocks, field observations and geochemical and petrographic data argue against wholesale diapiric rise of large melt volumes. For example, some granulites preserve textural, structural, and geochemical evidence suggesting that melts segregated without disruption of the lithological layering (e.g., Brown and Earle, 1983; Clemens, 1989). Field and geochronological data from many high-grade gneiss terranes show that

73

partial melting accompanied deformation; observations relevant to the present study include the close association between leucosomes and structures such as fold axial planes, boudin necks, and shear bands. As a result of these observations, deformation-driven melt segregation has gained widespread acceptance as an alternative segregation mechanism (e.g., Sawyer, 1994; Brown *et al.*, 1995; Watt *et al.*, 1996; Sawyer, 2001), and deformation is now believed to be one of the key factors controlling the separation of melt from its residue in migmatites.

In principle, the idea of deformation-driven melt segregation is simple. Deformation of an anisotropic rock with competency contrasts produces mechanical instabilities because the various layers or structures deform at different rates (Stromgard, 1973). These mechanical instabilities create pressure gradients that act as a driving force for melt segregation, and lead to the formation of dilational structures, such as shear bands and boudin necks, that act as sinks into which melts can migrate (Sawyer, 1994). Field evidence of deformation-driven melt segregation in the Muskoka domain is presented below.

The rate of melt segregation is one of several factors controlling the degree of equilibrium between a melt and its residue. If the rate of segregation is greater than the rate of diffusion in the residual minerals, trace elements hosted by major phases involved in the melting reaction, e.g., Ba, Rb, and Sr in feldspars and biotite, will be depleted in the melt relative to that expected for an equilibrium melt. Other elements, for example the rare earth elements, show a more complex behavior. These elements are commonly hosted by accessory phases, e.g., zircon, allanite, and apatite, which means that in addition to the rate of segregation, their behavior also depends on factors such as the rate of dissolution (in turn controlled by temperature, composition, and water content of the melt, e.g., Watson and Harrison, 1984) and armoring by residual minerals such as biotite, hornblende, and pyroxenes (Bea *et al.*, 1994; Nabelek and Glascock, 1995).

The above discussion shows that melts formed in rocks undergoing deformation may be expected to have disequilibrium compositions whereas the slower melt segregation rates anticipated in rocks not undergoing deformation could result in melts

with equilibrium compositions. Here, we present field, petrographic, and geochemical data from two types of migmatite that are interpreted to demonstrate the effects of deformation-driven melt segregation on the composition of partial melts. Leucosome compositions are inferred to represent melt compositions, with some exceptions as discussed further below. Based on field observations, one type of migmatite is interpreted to have formed during syn-melting deformation, and appears to preserve leucosomes with disequilibrium compositions. The other type of migmatite formed in more mafic host rocks that were stronger and, therefore, less affected by deformation during melting; this type contains leucosomes that preserve equilibrium compositions and appear to have undergone significant fractional crystallization. We ascribe the differences in leucosome compositions between these two types of migmatite to rapid, deformation-driven melt segregation and lack of it, respectively.

3.2. Geological setting

The Mesoproterozoic Grenville Province in Ontario exposes large tracts of upper amphibolite- to granulite-facies migmatitic gneisses of dominantly Laurentian affinity. It is widely accepted that deformation, high-grade metamorphism, and reworking of the Laurentian margin during the Grenvillian orogeny resulted from continent-arc(s) and/or continent-continent collision(s) along the southeastern margin of Laurentia between 1200 and 1000 Ma (e.g., Rivers, 1997; Carr et al., 2000). At the western end of the orogen (Fig. 3.1), the Central Gneiss Belt (CGB; Wynne-Edwards, 1972) comprises pre-1350 Ma high-grade gneisses, formed along the active southeastern margin of the pre-Grenvillian Laurentian craton (Culshaw and Dostal, 1997; Rivers, 1997; Rivers and Corrigan, 2000; Culshaw and Dostal, 2002; Chapter 2). In the study area the CGB consists of discrete lithotectonic domains assembled during multiple stages of northwest-directed convergence and now recognized as lithologically distinct domains separated by strongly sheared boundaries interpreted as thrust zones (e.g., Davidson et al., 1982; Culshaw et al., 1997). The earliest stage of convergence, termed the 'Elzevirian orogeny' (ca. 1200-1160 Ma; Moore and Thompson, 1980), involved assembly of arc
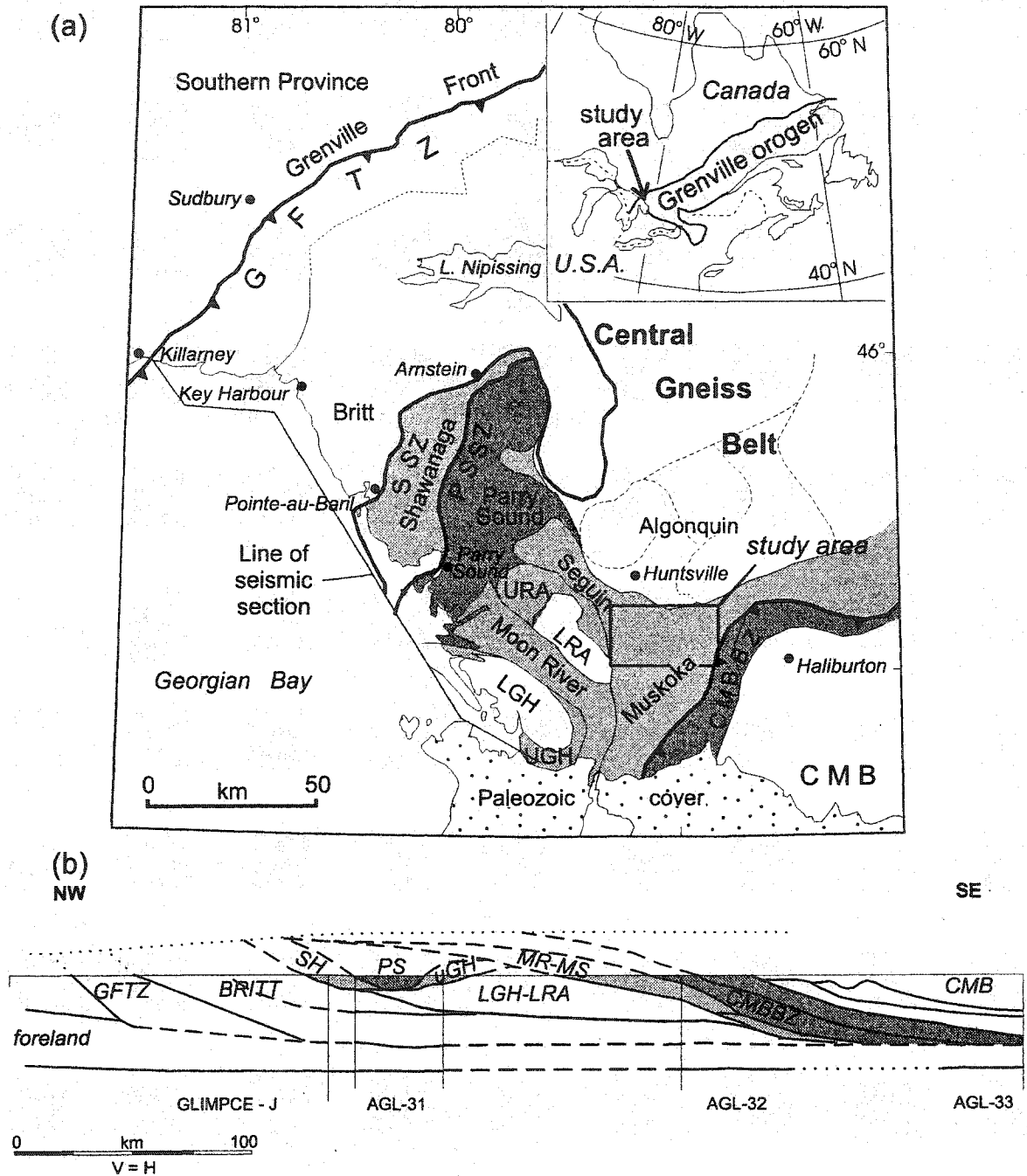
Fig. 3.1 (a) Location and geology of the study area. Heavy barbed lines indicate major thrust-boundaries and heavy non-barbed lines indicate other important structural contacts. Thin lines represent domain boundaries after Culshaw *et al.* (1983, 1988, 1989), Davidson (1984), and Davidson and van Breemen (1988), with minor modifications by Culshaw *et al.* (1997). (b) Seismic interpretationafter White *et al.* (2000).

Abbreviations: GFTZ=Grenville Front Tectonic Zone, SSZ=Shawanaga Shear Zone, PSSZ=Parry Sound Shear Zone, URA=Upper Rosseau domain, LRA=Lower Rosseau domain, UGH=Upper Go Home domain, LGH=Lower Go Home domain, CMBBZ=Central Metasedimentary Belt boundary thrust zone, CMB=Central Meta-sedimentary Belt, PS=Parry Sound domain.

terranes offshore from, or at the distal southeastern edge of, Laurentia (e.g., Carr *et al.*, 2000). In the study area, the main collisional event, termed the 'Ottawan orogeny' (Moore and Thompson, 1980), began sometime between 1120 and 1080 Ma with emplacement of post-1400 Ma arc and back-arc assemblages of the Central Metasedimentary Belt (CMB) over the CGB along a crustal-scale shear zone termed the Central Metasedimentary Belt boundary thrust zone (CMBBZ, Hanmer and McEachern, 1992). The Ottawan orogeny was associated with foreland-propagating convergence and widespread upper amphibolite- to granulite-facies metamorphism at 1085-1035 Ma (e.g., Culshaw *et al.*, 1997; Timmermann *et al.*, 1997; McMullen, 1999; Carr *et al.*, 2000; Wodicka *et al.*, 2000), followed by a regionally significant phase of ductile extension at ca. 1020 Ma (Culshaw *et al.*, 1994; Ketchum *et al.*, 1998). There is evidence for both earlier and later extensional deformation in some parts of the region (Culshaw, 1986; van der Pluijm and Carlson, 1989; Timmermann *et al.*, 2002). A final stage of orogen-wide convergence affected the Grenville Front Tectonic Zone at ca. 1000 Ma (e.g., Haggart *et al.*, 1993).

3.3. Study area

The Muskoka domain (Figs. 3.1 and 3.2) lies immediately beneath the CMBBZ, close to the boundary between polycyclic Laurentian rocks and monocyclic rocks that do not record evidence of pre-Grenvillian high-grade metamorphism (e.g., Culshaw *et al.*, 1997; Ketchum and Davidson, 2000). The Muskoka domain is characterized by highly migmatitic orthogneisses the protoliths of which formed during a regionally significant episode of arc magmatism at ca. 1450 Ma (e.g., Carr *et al.*, 2000; Chapter 2). Peak metamorphic conditions of 750-850°C at 0.9-1.15 GPa (Fig. 3.3) were attained at ca. 1080-1060 Ma (Timmermann, 1998; Timmermann *et al.*, 2002; S. Gagné and J. Hawken, unpublished data). Timmermann *et al.* (1997) dated a foliation-parallel leucosome in the Muskoka domain at 1064 ± 18 Ma, and this age has been confirmed by recent SHRIMP dating (Chapter 5). Northwest-directed, thrust-sense shear zones along the northwestern margin of the CMBBZ cut Muskoka domain migmatites, and within the Muskoka domain
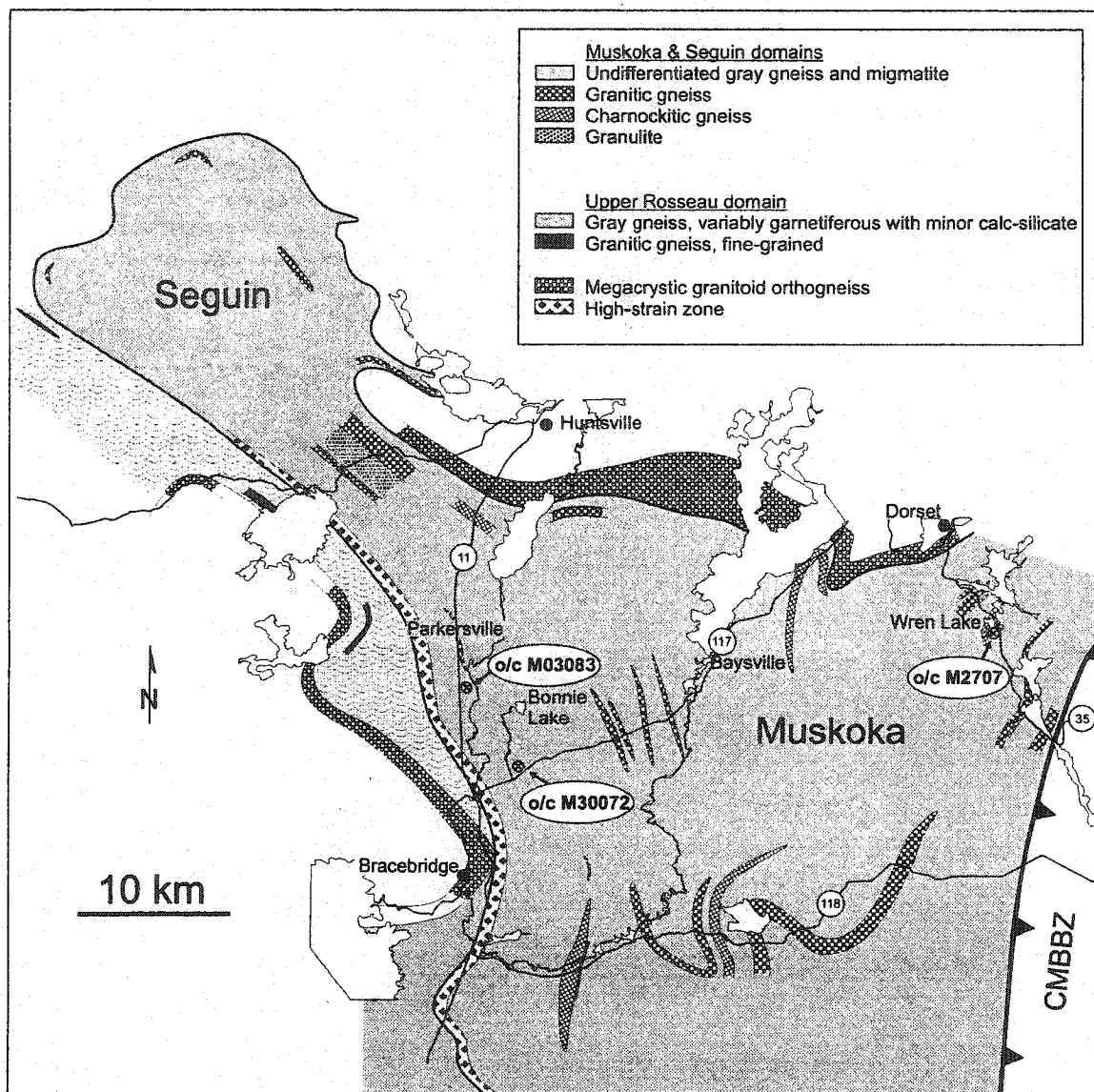
Fig. 3.2 Geological map of the Muskoka domain showing dominant lithological units (see Chapter 2) and the location of the investigated outcrops. UTM coordinates (UTM zone 17) of the investigated outcrops: o/c M03083 (Parkersville): 632 700E 5002 400N, o/c M30072 (Bonnie Lake): 636 500E 4995 500N, o/c M2707 (Wren Lake): 668 550E 5005 430N.
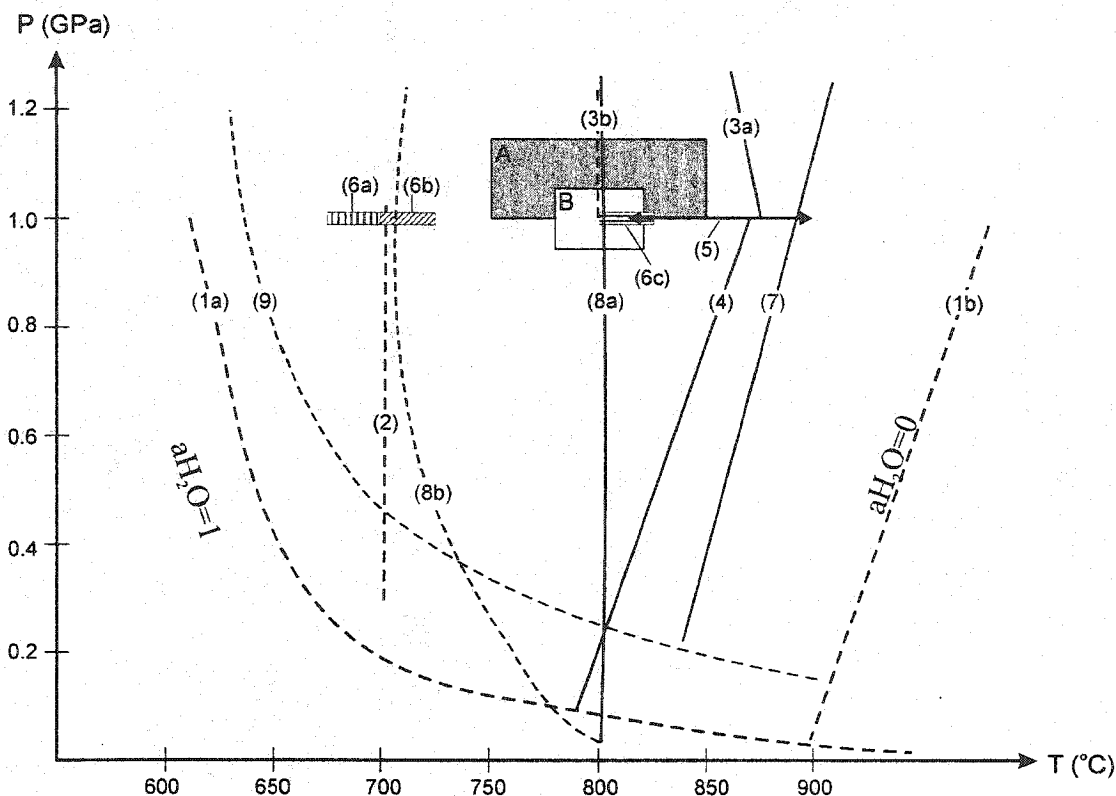
Fig. 3.3 P-T diagram summarizing some relevant melting reactions and results from experimental melting studies. For clarity, divariant reactions are illustrated using a single line. Solid lines denote fluid-absent melting reactions, dashed lines denote fluid-present reactions. (1a) and (1b) illustrate the reaction $Qtz+Pl\pm Kfs+Fl=M$ in the presence of a pervasive H_2O-rich ($aH_2O=1$) and CO_2-rich ($aH_2O=0.1$) fluid, respectively (Stevens and Clemens, 1993). (2) Water-saturated melting of tonalite $Bt+Pl+Qtz+Fl$ (water-rich)=$Hbl+M$ (Busch *et al.*, 1974). (3) Partial melting of a biotite-plagioclase-quartz gneiss (Gardien *et al.*, 2000). (3a) Biotite-out with no H_2O added to the system. At pressures between 1 and 2 GPa and no H_2O added, <4 vol.% melt was produced at T=900°C. (3b) Biotite-out with >2 wt.% H_2O added. At pressures between 1 and 2 GPa and 4 wt.% H_2O added, between 50 and 60 vol.% melt was produced at T as low as 800°C. (4) Fluid-absent melting $Bt+Pl+Qtz=Opx+Kfs+M$ (Stevens and Clemens, 1993). (5) Fluid-absent biotite dehydration melting of a tonalite at 1 GPa (Rutter and Wyllie, 1988). Between 825 and 900°C (indicated by double-pointed arrow) the biotite melting reaction produced 20% melt. (6) Partial melting of dacite at 1 GPa (Conrad *et al.*, 1988). Boxes with vertical (6a), diagonal (6b), and horizontal (6c) lines represent the solidus at 1 GPa with $aH_2O=0.75$, 0.5, and 0.25, respectively. (7) Beginning of biotite dehydration melting in a biotite gneiss according to the reaction $Bt+Pl+Qtz=M+Opx+Ox$ (Patiño Douce and Beard, 1995). (8a) $Bt+Qtz+Kfs=Opx+M$ (reaction [V] of Peterson and Newton (1989)), and (8b) $Bt+Qtz+Kfs+Fl$ (water-rich)=M (reaction [O] of Peterson and Newton (1989)). (9) Wet basalt solidus (Green 1982). Boxes A (shaded) and B (white) indicate range of P-T conditions in the Muskoka domain determined by Timmermann *et al.* (2002) and S. Gagné and J. Hawken (unpublished data, 2002), respectively. Abbreviations: minerals after Kretz (1983), M=melt, Fl=fluid, Ox=oxides. Note that in Fig. 3.3 and later in the text we use the term 'fluid' to describe phases such as H_2O and CO_2, whereas 'melt' (*s.l.*) is used to describe melts and magmas.

field evidence suggests that leucosome was present during southeast-directed shear (Timmermann *et al.*, 2002). Rocks at both higher and lower structural levels are significantly less migmatitic (Fig. 3.1), leading Jamieson *et al.* (1992) and Culshaw *et al.* (1997) to speculate that the presence of these highly migmatitic rocks may have influenced the rheology and tectonic evolution of the western part of the orogen.

3.4. Migmatites

The dominant lithology in the Muskoka domain is gray, migmatitic orthogneiss, ranging in composition from gabbro to granite, although quartz monzodiorite and granodiorite predominate (Timmermann, 1998; Timmermann *et al.*, 2002; Chapter 2). We have identified two main types of migmatite based on leucosome morphology and type of protolith, referred to as stromatic and patchy migmatite. The stromatic migmatites typically have light gray, quartz monzodioritic to granodioritic mesosomes, and are by far the dominant type of migmatite in the Muskoka domain. The patchy migmatites have dioritic mesosomes.

Three representative outcrops were investigated in detail (Fig. 3.2). The first two outcrops are located south of Parkersville (o/c M03083) and Bonnie Lake (o/c M30072), respectively, in the western part of the Muskoka domain. The Parkersville and Bonnie Lake outcrops display stromatic and patchy migmatites, respectively. The third outcrop is located at Wren Lake (o/c M2707) in the eastern part of the Muskoka domain and comprises both stromatic and patchy migmatites separated by sharp, foliation-parallel contacts. All the investigated migmatites preserve pre-migmatite compositional banding and foliation, and can, therefore, be classified as metatexite (Brown, 1973). Although leucosome abundances locally exceed 40-50 vol.%, no diatexites, in which pre-migmatite structures are largely destroyed (Brown, 1973; Sawyer, 1998), are present in this area. The migmatite terminology used herein is after Ashworth (1985).

3.4.1. Stromatic migmatite

Leucosome in the stromatic migmatites at Parkersville and Wren Lake is granitic and concordant to slightly discordant to the host-rock foliation (Fig. 3.4a); for

convenience it is referred to here as concordant leucosome. The concordant leucosomes constitute 20-30 vol.%, and rarely up to 40-50 vol.%, of the stromatic migmatites, measured on a series of vertical cross-sections through the outcrops at high angles to the gently southeast-dipping foliation. The leucosomes are fine- to medium-grained, forming 0.5-5 cm thick layers a few meters long, and are generally rimmed by thin, discontinuous melanosomes, referred to as concordant melanosome below. The concordant leucosomes are variably deformed and in places younger leucosomes cut older, deformed leucosomes; thus, the estimate of 20-50 vol.% leucosome does not represent the amount of melt present in these rocks at any one time. The concordant leucosomes are commonly associated with small shear bands that generally display top-to-southeast, normal-sense displacement (Timmermann *et al.*, 2002). Locally, the melts appear to have migrated along the foliation and accumulated within the shear bands (Fig. 3.4b) or in larger melt collection zones (Fig. 3.4c) that are locally associated with boudin necks (Fig. 3.4d). These observations suggest that melt was present during deformation.

3.4.2. Patchy migmatite

The patchy migmatites range from small, irregular patches, <10-20 cm across, to dikes or dike/fracture networks, 30-40 cm across and 3-4 m long (Fig. 3.5a). For clarity, we refer to these morphological end-members as patches and dikes, respectively, but emphasize that the field, petrographic, and geochemical data strongly suggest that they are part of a continuum. The patches typically contain coarse-grained granitic to pegmatitic leucosome, with up to 5 cm subhedral to euhedral, poikilitic hornblende (Fig. 3.5b, c). The mineralogy of the patches varies from hornblende-dominated, with seam-like networks of granitic material, to leucosome-dominated, with little or no hornblende. The dikes are pegmatitic and typically zoned, with quartz-rich cores, resembling typical pegmatite zonation suggesting crystallization from relatively water-rich melts (e.g., Jahns and Burnham, 1969). Large hornblende crystals, resembling those in the patches, are common along the dike margins (Fig. 3.5d) or form local accumulations within the dikes. Commonly, patches and dikes are connected by thin seams of granitic material. Immediately adjacent to the patches, and locally to the dikes, the host rock is enriched in
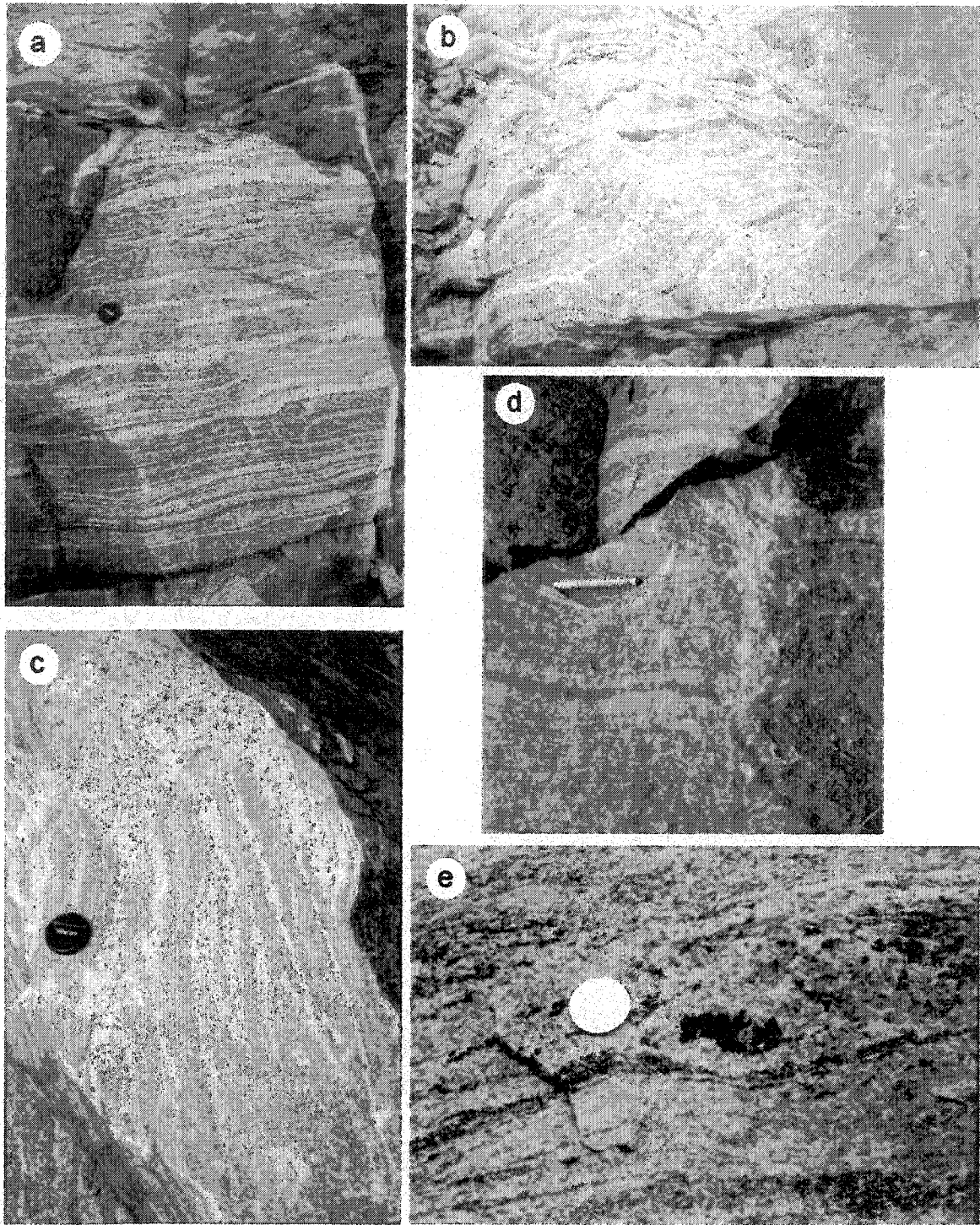
Fig. 3.4 (a) Concordant leucosome in stromatic migmatite; lens cap for scale ca. 5 cm across. From Parkersville outcrop. (b) Top-to-southeast directed shear band containing leucosome. From Hw 117, ca. 5 km east of Dorset. (c) Concordant leucosome apparently feeding into a larger leucosome patch, interpreted to represent a melt collection zone; lens cap for scale ca. 5 cm across. From Parkersville outcrop. (d) Small leucosome patch in boudin neck; pen for scale ca. 13 cm long. From Hw 117, ca. 5 km north-northeast of Baysville. (e) Large Hbl porphyroblast in stromatic migmatite, Parkersville outcrop.
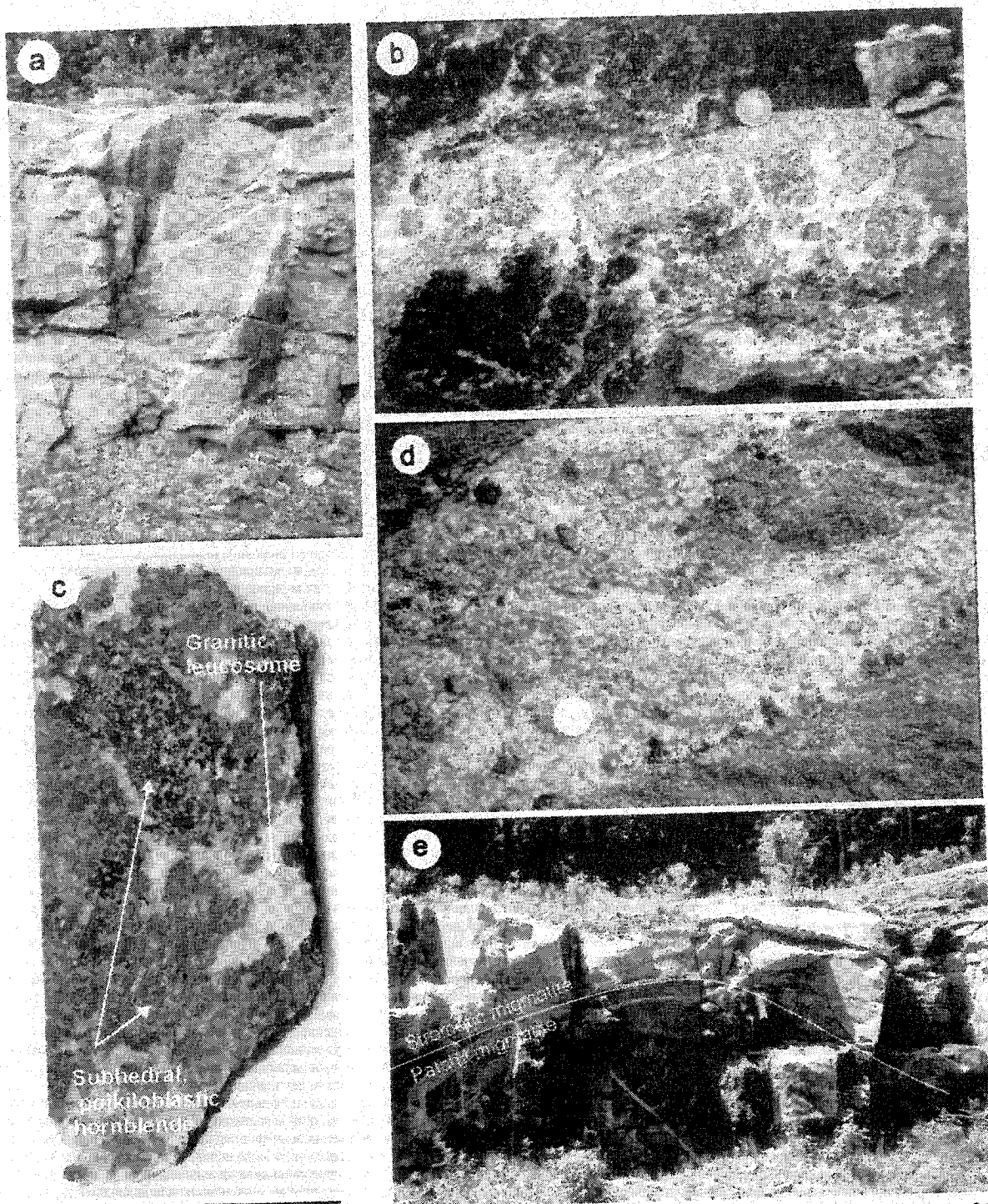
Fig. 3.5 (a) Network of dikes and patches in a patchy migmatite; hammer for scale ca. 30 cm long. (b) Hornblende-rich patch comprising subequal amounts of granitic leucosome and coarse hornblende; coin for scale ca. 2 cm across. (c) Close-up of hornblende-rich patch showing coarse, subhedral, poikiloblastic hornblende and leucosome; scale-bar is 5 cm long. (d) Close-up of pegmatite dike showing how hornblende porphyroblasts, similar to those depicted in (b) and (c), concentrate along the margins of the dikes; coin for scale ca. 2 cm across. (e) Photo showing the foliation in the stromatic migmatites wrapping around an enclave of patchy migmatite, forming a pinch-and-swell structure; photo ca. 5 m across. All photos from Wren Lake outcrop.

subhedral, medium-grained (ca. 0.5 cm) hornblende, interpreted as melanosome (referred to as patchy melanosome below). Despite clear petrographic and geochemical differences, discussed below, the patchy melanosomes are difficult to distinguish from the dioritic mesosome in the field. The distribution of melanosome is, therefore, unclear; in particular, some of the dikes appear to be locally (meter-scale or less) intrusive and may lack associated melanosomes. We note, however, that several of the patchy melanosome samples were taken immediately adjacent to the dikes, thus, melanosome is associated with both dikes and patches. Leucosome abundances are difficult to estimate in the patchy migmatites as a result of their irregular distribution, but appear to be lower than in the stromatic migmatites.

3.4.3. Structural relationship between stromatic and patchy migmatite

In outcrops containing both stromatic and patchy migmatites (e.g., Wren Lake outcrop), the foliation in the former wraps around the latter, forming a pinch-and-swell structure (Fig. 3.5e). Furthermore, unlike in the stromatic migmatites, there is no evidence that the location of leucosomes in the patchy migmatites is structurally controlled. These observations suggest significant rheological contrast between the two types of migmatite. Whether the difference in strength results from the proportion of melt present in the rocks or the type of host rock (mesosome) is not clear. Available experimental data show that granitic rocks are generally weaker than dioritic rocks (Hansen and Carter, 1982; Kirby, 1983), and it appears likely that, for similar degrees of partial melting, the dioritic mesosomes (patchy migmatites) would have been stronger than the granodioritic mesosomes (stromatic migmatites). As discussed in the Introduction (section 3.1.2), the higher degree of partial melting in the stromatic migmatites probably would have enhanced the difference in strength, but this cannot be demonstrated. None of the patches or dikes cuts the patchy-stromatic migmatite contact, thus, the relative age of and relationship between stromatic and patchy migmatite is not known.

3.5. Petrography and geochemistry

3.5.1. Analytical procedures

Major and trace elements were determined on fused glass beads and pressed powder pellets, respectively, using standard X-ray fluorescence (XRF) techniques at St. Mary's University, Halifax, Nova Scotia. Rare earth elements (REEs), Hf, and Th were determined by inductively coupled plasma-mass spectrometry (ICP-MS) using a Na_2O_2 sintering technique at Memorial University, St. John's, Newfoundland. Dostal *et al.* (1986) and Longerich *et al.* (1990) discussed the analytical procedures, accuracy, and precision of the XRF and ICP-MS analyses, respectively (see also Appendix A). The geochemical and mineral compositional data are presented in Appendix C. Mineral abbreviations used in the text and figures are from Kretz (1983).

3.5.2. Stromatic migmatites

The concordant leucosomes and granodioritic mesosomes were sampled by serial cutting of large slabs. The concordant melanosomes were too thin to be sampled for geochemical analysis. Timmermann (1998) and Timmermann *et al.* (2002) described the petrography of the stromatic migmatites in the Muskoka domain in detail, and the petrographic description of these migmatites, therefore, focuses on the points pertinent to their petrogenesis.

Granodioritic mesosome

The granodioritic to quartz monzodioritic mesosome (for simplicity referred to as granodioritic) is fine- to medium-grained and moderately foliated. The modes of representative samples are given in Table 3.1. Minor 'melt' films (cf., Sawyer, 2001) along some grain boundaries (Fig. 3.6a) and rare, small (<1 cm) quartz-feldspar patches, interpreted to represent former melt pockets, suggest some melting in the mesosome; there are, however, no indications (petrographic or geochemical) that melts were extracted from the mesosome. The proportion of melt films in the granodioritic mesosome was estimated by point counting of 2000 points as < 0.5 vol.‰, thus, they are volumetrically insignificant. Apatite, zircon, and allanite are common accessory phases.
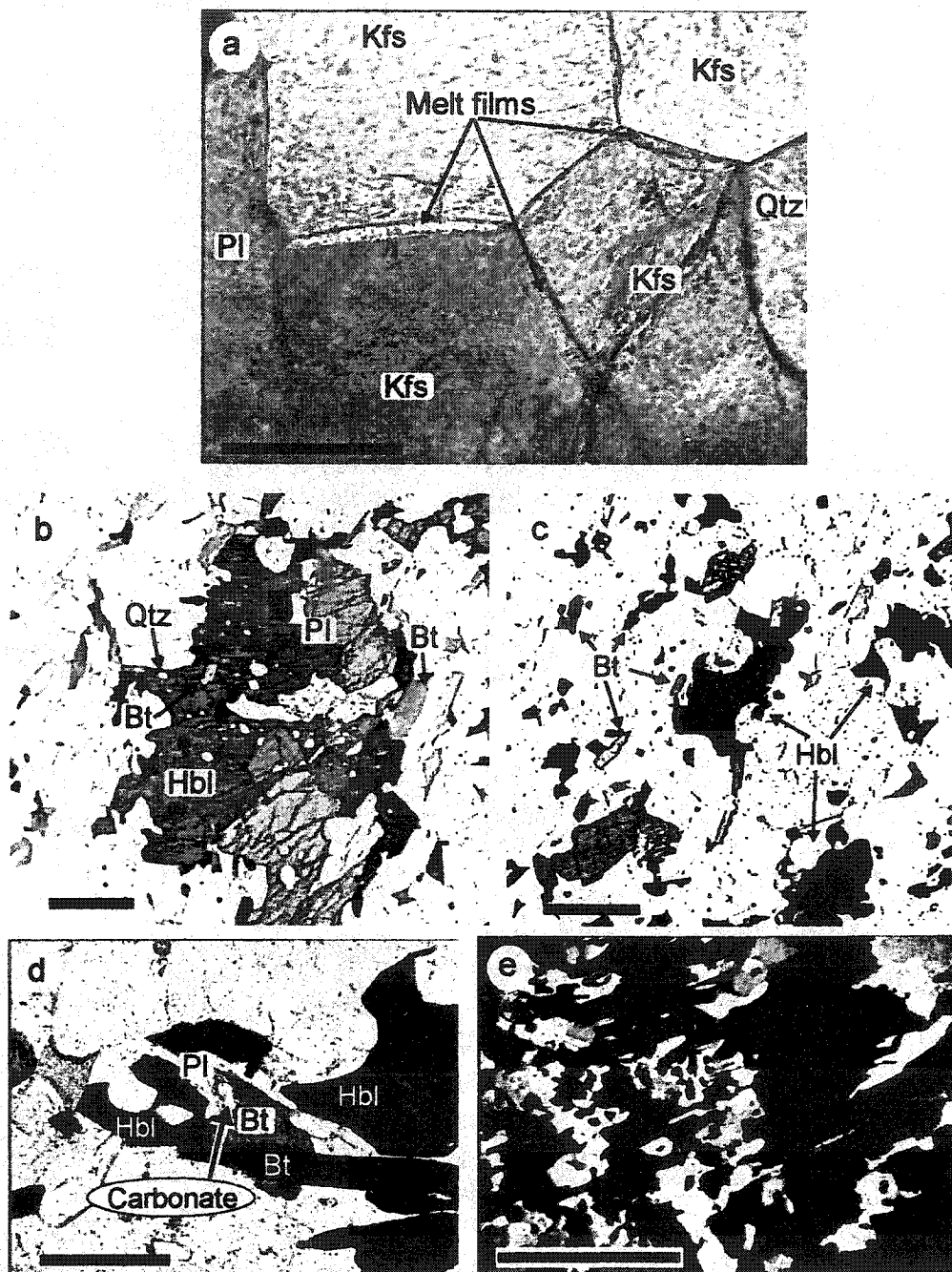
Fig. 3.6 (a) 'Melt' films along K-feldspar grain boundaries in granodioritic mesosome. Similar 'melt' films have been observed in the dioritic mesosome. (b) Coarse hornblende with rounded inclusions of plagioclase, biotite, and quartz from the concordant melanosome. Notice also coarse biotite on the right-hand side of the photo, apparently in equilibrium with the hornblende. (c) Typical hornblende and biotite texture in the granodioritic mesosome, shown for comparison; note that scale is similar in (b) and (c). (d) Two small carbonate grains associated with biotite; from the granodioritic mesosome, (e) Coarse, subhedral hornblende (black) in hornblende-rich patch, interpreted to be a cumulate phase. The hornblende is optically continuous. White/gray phase is plagioclase. Scale bar in (a) is 0.1 mm, in (b) and (c) 1 mm, in (d) 0.5 mm, and in (e) 5 mm. All photos from Parkersville outcrop except (e) from Wren Lake outcrop

The granodioritic mesosome ranges from 65 to 68 wt.% SiO_2. Samples from the two investigated outcrops at Parkersville and Wren Lake have essentially similar major and trace element contents (Figs. 3.7 and 3.8). The granodioritic mesosome from Wren Lake is slightly higher in total REE content with more pronounced negative Eu anomalies $((Eu/Eu^*)_N=0.40-0.45)$ than mesosome from Parkersville $((Eu/Eu^*)_N=0.58)$, but the REE patterns are similarly fractionated $((La/Yb)_N=5-12)$ (Fig. 3.8).

Concordant leucosome

The concordant leucosomes are medium- to coarse-grained and granitic (Table 3.1), with small amounts (ca. 1-5 vol.%) of hornblende porphyroblasts and flakes of biotite. The hornblende in the leucosomes is texturally similar to that in the associated concordant melanosomes (see below), and probably represents residual hornblende that was mechanically incorporated into the melt.

The concordant leucosomes range in SiO_2 from 70 to 73 wt.%, and most major elements decrease with increasing SiO_2, whereas K_2O and most trace elements show little systematic variation and tend to plot in clusters. The REE patterns (Fig. 3.8) are moderately fractionated, with $(La/Yb)_N$ increasing from 8 to 24 with increasing SiO_2 (Fig. 3.7f). Total REE contents and Eu anomalies $((Eu/Eu^*)_N=0.7-1.3)$ are not correlated with SiO_2.

Relative to the granodioritic mesosome, the concordant leucosomes are depleted in all major elements except SiO_2 and K_2O. Barium, Rb, and Sr are enriched in the leucosomes. Yttrium, Zr, Hf, and Nb are lower in the leucosomes and Th is similar in leucosomes and granodioritic mesosomes. Total REE contents are lower, REE patterns more fractionated, and Eu anomalies are more positive in the leucosomes than in the mesosomes (Fig. 3.8).

Table 3.1 Modes of representative migmatite samples.

Sample	Granodioritic mesosome M03083B-M	Concordant leucosome M2707-16	Concordant melanosome M2707-16B-5	Concordant melanosome M03083B-L	Dioritic mesosome M2707-10	Patchy leucosome M2707-5-L2	Patchy melanosome M2707-5B-M
Quartz	15.0	31.3	5.5	8.0	acc.	25.8	
Plagioclase	53.8	21.8	56.0	74.5	46.3	4.0	23.0
K-feldspar	11.0	37.8	1.0	1.0		62.0	
Hornblende	11.6	0.8	16.5	8.8	37.5	4.0	56.0
Biotite	6.8	4.0	20.0	7.8	8.0	1.0	17.0
Titanite				acc			
Opaques	1.6	1.8	acc	acc	8.3		3.8
Apatite	acc.		acc	acc	acc.		acc.
Zircon	acc.	acc.	acc	acc	acc.		acc.
Allanite	acc.		acc.	acc			
Myrmekite							acc.
Saussurite		2.3					acc.

Based on 400-600 counts per sample. acc.=accessory phase (<0.25 vol.%).
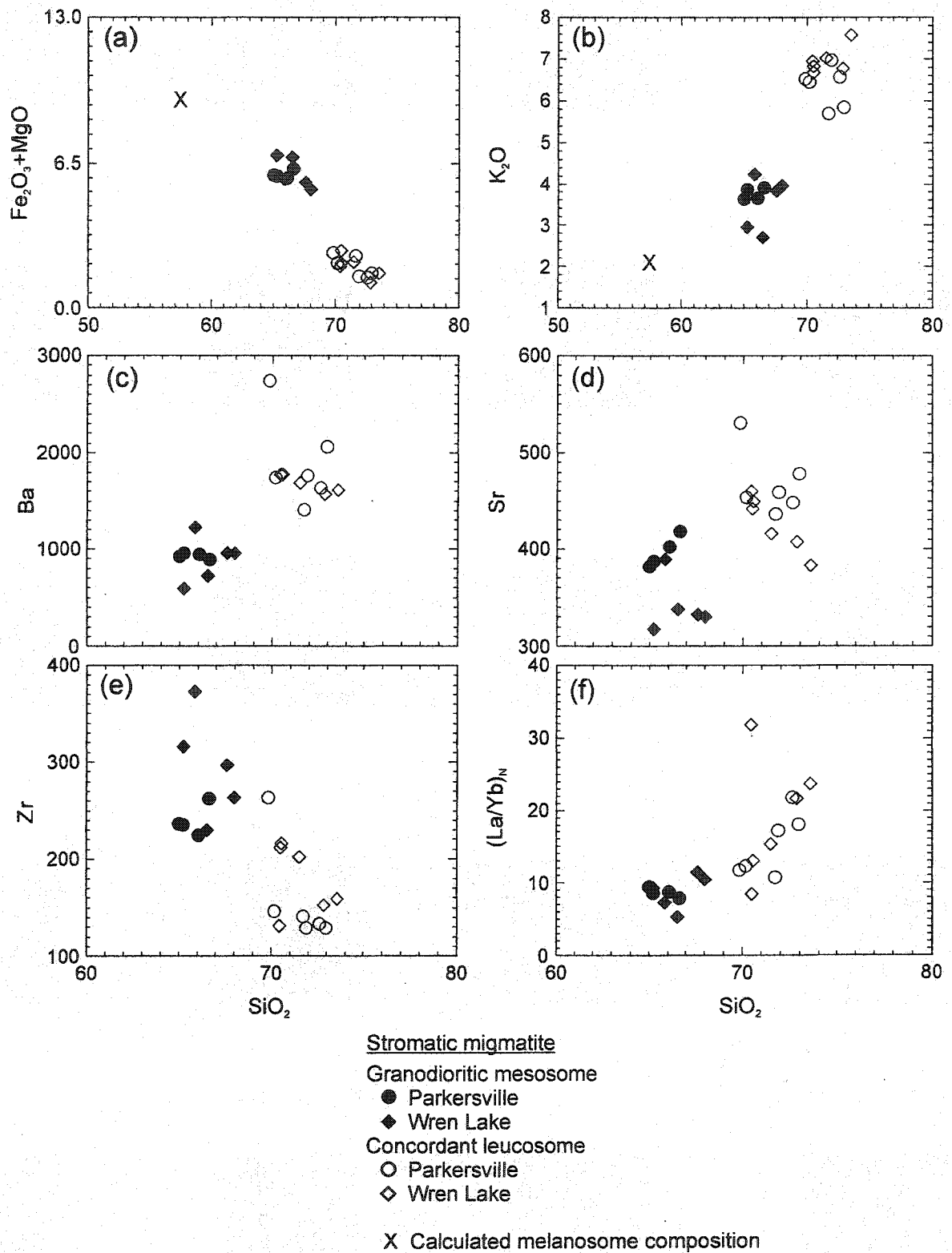
Fig. 3.7 (a-f) Harker variation diagrams, stromatic migmatites. Major elements are in wt% and trace elements in ppm.
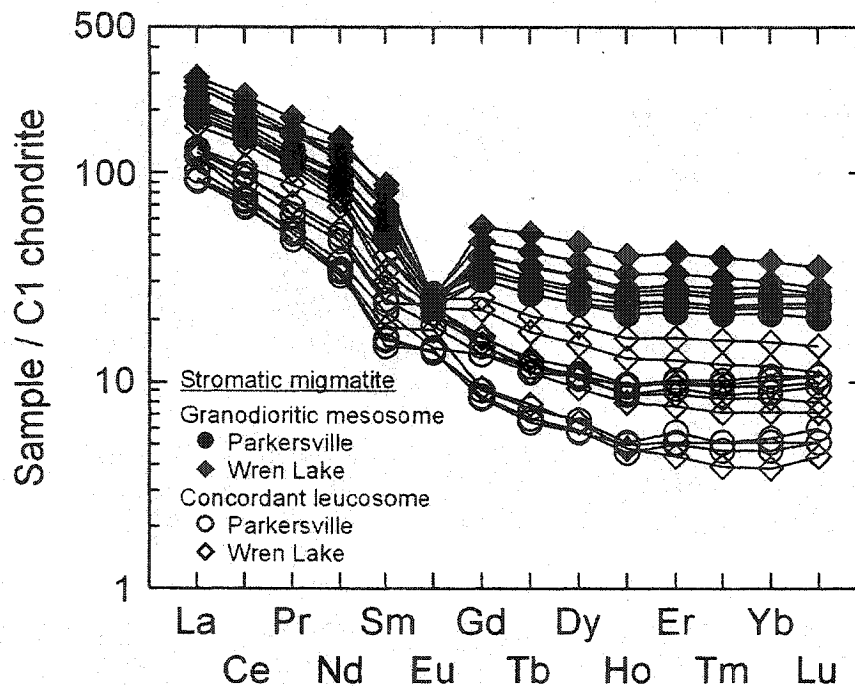
Fig. 3.8 Chondrite-normalized REE patterns, stromatic migmatite.

Concordant melanosome

The concordant melanosomes are generally <5-10 mm thick and consist of plagioclase, hornblende, and biotite. Accessory minerals include apatite, zircon, allanite, and titanite. Much of the hornblende in the concordant melanosome is similar to hornblende in the granodioritic mesosome (Fig. 3.6c), however, a significant portion is coarser-grained with rounded inclusions of plagioclase, quartz, and biotite (Fig. 3.6b). Similar coarse hornblende is generally absent from the granodioritic mesosome and is considered related to formation of the concordant leucosomes, probably through a reaction involving biotite, plagioclase, and quartz, discussed further below. Biotite in the concordant melanosome is compositionally similar to biotite in the granodioritic mesosome (Appendix C); however, melanosome biotite is coarser, and forms clusters intergrown and apparently in equilibrium with hornblende (Fig. 3.6b). However, the P-T conditions experienced by these rocks (Timmermann *et al.*, 2002; S. Gagné and J. Hawken, unpublished data) suggest that biotite is unlikely to have been stable during peak metamorphism (Fig. 3.3). In addition, the marked Rb enrichment in the concordant

leucosomes relative to the granodioritic mesosome is at variance with a significant proportion of biotite in the residue. It seems more likely that the biotite in the concordant melanosomes grew as result of back-reaction as the melts crystallized.

The major element composition of the concordant melanosomes was estimated using modal analysis and anhydrous mineral compositions (cf., Olsen, 1982). The calculated composition is plotted in Figs. 3.7a, b. The granodioritic mesosome, concordant leucosome, and concordant melanosome define a roughly straight line with melanosome and leucosome plotting at lower and higher SiO_2, respectively, relative to the mesosome. This observation is consistent with the concordant melanosomes representing the residue after extraction of granitic melt (~concordant leucosome) from the granodioritic mesosome.

3.5.3. Patchy migmatite

Dioritic mesosome

The dioritic mesosome is fine-grained and weakly foliated relative to the granodioritic mesosome. The modes of representative samples are given in Table 3.1. The dioritic mesosome has a recrystallized granoblastic texture, dominantly comprising hornblende and plagioclase with minor biotite and quartz. Biotite needles or laths, typically 1-3 mm long, define a weak foliation. Apatite and zircon are the main accessory minerals; allanite was not observed.

The dioritic mesosome ranges from 47.7 to 54.2 wt.% SiO_2 (Fig. 3.9). Chondrite-normalized REE patterns (Fig. 3.10) are slightly fractionated with $(La/Yb)_N$ between 2.5 and 5.8, and $(Eu/Eu^*)_N$ between 0.56 and 0.79.

Patches

We analyzed bulk hornblende-rich patches (granitic material with variable, but generally large, proportions of hornblende), as well as the granitic portions of the patches, separated using a rock-saw. The patches can be separated into two components: a granitic component referred to as patchy leucosome, and a mafic component made up of large, euhedral to subhedral hornblende referred to as hornblende-rich patches. The

samples of hornblende-rich patches contain small amounts of granitic material (leucosome) that could not be separated.

Hornblende-rich patches. The hornblende-rich patches are distinguished by large, typically 5 cm long, randomly oriented, euhedral to subhedral, strongly poikilitic or skeletal hornblendes (Fig. 3.6d). The inclusions in these hornblendes are dominantly plagioclase, with minor quartz and biotite, and, unlike inclusions in hornblende from the concordant and patchy melanosomes, are irregular and oriented parallel to the cleavage of the hornblende.

The hornblende-rich patches are slightly more silicic than the dioritic mesosome, with SiO_2 ranging from 50.3 to 58.4 wt.% (Fig. 3.9). The mafic components (TiO_2, Fe_2O_3, MnO, MgO) are similar to or slightly lower than the dioritic mesosome, whereas CaO and Na_2O are lower and K_2O higher. Trace elements are generally similar in the hornblende-rich patches and dioritic mesosome (Fig. 3.9), except V and Th that are lower and slightly higher, respectively, in the patches. The REE patterns (Fig. 3.10) are more strongly fractionated (($La/Yb)_N$=5.2-12.7) than that of the dioritic mesosome, whereas total REE contents and Eu anomalies are similar to the mesosome.

Patchy leucosomes. The patchy leucosomes are medium- to coarse-grained, comprising dominantly K-feldspar, plagioclase, and quartz (Table 3.1). The patchy leucosomes contain between 64.3 and 73.8 wt.% SiO_2 (Fig. 3.9). Total REE contents decrease with increasing SiO_2, whereas REE fractionation increases (($La/Yb)_N$=6-13) and Eu anomalies ($Eu/Eu^*)_N$=0.8-1.8) become more positive (Fig. 3.9e, f).

Relative to the dioritic mesosome, the patchy leucosomes are depleted in all major elements except SiO_2 and K_2O; Ba is significantly higher in the patchy leucosomes, and Rb and Sr slightly higher. Other trace elements (including the REEs) are lower in the patchy leucosomes than in the dioritic mesosome (Fig. 3.10).

Dikes

The dikes are pegmatitic but otherwise petrographically similar to the patchy leucosomes. Along the margins, the dikes contain significant amounts of hornblende,
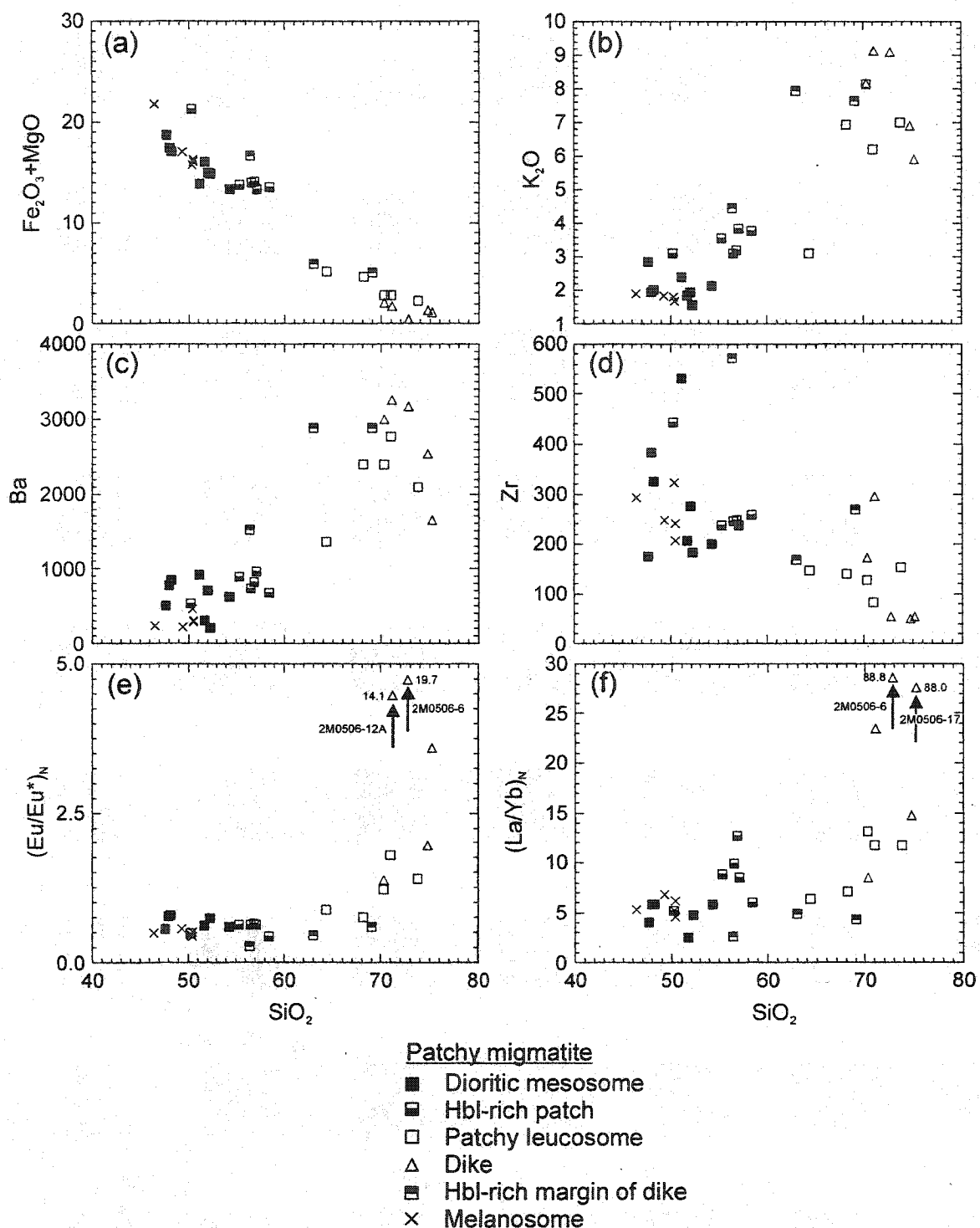
Fig. 3.9 (a-f) Harker variation diagrams, patchy migmatite. Arrows in (e) and (f) indicate samples with $(Eu/Eu^*)_N$ and $(La/Yb)_N$ values outside the range covered by the diagram.
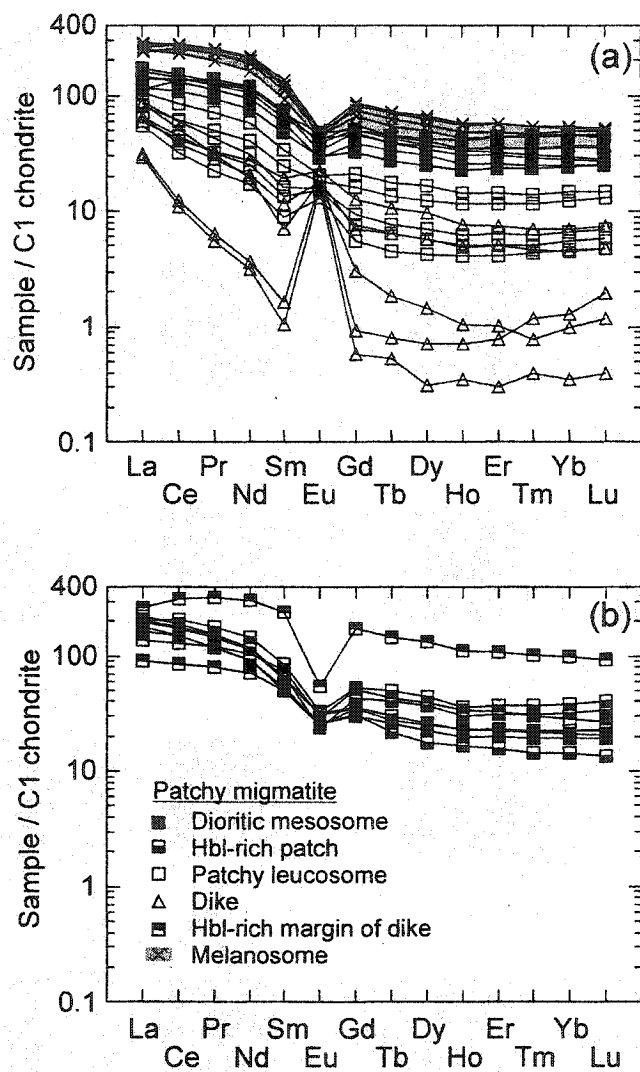
Fig. 3.10 Chondrite-normalized REE patterns for the patchy migmatites. (a) dioritic mesosome, patchy leucosome, dike, and melanosome (shaded for readability), (b) hornblende-rich patch and hornblende-rich margin of dike. Normalized to values of Sun and McDonough (1989).

some of which is texturally similar to the large, cumulate hornblendes in the patches, and some which is similar to hornblende in the patchy melanosome (described below).

Samples from the dikes include the hornblende-rich margins as well as more central, pegmatitic portions. The quartz-dominated centers of the dikes were not sampled. The hornblende-free portions of the dikes are similar to the patchy leucosomes for most major and trace elements, although generally slightly more silicic (Fig. 3.9). The REE patterns (Fig. 3.10), however, display much greater variation in terms of fractionation ((La/Yb)$_N$=8.5-88.8) and Eu anomalies ((Eu/Eu*)$_N$=1.4-19.7). Although we collected relatively large samples of pegmatite to ensure that the samples were representative of the dike composition, it is likely that the two samples with the most extreme Eu anomalies (2M0506-6 and 2M0506-12A) are biased toward K-feldspar. This interpretation is corroborated by the very high K_2O content of these samples (~9.1 wt.%), significantly higher than most granitic rocks. We therefore regard these samples as unrepresentative of the dike composition and they are not included in the ensuing discussion on migmatite petrogenesis. The hornblende-rich margins of the dikes display a range of compositions from similar to hornblende-rich patches to compositions that are more similar to the patchy leucosomes, reflecting the amount of hornblende in the samples.

Patchy melanosome

The hornblende-rich patches typically grade into melanosome comprising medium-grained (~0.5 cm) hornblende, plagioclase, and biotite (Table 3.1). This type of melanosome is referred to as patchy melanosome to distinguish it from the concordant melanosome in the stromatic migmatites. Hornblende in the patchy melanosome is texturally similar to that in the concordant melanosome, typically containing rounded inclusions of plagioclase, biotite, and quartz. Biotite typically occurs as dark red to nearly opaque, irregular grains, in contrast to the more needle-like biotite in the dioritic mesosome. The patchy melanosomes typically contain a small proportion of granitic material, interpreted as representing unsegregated melt.

The patchy melanosome is somewhat higher in Fe_2O_3, MgO, MnO, CaO, Y, Nb, Zn, Ni, Cr, and Th, and slightly lower in Rb and Ba than the dioritic mesosome, but with essentially similar SiO_2, TiO_2, Al_2O_3, and Na_2O content (Fig. 3.9). Total REE contents are higher than in the dioritic mesosome, with larger negative Eu anomalies (($Eu/Eu^*)_N$=0.43-0.55), and similar or slightly higher $(La/Yb)_N$ between 4.5-6.8 (Fig. 3.10). The higher $(La/Yb)_N$ of the melanosome is caused by enrichment in LREEs.

3.6. Migmatite petrogenesis

3.6.1. Incongruent biotite breakdown

Based on petrographic evidence, Timmermann *et al.* (2002) proposed that formation of voluminous leucosome in the Muskoka domain took place by incongruent, fluid-absent biotite melting, producing granitic melt and residual hornblende, according to reaction (3.1).

$$Bt + Pl + Qtz = Hbl + \text{Granitic melt} \qquad (3.1)$$
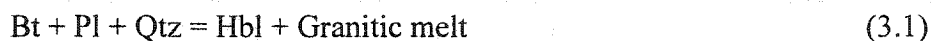
The petrographic observations described above are similar to those of Timmermann *et al.* (2002) and support their interpretation that biotite reacted with plagioclase and quartz to produce granitic melt and residual hornblende. However, instead of, or perhaps in addition to, the fluid-absent reaction proposed by Timmermann *et al.* (2002), we suggest that partial melting took place under fluid-present conditions, according to reaction (3.2).

$$Bt + Pl(I) + Qtz + Fluid = Hbl + Pl(II) + \text{Granitic melt} \qquad (3.2)$$
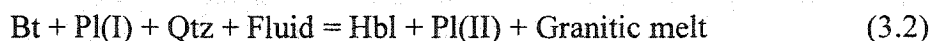
Some of the concordant leucosomes may also have formed by eutectic melting of plagioclase, quartz, and K-feldspar (reaction (3.3)), probably in addition to reaction (3.2).

$$Qtz + Pl + Kfs + Fluid = \text{Granitic melt} \qquad (3.3)$$

Our reasons for invoking fluid-present partial melting are explained below, and we also attempt to place some constraints on the composition of the hypothesized fluid.

3.6.2. The role of fluids

As shown above, partial melting in both stromatic and patchy migmatite was

associated with growth of new hornblende. Some experimental studies (e.g., Naney, 1983; Gardien *et al.*, 2000) have shown that the stabilization and growth of new hornblende during partial melting of a biotite-plagioclase-quartz assemblage requires addition of at least 3-4 wt.% H_2O. Other experimental studies found that new hornblende can form by biotite dehydration melting under fluid-absent conditions (e.g., Skjerlie and Johnston, 1996); however, in the case described by Skjerlie and Johnston (op. cit.), the breakdown of biotite to form hornblende produced insignificant amounts of melt (<5 vol.%) at 850°C. Significant melting took place only at higher temperatures when hornblende reacted to form melt and residual pyroxene. Pyroxene is generally absent in the investigated rocks (Timmermann *et al.*, 2002; this study).

In order to determine if biotite dehydration melting (reaction 3.1) can solely account for formation of the observed leucosomes, we made some simple calculations. If the granodioritic and dioritic mesosomes are representative of the mineralogy of the source to the concordant and patchy leucosomes, respectively, the relatively low abundance of biotite (<10 vol.%) is insufficient to produce significant amounts of melts. For example, if the mode of biotite (with 3.9 wt.% H_2O, Clemens and Vielzeuf, 1987) is 10 vol.%, and assuming that the specific gravity of biotite is 3.0, and that of the source rock is 2.7; 0.4 wt.% H_2O can be made available to the melting reaction by biotite breakdown. According to Clemens and Vielzeuf (1987), this amount of H_2O can produce ca. 10 vol.% melt in a quartzofeldspathic source rock at 1 GPa at temperatures between 800 and 850°C. In fact, this number is an upper estimate of the amount of melt that could have been produced by biotite dehydration melting in the investigated rocks because in the calculations of Clemens and Vielzeuf (1987) all the fluid liberated by hydrous phase breakdown entered the melt (i.e., the residue was anhydrous). In contrast, partial melting in the Muskoka domain involved growth of a new hydrous phase (hornblende), thus significantly reducing the amount of fluid available to the melt. Fluid-absent, biotite dehydration melting, therefore, is unlikely to produce large amounts of melt if a new water-rich phase such as hornblende is a dominant residual phase (cf., Conrad *et al.*, 1988; Skjerlie and Johnston, 1996). Biotite dehydration melting to produce an anhydrous residual phase (e.g., orthopyroxene) would be more efficient for producing significant

amounts of melt, and the calculations above suggest that in this case ca. 10 vol.% melt could be produced from a source with 10 vol.% biotite. However, the lack of orthopyroxene and the peak temperatures estimated from Muskoka domain rocks (cf. Fig. 3.3) argue against a leucosome-forming reaction producing residual orthopyroxene. We therefore believe that partial melting took place in the presence of a H_2O-bearing fluid (cf., (6c) and (3b) in Fig. 3.3), with further melting at progressively lower aH_2O or possibly fluid-absent conditions (cf., Sawyer, 1998). A similar model to that proposed here was invoked by McMullen (1999) for the eastern Muskoka domain and has also been proposed to account for partial melting of similar lithologies elsewhere (e.g., Lappin and Hollister, 1980; Kenah and Hollister, 1983; McLellan, 1988; Mogk, 1992; Nédélec *et al.*, 1993; Sawyer, 1998; Escuder Viruete, 1999).

The composition of the initial fluid is impossible to constrain without isotopic and/or fluid inclusion data. Phase equilibrium evidence from high-grade metamorphic rocks suggests that pure aqueous fluids are generally not present in excess (see Stevens and Clemens, 1993 and references therein), thus, aH_2O was most likely <1 during migmatization. This interpretation is also consistent with the lack of leucosome in common metabasites in the area (cf., (9) in Fig. 3.3). The two most likely scenarios for achieving $aH_2O<1$ are (Clemens and Watkins, 2001) (i) that the system initially contained an H_2O-rich fluid, but in insufficient quantities to saturate the melt, or, (ii) that the fluid was a mix of H_2O and another component such as CO_2 (e.g., Newton *et al.*, 1980). Several features argue for the latter case. For example, some of the migmatites contain small amounts of carbonate associated with skeletal biotite and biotite-hornblende intergrowths that appear to have been involved in melting (Fig. 3.6e; Jamieson, unpublished data). In addition, patches of greenish granulite, also containing small amounts of carbonate (Slagstad, unpublished data), are common in parts of the Muskoka domain, and were interpreted by Timmermann *et al.* (2002) to have formed by influx of low-aH_2O, CO_2-rich fluids coeval with formation of the migmatites, although new field and geochronological data, discussed in Chapter 5, may argue against this interpretation. Recent work on fluid inclusions in garnet in a paragneiss from the Algonquin domain, immediately underlying the Muskoka domain, identified single-phase

inclusions consisting of nearly pure CO_2 (Layman *et al.*, 2003). Although the source of this CO_2-rich fluid and its relationship to the migmatization is unknown it demonstrates local presence of CO_2-rich fluid at high metamorphic grade. Infiltration of similar fluids was also invoked by Pattison (1991) to explain the development of light-colored veins (net veins) rich in pyroxene, plagioclase, and locally quartz, in small metagabbro boudins in the Seguin subdomain, contiguous with the Muskoka domain (Fig. 3.2). It is possible that influx of a mixed H_2O-CO_2 fluid during high-grade Grenvillian metamorphism can account for both extensive partial melting (cf., Giorgetti *et al.*, 1996) as well as local development of granulite-facies assemblages. In this model, H_2O would have been partitioned into the melts, whereas most of the CO_2 would have remained in the rocks (cf., Clemens, 1993), forming the patchy granulites and small accumulations of carbonate. During cooling and melt crystallization, back-reaction between H_2O and orthopyroxene could have formed the hornblende-rimmed orthopyroxenes typically observed in the patchy granulites (Timmermann *et al.*, 2002). Detailed isotopic and fluid inclusion analysis on both migmatites and patchy granulites is needed in order to determine the role and nature of fluids during high-grade metamorphism in these rocks.

3.6.3. Mesosome: a good approximation to protolith composition?

In contrast to hornblende in the melanosome, hornblende in the mesosome generally lacks textural evidence of having formed by incongruent breakdown of biotite, although in rare samples such textures are associated with tiny pockets of leucosome, generally <1 cm long and unnoticeable in the field. These minuscule leucosomes, along with thin 'melt' films suggest the retention of small amounts of melt in the mesosome. However, these melt pockets and films are volumetrically insignificant (<0.5 vol.‰), and the petrographic and geochemical data suggest that these melts were segregated on a mm-scale at most, and were not extracted from the mesosomes. We therefore conclude that the mineralogical and chemical composition of the mesosomes approximates the composition of the source to the leucosomes.

3.6.4. Trace element modeling

Trace element modeling of magmatic processes was first applied to mantle-related

systems, where it has found undeniable success (e.g., Bédard, 2001). It was then applied to crustal systems, where it is used for studying the petrogenesis of migmatites (e.g., Sawyer, 1987, 1991; Barbey *et al.*, 1989). A well known problem, however, in applying trace element modeling to crustal rocks is the common presence of accessory phases such as apatite, zircon, allanite, and monazite. These phases are extremely rich in certain trace elements (e.g., LREEs in allanite and monazite, HREEs in zircon) and in many cases can obscure the effects produced by major phases during partial melting and fractional crystallization (e.g., Bea, 1996 and references therein). All of the rocks investigated here contain accessory phases, in particular zircon, apatite, allanite, and titanite. For this reason, elements such as Ba, Rb, and Sr that are hosted by the major phases involved in partial melting may be better indicators of petrogenesis. There are, however, significant problems inherent in modeling these elements as well. One problem is the large variation in measured partition coefficients, in some cases varying by an order of magnitude (see Appendix F). As summarized by Solar and Brown (2001), this variation reflects a number of important controls on partition coefficients, for example structure and composition of the melt (e.g., Mahood and Hildreth, 1983; Nash and Crecraft, 1985), mineral composition (e.g., Blundy and Wood, 1991; Icenhower and London, 1996), temperature (Icenhower and London, 1995; Chappell, 1996), and water content (Mahood and Hildreth, 1983). Assuming that the leucosomes, mesosomes, and melanosomes represent melt, source, and residue, respectively, another potential problem is to what degree the measured compositions reflect the compositions at the time of migmatization. Fourcade *et al.* (1992) and Berger and Rosenberg (2003) argued that the trace element distribution between leucosome and melanosome in some migmatites reflects mineral-mineral equilibrium rather than melt-mineral equilibrium, which they ascribed to reequilibration by diffusion during cooling of the migmatite terrane. The prolonged thermal history of the Grenville Province, followed by protracted cooling (Reynolds *et al.*, 1995), may, therefore, present a problem. Along the same lines, Nabelek (1999) suggested that migmatites in the Black Hills, South Dakota, have trace element distributions compatible with solid-solid equilibrium because the melt and residue maintained equilibrium during crystallization and subsolidus cooling.

In the succeeding sections the concentrations of Ba, Rb, Sr, and REEs in the leucosomes are modeled. Despite the inherent problems discussed above, Ba, Rb, and Sr appear to be relatively good indicators of various partial melting reactions (equilibrium vs. disequilibrium), whereas the REEs appear to be controlled by accessory phases.

Two types of melting reaction are modeled: batch equilibrium and disequilibrium melting (see Appendix F for equations and a discussion of the robustness of the model results). Equilibrium partial melting requires that the melt and the solid from which it was derived maintained thermodynamic and compositional equilibrium, and that the partitioning of trace elements between the melt and the solid followed Henry's law, i.e., can be described by an equilibrium partition coefficient (e.g., Hanson, 1978). Maaløe (1982) described three types of equilibrium partial melting: batch melting, where batches of magma segregate when the permeability threshold is reached; perfect fractional melting, where infinitesimally small amounts of melt leave the system immediately after they are formed; and an intermediate case referred to as critical melting. Sawyer (1991) pointed out that for small degrees of partial melting (F<0.4), these melting models yield comparable results; thus, only batch melting is considered here. During disequilibrium partial melting, equilibrium is not maintained between the melt and the solid residue, and the concentration of an element in the melt is proportional to the concentrations in and proportions of phases entering the melt (Allègre and Minster, 1978; Prinzhofer and Allègre, 1985; Barbey et al., 1989). Strictly, solid-solid partition coefficients should be used in the disequilibrium modeling. The solid-solid partition coefficients are not known; however, Barbey et al. (1989) suggested that they can be estimated from solid-melt partition coefficients (see Barbey et al., 1989 for derivation). Although many workers, dealing with similar problems as those described here, have used this approximation (Sawyer, 1991; Chavagnac et al., 1999; Jung et al., 1999), it introduces an undetermined level of uncertainty. Uncertainties related to analytical error and the use of different partition coefficients are discussed in Appendix F. Partition coefficients used here are given in Table 3.2.

3.6.5. Stromatic migmatites

Trace element modeling

The stromatic migmatites at Parkersville and Wren Lake are compositionally similar, and yield similar trace element model results. Therefore, only the Parkersville outcrop is considered here. The field observations and petrographic data suggest that the concordant leucosomes formed by partial melting of granodioritic mesosome by incongruent breakdown of biotite, reacting with quartz, plagioclase, and probably K-feldspar, leaving a hornblende-plagioclase-dominated residue. The average geochemical and mineralogical composition of the granodioritic mesosome is used as the source in the modeling.

Table 3.2 Partition coefficients used in trace element modeling of migmatite petrogenesis.

	Plagioclase	K-feldspar	Hornblende	Biotite	Apatite	Allanite	Zircon
Ba	0.36	6.12	0.044	6.36	n.d.	n.d.	n.d.
Rb	0.048	0.34	0.014	3.26	n.d.	n.d.	n.d.
Sr	2.84	3.87	0.022	0.120	n.d.	n.d.	n.d.
La	0.26	n.d.	$0.74^{\S}$ (0.6)	$0.32^{\S}$	$20^{\S}$	960	n.d.
Ce	0.24	0.044	1.52 (0.9)	0.32	34.7	940	2.64
Nd	0.17	0.025	4.26 (2.8)	0.29	57.1	750	2.2
Sm	0.13	0.018	7.77 (4)	0.26	62.8	620	3.14
Eu	0.814	1.13	5.14 (3.5)	0.24	30.4	56	3.14
Gd	0.09	0.011	10 (5)	0.28	56.3	440	12
Tb	0.09*	0.009*	12* (6)	0.29*	54*	270	25*
Dy	0.086	0.006	13 (6.2)	0.29	50.7	200	45.7
Ho	0.085*	0.006*	12* (6.1)	0.33*	45*	n.d.	100*
Er	0.084	0.006	12 (6)	0.35	37.2	100	135
Tm	0.08*	0.009*	10* (6)	0.39*	30*	75*	200*
Yb	0.077	0.012	8.38 (3.7)	0.44	23.9	54	270
Lu	0.062	0.006	5.5 (3)	0.33	20	41	323

Data from Arth (1976) and Arth and Barker (1976), except *determined by extrapolation and §Barbey *et al.* (1989). Allanite data from Martin (1987), zircon data from Arth and Hanson (1975). Hornblende data in parentheses used in section 3.8 Alternative interpretation of migmatite petrogenesis, compiled by Borg and Clynne (1998).n.d.=no data.

Equilibrium melting. The modeled composition of a melt formed by 10 to 50% partial melting of the average granodioritic mesosome at the Parkersville outcrop, in

equilibrium with a plagioclase-dominated residue ($Pl_{56}Hbl_{39}Qtz_5$) as indicated by the petrography, is shown in Fig. 3.11a. The large proportion of plagioclase in the residue yields model melts that are strongly depleted in Sr relative to the concordant leucosome, and the lack of a Rb-bearing phase (biotite) in the residue results in strong Rb enrichment in the model melt. The Ba contents of the model melts are similar to the concordant leucosome, but the resulting Ba/Rb and Rb/Sr ratios differ significantly from the leucosomes. Reducing the proportion of plagioclase and adding biotite to the residue yields model melts that have Sr and Rb contents similar to those observed in the leucosomes; however, the presence of biotite in the residue produces model melts that are strongly depleted in Ba relative to the leucosomes. The model melts have moderately negative Eu anomalies, controlled by the proportion of plagioclase in the residue, in contrast to the predominantly positive Eu anomalies observed in the leucosomes. The other MREEs are similar between the model melts and leucosomes. The LREEs are controlled by the proportion of allanite in the residue; for example, adding 0.1 wt.% allanite reduces the concentration of La in the model melt from 98 to 35 ppm. The modeling results are, therefore, interpreted to suggest that the concordant leucosomes did not form by equilibrium melting of the granodioritic mesosome.

Disequilibrium melting. The results of the disequilibrium melting models are shown in Fig. 3.11b. The model melt has similar Ba, Rb, and Sr contents to the concordant leucosome if the dominant phase entering the melt is plagioclase, followed by K-feldspar, quartz, and biotite (Model melt 1; details given in Fig. 3.11b and caption). The model melt is strongly depleted in REEs relative to the concordant leucosomes, and has a much larger, positive Eu anomaly. However, adding 0.8 wt.% apatite to the model melt produces MREE and HREE contents similar to the leucosomes (Model melt 2, Fig. 3.11b). The LREE contents of the model melt are too high, but adding 0.04 wt.% allanite to the source produces a good fit. Although involvement of accessory minerals is feasible considering the petrographic data, for example as residual phases or entering the melt by melting or dissolution or as xenocrysts, it is clear that the REEs are poor indicators of petrogenesis in these rocks as they probably do not reflect the behavior of the major phases. In contrast, the modeled Ba, Rb, and Sr contents are consistent with
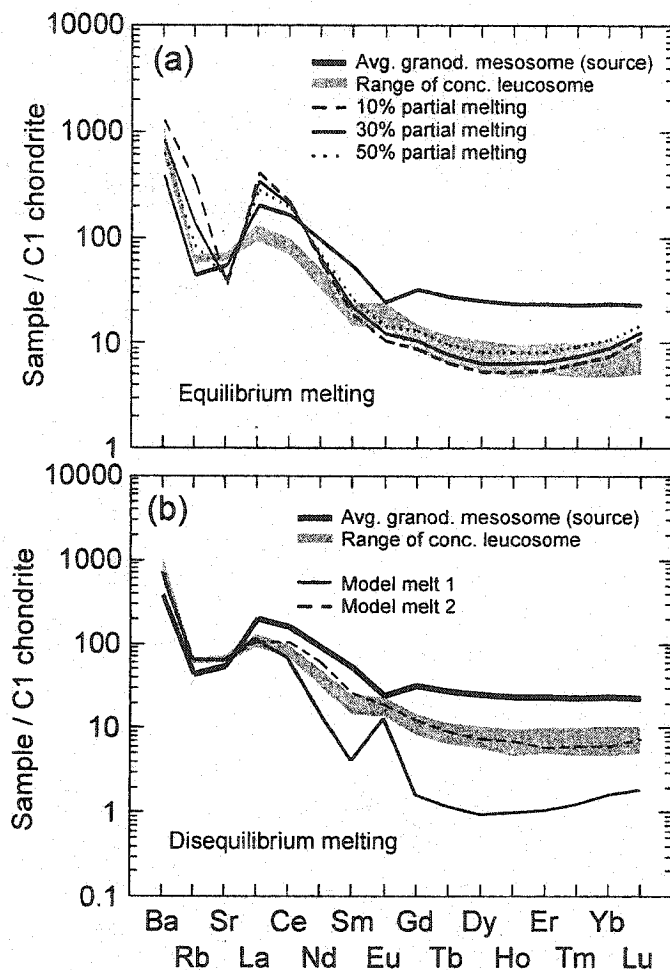
Fig. 3.11 Trace element modeling of stromatic migmatite. (a) Equilibrium melting of average granodioritic mesosome, Parkersville outcrop; model residue: Pl (56 wt.%) Hbl (39 wt.%), and Qtz (5 wt.%). (b) Disequilibrium melting of average granodioritic mesosome. The mode of the mesosome is Qtz (15 vol.%), Pl (55 vol.%), Kfs (11 vol.%), Hbl (12 vol.%), and Bt (7 vol.%). Model melt 1 does not take accessory phases into account; phases and their weight proportions entering the melt are Pl (45 wt.%), Kfs (26 wt.%), Qtz (18 wt.%), Bt (11 wt.%). Model melt 2 is similar to model melt 1 except that 0.8 wt.% apatite is added to the melt and 0.04 wt.% allanite is added to the residue, in order to demonstrate the effects of accessory phases on the model result.

the petrographic observations. We therefore interpret the concordant leucosomes to have formed by disequilibrium partial melting of granodioritic mesosome.

With the composition of the source (granodioritic mesosome), residue (calculated concordant melanosome) and melt (concordant leucosome) known, it is possible to calculate the degree of melting using the mass-balance calculation $C_s=FC_m+(1-F)C_r$, where C_s is the composition of the source, C_m is the composition of the melt, and C_r is the composition of the residue (Sawyer, 1991). An alternative approach is to use only elements that are strongly partitioned into the residue, reducing the mass-balance equation to $F=(C_r-C_s)/C_r$ (Sawyer, 1991). For the mafic oxides (TiO_2, Fe_2O_3, MnO, and MgO) this method yields estimates of F between 0.33 and 0.64. If the melt is contaminated by residual phases, as indicated by the petrography, F is overestimated (Sawyer, 1991). In addition, the accuracy of the calculated melanosome composition is unknown.

3.6.6. Patchy migmatites

The patches are typically randomly distributed, have complex shapes (cf., McLellan, 1988) with associated melanosomes, and lack evidence of feeder dikes or shear bands that could have acted as conduits for externally derived melts. We therefore conclude that the leucosomes most likely represent *in situ* (on the outcrop scale) melts. Field and petrographic observations from the patchy migmatites provide some clues as to their petrogenesis. The patchy leucosomes appear to represent locally derived melts that formed by partial melting of dioritic mesosome, leaving a residue (patchy melanosome) comprising hornblende, plagioclase, and biotite. Much of the biotite is probably retrograde. The coarse, subhedral to euhedral hornblendes in the patches are interpreted to have crystallized from a melt, and, because the hornblendes contain a significant proportion of plagioclase (+some biotite), evolved melts and cumulates should have compositions compatible with removal and accumulation of hornblende+plagioclase±biotite, respectively. Thin seams of granitic material typically connect the patches and dikes. We interpret these seams to represent former melt conduits along which granitic melts migrated from the patches, leaving melt-depleted

hornblende-rich patches (cumulates). Melt migration distances are inferred to have been short, on the order of a few dm to 1-2 m. In this interpretation, the dikes represent the evolved melts expelled from the patches. The zoning in the dikes, with quartz-rich centers, probably implies that none of the samples from the dikes represents melt compositions. Although we have not investigated the process by which the zoning developed, we can make some generalizations as to the geochemical effects. The most obvious effect is that, because most of the quartz is concentrated in the center, the surrounding, feldspar-rich material will be depleted in SiO_2 and enriched in other major elements relative to the original melt. In addition, because the partition coefficients for trace elements in quartz are exceedingly small, the surrounding pegmatitic material is probably enriched in trace elements relative to the original melts. In contrast, trace element ratios will be less affected and the shape of the REE pattern is probably representative of the original melt composition.

Major elements

The major elements are presented in a (Na+Ca)-(Fe+Mg+Ti)-(K*10) ternary diagram (Fig. 3.12) (cf., Solar and Brown, 2001; Barnes *et al.*, 2002). K*10 is used in order to bring the points toward the center of the triangle to increase the legibility. Note that although this does not alter the relative position of the points (cf., Pearce and Cann, 1973) it affects the distance between them, in particular, points plotting close to the (Na+Ca)-(Fe+Mg+Ti) tie-line will move significantly toward the K*10 corner whereas points with high K contents (i.e., leucosomes) are less affected. The petrography of the patchy melanosomes suggests that hornblende and, to a lesser degree, plagioclase were the dominant residual minerals. The residue, source, and granitic melts should form a straight line with the residue displaced toward the hornblende-plagioclase tie-line and the granitic melts plotting close to the K*10 corner. The results from this diagram are, therefore, consistent with the model proposed above. The hornblende/plagioclase ratio of the residue can be estimated by extending the straight line so that it intersects the hornblende-plagioclase tie-line. From this procedure we estimate that the residue comprised between 80 and 85 wt.% hornblende and 15 to 20 wt.% plagioclase, which is
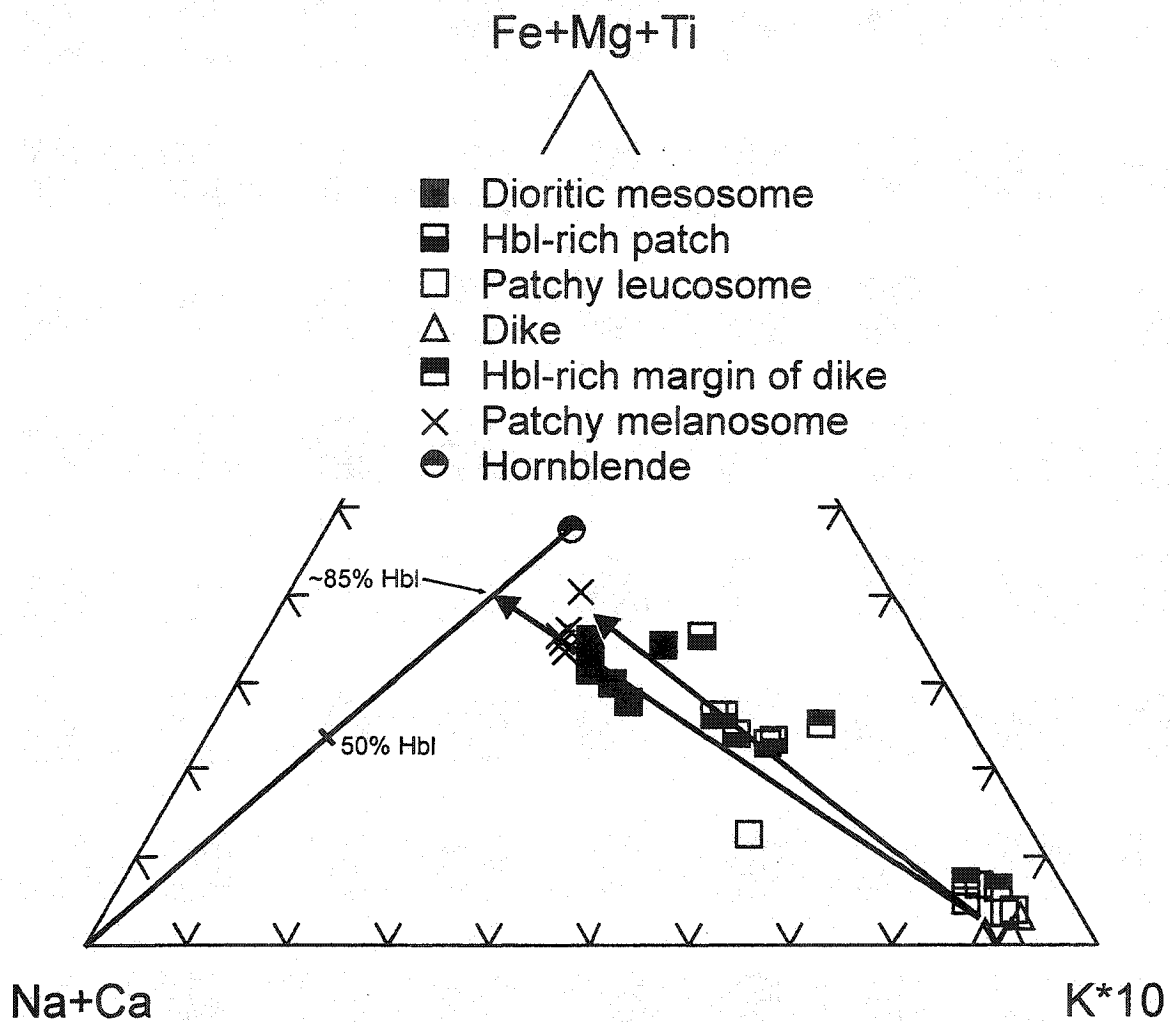
Fig. 3.12 Patchy migmatite components plotted in a molar (Fe+Mg+Ti)-(Na+Ca)-(K*10) ternary diagram (modified after Solar and Brown, 2001). The hornblende composition was measured on a grain in a Hbl-rich patch (Appendix C).

significantly lower than the plagioclase/hornblende ratio determined from the petrography (Table 3.1). The lack of significant scatter in any of the major elements used argues against secondary element mobilization, and the reason for the discrepancy between major elements and petrography remains unclear. The hornblende-rich patches plot on a line connecting the most felsic patchy leucosomes+dikes and hornblende+minor plagioclase, suggesting that they represent a mix of hornblende, some plagioclase, and melt, as indicated by the field and petrographic observations. The hornblende-rich patches plot close to the center of this line, suggesting that the patches constitute subequal amounts of hornblende+plagioclase and melt; however, this is a result of using K*10 rather than K in the lower right-hand corner as discussed above. In reality, the hornblende-rich patches plot close to the hornblende-plagioclase tie-line and the estimated proportion of melt is only 10-20 wt.%, consistent with the field and petrographic observations.

Trace element modeling

The patchy leucosomes show a greater range in composition than the concordant leucosomes, interpreted to reflect a greater influence of fractional crystallization in the former. Here, we take the average of the three most felsic patchy leucosomes to represent the closest approximation to the primary melt composition. The average dioritic mesosome is taken to represent the composition of the source.

Estimates of the degree of melting, using the same method as described for the stromatic migmatites, and taking the average dioritic mesosome to represent the source and the most mafic patchy melanosome to represent the residue, yield values of F between 0.27 and 0.34 for Fe_2O_3, MgO, and MnO.

Equilibrium melting. 10 to 50% partial melting of dioritic mesosome, leaving a residue comprising 85 wt.% hornblende and 15 wt.% plagioclase, as indicated by Fig. 3.12, yields model melts that are strongly enriched in Sr, but similar in Ba and Rb, relative to the most felsic patchy leucosomes (Fig. 3.13a). A more plagioclase-rich residue comprising 69 wt.% hornblende and 31 wt.% plagioclase, more in line with the

petrographic observations from the patchy melanosomes, shows that the Ba, Rb, and Sr composition of the patchy leucosomes could have resulted from 30% equilibrium partial melting (Fig. 3.13b). The MREE contents of the model melt are similar to the patchy leucosomes, except that the modeled Eu anomalies are less positive than those observed in the leucosomes. The modeled LREE contents are significantly higher than observed in the leucosomes and the HREE pattern is positively sloping, in contrast to the flat HREE patterns of the leucosomes. However, as was the case with the concordant leucosomes, taking accessory phases into account produces a model melt (30% melting) that perfectly matches the observed leucosome composition (Fig. 3.13b). The resulting model melt has a positive Eu anomaly (1.33 at 30% melting), similar to patchy leucosomes. In contrast, the modeled MREE contents are little influenced by accessory phases; adding as much as 5 wt.% apatite to the residue does not significantly affect the MREE contents of the model melt. Thus, the modeled MREE contents are determined dominantly by the proportion of hornblende and, to a lesser degree, plagioclase in the residue. The trace element modeling shows that the patchy leucosomes could have formed by 30% partial melting of dioritic mesosome.

Disequilibrium melting. The patchy leucosomes probably formed by a melting reaction involving plagioclase, biotite, and quartz as reactants. Assuming that the degree of melting was ca. 30%, as estimated above, the modal composition of the dioritic mesosome imposes some constraints on the weight proportions of these phases entering the melt. Quartz constitutes ca. 2 wt.% of the source, thus, quartz cannot constitute more than 6 wt.% of the assemblage entering the melt or the source will become exhausted in quartz at <30% melting. Similarly, the proportion of biotite entering the melt is limited to 25 wt.%. Thus, plagioclase must constitute at least 69 wt.% of the phases entering the melt, producing model melts that are strongly enriched in Sr relative to the patchy leucosomes (Fig. 3.13c). The modeled REE contents are much lower than in the leucosomes, and the Eu anomaly is much more positive, but as above, taking accessory phases into account produces a better fit.
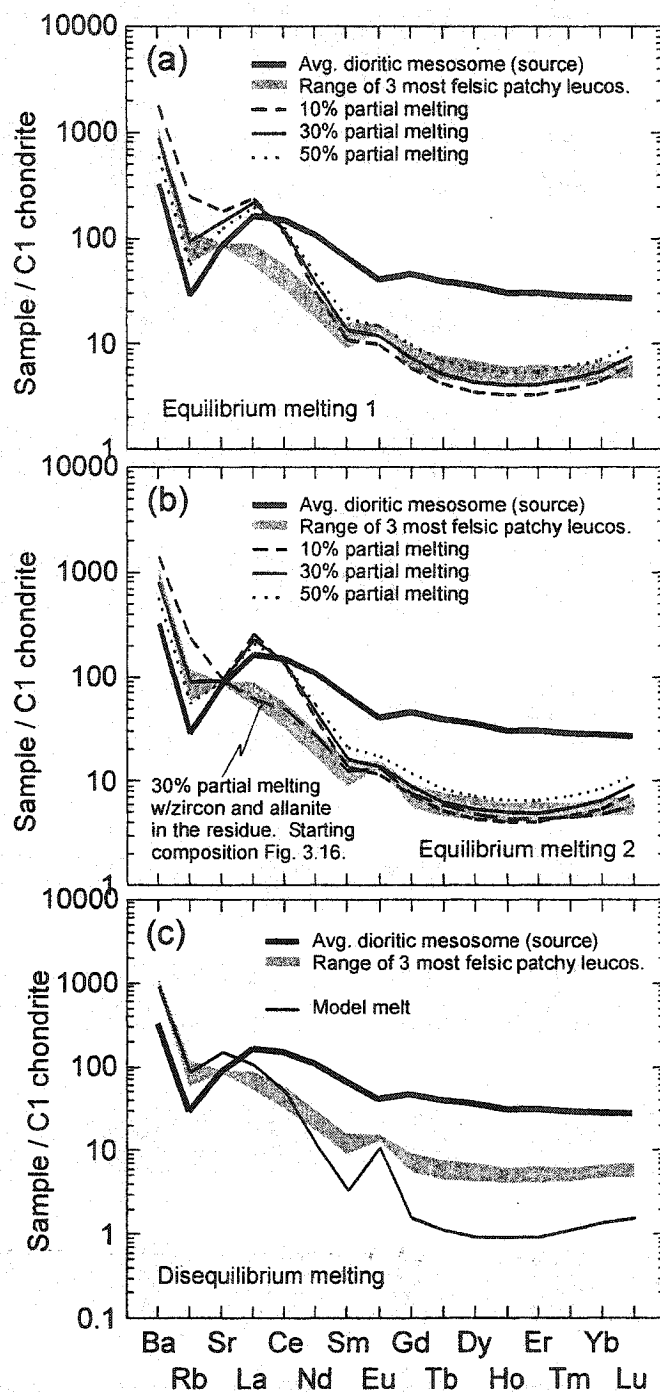
Fig. 3.13 Trace element modeling of patchy migmatite. (a) Equilibrium melting of average dioritic mesosome; model residue (wt.%): Hbl (85 wt.%) and Pl (15 wt.%). (b) Same as (a) but with different proportions of hornblende and plagioclase in the model residue, Hbl (69 wt.%) and Pl (31 wt.%). Also shown is the model melt produced by 30% partial melting, with a small amount of zircon (0.8 wt.%) and allanite (0.3 wt.%) in the residue in addition to hornblende and plagioclase; apatite has little impact on the REE pattern. (c) Disequilibrium melting of average dioritic mesosome. The mode of the mesosome is Qtz (2 vol.%), Pl (45 vol.%), Hbl (37 vol.%), Bt (8 vol.%), and Mag (8 vol.%). Phases and weight proportions entering the melt are Pl (69 wt.%), Bt (25 wt.%), and Qtz (6 wt.%).

Although the results of the trace element modeling do not exclude disequilibrium melting, the trace element composition of the patchy leucosomes appears to fit the equilibrium model more closely. Based on the available geochemical data, we interpret the patchy leucosomes to have formed by equilibrium partial melting, in contrast to the concordant leucosomes that probably formed by disequilibrium melting.

Effects of fractional crystallization

Sawyer (1987) showed that fractional crystallization can have a great impact on leucosome compositions. In the case investigated by Sawyer (1987), feldspar-dominated fractionation produced fractionated liquids with higher REE abundances and greater negative Eu anomalies than the unfractionated melt, and cumulates with lower REE abundances and more positive Eu anomalies. However, if the compositional variation in the patchy leucosomes is a result of fractionation, several lines of evidence suggest that feldspar was not the dominant fractionating phase. For example, total REE contents decrease whereas $(La/Yb)_N$ increases and $(Eu/Eu^*)_N$ becomes more positive with increasing SiO_2, suggesting fractionation of a REE-rich phase with an affinity for HREEs and a negative Eu anomaly. Given the petrographic evidence for cumulate hornblende with inclusions of plagioclase and biotite in the hornblende-rich patches, we believe that the patchy leucosomes evolved by fractional crystallization of these phases and that the hornblende-rich patches represent cumulates mixed with variable proportions of interstitial melt. The complementary evolved melt must have been felsic, with a low total REE content, a large positive Eu anomaly, and high $(La/Yb)_N$. The best candidate for this melt is the pegmatitic material in the dikes; if so, the dikes probably represent melt collection zones.

3.7. Discussion

There are a number of sources of uncertainty in the above interpretations. Textures indicating that a small amount of melt was retained in the mesosomes lead to some uncertainty as to whether the mineralogical and geochemical composition of the mesosome represents a good approximation to the protolith composition. Small amounts

of residual material, mechanically incorporated into the leucosomes, would affect their composition to various degrees. Small amounts of remaining interstitial melt in the melanosomes, and problems related to the physical separation of melanosome from mesosome and leucosome, means that the composition of the melanosome is somewhat removed from true residual compositions. In addition, primary processes such as melt loss/gain and secondary processes such as element mobility are difficult to quantify and add to the overall uncertainties. Despite these complexities, which are inherent in most studies of migmatites, a combination of field observations, geochemistry, and petrography has proven fruitful in constraining leucosome-forming processes (e.g., Sawyer, 1987, 1991; Jung et al., 1999; Mengel et al., 2001; Otamendi and Patiño Douce, 2001).

3.7.1. Role of fluid during melting

Several lines of evidence argue for the involvement of a mixed H_2O-CO_2 fluid in the formation of the Muskoka migmatites. Calculations on the availability of water through biotite breakdown and experimental evidence (Conrad et al., 1988; Skjerlie and Johnston, 1996) show that incongruent, fluid-absent biotite melting is an inefficient melt-producing reaction when a hydrous residual phase is produced. This is because a significant proportion of the released water enters the new phase rather than partaking in the melting reaction. In addition, observations in the Muskoka domain such as net-veining in some gabbroic bodies (Pattison, 1991), and patchy granulites possibly coeval with the migmatites (Timmermann et al., 2002) have been ascribed to the presence of a relatively low-aH_2O fluid. The presence of small amounts of carbonate associated with the migmatites may also be the result of a CO_2-bearing fluid, and is supported by the recent identification of fluid inclusions consisting of nearly pure CO_2 in garnet in the Algonquin domain (Layman et al., 2003). Further field, petrographic, geochemical, and isotopic work is needed in order to answer questions such as source, composition, fluid-rock ratio, and mode of migration of the fluid.

3.7.2. Effects of deformation on petrogenesis

Deformation can significantly enhance melt segregation rates (e.g., Brown et al.,

1995; Watt *et al.*, 1996), and the presence of melt weakens rocks and, thus, affects their deformation behavior (van der Molen and Paterson, 1979; Rutter, 1997; Rushmer, 2001). Rushmer (1996) and Rosenberg (2001) present recent summaries of the deformation of partially molten rocks, and parts of the following section are based on these publications.

The first experimental investigations of deformation of partially molten granite were those of Murrel and Chakravarty (1973) and Murrel and Ismail (1976). These workers showed that partial melting dramatically reduces the strength of a rock; however, the melt fractions in the experiments were poorly constrained. Later work by Arzi (1978) and van der Molen and Paterson (1979) on deformation of water-saturated, partially molten granite at temperatures between 860 and 1020°C and a pressure of 200 MPa, showed a sharp drop in strength at melt fractions between 10 and 35 vol.% (Fig. 3.14). Arzi (1978) suggested that the sharp drop in strength represents the transition between a flow regime controlled by the solid to a flow regime controlled by the melt, and termed this transition the rheologic critical melt fraction (RCMP). Van der Molen and Paterson (1979) termed the point of maximum rate of strength reduction, i.e., the inflection point of the melt fraction vs. viscosity curve in Fig. 3.14, the critical melt fraction (CMF). Because of the low melt fractions used in the experiments of Arzi (1978) and van der Molen and Paterson (1979), the upper boundary (i.e., highest melt fraction) of the RCMP and the CMF had to be estimated by semi-empirical laws that describe the viscosity of suspensions at different solid fractions (Roscoe, 1952) (Fig. 3.14). More recently, Rutter and Neumann (1995) reinvestigated the mechanical behavior of partially molten granite as a function of melt fraction for melt fractions up to ca. 50 vol.%, under similar P-T conditions and strain rates as those used by Arzi (1978). In contrast to the results of Arzi (1978) and van der Molen and Paterson (1979), Rutter and Neumann (1995) found a nearly linear relationship between melt fraction and effective viscosity (Fig. 3.14).

As pointed out by Rutter and Neumann (1995), melt viscosity may also influence the rate at which a partially molten rock weakens. In the experiments conducted by Arzi (1978) and van der Molen and Paterson (1979), the melt fraction was controlled by adding water to the experimental charge; in contrast, Rutter and Neumann (1995)

increased the melt fraction by increasing the temperature. The experiments of Arzi (1978) and van der Molen and Paterson (1979) therefore simulate fluid-present melting, whereas the experiments of Rutter and Neumann (1995) simulate fluid-absent melting. In the experiments of van der Molen and Paterson (1979), the viscosity of the water-rich melt dropped by almost four orders of magnitude by 20 vol.% melt, which could account for the observed sharp decrease in strength (Rutter and Neumann, 1995). Experimental work by Lejenue and Richet (1995) appears to support the existence of an RCMP, but at higher melt fractions (40-60 vol.%) than found by earlier workers. In summary, the experimental conditions (i.e., 'wet' or 'dry' melting) determine whether an abrupt loss of strength (RCMP or CMF) or a gradual decrease in effective viscosity is observed in the experiments. In either case, the experimental investigations show that the strength of rocks ranging in composition from amphibolite to granite decreases with increasing melt fractions; the decrease is >2 orders of magnitude for melt fractions between 0 and 40 vol.% (Fig. 3.14).
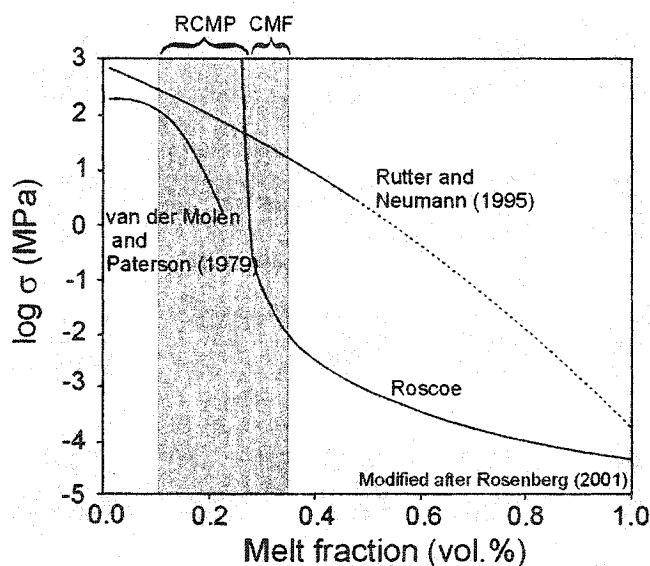
Fig. 3.14 Melt fraction vs. log strength.

Field observations from the stromatic migmatites, such as melt collection zones in boudin necks and syn-melting shear bands, suggest that melt was present during deformation (Timmermann et al., 2002). In contrast, the patchy migmatites lack evidence of syn-melting deformation although undulose extinction of quartz and feldspar

suggests some post-crystallization strain. Their host rocks are typically dioritic and would have been stronger, and would also have yielded less melt at a given temperature, than the granodioritic rocks that host the stromatic migmatites. Thus, the lower strain of the patchy migmatites may have resulted from both different host rocks as well as lower melt proportions. Several papers have emphasized the importance of deformation as a driving mechanism for melt segregation and migration (e.g., Sawyer, 1994; Brown *et al.*, 1995; Watt *et al.*, 1996), and differences in strain may have had a significant influence on melting processes in the Muskoka migmatites. We hypothesize that rapid, deformation-enhanced melt segregation in the stromatic migmatites resulted in melts with disequilibrium compositions. In contrast, lack of significant deformation in the patchy migmatites may have caused lower melt segregation rates, thus allowing a greater degree of equilibrium to be attained. The evidence of fractional crystallization in the patchy migmatites is also consistent with equilibrium melting (Brown, 1979; Sawyer, 1987; Sawyer and Barnes, 1988). The fracture-like geometry of the pegmatite dikes in the patchy migmatites could be a result of melt-enhanced embrittlement (Davidson *et al.*, 1994).

Although our interpretations regarding the relationship between petrogenesis and deformation appear to make sense intuitively, inherent problems such as post-migmatization deformation, influence of accessory phases, element mobility, variable gain/loss of melt, and the potential for solid state equilibrium make quantitative interpretation of partial melting reactions in these migmatites difficult.

3.8. An alternative interpretation of migmatite petrogenesis

The petrogenetic model presented above is appealing because of the apparent link between geochemical data and field observations. However, some of the interpretations, particularly for the stromatic migmatites, are clearly speculative. Here, we discuss the discrepancies between the petrogenetic model proposed above and the field and geochemical observations.

3.8.1. Stromatic migmatites - evidence of open-system processes?

The common occurrence of melanosome in the stromatic migmatites and the near-linear compositional relationship between concordant leucosome-granodioritic mesosome-concordant melanosome (Fig. 3.7) was interpreted above to suggest that the concordant leucosomes represent *in situ* melts formed by partial melting of the granodioritic mesosome, leaving a residue represented by the concordant melanosome. However, a mass balance calculation (Table 3.3) shows that this interpretation is unlikely to be correct. In particular, the sum of concordant leucosome/melanosome, assuming thicknesses of 2 and 0.2 cm, respectively, is too low in ferromagnesian components and too high in K_2O. Similarly, plotting the calculated concordant melanosome composition in Harker diagrams along with the granodioritic mesosome and concordant leucosome shows that the leucosomes fall below a line extending from the calculated melanosome-granodioritic mesosome composition with respect to the ferromagnesian components, and above the line with respect to K_2O. In the Qz-Ab-Or normative diagram (Fig. 3.16) the leucosomes (both concordant and patchy) are displaced toward the Qz-Or line relative to the eutectic composition.

Table 3.3 Mass balance calculation, stromatic migmatite.

	SiO_2	TiO_2	Al_2O_3	Fe_2O_3	MnO	MgO	CaO	Na_2O	K_2O
Granodioritic mesosome	66.6	0.7	15.2	4.5	0.1	1.6	3.2	4.0	3.5
Concordant melanosome. Thickness 0.2 cm	57.3	0.9	18.8	6.1	0.1	3.4	5.2	5.5	2.1
Concordant leucosome Thickness 2 cm	71.6	0.2	14.4	1.5	0.02	0.4	1.5	2.8	7.0
Sum, leucosome+melanosome	70.3	0.3	14.8	1.9	0.0	0.6	1.8	3.1	6.5
Sum-granodioritic mesosome	3.6	-0.4	-0.4	-2.6	0.0	-1.0	-1.3	-0.9	3.0
%	5	-58	-3	-57	-60	-60	-42	-22	84

Mode of concordant melanosome from Table 3.1 (average of two samples); mineral chemical data given in Appendix C.

The very high-leucosome proportions observed in some stromatic migmatites (e.g., in the Parkersville outcrop) can be interpreted in terms of injection of granitic melts from an external source, and this interpretation is consistent with the mass balance calculation
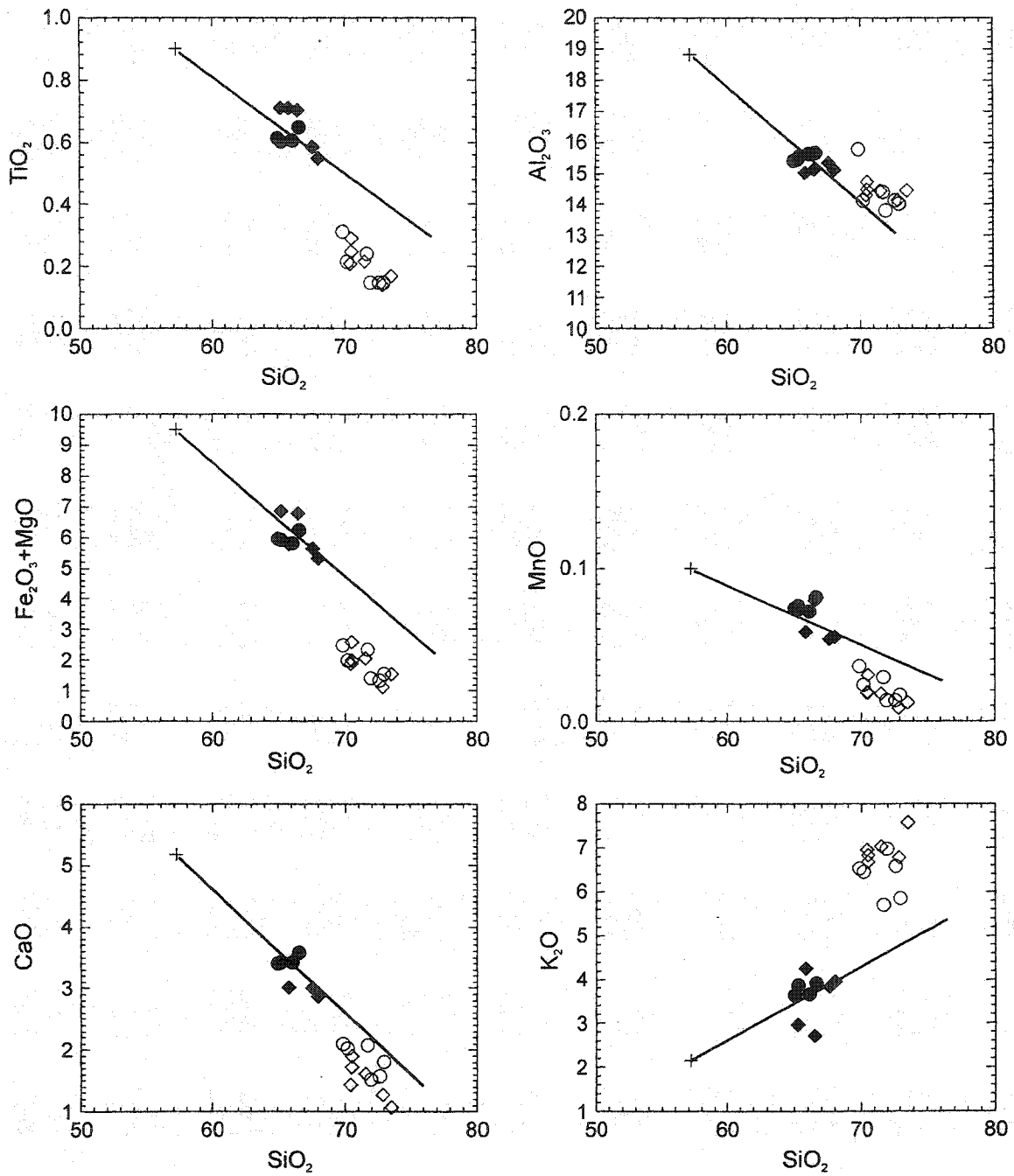
Stromatic migmatite
Granodioritic mesosome
  ● Parkersville
  ◆ Wren Lake
Concordant leucosome
  ○ Parkersville
  ◇ Wren Lake

  + Calculated melanosome composition

Fig. 3.15 Mass balance calculation, stromatic migmatite.

in Table 3.3. An unresolved problem with this interpretation is that despite analyzing a relatively large number of samples, no rocks with apparent residual compositions have been identified. A possible solution is that some of the externally derived melts came from sources outside the Muskoka domain or unexposed parts of the Muskoka domain.
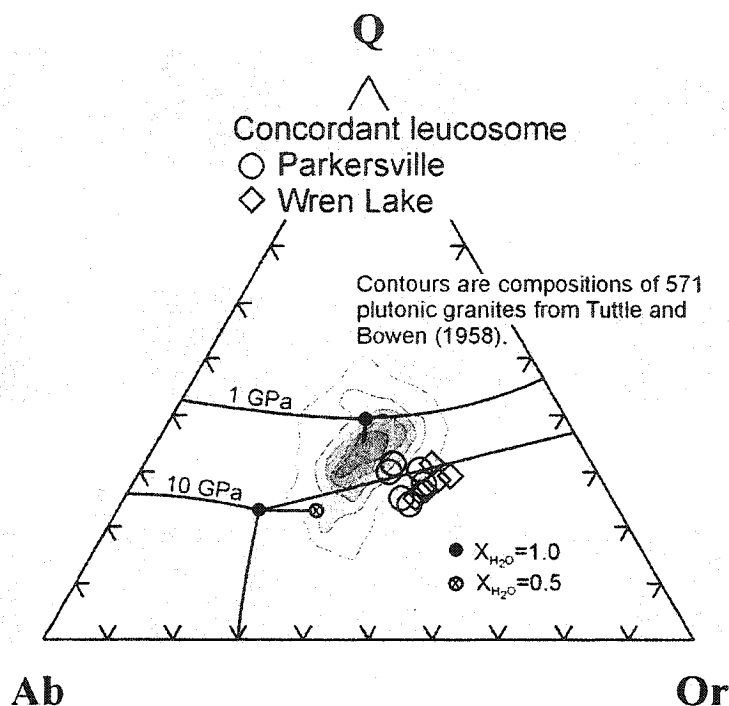
Fig. 3.16 Qz-Ab-An normative diagram.

Judging from the mass balance calculation in Table 3.3 and a comparison with the composition of 571 plutonic granites (Fig. 3.16, from Tuttle and Bowen, 1958, compiled by Herzberg, 1995) the leucosomes are enriched in K_2O relative to most granites. It was argued above that partial melting took place in response to influx of externally derived fluids, but apart from discussing whether the fluids were water-rich *vs.* mixed H_2O-CO_2, their possible composition was not discussed. Similar excess in K_2O and deficiency of ferromagnesian components was reported by Olsen (1984) for migmatites from the Colorado Front Range, near Denver. Olsen (1984) attributed the chemical characteristics of the migmatites to result from metasomatism and partial melting initiated by infiltrating fluids, and a similar interpretation appears feasible for the Muskoka migmatites.

3.8.2. Equilibrium or disequilibrium melting?

Based on experimental work, Watson and Harrison (1983) and Harrison and Watson (1984) derived mathematical expressions for calculating the solubility of Zr as a function of temperature and composition of the melt. Assuming that the concordant and patchy leucosomes represent melts saturated in Zr, it is possible to calculate the temperature of crystallization. The concordant leucosomes yield Zr saturation temperatures between 751 and 808°C, whereas the patchy leucosomes yield slightly lower temperatures between 721 and 774°C (4 of 5 patchy leucosomes yield temperatures between 742 and 774°C) (Appendix C). The calculated temperatures are within error of the peak metamorphic temperatures in the area (Timmermann, 1998; Timmermann *et al.*, 2002; S. Gagné and J. Hawken, unpublished data), indicating that both types of leucosome may be in equilibrium with respect to Zr.

The interpretation of disequilibrium melting in the stromatic migmatites was based on the Sr and Rb concentrations of the concordant leucosomes. The apparent disagreement between the Sr, Rb, and Zr contents is difficult to explain by geological processes because Sr and Rb, being large ion lithophile elements, have higher diffusion rates than Zr, which is a high field-strength element. Thus, equilibrium between melt and residue should have been attained relatively rapidly with respect to Sr and Rb, but would have taken longer for Zr. The apparent disagreement is, therefore, opposite to what would be expected for disequilibrium melting.

3.8.3. Petrogenesis of the patchy migmatites

The patchy migmatites are much less deformed than the stromatic migmatites and are, therefore, preferred targets for investigating migmatite petrogenesis. The petrographic and field observations suggest that the patchy migmatites formed by fluid-present, equilibrium partial melting of plagioclase+quartz+biotite, leaving a residue dominated by hornblende and plagioclase. The melts in the patchy migmatites apparently underwent fractional crystallization of hornblende+plagioclase+biotite, with the hornblende-rich patches and dikes representing accumulations of these phases and fractionated melts, respectively. In addition, the zoning in the dikes with feldspar-rich

rims and quartz-rich centers suggest that the melts underwent fractional crystallization of feldspar after separation from the patches. This interpretation is tested in Fig. 3.17 using trace element modeling. The modeling is done in three stages: stage 1 models partial melting of the dioritic mesosome leaving a hornblende-plagioclase dominated residue, producing the 'original' melt (30% melting); stage 2 models fractional crystallization in the patches and involves fractional crystallization of the 'original' melt with hornblende and plagioclase as the main fractionating phases; stage 3 models fractional crystallization of the melt after it has separated from the patches and collected in the dikes. Partition coefficients are given in Table 3.2; note that the partition coefficients for REEs in hornblende are 19-56% smaller than used in the previous modeling in this chapter. The reason for using a different set of partition coefficients is that although a difference of 19-56% does not significantly influence the results for each stage of the model, the accumulated effects are significant for the second and third stage. Both sets of partition coefficients are appropriate for granitic melts.

Stage 1 - Equilibrium melting of dioritic mesosome

The first stage of the model involves equilibrium batch melting of the average dioritic mesosome. Model melts produced by 10, 30, and 50% partial melting, and model restites produced by 30 and 50% partial melting are compared to the compositions of the patchy leucosomes and patchy melanosomes, respectively (Fig. 3.17a). The resite consists dominantly of hornblende and plagioclase, with small amounts of biotite and trace amounts of zircon and allanite (see Fig. 3.17 for details). The model melts resemble the least silicic, most REE-rich patchy leucosomes with the exception that the model melts have slightly positive Eu anomalies in contrast to the slightly negative Eu anomalies observed in the leucosomes. The model restite is similar to the patchy melanosome in composition, except for the modeled Eu anomalies, which are slightly less negative in the model restite. The modeled Eu anomalies are strongly dependent on the Eu anomaly of the source. The dioritic mesosome has an average $(Eu/Eu^*)_N$ of 0.73, but ranges between 0.56 and 0.79, and selecting a starting composition with a lower $(Eu/Eu^*)_N$ would produce a better fit between model melt/resite and patchy

leucosome/melanosome. The calculation presented in Fig. 3.18 shows that the major element composition of the model restite is similar to the patchy melanosomes. The model melt produced by 30% partial melting was used as the 'original' melt in stage 2.

Stage 2 - Fractional crystallization in the patches

Stage 2 models equilibrium fractional crystallization of the 'original' melt produced in stage 1, fractionating hornblende and plagioclase along with small amounts of biotite and trace amounts of zircon and allanite (Fig. 3.17b). The model melts produced by 10-60% fractional crystallization resemble the silicic patchy leucosomes; in particular, the total REE contents decrease with increasing fractionation, Eu anomalies become more positive, and Ba and Rb increase. Thus, many of the patchy leucosomes appear to represent fractionated melts, rather than melts formed directly by partial melting of the dioritic mesosome. The model cumulates are compositionally similar to the hornblende-rich patches, except for the negative Eu anomaly of the patches that is not reproduced in the model. Selecting a different starting composition in stage 1 would have yielded a better fit for Eu, but is unlikely to be the sole reason for the observed discrepancy. The LREE and HREE contents of the model cumulate depend largely on the amount of allanite and zircon in the fractionating assemblage; in contrast, the MREE contents are largely determined by the major phases, and suggest that the hornblende-rich patches represent accumulations of hornblende+plagioclase+biotite mixed with 10-50% melt. The calculation in Fig. 3.19 is consistent with the trace element modeling and field observations, suggesting that the hornblende-rich patches consist of accumulations of cumulate hornblende+plagioclase+biotite mixed with ca. 40-50 wt.% melt (patchy leucosome).

Stage 3 - Fractional crystallization in the dikes

The third stage of the model simulates fractional crystallization of the melt in the dikes, after it separated from the patches. The field observations and petrographic data suggest fractionation of feldspar; samples with strongly positive Eu anomalies are enriched in K_2O and depleted in Na_2O+CaO relative to other dike samples, suggesting accumulation of K-feldspar and lesser amounts of plagioclase. The starting composition
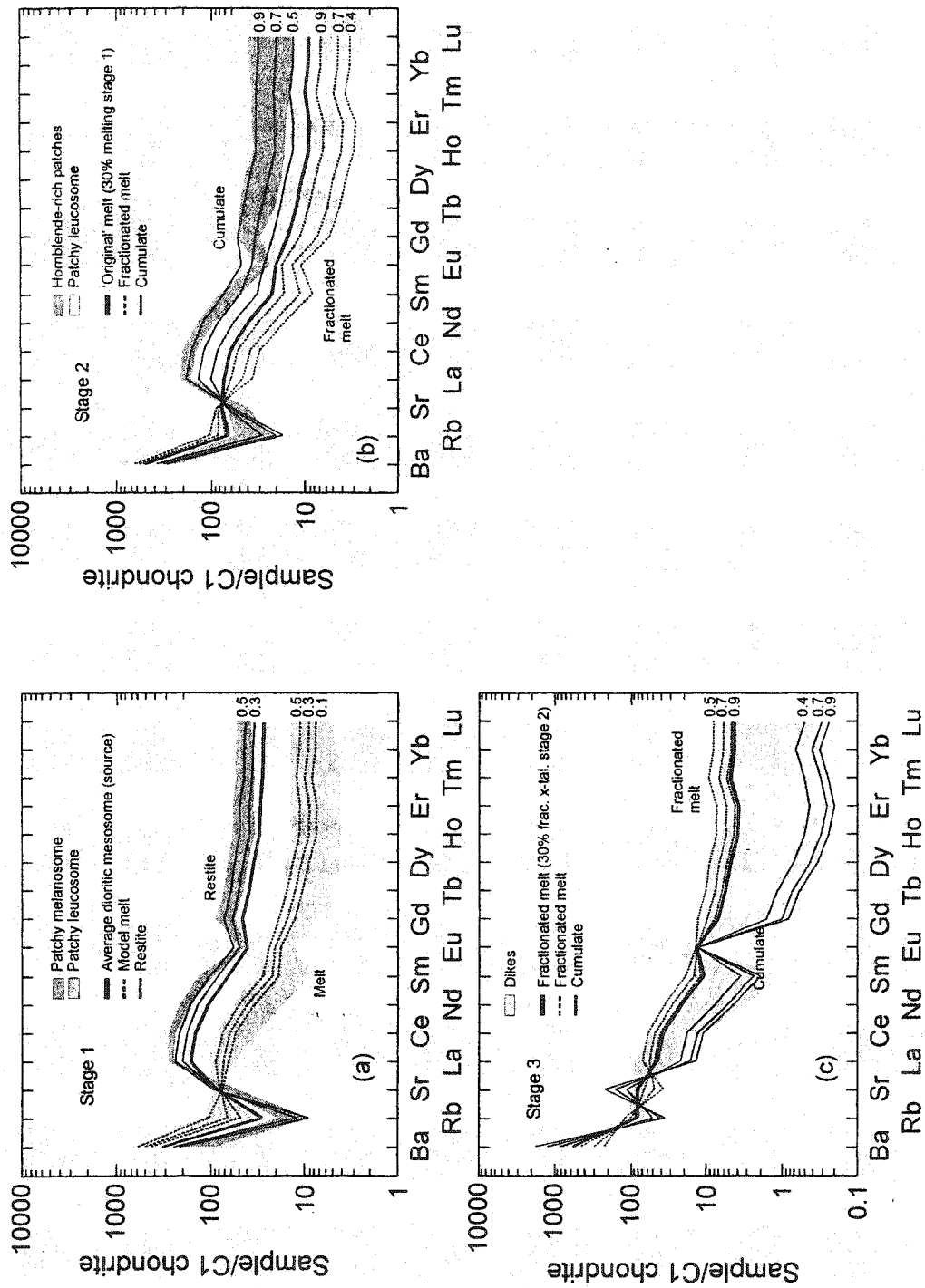
Fig. 3.17 Trace element modeling, patchy migmatite. (a) Stage 1, partial melting dioritic mesosome. Residue (wt.%): Hbl (53), Pl (41), Bt (5), Zrn (0.6), Aln (0.2). (b) Stage 2, fractional crystallization, hornblende-rich patches. Cumulate (wt.%): Hbl (66), Pl (26), Bt (7), Zrn (0.8), Aln (0.3). (c) Stage 3, fractional crystallization, dikes. Cumulate (wt.%): Kfs (59), Pl (36), Bt (6), Aln (0.02).
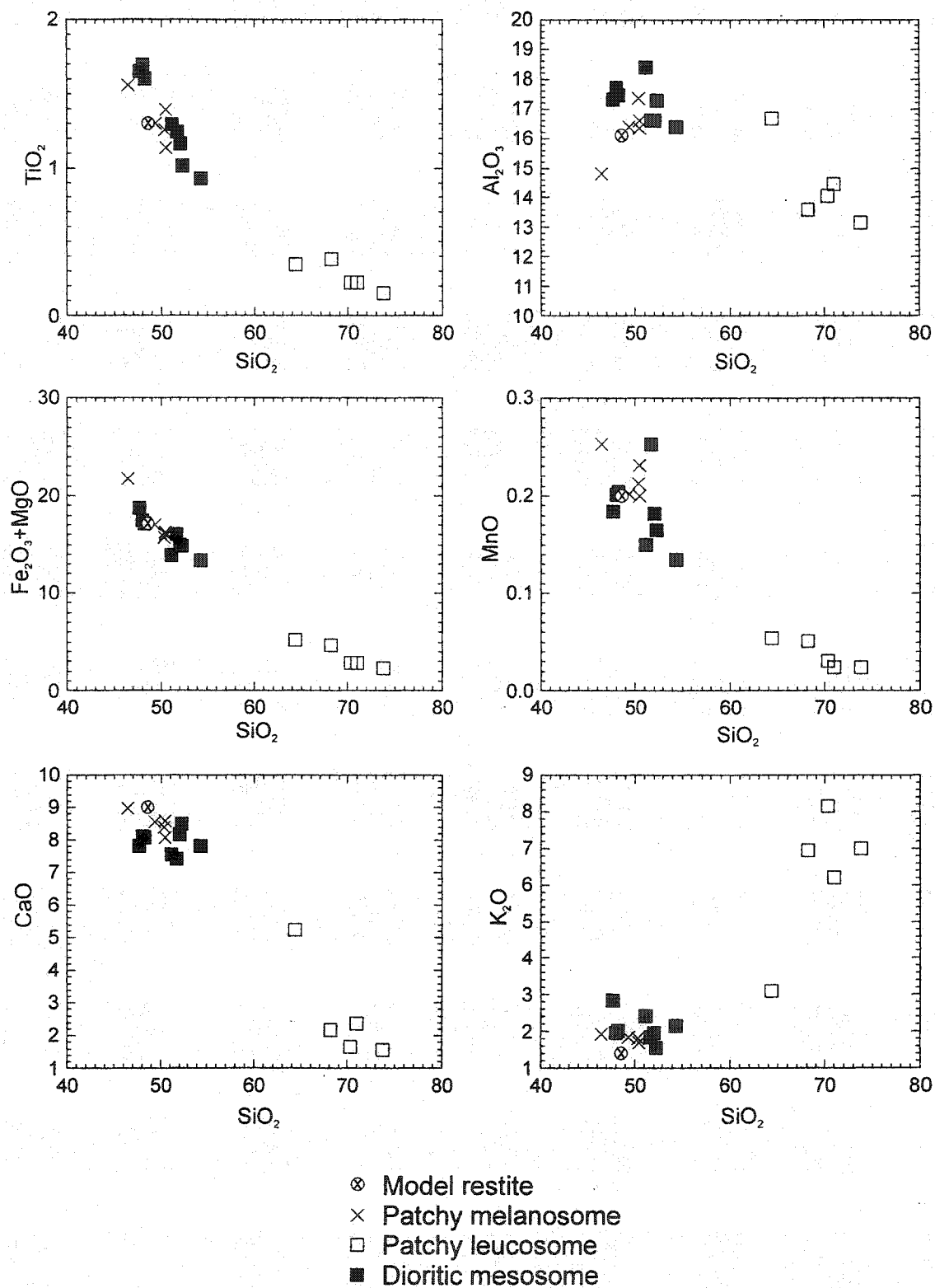
Fig. 3.18 Model restite, patchy migmatite, Hbl (53 wt.%), Pl (41 wt.%), Bt (5 wt.%).
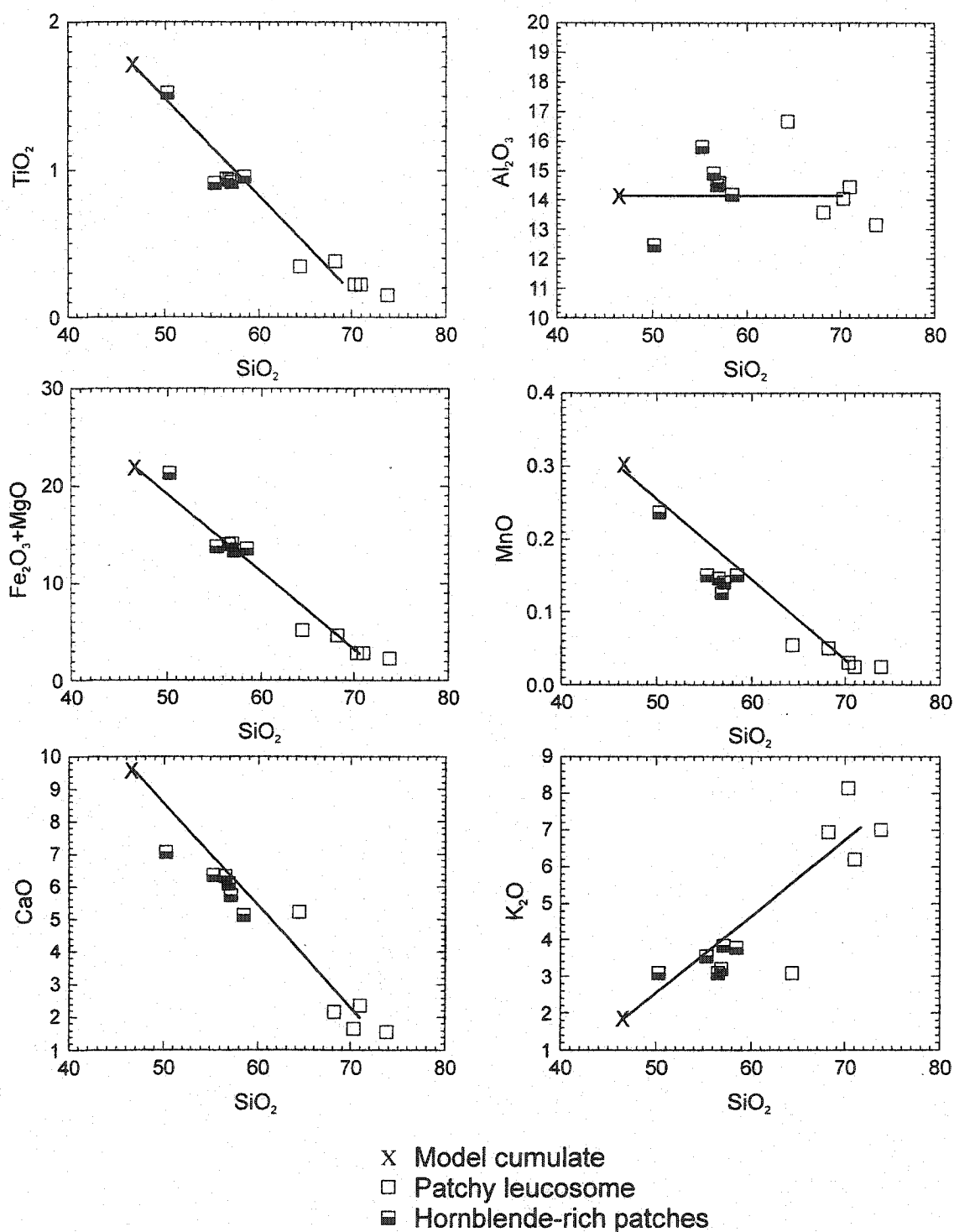
Fig. 3.19 Model cumulate, patchy migmatite, Hbl (67 wt.%), Pl (26 wt.%), Bt (7 wt.%).

in stage 3 is the fractionated melt from stage 2, formed by 30% fractional crystallization. The dominant fractionating phases are K-feldspar and plagioclase, with minor biotite and trace amounts of allanite (Fig. 3.17c). The model cumulates produced by 10-60% fractional crystallization are similar to the samples from the dikes with the lowest REE contents and most positive Eu anomalies, whereas the model melts are similar to the samples with higher REE contents and straighter REE patterns. This result is consistent with feldspar-dominated fractional crystallization in the dikes.

3.9. Conclusions

The following conclusions can be made based on the field, petrographic, and geochemical data presented above:

- The Muskoka domain migmatites appear to display a relationship between leucosome morphology, leucosome composition, and deformation. The patch-like geometry and random distribution of leucosomes in the patchy migmatites and the observation that stromatic migmatites wrap around smaller bodies of patchy migmatite are compatible with the interpretation that their dioritic host rocks were stronger than the surrounding highly migmatitic granodiorites.

- The concordant leucosomes in the granodioritic gneisses may represent disequilibrium melts, although the evidence for disequilibrium melting is debatable. In contrast, the patchy migmatites in the dioritic gneisses probably formed by equilibrium melting and were later modified by fractional crystallization of hornblende and feldspars. We ascribe the apparent differences in melting reaction to different degrees of syn-melting deformation; the rate of deformation-induced melt segregation in the stromatic migmatites outpaced the rate of diffusion in the residue, producing disequilibrium melts, and *vice versa* for the patchy migmatites.

- Melting in both types of migmatite probably involved incongruent, fluid-present biotite breakdown. The composition of the hypothetical fluid is unconstrained in the absence of isotopic and fluid-inclusion data, but a mixed H_2O-CO_2 fluid appears most likely. The fluids may have been K_2O-rich, possibly explaining the large

excess of K_2O suggested by mass balance calculations.

4. Migmatites and granite-pegmatite in the Shawanaga domain

4.1. Introduction and geological background

Previous mapping along the shores of Georgian Bay by Culshaw *et al.* (1988, 1989, 1990) identified extensive areas of migmatitic ortho- and paragneisses, with highly migmatitic rocks predominating in the southern Shawanaga domain, close to the overlying Parry Sound domain (Figs. 4.1 and 4.2). Culshaw *et al.* (1988, 1989, 1994) and Culshaw and Dostal (1997, 2002) divided the Shawanaga domain into five units or gneiss associations (Fig 4.1). The lowermost unit is the Shawanaga pluton, lying partly within the Shawanaga shear zone. Overlying the Shawanaga pluton are the Ojibway and Sand Bay gneiss associations, comprising dominantly ortho- and paragneisses, respectively. The ages of the Ojibway and Sand Bay gneiss associations have been determined at ca. 1460 and 1360 Ma, respectively (T. E. Krogh, unpublished data), and Culshaw *et al.* (1994) interpreted the contact to represent a deformed unconformity or décollement. The two uppermost units of the Shawanaga domain are the Lighthouse gneiss association, comprising dominantly pelitic/psammitic gneisses and amphibolites (Culshaw and Dostal, 2002), and the 'marginal orthogneiss', a megacrystic granitoid orthogneiss dated at 1346+69/-39 Ma (van Breemen *et al.*, 1986). Of these five units, only the Ojibway and Sand Bay gneiss associations are considered in detail here. The 'marginal orthogneiss' and Shawanaga pluton were discussed briefly in Chapter 2.

The Shawanaga domain is bounded below and above by ductile shear zones. The lower boundary against the Britt domain is marked by the shallow to moderately dipping Shawanaga shear zone (Culshaw *et al.*, 1994; Ketchum *et al.*, 1998). The Shawanaga shear zone contains dominantly top-to-southeast extensional kinematic indicators, and dating of pre- or syn-kinematic (1042 Ma), late syn-kinematic (1019 Ma), and post-kinematic (988 Ma) pegmatite dikes (Ketchum *et al.*, 1998) suggests extensional shear at ca. 1020 Ma. Thus extension on the Shawanaga shear zone post-dated peak metamorphism (at ca. 1090-1050 Ma, see below) by 10-30 My (cf., Tuccillo *et al.*, 1992). Evidence of thrusting along the Shawanaga shear zone comes from thrust-sense

127

kinematic indicators preserved along strike further inland where extensional shear fabrics are less penetrative (Ketchum, 1995), and from tectonostratigraphic evidence such as absence/presence of mafic dikes and ages of metaigneous rocks and metamorphism (Culshaw *et al.*, 1994). The age of thrusting on the Shawanaga shear zone is unknown but geochronological data discussed in Chapter 5 may indicate thrusting at ca. 1090 Ma. The upper boundary, between the Shawanaga and Parry Sound domains, is marked by the basal Parry Sound shear zone, which is a very wide (several hundred meters thick) zone of high strain fabric. The basal Parry Sound shear zone was interpreted by Culshaw *et al.* (1994) and Wodicka (1994) as a cryptic thrust overprinted by a discrete extensional shear zone. Thrusting on the basal Parry Sound shear zone probably took place at ca. 1120 Ma (Wodicka, 1994; Krogh, 1997), whereas the timing of extension may be similar to extension on the Shawanaga shear zone, indicated by titanite cooling ages in the footwall (Wodicka, 1994; Ketchum, 1995).

Although there is tenuous evidence for a ca. 1120 Ma event in the Shawanaga domain (Tuccillo *et al.*, 1992; Wodicka, 1994; Bussey *et al.*, 1995), the main phase of metamorphism and deformation took place between ca. 1090 and 1050 Ma (Krogh *et al.*, 1993a; T. E. Krogh, unpublished data; Wodicka *et al.*, 2000; Chapter 5), and involved partial melting at ca. 1082 Ma (T. E. Krogh, unpublished data). P-T estimates for this stage of metamorphism are 1050-1100 MPa and 830°C for the uppermost structural level of the Shawanaga domain (Lighthouse gneiss association), and 750-850 MPa and 685-700°C for the structurally lower Ojibway gneiss association (Wodicka *et al.*, 2000). Sillimanite-grade conditions were maintained until at least ca. 1020 Ma (Wodicka *et al.*, 2000). Ketchum *et al.* (1998) obtained U-Pb titanite ages of 1028-1018 Ma from the Shawanaga domain, and, because metamorphic temperatures in the Shawanaga domain exceeded the closure temperature of titanite, Wodicka *et al.* (2000) argued that the initial stages of decompression and cooling must have occurred prior to extensional displacement along the Shawanaga shear zone at 1020 Ma. This interpretation requires that extension on the Shawanaga shear zone did not commence until ca. 1020 Ma, which cannot be excluded based on the existing data (Ketchum *et al.*, 1998).
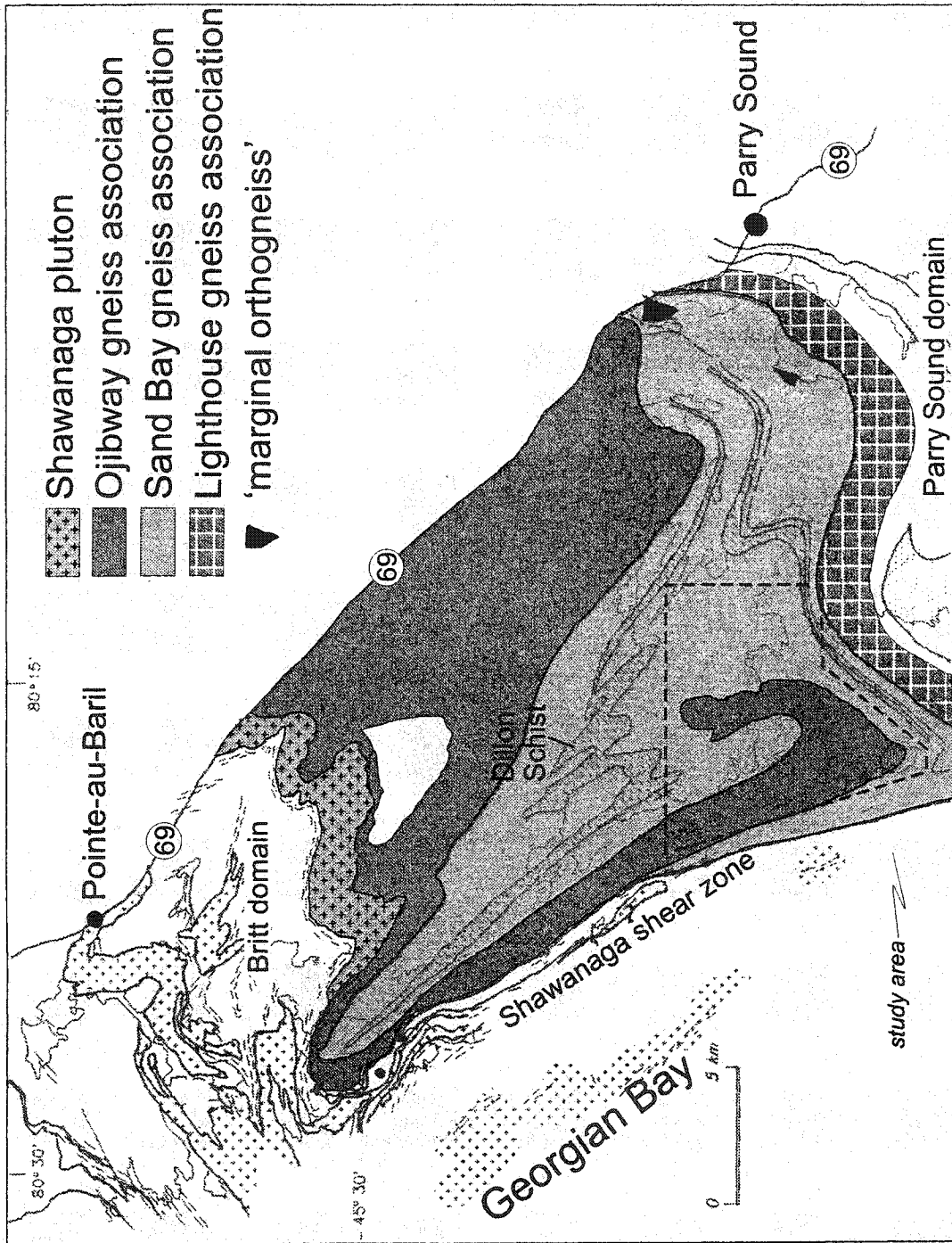
Fig. 4.1 Simplified map of southern Shawanaga domain. Modified after Culshaw *et al.* (1994).
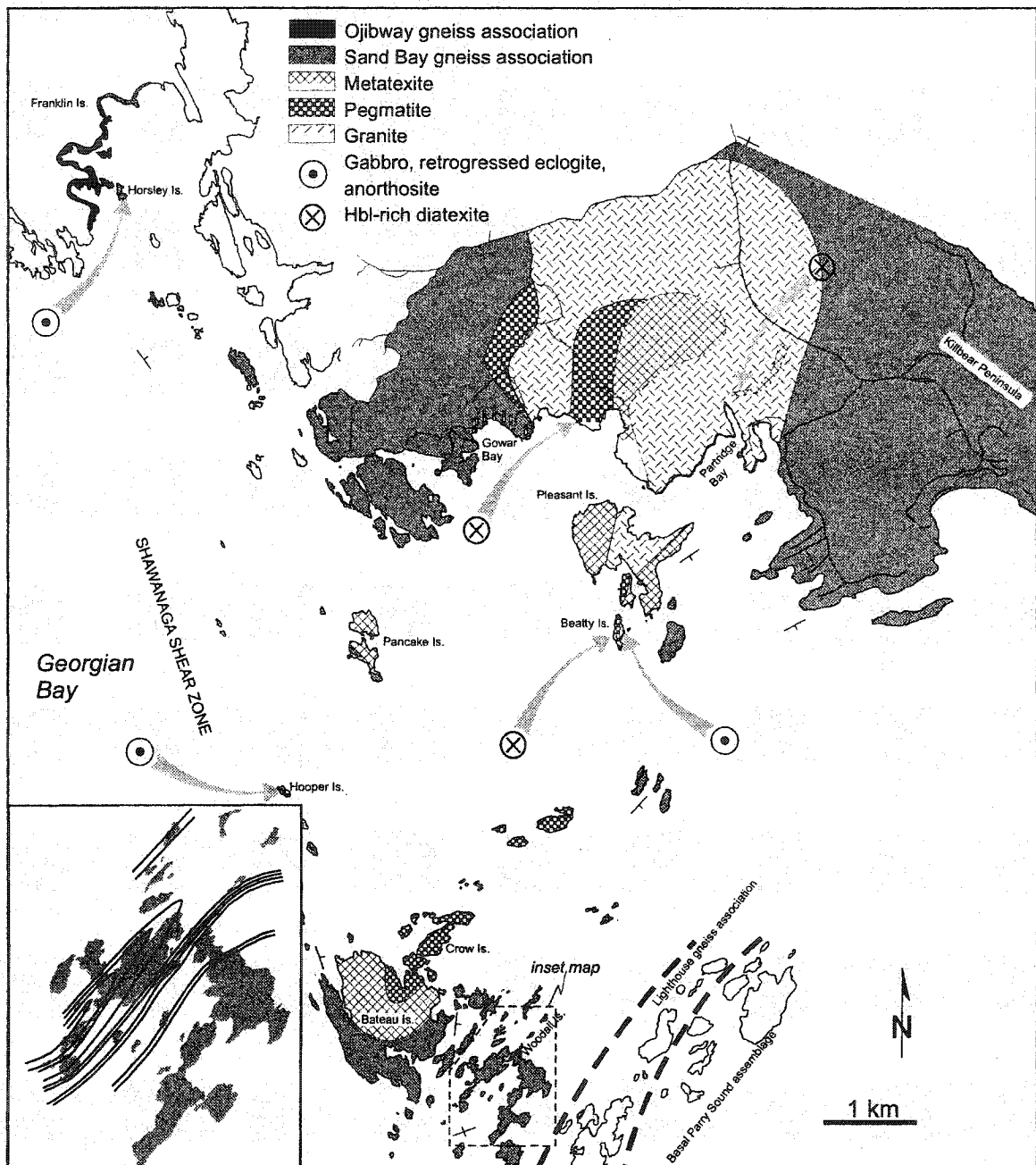
Fig. 4.2 Map of southwestern Shawanaga domain (study area). Inset map from Woodall Island shows how much of the original stratigraphy is affected by isoclinal folding. The Woodall Island pegmatite dikes are dominantly located within the area outlined by the inset map.

Culshaw *et al.* (1989, 1994) interpreted the highly migmatitic rocks in southern Shawanaga domain to represent orthogneisses of the Ojibway gneiss association, and the contact with less migmatitic Sand Bay gneisses was interpreted to define the closure of a large, early fold, refolded about northwest-trending axes (Fig. 4.1). Culshaw *et al.* (1989, 1994) suggested that the early fold formed as a result of early orogenic convergence, whereas the refold was related to late-orogenic extensional shear.

4.2. Geology of the southern Shawanaga domain

4.2.1. Sand Bay gneiss association

In the investigated area (Fig. 4.2), the Sand Bay gneiss association consists of a layered assemblage, with variable proportions of fine-grained, pink rhyolitic and gray quartzofeldspathic gneisses (Fig. 4.3a). Culshaw and Dostal (1997) interpreted the former to represent rhyolites based on compositional data (see Chapter 2). Geochemical data, discussed below, and geochronological data, discussed in Chapter 5, suggest that the gray quartzofeldspathic gneisses could represent detritus from the protoliths to the Ojibway gneiss association. The present thickness of individual pink and gray layers varies from several hundred meters to less than a meter, but, considering the large amounts of strain recorded in the investigated rocks (Culshaw *et al.*, 1994), original stratigraphic thicknesses must have been significantly greater. Detailed mapping in well exposed areas reveals that much of the original stratigraphy is affected by isoclinal folding (Fig. 4.2 inset). In addition to pink rhyolitic and gray quartzofeldspathic gneisses, the Sand Bay gneiss association comprises lesser amounts of gray plagioclase-quartz-biotite gneiss (Dillon schist, Culshaw *et al.*, 1989) and minor calc-silicate, quartzite, and amphibolite. Outside the main study area, for example on Killbear Peninsula (Fig. 4.2) and south of Point-au-Baril (Fig. 4.1) (Culshaw and Dostal, 1997), pink rhyolitic gneiss predominates.

Detrital zircons from quartzites in the Sand Bay gneiss association yield ages ranging from >2000-1382 Ma (T. E. Krogh, unpublished data), indicating a Laurentian source. Recent work in the lower Lighthouse gneiss association reached a similar

conclusion (Raistrick, 2003). Detrital zircons from the Dillon schist suggest that a proximal, ca. 1364 Ma, volcanic source contributed some of the detritus (T. E. Krogh, unpublished data); Culshaw and Dostal (1997) inferred a depositional age of ca. 1360 Ma for the Sand Bay gneiss association.

4.2.2. Ojibway gneiss association

The Ojibway gneiss association was not a primary target of this study and is discussed only briefly. The Ojibway gneiss association is dominated by gray, migmatitic, upper amphibolite-facies dioritic to granodioritic orthogneiss (Culshaw *et al.*, 1994; Chapter 2) and extends southeastward to within a few kilometers of the Parry Sound domain (Culshaw *et al.*, 1994). Petrographically, geochemically, and in terms of migmatite morphology, the Ojibway gneiss association is similar to the Muskoka domain, as described in Chapters 2 and 3. The migmatites are generally stromatic and leucosome abundances range between 15 and 35 vol.%. However, the general increase in leucosome abundance within the Ojibway gneiss association from northwest to southeast suggested by Culshaw *et al.* (1989) was not confirmed during this study.

4.3. Migmatite, granite, and pegmatite in southern Shawanaga domain

The focus of the work in this area was a distinct, spatially associated group of highly migmatitic gneisses (metatexites and diatexites), granite, and pegmatite. The terminology used below to describe the migmatites is after Ashworth (1985). Metatexite and diatexite were defined by Brown (1973) as migmatites that do and do not, respectively, preserve pre-migmatite layering, foliation, and/or banding.

4.3.1. Metatexites

In most places, the metatexites contain high proportions of white to pink, hornblende-rich leucosome, typically strongly deformed (Fig. 4.3b, c). The metatexites generally cannot be separated into leucosome-mesosome-melanosome components, and the proportion of leucosome in the metatexites is difficult to estimate because of high, post- and syn-crystallization strain and generally large leucosome abundances. A rough estimate of leucosome proportions suggests in excess of 40-50 vol.% leucosome, and

locally the metatexites grade into hornblende-rich diatexite (see below).

Strongly deformed rocks on Pancake Island (Fig. 4.2), immediately above the Shawanaga shear zone, show a nearly complete transition from sparsely to moderately migmatitic, interlayered pink and gray Sand Bay gneisses, to metatexite, the latter locally preserving a strongly disrupted, pink and gray layering (Fig. 4.3c), and rare, rotated calc-silicate fragments (Fig. 4.3d). In several other localities, enclaves that can be correlated with Sand Bay gneiss association lithologies, in particular the interlayered pink and gray quartzofeldspathic gneiss, are associated with the metatexites. The protolith to the metatexites is, therefore, interpreted as Sand Bay gneiss, in particular the gray quartzofeldspathic gneiss. SHRIMP dating of a hornblende-rich leucosome from the north end of Pleasant Island (Fig. 4.2) (Chapter 5) revealed a dominant population of inherited cores with an age of ca. 1450 Ma, and two younger cores at ca. 1410 and 1350 Ma. These geochronological data are consistent with the geochemical data, discussed below, suggesting that the ca. 1450 Ma protoliths of gray orthogneisses of the Ojibway gneiss association could have been the main source of the gray quartzofeldspathic Sand Bay gneiss. The younger cores probably reflect minor input from younger volcanic sources.

In some outcrops, the hornblende-rich leucosomes are folded by open to tight folds with southeast-plunging axes. Associated with many of these folds are small, axial-planar top-to-southeast, leucosome-bearing shear bands (Fig. 4.3e). Similar leucosome-bearing shear-bands have commonly been reported from other migmatite terranes, and are generally interpreted to represent melt migration structures (Brown, 1994b; Oliver *et al.*, 1999; Chapter 3). On Beatty Island (Fig. 4.2), these shear bands end in discordant, meter-sized patches of medium- to coarse-grained granite with very little hornblende. I interpret this observation to suggest that melts segregated from the hornblende-rich leucosomes, migrated along the shear bands, and collected in the hornblende-poor granitic patches. The relatively low hornblende content in the granitic patches contrasts with its abundance in the associated hornblende- rich leucosomes, suggesting that melt-residue separation was highly effective. It is commonly held that differential stress is an
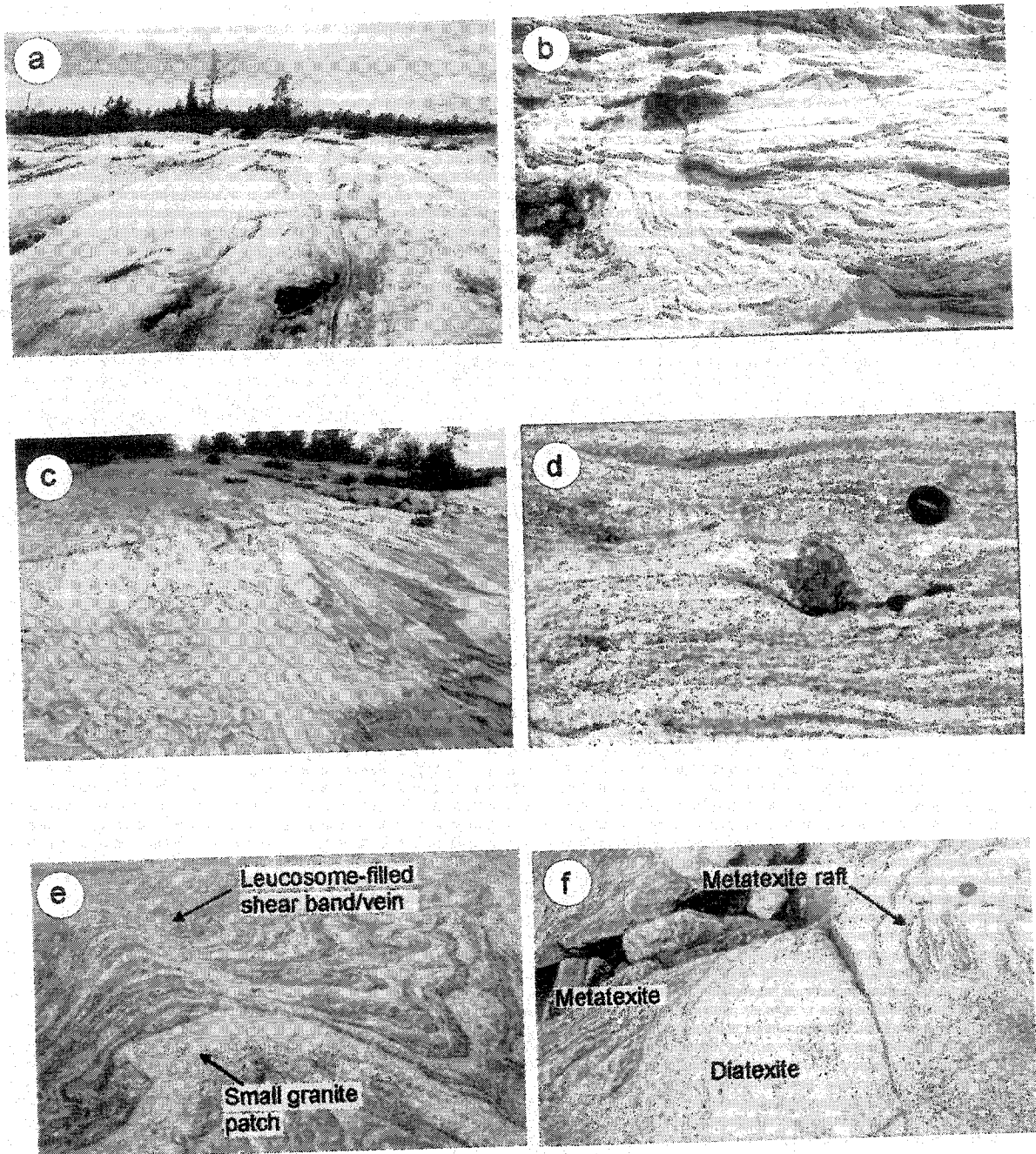
Fig. 4.3 (a) Interlayered pink and gray Sand Bay gneiss, Franklin Island. (b) Metatexite with abundant hornblende-rich leucosome, Richard's Bay. (c) Metatexite, preserving strongly disrupted pink and gray layering, Pancake Island. (d) Rotated calc-silicate fragment in metatexite, Pancake Island. (e) Leucosome-filled shear band or vein, possibly indicating syn-tectonic melt migration, Beatty Island. (f) Raft of metatexite 'floating' in hornblende-rich diatexite, Beatty Island.
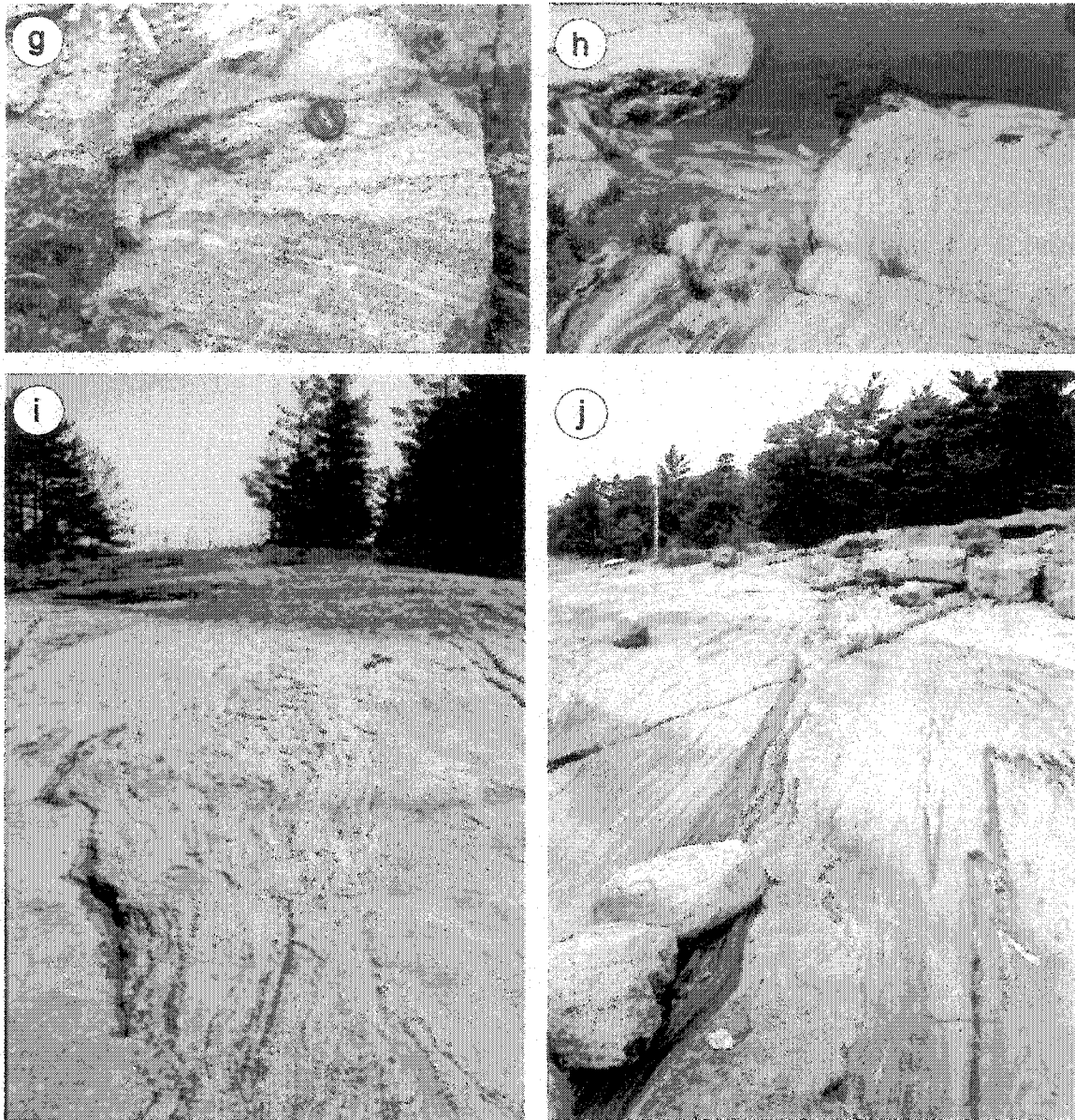
Fig. 4.3 continued. (g) Granite sheets, cutting strong fabric and older leucosome in Sand Bay gneiss, Partridge Bay. (h) Example of disaggregation of enclave into pegmatite, Crow Island. (i) Schlieren in pegmatite, Pleasant Island. (j) Folded and boudinaged pegmatite dikes cutting relatively strong fabric in Sand Bay gneiss, Gowar Bay.
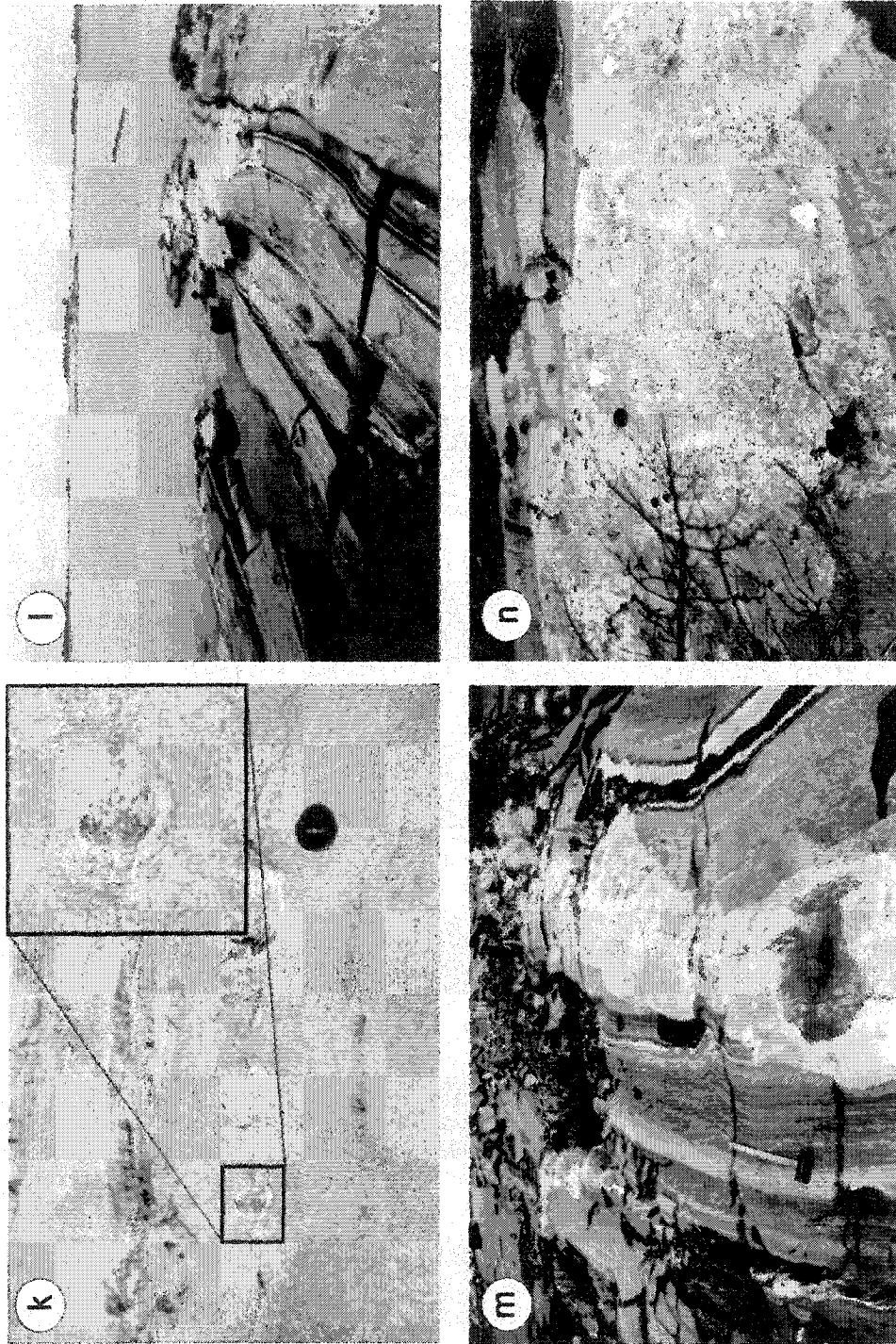
Fig. 4.3 continued. (k) Top-to-northeast (sinistral) kinematic indicators in Sand Bay gneiss association, Gowar Bay. Foliation 326/vertical, fold axes plunging shallowly (difficult to measure) toward 170-175°. (l) and (m) Woodall Island pegmatite dikes cutting fabric in Sand Bay gneiss. (n) Folded and boudinaged Woodall Island pegmatite dikes, cutting fabric in Sand Bay gneiss.

important driving force for melt segregation and that heterogeneous deformation, indicated for example by the development of boudins and shear bands, can provide low-pressure sinks into which melts can flow (Sawyer, 1994; Brown *et al.*, 1995; Rutter and Neumann, 1995). Brown (1994a) considered this process to be highly effective in producing leucosomes with little restite component, consistent with the above observations.

Hornblende in the leucosomes defines a weak lineation parallel to the southeast-plunging fold axes, suggesting that deformation continued beyond leucosome formation and crystallization. Similar metatexites south of the Parry Sound domain, in the Upper Go Home domain (Culshaw *et al.*, 1990; this study), suggest that highly migmatitic rocks extend beneath the Parry Sound domain.

4.3.2. Hornblende-rich diatexite

Hornblende-rich diatexites are locally intimately associated with the metatexites. The hornblende-rich diatexites are relatively rare and appear to be confined to random 'patches' or small bodies ranging from a few meters up to several tens of meters across, too small to be mapped on the scale of this study (Fig. 4.2). The transition from metatexite to hornblende-rich diatexite takes place over a few decimeters and appears to be related to an increasing melt proportion in the latter. Locally, rafts of metatexite appear to 'float' in the hornblende-rich diatexite (Fig. 4.3f) and the diatexites typically cut across hornblende-rich leucosome in the metatexite, suggesting that the diatexite behaved as a magma.

4.3.3. Granite

The granites are medium- to coarse-grained and contain significantly fewer, but similar, enclaves and schlieren than the pegmatites (discussed below). Although relatively homogeneous, they locally contain scattered pegmatitic K-feldspar crystals (5-10 cm) and pegmatitic pockets (<1 m). Granite predominates in the northern part of the investigated area where it forms an irregular body or pluton several kilometers across. In addition, several smaller, irregular bodies or patches of granite grade into the pegmatites

in areas where the latter predominate.

The transition between pegmatite and granite takes place over a few meters, with decreasing proportions of pegmatitic K-feldspar crystals in the granite, rather than a gradual decrease in overall grain size. Placing the contact between pegmatite and granite on the basis of grain size is, therefore, subjective.

The contact between the granites and the Sand Bay gneiss association is poorly exposed. Granite dikes or sheets locally cut the same early fabric in pink and gray Sand Bay gneisses (Fig. 4.3g) that is cut by the pegmatites (see below).

4.3.4. Pegmatite

Heterogeneous pegmatite forms relatively large bodies and irregular sheets throughout the investigated area. The pegmatites comprise coarse-grained, K-feldspar-rich bodies with significant proportions of variably disaggregated enclaves and schlieren (Figs. 4.3h, i). The contact between sparsely to moderately migmatitic Sand Bay gneisses and pegmatite is well exposed along the shores of Gowar Bay (Fig. 4.2), where it is characterized by increasing proportions of pegmatitic dikes or sheets (Fig. 4.3j) over a distance of a few hundred meters, to the point where Sand Bay gneisses form small enclaves or disappear entirely. The pegmatite sheets typically cut an older fabric in the Sand Bay gneisses. The fabric is isoclinally folded and contains small amounts of leucosome, however, due to the sparsity of observable cross-cutting relationships between this fabric and the pegmatite and granite it is not clear whether the isoclinal folds and leucosomes formed prior to or after intrusions of the pegmatite and granite. Locally, within the early fabric, rotated pegmatite fragments (probably from an earlier generation of pegmatite) show a top-to-northeast sense of shear (Fig. 4.3k). The pegmatites generally carry a weak, shallow, southeast-plunging lineation, and are locally folded by southeast-trending isoclinal folds. Although there is a close spatial relationship between the metatexites and pegmatites, the latter do not appear to cut the metatexites, but rather form deformed sheets within them. Close to the Shawanaga shear zone, the pegmatites were strongly deformed in a solid state, indicated by the development of augen textures; thus, they crystallized prior to ca. 1020 Ma deformation along this shear zone.

The source to the granite and pegmatite could not be determined in the field. Enclaves and schlieren are common, particularly in the pegmatite, and in many cases are identifiable as Sand Bay gneiss (pink-gray layering ± calc-silicate/quartzite layers). I regard the enclaves as variably disaggregated and assimilated xenoliths rather than remnants of unmelted protolith, based on textural evidence discussed below. Evidence of disaggregation and assimilation of the enclaves and schlieren is ubiquitous (Fig. 4.3h). In less deformed pegmatites and granites, the schlieren are locally at high angles to the regional foliation, suggesting magmatic flow.

4.3.5. Woodall Island pegmatite dikes

A number of pegmatite dikes on Woodall Island (Fig. 4.2), in the southern part of the study area, display field characteristics similar to the pegmatite dikes in Gowar Bay. In order to distinguish these dikes from the pegmatites located between Bateau Island and Gowar Bay (Fig. 4.2), they are referred to as Woodall Island pegmatite dikes. The Woodall Island pegmatite dikes cut an older fabric containing sparse leucosome in the Sand Bay gneisses (Figs. 4.3l, m) and were boudinaged and later folded by tight to isoclinal, southeast-trending folds (Fig. 4.3n). The age of the Woodall Island pegmatite dikes is unconstrained, but is inferred to be similar to the pegmatites elsewhere in the area based on structural similarities to the pegmatite dikes in Gowar Bay.

4.4. Petrography and geochemistry

4.4.1. Analytical procedure

Major and trace elements were determined on fused glass beads and pressed powder pellets, respectively, using standard X-ray fluorescence (XRF) techniques at St. Mary's University, Halifax, Nova Scotia. Rare earth elements (REEs), Hf, and Th were determined by inductively coupled plasma-mass spectrometry (ICP-MS) using a Na_2O_2 sintering technique at Memorial University, St. John's, Newfoundland. Dostal *et al.* (1986) and Longerich *et al.* (1990) discussed the analytical procedures, uncertainties, and precision of the XRF and ICP-MS analyses, respectively (see also Appendix A). The geochemical data are presented in Appendix D. Mineral abbreviations used in the text

and figures are from Kretz (1983).

4.4.2. Ojibway and Sand Bay gneiss associations

The petrography and geochemistry of the orthogneisses in the Ojibway gneiss association and the pink rhyolitic gneisses in the Sand Bay gneiss association were briefly outlined in Chapter 2. This section is limited to discussing the gray quartzofeldspathic gneisses in the Sand Bay gneiss association.

The fine-grained, gray quartzofeldspathic gneisses in the Sand Bay gneiss association consist of plagioclase, K-feldspar, quartz, and biotite, with little or no hornblende (Table 4.1). Irregular muscovite and euhedral to subhedral epidote, typically associated with biotite, are common in small amounts (1-3 vol.%). Epidote is commonly cored by allanite. Other accessory phases include titanite, apatite, zircon, and rare carbonate. The gray quartzofeldspathic gneisses range in composition from 64 to 70 wt.% SiO_2 and resemble the gray orthogneisses in the Ojibway gneiss association and Muskoka domain with respect to most major and trace elements. Exceptions include Zr, Hf, and the MREEs and HREEs, which are lower in the gray quartzofeldspathic gneisses (Fig. 4.4). The REE patterns are moderately fractionated, with $(La/Yb)_N$ between 7.4 and 13.3, and moderately negative Eu anomalies $((Eu/Eu^*)_N=0.6-0.8)$. The compositional similarities between the gray orthogneisses in the Ojibway gneiss association and the gray quartzofeldspathic paragneisses could indicate that the latter represent detrital material derived from the protolith to the Ojibway gneisses. This interpretation is supported by the geochronological results (Chapter 5).

4.4.3. Metatexites

The hornblende-rich leucosomes are medium- to coarse-grained and comprise plagioclase, quartz, K-feldspar, and ≥20 vol.% hornblende. Biotite is rare. The mode of some representative samples is given in Table 4.1. Equant to slightly elongate, anhedral to subhedral hornblende defines a weak, shallowly southeast-plunging lineation. Plagioclase, biotite, and locally abundant euhedral to subhedral titanite are commonly included in the hornblende. Smaller amounts of titanite are also present in the leucosome matrix. Subhedral to euhedral epidote is common although volumetrically insignificant,

and mostly occurs as inclusions in hornblende. The epidote is typically cored by allanite, and allanite also occurs alone as inclusions in hornblende.
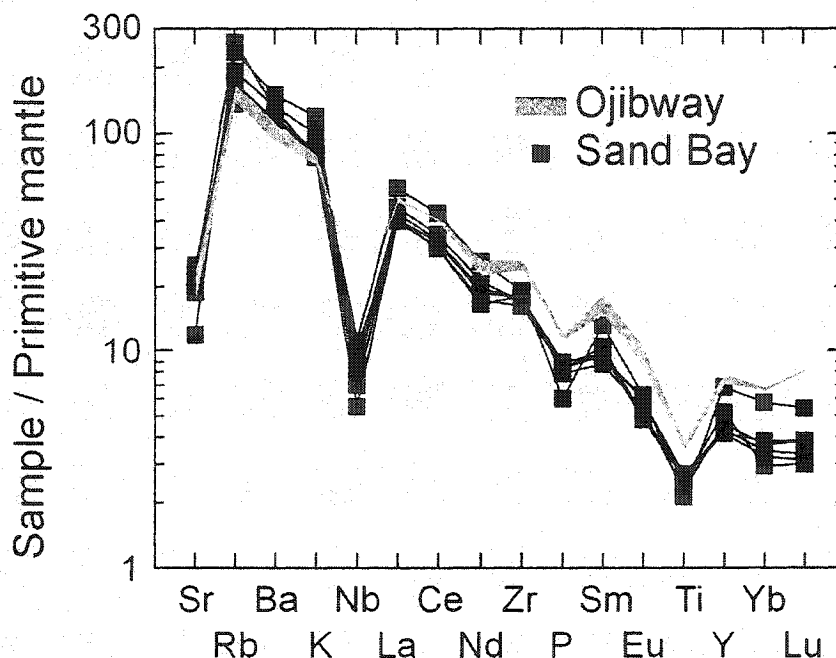
Fig. 4.4 Primitive mantle-normalized diagram comparing the composition of the gray, quartzofeldspathic Sand Bay gneiss with the Ojibway gneiss association.

The hornblende-rich leucosomes range in SiO_2 from 61 to 70 wt.%, and most major elements decrease with increasing SiO_2, except K_2O, which increases. Barium and Rb are also positively correlated with SiO_2, whereas the other trace elements are independent of SiO_2 (Fig. 4.5a-d). The REE patterns (Fig. 4.5f) are variable, ranging from slightly LREE-depleted to LREE-enriched ($(La/Yb)_N$=0.2-2.6), with small to moderate negative Eu anomalies ($(Eu/Eu^*)_N$=0.5-0.9). The variation in REE fractionation is not correlated with any major or trace elements, whereas Eu anomalies become more negative with increasing K_2O, Ba, and Rb, and broadly more positive with increasing CaO. Total REE contents increase with increasing P_2O_5, Y, Zr, Nb, Th, and Hf (Fig. 4.5e), suggesting that the REEs are hosted by accessory phases such as zircon, allanite, and apatite. Several of the hornblende-rich leucosomes are enriched in MREEs, a feature compatible with accumulation of hornblende (cf., Arth and Barker, 1976).

The granitic patches on Beatty Island are medium- to coarse-grained, comprising

K-feldspar, quartz, and plagioclase with minor hornblende, biotite, and epidote. Accessory phases include titanite, apatite, zircon, and allanite. The granitic patches are slightly more silicic than the most silicic hornblende-rich leucosomes and hornblende-rich diatexites (Fig. 4.5), with highly variable REE contents (Fig. 4.5g) apparently controlled by accessory phases.

4.4.4. Hornblende-rich diatexite

A close association between the metatexites and hornblende-rich diatexite is apparent from the field observations, and is corroborated by the petrographic and geochemical data. Petrographically, the hornblende-rich diatexites are slightly coarser-grained, with overlapping to slightly lower proportions of hornblende than the hornblende-rich leucosomes (Table 4.1). Hornblende is texturally similar in the two rock types. Geochemically, the hornblende-rich diatexites are similar to and span the same range as the hornblende-rich leucosomes, although the hornblende-rich diatexites are generally more silicic than the hornblende-rich leucosomes (Fig. 4.5), interpreted to indicate slightly higher melt proportions in the diatexites.

4.4.5. Granite

The granites are generally coarse- to medium-grained, and consist of K-feldspar, quartz, and plagioclase. Mafic phases are sparse and include magnetite or magnetite-ilmenite intergrowths, biotite, and titanite. Other accessory phases include muscovite, zircon, and apatite. The granites typically carry a weak fabric defined in the field by biotite-rich schlieren; no fabric could be discerned petrographically.

The granites contain between 71 and 79 wt.% SiO_2, and most major and trace elements plot in a cluster or display broad negative trends with increasing SiO_2. The A/CNK ratios (mole $Al_2O_3/(CaO+Na_2O+K_2O)$) range from 1.00 to 1.09. Total REE contents are variable, ranging from 6 to 204 ppm (Fig. 4.6a), $(La/Yb)_N$ ranges from 1-10, and total REE contents correlate positively with Fe_2O_3, P_2O_5, Y, Zr, Th, and Hf (Fig. 4.6e, f). A number of the samples have non-parallel, crossing REE patterns. Europium anomalies are moderately to strongly negative (($Eu/Eu^*)_N$=0.3-0.7), except for sample 2S19063, which has a positive Eu anomaly (Fig. 4.6d). In the Y+Nb vs. Rb

discrimination diagram of Pearce *et al.* (1984), the granites straddle the boundary between volcanic arc and syn-collision granite compositions.

4.4.6. Pegmatite

The pegmatites vary in grain size from 2 to 20 cm, but do not display any systematic spatial variation in grain size. The pegmatites classify as 'simple', dominated by K-feldspar, plagioclase, and quartz, with no discernible zoning on the scale of the granite-pegmatite pluton. Biotite is the dominant mafic phase, forming small clusters of needle- or lath-shaped grains reminiscent of textures in the gray quartzofeldspathic Sand Bay gneiss. Field evidence and textures suggest that the biotite may represent xenocrysts formed by disaggregation of enclaves of gray quartzofeldspathic Sand Bay gneiss. Consequently, biotite contents vary widely from 10-20 vol.% near former enclaves to accessory amounts in areas lacking enclaves and schlieren. These observations suggest that assimilation of country rocks took place by fracturing and digestion (e.g., Marsh, 1982) rather than by partial melting of the country rocks and incorporation of the melt into the magma. Titanite occurs in trace amounts and hornblende is generally lacking. Muscovite, apatite, and zircon occur as accessory phases; allanite was not observed.

The pegmatites display a narrow range in SiO_2 from 71.4 to 74.8 wt.%. Most major elements display no or broadly negative trends against SiO_2. A/CNK ratios range from 0.98 to 1.05, i.e., slightly lower than the granite. Total REE contents are low (<61 ppm) (Fig. 4.6b) and correlate positively with P_2O_5, Y, Zr, Th, and TiO_2 (Fig. 4.6e, f). Six of the 10 samples have no or a positive Eu anomaly (($Eu/Eu^*)_N$>0.99), whereas the other four have $(Eu/Eu^*)_N$ between 0.64 and 0.70 (Fig. 4.6d). I will refer to these two groups of pegmatite as the positive and negative Eu anomaly-group, respectively. The two groups of pegmatite have indistinguishable major element compositions, however, the negative Eu anomaly-group has slightly lower K_2O and higher total REE contents and Y, very similar to the granite. Like the granites, both groups of pegmatite are characterized by crossing REE patterns.

Table 4.1 Modes of selected representative samples, gray quartzofeldspathic gneiss, Ojibway gneiss association, hornblende-rich leucosome, and hornblende-rich diatexite.

Sample	Gray quartzofeldspathic gneiss				Ojibway gneiss association		Hbl-rich leucosome		Hbl-rich diatexite
	S16064-2	2S21067	2S21068	S17062-2	S31052-H	S11064-2	S20066-1	2S2006-3	2S19061
n	1000	1000	1000	1000	1000	1000	500	500	500
Qtz	26.0	20.8	22.7	23.5	24.5	11.8	11.2	19.0	31.4
Pl	39.6	40.0	49.2	46.7	47.3	53.5	51.2	46.2	43.2
Kfs	21.3	22.0	13.9	8.3	11.1	9.8	0.6	18.4	17.2
Hbl	0.1	acc.	acc.	2.1	2.7	7.2	30.6	14.0	5.4
Bt	10.6	16.6	11.9	17.9	11.7	15.5	2.2	acc.	2.2
Opaques	0.5								
Ttn	acc.	acc.	acc.	0.6	1.1	1.4 (?)	1.6	1.2	acc.
Ep	acc.	0.3	1.7	0.9	0.9	0.6	1.6	0.8	acc.
Ms	1.9								
Zrn	acc.	acc.	acc.	acc.	acc.	acc.	acc.	acc.	acc.
Ap	acc.	acc.	acc.	acc.	acc.	acc.	acc.	acc.	acc.
Aln	acc.		acc.		acc.	acc.	acc.	acc.	acc.
Carbonate	acc.	acc.	acc.		acc.	acc.	acc.		acc.

Acc=Accessory phase (<0.25 vol.%).
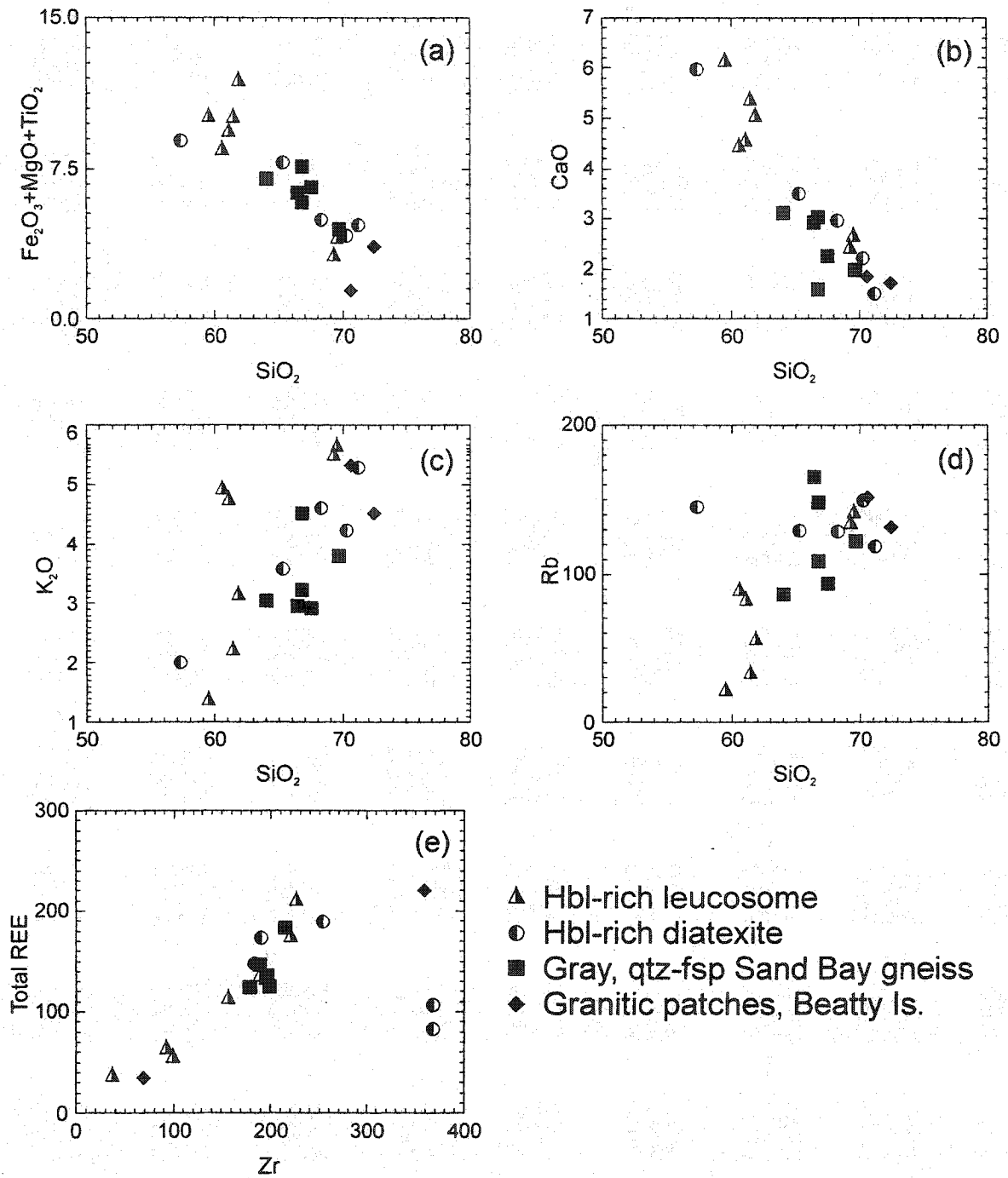
Fig. 4.5 Selected variation diagrams of hornblende-rich leucosome, hornblende-rich diatexite, gray quartzofeldspathic Sand Bay gneiss, and granitic patches on Beatty Island.
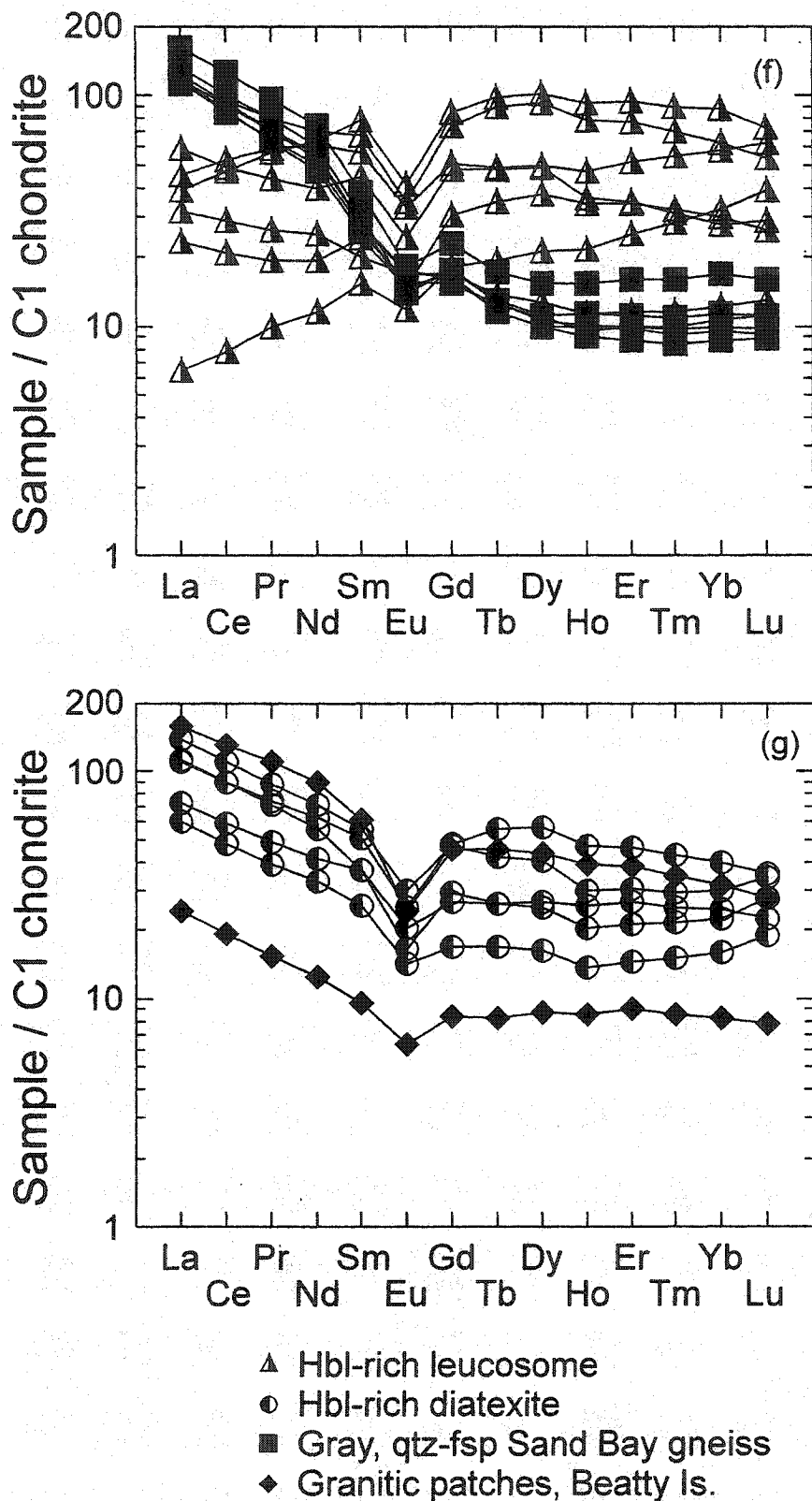
Fig. 4.5 continued. Chondrite-normalized REE plot of hornblende-rich leucosome, hornblende-rich diatexite, gray quartzofeldspathic Sand Bay gneiss, and granitic patches on Beatty Island. Chondrite normalization factors from Sun and McDonough (1989).

4.4.7. Woodall Island pegmatite dikes

The Woodall Island pegmatite dikes are petrographically similar to the pegmatites but are enriched in Rb, Y, Nb, Th, Pb, U, and HREEs, and depleted in CaO, Ba, Sr, and Zr relative to the pegmatite and granite (Fig. 4.6). The A/CNK ratios display a narrow range between 0.99 and 1.01. The Eu anomalies are strongly negative (($Eu/Eu^*)_N$=0.15-0.24).

4.5. Petrogenesis

4.5.1. Hornblende-rich leucosomes

The field observations suggest that the hornblende-rich leucosomes formed by partial melting of gray quartzofeldspathic Sand Bay gneiss. The large variation in leucosome abundance in these gneisses, from ca. 10-15 vol.% to ca. 50 vol.%, indicates significant differences in fertility. The gray quartzofeldspathic gneisses typically contain ca. 10 vol.% biotite and trace amounts of hornblende and titanite. In contrast, the hornblende-rich leucosomes contain only trace amounts of biotite, but significant proportions of hornblende and titanite (Table 4.1). Similar to the migmatites in the Muskoka domain (Chapter 3), rounded inclusions of biotite, plagioclase, and quartz are common in the hornblende. A possible interpretation is that the hornblende and titanite are residual after incongruent breakdown of biotite. Field observations and geochemical data (discussed below) indicate that the hornblende-rich leucosomes lost granitic melt and may be considered residual. The petrographic observations, therefore, suggest a melting reaction involving biotite, plagioclase, and possibly quartz, to produce granitic melt, hornblende, and titanite. Subsequent deformation-induced melt loss then formed leucosomes enriched in residual and cumulate phases, particularly hornblende.

4.5.2. Transition from metatexite to hornblende-rich diatexite

The transition from metatexite to hornblende-rich diatexite is well exposed on Beatty Island. Here, the metatexites grade into hornblende-rich diatexite containing rafts of the former, suggesting that the metatexites and diatexites behaved as rock and magma, respectively. The higher melt fraction in the diatexites may have resulted from either

higher degrees of partial melting (Brown, 1973), local redistribution of melts (Sawyer, 1998), or injection of externally derived melts (Greenfield *et al.*, 1996). Field evidence of melt extraction and local redistribution is common, and the extracted melt is probably best represented by the granitic patches on Beatty Island. The gray quartzofeldspathic Sand Bay gneisses, hornblende-rich leucosomes, hornblende-rich diatexites, and granite patches display linear relationships on major element variation diagrams, suggesting that they could represent protolith, melt-depleted magmas, melt-enriched magmas, and melt, respectively (Fig. 4.5). The straight, relatively well defined linear arrays are consistent with closed system (except for fluid) partial melting on the scale of the outcrop. Most hornblende-rich leucosomes plot on the low-SiO_2 side of the protolith, whereas most hornblende-rich diatexites have major element compositions similar to, but slightly more silicic than, the protolith. Thus, the field observations and geochemical data suggest that the hornblende-rich leucosomes formed by partial melting of gray quartzofeldspathic Sand Bay gneiss but lost much of their melt, probably as a result of deformation-assisted segregation. The hornblende-rich diatexites formed where the melt proportion were higher than in the metatexites, possibly exceeding the critical melt fraction (cf., Brown, 1994a; see also Chapter 3), probably as a result of melt injection from nearby hornblende-rich leucosomes (akin to 'closed-system melt redistribution' of Sawyer, 1998).

4.5.3. Pegmatite-granite relationship

Fractional crystallization

One of the most commonly proposed mechanisms to explain the origin of the parental liquids to granitic pegmatites is fractionation of less evolved granitic melts (e.g., Jahns and Burnham, 1969; Simmons *et al.*, 1987; Walker *et al.*, 1989). This model is based on the common spatial association between pegmatites and granites and on the observation that trace elements that are incompatible in granitic assemblages are commonly enriched in the pegmatites (Walker *et al.*, 1989). In the study area, the field observations suggest an intimate relationship between the granites and pegmatites, corroborated by the geochronological data (Chapter 5). However, the geochemical data are not compatible with formation of the pegmatites by fractional crystallization of a
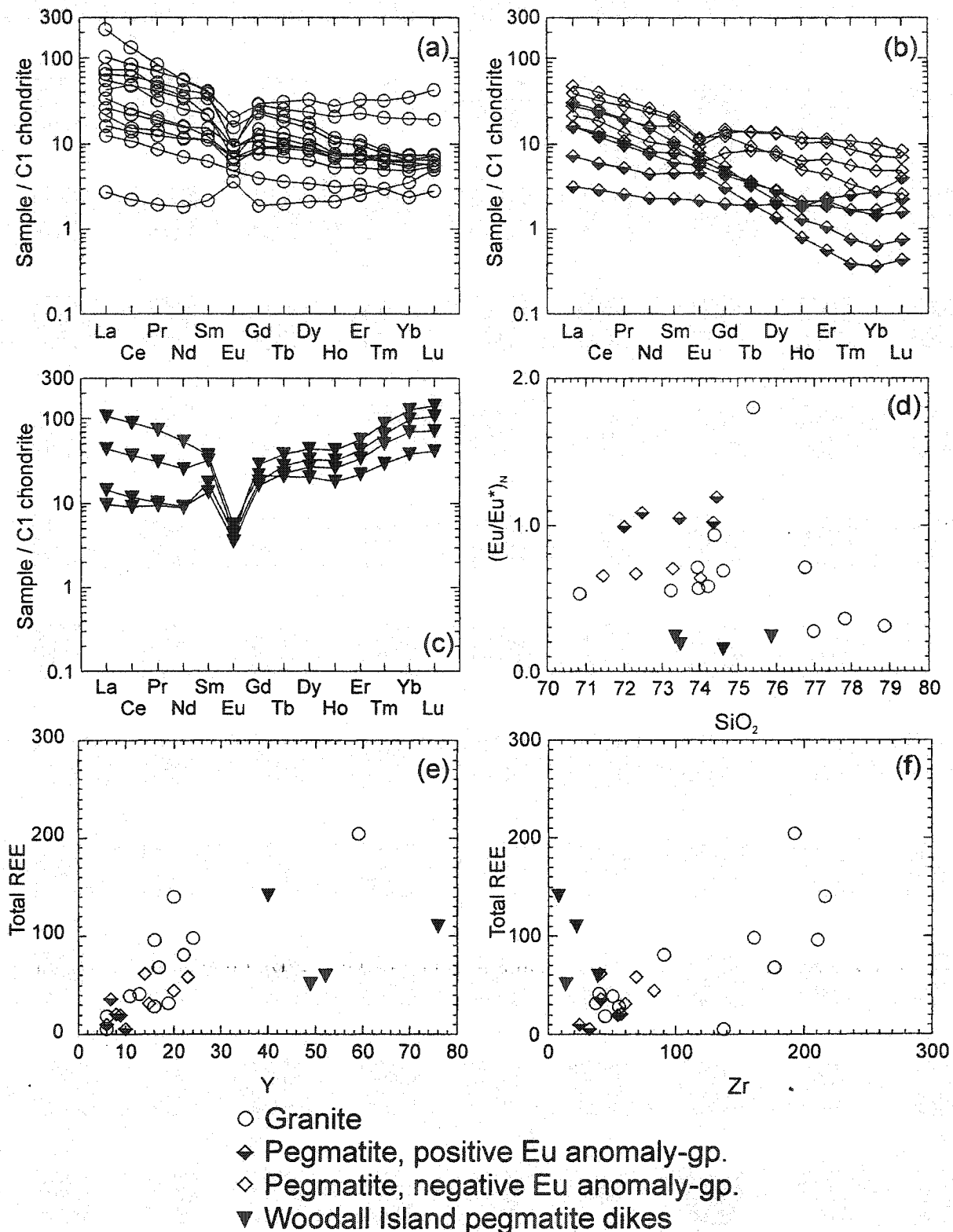
Fig. 4.6 (a-f) Chondrite-normalized REE-patterns and selected variation diagrams for the granites, pegmatites (positive and negative Eu anomaly-groups) and Woodall Island pegmatite dikes. Chondrite-normalization factors from Sun and McDonough (1989).
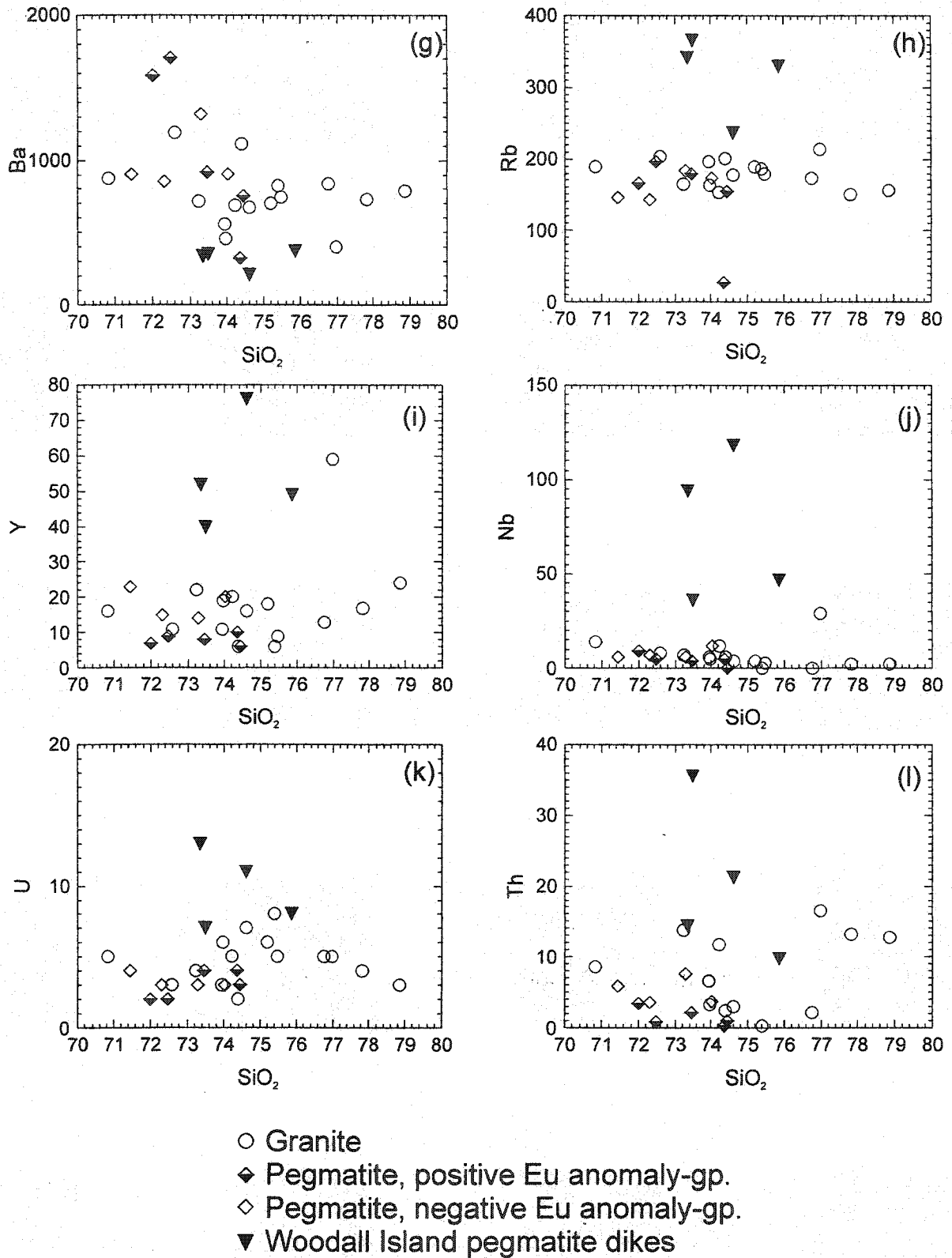
Fig. 4.6 continued. (g-l) Selected variation diagrams illustrating the compositional differences between the granites, pegmatites, and Woodall Island pegmatite dikes.

granitic magma. Differentiation of granitic magmas typically involves fractional crystallization of feldspars. Barium and Sr partition into feldspar whereas elements that are incompatible in feldspar such as Rb, Pb, and Ga become enriched in the melt (e.g., Icenhower and London, 1996; Larsen, 2002). In contrast to this predicted evolution, the pegmatites are enriched in Ba and Sr relative to the granites, Rb is similar, and Pb and Ga are higher in the granites. Ratios between assumed compatible and incompatible elements display the same inconsistency with respect to the predicted variation between primitive and evolved melts; for example, Ba/Rb and K/Rb are higher in the pegmatite than in the granite, and Rb/Sr is lower (Figs. 4.7a, b), opposite to the expected evolution of a granitic magma (e.g., Shaw, 1968).

In contrast to the pegmatites, the Woodall Island pegmatite dikes have compositions that can be interpreted as reflecting derivation from the granitic magma. For example, Ba/Rb and K/Rb ratios are lower and Rb/Sr ratios are higher in the Woodall Island pegmatite dikes than in the granite (Figs. 4.7a, b), Rb, Ga, Pb, and Nb are higher and Sr and Ba lower, consistent with the effects of alkali-feldspar fractionation. In order to test the effects of feldspar fractionation, the Ba, Rb, Sr, and REE compositions were modeled using the equation for equilibrium fractional crystallization (Appendix F); partition coefficients are presented in Table 4.2. The Ba, Rb, and Sr contents of the starting composition (i.e., 'least evolved melt') were taken to be similar to the granite with the highest Ba/Rb ratio (5.88, sample S02065-2); however, because REE concentrations are unavailable for this sample, the REE content of the starting composition was taken to be similar to the sample with the second highest Ba/Rb ratio (5.53; sample S13066). The modeling shows that the Ba, Rb, and Sr contents of the granites (excluding one outlier; sample S08067) are consistent with fractional crystallization of K-feldspar (Fig. 4.7c). The partition coefficient for Ba in plagioclase is more than an order of magnitude smaller than in K-feldspar, thus, adding plagioclase to the fractionating assemblage lowers the rate at which Ba is removed, producing a trajectory in the Rb/Sr vs. Ba/Rb diagram with a shallower slope than if K-feldspar is the only fractionating phase. The Woodall Island pegmatite dikes have Rb/Sr ratios similar

Table 4.2 Partition coefficients used in modeling fractional crystallization of a granitic magma.

	Plagioclase	K-feldspar	Allanite
Ba	0.36	6.12	n.d.
Rb	0.048	0.34	n.d.
Sr	2.84	3.87	n.d.
La	0.26	0.05	960
Ce	0.24	0.044	940
Nd	0.17	0.025	750
Sm	0.13	0.018	620
Eu	0.814	1.13	56
Gd	0.09	0.011	440
Tb	0.09*	0.009*	270
Dy	0.086	0.006	200
Ho	0.085*	0.006*	150*
Er	0.084	0.006	100
Tm	0.08*	0.009*	75*
Yb	0.077	0.012	54
Lu	0.062	0.006	41

Data from Arth (1976) and Arth and Barker (1976), except *determined by extrapolation. Allanite data from Martin (1987). n.d.=no data.

to those produced by 50-60% fractional crystallization of K-feldspar. Fig. 4.7d shows modeled Ba/Rb ratios vs. modeled $(Eu/Eu^*)_N$. Europium anomalies in the granites are not correlated with Ba/Rb, at odds with a model involving fractional crystallization of feldspar. The Woodall Island pegmatite dikes have compositions compatible with ca. 70-80% fractional crystallization of K-feldspar. The distinct HREE-enriched pattern of the Woodall Island pegmatite dikes, however, cannot be produced by fractional crystallization of K-feldspar alone (Fig. 4.7e). Only if a LREE-enriched phase such as allanite is added to the fractionating assemblage does the modeled REE pattern resemble the observed pattern.

Zircon morphology

As discussed in Chapter 5, the zircons in the granite and pegmatite are typically metamict and appear to have reacted with U-rich fluids (M. Hamilton, personal communication, 2002). The similarities in morphology of zircons from the granite and pegmatite support a genetic relationship. The dominant population of zircon in the pegmatites is metamict, with high-U+Th cores yielding an age of ca. 1090 Ma. Compositionally similar cores in the granite yield a similar age, but in addition, the granite contains medium-U+Th zircons
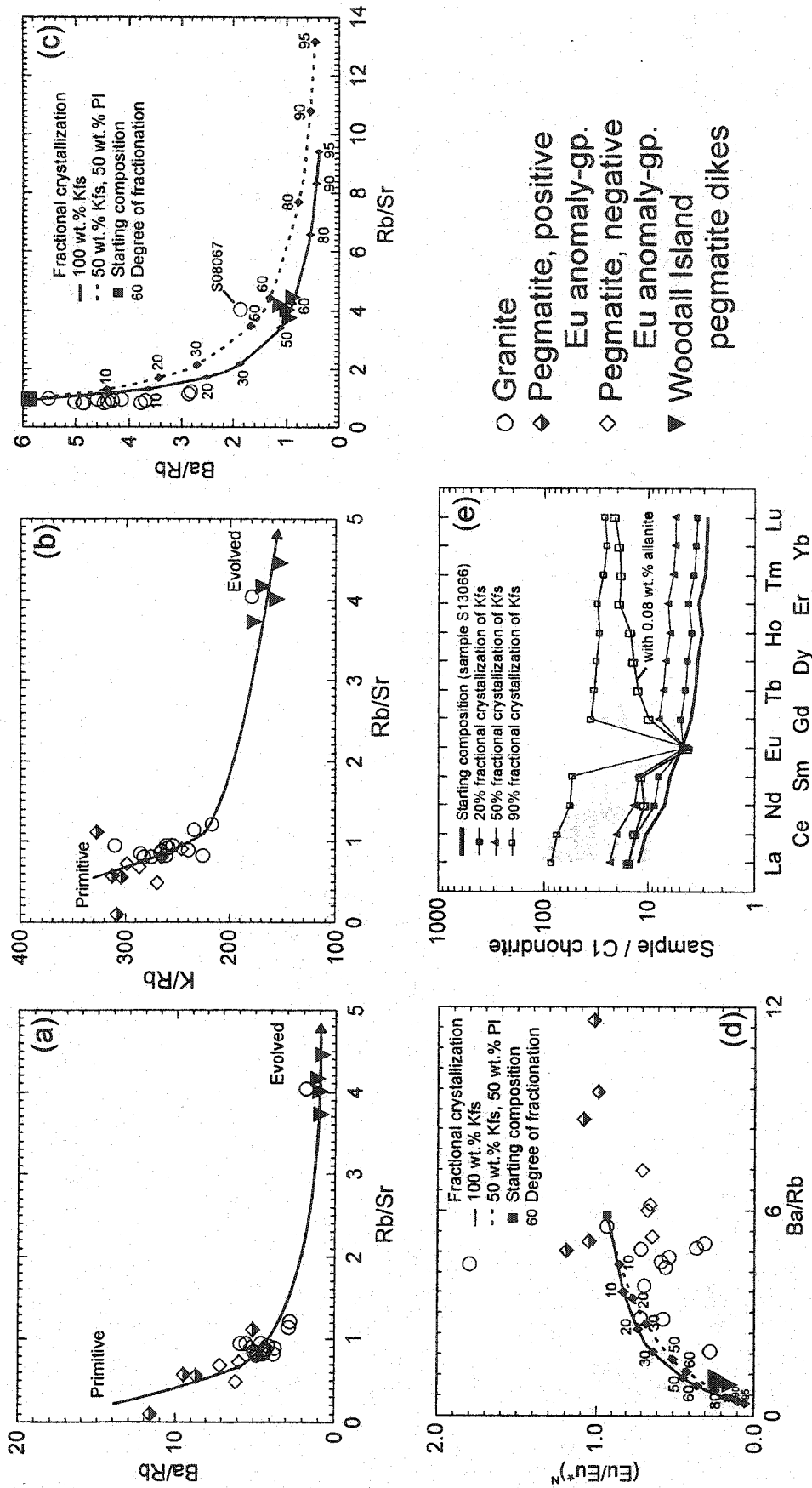
Fig. 4.7 (a) Rb/Sr vs. Ba/Rb diagram and (b) Rb/Sr vs. K/Rb diagram, granites, pegmatites, and Woodall Island pegmatite dikes. (c) Rb/Sr vs. Ba/Rb diagram, granites, and Woodall Island pegmatite dikes, with model melt compositions produced by 10 to 95% fractional crystallization of K- feldspar and K-feldspar+plagioclase. (d) Ba/Rb vs. $(Eu/Eu^*)_N$, granites, pegmatites, and Woodall Island pegmatite dikes, with model melt compositions similar to (c). (e) Model melt compositions produced by 20 to 90% fractional crystallization of K-feldspar; the effect of allanite crystallization is also shown.

and medium-U+Th rims on high-U+Th cores that also yield an age of ca. 1090 Ma (Fig. 4.8a). The most likely interpretation is that the high-U+Th cores in the granite grew from a magma rich in both elements. As fractional crystallization progressed, the evolved melt became enriched in U, Th, and other incompatible elements, and further zircon growth in the more primitive granitic melt produced medium-U+Th zircon rims and new cores. Fig. 4.8b (steps 1-3) illustrates this evolution schematically.

Open-system processes

Open-system processes during fractional crystallization, including magma replenishment, magma tapping, and assimilation, can produce magmas with compositions that deviate significantly from those expected from fractional crystallization processes alone (e.g., O'Hara and Mathews, 1981; Norman and Leeman, 1990). Numerous schlieren in the pegmatites and, to a lesser extent, in the granites suggest significant assimilation of country rocks. The country rocks (Sand Bay gneiss association) have higher REE contents than the pegmatites and the majority of granites; if assimilation were the only open-system process operating along with feldspar fractionation, the pegmatites should be enriched in REEs relative to the granites.

Interestingly, the Woodall Island pegmatite dikes show a nearly complementary relationship to the other pegmatites for a number of elements (Figs. 4.6 and 4.7). For example, the pegmatites are enriched in Sr and Ba and have positive Eu anomalies, whereas the Woodall Island pegmatite dikes display the opposite effects relative to the granites. Furthermore, the Woodall Island pegmatite dikes are enriched in Rb, Y, Nb, Pb, Ga, Th, U, Th/U, and HREEs relative to the granites, whereas the pegmatites are depleted in these elements. Relatively late removal of U and Th from the pegmatites, most likely in exsolving fluids, explains why they have U+Th contents similar to or lower than the granites, yet did not grow medium U+Th zircon (Fig. 4.8b step 4). Notably, the elements enriched in the pegmatites are compatible in feldspar, whereas the elements enriched in the Woodall Island pegmatite dikes are incompatible in feldspar (Table 4.2). It is, therefore, possible that the Woodall Island pegmatite dikes represent evolved melts extracted from the pegmatites, and intruded the roof above the granite-pegmatite pluton.
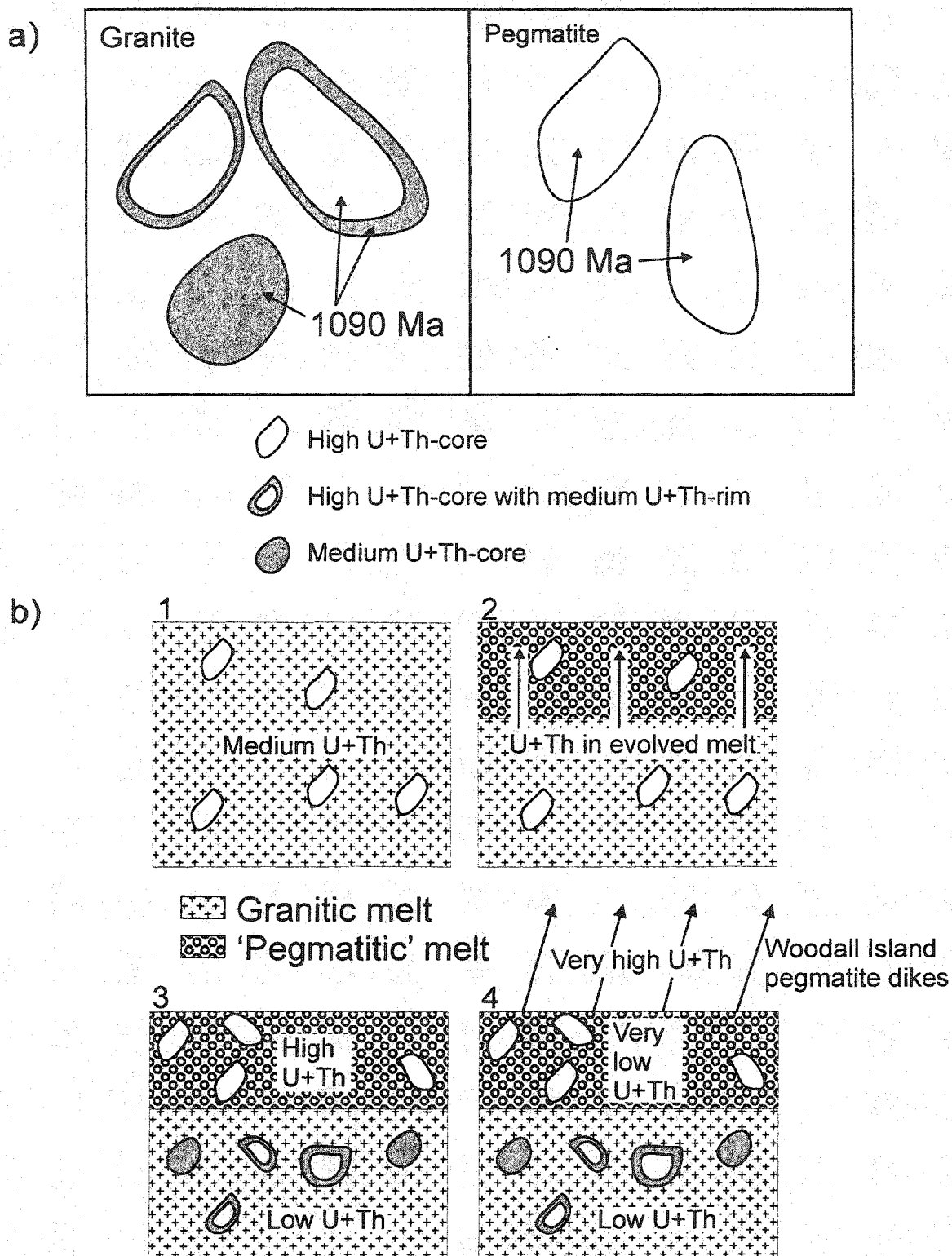
Fig. 4.8 (a) Illustration demonstrating the zircon morphological differences between the granite and pegmatite. (b) Cartoon illustrating how the 'cores' and 'rims' in the granite may have developed. See text for details.

According to this interpretation, the pegmatites (the positive-Eu-anomaly group at least) are accumulations mainly of K-feldspar.

4.6. Discussion

Culshaw *et al.* (1994) interpreted the metatexite protolith to be Ojibway orthogneiss, whereas I interpret it to be the gray quartzofeldspathic Sand Bay gneiss. It is, however, possible that both of these hypotheses are partly correct. In many outcrops a Sand Bay protolith is positively identified, particularly where the migmatites are associated with the characteristic interlayered pink and gray assemblage or contain fragments, such as calc-silicate, typical of the Sand Bay gneiss association. Geochronological data from a hornblende-rich leucosome from the north end of Pleasant Island (Chapter 5) are also interpreted in terms of a Sand Bay protolith. Elsewhere, an Ojibway protolith can be inferred based on petrographic evidence; in particular, the presence of hornblende with biotite is characteristic of the Ojibway gneiss association, in contrast to the gray quartzofeldspathic Sand Bay gneisses that lack significant hornblende. In general, metatexites with a Sand Bay protolith appear to contain a larger proportion of hornblende-rich leucosome. Using this distinction, metatexites with a Sand Bay protolith appear to dominate. The field evidence, therefore, suggests that the Sand Bay and Ojibway gneiss associations are tectonically interlayered in the study area.

The pegmatite and granite cut an older fabric in the Sand Bay gneiss association, and their ages provide a minimum estimate for the onset of Grenvillian orogenesis in the Sand Bay gneiss association. The fabric contains kinematic indicators suggesting top-to-northwest movement, given present-day orientations, that could be interpreted to reflect northwest-directed thrusting. This interpretation is, however, uncertain considering that the amount of post-shear folding is unconstrained. Culshaw *et al.* (1989, 1994) inferred the presence of a large, refolded fold in the study area, interpreted to have formed during early convergence. If this interpretation is correct, the intrusive contacts between the pegmatite/granite and Sand Bay gneiss association suggest that the pegmatite/granite transects this early fold, and, therefore, post-dates early thrusting and folding in the Sand

Bay gneiss association. Together with geochronological data from the pegmatite and granite (Chapter 5), these observations suggest that early fabric development and folding in the Sand Bay gneiss association took place >1090 Ma, thus supporting the possibility of a cryptic event at ca. 1120 Ma as proposed by Tuccillo *et al.* (1992), Wodicka (1994), and Bussey *et al.* (1995).

Judging from the geochronological data in Chapter 5, the granite and pegmatite had solidified by the time the metatexites formed. This interpretation is consistent with several observations; for example, the pegmatites and granite are clearly intrusive but do not cut the metatexites, and the pegmatites contain a number of enclaves and schlieren of Sand Bay gneiss, but no enclaves of metatexites.

4.7. Conclusions

- In several localities, the metatexites appear to have formed by partial melting of gray quartzofeldspathic Sand Bay gneiss, whereas in others the metatexites may have formed by partial melting of Ojibway orthogneiss. Distinguishing between the two is difficult in the absence of characteristic marker lithologies.

- The metatexites formed syn-tectonically, evident from melt migration along shear bands and geochronological data.

- The Sand Bay gneiss association already carried a relatively strong, possibly thrust-related fabric when the granite and pegmatite were intruded.

- Based on field observations and geochronological data, the investigated granites and pegmatites appear to be related. Their compositions are incompatible with fractional crystallization processes alone, which may indicate that open-system processes including assimilation and tapping of evolved, probably water-rich, melts were involved.

5. Geochronology, Muskoka and Shawanaga domains

5.1. Introduction

Conventional TIMS U-Pb ages on zircon and other U-bearing minerals from migmatitic orthogneisses in the Central Gneiss Belt suggest that the protoliths formed between 1480 and 1350 Ma, with high-grade Grenvillian (Ottawan) metamorphism at 1080-1040 Ma (see Table 5.2 for summary). However, the TIMS data are generally discordant, with large errors (typically on the order of ±10-30 My) on both upper and lower intercepts. The discordance may result from complex zoning in the dated minerals, Pb loss during high-grade metamorphism, or both, and represents a major impediment in our understanding of the timing and tectonic processes related to (1) protolith formation and (2) Grenvillian metamorphism.

As discussed in Chapter 2, the geochemical data indicate that most orthogneisses in the Muskoka and Shawanaga domains have protoliths with calc-alkaline affinities and probably formed in one or more continental arcs at ca. 1450 Ma. In contrast, a smaller group of orthogneiss bodies, including A-type granitic and charnockitic gneiss in the Muskoka domain and rhyolitic gneiss in the Shawanaga domain, have protolith compositions indicative of an extensional setting such as an ensialic back-arc or rifted arc. Conventional TIMS dating of an A-type granitic gneiss in the Muskoka domain yielded a strongly discordant age of 1394 ± 13 Ma, interpreted to represent the age of crystallization (Timmermann et al., 1997), and dating of detrital zircons from paragneisses interlayered with the rhyolitic gneiss suggested an age of ca. 1360 Ma for the rhyolite (T. E. Krogh, unpublished data). However, no other data have been acquired from A-type granitoid rocks in the region, including the charnockitic gneiss. Based on the geochemical data in Chapter 2 and previously published geochronological data, the calc-alkaline and A-type rocks may be interpreted to represent two distinct tectono-magmatic events. However, taking the scarcity and discordance of the available geochronological data from the A-type rocks into account, a continuous evolution from calc-alkaline to A-type magmatism cannot be discounted; it is also possible that the calc-

alkaline and A-type rocks are coeval. Here, we present new geochronological data from the A-type granitic and charnockitic gneiss in the Muskoka domain that shed new light on the tectonic evolution of the southeastern Laurentian margin between ca. 1480 and 1400 Ma.

As discussed in the introduction to this thesis, the Muskoka and Shawanaga domains occupy structural positions within the Central Gneiss Belt that make them primary targets for investigations of Grenvillian orogenesis. Grenvillian metamorphic ages in the Muskoka and Shawanaga domains typically range from ca. 1080-1040 Ma, with associated errors of ±10-50 My. Zircons in the migmatites are typically strongly zoned due to a combination of inheritance, dissolution during partial melting, and new growth during crystallization. A key question is whether the large range in metamorphic ages reflects a single protracted metamorphic episode, or multiple events that are masked by the discordant data? Crustal weakening associated with partial melting can have a profound effect on tectonic style on timescales of < 20 My (e.g., Jamieson *et al.*, 2002). In order to develop and test quantitative tectonic models for the southwestern part of the Grenville orogen, times of leucosome formation within the Muskoka and Shawanaga domains, and any differences in the ages of migmatite between the two domains, must be known more precisely than is possible with existing TIMS data. The spatial resolution of the SHRIMP allows us to separate multiple zircon-forming episodes, which in turn allows us to refine our understanding of the timing and duration of pre-Grenvillian and Grenvillian magmatic and tectonic processes.

Nine samples from the Muskoka and Shawanaga domains were selected for geochronological analysis. Mike Hamilton analyzed eight samples on the Sensitive High-Resolution Ion Microprobe (SHRIMP) at the Geological Survey of Canada in Ottawa, and John Ketchum analyzed one sample by Isotope Dilution-Thermal Ionization Mass Spectrometry (ID-TIMS) at the Royal Ontario Museum in Toronto. The majority of the samples were selected to constrain the Grenvillian evolution of the area (Chapters 3 and 4); only two protolith samples, the charnockitic and granitic gneiss in the Muskoka domain (Chapter 2), were analyzed. In addition, zircon cores from *in situ* leucosomes

were expected to yield information about the age of the migmatite protolith. The geochronological methods are discussed in Appendix E. Sample locations are shown in Fig. 5.1, and UTM coordinates for each sample are given in Table 5.1. The complete dataset is presented in Appendix E (Tables E.1-E.9). The SHRIMP data are presented first by a regression through or weighted mean $^{207}Pb/^{206}Pb$ of all the data points obtained from each sample. Next, morphological and compositional data are used to identify different populations of cores and/or rims. Numbers in the text referring to specific SHRIMP spot analyses are in italics; spot locations and the $^{207}Pb/^{206}Pb$ age of each spot analysis are shown in Appendix E.

5.2. Sample preparation

Large samples (5-30 kg) were cut and crushed in jaw crusher. The sample material was reduced to sand-sized particles in a disk mill. Zircons were separated using standard separation techniques, including Wilfley water-table and heavy liquids. Zircons used for dating were immersed in alcohol and hand-picked with tweezers under a binocular microscope from the least paramagnetic fraction at 1.7 A, 15° forward slope, and 0° side tilt on a Frantz isodynamic separator. Mounting of zircons for SHRIMP analysis and sample preparation for ID-TIMS analysis were performed by Mike Hamilton and John Ketchum, respectively. All back-scatter electron and cathodoluminescence images (Figs. E.3-E.10) were taken by Mike Hamilton.

5.3. Sample descriptions and results

5.3.1. M300617 – charnockitic gneiss, Muskoka domain (ID-TIMS)

This sample of charnockitic gneiss was collected along Hw 118, west of Mathiasville (Figs. 5.1a, 5.2a). The charnockitic gneiss was described in Chapter 2. This rock type was previously undated, and the geochemistry suggests that its petrogenesis differed significantly from that of the ca. 1450 Ma gray gneisses that dominate in the area. The purpose of dating this rock type was to determine its crystallization age and thereby better constrain its tectonic significance, specifically, the goal was to determine whether or not it represents a stage of magmatism distinct from that forming the gray
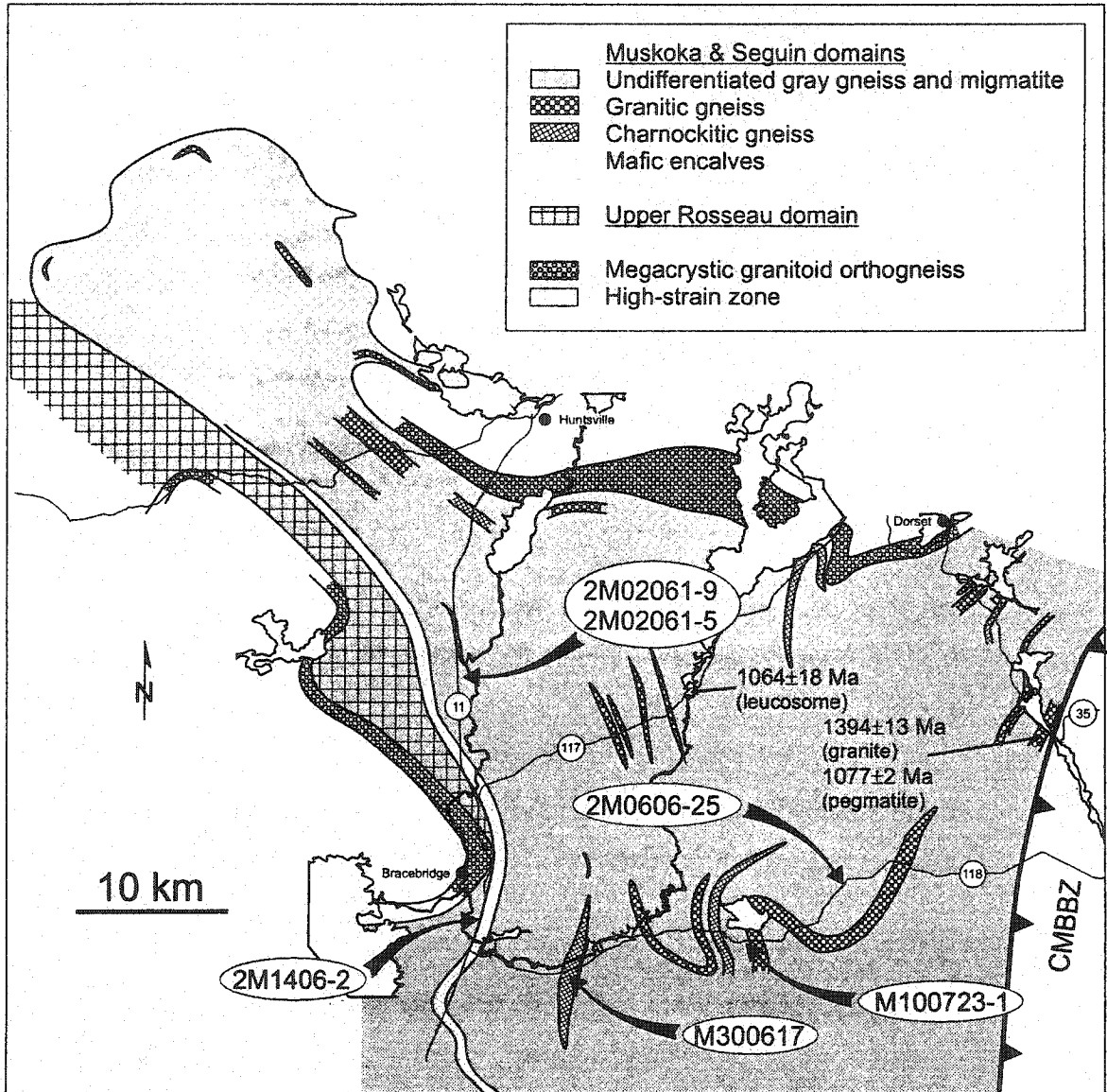
Fig. 5.1a Sample locations for geochronology, Muskoka domain. UTM coordinates given in Table 5.1. The three unframed dates refer to Timmermann *et al.* (1997).
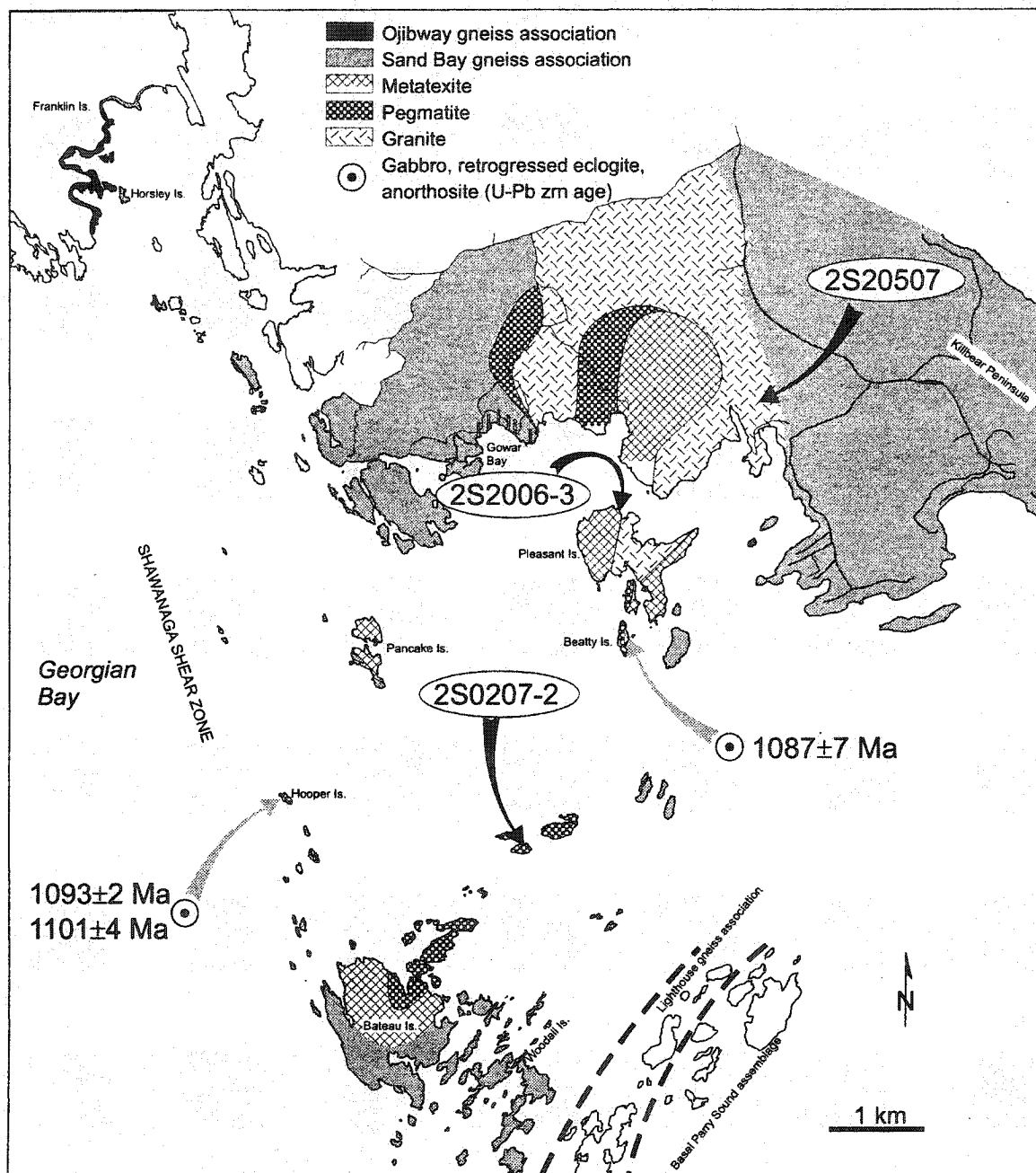
Fig. 5.1b Sample locations for geochronology, Shawanaga domain. UTM coordinates given in Table 5.1. Dates from retrogressed eclogites from Ketchum and Krogh (1998) and J. Ketchum, pers. comm., 2002).
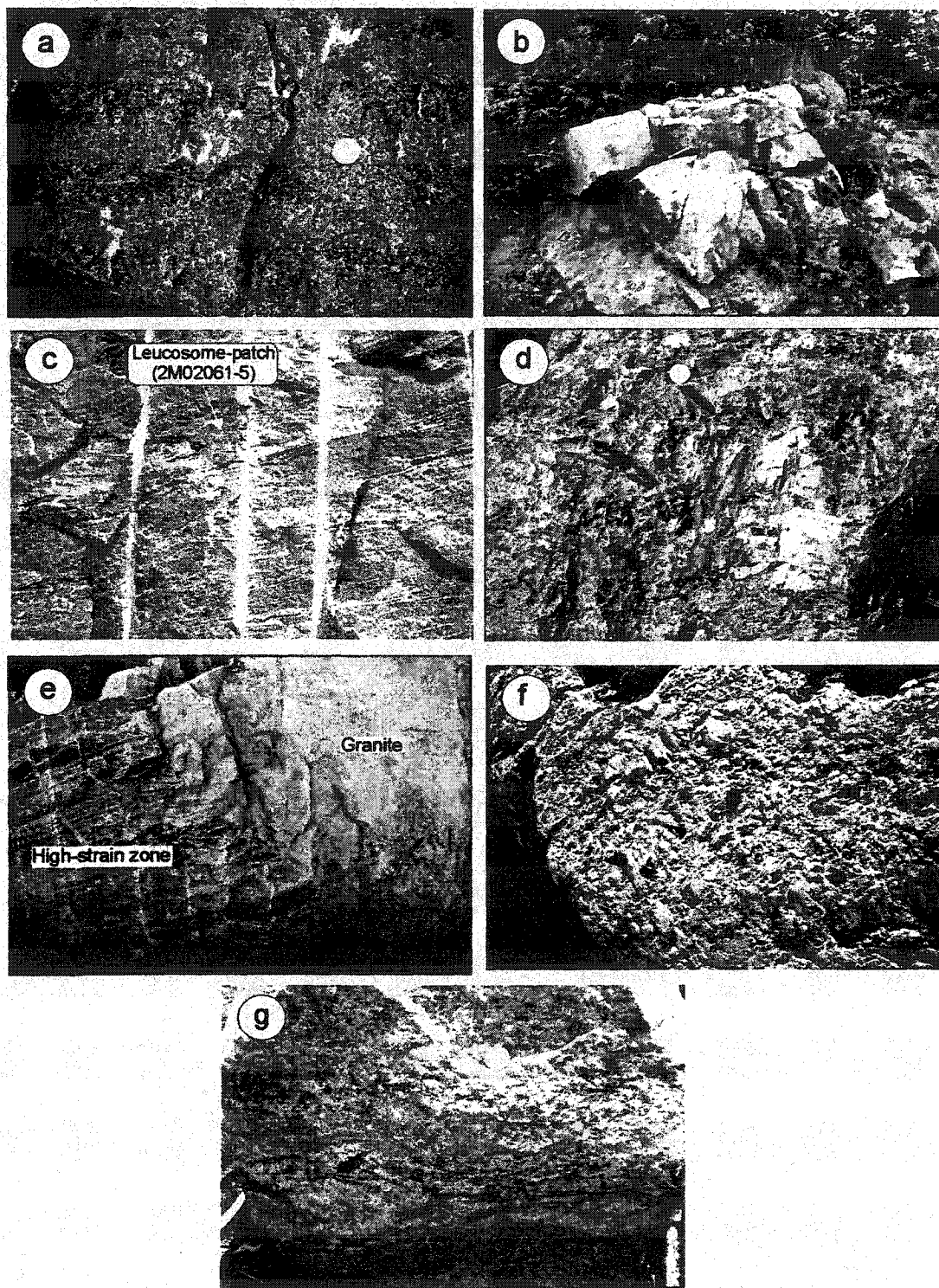
Fig. 5.2 (a) Charnockitic gneiss (M300617), Hw 118 Mathiasville. (b) Granitic gneiss (M100723-1), Hw 118 Wood Lake. (c) Pegmatitic infill in boudin neck (2M02061-5), Parkersville outcrop. (d) Orthopyroxene-bearing pegmatitic syenite (2M0606-25), Black River. (e) Post-tectonic granite dike cutting fabric in high-strain zone between Muskoka and Upper Rosseau domains (2M1406-2), Hw 11 south of Bracebridge. (f) Pegmatite (2S0207-2), Reid Island, Georgian Bay. (g) Granite with biotite-rich schlieren (2S0507), Killbear Marina.

gneisses.

Preliminary observations suggested that the zircons in this sample lacked distinct cores and rims, resembling primary, igneous zircons (e.g., Poldervaart, 1956); ID-TIMS therefore seemed suited for obtaining a precise crystallization age for the charnockitic gneiss.

The Pb and U isotopic compositions of four colorless, subhedral to euhedral, prismatic grains (Z1-Z4, single-grain analyses), a fraction consisting of 3 colorless, euhedral grains (Z5), and a fraction consisting of two pristine zircons following HF acid treatment (Z6) are shown in Fig. 5.3a. The HF acid treatment was performed by placing a large number of grains in a dissolution capsule with concentrated HF for four hours at 195°C. The six analyses are between 1.8 and 3.4% discordant, and a regression (York, 1969) through the six points yields an upper intercept age of 1449+20/-17 Ma and a lower intercept age of 1072+28/-31 Ma, interpreted to represent the ages of crystallization of the charnockitic magma and Grenvillian metamorphic overprinting, respectively. It is not clear whether the discordance is due to Pb loss during Grenvillian metamorphism or to mixtures of primary and metamorphic (recrystallized?) zircon within individual grains. Both the upper and lower intercept age are similar to previously reported crystallization and metamorphic ages from the surrounding gray gneisses (e.g., Timmermann *et al.*, 1997).

5.3.2. M100723-1 – granitic gneiss, Muskoka domain

This sample is from a fine- to medium-grained, sparsely migmatitic granitic gneiss, described in detail in Chapter 2. The sample was collected from a small outcrop along Hw 118, south of Wood Lake (Figs. 5.1a, 5.2b). Earlier TIMS dating of granitic gneiss in the Muskoka domain (Timmermann *et al.*, 1997) (Fig. 5.1a) yielded a strongly discordant age of 1394 ± 13 Ma, interpreted to represent the age of crystallization. Sample M100723-1 is from a different locality than the granitic gneiss dated by Timmermann *et al.* (1997) (Fig. 5.1a), but is petrographically and geochemically similar.

Images of the analyzed grains are shown in Fig. E.3. A regression through all 32
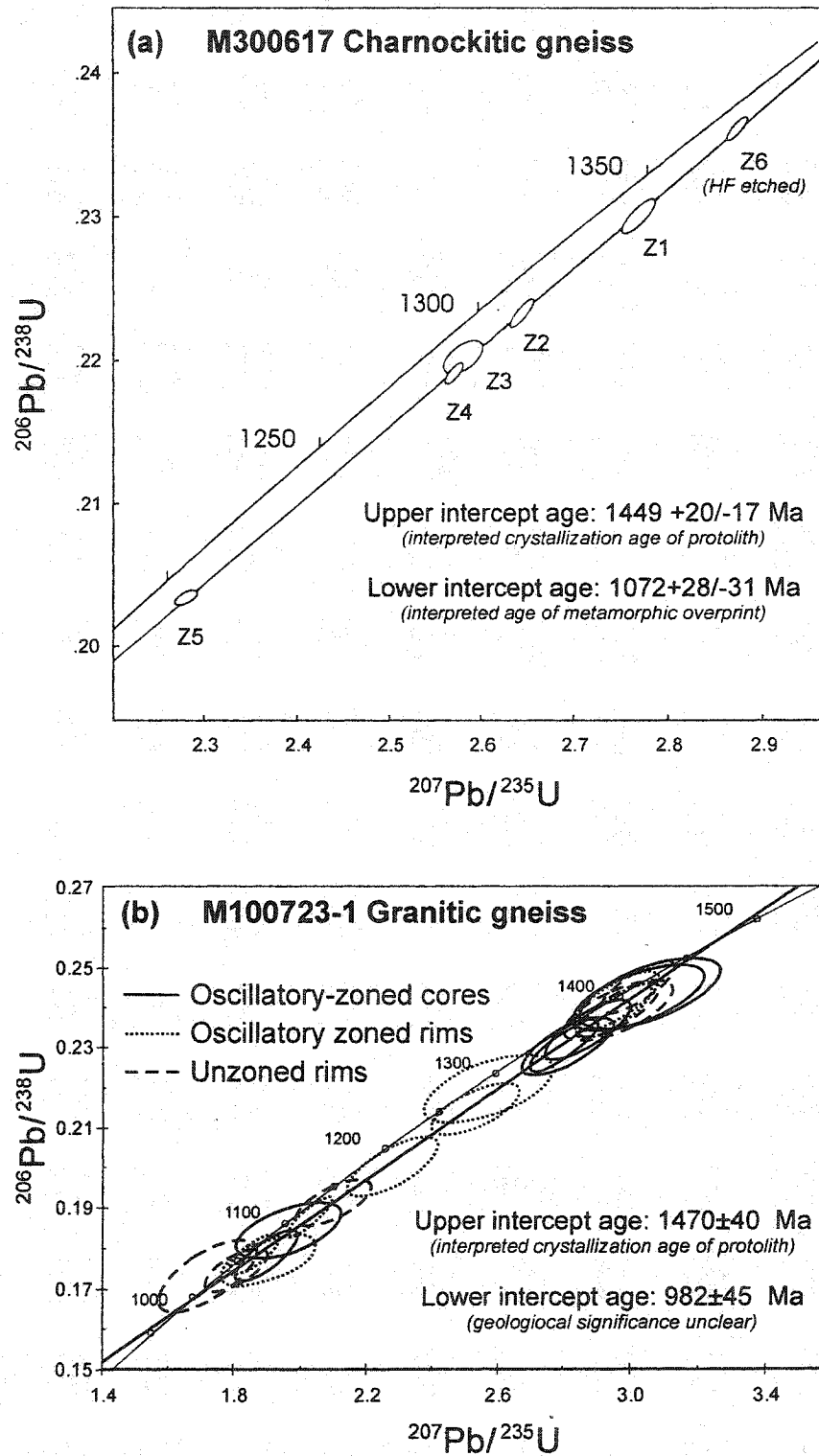
Fig. 5.3 Concordia diagrams, (a) sample M300617 (charnockitic gneiss) and (b) sample M100723-1 (granitic gneiss).

data points (Table E.2) yields an upper intercept of 1471±40 Ma and a lower intercept of 1000±40 Ma (MSWD=0.55, p=0.98). See Appendix E for definitions of MSWD and probability (p). Two types of core appear to be present in the zircons from this sample. The first type is unzoned and characterized by very low U, appearing bright white in cathodoluminescent (CL) images (e.g., grains 14 and 24). Three such cores (*5.1, 16.2, 20.1*) yielded strongly discordant and reversely discordant ages between ca. 1537 and 1112 Ma with large errors. This type of core is referred to as low-U core below. The other type of core shows generally well-developed oscillatory zoning (e.g., grains 7 and 17) and yields 2.7-6.4% discordant $^{207}Pb/^{206}Pb$ ages between 1130 and 1450 Ma. This type of core is referred to as oscillatory-zoned core below.

The low-U cores typically have thick oscillatory-zoned rims which yielded slightly discordant ages between 1420 and 1090 Ma, i.e., similar to the oscillatory-zoned cores. The oscillatory-zoned rims are compositionally and morphologically indistinguishable from the oscillatory-zoned cores. Furthermore, the ages of the oscillatory-zoned cores and rims are similar. The oscillatory-zoned cores generally do not have significant rims. Two exceptions may be grains 2 and 4 where the cores yield a discordant ca. 1130 Ma age, and the unzoned rims yield ages of ca. 991 Ma (*2.2*) and 1073 Ma (*4.2*). These unzoned rims are compositionally similar to the oscillatory-zoned cores.

Based on the above observations, a likely hypothesis is that the low-U cores represent inherited zircon, and the oscillatory-zoned rims and cores represent new zircon that grew during crystallization of the granite. A regression through the oscillatory-zoned cores and rims yields an upper intercept age of 1475±50 Ma and a lower intercept age of 979±52 Ma (MSWD=0.38, p=0.98). Including the unzoned rims in the regression yields essentially similar results with an upper intercept of 1470±40 Ma and a lower intercept of 982±45 Ma (MSWD=0.43, p=0.99) (Fig. 5.3b), interpreted to represent the age of crystallization of the granitic magma and Pb-loss, respectively. Eleven analyses (*3.2, 5.1, 9.1, 10.1, 12.1, 13.1, 13.2, 15.1, 16.2, 20.1, 20.2*) with imprecise ^{207}Pb counts and a high proportion of common Pb were excluded from the regression; all other analyses were included.

The upper intercept age of ca. 1470 Ma falls in the range of the gray orthogneisses that dominate the Muskoka domain (Chapter 2), and, therefore, appears to be geologically reasonable, although not in agreement with the earlier work of Timmermann *et al.* (1997). The lower intercept age of ca. 980 Ma is younger than any reported zircon age from the Muskoka domain (Timmermann, 1998; McMullen, 1999), but is comparable to allanite and titanite ages from elsewhere in the Muskoka domain (1015 to 987 Ma; Timmermann, 1998), interpreted to reflect late fluid influx, and to zircon and titanite ages from lower structural levels in the Central Gneiss Belt (e.g., Ketchum *et al.*, 1998). Given the large error, the lower intercept age may represent the combined effects of several processes of broadly similar age.

An important question is whether or not the SHRIMP data from the granitic gneiss exclude crystallization at ca. 1400 Ma, as previously suggested by Timmermann *et al.* (1997). Two analyses, *5.3* (oscillatory-zoned rim) and *22.1* (unzoned rim) yield concordant ages of 1404 and 1413 Ma, respectively, and are the only analyses that could be taken to indicate crystallization at ca. 1400 Ma. Analysis *5.2*, from the same rim as analysis, *5.3* yielded a 6% discordant age of ca. 1333 Ma, suggesting relatively complex age systematics. Thus, the new SHRIMP data do not exclude crystallization at ca. 1400 Ma, but are interpreted here to reflect crystallization sometime between 1430 and 1500 Ma.

5.3.3. 2M02061-9 – concordant leucosome, Muskoka domain

This sample is from a fine- to medium-grained granitic leucosome with abundant hornblende and lesser amounts of biotite. The sample corresponds to the concordant leucosomes described in Chapter 3 (see photo Fig. 3.4a), and was collected from the Parkersville outcrop (o/c M03083). The purpose of dating this sample is to determine the age of migmatization in the Muskoka domain, in order to establish the relationship to migmatization in other parts of the southwestern Grenville Province (e.g., Shawanaga domain, Chapter 4) and orogenic evolution. Dating of apparently *in situ* leucosome can also be expected to yield information about the age of the protolith in the form of inherited grains or cores.

Most of the zircons in this sample contain small- to medium-sized, rounded to irregular cores, mantled by higher-U, relatively thick and delicately oscillatory-zoned rims (Fig. E.4). A regression through all 18 data points (Table E.3), yields an upper intercept of 1460 ± 61 Ma and a lower intercept of 1038 ± 59 Ma (MSWD=3.7, p=0.000). The cores typically contain numerous cracks and inclusions of apatite, plagioclase, quartz, Ti-magnetite (?), and biotite, whereas the rims contain few or no inclusions or cracks. Some grains (e.g., grain 6) show signs of a late metamorphic overgrowth.

Cores

The age of the cores is discussed below, along with the cores from sample 2M02061-5, which is from the same outcrop as sample 2M02061-9.

Rims

The 10 analyses from the thick, oscillatory-zoned rims yield a weighted mean $^{207}Pb/^{206}Pb$ age of 1068 ± 10 Ma (MSWD=1.6, p=0.097) (Fig. 5.4a). Two of the analyses (*5.1, 6.1*) yield significantly older ages than the other rims, and excluding these two analyses yields a slightly younger age of 1062 ± 8 Ma. There is, however, no textural or compositional basis for excluding these two analyses, and 1068 ± 10 Ma is therefore considered the best estimate for the age of leucosome crystallization.

Late overgrowth. One metamorphic overgrowth (*6.2*) was analyzed and yielded a $^{207}Pb/^{206}Pb$ age of 1059 ± 11 Ma. This metamorphic overgrowth may have formed during the same metamorphic event that led to partial melting, and may be taken to indicate protracted high-temperature conditions.

5.3.4. 2M02061-5 – pegmatitic infill in boudin neck, Muskoka domain

A small patch of pegmatitic material, located in a boudin neck (Fig. 5.2c) was sampled in order to determine the age of boudinage. The boudinaged layer is an amphibolite, compositionally similar to the mafic enclaves described in Chapter 2, and the boudins are concordant to the Grenvillian fabric. Like the concordant leucosome (2M02061-9), this sample is from the Parkersville outcrop; however, no clear relationship to the concordant leucosomes could be established based on petrography, geochemistry,
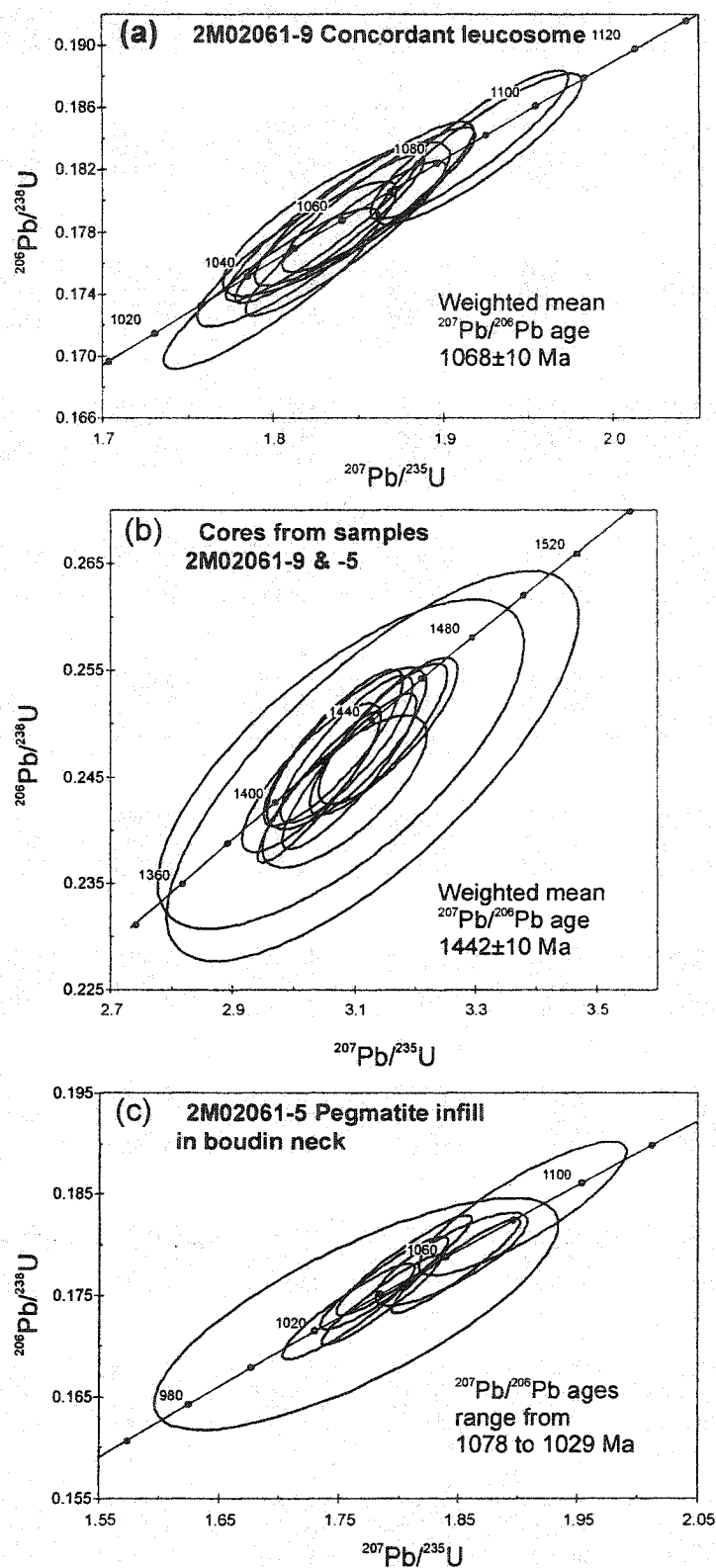
Fig. 5.4 Concordia diagrams, (a) zircon rims sample 2M02061-9 (concordant leucosome), (b) zircon cores samples 2M02061-9 and -5, both samples from the same outcrop, and (c) zircon rims sample 2M02061-5 (pegmatite infill in boudin neck).

or field relations.

The zircons comprise broad, oscillatory-zoned cores, surrounded by higher-U thin to thick, apparently metamorphic, overgrowths (Fig. E.5). A regression through all 22 data points (Table E.4) yields an upper intercept of 1537±41 Ma and a lower intercept of 1041±35 Ma (MSWD=2.4, p=0.001). The overgrowths or rims locally embay cores (e.g., grain 3). Inclusions, restricted to the cores, are dominated by quartz, plagioclase, and apatite.

Cores

Samples 2M02061-9 and -5 are from the same outcrop and their inherited cores can be expected to have come from the same source. The core analyses in these two samples are, therefore, combined. Analyses *3.2* and *12.1* (sample 2M02061-9) have unusually high U+Th and were excluded. In addition, analyses that are >4% discordant were excluded (*1.2, 11.1* from sample 2M02061-9 and *4.1, 9.1, 10.1* from sample 2M02061-5). The remaining 11 analyses yield a weighted mean $^{207}Pb/^{206}Pb$ age of 1442±10 Ma (MSWD=1.02, p=0.43) (Fig. 5.4b), interpreted to represent the crystallization age of the protolith to the gray orthogneiss host rock.

An interesting relationship is observed in grain 1 (sample 2M02061-5), where a ca. 1440 Ma oscillatory-zoned core is overgrown and truncated by what appears to be a metamorphic rim of similar age. This relationship may indicate that the ca. 1440 Ma orthogneisses were metamorphosed shortly after they formed; a similar idea was hinted at by Timmermann (1998). Previous ID-TIMS dating has typically yielded upper intercept ages with large errors, which can be explained if the rocks experienced a phase of metamorphism just after crystallization. Alternatively, the large errors associated with the protolith ages could reflect protracted and variable Grenvillian Pb loss. Without the ability to relate age with zircon texture, previous geochronological work may have missed this inferred early, pre-Grenvillian phase of metamorphism. An alternative explanation to the observed core-rim relationship in grain 1 is that the oscillatory zoned core was corroded by the magma and the 'rim' grew from a slightly more evolved

magma with a different composition; i.e., they may both be magmatic.

Rims

Excluding the three most discordant analyses (*3.2, 5.2, 11.1*), the overgrowths range in age ($^{207}Pb/^{206}Pb$) from 1078±9 Ma (*7.2*) to 1029±11 Ma (*13.1*) (Fig. 5.4c). The overgrowths apparently cannot be subdivided into distinct populations based on texture or composition, meaning that none of the analyses can be interpreted to represent the age of crystallization of the pegmatite. The most likely interpretation appears to be that the boudin neck and pegmatitic infill formed at the onset of ductile deformation, probably around ca. 1080 Ma (Timmermann *et al.*, 1997) and remained a low-pressure sink from that time. Therefore, whenever fluids were generated in the surrounding rocks, the boudin neck was a favored location for continued zircon growth during high-grade metamorphism. The results are therefore compatible with previous geochronology from the area (e.g., Timmermann *et al.*, 1997; McMullen, 1999; Timmermann *et al.*, 2002), suggesting a long-lived high-temperature Grenvillian metamorphic history.

5.3.5. 2M0606-25 – pegmatitic syenite, Muskoka domain

Pegmatitic syenite bodies and dikes, typically <1m up to a few meters across, are common in the eastern Muskoka domain and appear to be spatially associated (Slagstad, unpublished field data) with patchily developed granulites (Timmermann *et al.*, 2002). The pegmatitic syenites are characterized by coarse orthopyroxene (Fig. 5.2d), suggesting that they were 'dry', in contrast to most other pegmatites in the Muskoka domain that typically have retrogressed margins. Timmermann *et al.* (2002) suggested that the patchy granulites formed in response to influx of CO_2-rich fluids during Grenvillian metamorphism, derived from rare marble layers intercalated with the Muskoka orthogneisses or from more voluminous marble in the overlying Central Metasedimentary Belt boundary thrust zone (CMBBZ) and Bancroft terrane (Fig. 1.5). However, the recognition that the patchy granulites are spatially associated with pegmatitic syenites raises the possibility that the CO_2-rich fluids that produced the patches were transported from relatively deep crustal levels by magmatic processes (cf., Frost and Frost, 1987).

The dated sample is from a pegmatitic syenite at the intersection between Hw 118

and Black River (Fig. 5.1a), dominantly comprising K-feldspar, with variably, but generally large (2-30 cm), equant to elongate orthopyroxene (Fig. 5.2d). A similar pegmatite from a different locality (Fig. 5.1a) yielded a zircon age of 1077±2 Ma and titanites ranging in age from 1063 to 1079 Ma (Timmermann et al., 1997).

Zircons from the pegmatitic syenite are coarse and typically irregular and angular, possibly as a result of crushing during separation (Fig. E.6). The zircons show faint, broad zoning and are inclusion-free. The weighted mean $^{207}Pb/^{206}Pb$ age of the 18 data points (Table E.5) is 1033±9 Ma (MSWD=1.5, p=0.079). In most grains, no core-rim relationship was apparent, a possible exception being grain 2 with a faintly oscillatory-zoned core, and a higher-U, apparently unzoned rim. The age of core and rim are the same within error (analyses 2.1 and 2.2). There is no basis for dividing the zircons into more than one population. Excluding the 5 most discordant analyses (>2.4%; 3.1, 12.1, 13.1, 14.1, 16.1) the remaining 12 analyses (<2.1% discordant) yield a weighted mean $^{207}Pb/^{206}Pb$ age of 1036±7 Ma (MSWD=0.26, p=0.992) (Fig. 5.5a), taken to represent the crystallization age of the pegmatitic syenite. This pegmatite is ca. 30-40 My younger than the apparently similar pegmatite dated by Timmermann et al. (1997).

5.3.6. 2M1406-2 – post-tectonic granite dike, Muskoka domain

This sample is from a large (>10 m), apparently undeformed granite dike a few kilometers south of Bracebridge along Hw 11 (Fig. 5.1a). The dike cuts the foliation and concordant leucosomes in a high-strain shear zone marking the boundary between the Muskoka domain and underlying Upper Rosseau domain (Fig. 5.2e). The age of the granite provides a minimum estimate of the age of movement along this shear zone, and thus, assembly of this part of the orogen. Similar, smaller bodies have been observed elsewhere in the Muskoka domain. Geochemically, the granite is distinct from any of the surrounding leucosomes; in particular the REE pattern is more strongly fractionated with $(La/Yb)_N>28$. The high $(La/Yb)_N$ suggests that a phase incorporating HREEs, e.g., garnet, may have been present in the source, indicating a source outside the Muskoka domain where garnet is generally absent.
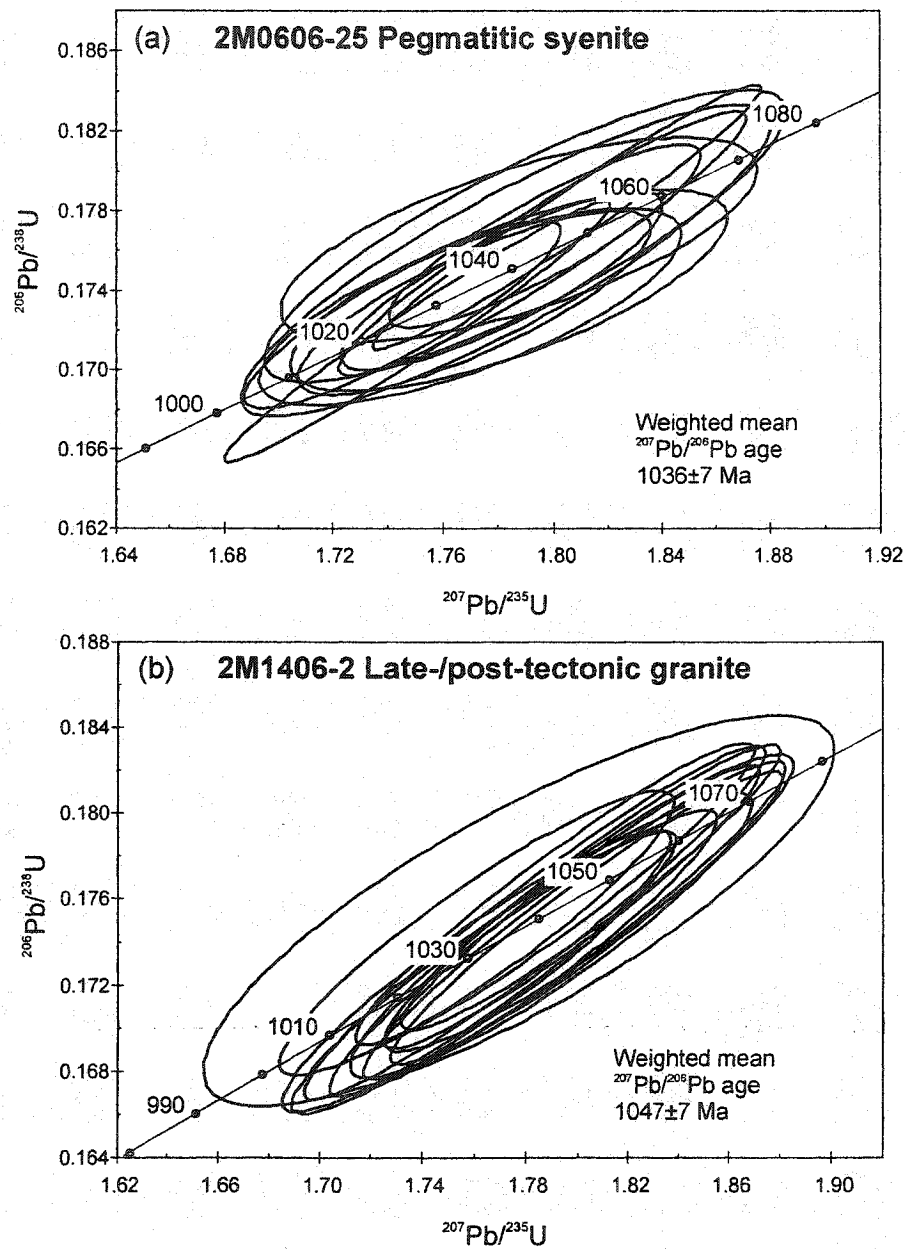
Fig. 5.5 Concordia diagrams, (a) sample 2M0606-25 (pegmatitic syenite), and (b) sample 2M1406-2 (late- or post-tectonic granite dike).

The zircons from this granite are generally large and prismatic, dominantly showing magmatic, oscillatory zoning (Fig. E.7). The weighted mean $^{207}Pb/^{206}Pb$ age of the 15 data points (Table E.6) is 1049±6 Ma (MSWD=0.58, p=0.88). A few grains show relatively thin rims that give the grains a somewhat rounded appearance and suggest overgrowth or recrystallization; it is, however, possible that the rims are magmatic. Apart from these rims, which were too thin to analyze, distinct rims and cores could not be identified. There are no morphological or compositional characteristics that allow the zircons to be subdivided into more than one population.

Two of the analyses (*6.1, 12.1*) are moderately discordant (3.3-3.4%), whereas the other analyses are <2% discordant. Excluding *6.1* and *12.1*, the remaining 13 analyses yield a weighted mean $^{207}Pb/^{206}Pb$ age of 1047±7 Ma (MSWD=0.75, p=0.70) (Fig. 5.5b), taken to represent the crystallization age of the granite.

5.3.7. 2S0207-2 – pegmatite, Shawanaga domain

This sample is from pegmatite on Reid Island, a few kilometers northeast of Bateau Island (Figs. 5.1b, 5.2f) on Georgian Bay. The island is composed almost entirely of pegmatite. The sample was collected in an area where schlieren are comparatively rare, in order to minimize the effects of inherited or xenocrystic zircon. Field relationships, petrography, and geochemistry of the pegmatites were described in Chapter 4. The purpose of dating this sample is to determine the age of crystallization and to establish the age relationship to migmatites and granite in and around Parry Sound, as outlined in Chapter 4, and elsewhere in the southwestern Grenville Province (e.g., Muskoka domain, Chapter 3). The age of the pegmatite also represents a minimum age for the development of an older, isoclinally folded fabric in the Sand Bay gneisses (Chapter 4).

Zircons are predominantly large prismatic or needle-like (Fig. E.8). The weighted mean $^{207}Pb/^{206}Pb$ age of the 16 data points (Table E.7) is 1079±14 Ma (MSWD=17, p=0.000). The grains are typically altered and cracked, and appear metamict, consistent with the generally very high U concentrations (up to 9000 ppm). The zircons can generally be subdivided into distinct populations on the basis of morphology. A useful

subdivision for interpreting the age systematics of this sample is one group comprising magmatic cores (*3.1, 6.2, 7.1, 9.1, 9.2, 13.1, 13.2*), non-rimmed grains (*2.1, 10.1*), and a magmatic overgrowth (*4.1*), and a second group of metamorphic overgrowths, typically zircon tips (*1.1, 5.1, 6.1, 8.1, 11.1, 12.1*). The two groups are referred to as 'cores' and 'rims', respectively.

Cores

The cores are high in U (1300-5000 ppm) and Th (12-80 ppm), and, excluding analyses *9.1* (3.6% discordant) and *13.2* (27% discordant), yield a weighted mean $^{207}Pb/^{206}Pb$ age of 1086±7 Ma (MSWD=2.0, p=0.053). The two youngest analyses (*4.1, 10.1*) are significantly lower in U and Th than the other cores (similar to the rims). The remaining 6 analyses yield a weighted mean $^{207}Pb/^{206}Pb$ age of 1088±7 Ma (MSWD=1.7, p=0.14) (Fig. 5.6a), which is considered to be the best estimate of the age of pegmatite crystallization.

The moderately discordant analysis 9.*1* yields a $^{207}Pb/^{206}Pb$ age of 1126±6 Ma. In light of the discordance, the significance of this age is unclear. However, the age is similar to the suggested age (ca. 1120 Ma) of initial thrusting in the basal Parry Sound domain (Tuccillo *et al.*, 1992; Wodicka, 1994), immediately overlying the Shawanaga domain.

Rims

The metamorphic rims are typically lower in U and Th than the cores; an exception is analysis *5.1* which is an 'overgrowth' truncating the internal oscillatory-zoning of a magmatic core. Analysis *5.1* is discussed separately below. Excluding analysis *11.1*, which is 3.2% discordant, the weighted mean $^{207}Pb/^{206}Pb$ age of the rims is 1072±8 Ma (MSWD=0.111, p=0.95) (Fig. 5.6a). This age is taken to represent the age of metamorphism of the pegmatites; including the two cores (*4.1, 10.1*) that are compositionally similar to the rims yields the same result.

Analysis *5.1* yields a 1.8% reversely discordant $^{207}Pb/^{206}Pb$ age of 1051±4 Ma. Compositionally, *5.1* is characterized by high U+Th, similar to the cores, thus it is
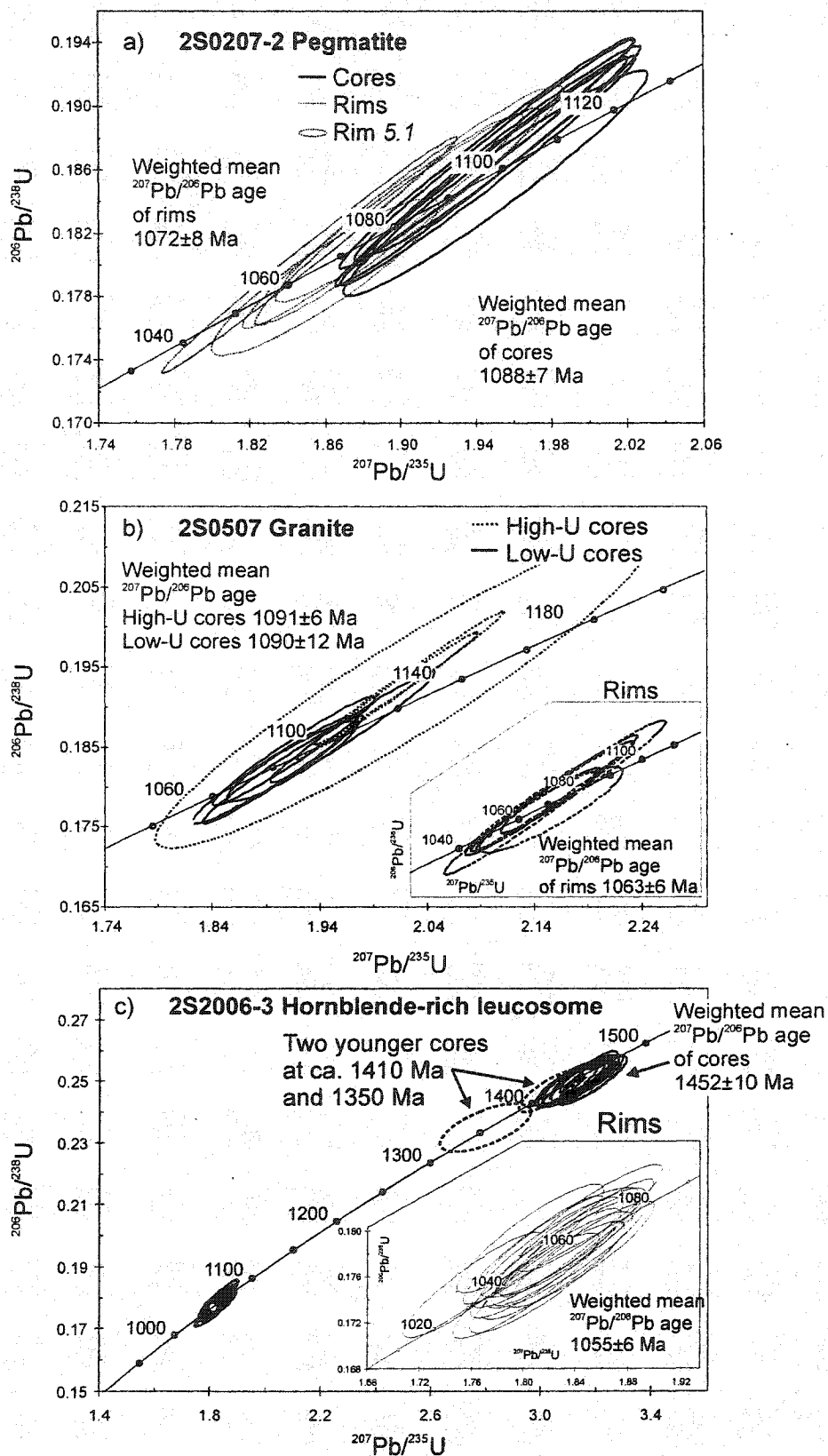
Fig. 5.6 Concordia diagrams, (a) sample 2S0207-2 (pegmatitic diatexite), (b) sample 2S0507 (granite), and (c) sample 2S2006-3 (hornblende-rich leucosome).

possible that the 'overgrowth' represents recrystallization of a magmatic core, induced for example by fluid influx along a crack. Similar features may be present in some of the other zircons from this sample, e.g., the grain to the left of grain 13 and in the core of the equant grain to the right of grain 3 (Fig. E.8). The age of 1051±4 Ma overlaps with the crystallization age of the spatially associated hornblende-rich leucosomes (2S2006-3) discussed below, and is therefore considered to represent a geologically significant metamorphic event or part of an extended period of continuous metamorphism.

5.3.8. 2S0507 –granite, Shawanaga domain

This sample is from a homogeneous granite body in the Shawanaga domain (Figs. 5.1b, 5.2g), described in Chapter 4. The sample was collected just north of Killbear Marina, in the central part of the granite. The purpose of dating this granite is to establish the relationship to the pegmatite and surrounding migmatites as well as to constrain the age of deformation in the Sand Bay gneiss association (cf., Chapter 4).

The zircons from this sample are morphologically and texturally similar to those in the pegmatite (2S00207-2) (Fig. E.9). The weighted mean $^{207}Pb/^{206}Pb$ age of all of the 22 obtained data points (Table E.8) is 1084±18 Ma (MSWD=37, p=0.000). Generally, elongate prisms predominate, and the grains, though commonly displaying delicate oscillatory zoning, are pervasively altered and cracked. Local replacement, possibly to uraninite, is visible, and a few grains show synneusis twins. Inclusions are K-feldspar, magnetite or hematite, biotite, apatite, and sodic plagioclase.

Zircons in the granite and pegmatite (2S0207-2) have several morphological features in common. The granite can be considered in terms of one group encompassing cores and non-rimmed grains on the one hand, and metamorphic overgrowths on the other.

Cores

The cores and non-rimmed grains are characterized by variable U and Th contents, and may be subdivided into two populations based on composition. One group of cores (*1.1, 7.1, 9.1, 10.1, 13.1*) is characterized by very high U (3700-9000 ppm) and Th (27-

200 ppm), and yields relative strong reversely discordant results. The other group (*2.1, 4.1, 12.1, 13.2, 14.1*) is lower in U (800-2100 ppm) and Th (3-26 ppm) and yields near-concordant results. The age of the high-U cores is difficult to determine because of the large discordance; excluding analyses *1.1* and *9.1* with ≥5% discordance yields a weighted mean $^{207}Pb/^{206}Pb$ age of 1091±6 Ma (MSWD=0.104, p=0.90) (Fig. 5.6b). The lower-U cores yield a similar weighted mean $^{207}Pb/^{206}Pb$ age of 1090±12 Ma (MSWD=1.5, p=0.2) (Fig. 5.6b). Here, 1090±12 Ma is considered to represent the crystallization age of the granite, which is essentially identical to the pegmatite. The high-U cores from the granite, in addition to being similar in age to the zircons from the pegmatite, are also compositionally and texturally similar.

Analysis *4.2* targeted an oscillatory-zoned core characterized by low U (490 ppm) but high Th (200 ppm) that yielded a 7% discordant weighted mean $^{207}Pb/^{206}Pb$ age of ca. 1347 Ma. The age of this core is similar to an inherited core in the hornblende-rich leucosome (2S2006-3) from the same area (discussed below), and may represent an inherited or xenocrystic core from the Sand Bay gneiss association.

Analysis *17.1* targeted a core characterized by high U (3400 ppm) and Th (2200 ppm), and yielded an 8% reversely discordant weighted mean $^{207}Pb/^{206}Pb$ age of ca. 1291 Ma. This analysis is high in common lead (^{204}Pb=250 ppb) and the age is considered geologically meaningless.

Rims

Most metamorphic overgrowths or rims yield near-concordant results (<2.5%); two analyses (*1.2, 15.1*) yielding more discordant results (3.7-6.6%) were excluded. Most of the rims fall within a relatively restricted range of $^{207}Pb/^{206}Pb$ ages from 1059 to 1078 Ma (*3.1, 5.1, 6.1, 8.1, 11.1, 16.1*), yielding a weighted mean $^{207}Pb/^{206}Pb$ age of 1063±6 Ma (MSWD=0.44, p=0.82) (Fig. 5.6b inset). This age is interpreted as the age of metamorphism of the granite.

Two rims yield significantly younger ages at 1042±7 Ma (*3.2*) and 1032±13 Ma (*7.2*). Ketchum *et al.* (1998) showed that tectonism related to extensional movement

along the Shawanaga shear zone lasted until at least 1020 Ma, thus, it is possible that the two younger ages represent geologically significant events or part of a continuum of high-grade metamorphism.

5.3.9. 2S2006-3 – hornblende-rich leucosome, Shawanaga domain

This sample is from a hornblende-rich leucosome on Pleasant Island, Georgian Bay (Fig. 5.1b), as described in Chapter 4 (see photo Fig. 4.3b). The hornblende-rich leucosomes are spatially associated with the pegmatites and less commonly with the granite. The purpose of dating the hornblende-rich leucosome is to determine the age of leucosome formation, to establish whether or not there is an age relationship between these metatexites and the pegmatitic/granite in the Shawanaga domain, and to determine the timing of migmatization in the Shawanaga and Muskoka domains.

The zircons from this sample are generally slightly to moderately prismatic with abundant low-U cores surrounded by high-U mantles or rims (Fig. E.10). A regression through the 31 data points (Table E.9) yields an upper intercept of 1486±31 Ma and a lower intercept of 1070±31 Ma (MSWD=1.6, p=0.029). The cores are typically oscillatory-zoned and may be either irregular or prismatic, and are normally rich in inclusions (quartz, biotite, K-feldspar, plagioclase, and unidentified silicate) and cracks. Although the rims appear relatively structureless in CL images, back-scatter electron (BSE) images reveal delicate oscillatory zoning, suggesting precipitation from a melt.

Cores

Fourteen analyses from the oscillatory-zoned cores yielded near-concordant results. Although no distinction between different populations of cores could be made based on morphology and composition, there appears to be a dominant population of old cores and two significantly younger cores.

Fourteen analyses targeted the older population of cores, two of which (*1.3* and *6.1*) were 4-5% discordant. Excluding these two analyses yields a weighted mean $^{207}Pb/^{206}Pb$ age of 1452±10 Ma (MSWD=1.4, p=0.15) (Fig. 5.6c). The two younger cores yielded concordant ages of ca. 1410 Ma (*5.1*) and 1350 Ma (*12.1*) (Fig. 5.6c).

Rims

Fifteen rims were analyzed. Excluding the three most discordant analyses (>2.8%, spots *2.1, 3.2, 9.2*) the weighted mean $^{207}Pb/^{206}Pb$ age is 1055±6 Ma (MSWD=0.70, p=0.74) (Fig. 5.6c), taken to be the crystallization age of the hornblende-rich leucosomes.

Table 5.1 Summary table of geochronological data, Muskoka domain.

Sample #	Rock type	Domain/UTM	Age	Interpretation
M300617	Charnockitic gneiss	Muskoka 640 050 E 4980 550 N	1449+20/-17 Ma (UI)	Crystallization of charnockite
			1072+28/-31 Ma (LI)	Metamorphism
M100723-1	Granitic gneiss	Muskoka 651 650 E 4984 450 N	1470±40 Ma (UI)	Crystallization of granite
			982±45 Ma (LI)	Metamorphism?/ Pb-loss?
2M02061-9	Concordant leucosome	Muskoka 668 550 E 5002 400 N	1440±10 Ma	Age of host rock
			1068±10 Ma	Partial melting/ metamorphism
			1059±11 Ma	Metamorphism
2M02061-5	Leucosome, boudin neck	Muskoka 668 550 E 5002 400 N	1440±10 Ma	Age of host rock
			1080-1030 Ma	Protracted, near-continuous high-grade metamorphism
2M0606-25	Pegmatitic syenite	Muskoka 658 200 N 4988 250 E	1036±7 Ma	Crystallization of pegmatitic syenite
2M1406-2	Post-tectonic granite dike	Muskoka 634 150 E 4985 550 N	1047±7 Ma	Crystallization of granite

Table 5.1 cont. Summary table of geochronological data, Shawanaga domain.

2S0207-2	Pegmatite	Shawanaga 556 900 E 5018 700 N	1088±7 Ma	Crystallization of pegmatite
			1072±8 Ma	Metamorphism
			1051±4 Ma	Metamorphism
2S0507	Granite	Shawanaga 559 500 E 5023 450 N	~1347 Ma	Inherited core
			1090±12 Ma	Crystallization of granite
			1063±6 Ma	Metamorphism
			1042±7 Ma	
			1032±13 Ma	Metamorphism
2S2006-3	Hornblende-rich leucosome	Shawanaga 557 880 E 5022 280N	1452±10 Ma ~1410 Ma ~1350 Ma	Inherited cores from protolith
			1055±6 Ma	Crystallization of leucosome

Coordinates apply to UTM zone 17.

5.4. Discussion

5.4.1. Implications for the pre-Grenvillian evolution of the Laurentian margin

The dates for the charnockitic and granitic gneiss were incorporated in the discussion in Chapter 2, and their significance is therefore not discussed further here.

5.4.2. Early Grenvillian tectonic evolution

The earliest recorded Grenvillian metamorphism in the CGB took place in the Parry Sound domain at ca. 1160 Ma (van Breemen *et al.*, 1986; Tuccillo *et al.*, 1992; Wodicka, 1994). There is, however, compelling evidence that the earliest phase of metamorphism in the Parry Sound domain took place offshore of the Laurentian margin (Wodicka *et al.*, 1996), thus, the earliest recorded metamorphic overprint of the Laurentian margin post-dates 1160 Ma. The oldest 'Grenvillian' dates obtained in this study come from the pegmatite (sample 2S02072) and granite (sample 2S0507) in the Shawanaga domain, both dating at ca. 1090 Ma. The ages of the granite and pegmatite are important because 1) they provide a minimum age for deformation and metamorphism of the Sand Bay gneiss association, as discussed in Chapter 4, and 2) they are similar to metamorphic ages

from garnet-clinopyroxene-rich rocks, interpreted to represent retrogressed eclogite (referred to as r-eclogite below), in the interior Shawanaga domain and its bounding shear zones (Ketchum and Krogh, 1997; J. Ketchum, pers. comm., 2002). Ketchum and Krogh (1997, 1998) interpreted the 1085-1100 Ma ages from the r-eclogites to reflect high-pressure metamorphism, whereas Jamieson et al. (2003) interpreted the ages to represent later, high-temperature metamorphic overprinting.

Deformation and metamorphism at ca. 1120 Ma?

Geochronological data from the uppermost Shawanaga domain and basal Parry Sound assemblage suggest that an early phase of deformation and metamorphism in the Shawanaga domain may have taken place at ca. 1120 Ma (Tuccillo et al., 1992; Wodicka, 1994; Bussey et al., 1995). One zircon from the pegmatite yielded an age of ca. 1126 Ma, and may represent an inherited grain that formed during the postulated tectonic event at ca. 1120 Ma. However, the new geochronological data presented herein show no indications of a strong metamorphic overprint at ca. 1120 Ma. The data do, however, suggest a significant tectonic event in the Sand Bay gneiss association sometime before 1090 Ma. Although we have no constraints for an upper age limit, it is possible that the pre-1090 Ma fabric in the Sand Bay gneiss association is related to the postulated event at ca. 1120 Ma. This interpretation is also consistent with the tectonic reconstruction of Culshaw et al. (1997), who placed the Shawanaga domain at the outermost margin of Laurentia at ca. 1120 Ma. The Sand Bay gneiss association, in particular leucosome associated with the pre-1090 Ma fabric, is a key target for further work aimed at constraining the early Grenvillian evolution of the CGB.

Intrusion of granite-pegmatite coeval with or after high-pressure metamorphism?

The majority of the r-eclogites are associated with high-strain zones, interpreted to represent shear zones (Davidson et al., 1982; Culshaw et al., 1983), and it is possible that many of them represent tectonically incorporated fragments from deeper crustal levels However, on Beatty Is. (see Chapter 4 and Fig. 5.1b), a ca. 15 m wide pod of r-eclogite (Jamieson et al., 2003) dated at 1087±2 Ma (J. Ketchum, pers. comm., 2002) is closely associated with pegmatite and migmatite. Although the pegmatite and gabbro are not in

direct contact, it is clear that they are not separated by a shear zone. If the ages from the r-eclogites reflect high-pressure metamorphism, as suggested by Ketchum and Krogh (1997), and the ca. 1090 Ma age from the granite-pegmatite reflects intrusion of the granite-pegmatite magma, this observation means that the pegmatite-granite intruded crust that was either undergoing eclogite-facies metamorphism, or had done so within error of the geochronological data. Gebauer (1999) showed that high-pressure and ultra-high pressure metamorphism in the central and western Alps preceded granitoid magmatism by only ca. 5 My, after a phase of very rapid exhumation, and a similar interpretation is possible for the r-eclogite-granite-pegmatite relationship in the Shawanaga domain. Recent results from numerical modeling show that exhumation of rocks from peak pressure (ca. 1.9 GPa) to mid-crustal levels (35-40 km, 1-1.1 GPa) can take less than 10 My in entirely convergent orogens (R. A. Jamieson, pers. comm., 2003). In the models, the rocks spend ca. 5-15 My in the eclogite field and end up as high-P granulites (800-900°C, 1-1.2 GPa), apparently similar to the rocks investigated here.

An alternative interpretation of the metamorphic ages from the r-eclogites is that only the older metamorphic ages (1093-1101 Ma, Hooper Is. Fig. 5.1b) obtained by Ketchum and Krogh (1997) reflect high-pressure metamorphism whereas the younger ages (1085-1090 Ma) represent high-temperature metamorphism (Jamieson et al., submitted). According to this interpretation, intrusion of the granite-pegmatite magma was unrelated to high-pressure metamorphism. Distinguishing between these two interpretations requires further investigations into the significance of the ca. 1085-1100 Ma metamorphic ages obtained from the r-eclogites and better constraints on the age of granite-pegmatite magmatism.

5.4.3. Main phase of Grenvillian metamorphism

A number of geochronological analyses, summarized in Table 5.2, show that by ca. 1080 Ma, high-grade metamorphism had affected all the domains in the hanging wall to the Allochthon Boundary Thrust (ABT) (e.g., Shawanaga, Algonquin, Muskoka). In contrast, the earliest recorded Grenvillian metamorphism in the Britt domain, in the immediate footwall to the ABT, was at <1060 Ma (van Breemen and Davidson, 1990;

Krogh *et al.*, 1993a).

An important question is whether high-grade Grenvillian metamorphism in the CGB was continuous or episodic. Table 5.2 presents a summary of available geochronological data from the CGB, and Fig. 5.7 presents metamorphic (zircon) age data for the Muskoka and Shawanaga domains, suggesting one, protracted Grenvillian event between ca. 1080 and 1050 Ma in the Muskoka domain and 1080 and 1040 Ma in the Shawanaga domain. No distinct episodes of metamorphism can be distinguished within error of the data, suggesting that the rocks remained in the middle crust for more than 30 My, and possibly as long as 50 My (e.g., sample 2M02061-5). The slightly longer duration of metamorphism in the Shawanaga domain is consistent with forward (northwest) propagation of the orogen (Jamieson *et al.*, 1992).

In the Muskoka domain, the main phase of melting appears to have taken place at ca. 1065 Ma (Fig. 5.7a), indicated both in this study (1068±10 Ma, sample 2M02061-9) and by Timmermann *et al.* (1997), who obtained an age of 1064+18/-19 Ma from a concordant leucosome in a different part of the Muskoka domain (Fig. 5.1a). McMullen (1999) obtained an age of 1046+34/-39 Ma for partial melting in the eastern Muskoka domain (Fig. 5.7a), which may indicate a somewhat younger partial melting event, although the age is within error of those noted above. In the Shawanaga domain, T. E. Krogh (unpublished data) dated a leucosome in a boudin neck in the Ojibway gneiss association at ca. 1082 Ma (Fig. 5.7b), and a later age of partial melting at ca. 1055 Ma was obtained in this study (Fig. 5.7b) (sample 2S2006-2) from the Sand Bay gneiss association. These data suggest: 1) that partial melting in the Muskoka domain probably succeeded the onset of high-grade metamorphism at ca. 1080 Ma by several million years, and, 2) that melting may have been episodic. Both of these observations are consistent with partial melting as a result of pulses of fluid influx, as suggested in Chapter 3. However, several studies (e.g., Zeitler and Chamberlain, 1991; Vance and O'Nions, 1992) have shown that discrete events may form part of a continuous process within the crust. Brown *et al.* (1995) suggested that melt segregation probably takes place on timescales of <1 My, even though the source rocks on a regional scale are at

near-peak metamorphic conditions for several tens of millions of years. Thus, considering the field evidence for several generations of leucosome (Timmermann *et al.*, 2002; Chapter 3), it is conceivable that further geochronological work will reveal a more continuous record of partial melting. It is nevertheless clear that melt was present throughout much of the Grenvillian history of the CGB, although the amount and potential effect on crustal strength (cf., van der Molen and Paterson, 1979; Rutter, 1997; Rushmer, 2001) are difficult to estimate. The potential significance of partial melting on the orogenic evolution in this area is discussed further in Chapter 6.
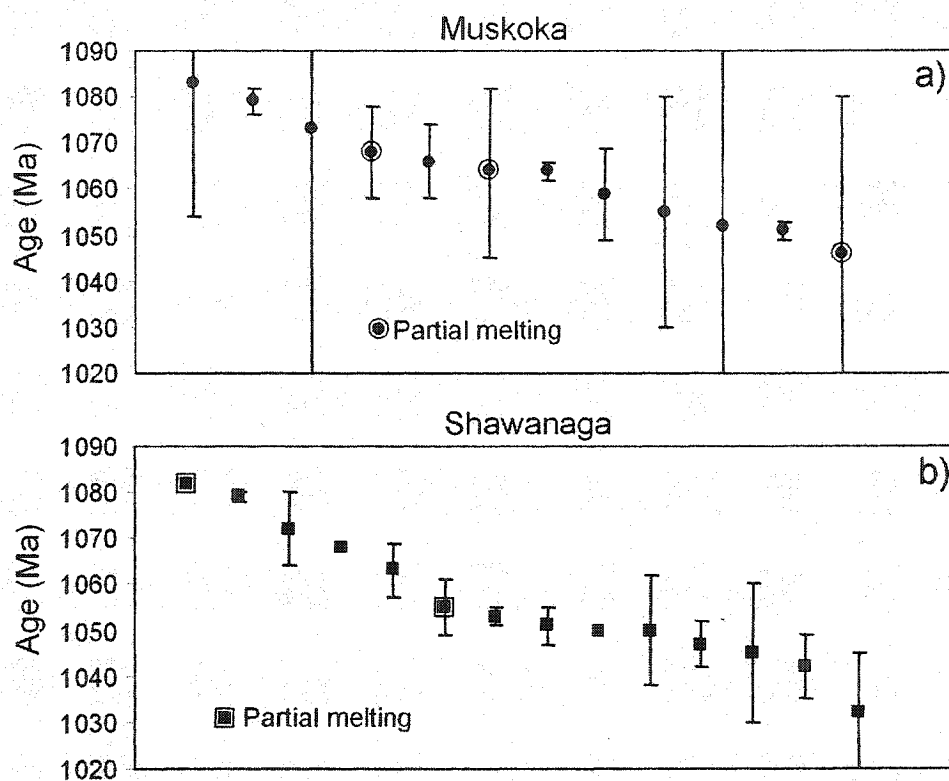
Fig. 5.7   Metamorphic ages from the Muskoka and Shawanaga domains.

Thrust assembly along the Muskoka-Upper Rosseau domain boundary apparently ceased at ca. 1047 Ma, indicated by the age of the late- or post-tectonic granite dike at the boundary (sample 2M1406-2), however, high-grade metamorphic conditions persisted until ca. 1030 Ma. In the eastern Muskoka domain, deformation persisted until ca. 1036 Ma (McMullen, 1999). It follows from these interpretations that significant orogenic extension at ca. 1020 Ma, recorded in structurally lower parts of the CGB (e.g.,

Shawanaga shear zone, Ketchum *et al.*, 1998), did not include reworking of the Muskoka-Upper Rosseau boundary or the interior Muskoka domain. Unfortunately, kinematic indicators are scarce in the high-strain zone separating the Muskoka and Upper Rosseau domains, thus, the kinematic significance of this zone is unclear.

The pegmatitic syenite, dated at ca. 1036 Ma (sample 2M0606-25), is nearly 40 My younger than an apparently similar pegmatite dike from a different part of the Muskoka domain (Fig. 5.1a) (Timmermann *et al.*, 1997). This study suggests that these very distinct pegmatites are related to the development of patchy granulites in the eastern Muskoka domain. However, further work including field work and stable isotope and fluid inclusion analysis is needed in order to determine the significance of these pegmatites and their relationship, if any, to the patchy granulites.

Table 5.2 Summary of U-Pb ages from the Central Gneiss Belt and Grenville Front Tectonic Zone. Updated from Ketchum (1995).

Abbreviations

Domains
- A - Ahmic
- Br - Britt
- Bu - Burwell
- GFTZ - Grenville Front Tectonic Zone
- LGH/UGH - Lower/Upper Go Home
- H - Huntsville
- K - Kiosk
- MCl - McClintock
- MR - Moon River
- N - Novar
- NE - Nepewassi
- O - Opeongo
- PS - Parry Sound
- R - Rosseau
- S - Seguin
- Sh - Shawanaga
- T - Tomiko

Unit / Rock type
- amph. - amphibolite
- anorth. - anorthosite
- g.a. - gneiss association
- gnd. - granodiorite
- mig. - migmatite
- ogn. - orthogneiss
- peg. - pegmatite
- pgn. - paragneiss
- P.-au.-B. complex - Pointe-au-Baril complex
- R-eclogite - retrogressed eclogite

Mineral
- a - allanite
- b - baddeleyite
- g - garnet
- m - monazite
- t - titanite
- ur - uraninite
- wr - whole rock (Pb-Pb age)
- z - zircon

Other
- def. - deformation
- leucos. - leucosome
- metam. - metamorphism
- min. - mineral

1. Grenville Front Tectonic Zone, Killarney area, Burwell and Tomiko domains

Age (Ma), mineral	Domain	Locality	Unit / Rock type	Significance	Reference
~2737 (z, t)	Bu	Hagar	Paragneiss	Metamorphism	Krogh (1989)
2679±2 (z, t)	Bu	WNW of L. Nipissing	Warren trondhjemite	Plutonism	Chen et al. (1995)
2680±2 (z)	Bu	N of L. Nipissing	Gray orthogneiss	Plutonism	Krogh et al. (1992)

Age	Terrane	Location	Rock type	Interpretation	Reference
2672±3 (z)	Bu	N of L. Nipissing	Gray orthogneiss	Plutonism	Krogh et al. (1992)
2669±4 (z, t)	Bu	WNW of L. Nipissing	Tilden tonalite	Plutonism	Chen et al. (1995)
2671±3 (z)	Bu	N of L. Nipissing	Gray orthogneiss	Plutonism	Krogh et al. (1992)
~2660 (z)	GFTZ	N. of North Bay	Pegmatite in ogn.	Min. metam./def.	Krogh and Davis (1970)
2650±5 Ma (z, m)	GFTZ	N of North Bay	Dike	Min. metam. age	Krogh (1991)
2647+/-12 (z)	GFTZ	N of North Bay	Orthogneiss	Plutonism	Steiger and Wasserburg (1969)
~2600 (z)	GFTZ	N of North Bay	Pegmatite	Min. metam. age	Krogh and Davis (1974)
~2600 (z)	GFTZ	N of North Bay	Pegmatite in gneiss	Min. def./metam.	Krogh and Wardle (1984)
2560±155 (wr)	GFTZ	River Valley	River Valley anorth.	Plutonism	Ashwal and Wooden (1989)
1747+6/-5 (z)	GFTZ	Coniston	Wanapitei ogn.	Plutonism	Prevec (1992)
1744±11 (z)	Bu	French River	Gneiss	Max. deposition age?	Krogh (1989)
1742±1 (z)		Killarney	Killarney ogn.	Plutonism	van Breemen and Davidson (1988)
~1740 (z)	GFTZ	Killarney	Orthogneiss	Plutonism	Krogh and Wardle (1984)
1732+7/-6 (z)		Collins Inlet	Killarney porphyry	Plutonism	van Breemen and Davidson (1988)
1715+6/-5 (z)	GFTZ	Beaverstone Bay	Grodine ogn.	Plutonism	Davidson et al. (1992)
1711+10/-8 (z)	GFTZ	Beaverstone Bay	Grodine ogn.	Plutonism	Davidson et al. (1992)
~1703 (z)	GFTZ	Collins Inlet	Fox Island granite	Plutonism	Davidson et al. (1992)
~1700 (z)	GFTZ	S of Bell Lake	Orthogneiss	Plutonism	Krogh et al. (1971)
1686+19/-16 (z)	T	NW of Mattawa	Quartzite	Max. deposition age	Krogh (1989)
~1626 (z)	GFTZ	SE of Sudbury	Chief Lake ogn.	Plutonism	Krogh and Davis (1969)
~1523 (z)	GFTZ	Tyson Lake	Bell Lake granite	Plutonism	Krogh et al. (1971)
1471±3 (z)	GFTZ	Tyson Lake	Bell Lake granite	Plutonism	van Breemen and Davidson (1988)
1454±8 (z, t)	GFTZ	Killarney	Ogn., amph. dikes	Metamorphism	Haggart et al. (1993)
1453±7 (z)	GFTZ	Killarney	Paragneiss	Metamorphism	Krogh (1989)
1450±50 (z)	GFTZ	Collins inlet	Pegmatite dike	Min. def. age	van Breemen and Davidson (1988)
~1445 (z)	GFTZ	Tyson Lake	Paragneiss	Metamorphism	Bethune et al. (1990)
~1400 (z)	Bu	W of L. Nipissing	Cosby ogn.	Plutonism	Silver in Lumbers (1975)

Age	Code	Location	Unit	Event	Reference
~1380 (z)	?	L. Nipissing	Powassan ogn.	Plutonism	Kamo et al. (1989)
1270±3 (z)	NE	N of L. Nipissing	Powassan batholith	Plutonism (A-type)	Davidson and van Breemen (2001)
~1250 (z)	T	E of L. Nipissing	Mulock batholith	Plutonism (A-type)	Davidson and van Breemen (2001)
1244+4/-3 (z)	T	NE of L. Nipissing	Mulock ogn.	Plutonism (A-type)	Lumbers et al. (1991)
1238±4 (b)	?	Espanola	Sudbury diabase	Dike emplacement	Krogh et al. (1987)
1222±2 (z)	Bu	SW of L. Nipissing	Mercer anorth.	Plutonism	Prevec (1992)
1206±18 (z)	Bu	NW of L. Nipissing	St. Charles anorth.	Plutonism	Prevec (1992)
~1150 (z)	GFTZ	Wanapitei	Pegmatitic leucos.	Metamorphism	Krogh and Wardle (1984)
1062±15 (z)	Bu	French River	Gneiss	Metamorphism	Krogh (1989)
~1032-985 (z)	GFTZ	Tyson Lake	Coronitic dikes	Metamorphism	Bethune (1993)
1007±43 (z)	T	NW of Mattawa	Quartzite	Metamorphism	Krogh (1989)
1000±2 (m)	GFTZ	Hagar	Paragneiss	Metam. or cooling	Mezger et al. (1993)
~1000 (z)	GFTZ	Tyson Lake	Coronitic dikes	Metamorphism	Bethune et al. (1990)
996-975 (z, t)	Bu	WNW of L. Nipissing	Warren trondhjemite	Metamorphism	Chen et al. (1995)
~992 (z, t)	Bu	Hagar	Paragneiss	Metamorphism	Krogh (1989)
~991 (z)	Bu	French River	Pegmatite in pgn	Syn-tectonic/metam.	Krogh and Davis (1974)
~991 (t)	GFTZ	N or North Bay	Leucosome	Metamorphism	Krogh et al. (1993b)
988±26	Bu	WNW of L. Nipissing	Tilden tonalite	Metamorphism	Chen et al. (1995)
988±10 (m)	GFTZ	N or North Bay	Dike	Mylonitization	Krogh (1991)
988±5 (m)	GFTZ	N or North Bay	Leucosome	Deformation	Krogh (1991)
988 (m)	GFTZ	S of Sudbury	Pegmatite	Metam./def.	Krogh et al. (1993b)
987-986 (z)	GFTZ	N of North Bay	Leucosome	Metam./def.	Krogh et al. (1993b)
~985 (z)	GFTZ	Tyson Lake	Coronitic dikes	Metamorphism	Bethune (1991)
982±27 (t)	GFTZ	Killarney	Orthogneiss	Metamorphism	Krogh (1989)
~980-963 (t)	GFTZ	Key Harbour	Orthogneiss dike	Cooling ages	Corrigan (1990)
978±13 (t, z)	GFTZ	Killarney	Ogn., amph. dikes	Metamorphism	Haggart et al. (1993)

2. Britt domain

Age (Ma), mineral	Domain	Locality	Unit / Rock type	Significance	Reference
1739±34 (z)	Br	Pointe-au-Baril	Bayfield g.a.	Plutonism	Krogh et al. (1993a)
1694±3 (z)	Br	Key Harbour	Key Harbour ogn.	Plutonism	Corrigan et al. (1994)
1606±2 (z)	Br	Pointe-au-Baril	Nadeau Is. g.a.	Plutonism	T. E. Krogh (unpub. data)
1457+9/-6 (z)	Br	Britt	Britt orthogneiss	Plutonism	van Breemen et al. (1986)
1456+12/-11 (z)	Br	Key Harbour	Britt pluton	Plutonism	Corrigan et al. (1994)
1450±1 (z)	Br	Pointe-au-Baril	Nadeau Is. g.a./Pgn.	Metamorphism	Tuccillo et al. (1992)
1450-1420 (z, t)	Br	Pointe-au-Baril	Bayfield g.a./Ogn.	Metamorphism	Krogh et al. (1992)
1442+7/-6 (z)	Br	Key Harbour	Mann Island gnd.	Plutonism	Corrigan et al. (1994)
~1442 (z)	Br	Key Harbour	Dike	Dike emplacement	Corrigan (1990)
1430±23 (t)	Br	Pointe-au-Baril	Bayfield g.a.	Metamorphism	Krogh et al. (1993a)
1430±17 (z)	Br	Pointe-au-Baril	P.-au-B. complex	Plutonism	Krogh et al. (1993a)
~1420 (z)	Br	Pointe-au-Baril	P.-au-B. complex	Plutonism	Krogh et al. (1992)
1062-1050 (z)	Br	Pointe-au-Baril	Bayfield g.a. (ogn.)	Mylonitization	Krogh et al. (1992)
~1062 (z)	Br	Pointe-au-Baril	Bayfield g.a. (ogn.)	New zircon growth	Krogh et al. (1993a)
1062±2 (m)	Br	Pointe-au-Baril	Nadeau Is. g. a. (pgn.)	Reset or cooling	Tuccillo et al. (1992)
1053±2 (m)	Br	Pointe-au-Baril	Nadeau Is. g. a. (pgn.)	Reset or cooling	Tuccillo et al. (1992)
~1047 (z)	Br	Pointe-au-Baril	Bayfield g.a. (ogn.)	New zircon growth	Krogh et al. (1993a)
1043 (ur)	Br	Britt	Pegmatite	Peg emplacement	Wanless and Lowdon (1961)
1037±1 (m)	Br	Key Harbour	Paragneiss	Cooling age	Corrigan et al. (1994)
1035±1 (m)	Br	Key Harbour	Paragneiss	Cooling age	Corrigan et al. (1994)
1015+16/-17 (z)	Br	Key Harbour	Leucosome in ogn.	Metamorphism	Corrigan et al. (1994)
1003±9 (t)	Br	Key Harbour	Leucosome in ogn.	Cooling ages	Corrigan et al. (1994)
998±15 (t)	Br	Pointe-au-Baril	Bayfield g.a. (ogn.)	Metamorphism	Krogh et al. (1993a)
990+2/-1 (z)	Br	Key Harbour	Pegmatite	Dike emplacement	Corrigan et al. (1994)

3. Algonquin (Huntsville, McClintock, Novar), Lower Rosseau, Lower Go Home, and Opeongo domains

Age (Ma), mineral	Domain	Locality	Unit / Rock type	Significance	Reference
1714+123/-71 (z)	H	Huntsville	Orthogneiss	Plutonism	Nadeau (1990)
1478+34/-27 (z)	MCl	Dorset	Metapelite	Metamorphism?	Timmermann (1998)
1460±60 (z)	H	Huntsville	Orthogneiss	Plutonism	van Breemen et al. (1986)
1460±5 (z)	GH	Go Home River	Migmatitic ogn.	Plutonism or Metam.	Krogh et al. (1993a)
1458±9 (z)	GH	Go Home River	Orthogneiss	Plutonism	Krogh et al. (1993a)
1444-1466 (z)	MCl	Go Home River	Megacrystic ogn.	Plutonism	Timmermann (1998)
1444+12/-8 (z)	N	Huntsville	Orthogneiss	Plutonism	Nadeau and van Breemen (1998)
1442+9/-8 (z)	H	Huntsville	Orthogneiss	Plutonism	Nadeau and van Breemen (1998)
1432+54/-98 (z)	H	Huntsville	Orthogneiss	Metamorphism	Nadeau and van Breemen (1998)
1426±5(z)	MCl	N of Dorset	Megacrystic ogn	Metamorphism	Timmermann (1998)
~1414 (z)	R	Lake Muskoka	Muskoka ogn	Plutonism	Krogh and Davis (1969)
1375+13/-12 (z)	O	Whitney	Orthogneiss	Plutonism	van Breemen and Davidson (1990)
1100±1 (m)	O	Madawaska	Paragneiss	Metam. or cooling	Mezger et al. (1993)
1080±1 (z)	O	Huntsville	Pegmatite	Late syn-thrusting	Nadeau (1990)
1074±2 (m)	H	Algonquin Park	Paragneiss	Metam. or cooling	Mezger et al. (1993)
1069+69/-70	MCl/O	Dorset	Megacrystic ogn	Pb-loss (Metam.)	Timmermann (1998)
1068+51/-12 (m)	MCl	Huntsville	Orthogneiss	Cooling age	Nadeau (1990)
1063±3 (m)	H	Huntsville	Pegmatite	Cooling age	Nadeau (1990)
~1050 (z)	H	Dwight	Ogn dike	Dike emplacement	van Breemen and Davidson (1990)
1049+/-2 (m)	H	Huntsville	Pegmatite	Late syn-thrusting	Nadeau (1990)
1047±2 (z)	H	Honey Harbour	Mafic dike	Metamorphism	Bussey et al. (1995)
1047±2 (z)	GH	Honey Harbour	Pegmatite infill	Metamorphism	Bussey et al. (1995)
1046±2 (z)	GH	Huntsville	Pegmatite	Late syn-thrusting	Nadeau (1990)
1043+22/-23 (z)	H	Whitney	Orthogneiss	Metamorphism	van Breemen and Davidson (1990)
1041+55/-61 (z)	O	Dorset	Metapelite	Metamorphism	Timmermann (1998)
	MCl				

Age (Ma), mineral	Domain	Locality	Unit / Rock type	Significance	Reference
1039+4/-2 (z)	H	Huntsville	Pegmatite	Extensional shear	Nadeau (1990)
1039±2 (t)	N	Novar	Amphibolite	Cooling age	Mezger et al. (1993)
1030+50/-20 (z)	H	Huntsville	Orthogneiss	Metamorphism	van Breemen et al. (1986)
1027±2 (z)	MCl	Huntsville	Pegmatite	Late syn-thrusting	Nadeau (1990)
1018±45 (z)	H	Huntsville	Orthogneiss	Metamorphism	Nadeau (1990)
1008+9/-5 (z)	GH	Honey Harbour	Pegmatite	Late tectonic	Krogh (1991)

4. Shawanaga, Upper Rosseau, Upper Go Home, and Ahmic domains

Age (Ma), mineral	Domain	Locality	Unit / Rock type	Significance	Reference
2000-1382 (z)	Sh	Pointe-au-Baril	Sand Bay g.a./qtzite	Max. depositional age	T. E. Krogh (unpub. data)
1466±11 (z)	Sh	Pointe-au-Baril	Ojibway g.a.	Plutonism	T. E. Krogh (unpub. data)
1460+12/-8 (z)	Br/Sh	Pointe-au-Baril	Shawanaga pluton	Plutonism	T. E. Krogh (unpub. data)
1452±10 (z)	Sh	Parry Sound	Hbl-rich leucosome	Inherited cores	T. Slagstad, M. Hamilton (unpub. data)
<1417±5 (z)	Sh	Pointe-au-Baril	Sand Bay g.a./Pgn	Sedimentation	T. E. Krogh (unpub. data)
~1410 (z)	Sh	Parry Sound	Hbl-rich leucosome	Inherited core	T. Slagstad, M. Hamilton (unpub. data)
<1390-1360 (z)	Sh	Pointe-au-Baril	Sand Bay g.a./Pgn	Sedimentation	T. E. Krogh (unpub. data)
1372+18/-17 (z)	A	W of Magnetawan	Love Lake granite	Plutonism/Inherited core	Bussey et al. (1995)
~1364 (z)	Sh	Pointe-au-Baril	Dillon schist	Max. depositional age	Krogh (unpub. data)
~1350 (z)	Sh	Parry Sound	Hbl-rich leucosome	Inherited core	T. Slagstad, M. Hamilton (unpub. data)
~1347 (z)	Sh	Parry Sound	Granite	Inherited core	T. Slagstad, M. Hamilton (unpub. data)
1346+69/-39 (z)	Sh	Parry Sound	Marginal orthogneiss	Plutonism	van Breemen et al. (1986)
1333+32/-27 (z)	Sh	Pointe-au-Baril	Sand Bay g.a.	Volcanism?	T. E. Krogh (unpub. data)
1302±27 (z)	A	Magnetawan	Migmatite host rock	Protolith	Bussey et al. (1995)
1170±30 (b)	Sh	NW of Parry Sound	Coronitic gabbro	Plutonism	Davidson and van Breemen (1988)
1152±2 (z)	Sh	Hw 69/Pointe-au-Baril	Coronitic gabbro	Plutonism	Heaman and LeCheminant (1993)
1120-1110 (z)	Sh/bPS	N of Parry Sound	R-eclogite	Eclogite metamorphism	Ketchum and Krogh (1997)

Age		Location	Rock type	Event	Reference
1090±12 (z)	Sh	Parry Sound	Granite	Crystallization	T. Slagstad, M. Hamilton (unpub. data)
1090–1085 (z)	Sh/GH	N of Parry Sound	R-eclogite	Eclogite metamorphism	Ketchum and Krogh (1997)
1088±7 (z)	Sh	Parry Sound	Pegmatite	Peg emplacement	T. Slagstad, M. Hamilton (unpub. data)
~1082 (z)	Sh	NW of Parry Sound	Leucos. in boudin neck	Metam./def.	T. E. Krogh (unpub. data)
1080–1078 (z)	Sh	W of Parry Sound	Pegmatite	Deformation	Krogh et al. (1993a)
1078±2 (z)	A	Magnetawan	Migmatite host rock	Metamorphism	Bussey et al. (1995)
1072±8 (z)	Sh	Parry Sound	Pegmatite	Metamorphism	T. Slagstad, M. Hamilton (unpub. data)
1068 (t)	A	W of Magnetawan	Love Lake granite	Plutonism or metam.	Bussey et al. (1995)
~1068 (z)	Sh	W of Parry Sound	Anorthosite	Deformation	Krogh et al. (1993a)
1063±6 (z)	Sh	Parry Sound	Granite	Metamorphism	T. Slagstad, M. Hamilton (unpub. data)
1060–1030 (z)	Sh	NW of Parry Sound	Coronitic gabbro	Metamorphism	van Breemen and Davidson (1990)
1055±6 (z)	Sh	Parry Sound	Hbl-rich leucosome	Anatexis	T. Slagstad, M. Hamilton (unpub. data)
1053±2 (z)	Sh	Pointe-au-Baril	Sand Bay g.a. (pgn.)	Metamorphism	T. E. Krogh (unpub. data)
1051±4 (z)	Sh	Parry Sound	Pegmatite	Metamorphism	T. Slagstad, M. Hamilton (unpub. data)
~1050 (z)	Sh	Pointe-au-Baril	Coronite	Metamorphism	Heaman and LeCheminant (1993)
1050±12 (z)	Sh	Pointe-au-Baril	Ojibway g.a. (ogn.)	Metamorphism	T. E. Krogh (unpub. data)
1047±5 (z)	Sh	NW of Parry Sound	Coronitic metagabbro	Metamorphism	Davidson and van Breemen (1988)
1042±7 (z)	Sh	Parry Sound	Granite	Metamorphism	T. Slagstad, M. Hamilton (unpub. data)
1032±13 (z)	Sh	Parry Sound	Granite	Metamorphism	T. Slagstad, M. Hamilton (unpub. data)
~1006 (z)	Sh	Pointe-au-Baril	Sand Bay g.a. (pgn.)	New zircon growth	Krogh et al. (1993a)
~990 (z)	Sh	Pointe-au-Baril	Sand Bay g.a. (pgn.)	Metamorphism	T. E. Krogh (unpub. data)

5. Muskoka, Seguin, and Moon River domains

Age (Ma), mineral	Domain	Locality	Unit / Rock type	Significance	Reference
1613+123/-119 (z)	Mu	Hw 118	Two-px granulite	?	Timmermann (1998)
1514+40/-30 (z)	Mu	Barry's Bay	Gray orthogneiss	Plutonism	McMullen (1999)
1499+50/-35 (z)	Mu	Barry's Bay	Gray, Grt-Opx ogn.	Plutonism	McMullen (1999)
1470±40 (z)	Mu	E of Bracebridge	Granitic orthogneiss	Plutonism (A-type)	T. Slagstad, M. Hamilton (unpub. data)
1468+26/-17 (z)	Mu	Barry's Bay	Megacrystic ogn.	Plutonism	McMullen (1999)
1449+20/-17 (z)	Mu	E of Bracebridge	Charnockitic ogn.	Plutonism (A-type)	T. Slagstad, J. Ketchum (unpub. data)
1457+7/-6 (z)	Mu	Baysville	Gray orthogneiss	Plutonism	Timmermann et al. (1997)
1456+16/-12 (z)	Mu	Hw 118	Granulite	Plutonism	Timmermann et al. (2002)
1453±6 (z)	S	Huntsville	Orthogneiss	Plutonism	Nadeau and van Breemen (1998)
1440±10 (z)	Mu	N of Bracebridge	Gray orthogneiss	Plutonism	T. Slagstad, M. Hamilton (unpub. data)
1427+16/-13 (z)	S	Huntsville	Orthogneiss	Plutonism	Nadeau and van Breemen (1998)
1420-1430 (z)	Mu	Hw 118	Granulite	Metamorphism	Timmermann (1998)
~1413 (z)	Mu	Barry's Bay	Gray orthogneiss	Plutonism	McMullen (1999)
1394±13 (z)	Mu	Hw 35, Ox Narrows	Granite	Plutonism	Timmermann et al. (1997)
~1390 (z)	Mu	Hw 118	Granulite	Plutonism?	Timmermann (1998)
1097±3 (z)	S	Huntsville	Pegmatite	Syn-thrust/min. metam.	Nadeau (1990)
1080±4 (z)	S	Huntsville	Coronitic metagabbro	Metamorphism	van Breemen and Davidson (1990)
1080-1030 (z)	Mu	N of Bracebridge	Gray orthogneiss	Metamorphism	T. Slagstad, M. Hamilton (unpub. data)
1079±3 (z)	Mu	NE of Baysville	Amphibolite	Metamorphism	Timmermann et al. (1997)
1077±2 (z, t)	Mu	Hw 35, Ox Narrows	Charnockite vein	Vein formation	Timmermann et al. (1997)
1073+74/-86 (z)	Mu	Barry's Bay	Gray, Grt-Opx ogn.	Retrogression	McMullen (1999)
1072+28/-31 (z)	Mu	E of Bracebridge	Charnockitic ogn.	Metamorphism	T. Slagstad, J. Ketchum (unpub. data)
1068±10 (z)	Mu	N of Bracebridge	Leucosome	Anatexis	T. Slagstad, M. Hamilton (unpub. data)
1066±8 (z)	Mu	Ox Narrows	Granite	Metamorphism	Timmermann et al. (1997)
1064+18/-19 (z)	Mu	Baysville	Leucosome	Anatexis	Timmermann et al. (1997)

1064±2 (z)	MR	W of Bala	Mafic dike	Metamorphism	Bussey et al. (1995)
1063-1052 (z)	Mu	Hw 35, Eme's Hill	Granulite vein	Vein formation	Timmermann et al. (2002)
1059±10 (z)	Mu	N of Bracebridge	Leucosome	Metamorphism	T. Slagstad, M. Hamilton (unpub. data)
1058+8/-4 (z)	S/R	Bracebridge	Orthogneiss dike	Min. metam./thrusting	van Breemen and Davidson (1990)
1056±3 (t)	S	Dorset	Granite	Cooling age	Mezger et al. (1993)
1052+52/-55 (z)	Mu	Hw 118	Granulite	Pb-loss (metam.)	Timmermann (1998)
1051±2 (z)	MR	S of Parry Sound	Mafic dike	Metamorphism	Bussey et al. (1995)
1047±7 (z)	Mu	S of Bracebridge	Post-tectonic granite	Granite emplacement	T. Slagstad, M. Hamilton (unpub. data)
1046+34/-39 (z)	Mu	Barry's Bay	Gray ogn./leucosome	Metam./anatexis	McMullen (1999)
1044±3 (t)	Mu	Hw 35, Eme's Hill	Granulite vein	Cooling age	Timmermann et al. (2002)
1036+10/-2.5 (z)	Mu	Barry's Bay	Syn-tectonic peg.	Peg. emplacement	McMullen (1999)
1037±7 (z)	Mu	E of Bracebridge	Peg. syenite w/Opx	Peg. emplacement	T. Slagstad, M. Hamilton (unpub. data)
1024±2 (t)	S	Dorset	Amphibolite	Cooling age	Mezger et al. (1993)
1017 (ur)	MR	Blackstone Lake	Pegmatite	Peg emplacement	Nier et al. (1941)
1014 (ur)	MR	Blackstone Lake	Pegmatite	Peg emplacement	Tilton et al. (1960)
993±2 (z)	Mu	Barry's Bay	Post-tectonic peg	Peg emplacement	McMullen (1999)
984 (ur)	MR	Blackstone Lake	Pegmatite	Peg emplacement	Wanless in Stockwell (1982)
982±45 (z)	Mu	E of Bracebridge	Granitic ogn.	Metam./Pb-loss	T. Slagstad, M. Hamilton (unpub. data)
976 (ur)	MR	Blackstone Lake	Pegmatite	Peg emplacement	Wasserburg and Hayden (1955)
894+110/-116 (z)	Mu	Barry's Bay	Megacrystic ogn	Metam./Pb-loss	McMullen (1999)

6. Parry Sound domain and Twelve Mile Bay assemblage

Age (Ma), mineral	Domain	Locality	Unit / Rock type	Significance	Reference
1438-1120 (z)	PS	Parry Sound	Quartzite	Deposition	Wodicka (1994)
<1436±17 (z)	bPS	Parry Sound	Quartzite	Deposition	Wodicka et al. (1996)
1425±75 (z)	PS	Parry Sound	McKellar ogn.	Plutonism	van Breemen et al. (1986)
1394 - 1364 (z)	bPS	Parry Sound	Megacrystic gnd.	Plutonism	Wodicka et al. (1996)
1383 - 1332 (z)	bPS	Parry Sound	Tonalitic gneiss	Plutonism	Wodicka et al. (1996)
1383±14 (z)	bPS	Parry Sound	Isabella Island ogn.	Plutonism	Wodicka et al. (1996)
1360-1312 (z)	PS	Parry Sound	Orthogneiss	Plutonism	Wodicka (1994)
1350±50 (z)	PS	Parry Sound	Whitestone anorth.	Plutonism	van Breemen et al. (1986)
1350-1286 (z)	PS	Parry Sound	Isabella anorth.	Plutonism	Wodicka (1994)
1315-1288 (z)	PS	Parry Sound	Orthogneiss	Plutonism	Wodicka (1994)
1314+12/-9 (z)	iPS	Parry Sound	Tonalitic gneiss	Plutonism	Wodicka et al. (1996)
~1313 (z)	PS	Parry Sound	Orthogneiss	Plutonism	Macfie and Dixon (1992)
1280±7 (z)	PS	Twelve Mile Bay	Orthogneiss	Plutonism	Wodicka (1994)
1163±3 (z)	bPS	Parry Sound	Parry Island anorth	Plutonism	Wodicka et al. (1996)
1163 - 1151 (z)	bPS	Parry Sound	Mafic dike	Dike intrusion	Wodicka et al. (1996)
1161±3 (z)	PS	Parry Sound	Paragneiss	Metamorphism	van Breemen et al. (1986)
1159±1 (m)	PS	Parry Sound	Paragneiss	Max. cooling age	Wodicka (1994)
1159+5/-4 (z)	PS	Parry Sound	Pegmatite	Thrusting	van Breemen et al. (1986)
1158+58/-101 (z)	bPS	Parry Sound	Isabella Island ogn.	Metamorphism	Wodicka et al. (1996)
1157±3 (z)	PS	Parry Sound	Pegmatite dike	Syn-thrusting	Wodicka (1994)
1157±1 (m)	PS	Parry Sound	Paragneiss	Metamorphism	Tuccillo et al. (1992)
1156-1146 (m)	PS	Parry Sound	Aplite veins	Reset and/or cooling	Wodicka (1994)
1153±2 (m)	PS	Parry Sound	Paragneiss	Cooling age	Wodicka (1994)
1152±2 (z)	PS	Parry Sound	Mafic dike	Min. Metam. age	Wodicka (1994)
1148±6 Ma (z)	PS	Parry Sound	Amphibolite	Min. Metam. age	Wodicka (1994))

Age	Terrane	Terrane name	Rock type	Event	Reference
1146-1140 (m)	PS	Parry Sound	Pegmatite dike	Reset and/or cooling	Wodicka (1994)
1140-1120 (z)	TMB	Twelve Mile Bay	Quartzite	Deposition	Wodicka et al. (1996)
1123±3 (g)	PS	Parry Sound	Paragneiss	Metamorphism	Tuccillo et al. (1992)
1121±5 (z)	PS	Parry Sound	Pegmatite	Late thrusting	van Breemen et al. (1986)
1121-1025 (z)	PS	Twelve Mile Bay	Quartzite	Deposition interval	Wodicka (1994)
1119-1104 (t)	PS	Parry Sound	Leucogabbro	Isotopic resetting	Wodicka (1994)
1117-1107 (t)	PS	Parry Sound	Amphibolite	Isotopic resetting	Wodicka (1994)
1117-1116 (z)	PS	Parry Sound	Peg. in boudin	Deformation	Krogh et al. (1993a)
1116+16/-10 (m)	PS	Parry Sound	Paragneiss	Metamorphism	Wodicka (1994)
1114±2 (z)	PS	Parry Sound	Mafic dike	Metamorphism	Bussey et al. (1995)
1111-1089 (t)	PS	Parry Sound	Amphibolite dike	Isotopic resetting	Wodicka (1994)
1109±1 (t)	PS	Parry Sound	Parry Island anorth.	Isotopic resetting	Wodicka (1994)
1103+6/-4 (z)	MR/PS	Parry Sound	Pegmatite	Late thrusting	van Breemen and Davidson (1990)
1086-1049 (a)	PS	Twelve Mile Bay	Orthogneiss	Reset or cooling	Wodicka (1994)
1080±2 (t)	PS	Parry Sound	Isabella Island ogn.	Metamorphism	Wodicka (1994)
1078±4 (t)	PS	Parry Sound	Quartz vein	Late thrusting	Tuccillo et al. (1992)
1034-1024 (t)	PS	Twelve Mile Bay	Orthogneiss	Reset or cooling	Wodicka (1994)

6. Discussion and conclusions

This chapter is intended to place the results of the thesis in a broader tectonic framework than was done in previous chapters, and to propose topics for further research. The focus is on geodynamic processes; other important topics such as protolith and migmatite petrogenesis were discussed in detail in the respective chapters and are not repeated here

6.1. Pre-Grenvillian evolution of the southwestern Grenville Province

6.1.1. Main new result

The main new result from this work relevant to the pre-Grenvillian evolution of the Grenville Province is that orthogneisses with apparent arc-related, ca. 1450 Ma protoliths in the Central Gneiss Belt are spatially and temporally associated with A-type granitic and charnockitic rocks.

6.1.2. Tectonic evolution

The pre-Grenvillian Paleo- and Mesoproterozoic evolution of the Grenville Province is commonly described in terms of an 'Andean' model (e.g., Rivers and Corrigan, 2000). Although this model may be correct in a broad sense, it is based on comparison with one of the most tectonically complex and varied settings in the world, and is, therefore, of limited practical value for understanding the evolution of and similarities/differences between different parts of the province. One of the main contributions of this thesis, building on the work of Culshaw and Dostal (1997, 2002), is to show that despite high-grade metamorphic and deformational overprint, the rocks retain significant geochemical information about how and in what tectonic setting their protoliths formed (Chapter 2). As stated in Chapter 2, tectonic models for the Grenville Province need to incorporate geochemical data, as well as the geochronological data that have provided most of the basis for developing tectonic models up until now.

Detailed tectonic interpretations for the late Paleoproterozoic to early Mesoproterozoic evolution of the CGB are probably premature, and at the present time,

198

several models are feasible. Fig. 6.1 presents a cartoon summarizing the tectonic evolution of the Laurentian margin (L) between ca. 1450 and 1350 Ma, as described in Chapter 2. The conceptual model in Fig. 6.1 extends until ca. 1150 Ma in order to show that the processes operating between ca. 1450 and 1350 Ma may have continued outboard of the Laurentian margin until the onset of Grenvillian orogenesis at ca. 1200 Ma.

Arc-related magmatic activity in the Muskoka domain (M) at ca. 1450 Ma, most likely on the Laurentian margin, is relatively well established based on abundant geochronological data (e.g., Timmermann *et al.*, 1997; Nadeau and van Breemen, 1998; McMullen, 1999; Chapter 5) and recent geochemical data (McMullen, 1999; Chapter 2). A new finding of this study, discussed in Chapter 2, is that the arc-related rocks are temporally and spatially related to A-type granites and charnockites, interpreted to suggest that the arc underwent intra-arc extension during all or part of its evolution. Anorthosite is commonly spatially and temporally associated with A-type granites (e.g., Frost *et al.*, 2002), but has so far not been identified in the Muskoka domain. It is possible, however, that ca. 1450 Ma anorthosites may be identified during future investigations. In addition to intra-arc extension, the new geochemical data, coupled with published geochronological data, suggest back-arc magmatism in the Britt domain (B) at ca. 1450 Ma (van Breemen *et al.*, 1986; Corrigan *et al.*, 1994). Furthermore, Nadeau and van Breemen (1998) suggested, based on geochronological and Sm-Nd isotopic data, that the Algonquin domain (AL) was situated in the ensialic back-arc region of the Muskoka arc, thus, a broad extensional tectonic regime, for example related to slab roll-back, appears to have dominated at ca. 1450 Ma.

Between ca. 1450 and 1430 Ma, the Britt domain, and possibly Algonquin domain, underwent granulite-facies metamorphism. Ketchum *et al.* (1994) suggested that metamorphism may have been related to accretion of a juvenile arc at this time. Alternatively, the granulite-facies assemblage may have formed in response to slab roll-back resulting in intra-arc/back-arc extension and associated high heat flow (Sandiford and Powell, 1986; Collins, 2002), or from convergence related to flat subduction or subduction advance with heat derived from coeval arc magmatism and/or crustal
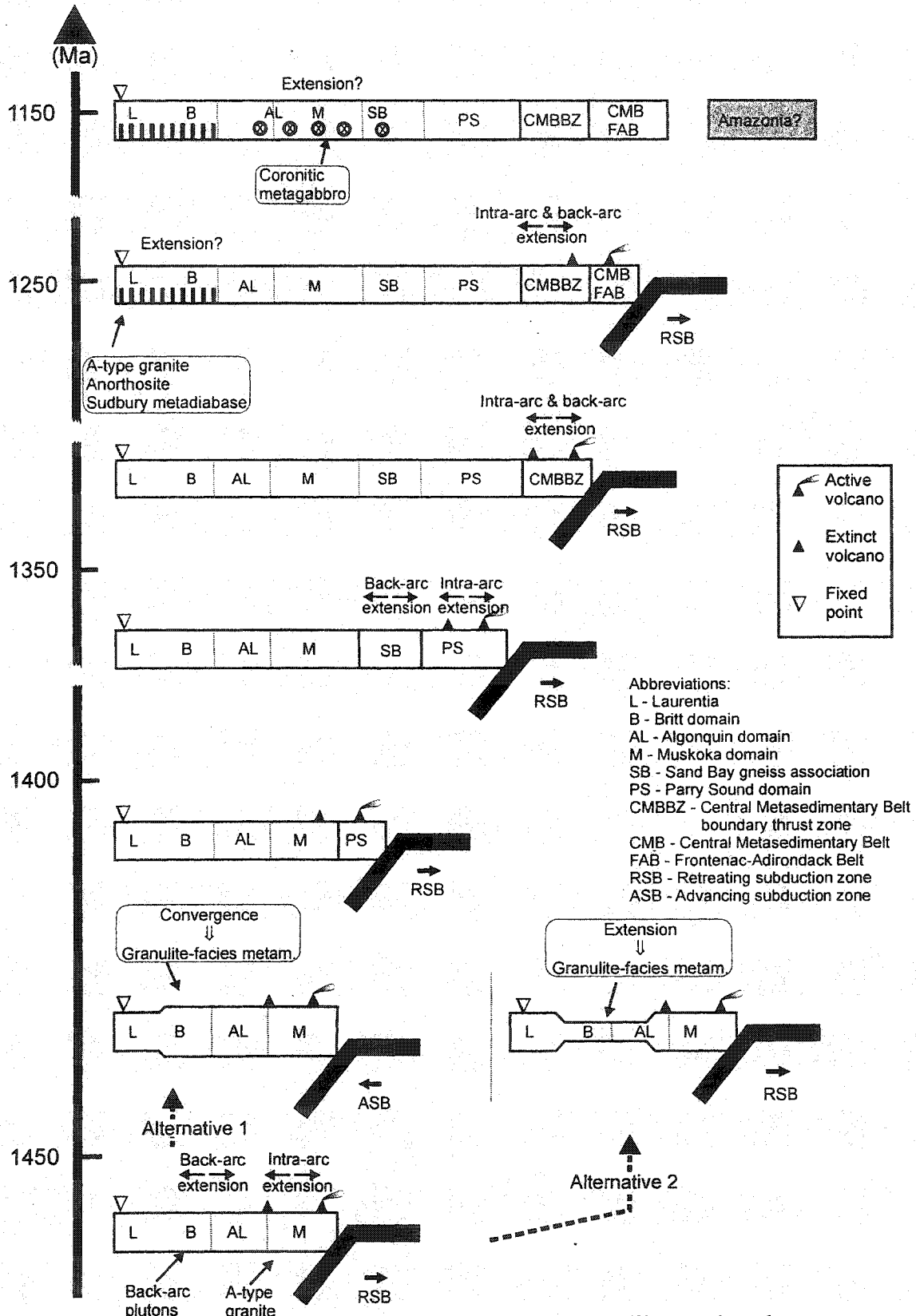
Fig. 6.1 Pre-Grenvillian tectonic evolution of the SW Grenville Province between ca. 1450 and 1150 Ma. ASB-advancing subduction boundary, RSB-retreating subdcution boundary (Royden, 1993).

thickening (e.g., Ross, 1985). The range of possible tectonic settings for this granulite-facies event, all consistent with an 'Andean' model, exemplifies the inherent problems in developing a tectonic model for this area. Fig. 6.1 illustrates two of the three possible interpretations; granulite-facies metamorphism as a result of accretion of a juvenile arc, as suggested by Ketchum *et al.* (1994), is not discussed further. Alternatives 1 and 2 in Fig. 6.1 illustrate granulite-facies metamorphism in response to convergence related to flat subduction or subduction advance and slab roll-back, respectively. Although the geodynamic implications of the two alternatives differ significantly, distinguishing between them is difficult. Both alternatives predict coeval arc magmatism and metamorphism, consistent with the geochronological data from the Muskoka domain, although the younger limit of arc magmatism (ca. 1430 Ma) is open to debate (Chapter 2). Distinction between the two interpretations can be made on the basis of further geochronological and petrographic work. Alternative 1 (convergence) implies i) that A-type magmatism, interpreted to reflect extension, ceased prior to metamorphism, and ii) that granulite-facies conditions were associated with an increase in pressure. In contrast, Alternative 2 (extension) implies i) that A-type magmatism may have been coeval with metamorphism, and ii) that granulite-facies conditions occurred at constant or decreasing pressure. Thus, better constraints on the timing of A-type magmatism and development of P-T-t paths for granulite-facies metamorphism may help distinguish between the two alternatives.

Magmatism in the Parry Sound domain (PS) began at 1425±75 Ma (van Breemen *et al.*, 1986) and may represent continuation of magmatism in the CGB (Culshaw *et al.*, 2002), or a new arc system developed outboard of the Laurentian margin or elsewhere. The former interpretation is preferred here (Fig. 6.1), based on dating of detrital zircons suggesting a Laurentian source for some of the metasedimentary rocks in the Parry Sound domain (Wodicka *et al.*, 1996). The magmatic evolution in the Parry Sound domain has not been studied in detail, but includes granitoid magmatism and intermittent anorthositic magmatism at ca. 1350 Ma, possibly at ca. 1280 Ma, and at ca. 1160 Ma (Table 5.2). The Sand Bay gneiss association formed at ca. 1360 Ma, possibly related to back-arc

extension during magmatism in the Parry Sound domain (Culshaw *et al.*, 2002), and dating of detrital zircons in the Sand Bay gneiss association suggests sediment input from a Laurentian source (T. E. Krogh, unpublished data; M. Raistrick, 2003). Anorthositic magmatism in the Parry Sound domain and rhyolitic volcanism in the Sand Bay gneiss association suggests intra-arc and/or back-arc magmatism at ca. 1350 Ma, i.e., similar to the geodynamic setting at ca. 1450 Ma.

Wodicka *et al.* (1996) interpreted the Parry Sound domain to represent a far-traveled allochthon that originated within the Central Metasedimentary Belt (CMB) or Central Metasedimentary Belt boundary thrust zone (CMBBZ). Magmatism in the CMB commenced later than in the Parry Sound domain, and involved intrusion of gabbro and anorthosite at 1280-1230 Ma, tonalite at 1280-1250 Ma, and 1250-1240 Ma leucogranite (Carr *et al.*, 2000 and references therein). Easton (1992) interpreted the CMB to represent arcs, rifted arcs, and continental fragments, and in Fig. 6.1 magmatism in the Parry Sound domain, CMB and CMBBZ is shown to be continuous with magmatism in the CGB. Magmatism in the Frontenac-Adirondack Belt (FAB) (see Carr *et al.*, 2000 for a review) is indicated in Fig. 6.1 to represent the last stage of outward growth of the Laurentian margin before and possibly overlapping with the onset of the Grenvillian orogeny.

Between ca. 1280 and 1235 Ma, the Sudbury diabase and A-type Powassan and Mulock batholiths intruded rocks now situated below the Allochthon Boundary Thrust (ABT) (Lumbers *et al.*, 1991; Dudás *et al.*, 1994; Davidson and van Breemen, 2001). Later, at ca. 1170-1150 Ma, podiform gabbro intruded rocks above the ABT (Davidson and van Breemen, 1988; Heaman and LeCheminant, 1993). The tectonic significance of these magmatic suites is unclear, although the available geochemical data (e.g., Ketchum and Davidson, 2000) suggest an extensional, continental setting. Their identification is, however, important for understanding the preceding geological history of the area because, as pointed out by Culshaw *et al.* (1997) and Ketchum and Davidson (2000), their apparent mutually exclusive presence in rocks above and below the ABT indicates significant original separation of terranes now juxtaposed along the ABT. Sudbury

metadiabase and coronitic metagabbro have not been identified in the Parry Sound domain or in units within and above the CMBBZ, however, mafic dikes in the Parry Sound domain, dated at between 1151 and 1163 Ma (Wodicka *et al.*, 1996), may represent the same phase of magmatism that produced the coronitic metagabbros.

6.1.3. Suggestions for further work

- Further geochronological and geochemical work, as outlined in Chapter 2, is needed to place tighter constraints on the timing and duration of arc magmatism in the Muskoka domain and to establish the temporal relationship between arc-related and A-type rocks.

- Petrographic work is needed to constrain the tectonic significance of granulite-facies metamorphism between ca. 1450 and 1430 Ma. In particular, determining the P-T-t path of metamorphism would be helpful, but may prove difficult (cf., Ketchum *et al.*, 1994).

- Sm-Nd isotopic analysis of the rocks investigated in Chapter 2 is needed to constrain the proportion of juvenile and older crust in the various lithologies. The isotopic data will have implications for petrogenetic as well as tectonic models, and can be used to establish the relationship (e.g., parent-daughter) between different rock types and to make inferences about the substrate to the magmatic arcs. An isotopic study of this sort is currently underway in the Shawanaga domain (Raistrick, 2003).

- Further geochemical work on rocks that were not targeted or only studied on a reconnaissance level here; e.g., the Mann Island granodiorite, Britt pluton, Parry Sound domain, CMB, FAB is needed to constrain the tectonic evolution of the Grenville Province between ca. 1400 and 1200 Ma.

6.2. Grenvillian tectonic evolution, 1100-1000 Ma

6.2.1. Main new results

The main new results from this work relevant to the Grenvillian evolution of the study area are that i) granite and pegmatite, dated at ca. 1090 Ma, cut what appears to be

a strong, leucosome-bearing fabric in the Sand Bay gneiss association, suggesting a pre-1090 Ma early Grenvillian history of deformation and high-grade metamorphism (but see cautionary note in Chapter 4), ii) partial melting in the CGB may represent discrete events, possibly related to fluid influx, although continuous, protracted partial melting is not ruled out, iii) improved constraints on the age of partial melting in the Muskoka domain, temporally and spatially associated with southeast-directed shear bands, allow new interpretations of Grenvillian geodynamic evolution.

6.2.2. Initial encounter between CGB and CMB

It is widely agreed that Grenvillian deformation in the CGB resulted from overthrusting of arc terranes now represented by the CMB (e.g., Carr *et al.*, 2000). As discussed in Chapter 1, however, there is significant controversy as to when the CMB was thrust onto the CGB. Hanmer and McEachern (1992) argued, based on dating of allegedly syntectonic pegmatite dikes in the CMBBZ, that the CMB was emplaced onto the Laurentian margin at ca. 1190 Ma, and that the shear zone was reactivated at ca. 1080-1060 Ma. This interpretation was disputed by Timmermann *et al.* (1997) who found no evidence of pre-1080 Ma metamorphism in the Muskoka domain in the immediate footwall to the CMBBZ. The results of Timmermann *et al.* (1997) are confirmed by this study. One aspect that should be kept in mind, however, is that although the Muskoka domain forms the immediate footwall to the CMBBZ at the present time, its structural position has been interpreted to be a result of relatively late (<1080 Ma) out-of sequence thrusting (Culshaw *et al.*, 1997; Nadeau and van Breemen, 1998). According to the reconstruction of Culshaw *et al.* (1997) and the conceptual model presented in Fig. 6.1, the Shawanaga domain (or Sand Bay gneiss association) and Parry Sound domain probably lay outboard of the Muskoka domain, consistent with geochronological data from the basal Parry Sound domain and Shawanaga domain, suggesting that the earliest recorded Grenvillian tectonic overprint was between 1160 and 1120 Ma (van Breemen *et al.*, 1986; Tuccillo *et al.*, 1992; Wodicka, 1994). The identification of a strong fabric in the Sand Bay gneiss association, cut by ca. 1090 Ma granite and pegmatite, supports the previously reported geochronological data. Thus,

although the new geochronological data from the Muskoka domain agree with Timmermann *et al.* (1997) that the onset of high-temperature metamorphism in the Muskoka domain was at ca. 1080 Ma, this age may record a stage of propagation of the orogen rather than initiation of Grenvillian orogenesis at the Laurentian margin.

6.2.3. Main phase of Grenvillian high-grade metamorphism and deformation

There is mounting evidence that succeeding an initial phase of high-pressure metamorphism, a prolonged history of high-grade metamorphism ensued in the CGB (Chapter 5). The main anatectic event in the Muskoka domain probably took place at ca. 1065 Ma (Timmermann *et al.*, 1997; Chapter 5), and a younger phase of anatexis may have taken place at ca. 1046 Ma in the eastern Muskoka domain (McMullen, 1999). Anatexis in the Shawanaga domain at ca. 1082 Ma (T. E. Krogh, unpublished data) and at ca. 1055 Ma (Chapter 5) suggests either several episodes of crustal melting throughout the study area, possibly related to pulses of fluid influx (e.g., Chapter, 3), or continuous, protracted melting. Deformation along the Muskoka-Upper Rosseau domain boundary appears to have ceased at ca. 1047±7 Ma, the age of undeformed granite dikes cutting the main Grenvillian foliation (Chapter 5). In contrast, deformation in the eastern Muskoka domain may have operated until at least 1036+10/-2.5 Ma (McMullen, 1999), as indicated by the age of a syn-tectonic pegmatite dike. These data suggest that significant late-tectonic extension at lower structural levels at ca. 1020 Ma (Ketchum *et al.*, 1998) did not affect the Upper Rosseau and Muskoka domains, i.e., the latter domains may have been carried along passively in the hangingwall to deeper structures.

6.2.4. Effects of melting on regional tectonic evolution

Melt weakening at mid-crustal orogenic levels may result in large-scale decoupling and localization of deformation (Hollister and Crawford, 1986; Royden, 1996; Clark and Royden, 2000). Beaumont *et al.* (2001b) and Jamieson *et al.* (2002) used numerical models to investigate the effects of melt weakening on crustal-scale deformation in large collisional orogens. Given a pressure gradient resulting from variation in crustal thickness, and a decrease in mid-crustal viscosity by a factor of <10 (Beaumont *et al.*, 2001b) resulting, for example, from incipient partial melting, narrow zones of gravity-

driven, outward-directed channel flow will develop in the mid-orogenic crust. Jamieson *et al.* (2002) speculated that the Muskoka domain could represent an example of mid-crustal channel flow.

The presence of melt in the Muskoka and Shawanaga domain migmatites must have reduced their strength, and would, therefore, have affected the deformation behavior of the migmatites both locally and regionally. Local differences in host rock composition, volume of leucosome, and strain are obvious in outcrop (Chapter 3). More mafic bulk compositions (metagabbros, dioritic mesosomes) contain less leucosome and the leucosome is less intensely deformed than in rocks of intermediate and felsic composition. The mafic lithologies typically form boudins or pinch-and-swell structures. These observations are compatible with the higher melting temperatures and higher mechanical strength of the metagabbros and diorites (Chapter 3). Once melting had begun, strain would have been strongly partitioned into the relatively weaker rocks with higher melt fractions. On a regional scale, the dominance of granodioritic compositions and leucosome-rich stromatic migmatites must have contributed to a significantly lower bulk effective viscosity for the Muskoka domain by comparison with rocks at both lower and higher structural levels, which contain significant volumes of mafic to intermediate granulite and typically have lower proportions of leucosome.

The effects of the inferred melt weakening on the local and regional structural evolution would have depended on the amount of melt present in the rocks at any one time, the duration of the melt-weakened state, and the regional tectonic regime at the time of melting (Beaumont *et al.*, 2001a). As noted above, outcrop proportions of leucosome range up to 40-50 vol.%. Although it seems unlikely that all the leucosome in these outcrops was molten at the same time, melt volumes of 10-20% are quite likely. At present, we have no constraints on the longevity of melting in these rocks. The observation that some leucosomes are strongly folded, others less folded, and yet others undeformed, suggests that leucosomes were present throughout much of the deformation history of the Muskoka domain, although not necessarily for a long time in any one place.

There is clear field evidence from the Muskoka and Shawanaga domains that melt

was present during top-to-southeast, normal-sense shear, as indicated by leucosomes in shear bands displaying southeast-directed displacement (Timmermann *et al.*, 2002; Chapters 3 and 4). At least three interpretations of this relationship are possible, depending on the tectonic regime associated with the top-to-southeast fabrics: i) the southeast-directed fabrics could be related to southeast-directed shear, syn-convergent extension. In this case, the extensional fabrics should be asymmetrical and demonstrably coeval with convergence, but could be either widely distributed or related to a specific shear zone (e.g., Shawanaga shear zone, Ketchum *et al.*, 1998); ii) the southeast-directed fabrics could be related to ductile thinning (flattening), in which case the fabrics should be symmetrical on a regional scale (but could be asymmetrical on a local scale), should post-date regional convergence (but could drive short-lived convergence at the margins of the orogen) and not restricted to a channel; iii) the southeast-directed fabrics could be related to channel flow (Beaumont *et al.*, 2001b; Jamieson *et al.*, 2002). In this case the fabrics should be restricted to a relatively thin but laterally extensive zone that had a lower viscosity than overlying and underlying regions, ductile flow would be concentrated in this zone and the flow direction in the upper part of the channel would appear to be opposite to the general transport direction. Fabrics related to channel flow should be demonstrably synchronous with convergent structures at lower structural levels.

Alternative i) is difficult to reconcile with the observation that the southeast-directed movement in the Muskoka domain coincides temporally with thrusting near the base of the CMBBZ at ca. 1060 Ma (van Breemen and Hanmer, 1986). The available geochronological data from the Muskoka and Shawanaga domains suggest that partial melting and southeast-directed, normal-sense shear was syn-convergent, and appear to rule out alternative ii) above that implies a post-orogenic age of fabric formation. Alternative ii) is also ruled out because the predicted symmetric structural pattern is not observed (i.e., there are no observations suggesting northwest-directed, normal-sense shear in the CGB). In contrast, a number of observations appear to support the suggestion by Jamieson *et al.* (2002) that the Muskoka (and Shawanaga?) domain represents a zone of Grenvillian channel flow. These domains are thin but laterally

extensive; the high degree of melting is likely to have reduced the viscosity of the rocks and the flow direction in these domains appears to have been opposite to the general transport direction in the CGB at the time of partial melting; flow was syn-tectonic. The study of channel flow in the Muskoka and Shawanaga domains has not been the focus of this thesis, however, as a tentative conclusion, based on results obtained here and from previous studies and following Jamieson *et al.* (2002), I suggest that the Muskoka and Shawanaga domains may represent zone(s) of Grenvillian channel flow.

6.2.5. Did partial melting facilitate thrusting in the study area?

Jamieson *et al.* (1992) suggested that partially molten rocks (migmatites) may have facilitated transport of allochthonous units in the study area by acting as thin, extremely weak, intra-crustal décollements. The geochronological data from the Shawanaga and Muskoka domains suggest that in many cases, partial melting took place several million years after peak metamorphic conditions had been attained, thus, partial melting probably did not facilitate early Grenvillian thrusting. However, as discussed above, leucosome-structure relationships and geochronological data suggest that partial melting in the Muskoka and Shawanaga domains may have been associated with channel flow. Thus, partial melting may have facilitated the assembly of the orogen into its present configuration, as discussed above.

6.2.6. Suggestions for further work

- Further detailed field, geochemical, and petrographic work is needed to understand the apparent differences in petrogenesis and possible relationship to deformation of the stromatic and patchy migmatites, as described in Chapter 3.

- Further field and geochronological work is needed to determine whether melting was episodic or continuous. This information is necessary in order to estimate the amount of melt present in these rocks at any one time, which has significance for the applicability of some tectonic models (for example channel flow).

6.3. The role of fluids in the middle crust during orogenesis

Fluids are powerful agents of metamorphism and their compositions, quantities, and modes of transport exert a fundamental control on melting, mineral stability, mass transport, deformation style, and heat flow. However, despite their potential effects on metamorphic and orogenic processes, the presence, nature, and role of fluids in the orogenic crust, particularly at mid- to lower crustal levels, are debated. Some authors have argued that massive, pervasive influx of CO_2-rich fluids can lead to formation of granulite-facies rocks (Touret, 1971; Jackson and Santosh, 1992), others have argued that flow of aqueous fluids may be important in the formation of greenschist- and amphibolite-facies rocks (Etheridge et al., 1983; Ferry, 1986), and yet others have argued that pervasive influx of fluids at mid- to lower crustal levels is nearly impossible (Stevens and Clemens, 1993).

The southwestern Grenville Province in Ontario exposes large tracts of upper amphibolite- to granulite-facies gneisses and migmatite. During the last five years, new field, petrographic, geochemical, and geochronological data have been obtained from the southwestern Grenville Province that provide some insight into the nature and role of fluids in the mid- to lower orogenic crust (Timmermann, 1998; Timmermann et al., 2002; Layman et al., 2003; this study). Although many more detailed studies on fluid activity during high-grade metamorphism have been conducted in other orogens e.g., the Reynolds Range, Australia (Vry et al., 1996; Williams et al., 1996), Deep Freeze Range, Antarctica (Giorgetti et al., 1996), Bamble Province, Norway (Touret, 1981), and the Limpopo belt, South Africa (Hoernes et al., 1995), the southwestern Grenville Province has the advantage that its metamorphic and deformational history is well constrained after more than 20 years of field, petrographic, and geochronological work (see recent reviews by Culshaw et al., 1997 and Carr et al., 2000, and references therein). This means that processes (e.g., partial melting and associated decrease in viscosity) related to the presence of fluids can be related to the tectonic and metamorphic history of the area to yield a better understanding of the role of fluids during high-grade metamorphism in the mid- to lower orogenic crust. Here, I review field observations, petrographic,

geochemical, and geochronological data from the southwestern Grenville Province that can be interpreted in terms of presence of fluids, and discuss the implications for the role of fluids during high-grade metamorphism in general. In particular, I will point out questions that have arisen from recent work (including this study) in the area.

6.3.1. Evidence of the presence of fluids in the CGB

Petrographic observations from the Muskoka domain suggest that partial melting took place under fluid-present conditions (Chapter 3), although breakdown of biotite probably also contributed to melting (Timmermann et $al.$, 2002). Petrographic observations from the migmatites (metatexites) in the Shawanaga domain (Chapter 4), in particular the relative scarcity of biotite in the host rocks (Sand Bay gneiss) and coarse hornblende in the leucosomes, suggest a similar petrogenesis to the migmatites in the Muskoka domain. In addition to apparent fluid-present melting in the Muskoka and Shawanaga domains, the heterogeneous development of migmatite in the Britt domain may be related to influx of externally derived fluids (N. G. Culshaw, pers. comm., 2003). The compositions, sources, and transport mechanisms of the hypothesized fluids are, however, poorly constrained. The identification of small amounts of carbonate associated with the Muskoka migmatites (Chapter 3), and the interpretation by Timmermann et $al.$ (2002) that some patchy granulites formed at the same time as the migmatites may indicate a mixed H_2O-CO_2 fluid. However, the age and possible genetic relations between migmatite and patchy granulite are not fully resolved, and it is possible that they formed at different times and/or were related to more than one influx of fluid. The geochemical data in Chapter 6 suggest that the hypothesized fluids present during partial melting contained K_2O.

Large mafic bodies, locally identifiable as coronitic metagabbro, are common in the Muskoka domain (see Fig. 2 in Ketchum and Davidson, 2000). A transect across a 45 m wide coronitic metagabbro located ca. 5 km north-northeast of Baysville along Hw 117, shows that the leucosome abundances in the granodioritic host rocks decrease from 39-50 vol.% at distances between 10 and 50 m from the metagabbro to <15 vol.% at distances <10 m from the granodiorite-metagabbro contact. The center of the metagabbro is

granulitic, whereas the outermost 5-8 m of the metagabbro are amphibolitized. Similar features are common elsewhere in the Muskoka domain (Timmermann *et al.*, 2002) and in the Britt domain (N. G. Culshaw, pers. comm., 2003). I interpret this observation to suggest that externally derived fluids were partitioned into the 'dry' mafic rocks where they caused retrogression rather than induce partial melting in the country rocks. In contrast, fluids derived by dehydration of hydrous phases in the country rocks would have caused partial melting at the site of dehydration, and would therefore not have caused retrogression of the metagabbro.

Granulites in the Parry Sound domain are retrogressed to amphibolite-facies toward the southern and southwestern margins (Culshaw *et al.*, 1989; Wodicka *et al.*, 2000). The retrogression is patchy in the more interior parts of the affected zone but becomes pervasive toward the margin (N. G. Culshaw, pers. comm., 2003) suggesting that retrogression resulted from influx of aqueous fluids. Similar examples of retrogression from granulite- to amphibolite-facies have been reported from a number of high-grade terranes e.g., the Scourie terrane, Scotland (Beach, 1976), the Fiskefjord region, Greenland (Garde, 1990), and the Limpopo belt, South Africa (van Reenen, 1986), and are generally interpreted to result from influx of externally derived fluids. The retrogressive fluids are typically interpreted to have been water-rich (e.g., Beach, 1976; Garde, 1990), but in some cases CO_2-rich fluids (van Reenen, 1986) or no fluids at all (Vennemann and Smith, 1992) are invoked.

6.3.2. Discussion

Although a few investigations targeting the nature and role of fluids in high-grade metamorphic rocks of the CGB have been undertaken in the study area (Pattison, 1991; Layman *et al.*, 2003), the observations summarized above suggest that a more systematic study could offer considerable insight on the role of fluid in the lower orogenic crust.

The results of the present study suggest that aqueous or mixed H_2O-CO_2 fluids can migrate through the mid-crustal levels (30-35 km depth) of large collisional orogens. In some migmatite terranes, formed at relatively shallow crustal levels (10-15 km depth), a meteoric fluid has been invoked (e.g., Wickham, 1987a). An atmospheric source is

extremely unlikely in the middle to lower crust, and dehydration of underlying rocks (cf., Le Fort, 1975) may be a more likely source. The Algonquin domain, immediately underlying the Muskoka domain, consists largely of granulites (Culshaw *et al.*, 1983) and may represent a possible source. However, at least some of these granulites formed prior to Grenvillian orogenesis (Nadeau, 1990) and are ruled out as a potential source, and it is not clear that the Algonquin domain was situated underneath the Muskoka domain at the time of partial melting in the latter. The mode of fluid transport also is not clear; for example, did dehydration of the Algonquin domain (or another source) involve partial melting and upward migration of hydrous melts, or were the fluids derived by subsolidus dehydration reactions and then migrated to higher structural levels where they induced partial melting? Was fluid transport pervasive or channelized, and what was the composition of the fluid?

Timmermann *et al.* (2002) suggested that patchy granulites in the eastern Muskoka domain formed in response to influx of low a_{H2O}-fluids during peak metamorphism. Their interpretation follows a large body of literature on apparently similar granulites in southern India (typically referred to as "arrested charnockite" Newton, 1992, and references therein). However, the observation that the patchy granulites are spatially related to orthopyroxene-bearing pegmatitic syenites (Chapter 5) allows an alternative petrogenetic interpretation to that proposed by Timmermann *et al.* (2002). Frost and Frost (1987) suggested that mantle-derived magmas could transport large amounts of CO_2 into the lower and middle crust to form granulite-facies assemblages, and experimental results by Peterson and Newton (1990) suggest that syenitic melts may dissolve relatively large amounts of CO_2. The spatial relationship between pegmatitic syenites and patchy granulite in the Muskoka domain may therefore indicate that the syenites transported CO_2 into the Muskoka domain, causing dehydration and formation of granulite-facies assemblages. The tectonic setting and evolution of the southern India "arrested charnockites" is poorly known. In contrast, the tectonic history of the Grenville Province is comparatively well known and may allow the formation of the patchy granulites to be linked with the tectonic evolution of the area. Several questions need to be answered first. In particular, did the patchy granulites form by influx of a CO_2-rich

fluid, and if so, what was the source of CO_2? Is the relationship between pegmatitic syenite and patchy granulite genetic as well as spatial? Were the pegmatites (and the CO_2 they may have contained) mantle-derived or did they contain a significant crustal component in the form of assimilated rock+associated fluids? If the pegmatites and CO_2 are mantle-derived, how did the mantle get involved?

Although the role of fluids during Grenvillian orogenesis has not been the focus of the present study, this work has highlighted the importance of the problem and has identified a number of specific targets for further study. Stable isotope (O, C, H) and fluid inclusion investigations of the migmatites, patchy granulites, and pegmatitic syenites could yield information about the compositions and sources of fluids during migmatization and formation of the patchy granulites (Hansen *et al.*, 1984; Jackson *et al.*, 1988). Such data are also needed to test the proposed genetic connection between patchy granulites and pegmatitic syenites. Geochemical and petrographic data are needed to test whether the formation of the patchy granulites was associated with compositional changes; for example, Powell (1983) and Clemens (1992) suggest that granulite may form by partial melting and extraction of the hydrous melt. This process should be possible to identify geochemically and petrographically in the patchy granulites. Combined with the large geochronological database from the CGB, further studies in this area, as briefly outlined above, presents an opportunity to relate the presence of fluids to the tectonic and metamorphic evolution of large orogenic systems.

6.4. Conclusions

- Calc-alkaline rocks in the Muskoka domain, probably formed in a continental magmatic arc, are spatially and temporally associated with A-type granites. Both suites of rock intruded at ca. 1450 Ma, and may have overlapped in age with granulite-facies metamorphism in the area.

- Partial melting in the Muskoka and Shawanaga domains may have been episodic, although continuous, protracted melting cannot be ruled out. The petrographic data suggest that partial melting may have taken place in response to influx of externally

derived fluids.

- Partial melting in the Muskoka and Shawanaga domains was coeval with the formation of southeast-directed structures. At the same time, the orogen as a whole was undergoing northwest-directed shortening. This relationship may indicate channel flow within the Muskoka and Shawanaga domains during Grenvillian orogenesis.

- Granite and pegmatite in the Shawanaga domain intruded at ca. 1090 Ma, cutting an older fabric in the Sand Bay gneiss association. The age of granite-pegmatite intrusion is similar to metamorphic ages from nearby retrogressed eclogites, which could represent either the time of high-pressure metamorphism or the high-temperature overprint. The field and geochronological data suggest that the Sand Bay gneiss association underwent Grenvillian deformation and metamorphism at least 10 My before the Muskoka domain.

7. References

Allègre, C. J. and Minster, J. F. (1978). Quantitative models of trace element behavior in magmatic processes. *Earth and Planetary Science Letters*, **38**, 1-25.

Anderson, J. L. and Cullers, R. L. (1978). Geochemistry and evolution of the Wolf River Batholith, a late Precambrian rapakivi massif in North Wisconsin, U.S.A. *Precambrian Research*, **7**, 287-324.

Anderson, J. L. (1983). Proterozoic anorogenic granite plutonism of North America. *Geological Society of America Memoir*, **161**, 133-154.

Arth, J. G. and Hanson, G. N. (1975). Geochemistry and origin of the early Precambrian crust of northeastern Minnesota. *Geochimica et Cosmochimica Acta*, **39**, 325-362.

Arth, J. G. (1976). Behaviour of trace elements during magmatic processes - a summary of theoretical models and their applications. *Journal of Research of the U.S. Geological Survey*, **4**, 41-47.

Arth, J. G. and Barker, F. (1976). Rare earth partitioning between hornblende and dacitic liquid and implications for the genesis of trondhjemitic-tonalitic magmas. *Geology*, **4**, 534-536.

Arzi, A. A. (1978). Critical phenomena in the rheology of partially melted rocks. *Tectonophysics*, **44**, 173-184.

Ashwal, L. D. and Wooden, J. L. (1989). River Valley pluton, Ontario: A late-Archean/early-Proterozoic anorthositic intrusion in the Grenville Province. *Geochimica et Cosmochimica Acta*, **53**, 633-641.

Ashworth, J. R. (1985). Introduction. In Ashworth, J. R. (ed.) *Migmatites*. Glasgow, Blackie, 1-35.

Bacon, C. R. and Druitt, T. H. (1988). Compositional evolution of the zoned calc-alkaline magma chamber of Mount Mazama, Crater Lake, Oregon. *Contributions to Mineralogy and Petrology*, **98**, 224-256.

Barbey, P., Bertrand, J.-M., Angoua, S., and Dautel, D. (1989). Petrology and U/Pb geochronology of the Telohat migmatites, Aleksod, Central Hoggar, Algeria. *Contributions to Mineralogy and Petrology*, **101**, 207-219.

Barnes, C. G., Shannon, W. M., and Kargi, H. (1999). Diverse Mesoproterozoic basaltic magmatism in west Texas. *Rocky Mountain Geology*, **34**, 263-273.

Barnes, C. G., Yoshinobu, A., Prestvik, T., Nordgulen, Ø., Karlsson, H., and Sundvoll, B. (2002). Crustal melting associated with emplacement of mafic arc plutons, Bindal Batholith, Norway. *Journal of Petrology*, **43**, 2171-2190.

Bea, F., Pereira, M. D., and Stroh, A. (1994). Mineral/leucosome trace-element partitioning in a peraluminous migmatite (a laser ablation-ICP-MS study). *Chemical Geology*, **117**, 291-312.

215

Bea, F. (1996). Residence of REE, Y, Th, and U in granites and crustal protoliths: Implications for the chemistry of crustal melts. *Journal of Petrology*, 37, 521-552.

Beach, A. (1976). The interrelations of fluid transport, deformation, geochemistry and heat flow in early Proterozoic shear zones in the Lewisian complex. *Philosophical Transactions of the Royal Society of London*, A280, 569-604.

Beaumont, C., Jamieson, R. A., Nguyen, M. H., and Lee, B. (2001a). Mid-crustal channel flow in large hot orogens: Results from coupled thermal-mechanical models. *Lithoprobe Report*, 79, 112-170.

Beaumont, C., Jamieson, R. A., Nguyen, M. H., and Lee, B. (2001b). Himalayan tectonics explained by extrusion of a low-viscosity crustal channel coupled to focused surface denudation. *Nature*, 414, 738-742.

Bédard, J. H. (2001). Parental magmas of the Nain Plutonic Suite anorthosites and mafic cumulates: A trace element modelling approach. *Contributions to Mineralogy and Petrology*, 141, 747-771.

Berger, A. and Rosenberg, C. L. (2003). Preservation of chemical residue-melt equilibria in natural anatexite: The effects of deformation and rapid cooling. *Contributions to Mineralogy and Petrology*, 144, 416-427.

Bethune, K. M., Davidson, A., and Dudás, F. Ö. (1990). Structure and metamorphism of the Sudbury dykes: Constraints on tectonic evolution of the Grenville Front south of Sudbury, Ontario. Geological Association of Canada - Mineralogical Association of Canada, Program with Abstracts, 15, A10.

Bethune, K. M. (1991). Fate of the Sudbury dykes in the Tyson Lake area south of Sudbury, Ontario: Implications for Grenville Front history and the origin of coronites of high-grade terranes. Geological Association of Canada - Mineralogical Association of Canada, Program with Abstracts, 16, A11.

Bethune, K. M. (1993). Evolution of the Grenville Front in the Tyson Lake area, southwest of Sudbury, Ontario, with emphasis on the tectonic significance of the Sudbury diabase dykes. *Unpublished Ph.D. Thesis, Queen's University, Kingston, Ontario*, 263 p.

Bickford, M. E. (1988). The formation of continental crust: Part 1. A review of some principles; Part 2. An application to the Proterozoic evolution of southern North America. *Geological Society of America Bulletin*, 100, 1375-1391.

Blein, O., Corriveau, L., and LaFlèche, M. (in press). Geochemistry and origin of cordierite-orthopyroxene gneiss in the hydrothermal system of a 1.4 Ga volcano-plutonic arc setting at granulite facies, Grenville Province. In Barthlolomew, M. J. (ed.) *Geological Society of America Memoir: Proterozoic tectonic evolution of the Grenville orogen in eastern North America*. Boulder, Colorado.

Blundy, J. D. and Wood, B. J. (1991). Crystal-chemical controls on the partitioning of Sr and Ba between plagioclase feldspar, silicate melts, and hydrothermal solutions. *Geochimica et Cosmochimica Acta*, 55, 193-209.

Borg, L. E. and Clynne, M. A. (1998). The petrogenesis of felsic calc-alkaline magmas from the southernmost Cascades, California: Origin by partial melting of basaltic lower crust. *Journal of Petrology*, **39**, 1197-1222.

Borg, S. G. and DePaolo, D. J. (1994). Laurentia, Australia, and Antarctica as a Late Proterozoic supercontinent: Constraints from isotopic mapping. *Geology*, **22**, 307-310.

Bowen, R. (1988). *Isotopes in the Earth Sciences*. London, Elsevier Applied Science Publishers Limited, 647 p.

Bowring, S. A., Housh, T. B., and Podosek, F. A. (1991). Nd isotopic constraints on the evolution of Precambrian "anorogenic" granites from Missouri. American Geophysical Union, Program and Abstracts, 1991 Spring Meeting, supplement to EOS Transactions of the American Geophysical Union, April 23, 296.

Brown, G. C., Thorpe, R. S., and Webb, P. C. (1984). The geochemical characteristics of granitoids in contrasting arcs and comments on magma sources. *Journal of the Geological Society of London*, **141**, 413-426.

Brown, M. (1973). The definition of metatexis, diatexis and migmatite. *Proceedings of the Geologists' Association*, **84**, 371-382.

Brown, M. (1979). The petrogenesis of the St. Malo migmatite belt, Armorican Massif, France, with particular reference to the diatexites. *Neues Jahrbuch fur Mineralogische Abhandlungen*, **135**, 48-74.

Brown, M. and Earle, M. M. (1983). Cordierite-bearing schists and gneisses from Timor, eastern Indonesia: P-T conditions of metamorphism and tectonic implications. *Journal of Metamorphic Geology*, **1**, 183-203.

Brown, M. (1994a). The generation, segregation, ascent and emplacement of granite magma: The migmatite-to-crustally-derived granite connection in thickened orogens. *Earth-Science Reviews*, **36**, 83-130.

Brown, M. (1994b). Melt segregation mechanism controls on the geochemistry of crustal melts. *Mineralogical Magazine*, **58a**, 124-125.

Brown, M., Averkin, Y. A., McLellan, E. L., and Sawyer, E. W. (1995). Melt segregation in migmatites. *Journal of Geophysical Research*, **100**, 15655-15679.

Bruhn, R. L., Stern, C. R., and de Wit, M. J. (1978). Field and geochemical data bearing on the development of a Mesozoic volcano-tectonic rift zone and back-arc basin in southernmost South America. *Earth and Planetary Science Letters*, **41**, 32-46.

Busch, W., Schneider, G., and Mehnert, K. R. (1974). Initial melting at grain boundaries. Part II: Melting in rocks of granodioritic, quartz dioritic, and tonalitic composition. *Neues Jahrbuch für Mineralogie, Monatshefte*, **8**, 345-370.

Bussey, F., Krogh, T. E., Klemens, W. P., and Schwerdtner, W. M. (1995). Tectonic and metamorphic events in the westernmost Grenville Province, central Ontario: new results from high-precision U-Pb zircon geochronology. *Canadian Journal of*

Earth Sciences, **32**, 660-671.

Carr, S. D., Easton, R. M., Jamieson, R. A., and Culshaw, N. G. (2000). Geologic transect across the Grenville orogen of Ontario and New York. *Canadian Journal of Earth Sciences,* **37**, 193-216.

Chappell, B. W. (1996). Compositional variation within granite suites of the Lachlan Fold Belt: Its causes and implications for the physical state of granite magma. *Transactions of the Royal Society Edinburgh: Earth Sciences,* **88**, 159-170.

Chavagnac, V., Nägler, T. F., and Kramers, J. D. (1999). Migmatization by metamorphic segregation at subsolidus conditions: Implications for Nd-Pb isotope exchange. *Lithos,* **46**, 275-298.

Chen, Y. D., Krogh, T. E., and Lumbers, S. B. (1995). Neoarchean trondhjemitic and tonalitic orthogneisses identified within the northern Grenville Province in Ontario by precise U-Pb dating and petrologic studies. *Precambrian Research,* **72**, 263-281.

Clark, M. K. and Royden, L. H. (2000). Topographic ooze: Building the eastern margin of Tibet by lower crustal flow. *Geology,* **28**, 703-706.

Clemens, J. D., Holloway, J. R., and White, A. J. R. (1986). Origin of an A-type granite: Experimental constraints. *American Mineralogist,* **71**, 317-324.

Clemens, J. D. and Vielzeuf, D. (1987). Constraints on melting and magma production in the crust. *Earth and Planetary Science Letters,* **86**, 287-306.

Clemens, J. D. (1989). The importance of residual source material (restite) in granite petrogenesis: A comment. *Journal of Petrology,* **30**, 1313-1316.

Clemens, J. D. (1992). Partial melting and granulite genesis: A partisan overview. In de Wit, M. J. (ed.) *The Archean Limpopo Granulite Belt: Tectonics and deep crustal processes. Precambrian Research,* **55**.

Clemens, J. D. (1993). Experimental evidence against CO_2-promoted deep crustal melting. *Nature,* **363**, 336-338.

Clemens, J. D. and Watkins, J. M. (2001). The fluid regime of high-temperature metamorphism during granitoid magma genesis. *Contributions to Mineralogy and Petrology,* **140**, 600-606.

Clifford, P. M. (1990). Mid-Proterozoic deformational and intrusive events along the Grenville Front in the Sudbury-Killarney area, Ontario, and their implications. In Ryan, A. B. (ed.) *Mid-Proterozoic Laurentia-Baltica: Geological Association of Canada Special Paper,* **38**, 335-350.

Clynne, M. A. (1990). Stratigraphic, lithologic, and major element geochemical constraints on magmatic evolution at Lassen volcanic center, California. *Journal of Geophysical Research,* **95**, 19651-19669.

Collins, W. J., Beams, S. D., White, A. J. R., and Chappell, B. W. (1982). Nature and

origin of A-type granites with particular reference to southeastern Australia. *Contributions to Mineralogy and Petrology*, **80**, 189-200.

Collins, W. J. (2002). Hot orogens, tectonic switching, and creation of continental crust. *Geology*, **30**, 535-538.

Condie, K. C. (1986). Geochemistry and tectonic setting of Early Proterozoic supracrustal rocks in the southwestern United States. *Journal of Geology*, **94**, 845-864.

Condie, K. C. and Chomiak, B. (1996). Continental accretion: Contrasting Mesozoic and Early Proterozoic tectonic regimes in North America. *Tectonophysics*, **265**, 101-126.

Coney, P. J., Jones, D. L., and Monger, J. W. H. (1980). Cordilleran suspect terranes. *Nature*, **288**, 329-333.

Conrad, W. K., Nicholls, I. A., and Wall, V. J. (1988). Water-saturated and - undersaturated melting of metaluminous and peraluminous crustal compositions at 10kb: Evidence for the origin of silicic magmas in the Taupo Volcanic Zone, New Zealand, and other occurrences. *Journal of Petrology*, **29**, 765-803.

Corrigan, D. (1990). Geology and U-Pb geochronology of the Key Harbour area, Britt Domain, Southwest Grenville Province. *Unpublished M.Sc. Thesis, Dalhousie University, Halifax, N.S.*

Corrigan, D., Culshaw, N. G., and Mortensen, J. K. (1994). Pre-Grenvillian evolution and Grenvillian overprinting of the Parautochthonous Belt in Key Harbour, Ontario: U-Pb and field constraints. *Canadian Journal of Earth Sciences*, **31**, 583-596.

Corriveau, L. and van Breemen, O. (2000). Docking of the Central Metasedimentary Belt to Laurentia in geon 12: Evidence from the 1.17-1.16 Ga Chevreuil intrusive suite and host gneisses, Québec. *Canadian Journal of Earth Sciences*, **37**, 253-269.

Cosca, M. A., Mezger, K., and Essene, E. J. (1998). The Baltica-Laurentia connection: Sveconorwegian (Grenvillian) metamorphism, cooling, and unroofing in the Bamble Sector, Norway. *Journal of Geology*, **106**, 539-552.

Creaser, R. A., Price, R. C., and Wormald, R. J. (1991). A-type granites revisited: Assessment of a residual-source model. *Geology*, **19**, 163-166.

Creaser, R. A. and White, A. J. R. (1991). Yardea dacite-Large-volume, high-temperature felsic volcanism from the Middle Proterozoic of South Australia. *Geology*, **19**, 48-51.

Cullers, R. L., Koch, R. J., and Bickford, M. E. (1981). Chemical evolution of magmas in the Proterozoic terrane of the St. Francois Mountains, southeastern Missouri 2. Trace element data. *Journal of Geophysical Research*, **86**, 10388-10401.

Cullers, R. L., Stone, J., Anderson, J. L., Sassarini, N., and Bickford, M. E. (1993). Petrogenesis of Mesoproterozoic Oak Creek and West McCoy Gulch plutons, Colorado: An example of cumulate unmixing of mid-crustal, two-mica granite of

orogenic affinity. *Precambrian Research*, **62**, 139-169.

Culshaw, N. G., Davidson, A., and Nadeau, L. (1983). Structural subdivisions of the Grenville Province in the Parry Sound-Algonquin region, Ontario. *Current Research, Part B, Geological Survey of Canada, Paper 83-1B*, 243-252.

Culshaw, N. G. (1986). Geology of the Drag Lake area, Haliburton County, Southern Ontario. Ontario Geological Survey, Open File Report, **5594**, 79 p.

Culshaw, N. G., Corrigan, D., Drage, J., and Wallace, P. (1988). Georgian Bay geological synthesis: Key Harbour to Dillon, Grenville Province of Ontario. *Current Research, Part C, Geological Survey of Canada, Paper 88-1C*, 129-133.

Culshaw, N. G., Check, G., Corrigan, D., Drage, J., Gower, R., Haggart, M. J., Wallace, P., and Wodicka, N. (1989). Georgian Bay geological synthesis: Dillon to Twelve Mile Bay, Grenville Province of Ontario. *Current Research, Part C, Geological Survey of Canada, Paper 89-1C*, 157-163.

Culshaw, N. G., Corrigan, D., Ketchum, J. W. F., and Wallace, P. (1990). Georgian Bay geological synthesis: Twelve Mile Bay to Port Severn, Grenville Province of Ontario. *Current Research, Part C, Geological Survey of Canada, Paper 90-1C*, 107-112.

Culshaw, N. G., Ketchum, J. W. F., Wodicka, N., and Wallace, P. (1994). Deep crustal extension following thrusting in the southwestern Grenville Province, Ontario. *Canadian Journal of Earth Sciences*, **31**, 160-175.

Culshaw, N. G. and Dostal, J. (1997). Sand Bay gneiss association, Grenville Province, Ontario: A Grenvillian rift- (and -drift) assemblage stranded in the Central Gneiss Belt? *Precambrian Research*, **85**, 97-113.

Culshaw, N. G., Jamieson, R. A., Ketchum, J. W. F., Wodicka, N., Corrigan, D., and Reynolds, P. H. (1997). Transect across the northwestern Grenville orogen, Georgian Bay, Ontario: Polystage convergence and extension in the lower orogenic crust. *Tectonics*, **16**, 966-982.

Culshaw, N. G., Ketchum, J. W. F., and Barr, S. (2000). Structural evolution of the Makkovik Province, Labrador, Canada: Tectonic processes during 200 Myr at a Paleoproterozoic active margin. *Tectonics*, **19**, 961-977.

Culshaw, N. G. and Dostal, J. (2002). Amphibolites of the Shawanaga domain, Central Gneiss Belt, Grenville Province, Ontario: Tectonic setting and implications for relations between the Central Gneiss Belt and Midcontinental USA. *Precambrian Research*, **113**, 65-85.

Culshaw, N. G., Jamieson, R. A., Slagstad, T., and Raistrick, M. (2002). The Pre-Grenville magmatic record of the Central Gneiss Belt, Grenville Province, Ontario: A long-lived continental arc. Geological Association of Canada - Mineralogical Association of Canada, Program with Abstracts, **27**, 25.

Dalziel, I. W. D. (1991). Pacific margins of Laurentia and East Antarctica as a conjugate

rift pair: Evidence and implications for an Eocambrian supercontinent. *Geology*, **19**, 598-601.

Davidson, A. and Morgan, W. C. (1980). Preliminary notes on the geology east of Georgian Bay, Grenville Structural Province, Ontario. *Current Research, Part A, Geological Survey of Canada, Paper 81-1A*, 291-298.

Davidson, A., Culshaw, N. G., and Nadeau, L. (1982). A tectono-metamorphic framework for part of the Grenville Province, Parry Sound region, Ontario. *Current Research, Part A, Geological Survey of Canada, Paper 82-1A*, 175-190.

Davidson, A. (1984). Identification of ductile shear zones in the southwestern Grenville Province of the Canadian Shield. In Greiling, E. (ed.) *Precambrian tectonics illustrated.* Stuttgart, Schweizerbart'sche Verlagsbuchhandlung, 263-279.

Davidson, A., Nadeau, L., Grant, S. M., and Pryer, L. L. (1985). Studies in the Grenville Province of Ontario. *Current Research, Part A. Geological Survey of Canada, Paper 85-1A*, 463-483.

Davidson, A. (1986). Grenville Front relationships near Killarney, Ontario. In Baer, A. J. (ed.) *The Grenville Province: Geological Association of Canada Special Paper*, **31**, 107-117.

Davidson, A. and van Breemen, O. (1988). Baddeleyite-zircon relationships in coronitic metagabbro, Grenville Province, Ontario: Implications for geochronology. *Contributions to Mineralogy and Petrology*, **100**, 291-299.

Davidson, A. (1990). Evidence for eclogite metamorphism in the southwest Grenville Province, Ontario. *Current Research, Part C, Geological Survey of Canada, Paper 90-1C*, 113-118.

Davidson, A., van Breemen, O., and Sullivan, R. W. (1992). Circa 1.75 Ga ages for plutonic rocks from the Southern province and adjacent Grenville Province: What is the expression of the Penokean orogeny? *Radiogenic Age and Isotopic Studies: Report 6. Geological Survey of Canada, Paper 92-2*, 107-118.

Davidson, A. (1995). A review of the Grenville orogen in its North American type area. *AGSO Journal of Australian Geology & Geophysics*, **16**, 3-24.

Davidson, A. (1998). An overview of Grenville Province Geology, Canadian Shield; Chapter 3. In St-Onge, M. R. (ed.) *Provinces and Precambrian Fossils in North America. Geological Survey of Canada No. 7*, **C-1**, 205-217.

Davidson, A. and van Breemen, O. (2001). Mid-Mesoproterozoic granitoid rocks in the North Bay area, Grenville Province, Ontario. *Radiogenic Age and Isotopic Studies: Report 14. Geological Survey of Canada, Current Research 2001-F8*, 15.

Davidson, C., Schmid, S. M., and Hollister, L. S. (1994). Role of melt during deformation in the deep crust. *Terra Nova*, **6**, 133-142.

Davidson, J. P., Dungan, M. A., Ferguson, K. M., and Colucci, M. T. (1987). Crust-magma interactions and the evolution of arc magmas: The San Pedro-Pellado

volcanic complex, southern Chilean Andes. *Geology*, 15, 443-446.

Davis, D. (1982). Optimum linear regression and error estimation applied to U-Pb data. *Canadian Journal of Earth Sciences*, 19, 2141-2149.

DePaolo, D. J. (1981). Trace element and isotopic effects of combined wallrock assimilation and fractional crystallization. *Earth and Planetary Science Letters*, 53, 189-202.

Derry, D. R. (1950). A tectonic map of Canada *Geological Association of Canada, Proceedings*, 3, 39-53.

Devine, J. D. (1995). Petrogenesis of the basalt-andesite-dacite association of Grenada, Lesser Antilles island arc, revisited. *Journal of Volcanology and Geothermal Research*, 69, 1-33.

Dewey, J. F. and Burke, K. C. (1973). Tibetan, Variscan, and Precambrian basement reactivation: Products of continental collisions. *Journal of Geology*, 81, 683-692.

Dickin, A. P. and McNutt, R. H. (1990). Nd model-age mapping of Grenville lithotectonic domains: Mid-Proterozoic crustal evolution in Ontario. In Ryan, B. (ed.) *Mid-Proterozoic Laurentian-Baltica: Geological Association of Canada Special Paper*, 38, 79-94.

Dorais, M. J., Whitney, J. A., and Roden, M. F. (1990). Origin of mafic enclaves in the Dinkey Creek Pluton, central Sierra Nevada Batholith, California. *Journal of Petrology*, 31, 853-881.

Dostal, J., Baragar, W. R. A., and Dupuy, C. (1986). Petrogenesis of the Natkusiak continental basalts, Victoria Island, Northwest Territories, Canada. *Canadian Journal of Earth Sciences*, 23, 622-632.

Dudás, F. O., Davidson, A., and Bethune, K. M. (1994). Age of the Sudbury diabase dykes and their metamorphism in the Grenville Province, Ontario. *Radiogenic Age and Isotopic Studies: Report 8. Geological Survey of Canada, Current Research 1994-F*, 97-106.

Dunphy, J. M. and Ludden, J. N. (1998). Petrological and geochemical characteristics of a Paleoproterozoic magmatic arc (Narsajuaq terrane, Ungava Orogen, Canada) and comparisons to Superior Province granitoids. *Precambrian Research*, 91, 109-142.

Easton, M. R. (1992). The Grenville Province and the Proterozoic history of central and southern Ontario. In Stott, G. M. (ed.) *Geology of Ontario, Ontario Geological Survey Special Volume 4, Part 2*, 715-904.

Easton, R. M. (1986). Geochronology of the Grenville Province. In Baer, A. J. (ed.) *The Grenville Province: Geological Association of Canada Special Paper*, 31, 127-173.

Eby, G. N. (1990). The A-type granitoids: A review of their occurrence and chemical characteristics and speculations on their petrogenesis. *Lithos*, 26, 115-134.

England, P. C. and Thompson, A. B. (1984). Pressure-temperature-time paths of regional metamorphism I. Heat transfer during the evolution of regions of thickened continental crust. *Journal of Petrology*, **25**, 894-928.

Escuder Viruete, J. (1999). Hornblende-bearing leucosome development during syn-orogenic crustal extension in the Tormes Gneiss Dome, NW Iberian Massif, Spain. *Lithos*, **46**, 751-772.

Etheridge, M. A., Wall, V. J., and Vernon, R. H. (1983). The role of the fluid phase during regional metamorphism and deformation. *Journal of Metamorphic Geology*, **1**, 205-226.

Faure, G. (1986). *Principles of Isotope Geology*. New York, John Wiley and Sons, 589 p.

Ferry, J. M. (1986). Reaction progress: A monitor of fluid-rock interaction during metamorphic and hydrothermal events. In Wood, B. J. (ed.) *Fluid-rock interactions during metamorphism*. New York, Springer, 60-88.

Fountain, J. C., Hodge, D. S., and Shaw, R. P. (1989). Melt segregation in anatectic granites: A thermo-mechanical model. *Journal of Volcanology and Geothermal Research*, **39**, 279-296.

Fourcade, S., Martin, H., and de Brémond d'Ars, J. (1992). Chemical exchange in migmatites during cooling. *Lithos*, **28**, 43-53.

Frost, B. R. and Frost, C. D. (1987). CO_2, melts and granulite metamorphism. *Nature*, **327**, 503-506.

Frost, B. R., Barnes, C. G., Collins, W. J., Arculus, R. J., Ellis, D. J., and Frost, C. D. (2001). A geochemical classification for granitic rocks. *Journal of Petrology*, **42**, 2033-2048.

Frost, C. D. and Frost, B. R. (1997). Reduced rapakivi-type granites: The tholeiite connection. *Geology*, **25**, 647-650.

Frost, C. D., Frost, B. R., Chamberlain, K. R., and Edwards, B. R. (1999). Petrogenesis of the 1.43 Ga Sherman batholith, SE Wyoming, USA: A reduced, rapakivi-type anorogenic granite. *Journal of Petrology*, **40**, 1771-1802.

Frost, C. D., Frost, B. R., Bell, J. M., and Chamberlain, C. P. (2002). The relationship between A-type granites and residual magmas from anorthosite: Evidence from the northern Sherman batholith, Laramie Mountains, Wyoming, USA. *Precambrian Research*, **119**, 45-71.

Fujimaki, H., Tatsumoto, M., and Aoki, K. (1984). Partition coefficients of Hf, Zr and REE between phenocrysts and groundmasses *Journal of Geophysical Research, Proceedings of the fourteenth lunar and planetary science conference, Part 2*, **89**, Supplement B662-B672.

Garde, A. A. (1990). Thermal granulite facies metamorphism with diffuse retrogression in Archean orthogneisses, Fiskefjord, southern West Greenland. *Journal of Metamorphic Geology*, **8**, 663-682.

Gardien, V., Thompson, A. B., and Ulmer, P. (2000). Melting of biotite+plagioclase+quartz gneisses: The role of H_2O in the stability of amphibole. *Journal of Petrology*, **41**, 651-666.

Gebauer, D. (1999). Alpine geochronology of the Central and Western Alps: New constraints for a complex geodynamic evolution. *Schweizerische Mineralogische Petrographische Mitteilungen*, **79**, 191-208.

Gertisser, R. and Keller, J. (2000). From basalt to dacite: Origin and evolution of the calc-alkaline series of Salina, Aeolian Arc, Italy. *Contributions to Mineralogy and Petrology*, **139**, 607-626.

Gill, J. B. (1984). Sr-Pb-Nd isotopic evidence that both MORB and OIB sources contribute to oceanic island arc magma sources in Fiji. *Earth and Planetary Science Letters*, **68**, 443-458.

Giorgetti, G., Frezzotti, M.-L.-E., Palmeri, R., and Burke, E. A. J. (1996). Role of fluids in migmatites: CO_2-H_2O fluid inclusions in leucosomes from the Deep Freeze Range migmatites (Terra Nova Bay, Antarctica). *Journal of Metamorphic Geology*, **14**, 307-317.

Govindaraju, K. (1994). 1994 compilation of working values and sample description for 383 geostandards. *Geostandards Newsletter*, **18**, 1-158.

Gower, C. (1992). Stage in the evolution of the southern margin of mid-Proterozoic Laurentia-Baltica. *Geologiska Föreningen i Stockhom Förhandlingar*, **114**, 455-457.

Gower, C. F., Rivers, T., and Ryan, A. B. (1990). *Mid-Proterozoic Laurentia-Baltica: Geological Association of Canada Special Paper 38*, 581 p.

Green, A. G., Milkereit, B., Davidson, A., Spencer, C., Hutchinson, W. F., Cannon, W. F., Lee, M. W., Agena, W. F., Behrendt, J. C., and Hinze, W. J. (1988). Crustal structure of the Grenville Front and adjacent terranes. *Geology*, **16**, 788-792.

Green, T. H. (1982). Anatexis of mafic crust and high pressure crystallization of andesite. In Thorpe, R. S. (ed.) *Andesites*. London, John Wiley & Sons, 465-487.

Greenfield, J. E., Clarke, G. L., Bland, M., and Clark, D. J. (1996). In-situ migmatite and hybrid diatexite at Mt Stafford, central Australia. *Journal of Metamorphic Geology*, **14**, 413-426.

Grove, T. L. and Donnelly-Nolan, J. M. (1986). The evolution of young silicic lavas at Medicine Lake Volcano, California: Implications for the origin of compositional gaps in calc-alkaline series lavas. *Contributions to Mineralogy and Petrology*, **92**, 281-302.

Gutscher, M.-A., Spakman, W., Bijwaard, H., and Engdahl, E. R. (2000). Geodynamics of flat subduction: Seismicity and tomographic constraints from the Andean margin. *Tectonics*, **19**, 814-833.

Haggart, M. J., Jamieson, R. A., Reynolds, P. H., Krogh, T. E., Beaumont, C., and

Culshaw, N. G. (1993). Last gasp of the Grenville orogeny - thermochronology of the Grenville Front Tectonic Zone near Killarney, Ontario. *Journal of Geology*, **101**, 575-589.

Hanmer, S. (1988). Ductile thrusting at mid-crustal level, southwestern Grenville Province. *Canadian Journal of Earth Sciences*, **25**, 1049-1059.

Hanmer, S. and McEachern, S. J. (1992). Kinematical and rheological evolution of a crustal-scale ductile thrust zone, Central Metasedimentary Belt, Grenville orogen, Ontario. *Canadian Journal of Earth Sciences*, **29**, 1779-1790.

Hansen, E. C., Newton, R. C., and Janardhan, A. S. (1984). Fluid inclusions in rocks from the amphibolite-facies gneiss to charnockite progression in southern Karnataka, India: Direct evidence concerning the fluids of granulite metamorphism. *Journal of Metamorphic Geology*, **2**, 249-264.

Hansen, F. D. and Carter, N. L. (1982). Creep of selected crustal rocks at 1000 MPa. *Transactions of the American Geophysical Union*, **63**, 437.

Hanson, G. N. (1978). The application of trace elements to the petrogenesis of igneous rocks of granitic composition. *Earth and Planetary Science Letters*, **38**, 26-43.

Harris, N., Inger, S., and Massey, J. A. (1993). The role of fluids in the formation of High Himalayan leucogranites. In Searle, M. (ed.) *Himalayan tectonics: Geological Society of London Special Publication*, **74**, 391-400.

Harrison, T. M. and Watson, E. B. (1984). The behavior of apatite during crustal anatexis: Equilibrium and kinetic considerations. *Geochimica et Cosmochimica Acta*, **48**, 1467-1477.

Heaman, L. M. and LeCheminant, A. N. (1993). Paragenesis and U-Pb systematics of baddeleyite (ZrO_2). *Chemical Geology*, **110**, 95-126.

Herzberg, C. (1995). Phase equilibria of common rocks in the crust and mantle. In Ahrens, T. J. (ed.) *Rock Physics and Phase Relations. A Handbook of Physical Constants*, American Geophysical Union, **3**, 166-177.

Hildreth, W. (1981). Gradients in silicic magma chambers: Implications for lithospheric magmatism. *Journal of Geophysical Research*, **86**, 10153-10192.

Hochstaedter, A. G., Gill, J. B., and Morris, J. D. (1990). Volcanism in the Sumisu Rift, II. Subduction and non-subduction related components. *Earth and Planetary Science Letters*, **100**, 195-209.

Hoernes, S., Lichtenstein, U., van Reenen, D. D., and Mokgatlha, K. (1995). Whole-rock / mineral O-isotope fractionations as a tool to model fluid-rock interaction in deep seated shear zones of the Southern Marginal Zone of the Limpopo Belt, South Africa. *South African Journal of Geology*, **98**, 488-497.

Hoffmann, P. F. (1989). Precambrian geology and tectonic history of North America. In Palmer, A. R. (ed.) *The Geology of North America; An overview: Geological Society of America, The Geology of North America*, A, 447-511.

Hoffmann, P. F. (1991). Did the break-out of Laurentia turn Gondwana inside-out? *Science*, **252**, 1409-1412.

Hollister, L. S. and Crawford, M. L. (1986). Melt-enhanced deformation: A major tectonic process. *Geology*, **14**, 558-561.

Icenhower, J. and London, D. (1995). An experimental study of element partitioning among biotite, muscovite and coexisting peraluminous silicic melt at 200 MPa (H_2O). *American Mineralogist*, **80**, 1229-1251.

Icenhower, J. and London, D. (1996). Experimental partitioning of Rb, Cs, Sr and Ba between alkali feldspar and peraluminous melt. *American Mineralogist*, **81**, 719-734.

Irvine, T. N. and Baragar, W. R. A. (1971). A guide to the chemical classification of the common volcanic rocks. *Canadian Journal of Earth Sciences*, **8**, 523-548.

Jackson, D. H., Mattey, D. P., and Harris, N. B. W. (1988). Carbon isotope compositions of fluid inclusions in charnockites from southern India. *Nature*, **333**, 167-170.

Jackson, D. H. and Santosh, M. (1992). Dehydration reaction and isotope front transport induced by CO_2 infiltration at Nuliyam, South India. *Journal of Metamorphic Geology*, **10**, 365-382.

Jaffey, A. H., Flynn, K. F., Glendenin, W. C., Bentley, W. C., and Essling, A. M. (1971). Precision measurements of half-lives and specific activities of ^{235}U and ^{238}U. *Physical Reviews C: Nuclear Physics*, **4**, 1889-1906.

Jahns, R. H. and Burnham, C. W. (1969). Experimental studies of pegmatite genesis: I. A model for the derivation and crystallization of granitic pegmatites. *Economic Geology*, **64**, 843-864.

Jamieson, R. A., Culshaw, N. G., Wodicka, N., Corrigan, D., and Ketchum, J. W. F. (1992). Timing and tectonic setting of Grenvillian metamorphism-Constraints from a transect along Georgian Bay, Ontario. *Journal of Metamorphic Geology*, **10**, 321-332.

Jamieson, R. A., Culshaw, N. G., and Corrigan, D. (1995). North-west propagation of the Grenville Orogen: Grenvillian structure and metamorphism near Key Harbour, Georgian Bay, Ontario. *Journal of Metamorphic Geology*, **13**, 185-208.

Jamieson, R. A., Williams, M. L., Jercinovic, M. J., and Timmermann, H. (2001). Chemical and age zoning in monazite from polycyclic paragneiss, Central Gneiss Belt, Grenville Orogen, Ontario. Geological Association of Canada - Mineralogical Association of Canada, Program with Abstracts, **26**, 72.

Jamieson, R. A., Beaumont, C., Nguyen, M. H., and Lee, B. (2002). Interaction of metamorphism, deformation and exhumation in large convergent orogens. *Journal of Metamorphic Geology*, **20**, 9-24.

Jamieson, R. A., Ketchum, J. W. F., Slagstad, T., Rivers, T., and Culshaw, N. G. (2003). Omphacite and zircon in high-pressure metabasite, Shawanaga domain, western

Grenville Province: The truth about some beauties? Geological Association of Canada - Mineralogical Association of Canada, Program with Abstracts, **28**.

Jung, S., Hoernes, S., Masberg, P, and Hoffer, E. (1999). The petrogenesis of some migmatites and granites (Central Damara Orogen, Namibia): Evidence for disequilibrium melting, wall-rock contamination and crystal fractionation. *Journal of Petrology*, **40**, 1241-1269.

Kamo, S. L., Heaman, L. M., and Lumbers, S. B. (1989). Age for a lamprophyre dyke, Callander Bay, Ontario: Use of Ti-bearing minerals as a potential geochronometer. Geological Association of Canada - Mineralogical Association of Canada, Program with Abstracts, **14**, A41.

Kay, S. M., Ramos, V. A., Mpodozis, C., and Sruoga, P. (1989). Late Paleozoic to Jurassic silicic magmatism at the Gondwana margin: Analogy to the Middle Proterozoic in North America? *Geology*, **17**, 324-328.

Kay, S. M., Kay, R. B., Citron, G. P., and Perfit, M. R. (1990). Calc-alkaline plutonism in the intra-oceanic Aleutian arc, Alaska. In Rapela, C. W. (ed.) *Plutonism from Antarctica to Alaska: Geological Society of America Special Paper*, **241**, 233-255.

Kenah, C. and Hollister, L. S. (1983). Anatexis in the Central Gneiss Complex, British Columbia. In Gribble, C. D. (ed.) *Migmatites, Melting and Metamorphism*, Shiva Publishing Limited, 142-162.

Ketchum, J. W. F., Jamieson, R. A., Heaman, L. M., Culshaw, N. G., and Krogh, T. E. (1994). 1.45 Ga granulites in the southwestern Grenville province: Geologic setting, P-T conditions, and U-Pb geochronology. *Geology*, **22**, 215-218.

Ketchum, J. W. F. (1995). Extensional shear zones and lithotectonic domains in the southwest Grenville orogen: Structure, metamorphism, and U-Pb geochronology of the Central Gneiss Belt near Pointe-au-Baril, Ontario. *Unpublished Ph.D. Thesis, Dalhousie University, Halifax, Nova Scotia*, 341 p.

Ketchum, J. W. F., Culshaw, N. G., and Dunning, G. R. (1997). U-Pb geochronologic constraints on Paleoproterozoic orogenesis in the northwestern Makkovik Province, Labrador, Canada. *Canadian Journal of Earth Sciences*, **34**, 1072-1088.

Ketchum, J. W. F. and Krogh, T. E. (1997). U-Pb constraints on high-pressure metamorphism in the Central Gneiss Belt, southwestern Grenville orogen. Geological Association of Canada - Mineralogical Association of Canada, Program with Abstracts, **22**, A78.

Ketchum, J. W. F., Heaman, L. M., Krogh, T. E., Culshaw, N. G., and Jamieson, R. A. (1998). Timing and thermal influence of late orogenic extension in the lower crust: A U-Pb geochronological study from the southwest Grenville orogen, Canada. *Precambrian Research*, **89**, 25-45.

Ketchum, J. W. F. and Krogh, T. E. (1998). U-Pb constraints on high-pressure metamorphism in the southwestern Grenville orogen, Canada. Goldschmidt

Conference 1998. Mineralogical Magazine, **62A**, 775-776.

Ketchum, J. W. F. and Davidson, A. (2000). Crustal architecture and tectonic assembly of the Central Gneiss Belt, southwestern Grenville Province, Canada: A new interpretation. *Canadian Journal of Earth Sciences*, **37**, 217-234.

Kirby, E., Karlstrom, K. E., and Androconis, C. L. (1995). Tectonic setting of the Sandia pluton: An orogenic 1.4 Ga granite in New Mexico. *Tectonics*, **14**, 185-201.

Kirby, S. H. (1983). Rheology of the lithosphere. *Reviews of Geophysics and Space Physics*, **21**, 1458-1487.

Kisvarsanyi, E. B. and Kisvarsanyi, G. (1990). Alkaline granite ring complexes and metallogeny in the Middle Proterozoic St. Francois mountains. In Ryan, A. B. (ed.) *Mid-Proterozoic Laurentia-Baltica: Geological Association of Canada Special Paper*, **38**, 433-446.

Kretz, R. (1983). Symbols for rock-forming minerals. *American Mineralogist*, **68**, 277-279.

Krogh, T. E. and Davis, G. L. (1969). Old isotopic ages in the northwestern Grenville Province. In Wynne-Edwards, H. R. (ed.) *Age Relationships in High-grade Terrains: Geological Association of Canada Special Paper*, **5**, 189-192.

Krogh, T. E. and Davis, G. L. (1970). Isotopic ages along the Grenville Front in Ontario. *Carnegie Institution of Washington Yearbook*, **68**, 309-313.

Krogh, T. E., Davis, G. L., and Frarey, M. J. (1971). Isotopic ages along the Grenville Front in the Bell Lake area, southwest of Sudbury, Ontario. *Carnegie Institution of Washington Yearbook*, **69**, 337-339.

Krogh, T. E. (1973). A low contamination method for hydrothermal decomposition of zircon and extraction of U and Pb for isotopic age determinations. *Geochimica et Cosmochimica Acta*, **37**, 485-494.

Krogh, T. E. and Davis, G. L. (1974). The age of the Sudbury Nickel Irruptive. *Carnegie Institution of Washington Yearbook*, **73**, 567-569.

Krogh, T. E. (1982). Improved accuracy of U-Pb zircon ages by the creation of more concordant systems using an air abrasion technique. *Geochimica et Cosmochimica Acta*, **46**, 637-649.

Krogh, T. E. and Wardle, R. (1984). U-Pb isotopic ages along the Grenville Front. Geological Association of Canada - Mineralogical Association of Canada, Program with Abstracts, **9**, 80.

Krogh, T. E., Corfu, F., Davis, D. W., Dunning, G. R., Heaman, L. M., Kamo, S. L., Machado, N., Greenhough, J. D., and Nakamura, N. (1987). Precise U-Pb isotopic ages of diabase dykes and mafic to ultramafic rocks using trace amounts of baddeleyite and zircon. In Fahrig, W. F. (ed.) *Mafic Dyke Swarms: Geological Association of Canada Special Paper*, **34**, 147-152.

Krogh, T. E. (1989). U-Pb systematics of zircon and titanite in metasediments and gneisses near the Grenville Front, Ontario. Geological Association of Canada - Mineralogical Association of Canada, Program with Abstracts, 14, A52.

Krogh, T. E. (1991). U-Pb zircon geochronology in the western Grenville Province. Paper presented at Lithoprobe Abitibi-Grenville Transect, Workshop III.

Krogh, T. E., Chen, Y. D., Culshaw, N. G., and Ketchum, J. W. F. (1992). Terrane identification within the Grenville Province. Paper presented at Lithoprobe Abitibi-Grenville Transect, Workshop IV.

Krogh, T. E., Culshaw, N. G., and Ketchum, J. W. F. (1993a). Multiple ages of deformation and metamorphism in the Parry Sound-Pointe-au-Baril area. *Lithoprobe Abitibi-Grenville Project, Report no. 33*, 39.

Krogh, T. E., Kamo, S. L., and Nunn, G. (1993b). Dating the first metamorphic and frontal thrust near Killarney, Sudbury, North Bay (Ontario), Chibougamau (Quebec) and Churchill Falls (Labrador). *Lithoprobe Abitibi-Grenville Project, Report no. 33*, 165.

Krogh, T. E. (1994). Precise U-Pb ages for Grenvillian and pre-Grenvillian thrusting of Proterozoic and Archean metamorphic assemblages in the Grenville Front Tectonic Zone, Canada. *Tectonics*, 13, 963-982.

Krogh, T. E., Gower, C. F., and Wardle, R. J. (1996). Pre-Labradorian crust and later Labradorian, Pinwarian and Grenvillian metamorphism in the Mealy Mountains terrane, Grenville Province, eastern Labrador. In Gower, C. F. (ed.) *Program and Abstracts, Proterozoic Evolution in the North Atlantic Realm, COPENA ECSOOT-IBTA Conference, Goose Bay*, 106-107.

Krogh, T. E. (1997). Seventy-five million years of convergence recorded in the Parry Sound shear zone in the Central Gneiss Belt of the Grenville Province *Proterozoic Orogenies and Plate Interactions: The North Atlantic Region in Space and Time. COPENA Conference, Norges Geologiske Undersøkelse, Abstract Proceedings*.

Landenberger, B. and Collins, W. J. (1996). Derivation of A-type granites from a dehydrated charnockitic lower crust: Evidence from the Chaelundi complex, eastern Australia. *Journal of Petrology*, 37, 145-170.

Lappin, A. R. and Hollister, L. S. (1980). Partial melting in the Central Gneiss Complex near Prince Rupert, British Columbia. *American Journal of Science*, 280, 518-545.

Larsen, R. B. (2002). The distribution of rare-earth elements in K-feldspar as an indicator of petrogenetic processes in granitic pegmatites: Examples from two pegmatite fields in southern Norway. *Canadian Mineralogist*, 40, 137-151.

Layman, A. J., Kontak, D. J., and Jamieson, R. A. (2003). Fluid inclusions in garnet, migmatitic paragneiss, Algonquin domain, Grenville Province, Ontario. Geological Society of America, Northeast Section.

Le Fort, P. (1975). Himalayas: the collided range. Present knowledge of the continental arc. *American Journal of Science*, 275-A, 1-44.

Lejenue, A. and Richet, P. (1995). Rheology of crystal-bearing silicate melts: an experimental study at high viscosities. *Journal of Geophysical Research*, 100, 4215-4229.

Lewry, J. F. and Stauffer, M. R. (1990). *The Early Proterozoic Trans-Hudson Orogen of North America: Geological Association of Canada Special Paper 37*, 505 p.

Lidiak, E. G. (1996). Geochemistry of subsurface Proterozoic rocks in the eastern Midcontinent of the United States: Further evidence for a within-plate tectonic setting. In Catacosinos, P. A. (ed.) *Basement and Basins of Eastern North America: Geological Society of America Special Paper*, 308, 45-66.

Lindh, A. and Persson, P.-O. (1990). Proterozoic granitoid rocks of the Baltic Shield - trends of development. In Ryan, A. B. (ed.) *Mid-Proterozoic Laurentia-Baltica: Geological Association of Canada Special Paper*, 38, 23-40.

Loiselle, M. C. and Wones, D. R. (1979). Characteristics and origin of anorogenic granites. Geological Society of America, Abstracts with Programs, 11, 468.

Longerich, H. P., Jenner, G. A., Fryer, B. J., and Jackson, S. E. (1990). Inductively coupled plasma-mass spectrometric analysis of geological samples: A critical evaluation based on case studies. *Chemical Geology*, 83, 105-118.

Ludwig, K. R. (2001). Isoplot/Ex version 2.49. A geochronological toolkit for Microsoft Excel. *Berkeley Geochronological Center Special Publication*, 1a, 1-55.

Lumbers, S. B. (1975). Geology of the Burwash area, districts of Nipissing, Parry Sound and Ontario. Ontario Division of Mines Geological Report 116, 158 p.

Lumbers, S. B., Wu, T.-W., Heaman, L. M., Vertolli, V. M., and MacRae, N. D. (1991). Petrology and age of the A-type Mulock batholith, northern Grenville Province, Ontario. *Precambrian Research*, 53, 199-231.

Maaløe, S. (1982). Geochemical aspects of permeability controlled partial melting and fractional crystallization. *Geochimica et Cosmochimica Acta*, 46, 43-57.

Macfie, R. I. and Dixon, J. M. (1992). New U-Pb ages for rocks of Parry Sound domain, southwest Central Gneiss Belt: Some preliminary results. Lithoprobe Abitibi - Grenville Project, Workshop IV, Program with Abstracts.

Mahood, G. and Hildreth, W. (1983). Large partition coefficients for trace elements in high-silica rhyolites. *Geochimica et Cosmochimica Acta*, 47, 11-30.

Maniar, P. D. and Piccoli, P. M. (1989). Tectonic discrimination of granitoids. *Geological Society of America Bulletin*, 101, 635-643.

Marsh, B. D. (1982). On the mechanics of igneous diapirism, stoping, and zone melting. *American Journal of Science*, 282, 808-885.

Martin, H. (1987). Petrogenesis of Archean trondhjemites, tonalites, and granodiorites

from eastern Finland: Major and trace element geochemistry. *Journal of Petrology*, **28**, 921-953.

McEachern, S. J. and van Breemen, O. (1993). Age of deformation within the Central Metasedimentary Belt boundary thrust zone, southwest Grenville orogen: Constraints on the collision of the Mid-Proterozoic Elzevir terrane. *Canadian Journal of Earth Sciences*, **30**, 1155-1165.

McLellan, E. L. (1988). Migmatite structures in the Central Gneiss Complex, Boca de Quadra, Alaska. *Journal of Metamorphic Geology*, **6**, 517-542.

McMenamin, M. A. S. and McMenamin, D. L. S. (1990). *The emergence of animals. The Cambrian breakthrough.* New York, Columbia University Press, 217 p.

McMullen, S. M. (1999). Tectonic evolution of the Bark Lake area, eastern Central Gneiss Belt, Ontario Grenville: Constraints from geology, geochemistry and U-Pb geochronology. *Unpublished M.Sc. Thesis, Carleton University, Ottawa, Ontario*, 175 p.

Mengel, K., Richter, M., and Johannes, W. (2001). Leucosome-forming small-scale geochemical processes in the metapelitic migmatites of the Turku area, Finland. *Lithos*, **56**, 47-73.

Menuge, J. A., Brewer, T. S., and Seeger, C. M. (2002). Petrogenesis of metaluminous A-type rhyolites from the St. Francois Mountains, Missouri and the Mesoproterozoic evolution of the southern Laurentian margin. *Precambrian Research*, **113**, 269-291.

Mezger, K., Essene, E. J., van der Pluijm, B. A., and Halliday, A. N. (1993). U-Pb geochronology of the Grenville orogen of Ontario and New York: Constraints on ancient crustal tectonics. *Contributions to Mineralogy and Petrology*, **114**, 13-26.

Michael, P. J. (1988). Partition coefficients for rare earth elements in mafic minerals of high silica rhyolites: The importance of accessory mineral inclusions. *Geochimica et Cosmochimica Acta*, **52**, 275-282.

Miyashiro, A. (1974). Volcanic rock series in island arcs and active continental margins. *American Journal of Science*, **274**, 321-355.

Mogk, D. W. (1992). Ductile shearing and migmatization at mid-crustal levels in an Archean high-grade gneiss belt, northern Gallatin Range, Montana, USA. *Journal of Metamorphic Geology*, **10**, 427-438.

Molnar, P. and Atwater, T. (1978). Inter-arc spreading and Cordilleran tectonics as alternates related to the age of the subducted lithosphere. *Earth and Planetary Science Letters*, **41**, 330-340.

Moore, J. M. and Thompson, P. H. (1980). The Flinton group: A late Precambrian metasedimentary succession in the Grenville Province of eastern Ontario. *Canadian Journal of Earth Sciences*, **17**, 1685-1707.

Moores, E. M. (1991). Southwest U.S.-East Antarctic (SWEAT) connection: A

hypothesis. *Geology*, **19**, 425-428.

Murrel, S. A. F. and Chakravarty, S. (1973). Some new rheological experiments on igneous rocks at temperatures up to 1,120°C. *Geophysical Journal of the Royal Astronomical Society*, **34**, 211-250.

Murrel, S. A. F. and Ismail, I. A. H. (1976). The effects of temperature on the strength at high confining pressure of granodiorite containing free and chemically-bound water. *Contributions to Mineralogy and Petrology*, **55**, 317-330.

Nabelek, P. I. and Glascock, M. D. (1995). REE-depleted leucogranites; Black Hills, South Dakota: A consequence of disequilibrium melting of monazite-bearing schists. *Journal of Petrology*, **36**, 1055-1071.

Nabelek, P. I. (1999). Trace element distribution among rock-forming minerals in Black Hills migmatites, South Dakota: A case for solid-state equilibrium. *American Mineralogist*, **84**, 1256-1269.

Nadeau, L. (1990). Tectonic, thermal and magmatic evolution of the Central Gneiss Belt, Huntsville region, southwestern Grenville orogen. *Unpublished Ph.D. Thesis, Carleton University, Ottawa, Ontario*, 190 p.

Nadeau, L. and Hanmer, S. (1992). Deep-crustal break-back stacking and slow exhumation of the continental footwall beneath a thrusted marginal basin, Grenville orogen, Canada. *Tectonophysics*, **210**, 215-233.

Nadeau, L. and van Breemen, O. (1998). Plutonic ages and tectonic setting of the Algonquin and Muskoka allochthons, Central Gneiss Belt, Grenville Province, Ontario. *Canadian Journal of Earth Sciences*, **35**, 1423-1438.

Naney, M. T. (1983). Phase equilibria of rock-forming ferromagnesian silicates in granitic systems. *American Journal of Science*, **238**, 993-1033.

Nash, W. P. and Crecraft, H. R. (1985). Partition coefficients for trace elements in silicic magmas. *Geochimica et Cosmochimica Acta*, **49**, 2309-2322.

Nédélec, A., Minyem, D., and Barbey, P. (1993). High-P-high-T anatexis of Archean tonalitic grey gneisses: The Eseka migmatites, Cameroon. *Precambrian Research*, **62**, 191-205.

Nédélec, A., Stephens, W. E., and Fallick, A. E. (1995). The Panafrican stratoid granites of Madagascar: Alkaline magmatism in a post-collisional extensional setting. *Journal of Petrology*, **36**, 1367-1391.

Newton, R. C., Smith, J. V., and Windley, B. F. (1980). Carbonic metamorphism, granulites and crustal growth. *Nature*, **288**, 45-50.

Newton, R. C. (1992). Charnockitic alteration: Evidence for CO_2 infiltration in granulite facies metamorphism. *Journal of Metamorphic Geology*, **10**, 383-400.

Nier, A. O., Thompson, R. W., and Murphy, B. F. (1941). The isotopic constitution of lead and the measurement of geological time. III. *Physical Review*, **60**, 112-116.

Norman, M. D. and Leeman, W. P. (1990). Open-system magmatic evolution of andesites and basalts from the Salmon Creek volcanics, southwestern Idaho, U.S.A. *Chemical Geology*, **81**, 167-189.

Nyman, M. W. and Karlstrom, K. E. (1997). Pluton emplacement processes and tectonic setting of the 1.42 Ga Signal batholith, SW USA: Important role of crustal anisotropy during regional shortening. *Precambrian Research*, **82**, 237-263.

O'Hara, M. J. and Mathews, R. E. (1981). Geochemical evolution in an advancing, periodically replenished, periodically tapped, continuously fractionated magma chamber. *Journal of the Geological Society of London*, **138**, 237-277.

Okamura, S., Arculus, R. J., Martynov, Y. A., Kagami, H., Yoshida, T., and Kawano, Y. (1998). Multiple magma sources involved in marginal-sea formation: Pb, Sr, and Nd isotopic evidence from the Japan Sea region. *Geology*, **26**, 619-622.

Oliver, N. H. S., Bodorkos, S., Nemechin, A. A., Kinney, P. D., and Watt, G. R. (1999). Relationships between zircon U-Pb SHRIMP ages and leucosome type in migmatites of the Halls Creek Orogen, western Australia. *Journal of Petrology*, **40**, 1553-1575.

Olsen, S. N. (1982). Open- and closed-system migmatites in the Front Range, Colorado. *American Journal of Science*, **282**, 1596-1622.

Olsen, S. N. (1984). Mass-balance and mass-transfer in migmatites from the Colorado Front Range. *Contributions to Mineralogy and Petrology*, **85**, 30-44.

Otamendi, J. E. and Patiño Douce, A. E. (2001). Partial melting of aluminous metagraywackes in the northern Sierra de Comechingones, central Argentina. *Journal of Petrology*, **42**, 1751-1772.

Passchier, C. W., Myers, J. S., and Kröner, A. (1990). *Field geology of high-grade gneiss terrains*. Berlin, Springer-Verlag, 150 p.

Patiño Douce, A. E. and Beard, J. S. (1995). Dehydration-melting of biotite gneiss and quartz amphibolite from 3 to 15 kbar. *Journal of Petrology*, **36**, 707-738.

Patiño Douce, A. E. (1997). Generation of metaluminous A-type granites by low-pressure melting of calc-alkaline granitoids. *Geology*, **25**, 743-746.

Pattison, D. R. M. (1991). Infiltration-driven dehydration and anatexis in granulite facies metagabbro, Grenville Province, Ontario, Canada. *Journal of Metamorphic Geology*, **9**, 315-332.

Pearce, J. A. and Cann, J. R. (1973). Tectonic setting of basic volcanic rocks determined using trace element analyses. *Earth and Planetary Science Letters*, **19**, 290-300.

Pearce, J. A. (1982). Trace element characteristics of lavas from destructive plate boundaries. In Thorpe, R. S. (ed.) *Andesites*, John Wiley & Sons, 525-548.

Pearce, J. A., Harris, N. B. W., and Tindle, A. G. (1984). Trace element discrimination diagrams for the tectonic interpretation of granitic rocks. *Journal of Petrology*, **25**,

956-983.

Pearce, J. A. and Peate, D. W. (1995). Tectonic implications of the composition of volcanic arc magmas. *Annual Review of Earth and Planetary Sciences*, **23**, 251-285.

Pearce, T. H. (1968). A contribution to the theory of variation diagrams. *Contributions to Mineralogy and Petrology*, **19**, 142-157.

Peterson, J. W. and Newton, R. C. (1989). Reversed experiments on biotite-quartz-feldspar melting in the system KMASH: Implications for crustal anatexis. *Journal of Geology*, **97**, 465-485.

Peterson, J. W. and Newton, R. C. (1990). Experimental biotite-quartz melting in the KMASH-CO_2 system and the role of CO_2 in the petrogenesis of granites and related rocks. *American Mineralogist*, **75**, 1029-1042.

Poldervaart, A. (1956). Zircons is rocks 2: Igneous rocks. *American Journal of Science*, **254**, 521-554.

Pope, D. C. and Willett, S. D. (1998). Thermal-mechanical model for crustal thickening in the central Andes driven by ablative subduction. *Geology*, **26**, 511-514.

Powell, R. (1983). Processes in granulite-facies metamorphism. In Gribble, C. D. (ed.) *Migmatites, melting and metamorphism*. Nantwich, Shiva, 127-139.

Prevec, S. A. (1992). U-Pb constraints on early Proterozoic mafic magmatism from the southern Superior and western Grenville provinces, Ontario. *Radiogenic Age and Isotopic Studies: Report 6. Geological Survey of Canada, Paper 92-2*, 97-106.

Prinzhofer, A. and Allègre, C. J. (1985). Residual peridotites and the mechanisms of partial melting. *Earth and Planetary Science Letters*, **74**, 251-265.

Raistrick, M. (2003). Depleted mantle derived magmas and Laurentian detritus in the supracrustal Lighthouse Gneiss Association, Grenville Province, Ontario. *Unpublished M.Sc. Thesis, Dalhousie University, Halifax.*

Reynolds, P. H., Culshaw, N. G., Jamieson, R. A., Grant, S., and McKenzie, K. (1995). $^{40}Ar/^{39}Ar$ transect from the Grenville Front across the Parautochthonous Belt, western Grenville Orogen, Ontario. *Journal of Metamorphic Geology*, **13**, 209-222.

Rivers, T., Martignole, J., Gower, C. F., and Davidson, A. (1989). New tectonic divisions of the Grenville Province, southeast Canadian Shield. *Tectonics*, **8**, 63-84.

Rivers, T. (1997). Lithotectonic elements of the Grenville Province: Review and tectonic implications. *Precambrian Research*, **86**, 117-154.

Rivers, T. and Corrigan, D. (2000). Convergent margin on southeastern Laurentia during the Mesoproterozoic: Tectonic implications. *Canadian Journal of Earth Sciences*, **37**, 359-383.

Roberts, D., Nissen, A. L., and Walker, N. (1999). U-Pb zircon age and geochemistry of

the Blåfjellhatten granite, Grong-Olden culmination, central Norway. *Norsk Geologisk Tidsskrift*, 79, 161-168.

Rollinson, H. R. (1993). *Using geochemical data: Evaluation, presentation, interpretation*. Essex, Longman, 352 p.

Roscoe, R. (1952). The viscosity of suspensions of rigid spheres. *British Journal of Applied Physics*, 3, 267-269.

Rosenberg, C. L. (2001). Deformation of partially molten granite: A review and comparison of experimental and natural case studies. *International Journal of Earth Sciences (Geologische Rundschau)*, 90, 60-76.

Ross, D. C. (1985). Mafic gneissic complex (batholithic root?) in the southernmost Sierra Nevada, California. *Geology*, 13, 288-291.

Royden, L. H. (1993). The tectonic expression of slab pull at continental convergent boundaries. *Tectonics*, 12, 303-325.

Royden, L. H. (1996). Coupling and decoupling of crust and mantle in convergent orogens: Implications for strain partitioning in the crust. *Journal of Geophysical Research*, 101, 17679-17705.

Rushmer, T. (1996). Melt segregation in the lower crust: How have experiments helped us? *Transactions of the Royal Society Edinburgh: Earth Sciences*, 87, 73-83.

Rushmer, T. (2001). Volume change during partial melting reactions: Implications for melt extraction, melt geochemistry and crustal rheology. *Tectonophysics*, 342, 389-405.

Russell, J. K. and Nicholls, J. (1988). Analysis of petrologic hypotheses with Pearce element ratios. *Contributions to Mineralogy and Petrology*, 99, 25-35.

Rutter, E. H. and Neumann, D. H. K. (1995). Experimental deformation of partially molten Westerly granite under fluid-absent conditions, with implications for the extraction of granitic magmas. *Journal of Geophysical Research*, 100, 15697-15715.

Rutter, E. H. (1997). The influence of deformation on the extraction of crustal melts: A consideration of the role of melt-assisted granular flow. In Holness, M. B. (ed.) *Deformation-Enhanced Fluid Transport in the Earth's Crust and Mantle*. London, Chapman & Hall, 82-110.

Rutter, M. J. and Wyllie, P. J. (1988). Melting of vapour-absent tonalite at 10 kbar to simulate dehydration-melting in the deep crust. *Nature*, 331, 159-160.

Sandiford, M. and Powell, R. (1986). Deep crustal metamorphism during continental extension: Modern and ancient examples. *Earth and Planetary Science Letters*, 79, 151-158.

Saunders, A. D., Tarney, J., Stern, C. R., and Dalziel, I. W. D. (1979). Geochemistry of Mesozoic marginal basin floor igneous rocks from southern Chile. *Geological*

Society of America Bulletin, **90**, 237-258.

Sawyer, E. W. (1987). The role of partial melting and fractional crystallization in determining discordant leucosome compositions. *Journal of Petrology*, **28**, 445-473.

Sawyer, E. W. and Barnes, S.-J. (1988). Temporal and compositional differences between subsolidus and anatectic migmatite leucosomes from the Quetico metasedimentary belt, Canada. *Journal of Metamorphic Geology*, **6**, 437-450.

Sawyer, E. W. (1991). Disequilibrium melting and the rate of melt-residuum separation during migmatization of mafic rocks from the Grenville Front, Quebec. *Journal of Petrology*, **32**, 701-738.

Sawyer, E. W. (1994). Melt segregation in the continental crust. *Geology*, **22**, 1019-1022.

Sawyer, E. W. (1996). Melt segregation and magma flow in migmatites: Implications for the generation of granite magmas. In Zen, E. (ed.) *Third Hutton Symposium The Origin of Granites and Related Rocks: Geological Society of America Special Paper*, **315**, 85-94.

Sawyer, E. W. (1998). Formation and evolution of granite magmas during crustal reworking: The significance of diatexites. *Journal of Petrology*, **39**, 1147-1167.

Sawyer, E. W. (1999). Criteria for the recognition of partial melting. *Physics and Chemistry of the Earth (A)*, **24**, 269-279.

Sawyer, E. W. (2001). Melt segregation in the continental crust: Distribution and movement of melt in anatectic rocks. *Journal of Metamorphic Geology*, **19**, 291-309.

Shaw, D. M. (1968). A review of K-Rb fractionation trends by covariance analysis. *Geochimica et Cosmochimica Acta*, **32**, 573-601.

Shaw, D. M. (1970). Trace element fractionation during anatexis. *Geochimica et Cosmochimica Acta*, **34**, 237-243.

Simmons, W. B., Lee, M. T., and Brewster, R. H. (1987). Geochemistry and evolution of the South Platte granite-pegmatite system, Jefferson County, Colorado. *Geochimica et Cosmochimica Acta*, **51**, 455-471.

Sims, P. K. and Peterman, Z. E. (1986). Early Proterozoic Central Plains orogen: A major buried structure in the north-central United States. *Geology*, **14**, 488-491.

Skjerlie, K. P. and Johnston, A. D. (1996). Vapour-absent melting from 10 to 20 kbar of crustal rocks that contain multiple hydrous phases: Implications for anatexis in the deep to very deep continental crust and active continental margins. *Journal of Petrology*, **37**, 661-691.

Smith, S. E. and Humphris, S. E. (1998). Geochemistry of basaltic rocks from the TAG hydrothermal mound (26°08'N), Mid-Atlantic Ridge. In Zierenberg, R. A. (ed.) *Proceedings of the Ocean Drilling Program, Scientific Results*, **158**, 213-229.

Söderlund, U., Möller, C., Andersson, J., Johansson, L., and Whitehouse, M. (2002). Zircon geochronology in polymetamorphic gneisses in the Sveconorwegian orogen, SW Sweden: Ion microprobe evidence for 1.46-1.42 and 0.98-0.96 Ga reworking. *Precambrian Research*, **113**, 193-225.

Solar, G. S. and Brown, M. (2001). Petrogenesis of migmatites in Maine, USA: Possible source of peraluminous leucogranite in plutons. *Journal of Petrology*, **42**, 789-823.

Stacey, J. S. and Kramers, J. D. (1975). Approximation of terrestrial lead isotope evolution by a two-stage model. *Earth and Planetary Science Letters*, **26**, 207-221.

Steiger, R. H. and Wasserburg, G. J. (1969). Comparative U-Th-Pb systematics in 2.7×10^9 yr. plutons of different geologic histories. *Geochimica et Cosmochimica Acta*, **33**, 1212-1232.

Stern, R. A. (1997). The GSC Sensitive High Resolution Ion Microprobe (SHRIMP): Analytical techniques of zircon U-Th-Pb age determinations and performance evaluation. *Radiogenic Age and Isotopic Studies: Report 10. Geological Survey of Canada, Current Research 1997-F*, 1-31.

Stevens, G. and Clemens, J. D. (1993). Fluid-absent melting and the roles of fluids in the lithosphere: A slanted summary? *Chemical Geology*, **108**, 1-17.

Stockwell, C. H. (1982). Proposals for Time Classification and Correlation of Precambrian Rocks and Events in Canada and Adjacent Areas of the Canadian Shield. Part I: A Time Classification of Precambrian Rocks and Events. *Geological Survey of Canada, Paper 80-19*, 1-135.

St-Onge, M. R., Wodicka, N., and Lucas, S. B. (2000). Granulite- and amphibolite-facies metamorphism in a convergent-plate-margin setting: Synthesis of the Quebec-Baffin segment of the Trans-Hudson orogen. *Canadian Mineralogist*, **38**, 379-398.

Streckeisen, A. L. (1973). Plutonic rocks. Classification and nomenclature recommended by the IUGS subcommission on the systematics of igneous rocks. *Geotimes, 18 October*, 26-30.

Stromgard, K. E. (1973). Stress distribution during formation of boudinage and pressure shadows. *Tectonophysics*, **16**, 215-248.

Sun, S.-s. and McDonough, W. F. (1989). Chemical and isotopic systematics of oceanic basalts: Implications for mantle composition and processes. In Norry, M. J. (ed.) *Magmatism in the Ocean Basins: Geological Society of London Special Publication*, **42**, 313-345.

Tilton, G. R., Wetherill, G. W., Davis, G. L., and Bass, M. M. (1960). 1000 million year old minerals from eastern United States and Canada. *Journal of Geophysical Research*, **65**, 4173-4179.

Timmermann, H., Parrish, R. R., Jamieson, R. A., and Culshaw, N. G. (1997). Time of metamorphism beneath the Central Metasedimentary Belt boundary thrust zone, Grenville orogen, Ontario: Accretion at 1080 Ma? *Canadian Journal of Earth Sciences*, **34**, 1023-1029.

Timmermann, H. (1998). Geology, metamorphism, and U-Pb geochronology in the Central Gneiss Belt between Huntsville and Haliburton, southwestern Grenville Province, Ontario. *Unpublished Ph.D. Thesis, Dalhousie University, Halifax, Nova Scotia*, 410 p.

Timmermann, H., Jamieson, R. A., Parrish, R. R., and Culshaw, N. G. (2002). Coeval migmatites and granulites, Muskoka domain, southwestern Grenville Province. *Canadian Journal of Earth Sciences*, **39**, 239-258.

Tindle, A. G., McGarvie, D. W., and Webb, P. C. (1988). The role of hybridization and crystal fractionation in the evolution of the Cairnsmore of Carsphairn intrusion, southern Uplands of Scotland. *Journal of the Geological Society of London*, **145**, 11-21.

Touret, J. (1971). Le facies granulite en Norvege meridionale. II. Les inclusions fluides. *Lithos*, **4**, 423-436.

Touret, J. (1981). Fluid inclusions in high grade metamorphic rocks. In Crawford, M. L. (ed.) *Mineralogical Association of Canada. Short course in fluid inclusions: Applications to petrology*, 182-208.

Tuccillo, M. E., Mezger, K., Essene, E. J., and van der Pluijm, B. A. (1992). Thermobarometry, geochronology and the interpretation of P-T-t data in the Britt domain, Ontario, Grenville orogen, Canada. *Journal of Petrology*, **33**, 1225-1259.

Turner, S. P., Foden, J. D., and Morrison, R. S. (1992). Derivation of some A-type magmas by fractionation of basaltic magma: An example from the Padthaway Ridge, south Australia. *Lithos*, **28**, 151-179.

van Breemen, O., Davidson, A., Loveridge, W. D., and Sullivan, R. W. (1986). U-Pb zircon geochronology of Grenville tectonites, granulites and igneous precursors, Parry Sound, Ontario. In Baer, A. J. (ed.) *The Grenville Province: Geological Association of Canada Special Paper*, **31**, 192-207.

van Breemen, O. and Hanmer, S. (1986). Zircon morphology and U-Pb geochronology in active shear zones: Studies of syntectonic intrusions along the northwest boundary of the Central Metasedimentary Belt, Grenville Province, Ontario. *Current Research, Part B, Geological Survey of Canada, Paper 86-1B*, 775-784.

van Breemen, O. and Davidson, A. (1988). Northeast extension of Proterozoic terranes of mid-continental North America. *Geological Society of America Bulletin*, **100**, 630-638.

van Breemen, O. and Davidson, A. (1990). U-Pb zircon and baddeleyite ages from the Central Gneiss Belt, Ontario. *Radiogenic Age and Isotopic Studies: Report 3. Geological Survey of Canada, Paper 89-2*, 85-92.

van der Molen, I. and Paterson, M. S. (1979). Experimental deformation of partially melted granite. *Contributions to Mineralogy and Petrology*, **70**, 299-318.

van der Pluijm, B. A. and Carlson, K. A. (1989). Extension in the Central Metasedimentary Belt of the Ontario Grenville: Timing and tectonic significance. *Geology*, **17**, 161-164.

van Reenen, D. D. (1986). Hydration of cordierite and hypersthene and a description of the retrograde orthoamphibole isograd in the Limpopo Belt, South Africa. *American Mineralogist*, **71**, 900-915.

Van Schmus, W. R., Bickford, M. E., Anderson, J. L., Bender, E. E., Anderson, R. R., Bauer, P. W., Robertson, J. M., Bowring, S. A., Condie, K. C., Denison, R. E., Gilbert, M. C., Grambling, J. A., Mawer, C. K., Shearer, C. K., Hinze, W. J., Karlstrom, K. E., Kisvarsanyi, E. B., Lidiak, E. G., Reed Jr., J. C., Sims, P. K., Tweto, O., Silver, L. T., Treves, S. B., Williams, M. L., and Wooden, J. L. (1993). Transcontinental Proterozoic provinces. In Van Schmus, W. R. (ed.) *Precambrian: Conterminous U.S.: Boulder, Colorado, Geological Society of America, The Geology of North America*, **C-2**, 171-334.

Van Schmus, W. R., Bickford, M. E., and Turek, A. (1996). Proterozoic geology of the east-central Midcontinent basement. In Catacosinos, P. A. (ed.) *Basement and Basins of Eastern North America: Geological Society of America Special Paper*, **308**, 7-32.

van Staal, C. R., Dewey, J. F., Mac Niocaill, C., and McKerrow, W. S. (1998). The Cambrian-Silurian tectonic evolution of the northern Appalachians and British Caledonides: History of a complex west and southwest Pacific-type segment of Iapetus. In Scott, A. C. (ed.) *Lyell: the Past is the Key to the Present: Geological Society of London Special Publication*, **143**, 199-242.

Vance, D. and O'Nions, R. K. (1992). Prograde and retrograde thermal histories from the central Swiss Alps. *Earth and Planetary Science Letters*, **114**, 113-129.

Vennemann, T. W. and Smith, H. S. (1992). Stable isotope profile across the orthoamphibole isograd in the Southern Marginal Zone of the Limpopo Belt, South Africa. In de Wit, M. J. (ed.) *The Archean Limpopo Granulite Belt: Tectonics and deep crustal processes. Precambrian Research*, **55**, 365-397.

Vry, J., Compston, W., and Cartwright, I. (1996). SHRIMP II dating of zircons and monazites: reassessing the timing of high-grade metamorphism and fluid flow in the Reynolds Range, northern Arunta Block, Australia. *Journal of Metamorphic Geology*, **14**, 335-350.

Walker, R. J., Hanson, G. N., and Papike, J. J. (1989). Trace element constraints on pegmatite genesis: Tin Mountain pegmatite, Black Hills, South Dakota. *Contributions to Mineralogy and Petrology*, **101**, 290-300.

Wanless, R. K. and Lowdon, J. A. (1961). Isotopic age measurements on coeval minerals and mineral pairs. In Lowdon, J. A. (ed.) *Age Determinations by the Geological*

Survey of Canada, Report 2. Geological Survey of Canada, Paper 61-17, 119-124.

Wark, D. A. and Miller, C. F. (1993). Accessory mineral behavior during differentiation of a granite suite: Monazite, xenotime and zircon in the Sweetwater Wash pluton, southeastern California, USA. *Chemical Geology*, **110**, 49-67.

Waschbusch, P. and Beaumont, C. (1996). Effect of a retreating subduction zone on deformation in simple regions of plate convergence. *Journal of Geophysical Research*, **101**, 28133-28148.

Wasserburg, G. J. and Hayden, R. J. (1955). Ar^{40}-K^{40} dating. *Geochimica et Cosmochimica Acta*, **7**, 51-60.

Watson, E. B. and Harrison, T. M. (1983). Zircon saturation revisited: Temperature and composition effects in a variety of crustal magma types. *Earth and Planetary Science Letters*, **64**, 295-304.

Watson, E. B. and Harrison, T. M. (1984). Accessory minerals and the geochemical evolution of crustal magmatic systems: A summary and prospectus of experimental approaches. *Physics of Earth and Planetary Interiors*, **35**, 19-30.

Watt, G. R., Burns, L. M., and Graham, G. A. (1996). Chemical characteristics of migmatites: Accessory phase distribution and evidence for fast melt segregation rates. *Contributions to Mineralogy and Petrology*, **125**, 100-111.

Weil, A. B., Van der Voo, R., Mac Niocaill, C., and Meert, J. G. (1998). The Proterozoic supercontinent Rodinia: Paleomagnetically derived reconstruction for 1100 to 800 Ma. *Earth and Planetary Science Letters*, **154**, 13-24.

Wetherill, G. W. (1956). Discordant U-Pb ages. *Transactions of the American Geophysical Union*, **37**, 320-326.

Whalen, J. B., Currie, K. L., and Chappell, B. W. (1987). A-type granites: Geochemical characteristics, discrimination and petrogenesis. *Contributions to Mineralogy and Petrology*, **95**, 407-419.

White, D. J., Easton, R. M., Culshaw, N. G., Milkereit, B., Forsyth, D. A., Carr, S. D., Green, A. G., and Davidson, A. (1994). Seismic images of the Grenville Orogen in Ontario. *Canadian Journal of Earth Sciences*, **31**, 293-307.

White, D. J., Forsyth, D. A., Asudeh, I. A., Carr, S. D., Wu, H., Easton, R. M., and Mereu, R. F. (2000). Seismic-based cross-section across the Grenville Front in Ontario. *Canadian Journal of Earth Sciences*, **37**, 183-192.

Wickham, S. M. (1987a). Crustal anatexis and granite petrogenesis during low-pressure regional metamorphism: The Trois Seigneurs massif, Pyrenees, France. *Journal of Petrology*, **28**, 127-169.

Wickham, S. M. (1987b). The segregation and emplacement of granitic magmas. *Journal of the Geological Society of London*, **144**, 281-297.

Williams, I. S., Buick, I. S., and Cartwright, I. (1996). An extended episode of early Mesoproterozoic metamorphic fluid flow in the Reynolds Range, central Australia. *Journal of Metamorphic Geology*, 14, 29-47.

Wilson, M. E. (1918). The subprovincial limitations of pre-Cambrian nomenclature in the St. Lawrence basin. *Journal of Geology*, 26, 325-333.

Wilson, M. E. (1925). The Grenville pre-Cambrian subprovince. *Journal of Geology*, 33, 289-407.

Winchester, J. A. and Floyd, P. A. (1977). Geochemical discrimination of different magma series and their differentiation products using immobile elements. *Chemical Geology*, 20, 325-343.

Windley, B. F. (1986). Comparative tectonics of the western Grenville and the western Himalaya. In Baer, A. J. (ed.) *The Grenville Province: Geological Association of Canada Special Paper*, 31, 341-348.

Windley, B. F. (1993). Proterozoic anorogenic magmatism and its orogenic connections. *Journal of the Geological Society of London*, 150, 39-50.

Wodicka, N. (1994). Middle Proterozoic evolution of the Parry Sound domain, southwestern Grenville orogen, Ontario: Structural, metamorphic, U/Pb, and $^{40}Ar/^{39}Ar$ constraints. *Unpublished Ph.D. Thesis, Dalhousie University, Halifax, Nova Scotia*, 357 p.

Wodicka, N., Parrish, R. R., and Jamieson, R. A. (1996). The Parry Sound domain: A far-travelled allochthon? New evidence from U-Pb zircon geochronology. *Canadian Journal of Earth Sciences*, 33, 1087-1104.

Wodicka, N., Ketchum, J. W. F., and Jamieson, R. A. (2000). Grenvillian metamorphism of monocyclic rocks, Georgian Bay, Ontario, Canada: Implications for convergence history. *Canadian Mineralogist*, 38, 471-510.

Wood, D. A. (1979). A variably-veined sub-oceanic upper mantle: Genetic significance for mid-ocean ridge basalts from geochemical evidence. *Geology*, 7, 499-503.

Wynne-Edwards, H. R. (1972). The Grenville Province. In Douglas, R. J. W. (ed.) *Variations in tectonic styles in Canada: Geological Association of Canada Special Paper*, 11, 263-334.

Yin, A. and Harrison, T. M. (2000). Geologic evolution of the Himalayan-Tibetan Orogen. *Annual Review of Earth and Planetary Sciences*, 28, 211-280.

York, D. (1969). Least squares fitting of a straight line with correlated errors. *Earth and Planetary Science Letters*, 5, 320-324.

Zeitler, P. K. and Chamberlain, C. P. (1991). Petrogenetic and tectonic significance of young leucogranites from the northwestern Himalaya, Pakistan. *Tectonics*, 10, 729-741.

APPENDIX A. Geochemistry, precision and accuracy

A.1. Introduction

Precision. Precision refers to the repeatability of a measurement. It is a measure of the reproducibility of the method and is determined by making replicate measurements on the same sample. The limiting factor on precision is the counting statistics of the measuring device used (i.e., instrumental performance). Other important factors determining the precision are the homogeneity of the original sample material and the ability (for XRF analyses) to make homogenous beads. Precision can be defined by the coefficient of variation (c), also known as relative standard deviation, which is 100 times the standard deviation (σ) divided by the mean (μ):

$$c = 100 * \frac{\sigma}{\mu}$$

Accuracy. The accuracy is an estimate of how close the measured values is to the true value. Unlike precision, a definitive measure of the accuracy of geologic samples is not possible because the 'true value' is unknown. Therefore, determining the accuracy of an analysis is normally done by reference to a geochemical reference standard (e.g., Govindaraju, 1994), the value of which has been established by numerous analyses, using a variety of techniques, in a number of different labs. The accuracy is defined as the measured value relative to the standard or true value, given in percent.

A.2. Precision and accuracy

A.2.1. XRF analyses

The major elements and the following trace elements were analyzed by XRF: Ba, Rb, Sr, Y, Zr, Nb, V, Cr, Co, Ni, Cu, Zn, Ga, Pb, U. The precision and accuracy of the XRF analyses were determined by multiple analyses of published standards (AGV-1 and BE-N, Govindaraju, 1994), and one in-house standard (HFL-1). The results with calculated precision and accuracy are shown in Table A.1. The precision of the major

elements is better than 2%, and mostly better than 1%. The accuracy is generally better than 3% on average, with some exceptions: accuracy of Na_2O and P_2O_5 is 10% and 8%, respectively, in HFL-1, and accuracy of MnO is 7% in AGV-1. The precision for the trace elements is generally better than 16%, except for U with a precision of 23% and 29% in HFL-1 and BE-N, respectively. The accuracy is better than 15% on average for most trace elements. The accuracy of Zr and Rb is 24% and 33%, respectively, in BE-N; the accuracy of U is poorer than 25% in all three standards, and Pb is poorer than 35% in AGV-1 and BE-N.

A.2.2. ICP-MS analyses

The following elements were determined using ICP-MS: La, Ce, Pr, Nd, Sm, Eu, Gd, Tb, Dy, Ho, Er, Tm, Yb, Lu, Hf, and Th. Similar to the XRF analyses, the precision and accuracy of the ICP-MS analyses were determined by multiple analyses of published and unpublished standards (MRG-1 and BR-688). The results with calculated precision and accuracy are shown in Table A.2. On average, the precision of the ICP-MS analyses is better that 10% and 12% for MRG-1 and BR-688, respectively, whereas the accuracy is better than 12% and 13% for MRG-1 and BR-688, respectively. For reasons unknown, these results are poorer than those obtained by Longerich *et al.* (1990) who reported precision between 2 and 4% and accuracy between 6 and 10% using the same Na_2O_2 sintering technique that was used here.

Table A.1 Precision and accuracy of XRF analyses.

	Standard HFL-1	Sept. 2000 HFL-1	Accuracy HFL-1	Nov. 2000 HFL-1	Accuracy HFL-1	Jan. 2001 HFL-1	Accuracy HFL-1
SiO_2	59.86	60.25	0.65	60.17	0.52	60.25	0.65
TiO_2	0.96	0.97	1.04	0.97	0.52	0.97	1.04
Al_2O_3	21.89	22.06	0.78	22.00	0.50	22.06	0.78
Fe_2O_3	7.07	7.11	0.57	7.09	0.28	7.11	0.57
MnO	0.08	0.08	0.00	0.07	1.33	0.08	0.00
MgO	1.70	1.73	1.76	1.76	3.53	1.73	1.76
CaO	0.29	0.28	3.45	0.28	3.45	0.28	3.45
Na_2O	1.39	1.50	7.91	1.55	11.51	1.50	7.91
K_2O	4.37	4.38	0.23	4.37	0.00	4.38	0.23
P_2O_5	0.12	0.13	7.50	0.13	5.83	0.13	7.50
L.O.I.	-	-	-	-	-	-	-
V	120	126	5	129	8	126	5
Cr	85	88	4	82	4	88	4
Co	37	34	8	35	5	34	8
Zr	181	184	2	178	2	184	2
Ba	900	984	9	921	2	984	9
Ni	40	40	0	45	13	40	0
Cu	32	37	16	33	3	37	16
Zn	106	109	3	107	1	109	3
Ga	31	33	6	27	13	33	6
Rb	178	180	1	179	1	180	1
Sr	211	215	2	213	1	215	2
Y	35	42	20	35	0	42	20
Nb	20	19	5	21	5	19	5
Pb	35	28	20	34	3	28	20
U	2	3	50	2	0	3	50
Max - major			8		12		8
Avg. - major			2		3		2
Max - trace			50		13		50
Avg. - trace			10		4		10

Table A.1 continued.

	Feb. 2001 HFL-1	Accuracy HFL-1	HFL-1 overall				
			Accuracy Max	Accuracy Mean	Mean HFL-1	St. dev. HFL-1	Precision HFL-1
SiO_2	60.09	0.38	0.65	0.55	60.19	0.08	0.13
TiO_2	0.96	0.10	1.04	0.68	0.97	0.00	0.45
Al_2O_3	22.02	0.59	0.78	0.66	22.04	0.03	0.14
Fe_2O_3	7.08	0.14	0.57	0.39	7.10	0.01	0.21
MnO	0.07	1.33	1.33	0.67	0.07	0.00	0.77
MgO	1.78	4.71	4.71	2.94	1.75	0.02	1.40
CaO	0.29	0.00	3.45	2.59	0.28	0.00	1.77
Na_2O	1.57	12.95	12.95	10.07	1.53	0.04	2.33
K_2O	4.38	0.23	0.23	0.17	4.38	0.01	0.11
P_2O_5	0.13	9.17	9.17	7.50	0.13	0.00	1.27
L.O.I.	-	-	-	-	-	-	-
V	132	10	10	7	128	3	2
Cr	80	6	6	4	85	4	5
Co	33	11	11	8	34	1	2
Zr	179	1	2	2	181	3	2
Ba	956	6	9	7	961	30	3
Ni	42	5	13	4	42	2	6
Cu	35	9	16	11	36	2	5
Zn	107	1	3	2	108	1	1
Ga	29	6	13	8	31	3	10
Rb	180	1	1	1	180	1	0
Sr	212	0	2	1	214	2	1
Y	42	20	20	15	40	4	9
Nb	21	5	5	5	20	1	6
Pb	34	3	20	11	31	3	11
U	2	0	50	25	3	1	23
Max - major		13					2
Avg. - major		3					1
Max - trace		20					23
Avg. - trace		6					6

Table A.1 continued.

	Standard AGV-1	Sept. 2000 AGV-1	Accuracy AGV-2	Nov. 2000 AGV-3	Accuracy AGV-4
SiO_2	58.84	59.06	0.37	58.81	0.05
TiO_2	1.05	1.05	0.38	1.05	0.48
Al_2O_3	17.15	17.09	0.35	17.03	0.70
Fe_2O_3	6.77	6.75	0.30	6.73	0.59
MnO	0.09	0.10	6.67	0.10	6.67
MgO	1.53	1.53	0.00	1.56	1.96
CaO	4.94	4.92	0.40	4.90	0.81
Na_2O	4.26	4.25	0.23	4.36	2.35
K_2O	2.92	2.92	0.00	2.91	0.34
P_2O_5	0.49	0.50	2.04	0.50	1.63
L.O.I.	1.20	1.20	0.00	1.20	0.00
V	121	143	18	146	21
Cr	10	9	11	10	1
Co	15	20	31	20	31
Zr	227	245	8	239	5
Ba	1226	1339	9	1133	8
Ni	13	13	0	17	31
Cu	60	57	5	60	0
Zn	88	88	0	92	5
Ga	20	22	10	22	10
Rb	67	65	3	62	8
Sr	663	666	0	665	0
Y	20	16	20	20	0
Nb	15	14	7	12	20
Pb	36	21	42	18	50
U	2	1	48	1	48
Max - major			7		7
Avg. - major			1		1
Max - trace			48		50
Avg. - trace			14		16

Table A.1 continued.

	Jan. 2001 AGV-5	Accuracy AGV-6	Feb. 2001 AGV-7	Accuracy AGV-8	Sept. 2001 AGV-9	Accuracy AGV-10
SiO_2	59.06	0.37	58.75	0.15	59.82	1.67
TiO_2	1.05	0.38	1.04	0.86	1.07	1.71
Al_2O_3	17.09	0.35	17.03	0.70	17.24	0.52
Fe_2O_3	6.75	0.30	6.69	1.18	6.85	1.18
MnO	0.10	6.67	0.10	6.67	0.10	8.89
MgO	1.53	0.00	1.56	1.96	1.56	1.96
CaO	4.92	0.40	4.91	0.61	4.98	0.81
Na_2O	4.25	0.23	4.28	0.47	4.32	1.41
K_2O	2.92	0.00	2.91	0.34	2.95	1.03
P_2O_5	0.50	2.04	0.50	2.45	0.51	3.27
L.O.I.	1.20	0.00	1.20	0.00	1.20	0.00
V	143	18	147	21	143	18
Cr	9	11	12	19	10	1
Co	20	31	17	11	19	24
Zr	245	8	241	6	253	11
Ba	1339	9	1278	4	1122	8
Ni	13	0	17	31	15	15
Cu	57	5	61	2	73	22
Zn	88	0	86	2	94	7
Ga	22	10	20	0	19	5
Rb	65	3	61	9	60	11
Sr	666	0	664	0	682	3
Y	16	20	21	5	21	5
Nb	14	7	13	13	11	27
Pb	21	42	21	42	15	58
U	1	48	<1	-	1	48
Max - major		7		7		9
Avg. - major		1		1		2
Max - trace		48		42		58
Avg. - trace		14		12		18

Table A.1 continued.

	Accuracy		Mean	St. dev.	Precision
	Max	Mean	AGV-11	AGV-12	AGV-13
SiO$_2$	1.67	0.52	59.10	0.43	0.72
TiO$_2$	1.71	0.76	1.05	0.01	0.99
Al$_2$O$_3$	0.70	0.52	17.10	0.09	0.50
Fe$_2$O$_3$	1.18	0.71	6.75	0.06	0.87
MnO	8.89	7.11	0.10	0.00	0.93
MgO	1.96	1.18	1.55	0.02	1.06
CaO	0.81	0.61	4.93	0.03	0.64
Na$_2$O	2.35	0.94	4.29	0.05	1.11
K$_2$O	1.03	0.34	2.92	0.02	0.56
P$_2$O$_5$	3.27	2.29	0.50	0.00	0.61
L.O.I.	0.00	0.00	1.20	0.00	0.00
V	21	19	144	2	1
Cr	19	9	10	1	12
Co	31	25	19	1	7
Zr	11	8	245	5	2
Ba	9	8	1242	108	9
Ni	31	15	15	2	13
Cu	22	7	62	7	11
Zn	7	3	90	3	4
Ga	10	7	21	1	7
Rb	11	7	63	2	4
Sr	3	1	669	8	1
Y	20	10	19	3	14
Nb	27	15	13	1	10
Pb	58	47	19	3	14
U	48	48	1	0	0
Max - major					1
Avg. - major					1
Max - trace					14
Avg. - trace					7

Table A.1 continued.

	Standard BE-N	Sept. 2000 BE-N	Accuracy BE-N	Nov. 2000 BE-N	Accuracy BE-N
SiO_2	38.20	38.36	0.42	38.36	0.42
TiO_2	2.61	2.66	1.80	2.62	0.42
Al_2O_3	10.07	10.08	0.10	9.98	0.89
Fe_2O_3	12.84	12.94	0.78	12.79	0.39
MnO	0.20	0.20	0.00	0.20	0.50
MgO	13.15	13.28	0.99	13.17	0.15
CaO	13.87	13.95	0.58	13.86	0.07
Na_2O	3.18	3.32	4.40	3.18	0.00
K_2O	1.39	1.40	0.72	1.38	0.72
P_2O_5	1.05	1.06	0.76	1.05	0.19
L.O.I.	2.45	2.45	0.00	2.45	0.00
V	235	318	35	319	36
Cr	360	359	0	335	7
Co	60	54	10	54	10
Zr	260	323	24	318	22
Ba	1025	1127	10	1025	0
Ni	267	270	1	260	3
Cu	72	68	6	63	13
Zn	120	101	16	112	7
Ga	17	16	6	17	0
Rb	47	26	45	36	23
Sr	1370	1387	1	1376	0
Y	30	30	0	30	0
Nb	105	104	1	105	0
Pb	4	6	50	5	25
U	2	2	17	1	58
Max - major			4		1
Avg. - major			1		0
Max - trace			50		58
Avg. - trace			15		14

Table A.1 continued.

	Jan. 2001 BE-N	Accuracy BE-N	Feb. 2001 BE-N	Accuracy BE-N	Sept. 2001 BE-N	Accuracy BE-N
SiO_2	38.36	0.42	38.29	0.24	38.14	0.16
TiO_2	2.66	1.80	2.62	0.42	2.62	0.19
Al_2O_3	10.08	0.10	10.00	0.70	10.02	0.50
Fe_2O_3	12.94	0.78	12.71	1.01	12.73	0.86
MnO	0.20	0.00	0.20	0.50	0.20	1.00
MgO	13.28	0.99	13.21	0.46	13.16	0.08
CaO	13.95	0.58	13.85	0.14	13.75	0.87
Na_2O	3.32	4.40	3.18	0.00	3.24	1.89
K_2O	1.40	0.72	1.39	0.00	1.38	0.72
P_2O_5	1.06	0.76	1.04	0.76	1.04	0.76
L.O.I.	2.45	0.00	2.45	0.00	2.45	0.00
V	318	35	314	34	301	28
Cr	359	0	338	6	349	3
Co	54	10	53	12	56	7
Zr	323	24	320	23	322	24
Ba	1127	10	1150	12	784	24
Ni	270	1	257	4	266	0
Cu	68	6	63	13	64	11
Zn	101	16	113	6	114	5
Ga	16	6	16	6	19	12
Rb	26	45	36	23	34	28
Sr	1387	1	1375	0	1338	2
Y	30	0	23	23	24	20
Nb	104	1	106	1	102	3
Pb	6	50	5	25	5	25
U	2	17	2	17	<1	-
Max - major		4		1		2
Avg. - major		1		0		1
Max - trace		50		34		28
Avg. - trace		15		14		14

Table A.1 continued.

	BE-N overall				
	Accuracy		Mean	St. dev.	Precision
	Max	Mean	BE-N	BE-N	BE-N
SiO_2	0.42	0.33	38.30	0.10	0.25
TiO_2	1.80	0.93	2.63	0.02	0.80
Al_2O_3	0.89	0.46	10.03	0.05	0.46
Fe_2O_3	1.01	0.76	12.82	0.11	0.87
MnO	1.00	0.40	0.20	0.00	0.42
MgO	0.99	0.53	13.22	0.06	0.44
CaO	0.87	0.45	13.87	0.08	0.60
Na_2O	4.40	2.14	3.25	0.07	2.16
K_2O	0.72	0.58	1.39	0.01	0.72
P_2O_5	0.76	0.65	1.05	0.01	0.77
L.O.I.	0.00	0.00	2.45	0.00	0.00
V	36	34	314	8	2
Cr	7	3	348	11	3
Co	12	10	54	1	2
Zr	24	24	321	2	1
Ba	24	11	1043	152	15
Ni	4	2	265	6	2
Cu	13	9	65	3	4
Zn	16	10	108	7	6
Ga	12	6	17	1	8
Rb	45	33	32	5	16
Sr	2	1	1373	20	1
Y	23	9	27	4	13
Nb	3	1	104	1	1
Pb	50	35	5	1	10
U	58	27	2	1	29
Max - major					2
Avg. - major					1
Max - trace					29
Avg. - trace					8

Table A.2 Precision and accuracy of ICP-MS analyses.

	Standard MRG-1 (MUN run 78-108)	Feb. 2001 MRG-1-1	Accuracy MRG-1	Feb. 2001 MRG-1-3	Accuracy MRG-1	Feb. 2001 MRG-1-1*	Accuracy MRG-1	July 2001 MRG-1-32	Accuracy MRG-1
La	8.83	8.55	3.16	8.71	1.41	8.70	1.47	9.16	3.78
Ce	25.80	24.05	6.79	25.30	1.95	24.69	4.28	25.44	1.38
Pr	3.71	3.48	6.17	3.65	1.71	3.62	2.56	3.72	0.38
Nd	17.60	16.74	4.88	17.67	0.38	17.59	0.05	18.05	2.56
Sm	4.34	4.22	2.83	4.52	4.15	4.49	3.48	4.38	1.02
Eu	1.38	1.34	2.65	1.45	4.99	1.45	4.95	1.39	1.05
Gd	3.97	3.82	3.86	4.09	3.09	4.13	3.99	4.06	2.25
Tb	0.52	0.51	2.33	0.55	4.83	0.56	8.26	0.56	7.06
Dy	3.00	2.71	9.72	2.93	2.20	2.99	0.49	3.00	0.10
Ho	0.49	0.47	4.40	0.50	1.89	0.51	3.18	0.49	0.78
Er	1.16	1.21	4.26	1.29	10.92	1.30	12.30	1.20	3.07
Tm	0.14	0.14	2.18	0.15	4.67	0.15	4.20	0.14	1.97
Yb	0.79	0.75	5.69	0.81	2.75	0.80	1.60	0.81	2.95
Lu	0.11	0.10	10.58	0.11	0.93	0.11	1.82	0.11	0.89
Hf	3.89	4.60	18.29	5.43	39.47	4.74	21.96	3.99	2.61
Th	0.82	0.75	8.64	0.78	4.63	0.75	8.68	0.81	1.27
Max			18		39		22		7
Average			6		6		5		2

Table A.2 continued.

	July 2001 MRG-1-31	Accuracy MRG-1	July 2001 MRG-1-35	Accuracy MRG-1	July 2001 MRG-1-37	Accuracy MRG-1	July 2001 MRG-1-37	Accuracy MRG-1	July 2001 MRG-1-39	Accuracy MRG-1
La	9.48	7.31	8.62	2.39	8.46	4.17	9.74	10.34	9.54	8.09
Ce	26.74	3.62	24.05	6.79	23.83	7.62	26.80	3.89	26.99	4.60
Pr	3.87	4.22	3.48	6.28	3.46	6.80	4.04	8.82	3.89	4.95
Nd	18.50	5.10	17.61	0.08	16.83	4.40	19.84	12.74	19.27	9.48
Sm	4.51	3.86	4.96	14.20	4.86	11.88	4.66	7.27	4.73	9.01
Eu	1.45	5.31	1.61	16.55	1.56	12.73	1.51	9.19	1.51	9.56
Gd	4.11	3.55	4.73	19.16	4.52	13.83	4.59	15.51	4.13	3.92
Tb	0.55	5.21	0.64	23.13	0.62	20.03	0.62	18.60	0.58	11.90
Dy	2.95	1.67	3.34	11.19	3.27	9.03	3.36	12.05	3.09	2.90
Ho	0.49	0.44	0.53	7.24	0.48	2.32	0.55	11.35	0.55	11.55
Er	1.15	0.55	1.36	17.21	1.24	7.16	1.29	11.60	1.32	13.65
Tm	0.14	3.21	0.15	4.59	0.14	0.11	0.15	10.12	0.16	15.83
Yb	0.82	3.48	0.79	0.60	0.77	2.51	0.89	12.36	0.93	17.99
Lu	0.11	0.96	0.13	15.56	0.12	12.80	0.12	7.59	0.12	13.48
Hf	3.86	0.64	4.23	8.77	4.48	15.12	4.41	13.34	4.39	12.97
Th	0.83	1.44	0.92	11.94	0.77	5.66	0.85	3.49	0.90	9.69
Max		7		23		20		19		18
Average		3		10		9		11		10

Table A.2 continued.

	July 2001 MRG-1-41	Accuracy MRG-1	Jan 2002 MRG-1-67	Accuracy MRG-1	Jan 2002 MRG-1-69	Accuracy MRG-1	Jan 2002 MRG-1-71	Accuracy MRG-1	Jan 2002 MRG-1-73	Accuracy MRG-1
La	9.58	8.49	8.33	5.65	9.27	5.03	8.86	0.37	7.78	11.86
Ce	26.89	4.22	22.67	12.14	25.10	2.71	24.82	3.82	21.23	17.73
Pr	3.95	6.42	3.39	8.74	3.72	0.14	3.67	1.10	3.10	16.40
Nd	19.17	8.94	15.69	10.83	17.04	3.17	18.00	2.26	15.00	14.74
Sm	4.59	5.85	4.24	2.41	4.45	2.43	4.48	3.12	4.10	5.64
Eu	1.49	8.22	1.34	2.93	1.42	2.83	1.45	4.77	1.32	4.48
Gd	4.04	1.79	3.85	2.90	3.79	4.60	4.17	5.10	4.36	9.90
Tb	0.59	13.01	0.54	3.54	0.51	1.90	0.56	7.08	0.58	10.92
Dy	3.18	6.07	2.85	4.87	2.71	9.70	2.95	1.53	3.10	3.36
Ho	0.52	6.80	0.40	18.19	0.42	15.29	0.49	0.79	0.42	14.25
Er	1.26	8.66	0.98	15.33	1.00	13.39	1.18	1.84	1.01	13.33
Tm	0.16	11.30	0.12	16.27	0.13	9.80	0.14	1.28	0.12	14.99
Yb	0.88	11.94	0.71	9.67	0.72	8.31	0.81	2.84	0.69	12.87
Lu	0.11	3.45	0.10	6.83	0.11	4.30	0.11	4.23	0.11	1.94
Hf	4.01	3.18	3.72	4.44	3.94	1.21	4.43	13.98	3.65	6.16
Th	0.89	8.55	0.67	18.29	0.77	6.44	0.84	2.23	0.67	17.87
Max		13		18		15		14		18
Average		7		9		6		4		11

Table A.2 continued.

	Jan 2002 MRG-1-75	Accuracy MRG-1	Jan 2002 MRG-1-77	Accuracy MRG-1	Jan 2002 MRG-1-80	Accuracy MRG-1	MRG-1 overall				
							Accuracy Max	Accuracy Mean	Mean MRG-1	St. dev. MRG-1	Precision MRG-1
La	8.00	9.37	7.97	9.77	9.08	2.87	12	6	8.81	0.60	6.80
Ce	22.53	12.66	22.58	12.47	24.92	3.40	18	6	24.63	1.71	6.93
Pr	3.26	12.13	3.32	10.59	3.61	2.61	16	6	3.60	0.26	7.10
Nd	15.71	10.72	16.53	6.08	17.43	0.97	15	6	17.45	1.32	7.56
Sm	4.60	6.06	4.32	0.41	4.43	2.10	14	5	4.50	0.22	4.97
Eu	1.48	7.06	1.39	0.71	1.42	3.11	17	6	1.45	0.08	5.33
Gd	4.66	17.25	4.24	6.91	4.19	5.43	19	7	4.20	0.28	6.73
Tb	0.59	12.62	0.55	5.23	0.59	13.45	23	10	0.57	0.04	6.47
Dy	3.13	4.35	2.96	1.50	3.10	3.23	12	5	3.04	0.19	6.24
Ho	0.44	10.29	0.48	1.72	0.48	2.74	18	7	0.48	0.04	8.96
Er	1.04	10.48	1.13	2.44	1.14	1.41	17	9	1.18	0.12	10.07
Tm	0.13	9.30	0.14	1.18	0.14	1.04	16	7	0.14	0.01	8.76
Yb	0.72	9.24	0.82	3.80	0.79	0.12	18	6	0.80	0.07	8.30
Lu	0.12	6.73	0.11	2.94	0.12	4.68	16	6	0.11	0.01	6.86
Hf	4.63	19.09	4.14	6.54	4.69	20.64	39	12	4.32	0.45	10.32
Th	0.67	18.00	0.71	13.49	0.80	2.77	18	8	0.79	0.08	9.98
Max		19		13		21					10
Average		11		5		4					8

Table A.2 continued.

	Standard BR-688 (MUN run 161-191)	Feb. 2001 BR-688-1	Accuracy BR-688	Feb. 2001 BR-688-3	Accuracy BR-688	Feb. 2001 BR-688-1*	Accuracy BR-688	July 2001 BR-688-31	Accuracy BR-688
La	4.98	4.81	3.33	4.76	4.46	4.91	1.31	5.28	6.00
Ce	11.55	10.99	4.82	11.03	4.47	11.41	1.21	11.96	3.59
Pr	1.65	1.58	4.43	1.59	3.50	1.64	0.80	1.73	4.74
Nd	8.03	7.64	4.81	7.80	2.83	7.93	1.22	8.40	4.58
Sm	2.30	2.27	1.44	2.34	1.67	2.40	4.32	2.43	5.74
Eu	0.94	0.93	0.88	0.96	2.48	0.98	4.04	1.00	6.87
Gd	2.88	2.71	6.01	2.83	1.62	2.94	2.11	2.99	3.99
Tb	0.48	0.45	6.06	0.48	0.14	0.49	2.67	0.50	3.71
Dy	3.21	3.02	5.93	3.25	1.31	3.34	4.18	3.39	5.70
Ho	0.70	0.66	5.20	0.70	0.20	0.72	2.81	0.72	2.27
Er	2.10	2.09	0.70	2.26	7.65	2.29	8.95	2.12	0.89
Tm	0.30	0.29	4.09	0.30	0.63	0.31	2.31	0.31	4.21
Yb	2.00	1.84	8.05	1.94	2.89	2.01	0.38	2.09	4.63
Lu	0.30	0.28	8.08	0.30	0.42	0.31	2.51	0.32	5.56
Hf	1.54	2.04	32.51	2.13	38.33	1.93	25.26	1.50	2.63
Th	0.33	0.33	0.22	0.32	3.16	0.33	0.45	0.35	5.44
Max			33		38		25		7
Average			6		5		4		4

Table A.2 continued.

	July 2001	Accuracy	July 2001	Accuracy	July 2001	Accuracy	July 2001	Accuracy	July 2001	Accuracy
	BR-688-32	BR-688	BR-688-35	BR-688	BR-688-37	BR-688	BR-688-37	BR-688	BR-688-39	BR-688
La	5.22	4.87	4.60	7.66	4.49	9.77	5.37	7.86	5.32	6.84
Ce	11.79	2.05	10.38	10.16	10.19	11.76	12.08	4.57	12.16	5.32
Pr	1.69	2.31	1.48	10.45	1.46	11.70	1.76	6.87	1.75	6.24
Nd	8.30	3.40	7.51	6.47	7.16	10.82	8.73	8.70	8.68	8.08
Sm	2.32	0.98	2.46	7.10	2.38	3.60	2.40	4.53	2.49	8.19
Eu	0.96	2.35	1.03	9.31	0.99	5.49	0.98	4.64	1.04	10.26
Gd	2.94	1.95	3.14	9.03	3.01	4.44	3.16	9.75	2.93	1.59
Tb	0.50	4.92	0.53	10.23	0.51	6.34	0.54	12.47	0.52	8.28
Dy	3.44	7.02	3.49	8.71	3.46	7.85	3.72	15.99	3.43	6.93
Ho	0.72	2.19	0.69	1.54	0.64	8.50	0.75	7.42	0.77	10.57
Er	2.10	0.14	2.19	4.15	2.04	2.97	2.25	7.22	2.30	9.36
Tm	0.31	2.23	0.28	6.01	0.28	6.90	0.32	6.78	0.33	11.01
Yb	2.04	1.98	1.78	10.98	1.78	11.23	2.17	8.66	2.24	11.94
Lu	0.31	2.99	0.32	7.15	0.32	6.22	0.32	6.30	0.34	13.39
Hf	1.57	2.22	1.57	1.83	1.67	8.25	1.64	6.46	1.71	10.73
Th	0.37	11.35	0.38	15.65	0.30	9.22	0.34	3.06	0.37	11.59
Max		11		16		12		16		13
Average		3		8		8		8		9

Table A.2 continued.

	July 2001 BR-688-41	Accuracy BR-688	Jan 2002 BR-688-67	Accuracy BR-688	Jan 2002 BR-688-69	Accuracy BR-688	Jan 2002 BR-688-71	Accuracy BR-688	Jan 2002 BR-688-73	Accuracy BR-688
La	5.56	11.55	4.66	6.49	5.10	2.48	4.94	0.90	4.09	17.83
Ce	12.74	10.28	10.27	11.05	11.24	2.70	11.15	3.45	9.14	20.83
Pr	1.85	12.39	1.49	9.59	1.64	0.71	1.61	2.24	1.30	20.96
Nd	9.12	13.56	6.95	13.40	7.63	5.02	8.04	0.08	6.29	21.72
Sm	2.54	10.23	2.18	5.15	2.29	0.38	2.28	0.71	2.00	13.26
Eu	1.07	13.88	0.89	5.59	0.95	1.47	0.96	2.36	0.83	11.91
Gd	2.99	3.93	2.69	6.62	2.69	6.57	2.93	1.74	2.89	0.22
Tb	0.55	15.32	0.47	1.28	0.45	6.23	0.49	1.38	0.47	1.54
Dy	3.76	17.07	3.14	2.15	3.04	5.22	3.25	1.32	3.24	0.89
Ho	0.79	12.84	0.57	19.02	0.59	16.00	0.69	0.87	0.56	20.09
Er	2.36	12.18	1.70	19.25	1.78	15.41	2.04	2.68	1.65	21.45
Tm	0.35	15.44	0.25	15.43	0.26	13.98	0.30	1.17	0.24	20.65
Yb	2.29	14.71	1.75	12.61	1.77	11.64	1.98	1.06	1.57	21.32
Lu	0.34	13.25	0.28	6.38	0.30	0.18	0.31	3.91	0.27	8.68
Hf	1.70	10.12	1.44	6.41	1.53	0.34	1.71	11.08	1.40	9.04
Th	0.38	16.50	0.28	13.99	0.31	5.06	0.32	2.21	0.27	19.51
Max	17		19		16		11		22	
Average	13		10		6		2		14	

Table A.2 continued.

	Jan 2002 BR-688-75	Accuracy BR-688	Jan 2002 BR-688-77	Accuracy BR-688	Jan 2002 BR-688-80	Accuracy BR-688	Accuracy Max	Accuracy Average	Mean BR-688	St. dev. BR-688	Precision BR-688
La	4.49	9.82	4.64	6.81	5.17	3.83	18	7	4.91	0.39	7.93
Ce	10.18	11.83	10.71	7.27	11.74	1.67	21	7	11.13	0.91	8.22
Pr	1.49	9.86	1.53	6.98	1.67	1.13	21	7	1.60	0.14	8.52
Nd	7.29	9.24	7.68	4.37	8.13	1.21	22	7	7.84	0.71	9.00
Sm	2.48	8.02	2.29	0.41	2.38	3.51	13	5	2.35	0.13	5.55
Eu	1.04	10.43	0.97	3.32	1.01	6.93	14	6	0.98	0.06	5.94
Gd	3.41	18.52	3.05	6.06	3.07	6.73	19	5	2.96	0.18	6.19
Tb	0.54	11.91	0.50	4.10	0.54	11.94	15	6	0.50	0.03	6.20
Dy	3.65	13.64	3.36	4.56	3.63	12.93	17	7	3.39	0.22	6.48
Ho	0.63	9.56	0.69	0.94	0.70	0.38	20	7	0.68	0.07	9.78
Er	1.86	11.19	2.06	1.68	2.08	0.93	21	7	2.07	0.21	10.21
Tm	0.27	8.76	0.30	1.27	0.30	0.37	21	7	0.29	0.03	9.57
Yb	1.82	8.80	2.08	4.19	1.99	0.47	21	8	1.95	0.19	9.99
Lu	0.33	11.08	0.32	5.52	0.33	8.47	13	6	0.31	0.02	6.43
Hf	1.84	19.66	1.64	6.25	1.87	21.59	38	13	1.70	0.20	12.04
Th	0.29	11.80	0.31	5.55	0.36	7.60	20	8	0.33	0.03	10.45
Max		20		7		22					12
Average		12		4		6					8

BR-688 overall

APPENDIX B. Geochemical data, Chapter 2

Table B.1 Geochemistry of gray gneiss, Muskoka domain, Ojibway gneiss association, Upper Go Home domain, and Shawanaga pluton.

	Muskoka domain							
Sample	99.16-P	99.16-Pv	M06073-1	M080715	M08079	M09072	99.16-Pw	99.42
Easting	647 550	647 550	634 850	645 330	642 500	632 480	647 550	669 500
Northing	5000 500	5000 500	4994 050	4999 150	4997 990	5008 150	5000 500	5001 330
SiO_2 (wt.%)	61.54	69.91	71.29	61.90	67.63	53.92	53.29	51.09
TiO_2	0.77	0.67	0.36	1.22	0.43	1.12	1.07	1.37
Al_2O_3	17.36	15.36	14.62	15.62	15.54	17.42	17.30	19.69
Fe_2O_3	5.14	3.16	2.43	6.17	3.13	9.86	9.34	9.15
MnO	0.07	0.06	0.04	0.13	0.05	0.16	0.15	0.13
MgO	2.23	0.81	0.73	1.62	1.21	4.32	4.36	3.43
CaO	4.73	2.10	1.99	3.33	2.59	7.51	7.25	7.35
Na_2O	4.85	3.94	3.80	3.97	4.49	3.61	5.05	4.66
K_2O	2.57	4.44	4.36	4.85	3.38	2.53	1.92	1.86
P_2O_5	0.28	0.17	0.11	0.40	0.15	0.32	0.37	0.44
L.O.I.	0.29	0.20	0.10	0.00	0.30	0.45	0.48	0.76
Total	99.83	100.82	99.82	99.21	98.91	101.22	100.58	99.92
Ba (ppm)	1132	1266	979	1404	1134	999	647	1116
Rb	71	134	142	101	82	60	31	30
Sr	936	417	430	345	559	549	636	1148
Y	20	22	29	53	19	33	39	40
Zr	301	371	192	798	186	333	308	396
Nb	6	11	10	26	6	8	8	12
Th	n.a.	12.63	14.89	n.a.	n.a.	n.a.	3.07	n.a.
Ga	22	18	19	21	19	21	21	26
Zn	84	59	51	109	62	101	123	131
Ni	12	-	<3	78	30	21	19	12
V	-	-	50	131	62	187	-	-
Cr	-	-	4	<4	11	16	-	-
Hf	n.a.	13.23	5.11	n.a.	n.a.	n.a.	10.39	n.a.
Co	15	1	5	11	6	33	34	29
U	1	3	3	3	<1	1	2	1
La	n.a.	47.38	43.52	n.a.	n.a.	n.a.	40.13	n.a.
Ce	n.a.	102.96	84.11	n.a.	n.a.	n.a.	91.53	n.a.
Pr	n.a.	11.36	9.57	n.a.	n.a.	n.a.	11.82	n.a.
Nd	n.a.	41.85	34.73	n.a.	n.a.	n.a.	47.84	n.a.
Sm	n.a.	7.69	5.89	n.a.	n.a.	n.a.	10.03	n.a.
Eu	n.a.	1.62	0.96	n.a.	n.a.	n.a.	2.19	n.a.
Gd	n.a.	5.87	4.70	n.a.	n.a.	n.a.	8.45	n.a.
Tb	n.a.	0.84	0.70	n.a.	n.a.	n.a.	1.20	n.a.
Dy	n.a.	4.96	4.30	n.a.	n.a.	n.a.	7.07	n.a.
Ho	n.a.	1.01	0.87	n.a.	n.a.	n.a.	1.43	n.a.
Er	n.a.	3.18	2.60	n.a.	n.a.	n.a.	4.34	n.a.
Tm	n.a.	0.43	0.40	n.a.	n.a.	n.a.	0.58	n.a.
Yb	n.a.	2.68	2.73	n.a.	n.a.	n.a.	3.51	n.a.
Lu	n.a.	0.41	0.41	n.a.	n.a.	n.a.	0.53	n.a.

Abbreviations: g.a.=gneiss association, UGH=Upper Go Home domain, L.O.I.=Loss On Ignition, n.a.=not analyzed, <x=below detection limit where x=reported detection limit. UTM Zone 17.

Table B.1 continued.

Sample	M2707-11	M04073-HI	M050712-2	M05077	M05081-5	M06071	M08078	M100715	M100716
					Muskoka domain				
Easting	668 550	666 000	669 300	671 250	658 550	668 100	641 850	643 230	643 500
Northing	5005 430	4989 100	5002 700	4998 830	4988 350	5006 430	4997 700	4984 150	4984 380
SiO_2	60.76	58.16	55.77	54.72	60.48	55.58	56.95	53.71	58.51
TiO_2	0.84	0.92	1.10	1.10	0.88	1.05	1.36	1.16	0.98
Al_2O_3	15.86	18.05	17.90	18.86	16.60	16.16	15.12	18.07	19.14
Fe_2O_3	6.36	6.93	7.84	7.96	5.96	8.87	9.01	8.36	5.78
MnO	0.11	0.09	0.12	0.12	0.08	0.14	0.14	0.11	0.10
MgO	3.11	3.10	3.62	3.82	2.07	4.54	3.58	4.09	1.97
CaO	5.46	6.01	6.45	7.06	4.46	6.80	5.97	7.03	4.71
Na_2O	4.00	4.58	4.69	4.98	4.17	3.87	3.42	4.38	5.46
K_2O	2.43	2.00	2.06	1.76	3.45	2.63	2.79	2.13	2.76
P_2O_5	0.25	0.33	0.37	0.42	0.25	0.30	0.53	0.42	0.32
L.O.I.	0.56	0.48	0.39	0.31	0.39	0.65	0.27	0.67	0.41
Total	99.74	100.65	100.31	101.10	98.79	100.58	99.14	100.12	100.14
Ba	759	672	467	970	1266	1000	832	970	1519
Rb	59	51	48	34	89	55	38	40	75
Sr	616	735	687	1094	485	446	645	1106	868
Y	35	41	37	22	29	34	35	28	23
Zr	199	270	271	313	407	333	286	272	664
Nb	10	8	10	8	8	11	13	7	7
Th	5.51	3.77	0.91	1.78	0.68	7.41	n.a.	n.a.	n.a.
Ga	21	23	25	26	20	22	20	26	25
Zn	95	98	123	104	103	166	102	120	114
Ni	15	22	22	332	10	17	27	27	5
V	129	138	156	155	116	157	195	168	116
Cr	41	30	36	47	16	125	40	55	4
Hf	4.56	7.78	8.27	8.93	10.86	10.16	n.a.	n.a.	n.a.
Co	20	21	36	33	13	37	26	27	9
U	<1	<1	<1	<1	1	1	<1	<1	<1
La	32.95	46.42	47.61	29.30	30.62	32.47	n.a.	n.a.	n.a.
Ce	69.25	105.37	112.88	69.22	61.97	72.74	n.a.	n.a.	n.a.
Pr	8.50	14.06	14.78	9.72	7.94	9.39	n.a.	n.a.	n.a.
Nd	34.80	57.95	60.60	42.03	33.18	38.08	n.a.	n.a.	n.a.
Sm	8.09	11.27	12.28	8.85	6.38	8.04	n.a.	n.a.	n.a.
Eu	1.45	2.02	2.11	2.16	1.58	1.62	n.a.	n.a.	n.a.
Gd	7.27	9.34	10.18	7.37	5.75	7.35	n.a.	n.a.	n.a.
Tb	1.10	1.39	1.52	1.04	0.86	1.17	n.a.	n.a.	n.a.
Dy	6.78	8.49	9.10	6.06	5.26	7.32	n.a.	n.a.	n.a.
Ho	1.23	1.68	1.78	1.21	1.08	1.52	n.a.	n.a.	n.a.
Er	3.87	4.82	5.58	3.67	3.11	4.76	n.a.	n.a.	n.a.
Tm	0.52	0.70	0.75	0.48	0.45	0.64	n.a.	n.a.	n.a.
Yb	3.34	4.53	4.76	2.94	3.07	4.07	n.a.	n.a.	n.a.
Lu	0.57	0.65	0.72	0.43	0.47	0.61	n.a.	n.a.	n.a.

Table B.1 continued.

Sample	Muskoka domain						Ojibway g.a.	
	M10075-1	M130717	M13079	M2407-4	M050711	M2707-1	S11064-2	S31052-h
Easting	637 430	668 800	668 080	648 930	669 380	668 500	566 580	567 280
Northing	4982 500	5003 700	5005 150	5002 150	5002 650	5005 580	5033 780	5032 750
SiO_2	59.12	56.32	59.69	59.84	49.03	46.72	60.68	63.22
TiO_2	0.81	1.06	0.84	0.85	1.56	2.03	0.83	0.74
Al_2O_3	19.22	19.21	18.43	18.21	19.61	18.31	17.02	16.67
Fe_2O_3	5.41	7.55	5.71	5.72	10.73	12.34	6.17	5.72
MnO	0.09	0.12	0.11	0.12	0.13	0.18	0.11	0.12
MgO	2.01	2.91	1.82	1.84	4.42	4.30	2.04	1.75
CaO	4.67	6.17	4.90	4.53	8.63	7.95	4.65	3.98
Na_2O	4.93	4.98	4.96	4.90	4.22	3.76	4.48	4.71
K_2O	2.87	1.97	2.39	3.21	1.61·	2.47	2.92	2.66
P_2O_5	0.33	0.38	0.30	0.28	0.53	1.04	0.26	0.24
L.O.I.	0.30	0.17	0.20	0.49	0.45	0.45	0.50	0.29
Total	99.75	100.85	99.35	99.99	100.92	99.55	99.66	100.10
Ba	1872	703	790	1418	904	1469	760	630
Rb	69	45	85	81	34	50	86	103
Sr	1006	844	655	644	954	882	496	369
Y	21	27	30	39	35	40	35	32
Zr	603	398	410	412	352	578	287	263
Nb	6	11	14	14	12	14	13	13
Th	n.a.	1.67	10.57	9.40	1.54	1.94	8.42	9.54
Ga	21	29	26	22	27	23	23	21
Zn	101	111	114	105	114	140	96	102
Ni	7	9	5	6	7	6	7	13
V	100	142	98	110	216	239	113	104
Cr	7	16	<4	8	<4	4	9	9
Hf	n.a.	12.15	13.04	11.97	11.36	12.78	7.96	7.91
Co	12	33	27	12	38	30	15	14
U	<1	<1	<1	<1	<1	<1	2	3
La	n.a.	43.81	56.42	51.11	33.71	42.37	32.54	33.87
Ce	n.a.	98.64	123.96	107.75	83.08	102.98	70.21	69.52
Pr	n.a.	12.33	14.70	12.48	11.55	14.25	8.71	8.00
Nd	n.a.	48.13	55.22	48.92	50.56	65.51	34.85	29.70
Sm	n.a.	9.18	10.48	10.14	11.17	15.55	7.97	6.46
Eu	n.a.	1.98	1.81	2.13	2.36	3.95	1.71	1.38
Gd	n.a.	7.26	8.32	8.71	10.00	14.12	7.10	5.65
Tb	n.a.	1.07	1.21	1.21	1.51	1.92	1.07	0.85
Dy	n.a.	6.43	7.04	7.20	9.17	11.07	6.55	5.25
Ho	n.a.	1.30	1.40	1.34	1.81	1.94	1.18	0.94
Er	n.a.	4.00	4.26	4.38	5.56	5.75	3.68	3.12
Tm	n.a.	0.52	0.57	0.65	0.73	0.71	0.51	0.46
Yb	n.a.	3.31	3.65	4.58	4.45	4.21	3.32	3.18
Lu	n.a.	0.50	0.56	0.84	0.67	0.71	0.58	0.60

Table B.1 continued.

Sample	UGH domain	Shawanaga pluton	
	G18066-2	S31057	S31057-h
Easting	571 750	557 350	557 350
Northing	4991 050	5042 730	5042 730
SiO_2	68.50	66.43	65.38
TiO_2	0.51	0.53	0.56
Al_2O_3	15.04	17.08	16.55
Fe_2O_3	3.15	4.06	4.93
MnO	0.06	0.06	0.09
MgO	0.94	1.09	1.37
CaO	1.64	3.29	3.62
Na_2O	3.72	3.14	3.37
K_2O	5.12	4.96	3.83
P_2O_5	0.16	0.15	0.19
L.O.I.	0.30	0.29	0.29
Total	99.14	101.07	100.17
Ba	1175	2039	1138
Rb	126	100	107
Sr	243	374	370
Y	36	20	45
Zr	291	279	259
Nb	11	8	13
Th	12.49	2.33	12.10
Ga	18	20	20
Zn	60	174	73
Ni	<3	4	4
V	58	83	85
Cr	4	7	<4
Hf	7.21	7.78	7.16
Co	<5	7	12
U	3	3	3
La	50.00	26.93	42.74
Ce	102.49	51.59	88.59
Pr	12.37	6.05	11.38
Nd	47.28	23.67	45.62
Sm	8.71	5.01	11.72
Eu	1.42	1.98	1.51
Gd	7.08	4.38	10.69
Tb	1.04	0.60	1.69
Dy	6.25	3.62	10.47
Ho	1.21	0.65	1.83
Er	3.49	2.05	5.66
Tm	0.51	0.29	0.74
Yb	3.36	2.01	4.55
Lu	0.50	0.37	0.77

Table B.2 Geochemistry of megacrystic granitoid orthogneiss, Muskoka domain and Ojibway gneiss association (Lake of Bays suite), megacrystic sheets in the Sand Bay gneiss association and Mann Island granodiorite and Britt pluton in the Britt domain.

	Muskoka domain				Ojibway g.a.
Sample	M11072	M13071	M15078	2M0706-2-1	S31056-mg
Easting	629 700	665 150	624 800	625 200	561 280
Northing	4995 950	5011 450	5016 180	5005 600	5038 830
SiO_2	69.30	60.92	58.67	70.01	60.45
TiO_2	0.40	0.79	0.86	0.40	0.76
Al_2O_3	15.42	17.85	18.64	15.38	17.92
Fe_2O_3	3.17	6.23	6.47	3.28	6.12
MnO	0.05	0.09	0.11	0.07	0.10
MgO	0.83	1.81	1.82	1.00	1.66
CaO	2.79	4.88	5.23	2.45	4.77
Na_2O	3.13	3.40	4.08	4.11	3.79
K_2O	4.44	3.15	3.51	4.53	3.59
P_2O_5	0.10	0.19	0.29	0.12	0.22
L.O.l.	0.19	0.47	0.39	0.20	0.36
Total	99.81	99.78	100.07	101.54	99.73
Ba	973	1573	1835	662	1739
Rb	129	65	84	34	79
Sr	240	405	554	228	505
Y	24	20	33	37	23
Zr	180	342	380	162	385
Nb	11	13	13	11	13
Th	9.17	2.42	6.70	0.87	6.92
Ga	20	23	23	23	22
Zn	50	91	105	67	95
Ni	3	10	<3	20	6
V	62	120	111	53	103
Cr	5	14	<4	17	12
Hf	5.25	9.07	10.05	9.52	10.20
Co	16	16	16	42	15
U	3	1	1	2	1
La	43.01	29.20	37.52	32.91	45.21
Ce	83.79	57.79	81.37	72.11	87.47
Pr	9.57	6.68	10.07	9.36	9.66
Nd	35.56	27.68	40.94	40.45	35.04
Sm	5.96	5.70	9.15	9.88	6.62
Eu	1.31	2.38	2.20	2.16	1.97
Gd	4.73	5.03	8.10	10.64	5.35
Tb	0.69	0.70	1.15	1.52	0.75
Dy	4.06	4.01	6.84	8.99	4.45
Ho	0.80	0.73	1.22	1.37	0.76
Er	2.25	2.21	3.74	3.65	2.38
Tm	0.32	0.28	0.49	0.48	0.32
Yb	2.14	1.83	3.12	2.99	2.09
Lu	0.32	0.34	0.54	0.50	0.39

Table B.2 continued.

	'Marginal' orthogneiss'	Sand Bay g.a.		Mann Island granodiorite	Britt pluton	
Sample	2S30062	S17066	S25061-4	2S28062	2S28063	2S28064
Easting	573 630	556 730	557 980	519 080	521 950	-
Northing	5027 580	5016 500	5020 950	5081 200	5081 400	-
SiO_2	67.27	63.67	71.86	73.02	67.36	62.41
TiO_2	0.42	0.61	0.40	0.11	0.99	1.22
Al_2O_3	14.94	16.66	14.66	14.82	13.92	14.04
Fe_2O_3	3.69	4.78	2.44	1.02	6.24	7.74
MnO	0.08	0.08	0.03	0.01	0.15	0.18
MgO	1.15	1.54	0.64	0.16	1.11	1.34
CaO	2.92	3.76	2.54	1.14	2.69	3.43
Na_2O	4.16	4.22	5.14	3.82	3.24	3.57
K_2O	3.79	3.59	1.10	5.54	4.94	4.12
P_2O_5	0.13	0.19	0.11	0.03	0.32	0.41
L.O.I.	0.30	0.56	0.27	0.58	0.49	0.20
Total	98.84	99.66	99.18	100.24	101.45	98.66
Ba	536	1169	406	727	1884	2185
Rb	118	91	70	81	111	81
Sr	215	464	311	216	236	287
Y	43	33	35	54	75	73
Zr	136	263	205	59	586	607
Nb	16	10	12	3	23	26
Th	8.17	8.92	18.47	3.61	9.08	8.27
Ga	22	21	20	16	19	21
Zn	76	81	33	19	118	158
Ni	5	4	<3	5	14	13
V	56	85	52	23	102	125
Cr	9	9	<4	<4	4	5
Hf	9.81	7.05	8.37	15.92	12.18	16.87
Co	67	12	6	42	63	58
U	5	2	3	3	4	3
La	47.74	35.57	37.11	74.30	56.50	81.60
Ce	90.80	72.72	73.71	151.16	122.28	167.77
Pr	10.88	8.73	8.55	18.07	15.01	20.58
Nd	41.62	33.64	32.01	71.66	59.09	82.40
Sm	7.64	7.28	7.58	15.21	13.06	17.73
Eu	1.55	1.48	1.03	3.37	3.37	4.71
Gd	6.80	6.25	6.57	12.26	14.03	18.55
Tb	1.15	0.92	1.00	1.86	2.18	2.72
Dy	7.08	5.74	5.95	11.18	13.96	16.84
Ho	1.29	1.02	0.96	1.89	2.33	2.70
Er	3.84	3.19	2.88	5.25	6.97	7.74
Tm	0.58	0.45	0.40	0.73	1.04	1.10
Yb	3.95	2.92	2.63	4.71	6.98	7.17
Lu	0.61	0.50	0.48	0.83	1.22	1.25

Table B.3   Geochemistry of granitic gneiss, Muskoka domain and Ojibway gneiss association.

	Muskoka domain							
Sample	M04074-HI	M05075-H1	M05079-1	M100723-1	M100710-2	M100720	M080711	M150712
Easting	662 350	671 700	670 180	651 650	640 850	645 500	643 300	627 450
Northing	4989 650	4998 350	4999 950	4984 450	4982 800	4984 850	4998 150	5017 100
SiO_2	64.33	68.79	72.32	73.41	68.18	71.02	76.54	76.67
TiO_2	0.62	0.38	0.24	0.35	0.46	0.43	0.21	0.11
Al_2O_3	17.97	16.21	14.14	13.44	14.61	12.99	11.96	12.30
Fe_2O_3	3.69	3.55	2.69	3.57	3.80	4.08	2.74	1.81
MnO	0.09	0.06	0.06	0.06	0.08	0.06	0.03	0.02
MgO	0.87	0.46	0.12	0.18	0.29	0.14	0.06	0.07
CaO	2.56	1.05	0.74	0.83	1.17	0.87	0.26	0.32
Na_2O	4.76	4.72	4.17	3.41	4.03	3.03	2.23	1.58
K_2O	5.43	5.91	5.48	5.76	5.72	5.55	7.16	7.88
P_2O_5	0.18	0.07	0.02	0.07	0.11	0.04	0.02	0.01
L.O.I.	0.47	0.53	0.08	0.00	0.10	0.00	0.10	0.19
Total	100.97	101.73	100.06	101.08	98.55	98.21	101.31	100.96
Ba	2489	942	488	765	1038	479	383	325
Rb	88	100	81	89	67	92	211	108
Sr	403	137	30	64	127	45	72	162
Y	57	45	21	81	70	46	52	84
Zr	619	746	613	694	668	1046	551	370
Nb	11	36	6	14	38	12	23	3
Th	11.41	4.68	5.80	5.71	n.a.	n.a.	7.89	3.33
Ga	20	29	23	28	28	24	23	31
Zn	77	63	49	63	88	77	71	59
Ni	5	<3	9	<3	<3	<3	<3	10
V	72	43	27	40	50	43	27	18
Cr	<4	<4	<4	<4	<4	<4	<4	<4
Hf	13.38	25.64	20.26	14.43	n.a.	n.a.	12.41	7.70
Co	<5	17	29	<5	<5	<5	<5	<5
U	2	3	4	4	3	4	4	3
La	119.76	121.07	95.65	101.32	n.a.	n.a.	50.64	54.55
Ce	219.86	243.08	203.16	247.33	n.a.	n.a.	104.39	122.31
Pr	25.52	27.01	23.94	25.60	n.a.	n.a.	12.90	13.39
Nd	97.92	98.13	90.03	95.73	n.a.	n.a.	47.34	53.44
Sm	16.98	17.44	16.00	17.99	n.a.	n.a.	10.04	13.27
Eu	2.88	2.24	1.08	2.32	n.a.	n.a.	0.35	0.80
Gd	13.54	13.69	11.97	14.80	n.a.	n.a.	8.04	12.30
Tb	1.96	2.14	1.64	2.52	n.a.	n.a.	1.32	2.08
Dy	11.69	12.90	9.10	15.88	n.a.	n.a.	8.44	13.95
Ho	2.28	2.53	1.69	3.17	n.a.	n.a.	1.54	2.88
Er	6.44	7.80	4.88	9.18	n.a.	n.a.	4.67	9.92
Tm	0.92	1.04	0.63	1.27	n.a.	n.a.	0.71	1.34
Yb	6.01	6.60	4.18	7.62	n.a.	n.a.	4.77	8.23
Lu	0.87	1.02	0.71	1.02	n.a.	n.a.	0.75	1.30

Table B.3 continued.

Sample	Muskoka domain					Ojibway g.a.
	M07075-1	M160740	M150724	99.45-PM2	M30064	S11063-2
Easting	667 100	605 050	629 200	632 650	641 350	566 780
Northing	5007 600	5029 250	5022 300	5003 500	4989 650	5033 430
SiO_2	65.68	73.75	69.97	72.67	69.51	74.62
TiO_2	0.45	0.22	0.25	0.41	0.33	0.25
Al_2O_3	16.99	14.31	14.95	15.00	14.63	12.84
Fe_2O_3	4.00	1.99	2.13	2.38	2.57	1.47
MnO	0.10	0.01	0.04	0.05	0.01	0.02
MgO	0.39	0.43	0.22	0.64	0.61	0.32
CaO	1.30	0.85	1.12	1.64	1.11	0.80
Na_2O	4.48	2.79	3.58	4.38	2.80	2.93
K_2O	6.81	6.45	6.07	4.09	6.59	5.65
P_2O_5	0.07	0.08	0.05	0.09	0.11	0.03
L.O.I.	0.29	0.45	0.27	0.10	0.82	0.17
Total	100.55	101.33	98.65	101.45	99.10	99.10
Ba	720	3238	1077	707	2894	963
Rb	110	77	130	150	144	161
Sr	68	347	128	234	362	134
Y	32	15	29	21	18	28
Zr	789	308	287	300	317	228
Nb	11	<1	10	11	2	6
Th	8.25	18.79	15.46	16.94	34.50	14.76
Ga	19	13	17	19	20	14
Zn	49	33	56	48	43	26
Ni	373	6	<3	1	<3	<3
V	46	32	30	-	49	33
Cr	11	<4	<4	-	<4	4
Hf	17.49	7.62	7.13	12.32	7.93	6.49
Co	37	55	<5	0	<5	<5
U	6	4	4	3	2	4
La	73.98	155.06	21.40	59.43	198.55	46.10
Ce	141.78	292.85	73.33	118.92	341.46	91.95
Pr	16.17	31.40	5.37	13.77	33.18	10.57
Nd	59.02	103.54	22.10	48.55	104.69	39.90
Sm	8.84	13.39	5.40	8.60	12.40	8.02
Eu	1.13	1.63	1.24	1.07	2.08	0.93
Gd	6.51	6.87	5.12	6.38	6.35	6.36
Tb	0.89	0.69	0.83	0.91	0.63	0.82
Dy	5.23	2.92	5.30	5.36	2.92	4.49
Ho	1.00	0.39	1.00	1.07	0.44	0.70
Er	2.97	0.97	3.13	3.33	1.17	1.91
Tm	0.46	0.13	0.39	0.45	0.14	0.23
Yb	3.30	0.85	2.47	2.86	0.82	1.37
Lu	0.57	0.15	0.43	0.44	0.15	0.23

Table B.4 Geochemistry of charnockitic gneiss, Muskoka domain.

Sample	M050713	M05079-2	M080721-1	M18072	M300617	M01078	M100723-2
Easting	668 300	670 180	656 500	633 650	640 050	649 650	651 650
Northing	5006 180	4999 950	5010 300	5012 800	4982 550	4985 200	4984 450
SiO_2	64.06	62.65	61.86	67.66	63.23	64.91	57.31
TiO_2	0.47	0.50	0.73	0.56	0.77	0.72	1.14
Al_2O_3	17.59	16.48	17.08	14.22	15.49	16.42	16.12
Fe_2O_3	4.13	6.72	6.31	5.81	6.53	5.33	8.99
MnO	0.07	0.18	0.18	0.14	0.18	0.11	0.21
MgO	0.42	0.19	0.47	0.21	0.52	0.79	1.36
CaO	1.37	2.35	2.92	1.49	2.18	2.43	2.66
Na_2O	4.65	5.30	4.90	4.25	4.95	4.69	4.80
K_2O	6.78	5.72	4.87	5.58	5.28	5.00	5.05
P_2O_5	0.07	0.09	0.22	0.08	0.22	0.19	0.34
L.O.I.	0.48	0.13	0.00	0.16	0.28	0.30	0.39
Total	99.93	100.31	99.54	100.16	99.63	100.88	98.37
Ba	452	588	2232	648	1254	1569	2358
Rb	90	72	47	66	56	87	43
Sr	57	112	306	26	185	348	229
Y	20	67	45	120	59	124	140
Zr	886	1356	1364	1249	1526	954	1916
Nb	2	39	16	40	27	30	57
Th	5.65	3.48	3.82	4.36	2.01	12.93	3.31
Ga	20	33	28	30	29	26	30
Zn	16	145	123	187	175	148	129
Ni	7	<3	<3	<3	<3	16	<3
V	47	51	67	53	75	77	99
Cr	<4	<4	<4	<4	<4	13	<4
Hf	20.77	42.13	29.93	36.81	40.08	26.52	45.91
Co	11	19	5	5	21	33	32
U	4	4	3	4	2	4	3
La	51.31	74.15	75.10	177.43	92.32	170.73	136.97
Ce	103.97	182.34	152.22	398.72	206.99	365.03	302.19
Pr	12.11	25.53	19.27	51.13	27.97	42.85	40.53
Nd	44.99	109.72	78.48	211.28	115.51	162.72	166.91
Sm	6.80	23.65	14.36	46.23	23.52	30.64	33.62
Eu	0.92	2.93	6.80	4.11	5.14	3.35	5.73
Gd	4.54	20.95	12.06	38.96	19.18	26.28	30.68
Tb	0.62	3.28	1.80	5.64	2.93	3.90	4.60
Dy	3.57	20.25	11.00	33.34	17.42	24.07	28.32
Ho	0.72	4.20	2.22	5.76	3.45	4.45	5.43
Er	2.31	13.54	6.49	17.16	10.46	12.81	15.66
Tm	0.33	1.91	0.97	2.20	1.37	1.82	2.27
Yb	2.33	12.78	6.70	13.83	8.79	11.68	14.80
Lu	0.41	2.10	1.08	2.41	1.40	1.61	2.25

Table B.5 Geochemistry of rhyolitic gneiss, Sand Bay gneiss association and Upper Go Home domain.

	Sand Bay g.a.					
Sample	S02063	S04064	S04066-4	S06062	S06064	S12063
Easting	559 150	558 930	559 300	560 100	559 500	556 300
Northing	5025 980	5019 530	5021 930	5021 280	5021 550	5015 450
SiO_2	78.08	75.06	76.75	77.45	77.62	76.00
TiO_2	0.14	0.21	0.07	0.12	0.08	0.25
Al_2O_3	11.74	13.58	12.57	12.25	12.50	11.69
Fe_2O_3	0.87	1.40	1.07	0.91	0.79	2.51
MnO	0.04	0.01	0.00	0.01	0.00	0.02
MgO	0.03	0.23	0.02	0.09	<0.01	0.10
CaO	0.34	0.99	0.81	0.76	0.47	1.17
Na_2O	3.57	4.93	2.95	3.17	3.47	1.89
K_2O	4.50	2.96	5.24	4.68	4.78	5.38
P_2O_5	0.02	0.02	0.01	0.02	0.02	0.03
L.O.I.	0.00	0.07	0.13	0.10	0.25	0.93
Total	99.32	99.47	99.63	99.55	99.98	99.96
Ba	63	320	362	373	183	943
Rb	284	117	177	203	195	152
Sr	11	86	105	70	11	90
Y	34	17	15	28	17	70
Zr	225	217	143	163	173	470
Nb	35	14	7	15	17	19
Th	26.94	12.84	11.73	n.a.	16.17	11.85
Ga	27	21	20	17	22	20
Zn	22	26	15	24	27	42
Ni	<3	<3	<3	<3	<3	<3
V	16	26	15	19	13	30
Cr	<4	<4	<4	<4	<4	<4
Hf	17.87	8.10	5.79	n.a.	10.67	14.00
Co	36	43	32	42	23	31
U	8	4	3	3	6	5
La	50.51	36.55	15.03	n.a.	11.00	54.38
Ce	72.23	85.71	37.46	n.a.	30.75	117.53
Pr	5.47	10.16	5.02	n.a.	4.13	15.26
Nd	13.61	38.88	20.53	n.a.	16.84	61.98
Sm	2.08	8.27	5.41	n.a.	4.85	14.62
Eu	0.13	0.79	0.20	n.a.	0.05	1.99
Gd	1.75	6.54	4.63	n.a.	4.07	13.66
Tb	0.34	1.03	0.73	n.a.	0.74	2.20
Dy	2.72	6.27	4.33	n.a.	5.12	13.92
Ho	0.78	1.22	0.82	n.a.	1.09	2.89
Er	3.75	3.79	2.43	n.a.	3.78	9.19
Tm	0.76	0.55	0.31	n.a.	0.55	1.28
Yb	6.79	3.64	1.92	n.a.	3.49	8.17
Lu	1.35	0.54	0.27	n.a.	0.51	1.24

Table B.5 continued.

	Sand Bay g.a.				UGH domain
Sample	S27059	S29056	S30051	S30052	G18068
Easting	556 330	553 980	557 080	556 580	573 150
Northing	5017 050	5023 650	5017 050	5016 230	4990 480
SiO_2	78.78	76.20	75.84	67.13	75.75
TiO_2	0.17	0.19	0.16	0.76	0.23
Al_2O_3	11.59	11.82	12.64	15.57	12.25
Fe_2O_3	1.10	2.20	0.99	3.24	3.19
MnO	0.01	0.01	0.01	0.06	0.01
MgO	0.01	0.10	0.17	0.94	0.13
CaO	0.37	0.58	0.37	1.52	0.81
Na_2O	3.47	2.11	3.22	4.38	3.66
K_2O	4.18	6.09	5.71	5.23	3.86
P_2O_5	0.01	0.02	0.03	0.21	0.02
L.O.I.	0.08	0.09	0.08	0.18	0.14
Total	99.77	99.42	99.21	99.23	100.05
Ba	41	972	531	1254	289
Rb	155	153	201	140	93
Sr	15	86	52	239	70
Y	17	66	11	36	64
Zr	222	331	109	443	587
Nb	7	22	12	19	19
Th	17.22	13.64	13.60	12.18	13.75
Ga	20	22	18	22	26
Zn	19	48	23	47	20
Ni	<3	<3	204	<3	306
V	13	25	23	86	25
Cr	<4	<4	<4	<4	<4
Hf	14.48	11.98	5.51	15.18	21.53
Co	42	32	26	25	40
U	4	4	3	4	5
La	21.19	62.57	34.60	46.83	69.94
Ce	59.66	136.38	53.35	116.78	147.62
Pr	7.78	17.29	4.37	13.54	18.89
Nd	31.58	68.69	11.91	53.55	76.54
Sm	8.36	15.37	1.66	11.18	16.71
Eu	0.05	1.31	0.24	2.14	0.96
Gd	6.81	14.14	1.21	8.79	15.76
Tb	1.04	2.33	0.19	1.30	2.52
Dy	6.10	14.92	1.26	7.64	15.65
Ho	1.17	3.12	0.29	1.51	3.11
Er	3.52	9.91	1.07	4.71	9.70
Tm	0.46	1.39	0.18	0.64	1.30
Yb	2.82	8.90	1.37	4.07	8.04
Lu	0.40	1.34	0.24	0.63	1.18

Table B.6 Geochemistry of metabasites in the Muskoka and Upper Go Home domains, and Sand Bay gneiss association.

	Muskoka				
Sample	99.16-A	M03083-M	M06073-2	M070713	M08072
Easting	647 550	632 700	634 850	664 700	638 200
Northing	5000 500	5002 400	4994 050	5009 300	4996 800
SiO_2	46.90	46.64	45.31	45.10	50.13
TiO_2	1.91	1.71	3.48	2.67	1.99
Al_2O_3	16.54	16.20	16.44	15.36	13.86
Fe_2O_3	14.26	12.59	15.49	16.07	14.93
MnO	0.20	0.20	0.22	0.22	0.22
MgO	6.25	7.33	5.27	5.99	5.94
CaO	8.15	8.75	7.82	8.09	9.84
Na_2O	3.76	3.49	4.01	4.15	2.57
K_2O	1.46	1.96	1.52	1.02	0.87
P_2O_5	0.30	0.34	0.57	0.70	0.26
L.O.I.	0.06	0.82	0.29	0.19	0.24
Total	99.78	100.02	100.42	99.56	100.86
Ba	589	286	25	107	26
Rb	11	47	32	18	24
Sr	418	484	478	543	249
Y	40	23	26	28	29
Zr	119	121	198	194	134
Nb	5	4	14	9	7
Th	1.22	0.68	1.35	0.69	n.a.
Ga	20	19	21	20	23
Zn	135	116	102	133	106
Ni	84	126	58	69	49
V	256	245	376	339	330
Cr	55	120	32	54	96
Hf	4.00	2.65	4.70	4.59	n.a.
Co	62	47	52	52	44
U	2	<1	<1	<1	1
La	8.77	12.33	16.34	18.78	n.a.
Ce	21.80	29.62	40.71	46.42	n.a.
Pr	3.37	4.24	6.03	6.95	n.a.
Nd	16.40	19.76	28.51	33.78	n.a.
Sm	4.70	4.66	6.79	7.97	n.a.
Eu	1.65	1.72	2.40	2.76	n.a.
Gd	5.03	4.95	7.06	7.95	n.a.
Tb	0.78	0.76	1.07	1.16	n.a.
Dy	4.80	4.74	6.51	6.99	n.a.
Ho	0.99	0.93	1.30	1.38	n.a.
Er	3.02	2.62	3.65	3.84	n.a.
Tm	0.40	0.38	0.51	0.53	n.a.
Yb	2.42	2.42	3.25	3.36	n.a.
Lu	0.36	0.35	0.48	0.49	n.a.

Table B.6 continued.

Sample	Muskoka domain			Sand Bay g.a.			
	2M1406-3	M10079	M29072	S06069-2	S13067	S14063	S14064
Easting	656 500	639 480	666 350	559 530	558 400	556 100	556 400
Northing	5010 300	4982 350	5008 280	5023 450	5020 800	5016 630	5016 930
SiO_2	48.69	45.89	51.50	46.97	46.11	48.79	47.69
TiO_2	1.93	1.43	1.45	0.62	2.22	1.57	4.07
Al_2O_3	13.48	16.61	15.11	15.24	17.68	14.92	12.86
Fe_2O_3	14.88	12.87	10.53	12.76	12.74	13.42	17.20
MnO	0.23	0.19	0.17	0.21	0.16	0.22	0.24
MgO	5.99	7.71	5.34	8.93	6.99	5.95	3.99
CaO	9.42	9.07	7.07	10.23	7.97	8.13	8.44
Na_2O	4.09	3.23	4.71	3.02	3.66	4.24	2.80
K_2O	0.87	1.79	2.11	1.45	1.41	2.01	0.86
P_2O_5	0.26	0.17	0.58	0.05	0.38	0.34	0.72
L.O.I.	0.50	0.90	0.97	0.75	0.84	0.44	0.44
Total	100.33	99.86	99.53	100.23	100.16	100.02	99.31
Ba	66	<5	723	10	77	150	<5
Rb	15	35	32	26	26	87	13
Sr	254	304	648	157	496	305	222
Y	29	21	34	20	21	31	10
Zr	131	75	286	24	137	182	270
Nb	6	3	11	2	10	7	13
Th	1.36	1.05	n.a.	n.a.	0.90	1.26	n.a.
Ga	22	19	19	16	19	20	23
Zn	123	108	126	105	83	164	142
Ni	41	110	67	168	110	56	11
V	302	233	203	179	251	255	448
Cr	93	70	131	277	156	43	16
Hf	4.45	2.03	n.a.	n.a.	3.28	6.30	n.a.
Co	71	52	35	55	61	59	58
U	<1	1	<1	1	<1	<1	1
La	12.43	10.00	n.a.	n.a.	10.89	18.91	n.a.
Ce	28.96	22.27	n.a.	n.a.	27.04	45.41	n.a.
Pr	4.23	3.08	n.a.	n.a.	3.85	6.28	n.a.
Nd	20.12	13.95	n.a.	n.a.	17.64	27.79	n.a.
Sm	5.94	3.61	n.a.	n.a.	4.76	7.06	n.a.
Eu	1.90	1.35	n.a.	n.a.	1.91	1.92	n.a.
Gd	6.21	4.06	n.a.	n.a.	5.00	7.18	n.a.
Tb	1.07	0.68	n.a.	n.a.	0.74	1.12	n.a.
Dy	6.95	4.38	n.a.	n.a.	4.51	7.14	n.a.
Ho	1.27	0.88	n.a.	n.a.	0.79	1.48	n.a.
Er	3.68	2.56	n.a.	n.a.	2.35	4.60	n.a.
Tm	0.52	0.37	n.a.	n.a.	0.31	0.61	n.a.
Yb	3.38	2.44	n.a.	n.a.	1.91	3.84	n.a.
Lu	0.56	0.36	n.a.	n.a.	0.32	0.59	n.a.

Note: sample 2M1406-3 is the mafic dike cutting a charnockite.

Table B.6 continued.

Sample	Sand Bay g.a.					UGH domain
	S17065	S20066-2	S27051-A	S29055-A	2S020710-1	G18061-2
Easting	556 650	555 650	545 380	554 100	555 900	571 300
Northing	5016 300	5017 750	5019 150	5023 280	5021 830	4993 350
SiO_2	47.28	47.24	44.78	50.99	45.45	47.46
TiO_2	2.65	0.85	2.86	1.08	1.89	1.10
Al_2O_3	17.89	16.03	15.75	17.13	16.92	15.75
Fe_2O_3	13.47	12.85	16.12	11.14	14.07	11.88
MnO	0.18	0.18	0.22	0.15	0.21	0.22
MgO	4.34	7.99	6.10	4.68	8.07	7.85
CaO	9.42	9.68	7.90	8.59	8.48	9.76
Na_2O	3.98	3.21	3.13	4.16	3.36	3.67
K_2O	0.95	1.65	2.56	1.44	0.67	0.85
P_2O_5	0.44	0.10	0.48	0.35	0.27	0.17
L.O.I.	0.18	0.62	0.47	0.53	0.59	0.52
Total	100.77	100.41	100.37	100.24	99.98	99.23
Ba	<5	<5	72	157	<5	<5
Rb	17	32	65	28	16	15
Sr	342	235	303	515	342	378
Y	29	20	24	25	21	21
Zr	168	51	176	95	112	83
Nb	7	1	15	5	3	3
Th	0.74	0.27	0.93	1.92	n.a.	0.39
Ga	23	17	20	20	18	17
Zn	128	96	135	46	116	110
Ni	26	127	62	21	89	112
V	325	178	329	204	221	208
Cr	66	102	30	44	48	149
Hf	5.88	1.45	5.76	1.86	n.a.	1.86
Co	50	54	68	45	84	58
U	1	1	<1	<1	<1	<1
La	9.83	2.93	11.87	15.03	n.a.	7.37
Ce	27.10	7.47	32.37	34.24	n.a.	18.39
Pr	4.15	1.17	4.83	4.85	n.a.	2.78
Nd	20.55	5.90	23.13	21.91	n.a.	13.43
Sm	6.18	2.12	6.36	5.98	n.a.	3.50
Eu	2.19	0.82	2.20	1.66	n.a.	1.21
Gd	6.85	2.92	6.53	5.97	n.a.	3.94
Tb	1.06	0.52	0.99	0.88	n.a.	0.63
Dy	6.59	3.67	6.00	5.34	n.a.	4.10
Ho	1.31	0.71	1.18	0.91	n.a.	0.83
Er	3.91	2.32	3.52	2.74	n.a.	2.37
Tm	0.50	0.32	0.46	0.36	n.a.	0.35
Yb	3.00	2.14	2.78	2.22	n.a.	2.27
Lu	0.45	0.37	0.42	0.39	n.a.	0.34

APPENDIX C. Geochemical data, Chapter 3

Table C.1 Geochemistry of stromatic migmatites.

| | Granodioritic mesosome | | | |
| | Parkersville o/c | | | |
Sample	M03083B-M1	M03083B-M2	M03083B-M3	M03083B-M4
SiO$_2$ (wt.%)	65.25	65.03	66.62	66.11
TiO$_2$	0.60	0.61	0.65	0.61
Al$_2$O$_3$	15.45	15.42	15.67	15.64
Fe$_2$O$_3$	4.49	4.54	4.72	4.40
MnO	0.08	0.07	0.08	0.07
MgO	1.43	1.42	1.51	1.41
CaO	3.42	3.40	3.59	3.42
Na$_2$O	3.92	4.14	4.10	4.05
K$_2$O	3.87	3.63	3.90	3.65
P$_2$O$_5$	0.18	0.18	0.20	0.18
L.O.I.	0.28	0.44	0.50	0.40
Total	98.97	98.89	101.54	99.94
Ba (ppm)	957	924	890	945
Rb	104	102	100	102
Sr	387	382	418	402
Y	35	35	37	35
Zr	236	237	262	225
Nb	13	11	8	11
Th	11.11	13.33	11.11	11.09
Ga	19	17	18	17
Zn	68	70	72	69
Ni	9	8	7	10
V	85	82	90	83
Cr	<4	<4	<4	<4
Hf	7.40	6.28	7.56	5.80
Co	47	49	47	45
U	2	2	2	2
La	46.55	53.03	48.32	44.40
Ce	95.44	107.65	100.63	91.53
Pr	11.10	12.33	11.76	10.76
Nd	42.11	46.44	45.69	40.63
Sm	7.95	8.61	8.74	7.30
Eu	1.40	1.49	1.53	1.30
Gd	6.29	6.76	7.07	6.32
Tb	0.99	1.08	1.14	0.98
Dy	6.05	6.47	6.92	6.04
Ho	1.27	1.35	1.46	1.20
Er	3.79	4.01	4.33	3.55
Tm	0.57	0.59	0.65	0.54
Yb	3.84	4.02	4.38	3.63
Lu	0.58	0.60	0.66	0.52

Table C.1 continued.

| | Granodioritic mesosome | | | | |
| | Wren Lake o/c | | | | |
Sample	M2707-16B-M2	M2707-16B-M4	M2707-16B-M5	M2707-16B-M7	M2707-16B-M8
SiO_2	67.99	67.57	65.84	65.25	66.52
TiO_2	0.55	0.59	0.71.	0.71	0.70
Al_2O_3	15.12	15.33	15.01	15.54	15.14
Fe_2O_3	4.01	4.15	4.26	5.01	4.88
MnO	0.06	0.05	0.06	0.07	0.08
MgO	1.31	1.48	1.50	1.84	1.88
CaO	2.87	3.01	3.00	3.45	3.54
Na_2O	3.71	3.89	4.01	4.06	4.06
K_2O	3.96	3.84	4.25	2.97	2.70
P_2O_5	0.16	0.17	0.18	0.20	0.19
L.O.I.	0.38	0.10	0.57	0.40	0.46
Total	100.12	100.18	99.39	99.51	100.15
Ba	955	962	1231	598	721
Rb	98	99	99	88	79
Sr	330	332	389	317	338
Y	47	42	43	48	60
Zr	264	297	373	316	230
Nb	11	13	17	13	16
Th	8.84	8.62	4.62	8.39	3.99
Ga	16	18	15	21	19
Zn	60	67	66	78	80
Ni	8	<3	5	8	5
V	74	82	88	92	90
Cr	6	5	7	12	16
Hf	6.32	7.76	9.32	8.84	6.30
Co	69	54	78	65	64
U	2	2	2	2	2
La	64.94	61.27	49.41	67.32	48.20
Ce	127.51	123.14	110.54	142.31	110.88
Pr	15.08	14.46	14.27	17.43	15.02
Nd	56.66	54.16	56.97	68.09	62.65
Sm	10.76	10.09	10.65	12.51	13.56
Eu	1.40	1.35	1.41	1.50	1.43
Gd	8.57	7.86	8.18	9.68	11.28
Tb	1.31	1.19	1.35	1.57	1.91
Dy	8.14	7.26	8.18	9.56	11.73
Ho	1.53	1.36	1.61	1.86	2.31
Er	4.57	4.00	4.76	5.42	6.80
Tm	0.68	0.59	0.72	0.80	1.01
Yb	4.46	3.84	4.80	5.16	6.49
Lu	0.65	0.57	0.67	0.72	0.89

Table C.1 continued.

| | Concordant leucosome | | | | | |
| | Parkersville o/c | | | | | |
Sample	M03083B-L1	M03083B-L2	M03083B-L3	M03083B-L4	2M02061-9A	2M02061-9B
SiO_2	72.60	71.72	71.92	70.19	72.95	69.85
TiO_2	0.15	0.24	0.15	0.22	0.15	0.31
Al_2O_3	14.12	14.42	13.81	14.14	14.03	15.76
Fe_2O_3	1.14	1.86	1.22	1.61	1.31	1.94
MnO	0.01	0.03	0.01	0.02	0.02	0.04
MgO	0.20	0.46	0.19	0.38	0.22	0.54
CaO	1.58	2.08	1.53	2.02	1.81	2.09
Na_2O	2.89	3.29	3.02	3.41	3.24	3.23
K_2O	6.57	5.68	6.98	6.44	5.83	6.53
P_2O_5	0.03	0.05	0.03	0.05	0.03	0.08
L.O.I.	0.37	0.28	0.47	0.47	0.19	0.30
Total	99.67	100.11	99.33	98.95	99.59	100.36
Ba	1631	1411	1763	1741	2069	2741
Rb	153	132	158	142	136	152
Sr	448	437	459	454	479	531
Y	13	21	14	19	12	20
Zr	133	141	129	146	129	263
Nb	2	3	2	9	1	4
Th	13.12	9.91	12.24	11.48	10.21	9.91
Ga	14	14	15	15	15	18
Zn	19	30	21	29	20	31
Ni	11	19	18	7	14	<3
V	29	39	28	37	32	45
Cr	<4	<4	<4	<4	<4	<4
Hf	3.08	3.20	3.15	4.47	2.99	5.31
Co	77	73	83	72	92	46
U	3	2	2	2	4	4
La	24.10	22.46	21.89	31.05	22.03	28.51
Ce	46.57	45.53	42.92	60.60	42.49	53.52
Pr	4.90	5.13	4.62	6.61	4.63	5.96
Nd	16.07	17.70	15.22	23.59	15.84	21.98
Sm	2.44	3.33	2.46	3.82	2.25	3.59
Eu	0.80	0.84	0.80	1.08	0.83	1.37
Gd	1.75	2.76	1.88	2.79	1.71	3.06
Tb	0.25	0.42	0.28	0.44	0.24	0.44
Dy	1.49	2.71	1.66	2.63	1.44	2.73
Ho	0.26	0.49	0.29	0.55	0.28	0.54
Er	0.83	1.55	0.94	1.70	0.85	1.63
Tm	0.12	0.22	0.13	0.26	0.13	0.25
Yb	0.80	1.50	0.91	1.81	0.87	1.73
Lu	0.13	0.24	0.15	0.27	0.13	0.27
$Zr_{satT}(°C)$	761	761	751	754	774	778

Table C.1 continued.

	Concordant leucosome					
	Wren Lake o/c					
Sample	M2707-16-L1	M2707-16B-L1	M2707-16B-L3	M2707-16B-L4	M2707-16B-L5	2M0506-15
SiO_2	73.57	72.85	70.50	71.53	70.54	70.43
TiO_2	0.17	0.14	0.29	0.22	0.25	0.21
Al_2O_3	14.44	14.13	14.75	14.44	14.47	14.29
Fe_2O_3	1.33	0.91	2.00	1.73	1.62	1.36
MnO	0.01	0.01	0.03	0.02	0.02	0.02
MgO	0.23	0.21	0.59	0.33	0.37	0.51
CaO	1.08	1.27	1.89	1.62	1.72	1.43
Na_2O	2.52	2.64	2.99	2.97	3.20	2.59
K_2O	7.57	6.76	6.66	7.01	6.81	6.95
P_2O_5	0.04	0.04	0.07	0.05	0.07	0.05
L.O.I.	0.38	0.27	0.21	0.29	0.10	0.89
Total	101.34	99.22	99.98	100.21	99.16	97.84
Ba	1609	1565	1777	1689	1777	1771
Rb	157	139	124	129	128	138
Sr	383	408	442	416	450	460
Y	17	19	28	25	21	12
Zr	159	153	212	202	216	131
Nb	2	2	11	11	10	3
Th	11.58	13.84	6.66	14.59	10.55	6.09
Ga	13	13	14	15	16	14
Zn	21	14	30	26	26	24
Ni	5	5	<3	<3	<3	<3
V	29	26	43	36	41	36
Cr	<4	<4	<4	<4	<4	<4
Hf	3.68	4.35	6.02	4.74	6.03	3.00
Co	75	77	64	97	75	58
U	3	2	2	2	2	3
La	40.00	42.97	31.08	42.74	29.45	28.64
Ce	83.64	90.19	66.30	91.83	58.71	48.16
Pr	9.67	10.39	8.29	10.80	6.82	4.89
Nd	34.34	35.96	32.42	38.76	24.90	16.21
Sm	4.67	5.20	6.24	6.23	4.29	2.77
Eu	1.19	1.30	1.43	1.30	1.23	1.02
Gd	3.14	3.40	5.16	4.56	3.32	1.93
Tb	0.42	0.46	0.77	0.65	0.49	0.29
Dy	2.37	2.62	4.73	3.87	2.93	1.61
Ho	0.45	0.49	0.91	0.74	0.55	0.27
Er	1.26	1.44	2.66	2.12	1.62	0.72
Tm	0.18	0.21	0.40	0.31	0.24	0.10
Yb	1.21	1.42	2.64	2.00	1.62	0.65
Lu	0.18	0.20	0.38	·0.28	0.25	0.11
$Zr_{satT}(°C)$	781	779	795	791	794	

Table C.2 Geochemistry of patchy migmatites.

| | Dioritic mesosome | | | | |
| | Wren Lake o/c | | | | |
Sample	M2707-10-M1	M2707-10-M2	2M0506-10	2M0506-11	2M1506-2M
SiO_2	48.24	47.98	54.24	51.14	52.08
TiO_2	1.60	1.69	0.93	1.29	1.16
Al_2O_3	17.47	17.69	16.39	18.38	16.61
Fe_2O_3	12.60	12.88	8.50	10.00	10.37
MnO	0.20	0.20	0.14	0.15	0.18
MgO	4.52	4.50	4.88	3.83	4.54
CaO	8.05	8.11	7.80	7.56	8.17
Na_2O	3.95	4.01	3.92	4.17	3.93
K_2O	2.02	1.94	2.14	2.40	1.94
P_2O_5	0.49	0.51	0.28	0.38	0.34
L.O.I.	0.40	0.54	0.79	0.50	0.50
Total	99.54	100.05	106.86	108.30	108.65
Ba	854	771	613	925	710
Rb	54	123	46	72	32
Sr	537	567	603	854	562
Y	37	37	38	33	43
Zr	324	383	200	530	275
Nb	12	12	9	7	11
Th	2.91	2.81	3.22	n.a.	n.a.
Ga	23	24	21	23	22
Zn	138	138	118	115	133
Ni	9	7	34	13	7
V	250	248	151	191	191
Cr	7	<4	115	30	35
Hf	8.53	8.72	4.66	n.a.	n.a.
Co	36	54	57	47	61
U	<1	2	<1	<1	1
La	41.32	38.71	35.26	n.a.	n.a.
Ce	95.09	89.35	80.66	n.a.	n.a.
Pr	12.72	11.99	10.76	n.a.	n.a.
Nd	54.72	50.50	44.50	n.a.	n.a.
Sm	10.90	9.99	9.00	n.a.	n.a.
Eu	2.80	2.51	1.71	n.a.	n.a.
Gd	10.48	9.57	8.15	n.a.	n.a.
Tb	1.59	1.46	1.27	n.a.	n.a.
Dy	9.67	8.94	7.91	n.a.	n.a.
Ho	1.91	1.76	1.45	n.a.	n.a.
Er	5.46	5.08	4.32	n.a.	n.a.
Tm	0.78	0.74	0.65	n.a.	n.a.
Yb	5.11	4.76	4.33	n.a.	n.a.
Lu	0.72	0.69	0.64	n.a.	n.a.

Table C.2 continued.

Sample	Dioritic mesosome			Patchy leucosome		
	Bonnie Lake o/c			Wren Lake o/c		
	M30072-1-M	M30072-3-M1	M30072-3-M2	M2707-5-L1	M2707-5-L2	M2707-5B-L
SiO$_2$	51.72	52.30	47.65	73.77	70.26	68.15
TiO$_2$	1.24	1.01	1.65	0.16	0.22	0.38
Al$_2$O$_3$	16.60	17.26	17.32	13.16	14.04	13.60
Fe$_2$O$_3$	11.27	9.61	12.27	1.63	1.99	3.28
MnO	0.25	0.17	0.18	0.02	0.03	0.05
MgO	4.75	5.24	6.44	0.66	0.87	1.32
CaO	7.42	8.47	7.82	1.56	1.64	2.16
Na$_2$O	3.57	3.79	3.25	2.09	1.96	2.06
K$_2$O	1.83	1.56	2.84	6.99	8.14	6.93
P$_2$O$_5$	0.19	0.20	0.32	0.05	0.07	0.09
L.O.I.	0.54	0.38	0.52	0.72	1.18	0.88
Total	99.38	99.98	100.26	100.81	100.40	98.90
Ba	300	200	508	2087	2396	2399
Rb	55	31	90	249	281	225
Sr	488	531	456	609	657	612
Y	51	30	40	12	15	24
Zr	206	183	174	154	128	140
Nb	20	12	18	4	4	8
Th	1.91	2.46	2.41	1.54	49.45	3.04
Ga	26	22	24	10	9	14
Zn	171	112	150	24	31	44
Ni	4	13	37	23	16	24
V	236	186	272	33	42	66
Cr	6	30	37	8	9	26
Hf	5.73	4.63	4.54	3.11	2.17	2.82
Co	50	31	39	121	124	66
U	<1	1	1	1	4	<1
La	27.14	28.07	33.58	15.48	20.82	24.57
Ce	84.94	68.31	86.09	26.95	36.06	52.54
Pr	13.29	9.05	12.31	3.08	4.03	6.69
Nd	56.79	36.84	53.19	11.70	14.68	26.81
Sm	11.64	7.43	11.18	2.05	2.49	5.17
Eu	2.25	1.74	1.98	0.87	0.91	1.20
Gd	10.56	6.73	10.03	1.60	1.97	4.37
Tb	1.69	1.03	1.48	0.24	0.29	0.66
Dy	11.07	6.40	9.39	1.47	1.79	4.17
Ho	2.37	1.31	1.95	0.29	0.35	0.81
Er	7.32	3.88	5.89	0.85	1.06	2.38
Tm	1.15	0.60	0.89	0.13	0.16	0.36
Yb	7.94	4.20	6.06	0.95	1.14	2.48
Lu	1.14	0.65	0.92	0.15	0.18	0.37
Zr$_{satT}$(°C)				774	752	755

Table C.2 continued

Sample	Patchy leucosome		Hornblende-rich patches		
	Bonnie Lake o/c		Wren Lake o/c		
	M30072-3-L1	M30072-3-L2	2M0506-1	2M0506-2	2M0506-3
SiO_2	70.99	64.34	50.28	58.39	56.87
TiO_2	0.22	0.35	1.52	0.95	0.93
Al_2O_3	14.45	16.68	12.49	14.21	14.51
Fe_2O_3	1.83	3.39	15.05	9.77	9.81
MnO	0.02	0.05	0.24	0.15	0.13
MgO	0.97	1.76	6.27	3.76	4.24
CaO	2.37	5.24	7.05	5.14	6.09
Na_2O	2.42	3.83	2.22	3.04	3.11
K_2O	6.19	3.09	3.11	3.78	3.21
P_2O_5	0.04	0.16	0.23	0.21	0.28
L.O.I.	1.15	0.72	1.00	0.40	0.60
Total	100.66	99.61	98.46	99.40	99.17
Ba	2765	1365	533	673	818
Rb	136	64	87	129	58
Sr	649	657	292	406	416
Y	12	22	53	55	24
Zr	83	146	442	259	248
Nb	4	10	3	17	9
Th	6.57	1.44	7.36	23.34	6.11
Ga	11	17	28	25	27
Zn	22	50	190	149	163
Ni	<3	5	54	25	39
V	44	71	233	153	155
Cr	<4	<4	153	90	95
Hf	1.30	3.22	13.39	6.97	8.08
Co	91	79	71	54	56
U	2	<1	<1	4	1
La	12.77	18.74	47.81	46.55	43.00
Ce	19.67	37.65	126.61	107.42	92.04
Pr	2.15	4.73	16.93	13.65	11.37
Nd	8.08	19.13	67.09	53.34	44.11
Sm	1.38	3.77	12.88	10.33	7.64
Eu	0.76	1.04	1.93	1.39	1.50
Gd	1.15	3.30	10.94	8.80	6.32
Tb	0.17	0.50	1.84	1.50	0.81
Dy	1.09	3.11	11.30	9.35	4.51
Ho	0.23	0.65	2.02	1.70	0.94
Er	0.68	1.94	6.06	5.20	2.62
Tm	0.11	0.30	0.94	0.80	0.37
Yb	0.78	2.13	6.58	5.51	2.43
Lu	0.12	0.33	1.02	0.86	0.34
$Zr_{satT}(°C)$	721	742			

Table C.2 continued.

Sample	Hornblende-rich patches			Patchy melanosome	
	Wren Lake o/c			Wren Lake o/c	
	2M0506-3b1	2M0506-3b2	2M0506-3b3	M2707-5-M1	M2707-5-M2
SiO_2	55.31	56.56	57.14	50.47	49.33
TiO_2	0.91	0.94	0.92	1.13	1.30
Al_2O_3	15.80	14.90	14.59	16.35	16.39
Fe_2O_3	9.63	9.76	9.41	10.68	11.30
MnO	0.15	0.15	0.14	0.20	0.20
MgO	4.11	4.19	3.98	5.53	5.65
CaO	6.36	6.32	5.74	8.59	8.56
Na_2O	3.48	3.26	2.94	3.98	3.91
K_2O	3.55	3.11	3.84	1.68	1.83
P_2O_5	0.27	0.30	0.25	0.34	0.38
L.O.I.	0.20	0.48	0.70	0.50	0.57
Total	99.57	99.49	98.95	99.46	99.42
Ba	894	733	958	289	213
Rb	59	54	72	35	45
Sr	488	437	444	431	455
Y	36	33	34	50	43
Zr	236	245	237	204	245
Nb	12	12	12	21	17
Th	4.35	10.41	4.34	9.77	4.53
Ga	30	29	27	25	26
Zn	167	169	157	158	162
Ni	22	28	26	33	41
V	154	157	153	193	223
Cr	97	90	84	120	114
Hf	7.12	7.54	5.81	7.02	6.76
Co	50	55	55	35	36
U	1	2	2	1	1
La	47.41	51.69	38.89	67.44	58.90
Ce	111.03	117.43	90.43	166.64	144.71
Pr	14.02	14.44	11.37	21.98	19.23
Nd	53.49	54.82	43.78	88.10	77.52
Sm	9.70	9.88	8.14	16.89	14.45
Eu	1.80	1.83	1.51	2.61	2.41
Gd	7.28	7.36	6.19	13.61	11.40
Tb	1.11	1.13	0.96	2.04	1.68
Dy	6.55	6.57	5.68	12.52	10.17
Ho	1.31	1.29	1.13	2.42	1.96
Er	3.78	3.69	3.28	7.23	5.78
Tm	0.57	0.56	0.49	1.12	0.88
Yb	3.86	3.76	3.27	7.82	6.22
Lu	0.58	0.57	0.49	1.20	0.95

Table C.2 continued.

Sample	Patchy melanosome Wren Lake o/c			Pegmatite dikes Wren Lake o/c		
	M2707-5B-M	2M0506-12D	2M0506-14B	2M0506-17	2M0506-6	2M0506-7
SiO_2	46.43	50.40	50.44	75.21	72.74	70.23
TiO_2	1.56	1.26	1.39	0.12	0.03	0.17
Al_2O_3	14.80	17.35	16.60	14.42	14.62	14.92
Fe_2O_3	14.98	10.83	11.31	0.82	0.26	1.53
MnO	0.25	0.21	0.23	0.01	0.00	0.02
MgO	6.75	4.86	4.74	0.24	0.16	0.54
CaO	8.96	8.37	8.06	1.39	0.31	1.08
Na_2O	3.22	4.23	4.11	3.02	2.09	2.34
K_2O	1.91	1.80	1.68	5.92	9.08	8.15
P_2O_5	0.43	0.39	0.43	0.02	0.02	0.03
L.O.I.	0.87	0.70	0.20	0.30	0.55	0.91
Total	100.16	109.44	109.17	101.17	99.31	99.01
Ba	225	458	301	1653	3171	3002
Rb	42	27	21	150	235	208
Sr	370	553	535	493	647	670
Y	54	75	79	<5	<5	16
Zr	290	321	239	54	54	172
Nb	23	16	23	<1	<1	2
Th	3.84	3.78	2.50	3.96	0.86	4.38
Ga	31	26	24	16	11	16
Zn	201	161	158	16	<5	28
Ni	46	22	23	<3	11	16
V	259	190	214	27	16	35
Cr	151	73	66	<4	<4	<4
Hf	8.44	9.12	7.03	0.80	0.47	3.15
Co	57	50	55	85	101	66
U	<1	1	1	3	2	2
La	62.25	65.81	57.89	20.27	6.84	14.19
Ce	172.39	173.00	156.49	31.24	6.78	25.47
Pr	23.88	24.40	22.23	2.98	0.53	3.16
Nd	99.37	101.77	93.19	9.14	1.46	12.87
Sm	19.32	20.78	18.82	1.08	0.16	2.94
Eu	2.88	2.95	2.55	1.05	0.92	1.28
Gd	15.67	18.17	17.20	0.63	0.12	2.64
Tb	2.38	2.76	2.63	0.07	0.02	0.40
Dy	14.24	16.97	16.23	0.37	0.08	2.46
Ho	2.75	3.24	3.17	0.06	0.02	0.43
Er	8.08	9.50	9.44	0.17	0.05	1.25
Tm	1.21	1.40	1.40	0.02	0.01	0.18
Yb	8.39	9.07	9.20	0.17	0.06	1.19
Lu	1.27	1.33	1.29	0.03	0.01	0.19

Table C.2 continued.

Sample	Pegmatite dikes		Hornblende-rich margin of pegmatite dikes		
	Wren Lake o/c		Wren Lake o/c		
	2M0506-8	2M0506-12A	2M0506-12C	2M0506-14A	2M0506-12B
SiO_2	74.71	71.11	56.43	62.96	69.03
TiO_2	0.09	0.12	1.28	0.45	0.39
Al_2O_3	13.87	15.00	12.19	15.97	13.84
Fe_2O_3	0.94	1.55	11.92	4.32	3.80
MnO	0.01	0.01	0.24	0.08	0.06
MgO	0.32	0.15	4.70	1.61	1.22
CaO	1.08	0.55	5.37	2.51	1.53
Na_2O	2.34	2.09	1.77	2.53	1.95
K_2O	6.90	9.13	4.47	7.93	7.64
P_2O_5	0.02	0.02	0.31	0.17	0.08
L.O.I.	0.21	0.30	1.11	0.69	0.89
Total	100.29	99.72	98.69	98.53	99.53
Ba	2542	3252	1524	2883	2880
Rb	179	226	81	187	179
Sr	639	712	368	667	609
Y	11	<5	141	59	42
Zr	50	295	571	167	269
Nb	1	<1	33	10	5
Th	3.81	1.37	6.78	6.92	4.08
Ga	13	13	22	18	13
Zn	12	14	183	73	62
Ni	5	114	14	11	9
V	26	35	181	77	68
Cr	<4	26	16	11	4
Hf	0.32	5.91	17.84	3.81	7.14
Co	65	76	76	53	65
U	2	2	1	2	2
La	15.63	7.36	61.59	32.54	21.64
Ce	23.68	7.54	194.24	80.00	52.39
Pr	2.68	0.61	30.39	11.39	7.53
Nd	9.62	1.70	141.61	49.57	33.17
Sm	1.80	0.25	36.55	11.41	7.69
Eu	1.06	1.04	3.21	1.68	1.48
Gd	1.43	0.19	35.81	10.62	7.09
Tb	0.24	0.03	5.36	1.60	1.04
Dy	1.47	0.18	33.28	9.92	6.40
Ho	0.28	0.04	6.30	1.93	1.31
Er	0.83	0.13	18.06	5.41	3.81
Tm	0.12	0.03	2.61	0.77	0.55
Yb	0.76	0.22	16.99	4.81	3.57
Lu	0.12	0.05	2.38	0.68	0.52

Table C.3 Mineral compositional data, Muskoka migmatites.

Plagioclase in granodioritic mesosome (grain#11)

Spot	18	19	20	21	22
SiO_2	61.31	61.16	61.28	61.31	60.83
Al_2O_3	23.83	23.82	23.88	24.11	23.80
CaO	5.45	5.52	5.52	5.58	5.67
Na_2O	8.53	8.70	8.09	7.91	7.89
K_2O	0.31	0.25	0.32	0.25	0.22
Total	99.43	99.43	99.09	99.15	98.40

Plagioclase in conc. leucosome (grain#6)

Spot	66	67	68	69	70
SiO_2	61.34	60.87	60.65	61.23	60.69
Al_2O_3	24.27	23.91	23.50	23.94	23.85
CaO	5.63	5.56	5.44	5.61	5.52
Na_2O	8.09	8.23	8.27	8.14	8.01
K_2O	0.36	0.31	0.26	0.25	0.21
Total	99.69	98.88	98.12	99.16	98.28

Plagioclase at conc. melanosome/conc. mesosome transition (grain#3)

Spot	36	37	38	39	40	41
SiO_2	61.03	61.297	61.02	60.66	60.91	60.72
Al_2O_3	23.97	24.03	23.87	23.56	23.60	24.06
CaO	5.61	5.73	5.70	5.36	5.36	5.59
Na_2O	8.94	8.64	8.41	8.68	8.60	8.56
K_2O	0.26	0.25	0.36	0.30	0.34	0.36
Total	99.82	99.95	99.36	98.56	98.81	99.28

Plagioclase in dioritic mesosome

Spot	1	2	3
SiO_2	60.53	59.53	60.43
Al_2O_3	24.85	24.61	24.48
CaO	7.03	7.04	6.86
Na_2O	7.16	7.29	7.52
K_2O	0.31	0.15	0.32
Total	100.26	98.6	99.72

Plagioclase in patchy melanosome

Spot	1	2	3
SiO_2	63.32	63.47	63.91
Al_2O_3	24.15	24.04	23.62
CaO	5.90	6.21	6.16
Na_2O	8.10	8.15	8.11
K_2O	0.30	0.09	0.32
Total	102.15	102.24	102.11

Table C.3 continued.

Biotite in granodioritic mesosome (grain#8)

Spot	9	10	11	12	13
SiO_2	35.89	35.87	35.98	36.05	35.94
TiO_2	4.39	4.42	4.46	4.35	4.17
Al_2O_3	13.85	13.71	13.68	13.64	13.98
FeO_t	18.09	17.83	18.25	18.41	18.21
MnO	0.40	0.46	0.31	0.29	0.31
MgO	11.74	11.89	11.99	11.85	12.19
K_2O	9.70	9.22	9.10	9.90	9.52
Total	94.22	93.56	93.93	97.67	64.47

Biotite in concordant melanosome (grain#4a)

Spot	44	45	46	47	48
SiO_2	35.57	36.01	34.91	36.17	36.04
TiO_2	4.20	4.39	3.98	4.14	4.22
Al_2O_3	13.97	13.60	13.90	13.73	13.74
FeO_t	18.71	18.23	18.79	18.25	18.21
MnO	0.33	0.41	0.44	-	0.32
MgO	12.36	11.96	12.82	12.05	12.23
K_2O	9.40	9.78	8.34	10.02	9.92
Total	94.36	94.52	93.29	94.51	94.82

Biotite in concordant leucosome (grain#1)

Spot	60	61	62	63	64
SiO_2	36.27	36.33	36.22	35.82	35.94
TiO_2	4.74	4.69	4.82	4.79	4.71
Al_2O_3	13.69	13.84	13.67	13.72	13.62
FeO_t	18.72	18.53	18.98	18.92	18.36
MnO	0.40	0.309	0.31	0.31	0.41
MgO	11.50	11.61	11.44	11.47	11.31
K_2O	10.04	9.89	9.83	10.00	9.82
Total	95.52	95.70	95.46	95.20	94.32

Biotite in patchy melanosome

Spot	1	2
SiO_2	37.97	38.15
TiO_2	4.33	4.36
Al_2O_3	14.21	14.13
FeO_t	15.68	16.28
MnO	13.35	12.99
MgO	0.21	0.20
K_2O	0.30	0.33
Total	95.11	95.90

Table C.3 continued.

Hornblende in granodioritic mesosome (grain#10)

Spot	28	29	30	34	35
SiO_2	40.72	40.85	41.70	41.27	41.28
TiO_2	1.57	1.69	1.15	1.81	1.62
Al_2O_3	10.75	10.54	10.05	10.64	10.41
FeO_t	17.47	17.59	18.74	17.31	17.46
MnO	0.55	0.57	0.58	0.54	0.67
MgO	9.76	9.75	9.55	10.11	9.89
CaO	11.44	11.64	11.77	11.51	11.59
Na_2O	1.65	1.77	1.25	1.77	1.87
K_2O	1.58	1.55	1.29	1.61	1.57
Total	95.77	96.16	96.22	96.79	96.55

Hornblende in concordant melanosome (grain#4b)

Spot	50	51	52	53	54
SiO_2	40.93	40.72	40.64	41.03	41.01
TiO_2	1.61	1.71	1.81	1.77	1.80
Al_2O_3	10.87	10.73	10.83	10.45	10.73
FeO_t	18.03	17.82	17.56	17.24	17.30
MnO	0.38	0.68	0.48	0.68	0.47
MgO	9.45	9.46	9.91	9.88	9.77
CaO	11.63	11.51	11.74	11.47	11.59
Na_2O	1.77	1.67	1.73	1.81	1.58
K_2O	1.69	1.61	1.54	1.61	1.67
Total	96.55	96.06	96.42	96.15	96.08

Table C.3 continued.

Hornblende in dioritic mesosome

Spot	1	2	3
SiO_2	42.86	42.74	42.6
TiO_2	1.38	1.59	1.9
Al_2O_3	11.11	11.10	11.12
FeO_t	18.34	17.87	18.41
MgO	9.53	9.3	9.43
CaO	11.25	11.33	11.28
Na_2O	1.83	1.71	1.75
K_2O	1.42	1.69	1.65
Total	97.71	97.34	98.13

Hornblende in patchy melanosome

Spot	1	2	3
SiO_2	43.69	43.86	43.69
TiO_2	1.87	1.90	2.22
Al_2O_3	10.41	10.68	10.43
FeO_t	18.10	17.82	18.22
MgO	10.32	9.89	9.90
CaO	11.19	11.12	10.92
Na_2O	2.14	1.96	2.00
K_2O	1.62	1.56	1.73
Total	99.34	98.78	99.10

K-feldspar in granodioritic mesosome (grain#12)

Spot	1	2	3	4	5
SiO_2	66.08	65.10	63.41	63.65	64.03
Al_2O_3	18.98	18.62	18.15	18.28	18.40
Na_2O	1.32	1.28	1.24	1.09	1.17
K_2O	13.89	14.27	14.69	15.86	15.15
Total	100.27	99.27	97.49	98.88	98.75

APPENDIX D. Geochemical data, Chapter 4

Table D.1 Geochemistry of gray quartzofeldspathic gneiss.

	Gray quartzofeldspathic gneiss					
Sample	2S210611	2S21067	2S21068	2S24061	2S24062	S16065-3
Easting	556 100	556 330	556 280	556 280	556 500	556 480
Northing	5016 430	5016 000	5015 900	5016 000	5016 180	5023 200
SiO_2 (wt.%)	64.02	66.77	69.67	67.55	66.41	66.73
TiO_2	0.59	0.59	0.46	0.57	0.55	0.50
Al_2O_3	16.21	15.13	14.98	15.62	15.30	15.80
Fe_2O_3	4.09	4.62	2.82	3.95	3.72	3.66
MnO	0.07	0.07	0.05	0.09	0.08	0.07
MgO	2.30	2.39	1.20	2.07	2.00	1.66
CaO	3.11	1.59	1.97	2.24	2.92	3.02
Na_2O	4.92	3.89	4.53	5.06	4.77	4.50
K_2O	3.04	4.51	3.79	2.92	2.95	3.22
P_2O_5	0.20	0.18	0.13	0.18	0.18	0.17
L.O.I.	0.70	0.95	0.65	0.98	0.71	0.69
Total	98.55	99.74	99.60	100.25	98.88	99.33
Ba (ppm)	843	1035	916	813	901	806
Rb	86	148	122	93	165	108
Sr	523	252	395	405	469	469
Y	19	20	31	19	24	21
Zr	197	189	214	196	179	199
Nb	7	6	8	6	4	5
Th	7.97	10.79	13.34	6.47	6.34	9.06
Ga	20	19	20	19	19	20
Zn	79	65	50	85	85	68
Ni	22	9	10	24	46	12
V	84	82	64	77	76	73
Cr	34	21	10	34	30	15
Hf	4.76	4.50	6.01	4.72	4.30	4.75
Co	54	58	50	44	50	61
U	2	4	4	3	2	3
La	29.68	31.74	38.76	28.06	27.05	27.63
Ce	57.69	61.49	77.14	55.64	52.37	53.06
Pr	6.87	7.59	9.29	6.63	6.16	6.04
Nd	26.15	28.41	34.68	25.11	23.32	22.11
Sm	4.33	4.69	5.84	4.35	4.18	3.91
Eu	0.99	0.85	1.06	0.81	1.01	0.90
Gd	3.38	3.63	4.70	3.63	3.41	3.17
Tb	0.44	0.48	0.65	0.49	0.44	0.47
Dy	2.54	2.69	3.90	2.84	2.51	2.81
Ho	0.56	0.58	0.87	0.64	0.51	0.55
Er	1.61	1.64	2.65	1.83	1.46	1.66
Tm	0.24	0.25	0.41	0.28	0.22	0.26
Yb	1.63	1.71	2.86	1.92	1.47	1.81
Lu	0.23	0.25	0.41	0.29	0.22	0.29

Table D.2 Geochemistry of hornblende-rich leucosome.

Sample	Hornblende-rich leucosome						
	2S04071	2S2006-3	2S26062	2S26063	2S26064	S16065-2	S20066-1
Easting	557 950	557 880	557 630	556 080	556 080	556 480	555 650
Northing	5023 230	5022 280	5021 450	5017 100	5017 100	5023 200	5017 750
SiO_2	61.40	69.53	69.24	61.07	61.83	60.57	59.48
TiO_2	0.76	0.29	0.31	0.73	0.28	0.68	0.85
Al_2O_3	15.23	15.38	15.48	16.94	13.09	16.45	16.71
Fe_2O_3	6.93	2.94	2.32	6.47	7.70	5.58	6.36
MnO	0.12	0.07	0.06	0.13	0.18	0.14	0.15
MgO	2.42	0.87	0.60	2.19	3.94	2.23	2.96
CaO	5.38	2.69	2.45	4.56	5.06	4.47	6.17
Na_2O	4.14	3.33	3.75	4.40	3.13	3.90	5.20
K_2O	2.23	5.80	5.51	4.76	3.17	4.94	1.39
P_2O_5	0.16	0.10	0.11	0.15	0.03	0.24	0.21
L.O.I.	0.50	0.39	0.20	0.40	0.50	0.40	0.60
Total	98.77	101.00	99.83	101.40	98.42	99.19	99.48
Ba	660	1308	926	724	569	1151	104
Rb	34	142	135	83	57	90	22
Sr	350	304	241	247	177	419	270
Y	21	62	76	77	44	125	141
Zr	99	93	156	189	37	226	220
Nb	7	19	22	25	11	47	59
Th	1.06	1.72	4.13	2.50	0.15	8.99	2.48
Ga	18	20	20	26	25	26	29
Zn	70	57	58	67	109	107	100
Ni	18	5	<3	15	94	15	24
V	119	49	45	106	70	93	116
Cr	8	9	<4	22	308	21	39
Hf	2.37	3.38	4.43	4.52	1.86	6.33	7.80
Co	65	57	77	51	69	51	56
U	3	4	5	5	3	4	4
La	7.53	5.54	13.94	10.71	1.53	27.02	9.29
Ce	17.63	12.86	30.21	32.29	4.78	58.45	28.70
Pr	2.51	1.85	4.14	5.62	0.94	7.66	5.42
Nd	11.89	9.10	18.66	28.62	5.42	32.82	30.07
Sm	3.08	3.75	6.88	8.76	2.35	10.32	11.97
Eu	0.98	0.86	1.40	1.91	0.69	2.00	2.42
Gd	3.46	6.25	9.90	10.42	3.73	15.39	17.51
Tb	0.51	1.30	1.80	1.83	0.73	3.36	3.73
Dy	3.26	9.54	12.44	12.59	5.40	23.75	26.15
Ho	0.65	1.93	2.07	2.68	1.23	4.47	5.27
Er	1.91	5.65	5.80	8.57	4.20	12.79	15.87
Tm	0.29	0.82	0.79	1.39	0.72	1.79	2.31
Yb	2.08	5.12	4.76	9.93	5.48	10.75	14.47
Lu	0.33	0.67	0.74	1.59	0.99	1.36	1.87

Table D.3 Geochemistry of hornblende-rich diatexite and granitic patches on Beatty Island.

	Hornblende-rich diatexite					Granitic patches	
Sample	2S19061	2S1906-4	2S2006-1	2S25063	2S25065-3	S0306-P2	S0306-P3
Easting	559 500	559 500	557 850	557 480	559 500	557 850	557 850
Northing	5023 450	5023 450	5020 080	5023 200	5023 450	5020 080	5020 080
SiO_2	71.20	57.24	70.32	68.29	65.26	70.59	72.43
TiO_2	0.42	0.71	0.37	0.38	0.69	0.10	0.28
Al_2O_3	14.24	20.11	15.07	15.27	15.66	16.04	13.93
Fe_2O_3	3.73	6.56	2.86	3.53	5.42	1.00	2.90
MnO	0.05	0.12	0.06	0.09	0.11	0.02	0.04
MgO	0.53	1.63	0.91	1.02	1.71	0.32	0.45
CaO	1.49	5.97	2.21	2.96	3.50	1.84	1.71
Na_2O	3.52	4.75	3.93	3.69	4.45	4.11	3.68
K_2O	5.28	2.00	4.23	4.61	3.59	5.32	4.51
P_2O_5	0.10	0.20	0.10	0.12	0.21	0.04	0.06
L.O.I.	0.30	0.40	0.36	0.20	0.30	0.46	0.41
Total	100.55	99.29	100.06	99.96	100.60	99.39	99.99
Ba	1088	1075	741	599	394	978	912
Rb	118	145	149	128	129	151	131
Sr	135	493	230	208	223	262	225
Y	44	28	54	85	60	19	75
Zr	368	368	183	190	254	69	359
Nb	11	16	20	29	20	5	22
Th	5.97	5.75	8.04	11.22	12.36	1.96	12.03
Ga	18	25	21	23	26	21	19
Zn	62	152	75	76	114	28	55
Ni	33	9	5	7	16	5	11
V	51	102	50	56	89	25	47
Cr	<4	15	5	6	18	<4	<4
Hf	3.77	4.22	4.13	5.85	6.67	1.21	10.49
Co	63	56	67	61	54	71	95
U	5	5	5	6	4	4	5
La	17.31	14.33	26.60	26.49	33.29	5.73	37.99
Ce	36.55	29.63	55.32	55.15	68.15	11.75	81.02
Pr	4.67	3.73	6.80	7.03	8.39	1.47	10.48
Nd	19.42	15.25	26.25	29.04	33.55	5.88	42.29
Sm	5.64	3.90	5.64	7.83	8.53	1.46	9.41
Eu	1.18	0.83	0.96	1.46	1.72	0.37	1.42
Gd	5.52	3.49	6.01	9.91	9.76	1.74	9.27
Tb	0.98	0.63	0.99	2.11	1.59	0.31	1.72
Dy	6.46	4.15	6.74	14.48	10.27	2.20	11.20
Ho	1.17	0.79	1.46	2.66	1.69	0.48	2.21
Er	3.54	2.43	4.39	7.69	5.05	1.50	6.31
Tm	0.55	0.38	0.65	1.09	0.75	0.22	0.88
Yb	3.81	2.74	4.20	6.71	5.08	1.41	5.41
Lu	0.70	0.48	0.57	0.91	0.87	0.20	0.70

Table D.4 Geochemistry of granite, pegmatite, and Woodall Island pegmatite dikes.

	Granite							
Sample	S02062	S02064	S050615	S05069	S06068	S08067	S13066	S02065-2
Easting	559 900	559 000	557 950	557 750	559 430	558 550	558 630	558 730
Northing	5024 100	5023 430	5022 000	5022 300	5023 300	5025 900	5022 130	5022 950
SiO_2	73.95	74.21	77.83	78.86	73.25	76.98	74.39	72.60
TiO_2	0.12	0.28	0.08	0.08	0.15	0.22	0.10	0.13
Al_2O_3	14.20	13.86	12.65	12.23	13.80	12.03	14.18	14.59
Fe_2O_3	1.18	2.00	1.41	1.12	1.66	1.35	0.77	0.90
MnO	0.01	0.02	0.01	0.00	0.01	0.03	0.01	0.01
MgO	0.12	0.27	0.04	0.05	0.13	0.22	0.24	0.26
CaO	1.08	1.41	1.09	0.91	1.05	0.53	0.88	0.84
Na_2O	3.42	3.59	2.92	2.61	3.29	3.47	3.31	2.91
K_2O	5.57	4.20	4.97	5.41	5.27	4.62	6.34	7.61
P_2O_5	0.03	0.05	0.01	0.01	0.03	0.04	0.02	0.02
L.O.I.	0.14	0.31	0.19	0.09	0.27	0.38	0.36	0.36
Total	99.82	100.20	101.19	101.37	98.91	99.87	100.60	100.22
Ba	562	689	732	791	714	400	1111	1193
Rb	197	154	150	157	165	214	201	203
Sr	172	187	186	186	189	53	211	214
Y	11	20	17	24	22	59	6	11
Zr	50	217	177	161	90	193	44	19
Nb	6	12	2	2	7	29	6	8
Th	6.68	11.76	13.27	12.72	13.73	16.46	2.47	n.a.
Ga	17	19	16	15	16	20	17	14
Zn	27	33	17	12	24	33	23	23
Ni	3	<3	5	<3	9	<3	213	<3
V	17	33	20	21	27	31	19	21
Cr	4	<4	11	11	<4	5	<4	<4
Hf	2.21	9.43	6.76	5.14	1.78	6.24	1.86	n.a.
Co	45	46	<5	<5	<5	<5	40	103
U	3	5	4	3	4	5	2	3
La	6.13	24.73	10.13	15.58	13.16	51.02	2.97	n.a.
Ce	13.41	52.20	30.13	37.61	29.12	82.25	6.53	n.a.
Pr	1.76	6.68	3.01	4.93	3.91	8.10	0.81	n.a.
Nd	7.26	26.57	11.91	19.75	15.99	25.69	3.27	n.a.
Sm	2.30	6.40	3.39	5.83	5.18	6.10	0.97	n.a.
Eu	0.54	1.18	0.39	0.55	0.90	0.55	0.28	n.a.
Gd	2.26	5.88	3.01	5.00	4.70	6.04	0.82	n.a.
Tb	0.37	0.95	0.49	0.77	0.69	1.15	0.14	n.a.
Dy	2.22	5.93	2.78	4.39	3.91	8.27	0.87	n.a.
Ho	0.43	1.17	0.44	0.66	0.59	1.58	0.18	n.a.
Er	1.27	3.70	1.22	1.77	1.60	5.42	0.55	n.a.
Tm	0.17	0.52	0.16	0.21	0.19	0.83	0.08	n.a.
Yb	1.02	3.34	0.92	1.22	1.09	5.86	0.48	n.a.
Lu	0.14	0.49	0.15	0.19	0.16	1.08	0.07	n.a.

Table D.4 continued.

Sample	Granite					
	2S19063	2S25065-2	2S25065-5	2S25065-5B	2S25065-7	2S25065-8
Easting	559 500	559 500	559 500	559 500	559 500	559 500
Northing	5023 450	5023 450	5023 450	5023 450	5023 450	5023 450
SiO_2	75.40	76.77	74.61	75.19	75.47	64.39
TiO_2	0.07	0.08	0.13	0.14	0.14	1.28
Al_2O_3	14.26	13.58	14.70	14.16	13.69	14.27
Fe_2O_3	0.47	0.58	1.03	1.21	1.49	7.02
MnO	0.01	0.01	0.01	0.01	0.01	0.13
MgO	0.16	0.16	0.16	0.20	0.27	1.57
CaO	1.08	1.09	1.29	1.25	1.03	4.09
Na_2O	3.32	3.12	3.65	3.43	3.20	3.23
K_2O	6.00	5.89	5.61	5.45	5.60	4.19
P_2O_5	0.02	0.02	0.02	0.02	0.03	0.55
L.O.I.	0.30	0.20	0.20	0.10	0.50	0.37
Total	100.78	101.31	101.21	101.06	100.93	100.72
Ba	825	842	673	701	743	2246
Rb	187	173	178	189	179	180
Sr	220	213	217	213	196	441
Y	6	13	16	18	9	14
Zr	137	39	55	104	31	630
Nb	<1	<1	4	4	3	21
Th	0.28	2.14	3.07	n.a.	n.a.	5.25
Ga	16	15	18	17	15	21
Zn	17	16	24	17	22	126
Ni	15	<3	26	11	<3	3
V	19	21	23	24	26.00	143
Cr	<4	<4	<4	10	<4	8
Hf	5.03	1.19	1.42	n.a.	n.a.	1.46
Co	76	95	53	60	97	113
U	8	5	7	6	5	5
La	0.64	7.99	3.82	n.a.	n.a.	5.58
Ce	1.37	15.56	8.55	n.a.	n.a.	12.33
Pr	0.19	1.91	1.18	n.a.	n.a.	1.67
Nd	0.85	7.60	5.28	n.a.	n.a.	7.15
Sm	0.33	1.84	1.67	n.a.	n.a.	2.32
Eu	0.21	0.41	0.40	n.a.	n.a.	0.54
Gd	0.39	1.59	1.87	n.a.	n.a.	2.12
Tb	0.08	0.26	0.35	n.a.	n.a.	0.36
Dy	0.53	1.63	2.21	n.a.	n.a.	2.10
Ho	0.12	0.30	0.39	n.a.	n.a.	0.35
Er	0.42	0.87	1.10	n.a.	n.a.	0.91
Tm	0.08	0.13	0.16	n.a.	n.a.	0.12
Yb	0.59	0.82	1.02	n.a.	n.a.	0.74
Lu	0.13	0.14	0.14	n.a.	n.a.	0.11

Table D.4 continued.

Sample	Granite		Pegmatite				
	2S29062	2S29063	S04061-d2	S080610	S19068	2S02072	S13064
Easting	559 200	558 000	557 850	556 630	556 330	556 900	557 400
Northing	5025 330	5023 300	5020 080	5023 950	5017 880	5018 700	5022 130
SiO_2	73.96	70.84	74.02	72.31	73.30	71.44	74.45
TiO_2	0.07	0.31	0.23	0.12	0.11	0.16	0.09
Al_2O_3	14.92	14.67	13.06	14.34	15.30	16.21	14.49
Fe_2O_3	0.68	2.16	2.44	1.44	0.72	0.86	0.84
MnO	0.01	0.03	0.02	0.01	0.00	0.01	0.01
MgO	0.13	0.65	0.41	0.22	0.20	0.29	0.18
CaO	0.94	1.03	1.15	1.51	1.12	1.87	1.44
Na_2O	4.98	3.23	2.91	3.68	3.46	4.29	3.64
K_2O	4.27	5.84	5.16	5.14	6.36	4.74	4.95
P_2O_5	0.02	0.08	0.03	0.03	0.03	0.05	0.01
L.O.I.	0.20	0.39	0.34	0.17	0.54	0.40	0.28
Total	99.98	98.84	99.78	98.97	101.14	99.92	100.38
Ba	459	876	907	856	1321	902	750
Rb	163	190	174	143	184	146	155
Sr	134	200	191	199	272	301	192
Y	19	16	20	15	14	23	6
Zr	37	211	83	60	40	69	24
Nb	5	14	12	7	6	6	<1
Th	3.29	8.65	3.70	3.67	7.56	5.88	1.09
Ga	20	21	15	18	15	20	17
Zn	16	48	47	24	18	21	20
Ni	10	4	<3	<3	<3	4	9
V	18	42	37	25	21	29	16
Cr	7	<4	<4	<4	<4	<4	<4
Hf	1.06	5.91	2.13	1.19	0.70	1.50	0.38
Co	69	65	95	88	72	52	103
U	6	5	3	3	3	4	3
La	5.13	17.32	6.49	5.08	11.28	9.27	1.69
Ce	9.42	44.33	14.10	11.20	24.37	19.75	3.57
Pr	1.34	4.43	1.84	1.30	3.10	2.61	0.51
Nd	5.54	16.96	7.56	4.91	12.12	10.87	2.09
Sm	1.72	3.29	2.47	1.45	3.17	2.92	0.70
Eu	0.33	0.53	0.55	0.34	0.67	0.64	0.26
Gd	1.79	2.65	2.79	1.60	2.58	3.01	0.62
Tb	0.33	0.42	0.52	0.31	0.35	0.51	0.07
Dy	2.13	2.42	3.39	2.06	1.88	3.33	0.35
Ho	0.39	0.41	0.58	0.36	0.28	0.67	0.05
Er	1.10	1.19	1.71	1.08	0.74	1.90	0.09
Tm	0.17	0.18	0.22	0.14	0.08	0.27	0.01
Yb	1.08	1.26	1.21	0.82	0.47	1.70	0.06
Lu	0.18	0.18	0.18	0.12	0.07	0.21	0.01

Table D.4 continued.

Sample	Pegmatite				Woodall Island pegmatite dikes			
	S16066	S19062	S27051-d	S29055-d	2S21069-A	2S21069-B	S25062	2S210610
Easting	556 600	555 830	545 380	554 100	556 250	556 250	556 250	556 350
Northing	5023 200	5017 380	5019 150	5023 280	5015 100	5015 100	5015 100	5016 000
SiO_2	73.47	72.49	72.01	74.35	74.60	75.86	73.34	73.48
TiO_2	0.08	0.11	0.12	0.06	0.07	0.03	0.03	0.03
Al_2O_3	14.15	14.97	15.19	15.12	14.69	13.13	15.49	14.88
Fe_2O_3	1.50	0.96	0.86	0.58	0.75	0.37	0.22	0.27
MnO	0.01	0.01	0.01	0.00	0.01	<0.001	<0.001	<0.001
MgO	0.14	0.29	0.26	0.27	0.08	0.01	0.02	0.02
CaO	0.84	0.91	1.39	2.71	0.67	0.22	0.51	0.51
Na_2O	2.82	3.13	3.65	5.67	5.26	3.22	4.75	3.32
K_2O	7.12	7.19	6.29	1.04	4.34	6.69	6.43	7.82
P_2O_5	0.02	0.02	0.02	0.02	0.02	0.01	0.02	0.02
L.O.I.	0.23	0.39	0.31	0.58	0.09	0.19	0.00	0.00
Total	100.38	100.47	100.11	100.40	100.48	99.54	100.80	100.35
Ba	916	1703	1586	325	211	371	340	351
Rb	180	196	167	28	236	329	341	366
Sr	162	354	290	299	53	79	85	98
Y	8	9	7	10	76	49	52	40
Zr	57	54	41	32	22	13	38	7
Nb	4	5	9	5	118	47	94	36
Th	2.17	0.87	3.41	0.33	21.19	9.75	14.34	35.53
Ga	17	15	15	17	63	44	54	46
Zn	25	21	19	8	12	7	<5.	5
Ni	<3	4	<3	<3	7	18	5	9
V	21	27	23	19	18	16	14	16
Cr	<4	<4	<4	<4	<4	<4	<4	<4
Hf	1.51	0.76	0.63	0.63	1.75	0.90	4.24	0.27
Co	68	92	95	114	73	59	69	61
U	4	2	2	4	11	8	13	7
La	3.65	3.83	7.25	0.75	10.26	3.39	2.25	25.22
Ce	8.33	7.42	15.33	1.78	22.50	7.11	5.61	54.53
Pr	1.03	0.91	1.88	0.25	2.99	0.97	0.88	6.92
Nd	3.82	3.57	7.17	1.08	11.96	4.24	4.16	24.76
Sm	1.20	0.93	1.62	0.35	4.84	2.07	2.70	5.72
Eu	0.38	0.32	0.46	0.13	0.26	0.21	0.25	0.33
Gd	0.96	0.89	1.10	0.41	5.91	3.32	3.74	4.45
Tb	0.13	0.13	0.12	0.07	1.43	0.85	1.02	0.78
Dy	0.71	0.73	0.55	0.51	11.12	6.79	8.33	5.07
Ho	0.11	0.12	0.07	0.10	2.38	1.47	1.79	1.01
Er	0.31	0.35	0.17	0.38	9.43	5.64	7.02	3.62
Tm	0.04	0.04	0.02	0.06	2.20	1.28	1.67	0.75
Yb	0.29	0.25	0.11	0.46	21.23	11.91	16.47	6.50
Lu	0.06	0.04	0.02	0.10	3.60	1.83	2.74	1.04

APPENDIX E. Geochronological data, Chapter 5

E.1. Introduction

U-Pb zircon dating of rocks described in Chapters 2-5 involved two different methods: 1) Sensitive High Resolution Ion Microprobe (SHRIMP), and 2) Isotope Dilution Thermal Ionization Mass Spectrometry (ID-TIMS). The first part of this appendix briefly outlines the principles behind U-Pb dating, similar for both methods, whereas the second part describes the analytical and sample preparation techniques.

E.2. Principles behind U-Pb dating

The principles behind U-Pb dating are discussed in most geochemical textbooks (e.g., Faure, 1986; Bowen, 1988). The method is based on the radioactive decay of ^{238}U and ^{235}U to ^{206}Pb and ^{207}Pb, respectively, involving a number of intermediate reactions. The decay of ^{238}U to ^{206}Pb and ^{235}U to ^{207}Pb thus gives rise to two independent geochronometers. The decay-rates of these reactions can then be used to plot a curve in a $^{206}Pb/^{238}U$ vs. $^{207}Pb/^{235}U$ diagram; Wetherill (1956) called this curve the 'concordia'. At the time of formation, a uranium-bearing mineral with no initial radiogenic lead plots in the origin of such a diagram and with time, if the system remains closed, moves along the concordia (Fig. E.1a). After 1.5 billion years, the $^{206}Pb/^{238}U$ and $^{207}Pb/^{235}U$ ratios define a point on the concordia called a 'concordant age', in this example corresponding to an age of 1.5 Ga. At 1.5 Ga, the rock in which the zircon is hosted undergoes high-grade metamorphism and the zircons loose variable amounts of Pb, resulting in variable degree of resetting of the internal, radioactive 'clock' in the zircon. This is shown with varying degree of fill in Fig. E.1a; some zircons (black circles) remained closed during metamorphism, whereas others (white circles) lost all their Pb (complete resetting) or represent growth of new zircon during the metamorphic event. After the metamorphic event, the zircons again become closed with respect to diffusion of Pb and U, and evolves either along the concordia (non-reset and completely reset zircons) or along paths parallel to the concordia (partially reset zircons) (Fig. E.1b). If the analyzed zircons came from

an orthogneiss, a likely interpretation could be that the protolith to the orthogneiss crystallized at ca. 2 Ga, corresponding to *C*, and underwent high-grade metamorphism and deformation at ca. 500 Ma, corresponding to *M*.

a)

2) U decays to Pb; after 1.5 billion years, the Pb/U ratio in the zircon plots here

Concordia

2Ga

1 Ga

Discordia

3) **Metamorphism.** Zircon undergoes varaible Pb-loss, indicated by varying degree of fill

$^{206}Pb/^{238}U$

$^{207}Pb/^{235}U$

1) Zircon forms = 0 years

b)

Concordia

C

2Ga

1 Ga

M

4) U decays to Pb, similar to 2)

$^{206}Pb/^{238}U$

$^{207}Pb/^{235}U$
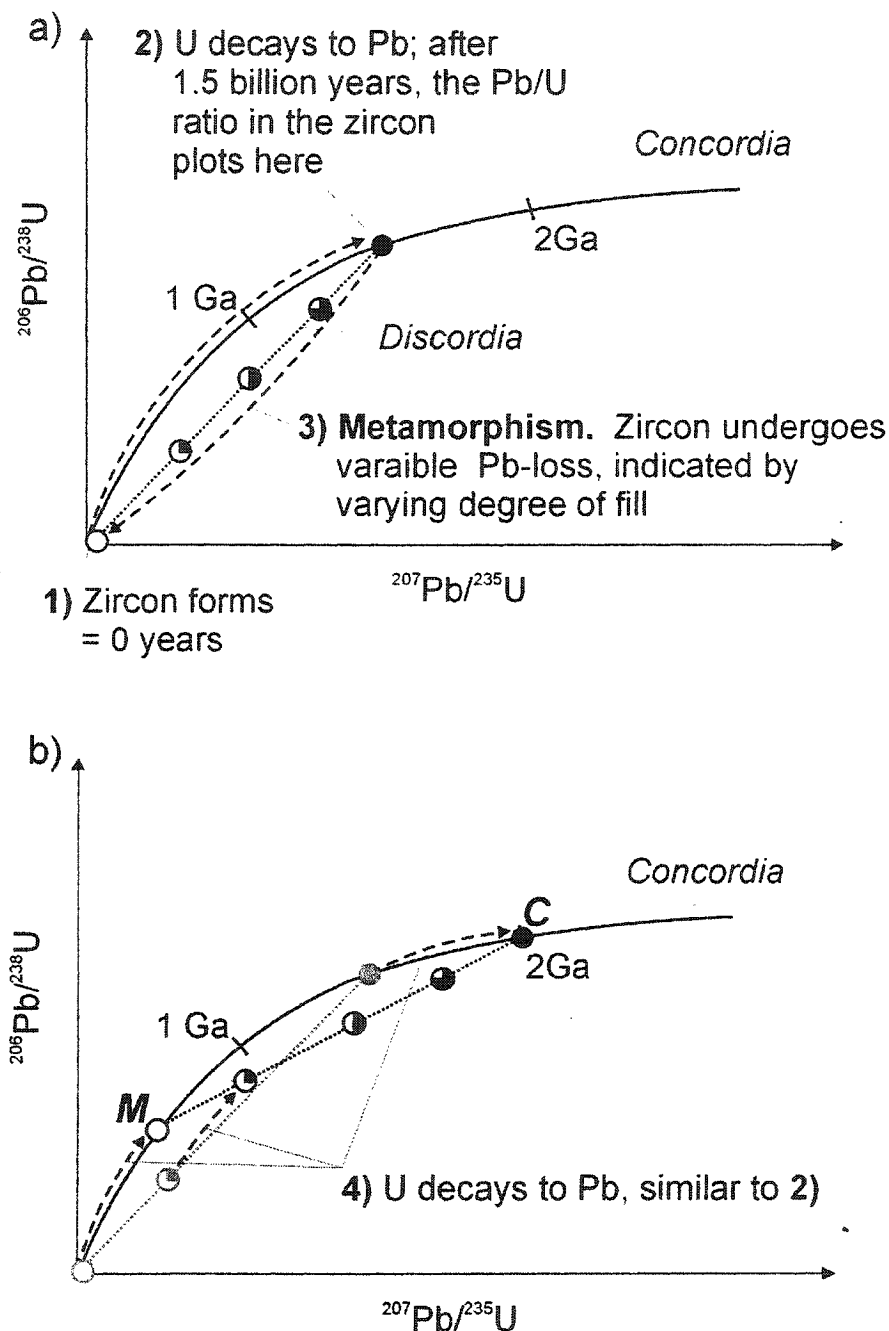
Fig. E.1 Principle behind the concordia diagram.

E.3. Sensitive High Resolution Ion Microprobe (SHRIMP)

E.3.1. Sample preparation

SHRIMP-analysis can be performed directly on polished thin-sections or the actual rock-slabs. More commonly, however, large rock specimens, weighing up to several 10s of kilos, are crushed and zircons extracted using heavy liquid separation, magnetic separation, and hand-picking, similar to that for ID-TIMS, discussed below. The selected grains are then mounted, together with zircon standards of known age, in epoxy and polished to reveal the central portions of the zircons. This was the procedure followed for the SHRIMP dating presented in this thesis. Following polishing, the mount is washed with soap by hand, rinsed with deionized water, air blown to remove water droplets, and allowed to dry under a heat lamp. The mount is then covered with 4 nm high purity gold to allow cathodoluminescence and back-scattered electron imaging. It is then repolished and cleaned to remove the Au, and recoated with 7 nm Au. The sample is then held under high vacuum for a minimum of 24 hours prior to analysis.

E.3.2. Analytical procedure

The SHRIMP II at the GSC in Ottawa was installed in 1995 in the J. C. Roddick Ion Microprobe Laboratory. A thorough discussion of the analytical techniques of U-Pb dating has been given by Stern (1997) and is briefly summarized here. Fig. E.2 shows schematically the SHRIMP II at the J. C. Roddick Ion Microprobe Laboratory, Geological Survey of Canada in Ottawa. The SHRIMP is a secondary mass spectrometer (SIMS) which means that it analyses secondary ions, ejected or 'sputtered' from the target zircon as it is hit by a beam of primary oxygen ions (O_2^-). The secondary ions are sputtered from the target in different directions at different velocities (kinetic energies), which necessitates both an energy focusing device (the electrostatic analyzer) and directional refocusing.

The primary column produces a beam of pure (ideally) O_2^- ions that can be focused to a spot on the target sample. The primary beam is mass filtered to prevent O^- or contamination such as NO_2^- or OH^- from reaching the target, and focused to yield radially

uniform beam density. Sputtering of the zircon produces pits that are typically ~13.5x19 µm (ellipse) and 0.5-1.0 µm deep, which in turn yields about 0.05 pg of Pb for analysis. This less than minute amount of analyzed Pb is one of the major reasons why SHRIMP ^{207}Pb / ^{206}Pb ages are less precise than those of ID-TIMS, discussed below. The spots are elliptical due to the 45° incident angle of the primary beam.
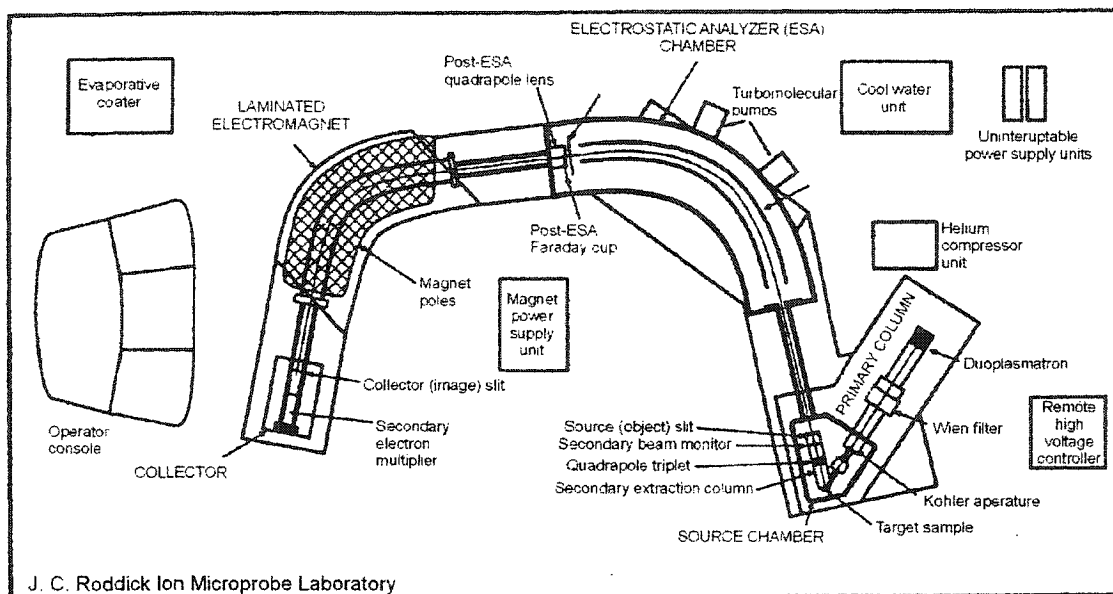
Fig. E.2 Schematic plan view of the GSC SHRIMP II, J. C. Roddick Ion Microprobe Laboratory. From Stern (1997).

The source chamber houses part of the primary column, the sample, and the secondary extraction column. Sputtering from the target zircon produces positive secondary ions (e.g. Zr^+, Pb^+, U^+, and Th^+) that are extracted from the sample by a 750 V potential and accelerated through a 10 kV potential. The quadropole triplet contains three lenses that focus and steer the secondary ions, and the secondary beam monitor is a Faraday plate that partially intersects the secondary beam, measuring its intensity. The source slit is the ion optical object of the analyzer system, focusing the secondary ions.

The electrostatic analyzer filters and focuses the ions according to kinetic energy. This is accomplished by two cylindrical plates (ESA electrodes), 2.5 cm thick and 30 cm high, spaced 6 cm apart, with a potential of 950 V between them (positive on the outer radius). Ions with identical kinetic energy will be focused at the same point on a plane

(energy focal plane) beyond the electrostatic field, and a mechanically adjustable slit (energy window) on this plane can then be used to allow only a particular portion of the energy spectrum to pass through the mass analyzer.

The magnetic sector (laminated electromagnet) focuses ions of identical mass (mass-dispersion) to the same point on the magnetic focal plane beyond the magnet. The mass-dispersed ions pass through the resolving (collector) slit located on the magnetic focal plane, and each arrival of an ion at the secondary electron multiplier generates a pulse of secondary electrons that, if above a selected threshold value, is converted into an ion count.

All calculations were made using the ISOPLOT program developed by Ken Ludwig at the Berkeley Geochronology Center, California (Ludwig, 2001).

MSWD=Mean Square of Weighted Deviates. The MSWD is calculated by the ISOPLOT program and is a measure of the ratio of the *observed* scatter of points from the best-fit line to the expected scatter, calculated from the assigned errors and error correlations (York, 1969). An MSWD close to unity indicates that the assigned errors are the only cause of scatter. MSWD values much higher than unity generally indicate either underestimated analytical errors, or the presence of non-analytical scatter, whereas MSWD values much lower than unity generally indicate either overestimated analytical errors, or unrecognized error-correlations (Ludwig, 2001).

p=Probability of Fit. The Probability of Fit was defined by Ludwig (2001) as "the probability that, if the only reason for scatter from a straight line is the analytical errors assigned to the data, the scatter of the data points will exceed the amount observed for the data". In other words, if the scatter of data points is greater than that expected from the assigned analytical errors, the Probability of Fit will be low.

E.4. Isotope Dilution Thermal Ionization Mass Spectrometry (ID-TIMS)

E.4.1. Sample preparation

After separation, zircons are air abraded, using the method of Krogh (1982), to

eliminate cracked grains and remove exterior surfaces. Final selection of the grains was then made. The weight of each fraction (typically single grains) was either measured with a microbalance, estimated by eye with visual reference to weighed grains, or determined using a spreadsheet program that estimates zircon weight based on photomicrograph measurements of grain length and width and estimation of maximum thickness (*the last method is now standard procedure*). As weights are normally small (generally <3 micrograms), all weighing methods are accurate to only about ±50%; however, measurement uncertainty only affects the calculation of Pb and U concentrations and has no influence on age data.

The selected grains were washed in 4N and then 7N HNO_3 and then loaded into Teflon bombs with HF/HNO_3 and a measured amount of ^{205}Pb - ^{235}U isotopic tracer solution (Krogh, 1973). Dissolution occurred over four to five days at 195°C. Due to small fraction sizes (<0.005 mg), chemical isolation and purification of U and Pb following dissolution is not essential and was not carried out.

Fractions were dried down with phosphoric acid and then loaded with silica gel onto outgassed rhenium filaments. The isotopic compositions of Pb and U were measured using a single Daly collector with a pulse counting detector in a solid source VG354 mass spectrometer. A detector mass discrimination of 0.14% per atomic mass unit (AMU) and a deadtime of 22.5 nsec were employed for Daly detector measurements. A thermal source mass discrimination correction of 0.1% per atomic mass unit for both Pb and U was also used.

The assigned laboratory blank for U was 0.2 pg. Total measured common Pb in samples was below 1 pg in most cases and was assigned the isotopic composition of lab blank (blank isotopic composition: $^{206}Pb/^{204}Pb=18.221$, $^{207}Pb/^{204}Pb=15.612$, $^{208}Pb/^{204}Pb=39.36$). Error estimates were calculated by propagating known sources of analytical uncertainty for each analysis including ratio variability (within run), uncertainty in the fractionation correction, and uncertainty in the isotopic composition of the laboratory blank. Decay constants used are those of Jaffey *et al.* (1971). All uncertainties in the text, tables, and concordia diagrams are given at the 95% confidence

level. Discordia lines and concordia intercept ages were calculated by the method of Davis (1982) using the in-house program ROMAGE. Average ^{207}Pb/^{206}Pb ages were also calculated using ROMAGE except in instances where the probability of fit was less than 30%, in which case a weighted ^{207}Pb/^{206}Pb age and uncertainty were calculated using the ISOPLOT program developed by Ken Ludwig. Probability of fit measures the scatter of analyses with respect to a Pb-loss line. A value of around 50% is expected for unimodal data sets with correctly chosen analytical errors. Significantly lower probabilities of fit suggest real differences in Pb loss history and/or zircon crystallization age.

Table E.1 U-Pb analytical data, charnockitic gneiss (M300617).

Fraction number and properties[a]	Weight (mg)[b]	U (ppm)	Pb[rad] (ppm)[c]	Th/U[d]	common Pb (pg)[d]	207Pb/204Pb[d]	206Pb/238U	2σ	207Pb/235U	2σ	207Pb/206Pb	2σ	Disc.[f] (%)
					Total						**Age (Ma)**		
								Corrected atomic ratios[e]					
Z1 subh clr 2:1 pr (1)	0.0036	15	3.5	0.41	0.38	195.3	0.2301	0.0012	2.770	0.018	1367.6	6.9	2.7
Z2 subh clr 2:1 pr (1)	0.0140	17	3.8	0.37	0.74	399.8	0.2233	0.0010	2.646	0.013	1336.5	4.9	3.1
Z3 subh clr 3:1 pr incl (1)	0.0070	13	3.0	0.38	1.14	114.6	0.2203	0.0012	2.582	0.022	1315.7	13.3	2.7
Z4 euh clr 2:1 pr (1)	0.0060	32	7.3	0.34	0.62	390.6	0.2191	0.0007	2.572	0.010	1318.2	4.7	3.4
Z5 euh clr 3:1 pr incl (3)	0.0080	41	8.6	0.39	2.49	155.3	0.2034	0.0005	2.281	0.012	1229.2	8.3	3.2

[a]Abbreviations: Z=zircon; subh=subhedral; euh=euhedral; clr=clear/colorless; pr=prism; incl=fluid and/or opaque inclusions; 2:1, 3:1=length:breadth ratio; number in brackets indicates number of grain analyzed.

[b]Weighing error ca. ±50%.

[c]Total radiogenic Pb after correction for blank, common Pb, and spike.

[d]Measured.

[e]Ratios corrected for blank and spike Pb, fractionation, and initial common Pb calculated for the age of the sample after Stacey and Kramers (1975).

[f]Percent discordance for the given 207Pb/206Pb age.

Table E.2 U-Pb analytical data, granitic gneiss (M100723-1).

Spot#	U (ppm)	Th (ppm)	Th/U	Pb^{rad} (ppm)	^{204}Pb (ppb)	$\frac{^{204}Pb}{^{206}Pb}$	$\frac{^{207}Pb}{^{235}U}$	1σ	$\frac{^{206}Pb}{^{238}U}$	1σ	Age $^{207}Pb/^{206}Pb$	1σ	Disc. (%)
Low-U cores													
5.1	18	8	0.471	4	9	0.0027	2.3489	0.2649	0.2171	0.0052	1158	229	109
16.2	10	6	0.584	3	9	0.0042	2.9176	0.5445	0.2217	0.0079	1537	380	84
20.1	29	12	0.410	6	10	0.0020	2.1701	0.1694	0.2053	0.0042	1112	153	108
Oscillatory-zoned cores													
1.1	220	42	0.195	50	8	0.0002	2.8130	0.0560	0.2302	0.0029	1396	27	96
2.1	103	4	0.044	18	3	0.0002	1.9666	0.0645	0.1845	0.0028	1130	55	97
3.2	48	22	0.480	12	7	0.0007	2.7391	0.1250	0.2259	0.0048	1381	75	95
4.1	217	7	0.032	36	5	0.0002	1.8989	0.0390	0.1782	0.0026	1129	25	94
6.1	216	78	0.372	52	9	0.0002	2.8725	0.0520	0.2343	0.0031	1402	21	97
7.1	98	70	0.731	27	5	0.0002	3.0245	0.0800	0.2422	0.0034	1437	40	97
10.1	90	63	0.720	23	11	0.0006	2.6683	0.3765	0.2306	0.0048	1291	293	104
12.1	137	85	0.644	33	13	0.0005	2.5388	0.0754	0.2198	0.0030	1288	49	100
13.1	54	33	0.633	13	9	0.0009	2.6316	0.1078	0.2270	0.0037	1295	71	102
17.1	352	105	0.309	82	6	0.0001	2.8024	0.0416	0.2305	0.0027	1387	16	96
23.1	84	12	0.143	20	5	0.0003	3.0581	0.0864	0.2435	0.0037	1448	43	97

Table E.2 continued.

Spot#	U (ppm)	Th (ppm)	Th/U	Pb^{rad} (ppm)	^{204}Pb (ppb)	$\frac{^{204}Pb}{^{206}Pb}$	$\frac{^{207}Pb}{^{235}U}$	1σ	$\frac{^{206}Pb}{^{238}U}$	1σ	Age ^{207}Pb/^{206}Pb	1σ	Disc. (%)
Oscillatory-zoned rims/magmatic overgrowths													
3.1	142	23	0.166	31	8	0.0003	2.5718	0.0810	0.2193	0.0035	1317	50	97
5.2	133	11	0.088	27	8	0.0003	2.5339	0.0554	0.2143	0.0026	1333	33	94
5.3	215	65	0.313	52	11	0.0002	2.9583	0.0528	0.2411	0.0030	1404	22	99
8.1	363	19	0.054	61	4	0.0001	1.8613	0.0313	0.1783	0.0021	1087	22	97
9.1	74	18	0.246	12	12	0.0010	1.7306	0.0853	0.1719	0.0025	1014	94	101
11.1	103	4	0.040	17	3	0.0002	1.9063	0.0579	0.1768	0.0025	1152	51	91
13.2	112	26	0.238	19	10	0.0006	1.7610	0.0569	0.1755	0.0024	1008	57	103
15.1	137	24	0.184	23	11	0.0006	1.7184	0.0540	0.1725	0.0021	993	57	103
16.1	236	32	0.140	55	5	0.0001	2.9521	0.0455	0.2386	0.0028	1420	17	97
20.2	141	31	0.230	24	14	0.0007	1.6963	0.0623	0.1719	0.0023	974	68	105
21.1	172	25	0.152	34	7	0.0002	2.2822	0.0562	0.2000	0.0030	1264	35	93
24.1	734	48	0.068	130	10	0.0001	2.0286	0.0270	0.1876	0.0020	1158	13	96
Unzoned rims													
2.2	124	37	0.307	21	6	0.0003	1.7214	0.0613	0.1730	0.0036	991	55	104
4.2	179	34	0.199	30	6	0.0002	1.8071	0.0385	0.1744	0.0021	1073	32	97
12.1	123	21	0.179	29	8	0.0003	2.9612	0.0658	0.2389	0.0031	1423	32	97
18.1	141	22	0.160	26	6	0.0003	2.0979	0.0464	0.1910	0.0025	1189	33	95
19.1	222	25	0.118	52	3	0.0001	2.9641	0.0496	0.2390	0.0029	1424	20	97
22.1	321	47	0.150	77	8	0.0001	3.0178	0.0456	0.2448	0.0027	1413	17	100

Table E.3 U-Pb analytical data, concordant leucosome (2M02061-9).

Spot#	U (ppm)	Th (ppm)	$\frac{Th}{U}$	Pb^{rad} (ppm)	204 ppb	$\frac{204Pb}{206Pb}$	$\frac{207Pb}{235U}$	1σ	$\frac{206Pb}{238U}$	1σ	Age $207Pb/206Pb$	1σ	Disc. (%)
Cores													
1.2	372	151	0.419	90	6	0.0001	2.8782	0.0455	0.2320	0.0027	1425	18	94
2.2	530	164	0.320	133	6	0.0001	3.0657	0.0467	0.2477	0.0030	1420	15	101
3.1	3180	1693	0.550	873	1	0.0000	3.0942	0.0499	0.2539	0.0039	1391	6	105
4.2	577	304	0.543	154	6	0.0000	3.0876	0.0444	0.2476	0.0028	1435	14	99
6.3	343	140	0.421	89	9	0.0001	3.0877	0.0534	0.2477	0.0031	1434	20	100
11.1	445	195	0.453	104	4	0.0000	2.7150	0.0434	0.2199	0.0026	1416	18	91
12.1	1308	472	0.373	339	3	0.0000	3.1796	0.0388	0.2508	0.0027	1466	8	98
Magmatic overgrowths													
1.1	1886	232	0.127	321	6	0.0000	1.8427	0.0241	0.1776	0.0020	1075	10	98
2.1	1869	206	0.114	319	5	0.0000	1.8307	0.0240	0.1786	0.0021	1051	10	101
3.1	1384	94	0.070	233	7	0.0000	1.8372	0.0273	0.1788	0.0020	1055	17	101
4.1	1683	35	0.021	282	1	0.0000	1.8622	0.0232	0.1801	0.0019	1069	11	100
5.1	1833	30	0.017	312	1	0.0000	1.9213	0.0248	0.1833	0.0020	1095	12	99
6.1	1412	10	0.008	240	11	0.0000	1.9156	0.0240	0.1836	0.0020	1086	11	100
7.1	1165	32	0.029	195	6	0.0000	1.8537	0.0263	0.1798	0.0022	1062	13	100
8.1	1180	83	0.073	194	5	0.0000	1.7992	0.0260	0.1744	0.0021	1064	13	97
9.1	2117	264	0.129	361	3	0.0000	1.8333	0.0227	0.1782	0.0020	1058	9	100
10.1	1162	68	0.060	193	7	0.0000	1.8138	0.0240	0.1766	0.0019	1055	13	99
Late metamorphic overgrowth													
7446-6.2	1850	154	0.086	307	7	0.0000	1.8094	0.0241	0.1758	0.0020	1059	11	99

Table E.4 U-Pb analytical data, pegmatitic infill in boudin neck (2M02061-5).

Spot#	U (ppm)	Th (ppm)	$\frac{Th}{U}$	Pb^{rad} (ppm)	^{204}Pb (ppb)	$\frac{^{204}Pb}{^{206}Pb}$	$\frac{^{207}Pb}{^{235}U}$	1σ	$\frac{^{206}Pb}{^{238}U}$	1σ	Age $^{207}Pb/^{206}Pb$	1σ	Disc. (%)
Cores													
1.1	112	102	0.941	33	2	0.0001	3.0785	0.1234	0.2462	0.0063	1440	54	99
2.1	126	78	0.643	34	3	0.0001	3.0847	0.0551	0.2436	0.0029	1464	23	96
3.1	173	115	0.685	48	3	0.0001	3.1400	0.0464	0.2485	0.0029	1460	15	98
4.1	189	97	0.529	49	1	0.0000	3.0711	0.0462	0.2404	0.0027	1481	16	94
5.1	242	184	0.785	68	2	0.0000	3.1307	0.1387	0.2460	0.0075	1474	55	96
6.1	447	320	0.739	123	4	0.0000	3.0426	0.0413	0.2440	0.0029	1434	10	98
7.1	189	117	0.638	51	3	0.0001	3.0296	0.0466	0.2449	0.0029	1420	17	100
8.1	246	122	0.510	66	4	0.0001	3.1561	0.0471	0.2493	0.0028	1464	16	98
9.1	218	149	0.704	60	0	0.0000	3.1248	0.0574	0.2431	0.0040	1492	12	94
10.1	247	72	0.301	55	6	0.0001	2.6303	0.0466	0.2207	0.0033	1348	15	95
Old metamorphic overgrowth													
1.2	603	33	0.056	141	3	0.0000	3.0926	0.0453	0.2455	0.0030	1454	13	97
Metamorphic overgrowth													
3.2	1062	74	0.072	175	1	0.0000	1.8098	0.0244	0.1741	0.0019	1079	14	96
4.2	1648	53	0.033	274	3	0.0000	1.8443	0.0261	0.1785	0.0019	1067	17	99
5.2	1348	95	0.073	230	3	0.0000	1.8386	0.0235	0.1809	0.0020	1034	10	104
7.2	1826	43	0.024	302	6	0.0000	1.8478	0.0221	0.1779	0.0019	1078	9	98
8.2	2100	97	0.048	343	5	0.0000	1.7860	0.0206	0.1745	0.0018	1048	8	99
8.3	1933	77	0.041	321	6	0.0000	1.8045	0.0232	0.1779	0.0020	1029	10	103
9.2	548	5	0.009	93	2	0.0000	1.9044	0.0357	0.1836	0.0027	1075	20	101
10.2	2162	91	0.044	350	4	0.0000	1.7654	0.0690	0.1732	0.0047	1040	52	99
11.1	1416	91	0.066	230	6	0.0000	1.7812	0.0223	0.1726	0.0018	1065	11	96
12.1	1431	62	0.045	235	5	0.0000	1.7882	0.0219	0.1762	0.0019	1031	10	102
13.1	1245	89	0.074	203	6	0.0000	1.7585	0.0226	0.1734	0.0019	1029	11	100

Table E.5 U-Pb analytical data, pyroxene-bearing pegmatite (2M0606-25).

Spot#	U (ppm)	Th (ppm)	Pb^{rad} (ppm)	^{204}Pb (ppb)	$\frac{^{204}Pb}{^{206}Pb}$	$\frac{^{207}Pb}{^{235}U}$	1σ	$\frac{^{206}Pb}{^{238}U}$	1σ	Age ^{207}Pb/^{206}Pb	1σ	Disc. (%)
1.1	640	548	130	5	0.0000	1.7967	0.0304	0.1764	0.0027	1038	11	101
2.1	221	176	44	6	0.0002	1.7834	0.0397	0.1755	0.0032	1033	22	101
2.2	945	84	159	5	0.0000	1.8057	0.0291	0.1777	0.0027	1033	7	102
3.1	547	169	97	5	0.0001	1.7640	0.0310	0.1765	0.0028	999	11	105
4.1	1011	7	161	4	0.0000	1.7506	0.0288	0.1719	0.0027	1037	7	99
5.1	173	110	34	2	0.0001	1.7903	0.0390	0.1767	0.0030	1027	24	102
6.1	342	333	70	2	0.0000	1.7845	0.0326	0.1740	0.0021	1052	25	98
7.1	1103	781	217	4	0.0000	1.7974	0.0233	0.1767	0.0019	1035	13	101
8.1	1123	30	180	3	0.0000	1.7449	0.0235	0.1728	0.0019	1021	13	101
9.1	262	296	57	3	0.0001	1.7880	0.0357	0.1766	0.0021	1026	30	102
10.1	651	483	127	4	0.0000	1.7716	0.0263	0.1734	0.0019	1044	18	99
11.1	434	310	84	8	0.0001	1.7701	0.0315	0.1732	0.0020	1045	25	99
12.1	333	213	63	3	0.0001	1.7866	0.0358	0.1725	0.0021	1071	29	96
13.1	333	324	68	7	0.0001	1.7348	0.0343	0.1744	0.0021	991	29	105
14.1	512	343	100	9	0.0001	1.8402	0.0290	0.1764	0.0020	1086	20	96
15.1	1110	158	186	5	0.0000	1.7816	0.0240	0.1745	0.0018	1043	15	99
16.1	528	410	105	3	0.0000	1.7535	0.0279	0.1744	0.0020	1012	19	102

Table E.6 U-Pb analytical data, post-tectonic granite dike (2M1406-2).

Spot#	U (ppm)	Th (ppm)	$\frac{Th}{U}$	Pb^{rad} (ppm)	^{204}Pb (ppb)	$\frac{^{204}Pb}{^{206}Pb}$	$\frac{^{207}Pb}{^{235}U}$	1σ	$\frac{^{206}Pb}{^{238}U}$	1σ	Age ^{207}Pb/^{206}Pb	1σ	Disc. (%)
1.1	514	237	0.477	95	2	0.0000	1.7778	0.0505	0.1755	0.0037	1027	34	102
2.1	695	318	0.473	128	0	0.0000	1.7920	0.0319	0.1763	0.0029	1034	11	101
3.1	570	231	0.418	103	2	0.0000	1.7842	0.0369	0.1749	0.0034	1041	11	100
4.1	448	170	0.392	80	4	0.0001	1.7612	0.0315	0.1744	0.0027	1020	14	102
5.1	503	200	0.410	89	4	0.0001	1.7641	0.0306	0.1726	0.0027	1045	12	98
6.1	537	228	0.438	97	1	0.0000	1.7909	0.0304	0.1734	0.0027	1066	11	97
7.1	473	199	0.435	85	3	0.0000	1.7611	0.0309	0.1727	0.0027	1041	13	99
8.2	483	187	0.401	87	4	0.0001	1.7906	0.0321	0.1743	0.0027	1055	15	98
9.1	679	314	0.478	126	1	0.0000	1.8060	0.0303	0.1766	0.0027	1047	10	100
10.1	465	210	0.466	84	2	0.0000	1.7797	0.0310	0.1735	0.0027	1052	12	98
11.1	701	316	0.465	129	1	0.0000	1.7998	0.0337	0.1750	0.0030	1057	11	98
12.1	319	73	0.236	55	0	0.0000	1.8020	0.0337	0.1741	0.0027	1071	17	97
13.1	715	316	0.456	131	2	0.0000	1.7990	0.0299	0.1756	0.0027	1049	10	99
14.1	433	164	0.391	78	3	0.0000	1.8054	0.0327	0.1758	0.0028	1054	13	99
15.1	489	190	0.402	88	2	0.0000	1.8045	0.0313	0.1751	0.0028	1061	11	98

Table E.7 U-Pb analytical data, pegmatite (2S0207-2).

Spot#	U (ppm)	Th (ppm)	Th/U	Pb^{rad} (ppm)	^{204}Pb (ppb)	$\frac{^{204}Pb}{^{206}Pb}$	$\frac{^{207}Pb}{^{235}U}$	1σ	$\frac{^{206}Pb}{^{238}U}$	1σ	Age ^{207}Pb/^{206}Pb	1σ	Disc. (%)
Cores, non-rimmed grains, and magmatic overgrowths													
2.1	2698	47	0.018	466	3	0.0000	1.9462	0.0321	0.1859	0.0030	1093	5	101
3.1	3468	44	0.013	602	2	0.0000	1.9454	0.0321	0.1871	0.0030	1080	5	102
4.1	1475	18	0.013	252	7	0.0000	1.9166	0.0323	0.1847	0.0029	1076	9	102
6.2	3239	63	0.020	560	2	0.0000	1.9428	0.0318	0.1859	0.0030	1090	5	101
7.1	2120	30	0.015	365	3	0.0000	1.9501	0.0330	0.1851	0.0029	1105	9	99
9.1	1832	25	0.014	312	3	0.0000	1.9521	0.0310	0.1834	0.0028	1126	6	96
9.2	2537	44	0.018	441	3	0.0000	1.9495	0.0306	0.1873	0.0029	1082	5	102
10.1	1279	12	0.009	217	2	0.0000	1.8973	0.0307	0.1833	0.0028	1071	8	101
13.1	4958	80	0.017	863	1	0.0000	1.9564	0.0290	0.1873	0.0027	1089	5	102
13.2	9076	198	0.023	942	19	0.0000	1.0896	0.0367	0.1122	0.0036	941	13	73
Metamorphic overgrowths													
1.1	994	8	0.008	168	3	0.0000	1.8907	0.0304	0.1828	0.0028	1069	8	101
6.1	977	7	0.008	166	2	0.0000	1.8985	0.0310	0.1830	0.0028	1075	8	101
8.1	1165	13	0.012	199	2	0.0000	1.9102	0.0312	0.1845	0.0028	1071	9	102
11.1	1228	11	0.009	207	79	0.0004	1.9133	0.0283	0.1813	0.0020	1109	17	97
12.1	1473	8	0.006	245	3	0.0000	1.8599	0.0246	0.1792	0.0020	1076	11	99
Young overgrowth/recrystallized core													
5.1	4184	39	0.010	700	3	0.0000	1.8519	0.0321	0.1806	0.0031	1051	4	102

Table E.8 U-Pb analytical data, granite (2S0507).

Spot#	U (ppm)	Th (ppm)	Th/U	Pb^{rad} (ppm)	^{204}Pb (ppb)	$\frac{^{204}Pb}{^{206}Pb}$	$\frac{^{207}Pb}{^{235}U}$	1σ	$\frac{^{206}Pb}{^{238}U}$	1σ	Age ^{207}Pb/^{206}Pb	1σ	Disc. (%)
Inherited core (ca. 1350 Ma)													
4.2	487	201	0.427	109	2	0.0000	2.5588	0.0402	0.2148	0.0025	1347	18	93
Inherited core (ca. 1290 Ma)													
17.1	3397	2218	0.675	863	247	0.0003	2.7952	0.0633	0.2415	0.0052	1291	10	108
High-U cores													
1.1	8039	136	0.017	1438	4	0.0000	2.0037	0.0417	0.1925	0.0040	1081	3	105
7.1	3769	51	0.014	670	3	0.0000	2.0022	0.0346	0.1914	0.0032	1092	4	103
9.1	9014	203	0.023	1696	299	0.0002	2.1048	0.3737	0.2023	0.0255	1081	239	110
10.1	3708	27	0.008	665	7	0.0000	2.0239	0.0363	0.1936	0.0034	1090	5	105
13.1	8839	178	0.021	1578	4	0.0000	2.0175	0.0940	0.1919	0.0080	1102	32	103
Lower-U cores and magmatic overgrowths													
2.1	1109	9	0.008	189	3	0.0000	1.9156	0.0309	0.1844	0.0028	1077	8	101
4.1	1395	3	0.002	242	4	0.0000	1.9706	0.0314	0.1874	0.0028	1102	7	101
12.1	1439	7	0.005	243	4	0.0000	1.9056	0.0305	0.1821	0.0028	1092	7	99
13.1	2075	26	0.013	353	6	0.0000	1.9139	0.0247	0.1831	0.0021	1090	10	99
14.1	810	6	0.008	137	3	0.0000	1.8986	0.0313	0.1821	0.0028	1085	9	99

Table E.8 continued.

Spot#	U (ppm)	Th (ppm)	$\frac{Th}{U}$	Pb^{rad} (ppm)	204 (ppb)	$\frac{204Pb}{206Pb}$	$\frac{207Pb}{235U}$	1σ	$\frac{206Pb}{238U}$	1σ	Age $207Pb/206Pb$	1σ	Disc. (%)
Metamorphic rims													
1.2	1697	9	0.006	267	16	0.0001	1.7551	0.0246	0.1696	0.0020	1070	12	94
3.1	1108	8	0.007	183	1	0.0000	1.8432	0.0298	0.1785	0.0027	1065	7	99
5.1	1377	12	0.009	231	15	0.0001	1.8641	0.0302	0.1811	0.0028	1059	8	101
6.1	1419	11	0.008	239	3	0.0000	1.8734	0.0298	0.1817	0.0028	1063	7	101
8.1	1698	18	0.011	286	2	0.0000	1.8731	0.0315	0.1820	0.0029	1059	6	102
11.1	1286	7	0.006	219	7	0.0000	1.9000	0.0311	0.1840	0.0028	1065	8	102
15.1	1434	31	0.022	230	12	0.0001	1.7862	0.0311	0.1727	0.0029	1069	8	96
16.1	1474	10	0.007	246	12	0.0001	1.8701	0.0271	0.1799	0.0022	1079	13	99
Younger metamorphic rims													
3.2	1334	12	0.009	223	4	0.0000	1.8395	0.0294	0.1802	0.0027	1042	7	103
7.2	1468	12	0.008	234	9	0.0000	1.7506	0.0232	0.1724	0.0019	1032	12	99

Table E.9 U-Pb analytical data, hornblende-rich leucosome (2S2006-3).

Spot#	U (ppm)	Th (ppm)	Th/U	Pb^{rad} (ppm)	^{204}Pb (ppb)	$\frac{^{204}Pb}{^{206}Pb}$	$\frac{^{207}Pb}{^{235}U}$	1σ	$\frac{^{206}Pb}{^{238}U}$	1σ	Age ^{207}Pb/^{206}Pb	1σ	Disc. (%)
Inherited cores (ca. 1450 Ma)													
1.1	897	339	0.390	231	8	0.0000	3.0951	0.0386	0.2482	0.0028	1435	8	100
1.3	177	82	0.477	47	1	0.0000	3.2693	0.0607	0.2508	0.0033	1519	22	95
3.1	523	331	0.654	146	12	0.0001	3.1529	0.0463	0.2507	0.0030	1451	14	99
4.1	569	224	0.407	149	3	0.0000	3.1661	0.0406	0.2496	0.0027	1467	11	98
6.1	354	239	0.697	93	4	0.0001	2.9226	0.0477	0.2355	0.0031	1426	15	96
7.1	375	295	0.812	108	3	0.0000	3.1858	0.0458	0.2513	0.0029	1466	14	99
7.2	730	388	0.549	198	8	0.0001	3.1427	0.0431	0.2500	0.0027	1450	14	99
8.1	672	546	0.840	196	10	0.0001	3.1742	0.0421	0.2527	0.0028	1448	12	100
9.1	246	114	0.480	65	3	0.0000	3.1186	0.0519	0.2490	0.0031	1443	19	99
10.1	289	237	0.847	84	6	0.0001	3.1580	0.0506	0.2510	0.0030	1452	17	99
11.1	339	218	0.663	94	4	0.0001	3.1212	0.0471	0.2498	0.0030	1438	15	100
13.1	375	352	0.968	111	2	0.0000	3.1893	0.0497	0.2504	0.0031	1475	15	98
14.1	465	286	0.636	128	2	0.0000	3.1771	0.0453	0.2493	0.0028	1476	14	97
15.1	440	322	0.757	124	0	0.0000	3.0951	0.0469	0.2489	0.0030	1430	15	100
Inherited core (ca. 1410 Ma)									(F				
5.1	351	211	0.623	95	9	0.0001	3.0360	0.0472	0.2467	0.0029	1410	17	101
Inherited core (ca. 1350 Ma)													
12.1	244	176	0.743	65	49	0.0010	2.8008	0.0679	0.2348	0.0032	1350	36	101

Table E.9 continued.

Spot#	U (ppm)	Th (ppm)	Th/U	Pb^{rad} (ppm)	204 (ppb)	$\frac{204Pb}{206Pb}$	$\frac{207Pb}{235U}$	1σ	$\frac{206Pb}{238U}$	1σ	Age $^{207}Pb/^{206}Pb$	1σ	Disc. (%)
Rims/magmatic overgrowths													
1.2	905	6	0.007	147	1	0.0000	1.8180	0.0242	0.1759	0.0020	1067	12	98
2.1	1407	7	0.005	228	6	0.0000	1.7616	0.0219	0.1753	0.0019	1011	11	103
3.2	1848	8	0.004	304	4	0.0000	1.8075	0.0221	0.1783	0.0019	1028	9	103
4.2	1656	5	0.003	272	7	0.0000	1.8182	0.0237	0.1781	0.0020	1043	11	101
5.2	1872	9	0.005	310	6	0.0000	1.8407	0.0240	0.1794	0.0021	1053	9	101
6.2	1290	7	0.005	209	6	0.0000	1.8017	0.0229	0.1752	0.0019	1057	11	98
7.3	1486	6	0.004	246	7	0.0000	1.8272	0.0250	0.1790	0.0020	1043	14	102
8.2	1312	8	0.006	220	3	0.0000	1.8503	0.0228	0.1811	0.0019	1044	10	103
9.2	1289	5	0.004	213	5	0.0000	1.8050	0.0230	0.1793	0.0019	1014	11	105
10.2	1203	7	0.006	199	23	0.0001	1.8364	0.0235	0.1790	0.0019	1052	12	101
11.2	1267	8	0.006	209	2	0.0000	1.8440	0.0229	0.1779	0.0019	1073	11	98
12.2	1159	8	0.007	190	7	0.0000	1.8253	0.0237	0.1770	0.0019	1063	12	99
13.2	1228	6	0.005	201	5	0.0000	1.8169	0.0235	0.1771	0.0020	1052	11	100
14.2	1221	7	0.006	201	2	0.0000	1.8309	0.0225	0.1781	0.0019	1057	10	100
16.1	1253	5	0.004	207	2	0.0000	1.8335	0.0255	0.1782	0.0020	1058	13	100
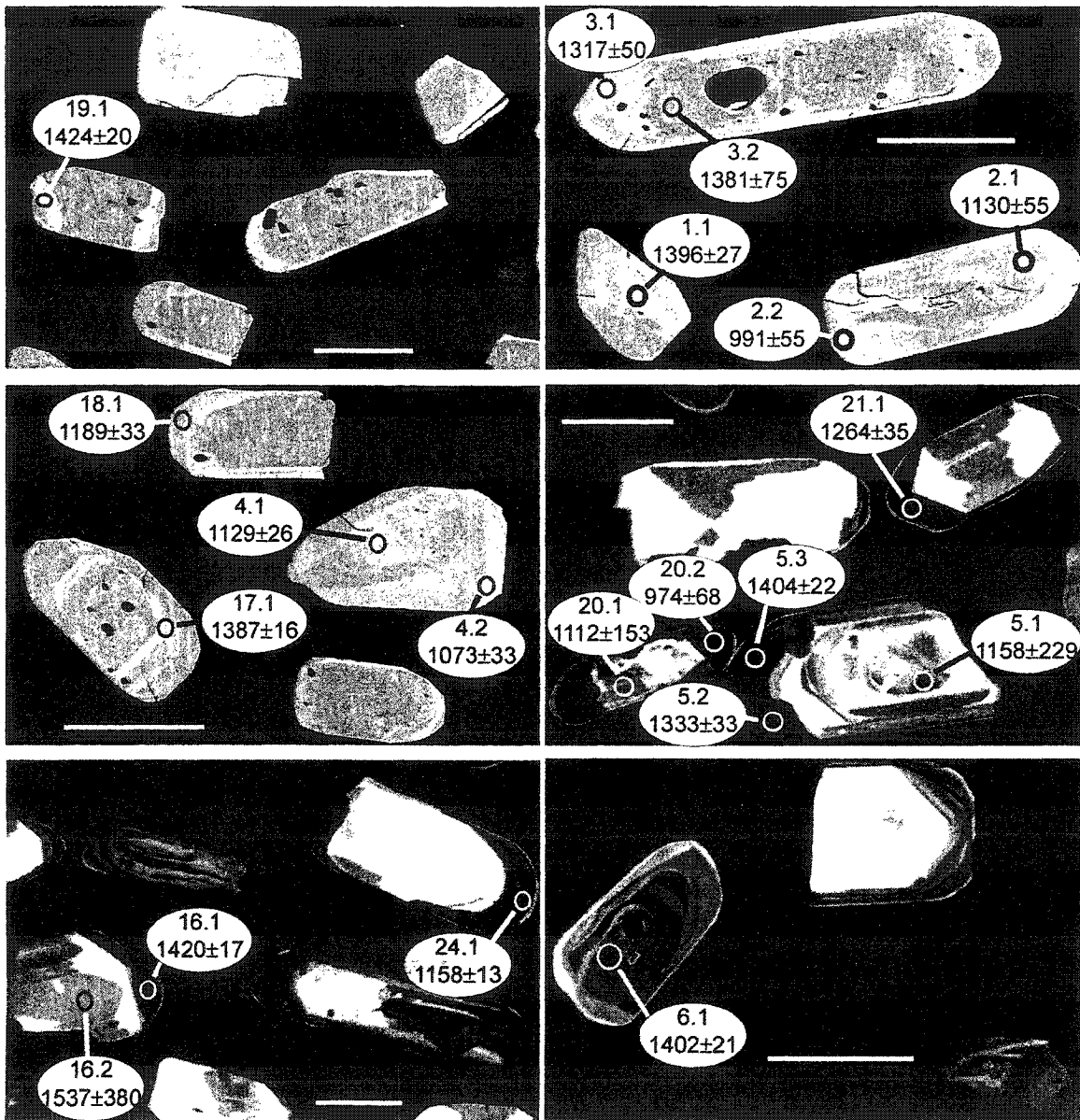
Fig. E.3 SHRIMP spot locations and $^{207}Pb/^{206}Pb$ ages with errors, granitic gneiss (M100723-1). Scale bar=100µm.
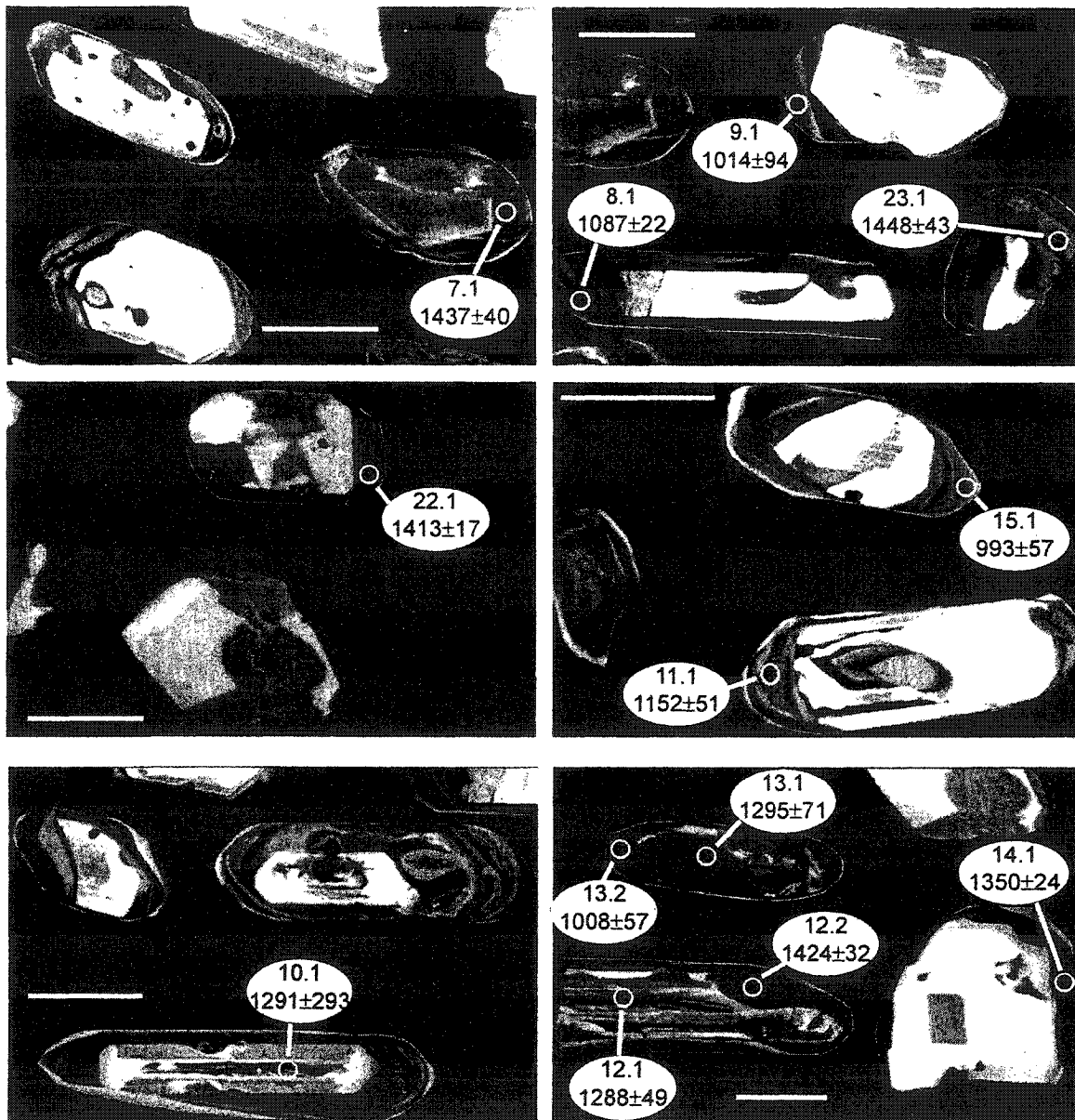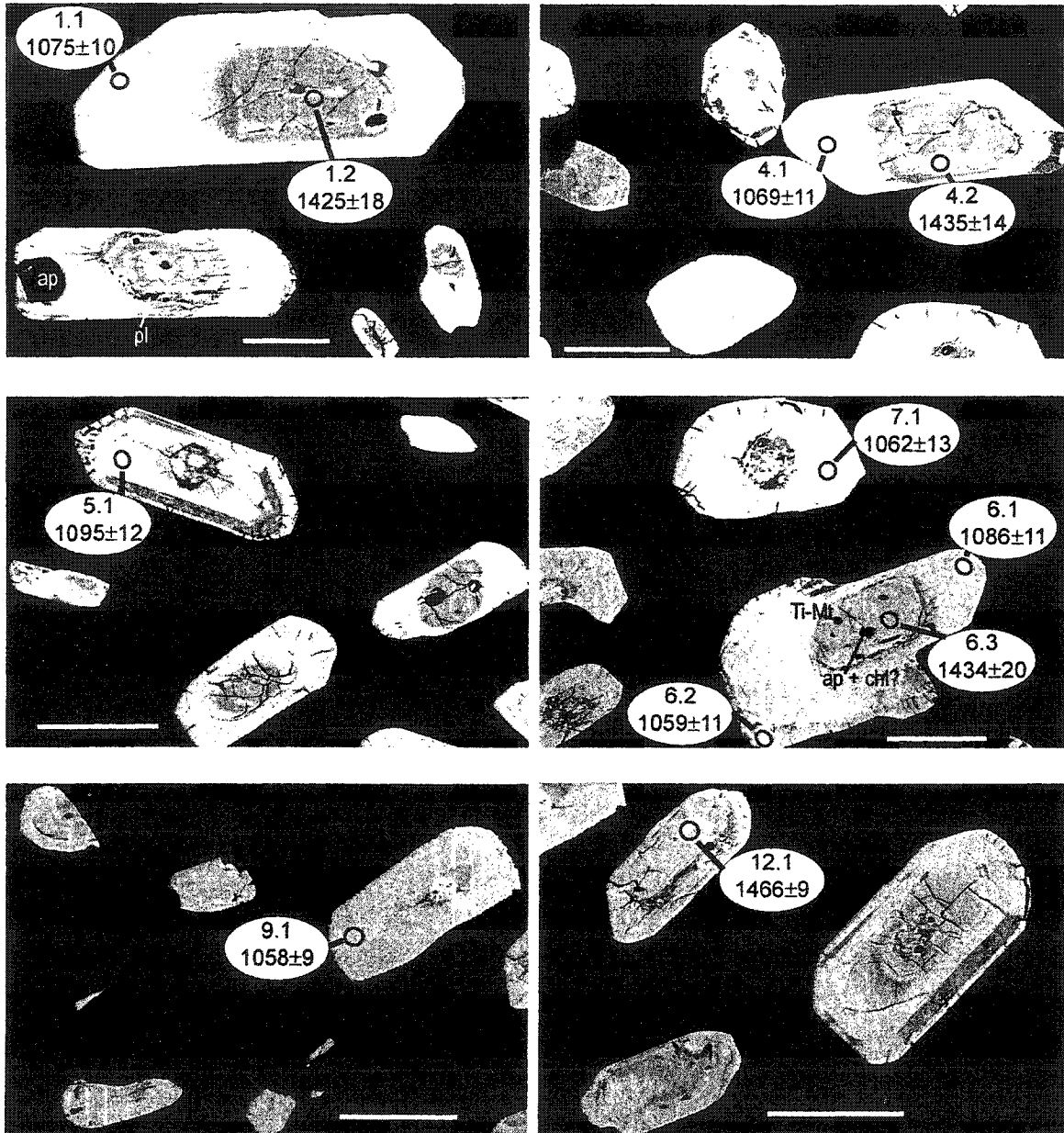
Fig. E.3 continued.

Fig. E.4 SHRIMP spot locations and $^{207}Pb/^{206}Pb$ ages with errors, concordant leucosome (2M02061-9). Scale bar=100µm.
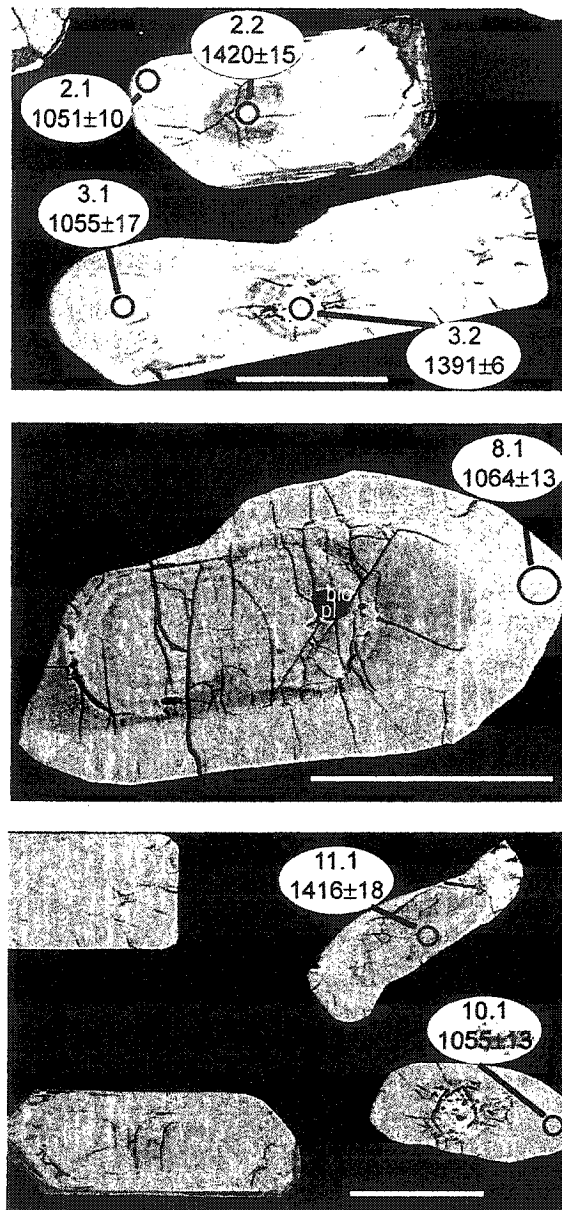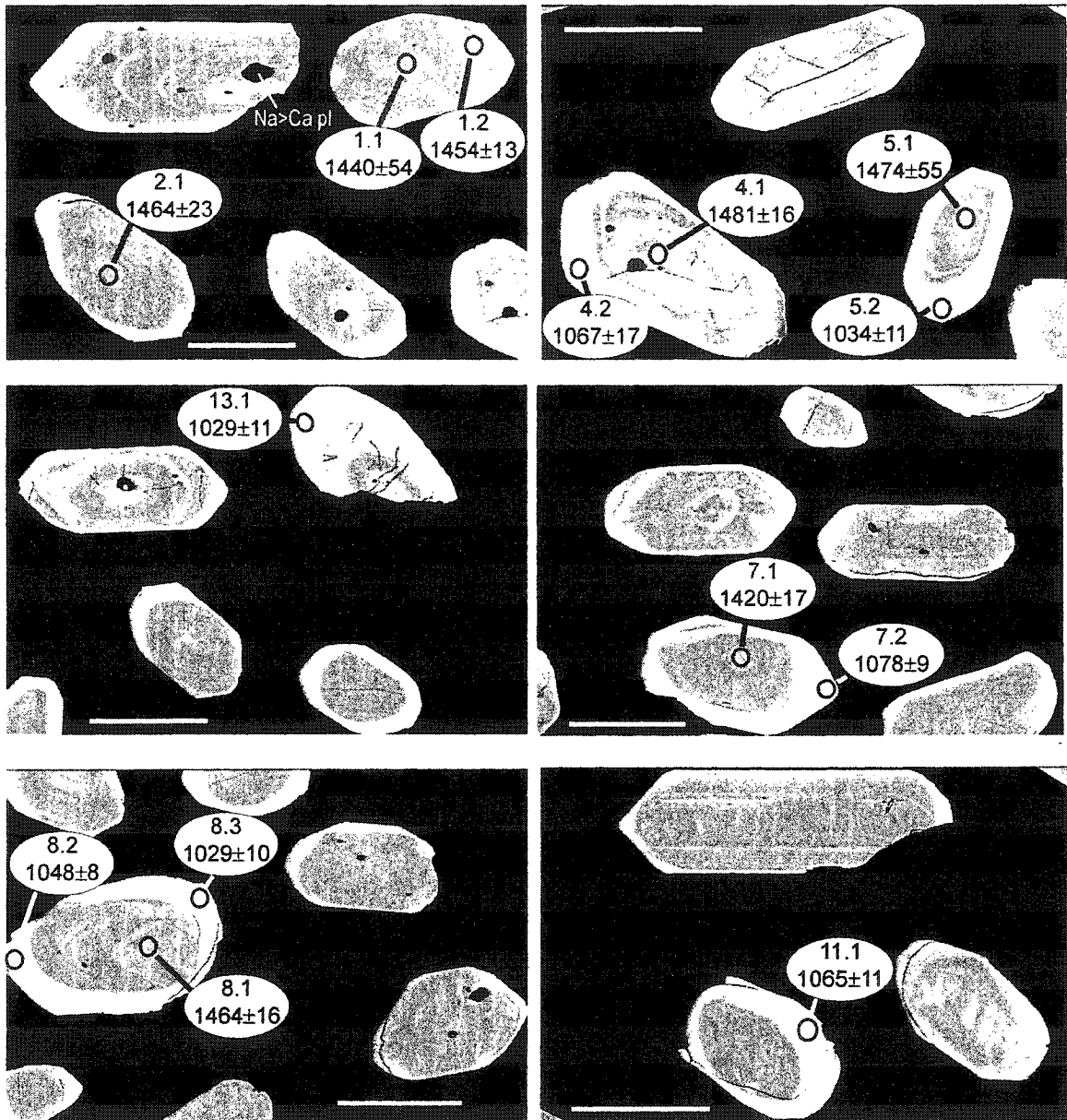
Fig. E.4 continued.

Fig. E.5 SHRIMP spot locations and $^{207}Pb/^{206}Pb$ ages with errors, pegmatitic infill in boudin neck (2M02061-5). Scale bar=100µm.
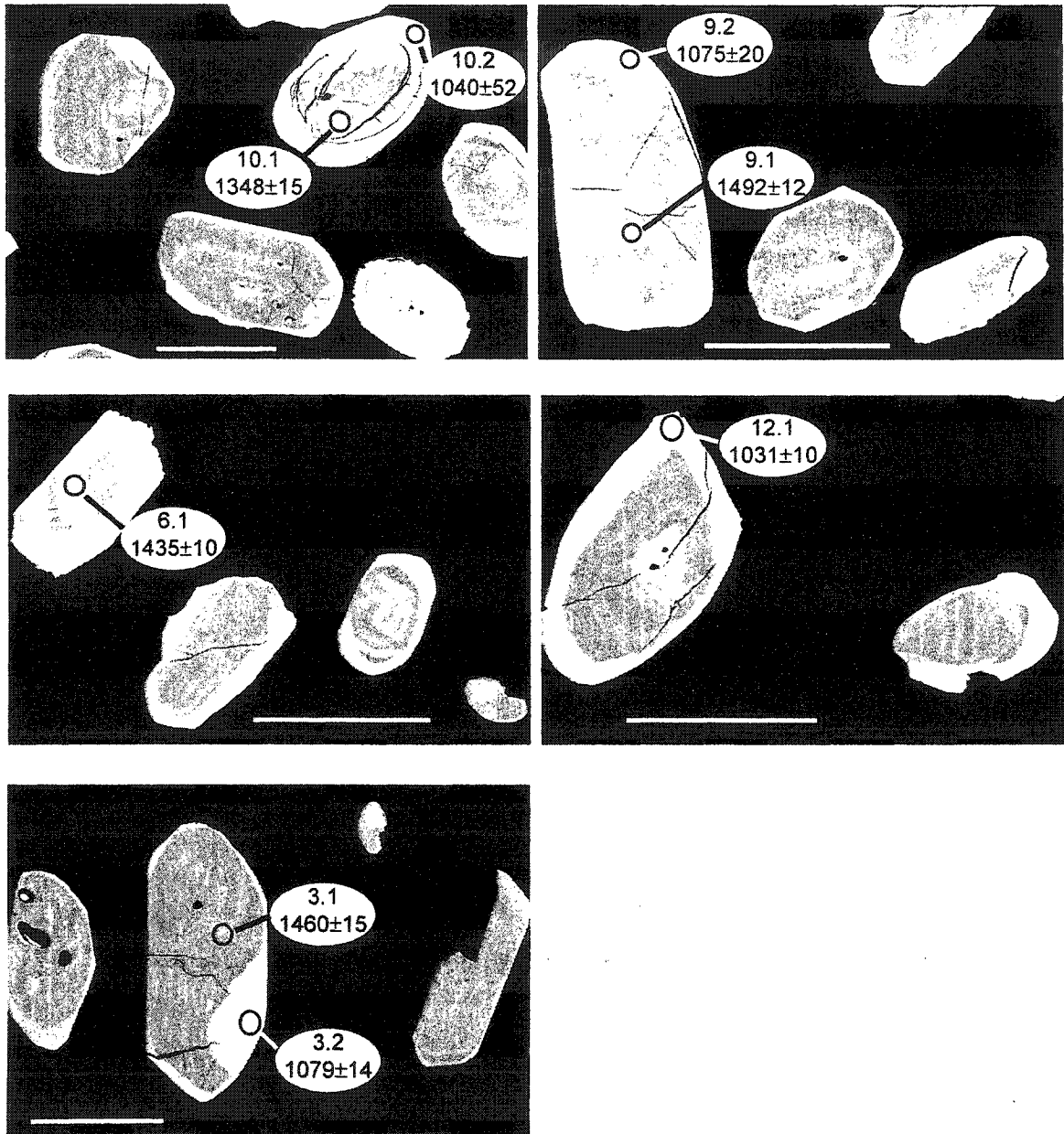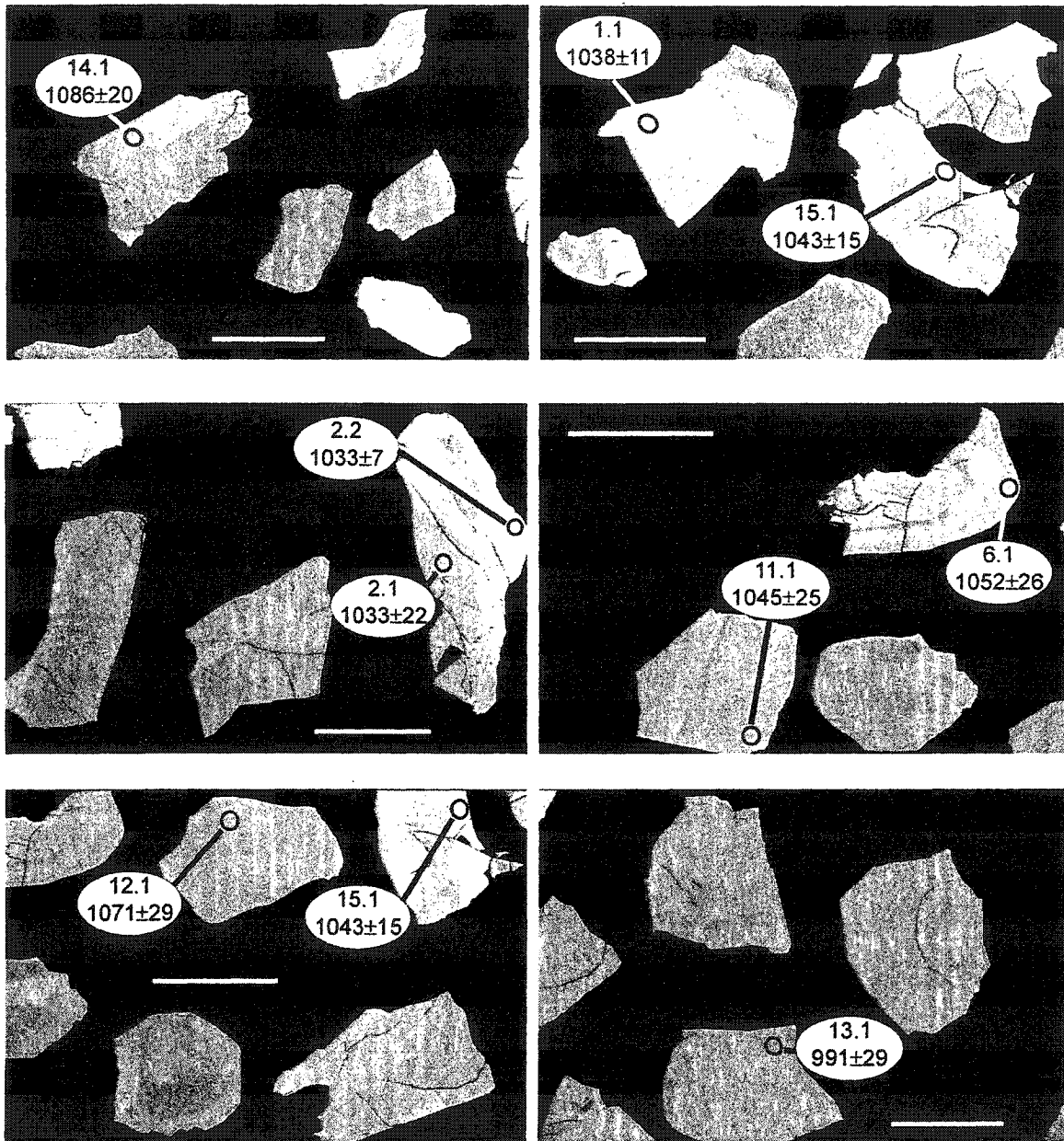
Fig. E.5 continued.

Fig. E.6 SHRIMP spot locations and $^{207}Pb/^{206}Pb$ ages with errors, pyroxene-bearing pegmatitic syenite (2M0606-25). Scale bar=200μm.
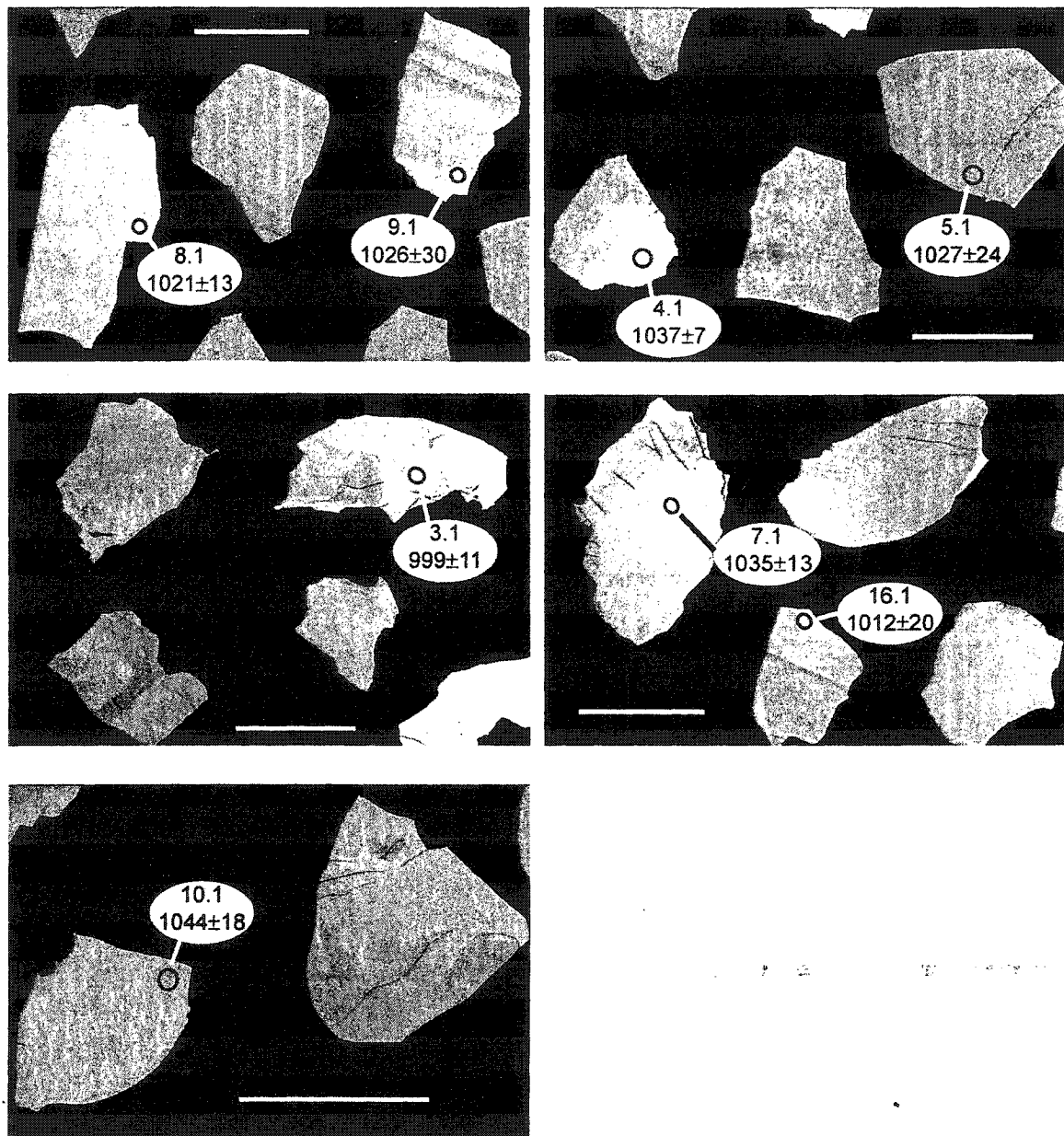
Fig. E.6 continued.
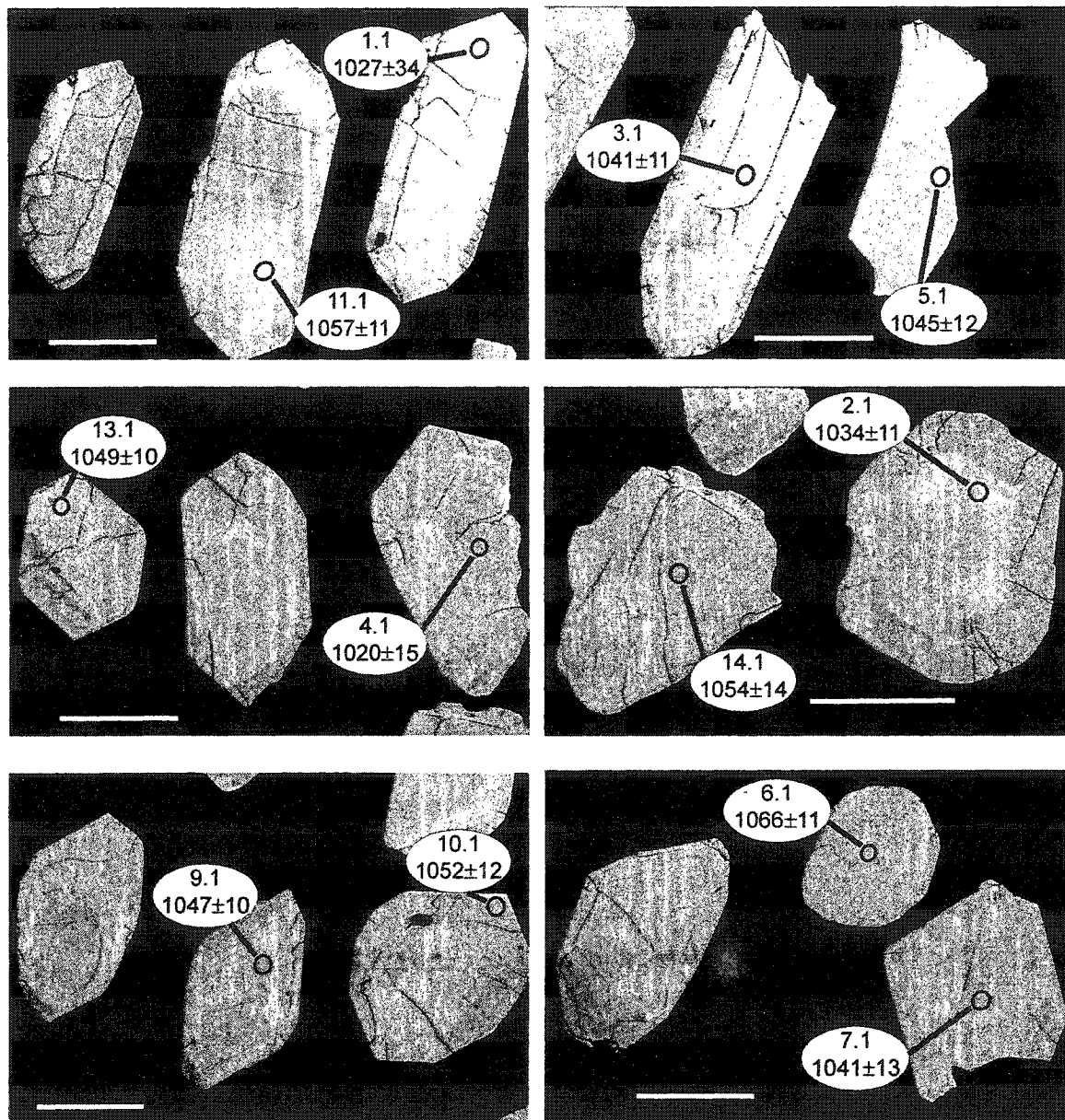
Fig. E.7 SHRIMP spot locations and $^{207}Pb/^{206}Pb$ ages with errors, post-tectonic granite dike (2M1406.2). Scale bar=200μm.
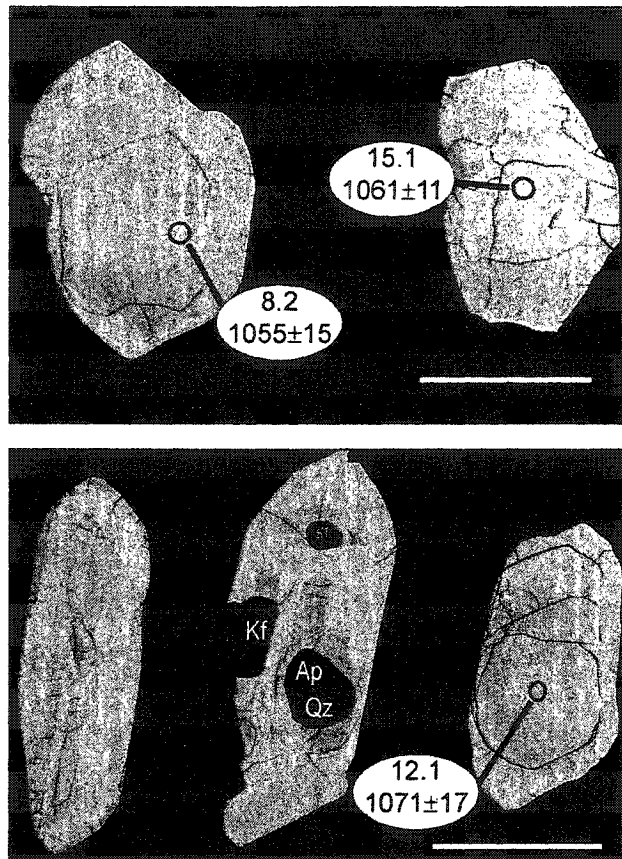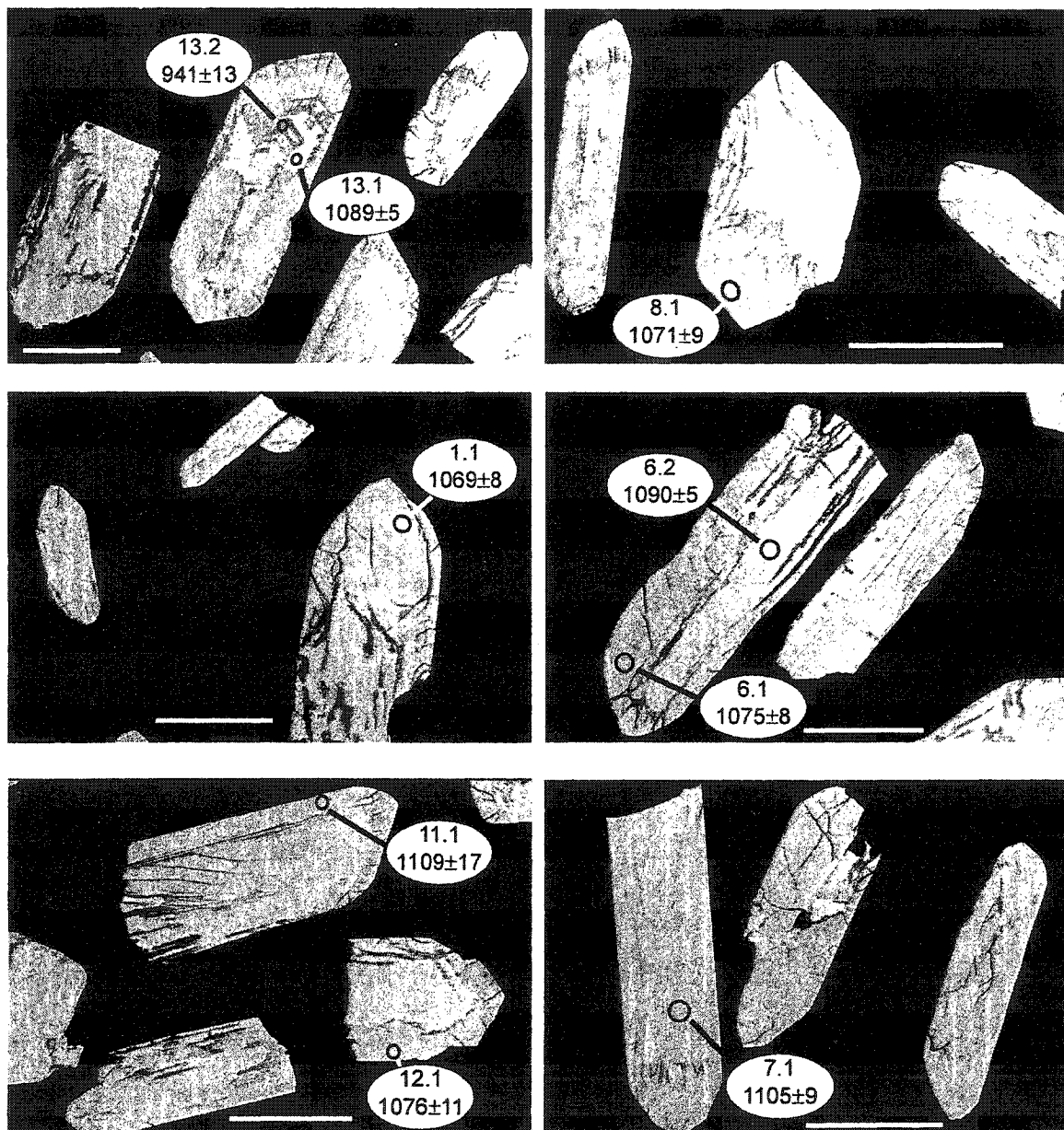
Fig. E.7 continued.

Fig. E.8 SHRIMP spot locations and ^{207}Pb/^{206}Pb ages with errors, pegmatite (2S0207-2). Scale bar=200μm.
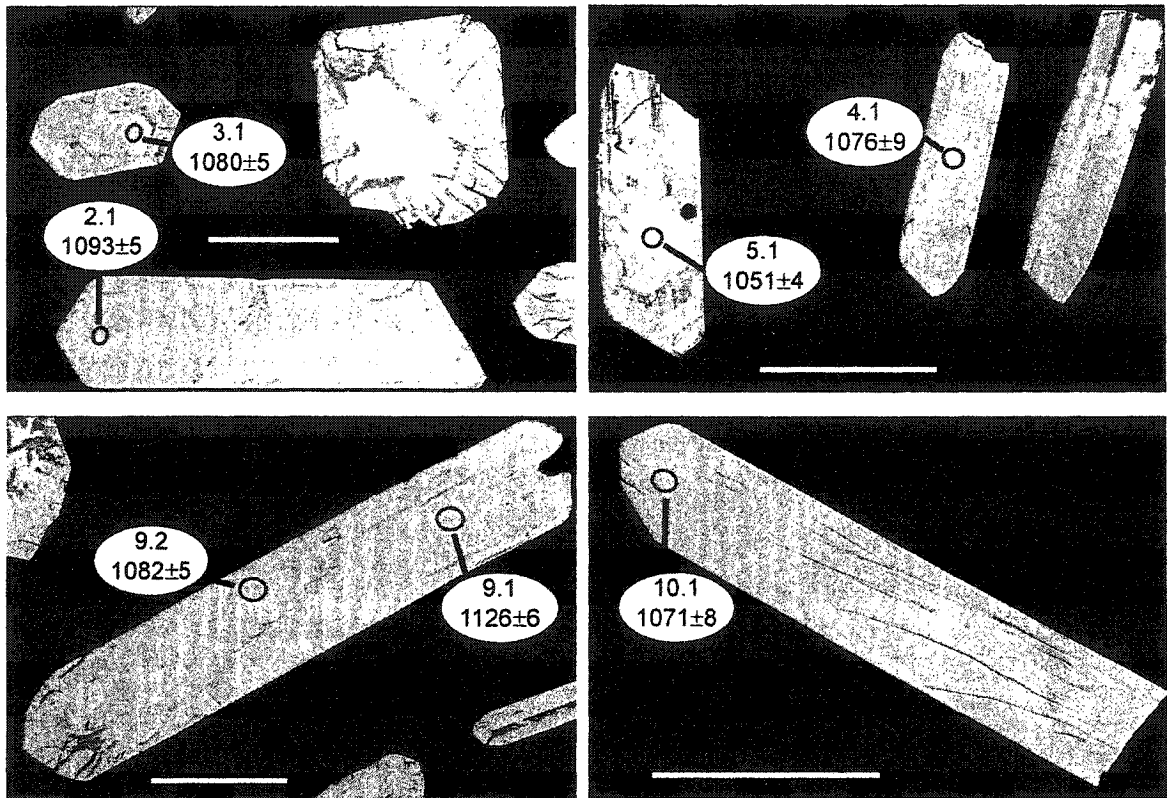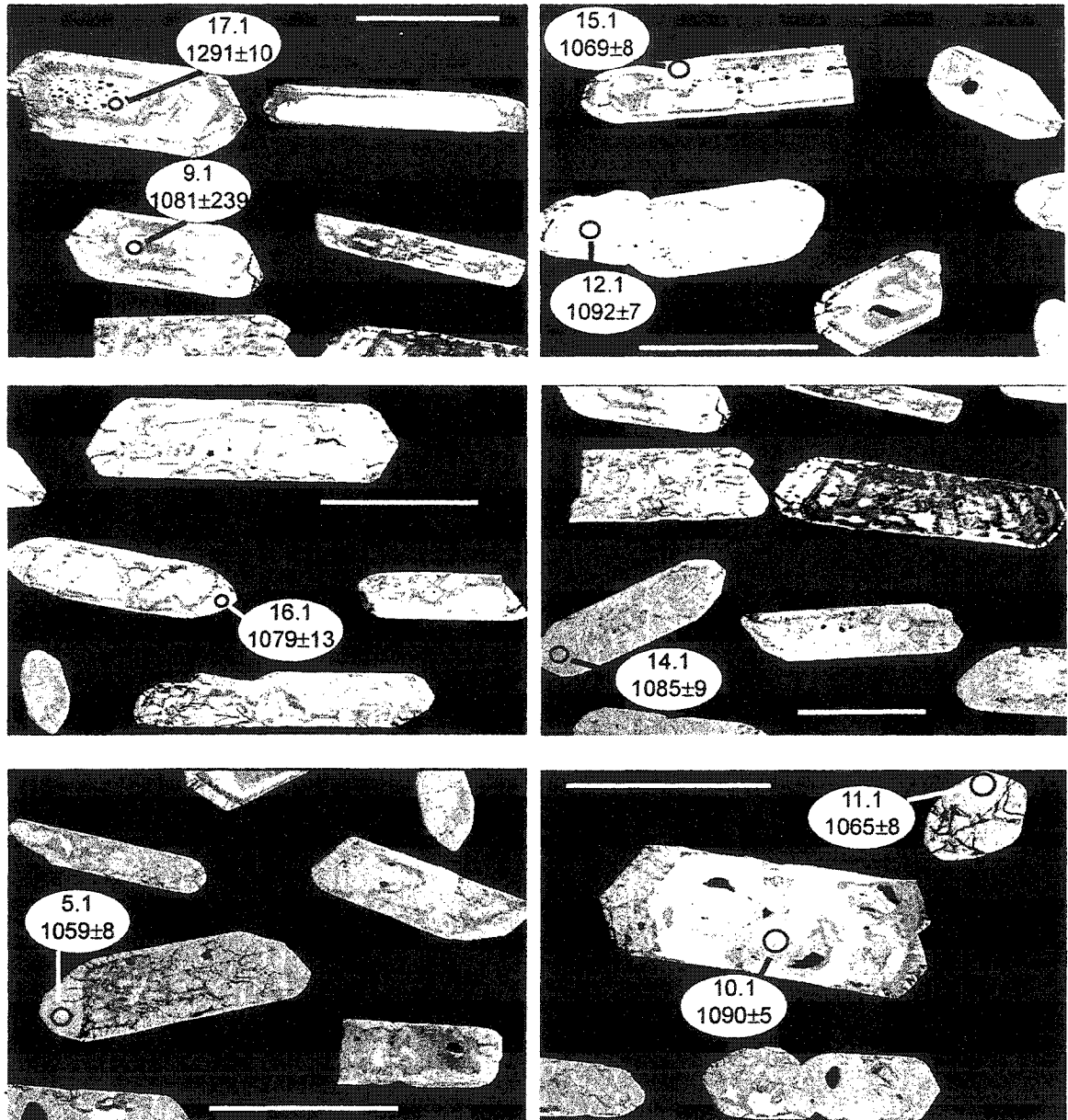
Fig. E.8 continued.

Fig. E.9 SHRIMP spot locations and $^{207}Pb/^{206}Pb$ ages with errors, granite (2S0507). Scale bar=200μm.
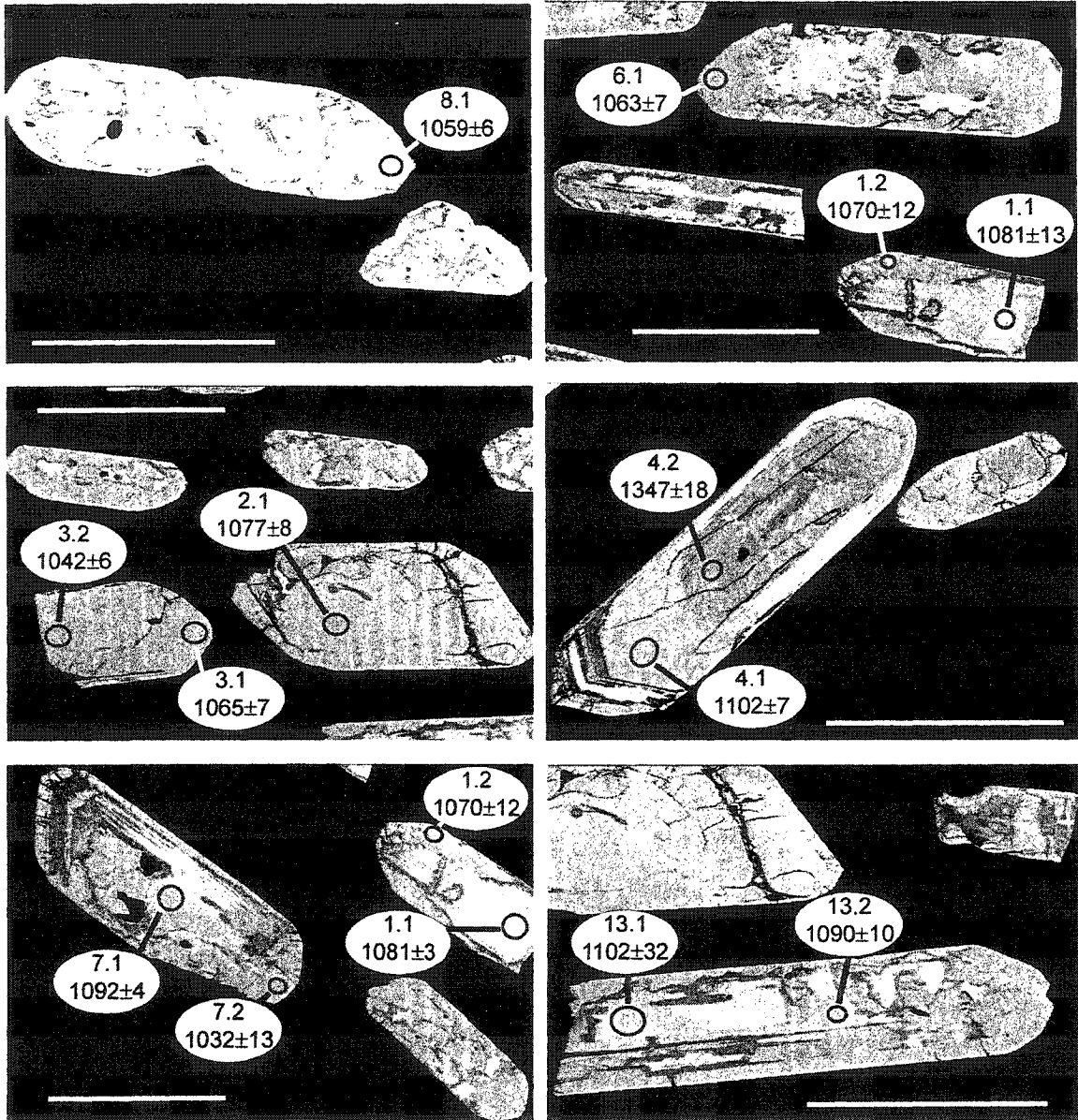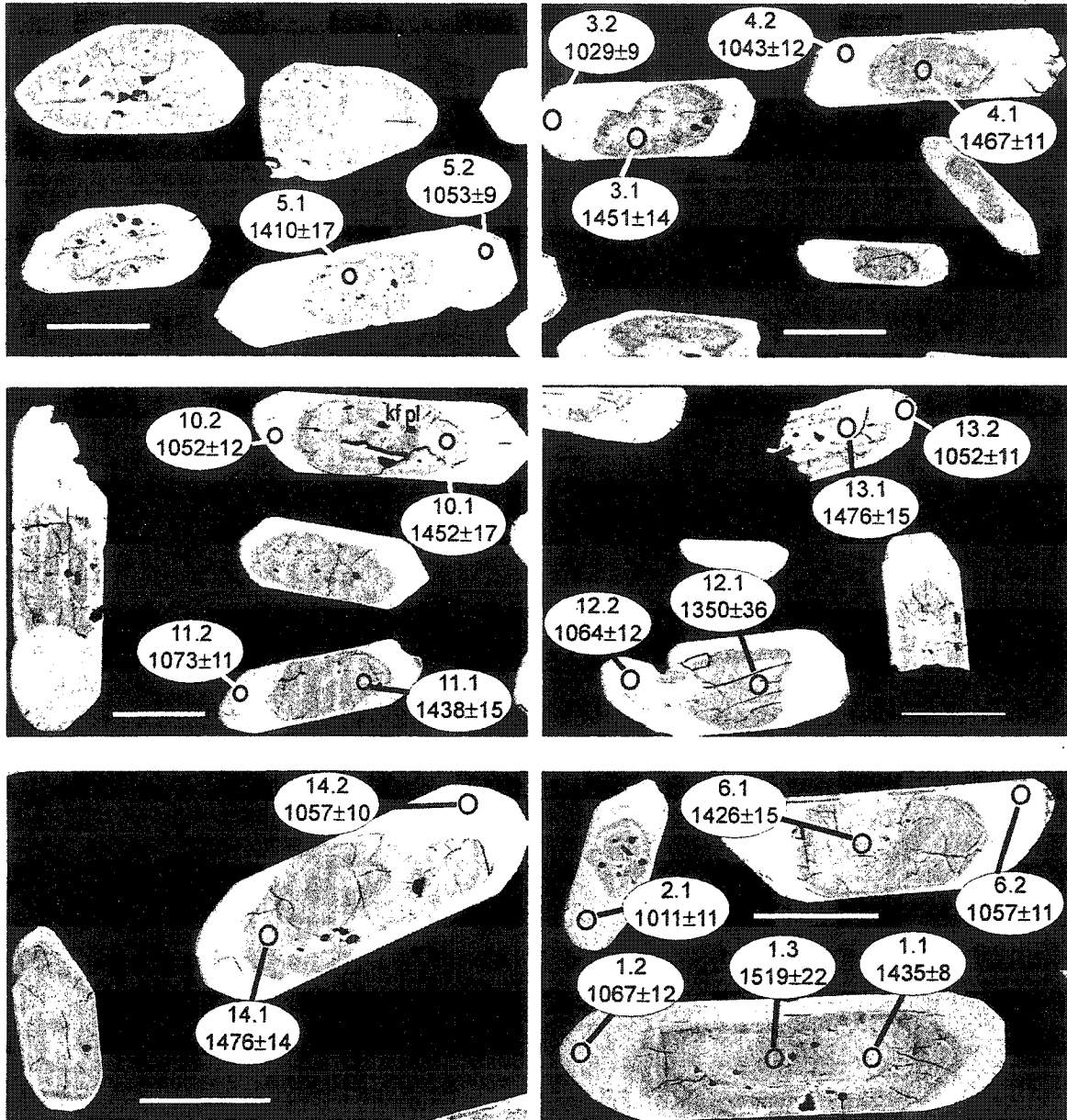
Fig. E.9 continued.

Fig. E.10 SHRIMP spot locations and $^{207}Pb/^{206}Pb$ ages with errors, hornblende-rich leucosome (2S2006-3). Scale bar=100μm.
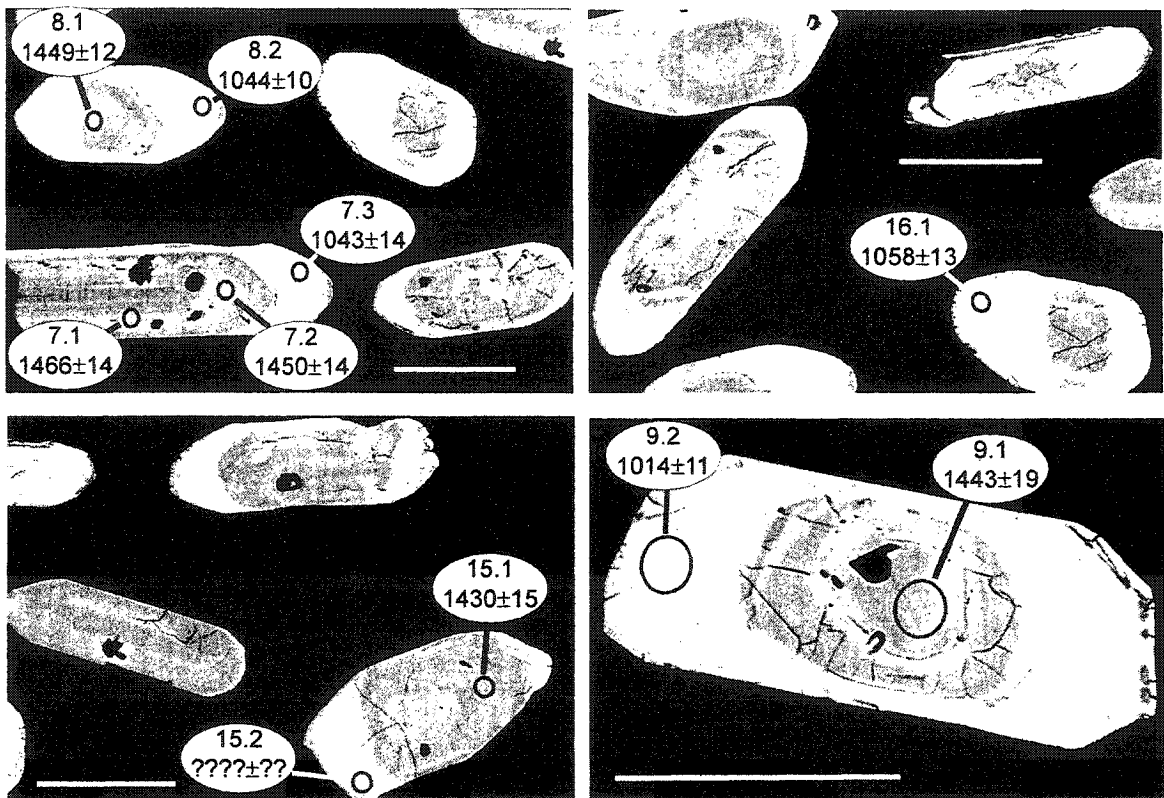
Fig. E.10 continued.

APPENDIX F. Trace element modeling-formulas and sources of uncertainty

F.1. Symbols

C_L^i = concentration of element i in the model melt.

C_0^i = concentration of element i in the original solid (unmelted source).

F = the weight proportion of melted material (i.e., degree of partial melting), or the weight proportion of remaining melt in the case of fractional crystallization.

F.2. Partial melting

F.2.1. Equilibrium batch melting

Equilibrium batch melting describes the formation of a partial melt in which the melt is continually reacting and reequilibrating with the solid residue at the site of melting until mechanical conditions allow it to escape as a single 'batch' of magma (Shaw, 1970). The concentration of a trace element in the model melt is given by:

$$C_L^i = \frac{C_0^i}{D_{RS}^i + F(1 - D_{RS}^i)} \qquad \text{(F.1)}$$

where $D_{RS}^i = \sum D_a^i X_{RS}$ where D_{RS}^i =the bulk partition coefficients of element i in the residual solid, D_a^i = the partition coefficient of element i between melt and mineral a, X_{RS} = the weight proportion of mineral a in the residual solid.

F.2.2. Rayleigh fractional melting

In Rayleigh fractional melting, any melt generated is instantly isolated from the source (Rollinson, 1993). Equilibrium is, therefore, only achieved between the melt and the surfaces of mineral grains in the source region. The concentration of a trace element in the model melt is given by:

$$C_L^i = \frac{C_0^i}{D_0^i}(1-F)^{(\frac{1}{D_0^i}-1)} \qquad \text{(F.2)}$$

330

where $D_0{}^i = \sum D_a{}^i X_0$ where $D_0{}^i$ = the bulk partition coefficient in the original solid phases prior to the onset of melting, $D_a{}^i$ = the partition coefficient of element i between melt and mineral a, X_0 = the weight proportion of mineral a in the source prior to melting.

Equation F.2 assumes that each fraction of melt is separated continuously from the source and collected in a melt collection zone, for example a leucosome or a pluton. The aggregate melt composition, $C_{aL}{}^i$, is given by

$$C_{aL}^i = \frac{C_0^i}{F}(1-(1-F)^{\frac{1}{D_0^i}})$$ (F.3)

F.2.3. Disequilibrium melting

The following description of disequilibrium partial melting as modified after Sawyer (1991). During disequilibrium melting, the concentration of element i in the melt (C_L^i) is given by (Allègre and Minster, 1978; Prinzhofer and Allègre, 1985):

$$C_L^i = x_1 C_1^i + x_2 C_2^i + ... + x_n C_n^i$$ (F.4a)

where x_j = the weight proportion of mineral j entering the melt, and C_j^i = the concentration of element i in mineral j.

Using solid-solid partition coefficients (D_S), equation F.4a can be written as:

$$C_L^i = C_1^i(x_1 + D_{2/1}^S x_2 + ... + D_{n/1}^S x_n)$$ (F.4b)

where $D_{2/1}{}^S$ = the partition coefficient for element i between solid 1 and solid 2.

The initial concentration of element i in the source rock is given by:

$$C_0^i = C_1^i(X_1 + D_{2/1}^S X_2 + ... + D_{n/1}^S X_n)$$ (F.4c)

where X_j is the weight proportion of mineral j in the source rock.

If

$$\frac{C_L^i}{C_1^i} = (x_1 + D_{2/1}^S x_2 + ... + D_{n/1}^S x_n) = M^i$$ (F.4d)

and

$$\frac{C_0^i}{C_1^i} = (X_1 + D_{2/1}^S X_2 + ... + D_{n/1}^S X_n) = Q^i$$ (F.4e)

then

$$C_L^i = C_0^i(\frac{M^i}{Q^i})$$ (F.4f)

Solid-solid partition coefficients are not known, but Barbey $et\ al.$ (1989) suggested that

they can be estimated from the solid-melt partition coefficients, thus:

$$D_{2/1}^S = \frac{D_2^i}{D_1^i}$$

(F.4g)

where D_j^i is the partition coefficient of element i between mineral j and the melt. Substituting in equations F.4b and F.4c, equation F.4f becomes (written in full):

$$C_L^i = C_0^i \left(\frac{x_1 + \dfrac{D_2^i x_2 + ... + D_n^i x_n}{D_1^i}}{X_1 + \dfrac{D_2^i X_2 + ... + D_n^i X_n}{D_1^i}} \right)$$

(F.4h)

F.3. Fractional crystallization

F.3.1. Equilibrium crystallization

During equilibrium crystallization of a magma, complete equilibrium is maintained between the melt and the crystallizing phases (Rollinson, 1993). The distribution of trace elements during equilibrium crystallization is the reverse of equilibrium batch melting (F.1), and the equation, therefore, is:

$$C_L^i = \frac{C_0^i}{F + D_{CP}^i(1-F)}$$

(F.5)

where $D_{CP}^i = \sum D_a^i X_{CP}$ where D_{CP}^i =the bulk partition coefficients of element i in the phases crystallized, D_a^i = the partition coefficient of element i between melt and mineral a, X_{RS} = the weight proportion of mineral a crystallized.

F.3.2. Rayleigh fractional crystallization

Rayleigh fractional crystallization describes a process in which crystals are instantly removed from the melt after crystallization, thus, the distribution of trace elements is not an equilibrium process (Hanson, 1978). The equation for Rayleigh fractional crystallization is:

$$C_L^i = C_0^i F^{(D_{CP}^i - 1)}$$

(F.6)

F.4. Sources of uncertainty

The two main sources of uncertainty in the trace element modeling in Chapters 2-4 are analytical error (Appendix A) and selected partition coefficients (Tables 2.2, 2.3, 2.4, 3.2, and 4.2).

F.4.1. Effects of analytical error

The precision of Ba, Rb, Sr, and the REEs was calculated in Appendix A and is summarized in Table F.1. Here, the analytical uncertainty of Ba is taken to be 15%, 16% for Rb, and 1% for Sr. The analytical uncertainty for the REEs is, for simplicity, taken to be 10%, although in reality it is somewhat lower for all REEs except Er.

Table F.1 Summary of calculated precisions (%) for elements used in trace element modeling.

Std.	Ba	Rb	Sr	La	Ce	Pr	Nd	Sm	Eu	Gd	Tb	Dy	Ho	Er	Tm	Yb	Lu
HFL-1	3	0	1														
AGV-1	9	4	1														
BE-N	15	16	1														
MRG-1				6.8	6.9	7.1	7.6	5.0	5.3	6.7	6.5	6.2	9.0	10.1	8.8	8.3	6.9
BR-688				7.9	8.2	8.5	9.0	5.6	5.9	6.2	6.2	6.5	9.8	10.2	9.6	10.0	6.4

Fig. F.1a illustrates the effects of analytical error on the results of trace element modeling, using the disequilibrium melting modeling (stromatic migmatite) from Chapter 3 as an example. The figure shows that the effects of analytical error are negligible in the trace element modeling. The conclusion regarding the granite-pegmatite relationship in Chapter 4 may appear counter-intuitive; for example, the higher Ba/Rb and lower Rb/Sr ratios of the pegmatites suggest that they are either more primitive than the granites or that they contain a significant proportion of cumulate material. Fig. F.1b shows that the difference in Ba/Rb and Rb/Sr ratios between the granite and pegmatite are statistically and petrogenetically significant. The upper limit of the Ba/Rb error bars in this diagram was calculated by (Ba+analytical error/Rb-analytical error) and the lower limit by Ba-analytical error/Rb+analytical error) and *vice versa* for the Rb/Sr ratios.
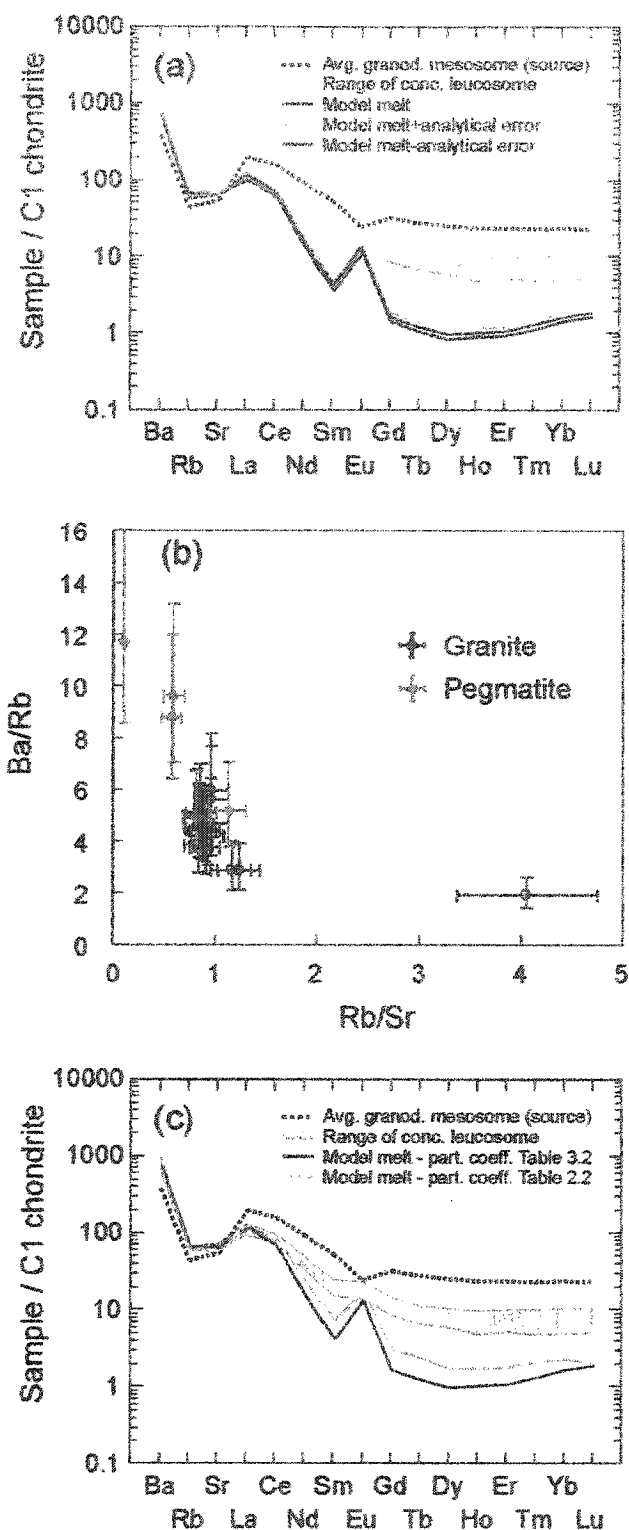
Fig. F.1 Effects of analytical errors on (a) partial melting calculations, stromatic migmatite (see Fig. 3.12b), and)b) Rb/Sr and Ba/Rb ratios of granites and pegmatites in Shawanaga domain (see Fig. 4.7a). (c) Effects of using different partition coefficients in the modeling. The same model is used in (a) and (c) but the partition coefficients are different.

F.4.2. Effects of using different partition coefficients

The inherent problems of selecting valid partition coefficients for the trace element modeling were discussed in Chapter 2 (section 2.5.1). The partition coefficients used in Chapters 2-4 were selected based on rough estimates of melt composition (e.g., basaltic, intermediate, granitic), water contents (e.g., dehydration melting, fluid-present melting), and oxygen fugacity. For most elements, the partition coefficients used in Chapters 2-4 are similar within an order of magnitude, there are, however, some important exceptions. Under reducing conditions (i.e., low oxygen fugacity), europium forms Eu^{2+}, which is compatible in plagioclase where it substitutes for Ca^{2+}. In contrast, under oxidizing conditions, europium forms Eu^{3+}, which is incompatible in plagioclase along with the other trivalent REEs. Petrogenesis of the granitic and rhyolitic gneiss in Chapter 2 and of the concordant leucosomes in Chapter 3 may both have involved partial melting of gray gneiss, but under very different conditions. As discussed in Chapter 2, the granitic and rhyolitic gneiss probably formed at high temperatures, under dry conditions with low oxygen fugacities. In contrast, the concordant leucosomes probably formed by fluid-present melting under relatively higher oxygen fugacities. Thus, despite similar whole-rock (~melt) compositions, the partition coefficients for Eu in plagioclase may have been very different. The selected partition coefficients, 2.15 (or higher) for granitic and rhyolitic gneiss and 0.814 for concordant leucosome reflect these differences; partition coefficients for the other REEs are nearly identical. Studies of partition coefficients in high-silica rhyolites (Mahood and Hildreth, 1983; Nash and Crecraft, 1985) show that partition coefficients of elements such as Eu and Sr may be an order of magnitude higher than in slightly less silicic systems. Mahood and Hildreth (1983) and Nash and Crecraft (1985) determined the partition coefficients on mineral separates, and their results were disputed by Michael (1988) who argued that the extreme partition coefficients resulted from inclusions of accessory phases. Michael (1988) focused on the mafic silicates, and because feldspars commonly contain significantly fewer inclusions than do mafic silicates, the extreme partition coefficients may be valid for high-silica rhyolites (G. Mahood, personal communication, 2002). Using such extreme partition coefficients

produces a model melt that is similar to the composition of the rhyolites, illustrating the profound effects of choosing different partition coefficients in some cases (see for example Fig. 2.15).

Fig. F.1c shows the result of redoing the trace element modeling presented in Fig. F.1a using partition coefficients for plagioclase and hornblende from Table 2.2 rather than 3.2 (except for Ba which was not used in Table 2.2). The most significant effect on the model result is that the MREE and HREE contents of the model melt are higher. The main conclusion, however, is not altered even though there is a ca. 50% difference in the partition coefficients for MREEs and HREEs in hornblende in Tables 2.2 and 3.2. I would, therefore, argue that the trace element modeling results presented herein are relatively robust, and not a result of choosing partition coefficient that yield some desired outcome.